NOAA Atlas NESDIS 70

WORLD OCEAN ATLAS 2009
Volume 3: Dissolved Oxygen, Apparent Oxygen Utilization, and Oxygen Saturation

Silver Spring, MD
March 2010

U.S. DEPARTMENT OF COMMERCE
National Oceanic and Atmospheric Administration
National Environmental Satellite, Data, and Information Service

National Oceanographic Data Center

Additional copies of this publication, as well as information about NODC data holdings and services, are available upon request directly from NODC.

National Oceanographic Data Center
User Services Team
NOAA/NESDIS E/OC1
SSMC III, 4th floor
1315 East-West Highway
Silver Spring, MD 20910-3282

Telephone: (301) 713-3277

Fax: (301) 713-3302

E-mail: NODC.Services@noaa.gov

NODC URL: http://www.nodc.noaa.gov/

For updates on the data, documentation, and additional information about the WOA09 please refer to:

http://www.nodc.noaa.gov/OC5/indprod.html

This document should be cited as:

Garcia, H. E., R. A. Locarnini, T. P. Boyer, J. I. Antonov, O. K. Baranova, M. M. Zweng, and D. R. Johnson, 2010. *World Ocean Atlas 2009 Volume 3: Dissolved Oxygen, Apparent Oxygen Utilization, and Oxygen Saturation*. S. Levitus, Ed., NOAA Atlas NESDIS 70, U.S. Government Printing Office, Washington, D.C., 344 pp.

This document is available on-line at http://www.nodc.noaa.gov/OC5/indprod.html

NOAA Atlas NESDIS 70

WORLD OCEAN ATLAS 2009
Volume 3: Dissolved Oxygen, Apparent Oxygen Utilization, and Oxygen Saturation

Hernan E. Garcia, Ricardo A. Locarnini, Timothy P. Boyer,
John I. Antonov, Olga K. Baranova, Melissa M. Zweng, and Daphne R. Johnson

Editor: Sydney Levitus

Ocean Climate Laboratory
National Oceanographic Data Center

Silver Spring, Maryland
March, 2010

U.S. DEPARTMENT OF COMMERCE
Gary Locke, Secretary

National Oceanic and Atmospheric Administration
Jane Lubchenco,
Under Secretary of Commerce for Oceans and Atmosphere

National Environmental Satellite, Data and Information Service
Mary E. Kicza, Assistant Administrator

Table of Contents

List of Figures

List of Tables

List of Maps in The Appendices

Appendix A: Maps of the annual number of observations and distribution of dissolved oxygen (O_2) at selected depth levels (Pages 29 to 52).

Appendix B: Maps of the seasonal (winter, summer, fall, spring) number of observations, seasonal distribution of dissolved oxygen (O_2), and seasonal minus annual distribution of O_2 at selected depth levels (Pages 53 to 92).

Appendix C: Maps of the monthly number of observations, monthly distribution of dissolved oxygen (O_2), and monthly minus annual distribution of O_2 at selected depth levels (Pages 93 to 152).

Appendix G: Maps of the annual distribution of oxygen saturation (O_2^S) at selected depth levels (Pages 249 to 264).

Appendix H: Maps of the seasonal (winter, summer, fall, spring) distribution of oxygen saturation (O_2^S), and seasonal minus annual distribution of O_2^S at selected depth levels (Pages 265 to 296).

Appendix I: Maps of the monthly distribution of oxygen saturation (O_2^S), and monthly minus annual distribution of O_2^S at selected depth levels (Pages 297 to 344).

Preface

The oceanographic analyses described by this atlas series expand on earlier works, *e.g.,* the *World Ocean Atlas 2005* (WOA05), *World Ocean Atlas 2001* (WOA01)*, World Ocean Atlas 1998* (WOA98)*, World Ocean Atlas 1994* (WOA94) and *Climatological Atlas of the World Ocean* (Levitus, 1982). Previously published oceanographic objective analyses have proven to be of great utility to the oceanographic, climate research, and operational environmental forecasting communities. Such analyses are used as boundary and/or initial conditions in numerical ocean circulation models and atmosphere-ocean models, for verification of numerical simulations of the ocean, as a form of "sea truth" for satellite measurements such as altimetric observations of sea surface height, for computation of nutrient fluxes by Ekman transport, and for planning oceanographic expeditions.

We continue preparing climatological analyses on a one-degree grid. This is because higher resolution analyses are not justified for all the variables we are working with and we wish to produce a set of analyses for which all variables have been analyzed in the same manner. High-resolution analyses as typified by the work of Boyer *et al.* (2004) will be published separately.

In the acknowledgment section of this publication we have expressed our view that creation of global ocean profile and plankton databases and analyses are only possible through the cooperation of scientists, data managers, and scientific administrators throughout the international scientific community. I would also like to thank my colleagues and the staff of the Ocean Climate Laboratory of NODC for their dedication to the project leading to publication of this atlas series. Their integrity and thoroughness have made this database possible. It is my belief that the development and management of national and international oceanographic data archives is best performed by scientists who are actively working with the historical data.

Sydney Levitus
National Oceanographic Data Center
Silver Spring, MD
March 2010

Acknowledgments

This work was made possible by a grant from the NOAA Climate and Global Change Program which enabled the establishment of a research group at the National Oceanographic Data Center. The purpose of this group is to prepare research quality oceanographic databases, as well as to compute objective analyses of, and diagnostic studies based on, these databases. Support is now from base funds and from the NOAA Climate Program Office.

The data on which this atlas is based are in *World Ocean Database 2009* and are distributed on-line and on DVD by NODC/WDC. Many data were acquired as a result of the IOC/IODE *Global Oceanographic Data Archaeology and Rescue* (GODAR) project, and the IOC/IODE *World Ocean Database* project (WOD). At NODC/WDC, data archaeology and rescue projects were supported with funding from the NOAA Environmental Science Data and Information Management (ESDIM) Program and the NOAA Climate and Global Change Program which included support from NASA and DOE. Support for some of the regional IOC/GODAR meetings was provided by the Marine Science and Technology (MAST) program of the European Union. The European Community has also provided support for the Mediterranean Data Archeology and Rescue (MEDAR/MEDATLAS) project which has resulted in the inclusion of substantial amounts of ocean profile data from the Mediterranean Sea. Additional Black Sea data have been acquired as a result of a NATO sponsored project.

We acknowledge the scientists, technicians, and programmers who have collected and processed data, those individuals who have submitted data to national and regional data centers as well as the managers and staff at the various data centers. We thank our colleagues at the NODC. Their efforts have made this and similar works possible.

WORLD OCEAN ATLAS 2009
Volume 3: Dissolved Oxygen, Apparent Oxygen Utilization, and Oxygen Saturation

ABSTRACT

This atlas consists of a description of data analysis procedures and horizontal maps of annual, seasonal, and monthly climatological distribution fields of dissolved oxygen, apparent oxygen utilization (AOU), and dissolved oxygen saturation at selected standard depth levels of the world ocean on a one-degree latitude-longitude grid. The aim of the maps is to illustrate large-scale characteristics of the distribution of dissolved oxygen as a function of depth. The oceanographic data used to generate these climatological maps were computed by objective analysis of all scientifically quality-controlled historical dissolved oxygen data in the *World Ocean Database 2009*. Maps are presented for climatological composite periods (annual, seasonal, monthly, seasonal and monthly difference fields from the annual mean field, and the number of observations) at selected standard depths.

1. INTRODUCTION

The distribution of dissolved oxygen (O_2) in the world ocean is affected by both biochemical and physical processes. Biochemical processes include sources and sinks of O_2 due to marine production, respiration, and oxidation of labile organic matter (*e.g.*, biological pump). Physical processes include sources and sinks of O_2 caused by water mass renewal, air-sea flux exchange, gas solubility (*e.g.*, thermal pump), and water mixing. The oceanic O_2 inventory is sensitive to local to global changes driven by the physical and biological state of the ocean as well as anthropogenic effects acting on different time scales (*e.g.*, Keeling and Garcia, 2001; Matear and Hirst, 2003; Stramma *et al.,* 2008; Shaffer *et al.,* 2009; Riebesell *et al.,* 2009; Hofmann and Schellnhuber, 2009).

This atlas includes an objective analysis of all scientifically quality-controlled historical O_2 (ml l^{-1}) measurements available in the *World Ocean Database 2009* (WOD09; Boyer *et al.,* 2009). We present data analysis procedures and horizontal maps showing annual, seasonal, and monthly climatologies and related statistical fields for O_2 (ml l^{-1}), Apparent Oxygen Utilization (AOU; ml l^{-1}, and dissolved oxygen saturation (O_2^S; %) at selected standard depth levels between the surface and the ocean bottom to a maximum depth of 5500 m. This atlas includes a subset of climatological maps. The complete set of maps, statistical and objectively analyzed data fields, and documentation are all available on Digital Video Disk (DVD) by sending an e-mail request to NODC.Services@noaa.gov and on-line at http://www.nodc.noaa.gov/OC5/indprod.html.

This atlas is part of the *World Ocean Atlas 2009* (WOA09) series. The WOA09 series include analysis for temperature (Locarnini *et al.,* 2010); salinity (Antonov *et al.,* 2010); dissolved oxygen, Apparent Oxygen Utilization, and oxygen saturation (this atlas); and dissolved inorganic nutrients (Garcia *et al.,* 2010a). Climatologies are

here defined as climatological data mean oceanographic fields at selected standard depth levels based on the objective analysis of historical oceanographic profiles and selected surface-only data. A profile is defined as a set of measurements for a single variable (temperature, salinity, O_2, *etc*.) at discrete depths taken as an instrument drops or rises vertically in the water column. All climatologies use all available data regardless of year of observation. The annual climatology was calculated using all data regardless of the month in which the observation was made. Seasonal climatologies were calculated using only data from the defined season (regardless of year). The seasons are here defined as follows. Winter is defined as the months of January, February, and March. Spring is defined as April, May, and June. Summer is defined as July, August, and September. Fall is defined as October, November, and December. Monthly climatologies were calculated using data only from the given month regardless of the day of the month in which the observation was made.

The O_2 data used are available from the National Oceanographic Data Center (NODC) and World Data Center (WDC) for Oceanography, Silver Spring, Maryland (Boyer *et al.,* 2009). Large volumes of oceanographic data have been acquired as a result of the fulfillment of several data management projects including:

a) the Intergovernmental Oceanographic Commission (IOC) Global Oceanographic Data Archaeology and Rescue (GODAR) project (Levitus *et al.,* 2005);

b) the IOC World Ocean Database project (WOD);

c) the IOC Global Temperature Salinity Profile project (GTSPP) (IOC, 1998).

The oceanographic data used in the WOA09 series have been analyzed in a consistent, objective manner on a one-degree latitude-longitude grid at standard depth levels from the surface to a maximum depth of 5500m. The procedures used in WOA09 are identical to those used in the World Ocean Atlas 2005 (WOA05) series (Locarnini *et al.,* 2006; Antonov *et al.,* 2006); Garcia *et al.,* 2006a,b), *World Ocean Atlas 2001* (WOA01) series (Stephens *et al.,* 2002; Boyer *et al.,* 2002; Locarnini *et al.,* 2002; Conkright *et al.,* 2002) and *World Ocean Atlas 1998* (WOA98) series (Antonov *et al.,* 1998 a, b, c; Boyer *et al.,* 1998 a, b, c; Conkright *et al.,* 1998, a, b, c; O' Brien *et al.,* 1998, a, b, c). Slightly different procedures were followed in earlier analyses (Levitus, 1982; *World Ocean Atlas 1994* series [WOA94, Levitus *et al.,* 1994; Levitus and Boyer 1994a, b; Conkright *et al.,* 1994]).

Objective analyses shown in this atlas are limited by the nature of the O_2 data base (data are non-uniform in space, time, and data quality), characteristics of the objective analysis techniques, and the grid used. These limitations and characteristics are discussed below.

Since the publication of WOA05, substantial amounts of additional historical and modern O_2 data have become available. However, even with these additional data, we are still hampered in a number of ways by a lack of oceanographic data. Because of the lack of O_2 data, we are forced to examine the annual cycle by compositing all data regardless of the year of observation. In some geographic areas, quality control is made difficult by the limited number of O_2 data collected in these areas. Data may exist in an area for only one season, thus precluding any representative annual analysis. In some areas there may be a reasonable spatial distribution of data points on which to base an analysis, but there may be only a few (perhaps only one) data values in each one-degree latitude-

longitude square.

We begin by describing the data sources and data distribution (Section 2). Then we describe the general data processing procedures (Section 3), the results (Section 4), summary (Section 5), and future work (Section 6). The appendices of this atlas include global maps for O_2, AOU, and O_2^S.

2. DATA AND DATA DISTRIBUTION

Data sources and quality control procedures are briefly described below. For further information on the data sources used in WOA09 refer to the *World Ocean Database 2009* (WOD09, Boyer *et al.,* 2009). The quality control procedures used in preparation of these analyses are described by Johnson *et al.* (2009).

2.1. Data sources

Historical oceanographic data used in this atlas were obtained from the NODC/WDC archives and include all data gathered as a result of the GODAR and WOD projects. All of the quality-controlled O_2 (ml l^{-1}) data used in this atlas were typically obtained by means of manual or automated chemical O_2 analysis of serial (discrete) water column samples (Garcia *et al.,* 2010b). The O_2 values were analyzed following various modifications of the Winkler titration method (Winkler, 1888) using visual, amperometric, or photometric end-detections (*e.g.*, Carpenter, 1965; Culberson and Huang, 1987; Knapp *et al.,* 1990; Culberson *et al.,* 1991; Dickson, 1994). We refer to the discrete water sample dataset in WOD09 as Ocean Station Data (OSD). Typically, each profile in the OSD dataset consists of 1 to 36 discrete O_2 observations collected at various depths between the surface and the bottom using Nansen or Niskin bottle water samplers. We note that WOD09 contains O_2 data obtained by electronic sensors mounted on the Conductivity-Temperature-Depth (CTD) rosette frame (*i.e.*, polarographic O_2 electronic sensors). However, in preparation of these climatologies we used O_2 data believed to be obtained by chemical titration methods only. We note that most (>75%) of the O_2 data in the WOD09 OSD dataset were collected on or after 1965. AOU (ml l^{-1}) and O_2^S (%) are derived (calculated) variables for an O_2 measurement when *in situ* temperature and salinity were also measured at the same geographic location, time, and depth (pressure). Section 2.2 describes the calculation of AOU and O_2^S.

To understand the procedures for taking individual oceanographic observations and constructing climatological fields, definition of the terms “standard level data” and “observed level data” are necessary. We refer to the actual measured value of an oceanographic variable *in situ* (Latin for “in place”) as an “observation”, and to the depth at which such a measurement was made as the “observed level depth”. We refer to such data as “observed level data”. Before the development of oceanographic instrumentation that measure at high frequencies along the vertical profile, oceanographers often attempted to make measurements at selected “standard levels” in the water column. Sverdrup *et al.* (1942) presented the suggestions of the International Association of Physical Oceanography (IAPSO) as to which depths oceanographic measurements should be made or interpolated to for analysis. Different nations or institutions have a slightly different set of standard depth levels defined. For many purposes, including preparation of the present climatology, observed level data are interpolated to standard depth levels, if observations did not occur at the desired standard depths. The levels at which the O_2, AOU, and O_2^S climatologies were calculated are given in

Table 1. Table 2 shows the depths of each standard depth level. Section 3.1 discusses the vertical interpolation procedures used in our work.

2.2. Data quality control

Quality control of the O_2 data is a major task, the difficulty of which is directly related to lack of data and metadata (for some areas) upon which to base statistical checks. Consequently certain empirical criteria were applied (see sections 2.2.1 through 2.2.4), and as part of the last processing step, subjective judgment was used (see sections 2.2.5 and 2.2.6). Individual data, and in some cases entire profiles or all profiles for individual cruises, have been flagged and not used further because these data produced features that were judged to be non-representative or questionable. As part of our work, we have made available WOD09 which contains both observed levels profile data and standard depth level profile data with various quality control flags applied. The flags mark individual measurements or entire profiles which were not used in the next step of the procedure, either interpolation to standard depth levels for observed level data or calculation of statistical means in the case of standard depth level data. Our knowledge of the variability of the world ocean in the instrumental record now includes a greater appreciation and understanding of the ubiquity of eddies, rings, and lenses in some parts of the world ocean as well as interannual and interdecadal variability of water mass properties associated with modal variability of the atmosphere such as the North Atlantic Oscillation, Pacific Decadal Oscillation, and El Niño Southern Ocean Oscillation. Therefore, we have simply flagged data, not eliminating them from the WOD09. Thus, individual investigators can make their own decision regarding the representativeness of the O_2 data. Investigators studying the distribution of features such as eddies will be interested in those data that we may regard as unrepresentative or questionable for the preparation of the analyses shown in this atlas.

2.2.1. Duplicate elimination

Because O_2 data are received from many sources, sometimes the same data set is received at NODC/WDC more than once but with slightly different time and/or position and/or data values, and hence are not easily identified as duplicate stations. Therefore, to eliminate the repetitive O_2 data values our databases were checked for the presence of exact and near exact replicates using eight different criteria. The first checks involve identifying stations with exact position/date/time and data values; the next checks involve offsets in position/date/time. Profiles identified as duplicates in the checks with a large offset were individually verified to ensure they were indeed duplicate profiles. All but one profile from each set of replicate profiles were eliminated at the first step of our processing.

2.2.2. Range and gradient checks

Range checking (*i.e.*, checking whether an O_2 value is within preset minimum and maximum values as a function of depth and ocean region) was performed on all O_2 values as a first quality control check to flag and withhold from further use the relatively few values that were grossly outside expected oceanic ranges. Range checks were prepared for individual regions of the world ocean. Johnson *et al.* (2009) and Boyer and Levitus (1994) detail the quality control procedures. Tables showing the O_2 ranges selected for each basin and depth can be found in Johnson *et al.* (2009).

A check as to whether excessive vertical gradients occur in the data has been

performed for O_2 data in WOD09 both in terms of positive and negative gradients. See Johnson *et al.* (2009) for limits for excessive gradients for O_2.

2.2.3. Statistical checks

Statistical checks were performed as follows. All data for O_2 (irrespective of year), at each standard depth level, were averaged within five-degree latitude-longitude squares to produce a record of the number of observations, mean, and standard deviation in each square. Statistics were computed for the annual, seasonal, and monthly compositing periods. Below 50 m depth, if data were more than three standard deviations from the mean, the data were flagged and withheld from further use in objective analyses. Above 50 m depth, a five-standard-deviation criterion was used in five-degree squares that contained any land area. In selected five-degree squares that are close to land areas, a four-standard-deviation check was used. In all other squares a three-standard-deviation criterion was used for the 0-50 m depth layer. For standard depth levels situated directly above the bottom, a four-standard-deviation criterion was used.

The reason for the weaker standard deviation criterion in coastal and near-coastal regions is the exceptionally large range of values in the coastal five-degree square statistics for O_2. Frequency distributions of O_2 values in some coastal regions are observed to be skewed or bimodal. Thus to avoid flagging possibly good data in environments expected to have large variability, the standard deviation criteria were broadened.

The total number of measurements in each profile, as well as the total number of O_2 observations exceeding the standard deviation criterion, were recorded. If more than two observations in a profile were found to exceed the standard deviation criterion, then the entire profile was flagged. This check was imposed after tests indicated that surface data from particular casts (which upon inspection appeared to be questionable) were being flagged but deeper data were not. Other situations were found where questionable data from the deeper portion of a cast were flagged, while near-surface data from the same cast were not flagged because of larger natural variability in surface layers. One reason for this was the decrease of the number of observations with depth and the resulting change in sample statistics. The standard-deviation check was applied twice to the O_2 data set for each compositing period.

In summary, first the five-degree square statistics were computed, and the data flagging procedure described above was used to provide a preliminary data set. Next, new five-degree-square statistics were computed from this preliminary data set and used with the same statistical check to produce a new, “clean” data set. The reason for applying the statistical check twice was to flag (and withhold from further use), in the first round, any grossly erroneous or non-representative data from the data set that would artificially increase the variances. The second check is then relatively more effective in identifying smaller, but questionable or non-representative, O_2 observations.

2.2.4. Subjective flagging of data

The O_2 data were averaged by one-degree squares for input to the objective analysis program. After initial objective analyses were computed, the input set of one-degree means still contained questionable data contributing to unrealistic distributions, yielding intense bull's-eyes or spatial gradients. Examination of these features indicated that some of them were due to profiles from particular oceanographic cruises. In such cases, data from an entire

cruise were flagged and withheld from further use by setting a flag on each profile from the cruise. In other cases, individual profiles or measurements were found to cause these features and were flagged.

2.2.5. Representativeness of the data

Another quality control issue is O_2 data representativeness. The general paucity of data forces the compositing of all historical data to produce "climatological" fields. In a given one-degree square, there may be data from a month or season of one particular year, while in the same or a nearby square there may be data from an entirely different year. If there is large interannual variability in a region where scattered sampling in time has occurred, then one can expect the analysis to reflect this. Because the observations are scattered randomly with respect to time, except for a few limited areas, the results cannot, in a strict sense, be considered a true long-term climatological average.

We present smoothed analyses of historical means, based (in certain areas) on relatively few observations. We believe, however, that useful information about the oceans can be gained through our procedures and that the large-scale features are representative of the real ocean. We believe that, if a hypothetical global synoptic set of ocean O_2 data existed and one were to smooth these data to the same degree as we have smoothed the historical means overall, the large-scale features would be similar to our results. Some differences would certainly occur because of interannual-to-decadal-scale variability.

Basically, the O_2 data diminish in number with increasing depth. In the upper ocean, the all-data annual mean distributions are quite reasonable for defining large-scale features, but for the seasonal periods, the data base is inadequate in some regions. With respect to the deep ocean, in some areas the distribution of observations may be adequate for some diagnostic computations but inadequate for other purposes. If an isolated deep basin or some region of the deep ocean has only one observation, then no horizontal gradient computations are meaningful. However, useful information is provided by the observation in the computation of other quantities (e.g., a volumetric mean over a major ocean basin).

2.3 Calculation of AOU and O_2^S

Apparent Oxygen Utilization (AOU, ml l^{-1}) and oxygen saturation (O_2^S, %) were estimated when quality-controlled *in situ* O_2 (ml l^{-1}), temperature (T, °C), and salinity (S) were all measured at the same geographic location, time, and depth (pressure). We note that not all O_2 observations included simultaneous temperature and salinity measurements (see section 2.2.4). Thus, the total number of observations available for calculating AOU and O_2^S is slightly smaller in number than the available number of O_2 observations.

AOU represents one estimate of the O_2 utilized due to biochemical processes relative to a preformed value. AOU (ml l^{-1}) was calculated as the difference between the O_2 gas solubility ($[O_2^*]$) and the measured O_2 concentrations and expressed as,

$$AOU = [O_2^*] - [O_2]$$

in which

$[O_2^*]$ is the O_2 solubility concentration (ml l^{-1}) calculated as a function of *in situ* temperature and salinity, and one atmosphere of total pressure. The $[O_2^*]$ values were calculated using the equation of Garcia and Gordon (1992) based on the $[O_2^*]$ values of Benson and Krause (1984); and $[O_2]$ is the measured O_2 concentration

(ml l^{-1}).

Apparent Oxygen Utilization is an approximate measure of True Oxygen Utilization (TOU). The calculation of AOU assumes that the amount of O_2 used during local biochemical processes can be estimated by the difference in concentration between the observed O_2 and the preformed O_2 values. However, AOU is affected by processes other than biochemical processes such water mixing, departures of $[O_2^*]$ from instantaneous full equilibration with the atmosphere, bubble gas injection, skin temperature effects, and other factors (*e.g.*, Broecker and Peng, 1982; Redfield *et al.,* 1963; Garcia and Keeling, 2001; Ito, 2004). We assume that these processes are small in magnitude when compared to the amplitude of the climatological seasonal O_2 signal on basin-scales.

The O_2 saturation (O_2^S, %) was estimated as 100% times the ratio of $[O_2]$ to $[O_2^*]$,

$$O_2^S = 100\%\left(\frac{[O_2]}{[O_2^*]}\right)$$

The calculated AOU and O_2^S values were processed following the same quality control methods outlined in section 2. Furthermore, if any of the O_2 (section 2) temperature (Locarnini *et al.,* 2010), or salinity (Antonov *et al.,* 2010) values were flagged during the quality control procedure, then AOU and O_2^S values were flagged also, and not used in the analysis.

3. DATA PROCESSING PROCEDURES

3.1. Vertical interpolation to standard levels

Vertical interpolation of observed depth level data to standard depth levels followed procedures in JPOTS Editorial Panel (1991). These procedures are in part based on the work of Reiniger and Ross (1968). Four observed depth level values surrounding the standard depth level value were used, two values from above the standard level and two values from below the standard level. The pair of values furthest from the standard level are termed "exterior" points and the pair of values closest to the standard level are termed interior points. Paired parabolas were generated via Lagrangian interpolation. A reference curve was fitted to the four data points and used to define unacceptable interpolations caused by "overshooting" in the interpolation. When there were too few data points above or below the standard level to apply the Reiniger and Ross technique, we used a three-point Lagrangian interpolation. If three points were not available (either two above and one below or vice-versa), we used linear interpolation. In the event that an observation occurred exactly at the depth of a standard level, then a direct substitution was made. Table 2 provides the range of acceptable distances for which observed level data could be used for interpolation to a standard level.

3.2. Methods of analysis

3.2.1. Overview

An objective analysis scheme of the type described by Barnes (1964) was used to produce the fields shown in this atlas. This scheme had its origins in the work of Cressman (1959). In *World Ocean Atlas 1994* (WOA94), the Barnes (1973) scheme was used. This required only one "correction" to the first-guess field at each grid point in comparison to the successive correction method of Cressman (1959) and Barnes (1964). This was to minimize computing time used in the processing. Barnes (1994) recommends a return to a multi-pass analysis when computing time is not an issue. Based on our own experience we agree with this assessment. The single

pass analysis, used in WOA94, caused an artificial front in the Southeastern Pacific Ocean in a data sparse area (Anne Marie Treguier, personal communication). The analysis scheme used in generating WOA98, WOA01, WOA05, and WOA09 analyses uses a three-pass "correction" which does not result in the creation of this artificial front.

Inputs to the analysis scheme were one-degree square means of data values at standard levels (for time period and variable being analyzed), and a first-guess value for each square. For instance, one-degree square means for our annual analysis were computed using all available data regardless of date of observation. For July, we used all historical July data regardless of year of observation.

Analysis was the same for all standard depth levels. Each one-degree latitude-longitude square value was defined as being representative of its square. The 360x180 gridpoints are located at the intersection of half-degree lines of latitude and longitude. An influence radius was then specified. At those grid points where there was an observed mean value, the difference between the mean and the first-guess field was computed. Next, a correction to the first-guess value at all gridpoints was computed as a distance-weighted mean of all gridpoint difference values that lie within the area around the gridpoint defined by the influence radius. Mathematically, the correction factor derived by Barnes (1964) is given by the expression:

$$C_{i,j} = \frac{\sum_{s=1}^{n} W_s Q_s}{\sum_{s=1}^{n} W_s} \qquad (1)$$

in which:

(i,j) - coordinates of a gridpoint in the east-west and north-south directions respectively;

$C_{i,j}$ - the correction factor at gridpoint coordinates (i,j);

n - the number of observations that fall within the area around the point i,j defined by the influence radius;

Q_s - the difference between the observed mean and the first-guess at the S^{th} point in the influence area;

$W_s = e^{-\frac{Er^2}{R^2}}$ (for $r \le R$; W_s =0 for $r > R$);

r - distance of the observation from the gridpoint;

R - influence radius;

$E = 4$.

The derivation of the weight function, W_s, will be presented in the following section. At each gridpoint we computed an analyzed value $G_{i,j}$ as the sum of the first-guess, $F_{i,j}$, and the correction $C_{i,j}$. The expression for this is

$$G_{i,j} = F_{i,j} + C_{i,j} \qquad (2)$$

If there were no data points within the area defined by the influence radius, then the correction was zero, the first-guess field was left unchanged, and the analyzed value was simply the first-guess value. This correction procedure was applied at all gridpoints to produce an analyzed field. The resulting field was first smoothed with a median filter (Tukey, 1974; Rabiner *et al.,* 1975) and then smoothed with a five-point smoother of the type described by Shuman (1957) (hereafter referred as five-point Shuman smoother). The choice of first-guess fields is important and we discuss our procedures in section 3.2.5.

The analysis scheme is set up so that the influence radius, and the number of five-point smoothing passes can be varied with each iteration. The strategy used is to begin

the analysis with a large influence radius and decrease it with each iteration. This technique allows us to analyze progressively smaller scale phenomena with each iteration.

The analysis scheme is based on the work of several researchers analyzing meteorological data. Bergthorsson and Doos (1955) computed corrections to a first-guess field using various techniques: one assumed that the difference between a first-guess value and an analyzed value at a gridpoint was the same as the difference between an observation and a first-guess value at a nearby observing station. All the observed differences in an area surrounding the gridpoint were then averaged and added to the gridpoint first-guess value to produce an analyzed value. Cressman (1959) applied a distance-related weight function to each observation used in the correction in order to give more weight to observations that occur closest to the gridpoint. In addition, Cressman introduced the method of performing several iterations of the analysis scheme using the analysis produced in each iteration as the first-guess field for the next iteration. He also suggested starting the analysis with a relatively large influence radius and decreasing it with successive iterations so as to analyze smaller scale phenomena with each pass.

Sasaki (1960) introduced a weight function that was specifically related to the density of observations, and Barnes (1964, 1973) extended the work of Sasaki. The weight function of Barnes (1964) has been used here. The objective analysis scheme we used is in common use by the mesoscale meteorological community. Several studies of objective analysis techniques have been made. Achtemeier (1987) examined the "concept of varying influence radii for a successive corrections objective analysis scheme." Seaman (1983) compared the "objective analysis accuracies of statistical interpolation and successive correction schemes." Smith and Leslie (1984) performed an "error determination of a successive correction type objective analysis scheme." Smith *et al.* (1986) made "a comparison of errors in objectively analyzed fields for uniform and non-uniform station distribution."

3.2.2. Derivation of Barnes (1964) weight function

The principle upon which the Barnes (1964) weight function is derived is that "the two-dimensional distribution of an atmospheric variable can be represented by the summation of an infinite number of independent harmonic waves, that is, by a Fourier integral representation". If *f(x,y)* is the variable, then in polar coordinates *(r,θ)*, a smoothed or filtered function *g(x,y)* can be defined:

$$g(x,y)=\frac{1}{2\pi}\int_0^{2\pi}\int_0^{\infty}\eta f(x+r\cos\theta, y+r\sin\theta)\, d\left(\frac{r^2}{4K}\right)d\theta \tag{3}$$

in which r is the radial distance from a gridpoint whose coordinates are *(x,y)*. The weight function is defined as

$$\eta = e^{-\frac{r^2}{4K}} \tag{4}$$

which resembles the Gaussian distribution. The shape of the weight function is determined by the value of K, which relates to the distribution of data. The determination of K follows. The weight function has the property that

$$\frac{1}{2\pi}\int_0^{2\pi}\int_0^{\infty}\eta\, d\left(\frac{r^2}{4K}\right)d\theta = 1 \tag{5}$$

This property is desirable because in the continuous case (3) the application of the weight function to the distribution *f(x,y)* will

not change the mean of the distribution. However, in the discrete case (1), we only sum the contributions to within the distance R. This introduces an error in the evaluation of the filtered function, because the condition given by (5) does not apply. The error can be pre-determined and set to a reasonably small value in the following manner. If one carries out the integration in (5) with respect to θ, the remaining integral can be rewritten as

$$\int_0^R \eta d\left(\frac{r^2}{4K}\right) + \int_R^\infty \eta d\left(\frac{r^2}{4K}\right) = 1 \qquad (6)$$

Defining the second integral as ε yields

$$\int_0^R e^{-\frac{r^2}{4K}} d\left(\frac{r^2}{4K}\right) = 1 - \varepsilon \qquad (7)$$

Integrating (7), we obtain

$$\varepsilon = e^{-\frac{R^2}{4K}} \qquad (7a)$$

Taking the natural logarithm of both sides of (7a) leads to an expression for K,

$$K = R^2 / 4E \qquad (7b)$$

where $E \equiv -\ln \varepsilon$

Rewriting (4) using (7b) leads to the form of weight function used in the evaluation of (1). Thus, choice of E and the specification of R determine the shape of the weight function. Levitus (1982) chose E=4 which corresponds to a value of ε of approximately 0.02. This choice implies with respect to (7) the representation of more than 98 percent of the influence of any data around the gridpoint in the area defined by the influence radius R. This analysis (WOA09) and previous analyses (WOA94, WOA98, WOA01, WOA05, WOA09) used E=4.

Barnes (1964) proposed using this scheme in an iterative fashion similar to Cressman (1959). Levitus (1982) used a four-iteration scheme with a variable influence radius for each pass. WOA94 used a one-iteration scheme. WOA98, WOA01, WOA05, and WOA09 employed a three-iteration scheme with a variable influence radius.

3.2.3. Derivation of Barnes (1964) response function

It is desirable to know the response of a data set to the interpolation procedure applied to it. Following Barnes (1964) and reducing to one-dimensional case we let

$$f(x) = A \sin(\alpha x) \qquad (8)$$

in which $\alpha = 2\pi/\lambda$ with λ being the wavelength of a particular Fourier component, and substitute this function into equation (3) along with the expression for η in equation (4). Then

$$g(x) = D\left[A \sin(\alpha x)\right] = Df(x) \qquad (9)$$

in which D is the response function for one application of the analysis and defined as

$$D = e^{-\left(\frac{\alpha R}{4}\right)^2} = e^{-\left(\frac{\pi R}{2\lambda}\right)^2}$$

The phase of each Fourier component is not changed by the interpolation procedure. The results of an analysis pass are used as the first-guess for the next analysis pass in an iterative fashion. The relationship between the filtered function $g(x)$ and the response function after N iterations as derived by Barnes (1964) is

$$g_N(x) = f(x) D \sum_{n=1}^{N} (1 - D)^{n-1} \qquad (10)$$

Equation (10) differs trivially from that given by Barnes. The difference is due to our first-guess field being defined as a zonal average, annual mean, seasonal mean, or monthly mean, whereas Barnes used the first application of the analysis as a first-guess. Barnes (1964) also showed that applying the

analysis scheme in an iterative fashion will result in convergence of the analyzed field to the observed data field. However, it is not desirable to approach the observed data too closely, because at least seven or eight gridpoints are needed to represent a Fourier component.

The response function given in (10) is useful in two ways: it is informative to know what Fourier components make up the analyses, and the computer programs used in generating the analyses can be checked for correctness by comparison with (10).

3.2.4. Choice of response function

The distribution of O_2 observations (see appendices) at different depths and for the different averaging periods, are not regular in space or time. At one extreme, regions exist in which every one-degree square contains data and no interpolation needs to be performed. At the other extreme are regions in which few if any data exist. Thus, with variable data spacing the average separation distance between gridpoints containing data is a function of geographical position and averaging period. However, if we computed and used a different average separation distance for each variable at each depth and each averaging period, we would be generating analyses in which the wavelengths of observed phenomena might differ from one depth level to another and from one season to another. In WOA94, a fixed influence radius of 555 kilometers was used to allow uniformity in the analysis of all variables. For the present analyses (as well as for WOA98 and WOA01), a three-pass analysis, based on Barnes (1964), with influence radii of 888, 666 and 444 km was used.

Inspection of (1) shows that the difference between the analyzed field and the first-guess field values at any gridpoint is proportional to the sum of the weighted-differences between the observed mean and first-guess at all gridpoints containing data within the influence area.

The reason for using the five-point Shuman smoother and the median smoother is that our data are not evenly distributed in space. As the analysis moves from regions containing data to regions devoid of data, small-scale discontinuities may develop. The five-point Shuman and median smoothers are used to eliminate these discontinuities. The five-point Shuman smoother does not affect the phase of the Fourier components that comprise an analyzed field.

The response function for the analyses presented in the WOA09 series is given in Table 4 and in Figure 1. For comparison purposes, the response function used by Levitus (1982), WOA94, and others are also presented. The response function represents the smoothing inherent in the objective analysis described above plus the effects of one application of the five-point Shuman smoother and one application of a five-point median smoother. The effect of varying the amount of smoothing in North Atlantic sea surface temperature (SST) fields has been quantified by Levitus (1982) for a particular case. In a region of strong SST gradient such as the Gulf Stream, the effect of smoothing can easily be responsible for differences between analyses exceeding 1.0°C.

To avoid the problem of the influence region extending across land or sills to adjacent basins, the objective analysis routine employs basin "identifiers" to preclude the use of data from adjacent basins. Table 5 lists these basins and the depth at which no exchange of information between basins is allowed during the objective analysis of data, *i.e.,* "depths of mutual exclusion." Some regions are nearly, but not completely, isolated topographically. Because some of these nearly isolated basins have water mass

properties that are different from surrounding basins, we have chosen to treat these as isolated basins as well. Not all such basins have been identified because of the complicated structure of the sea floor. In Table 5, a region marked with an ■*• can interact with adjacent basins except for special areas such as the Isthmus of Panama.

3.2.5. First-guess field determination

There are gaps in the data coverage and, in some parts of the world ocean, there exist adjacent basins whose water mass properties are individually nearly homogeneous but have distinct basin-to basin differences. Spurious features can be created when an influence area extends over two basins of this nature (basins are listed in Table 5). Our choice of first-guess field attempts to minimize the creation of such features. To provide a first-guess field for the annual analysis at any standard level, we first zonally averaged the observed O_2 data in each one-degree latitude belt by individual ocean basins. The annual analysis was then used as the first-guess for each seasonal analysis and each seasonal analysis was used as a first-guess for the appropriate monthly analysis if computed.

We then reanalyzed the O_2 data using the newly produced analyses as first-guess fields described as follows and as shown in Figure 2. A new annual mean was computed as the mean of the twelve monthly analyses for the upper 1500 m, and the mean of the four seasons below 1500 m depth for O_2, AOU, and O_2^S. The new annual mean for each variable was used as the first-guess field for new seasonal analyses. These new seasonal analyses in turn were used to produce new monthly analyses. This procedure produces slightly smoother means. More importantly we recognize that fairly large data-void regions exist, in some cases to such an extent that a seasonal or monthly analysis in these regions might not be realistic or meaningful. Geographic distribution of observations for the all-data annual periods (see appendices) is reasonable for upper layers of the ocean. By using an all-data annual mean, first-guess field regions where data exists for only one season or month will show no contribution to the annual cycle. By contrast, if we used a zonal average for each season or month, then, in those latitudes where gaps exist, the first-guess field would be heavily biased by the few data points that exist. If these were anomalous data in some way, an entire basin-wide belt might be affected.

One advantage of producing "global" fields for a particular compositing period (even though some regions are data void) is that such analyses can be modified by investigators for use in modeling studies. For example, England (1992) noted that the temperature distribution produced by Levitus (1982) for the Antarctic is too high (due to a lack of winter data for the Southern Hemisphere) to allow for the formation of Antarctic Intermediate Water in an ocean general circulation model. By increasing the temperature of the "observed" field the model was able to produce this water mass.

3.3. Choice of objective analysis procedures

Optimum interpolation (Gandin, 1963) has been used by some investigators to objectively analyze oceanographic data. We recognize the power of this technique but have not used it to produce analyzed fields. As described by Gandin (1963), optimum interpolation is used to analyze synoptic data using statistics based on historical data. In particular, second-order statistics such as correlation functions are used to estimate the distribution of first order parameters such as means. We attempt to map most fields in this atlas based on relatively sparse data sets. By necessity we must composite all data

regardless of year of observation, to have enough data to produce a global, hemispheric, or regional analysis for a particular month, season, or even yearly. Because of the paucity of data, we prefer not to use an analysis scheme that is based on second order statistics. In addition, as Gandin has noted, there are two limiting cases associated with optimum interpolation. The first is when a data distribution is dense. In this case, the choice of interpolation scheme makes little difference. The second case is when data are sparse. In this case, an analysis scheme based on second order statistics is of questionable value. For additional information on objective analysis procedures see Thiebaux and Pedder (1987) and Daley (1991).

3.4. Choice of spatial grid

The analyses that comprise WOA09 have been computed using the ETOPO5 land-sea topography to define ocean depths at each gridpoint (ETOPO5, 1988). From the ETOPO5 land mask, a quarter-degree land mask was created based on ocean bottom depth and land criteria. If four or more 5-minute square values out of a possible nine in a one-quarter-degree box were defined as land, then the quarter-degree gridbox was defined to be land. If no more than two of the 5-minute squares had the same depth value in a quarter-degree box, then the average value of the 5-minute ocean depths in that box was defined to be the depth of the quarter-degree gridbox. If three or more 5-minute squares out of the nine had a common bottom depth, then the depth of the quarter-degree box was set to the most common depth value. The same method was used to go from a quarter-degree to a one-degree resolution. In the one-degree resolution case, at least four points out of a possible sixteen (in a one-degree square) had to be land in order for the one-degree square to remain land and three out of sixteen had to have the same depth for the ocean depth to be set. These criteria yielded a mask that was then modified by:

a) Connecting the Isthmus of Panama,
b) Maintaining an opening in the Straits of Gibraltar and in the English Channel,
c) Connecting the Kamchatka Peninsula and the Baja Peninsula to their respective continents.

4. RESULTS

The appendices in this atlas include three types of black and white horizontal maps as a function of selected standard depth levels for O_2, AOU, and O_2^S, respectively:

a) Number of observations in each one-degree latitude-longitude grid used in the objective analysis binned into 1 to 5 and greater than 5 numbers of observations. Each map includes the total number of observations. We note that the number of observations is included for O_2 only. The number of observations for AOU and O_2^S is a subset of the number of O_2 observations used in the analysis.
b) Objectively analyzed distribution fields. One-degree grids for which there were less than three values available in the objective analysis defined by the influence radius are denoted by a "+" symbol.
c) Seasonal and monthly difference fields from the annual mean field. One-degree grids for which there were less than three values available in the objective analysis defined by the influence radius are denoted by a "+" symbol.

The maps are arranged by composite time periods (annual, seasonal, month) for O_2, AOU, and O_2^S, respectively. Table 5 describes all available O_2, AOU, and O_2^S maps and data fields. We note that the complete set of all climatological maps (in

color), objectively analyzed fields and associated statistical fields at all standard depth levels shown in Table 1 are available on DVD by sending an e-mail request to NODC.Services@noaa.gov and on-line at www.nodc.noaa.gov/OC5/indprod.html.

All of the figures use consistent symbols and notations for displaying information. Continents are displayed as solid black areas. Coastal and open ocean areas shallower than the standard depth level being displayed are shown as solid light gray areas. The objectively analyzed fields include the minimum and maximum values as well as the contour interval used. The maps may include additional contour lines displayed as dashed black lines. All of the maps were computer drafted using Generic Mapping Tools (Wessel and Smith, 1998). We describe next the computation of annual and seasonal fields (section 4.1) and available objective and statistical fields (section 4.2).

4.1. Computation of annual and seasonal fields

After completion of all of our analyses we define a final annual analysis as the average of our twelve monthly mean fields in the upper 1500 m of the ocean. Below 1500 m depth we define an annual analysis as the mean of the four seasonal analyses. Our final seasonal analyses are defined as the average of monthly analyses in the upper 1500 m of the ocean (see Figure 2).

4.2. Available objective and statistical fields

Table 5 lists all objective and statistical fields calculated as part of WOA09. Climatologies of oceanographic variables and associated statistics described in this document, as well as global figures of same can be obtained at the WOA09 webpage (http://www.nodc.noaa.gov/OC5/WOA09/pr_woa09.html) and on DVD by sending a request to NODC.Services@noaa.gov.

The sample standard deviation in a gridbox was computed using:

$$s = \sqrt{\frac{\sum_{n=1}^{N} (x_n - \overline{x})^2}{N - 1}} \qquad (11)$$

in which x_n= the n^{th} data value in the gridbox, $\overline{x}$=mean of all data values in the gridbox, and N= total number of data values in the gridbox. The standard error of the mean was computed by dividing the standard deviation by the square root of the number of observations in each gridbox.

In addition to statistical fields, the land/ocean bottom mask and basin definition mask are available on-line at http://www.nodc.noaa.gov/OC5/WOA09/pr_woa09.html. A user could take the standard depth level data from WOD09 with flags and these masks, and recreate the WOA09 fields following the procedures outlined in this document. Explanations and data formats for the data files are found under documentation on the WOA09 webpage.

4.3. Obtaining WOA09 fields online

The objective and statistical data fields can be obtained online in different digital formats at the WOA09 webpage (http://www.nodc.noaa.gov/OC5/WOA09/pr_woa09.html) and on DVD by sending a request to NODC.Services@noaa.gov. The WOA09 fields can be obtained in ASCII format (WOA native and comma separated value [CSV]) and netCDF through our WOA09 web page. For users interested in specific geographic areas, the World Ocean Atlas Select (WOAselect) selection tool can be used to designate a subset geographic area, depth, and oceanographic variable to view and optionally download

climatological means or related statistics in shapefile format which is compatible with GIS software such as ArcMap. WOA09 includes a digital collection of "JPEG" and high resolution graphic (PDF) images of the objective and statistical fields. In addition, WOA09 can be obtained in Ocean Data View (ODV) format (http://odv.awi.de/). WOA09 will be available through other online locations as well. WOA98, WOA01, and WOA05 are presently served through the IRI/LDEO Climate Data Library with access to statistical and objectively analyzed fields in a variety of digital formats (http://iridl.ldeo.columbia.edu/).

5. SUMMARY

In the preceding sections we have described the results of a project to objectively analyze all historical quality-controlled O_2 data in WOD09. We desire to build a set of climatological analyses that are identical in all respects for all variables in the WOA09 series including relatively data sparse variables such as nutrients (Garcia *et al.,* 2010a). This provides investigators with a consistent set of analyses to work with.

One advantage of the analysis techniques used in this atlas is that we know the amount of smoothing by objective analyses as given by the response function in Table 3 and Figure 1. We believe this to be an important function for constructing and describing a climatology of any parameter. Particularly when computing anomalies from a standard climatology, it is important that the data field be smoothed to the same extent as the climatology, to prevent generation of spurious anomalies simply through differences in smoothing. A second reason is that purely diagnostic computations require a minimum of seven or eight gridpoints to represent any Fourier component with statistical confidence. Higher order derivatives will require more smoothing.

We have attempted to create objectively analyzed fields and data sets that can be used as a "black box." We emphasize that some quality control procedures used are subjective. For those users who wish to make their own choices, all the data used in our analyses are available both at standard depth levels as well as observed depth levels (http://www.nodc.noaa.gov/OC5/WOA09/pr_woa09.html). The results presented in this atlas show some features that may be suspect and may be due to non-representative O_2 data that were not flagged by the quality control techniques used. Although we have attempted to identify as many of these features as possible by flagging the O_2 data which generate these features, some obviously could remain. Some may eventually turn out not to be artifacts but rather to represent "real" oceanic features, not yet capable of being described in a meaningful way due to lack of O_2 data. The views, findings, and any errors in this document are those of the authors.

6. FUTURE WORK

Our analyses will be updated when justified by additional O_2 observations. As more data are received at NODC/WDC, we will also be able to produce improved higher resolution climatologies for O_2, AOU, and O_2^S. Additional O_2 data will likely improve the results. For example, analysis of O_2 data collected by the broad-scale global array of temperature/salinity profiling floats (ARGO) equipped with automated O_2 sensors will help provide additional observational constraints on observed inter-annual to decadal-scale changes in both physical and biochemical O_2 processes (*e.g.*, Emerson *et al.,* 2002; Körtzinger *et al.,* 2004; Körtzinger *et al.,* 2005, Garcia *et al.,* 2005a,b; Garcia *et al.,* 1998; Keeling and Garcia, 2002; Bindoff and McDougall, 2002; Deutsch *et al.,* 2005; Stramma *et al.,* 2008; Shaffer *et al.,* 2009; Riebesell *et al.,* 2009; Hofmann and

Schellnhuber, 2009).

7. REFERENCES

Achtemeier, G. L., 1987. On the concept of varying influence radii for a successive corrections objective analysis. *Mon. Wea. Rev.,* 11, 1761-1771.

Antonov, J. I., R. A. Locarnini, T. P. Boyer, A. V. Mishonov, and H. E. Garcia, 2010. World Ocean Atlas 2009, Volume 2: Salinity. S. Levitus, Ed., NOAA Atlas NESDIS 69, U.S. Gov. Printing Office, Washington, D.C., 184 pp.

Antonov, J. I., S. Levitus, T. P. Boyer, M. E. Conkright, T.D. O' Brien, and C. Stephens, 1998a: *World Ocean Atlas 1998. Vol. 1: Temperature of the Atlantic Ocean.* NOAA Atlas NESDIS 27, U.S. Gov. Printing Office, Washington, D.C., 166 pp.

Antonov, J. I., S. Levitus, T. P. Boyer, M. E. Conkright, T.D. O' Brien, and C. Stephens, 1998b: *World Ocean Atlas 1998. Vol. 2: Temperature of the Pacific Ocean.* NOAA Atlas NESDIS 28, U.S. Gov. Printing Office, Washington, D.C., 166 pp.

Antonov, J. I., S. Levitus, T. P. Boyer, M. E. Conkright, T. D. O' Brien, C. Stephens, and B. Trotsenko, 1998c: *World Ocean Atlas 1998. Vol. 3: Temperature of the Indian Ocean.* NOAA Atlas NESDIS 29, U.S. Gov. Printing Office, Washington, D.C., 166 pp.

Antonov, J. I., R. A. Locarnini, T. P. Boyer, H. E. Garcia, and A.V. Mishonov, 2006: *World Ocean Atlas 2005, Vol. 2: Salinity*. S. Levitus, Ed., NOAA Atlas NESDIS 62, U.S. Gov. Printing Office, Washington, D.C. 182 pp.

Barnes, S. L., 1964. A technique for maximizing details in numerical weather map analysis. *J. App. Meteor.*, 3, 396-409.

Barnes, S. L., 1973. Mesoscale objective map analysis using weighted time series observations. *NOAA Technical Memorandum ERL* NSSL-62, 60 pp.

Barnes, S. L., 1994. Applications of the Barnes Objective Analysis Scheme, Part III: Tuning for Minimum Error. *J. Atmosph. and Oceanic Tech*., 11, 1459-1479.

Benson, B. B., and O. Krauss, 1984. The concentration and isotopic fractionation of oxygen dissolved in freshwater and seawater in equilibrium with the atmosphere. *Limnol. Oceanogr.*, 10, 264-277.

Bergthorsson, P. and B. Doos, 1955. Numerical Weather map analysis. *Tellus*, 7, 329-340.

Bindoff, N. L., and T. J. McDougall, 2000. Decadal changes along an Indian Ocean section at 32°S and their interpretation, *J. Phys. Oceanogr.*, 30, 1207–1222.

Boyer, T. P., J. I. Antonov , O. K. Baranova, H. E. Garcia, D. R. Johnson, R. A. Locarnini, A. V. Mishonov, T. D. O'Brien, D. Seidov, I. V. Smolyar, M. M. Zweng, 2009. World Ocean Database 2009. S. Levitus, Ed., NOAA Atlas NESDIS 66, U.S. Gov. Printing Office, Wash., D.C., 219 pp., DVDs.

Boyer, T. P. and S. Levitus, 1994. Quality control and processing of historical temperature, salinity and oxygen data. NOAA Technical Report NESDIS 81, 65 pp.

Boyer, T. P., S. Levitus, J. I. Antonov, M.E. Conkright, T.D. O' Brien, and C. Stephens, 1998a: *World Ocean Atlas 1998 Vol. 4: Salinity of the Atlantic Ocean*. NOAA Atlas NESDIS 30, U.S. Gov. Printing Office, Washington, D.C., 166 pp.

Boyer, T. P., S. Levitus, J. I. Antonov, M. E. Conkright, T.D. O' Brien, and C. Stephens, 1998b: *World Ocean Atlas 1998 Vol. 5: Salinity of the Pacific Ocean.* NOAA Atlas NESDIS 31, U.S. Gov. Printing Office, Washington, D.C., 166 pp.

Boyer, T. P., S. Levitus, J. I. Antonov, M. E. Conkright, T. D. O' Brien, C. Stephens, and B. Trotsenko, 1998c: *World Ocean Atlas 1998 Vol. 6: Salinity of the Indian Ocean*. NOAA Atlas NESDIS 32, U.S. Gov. Printing Office, Washington, D.C., 166 pp.

Boyer, T. P., C. Stephens, J. I. Antonov, M. E. Conkright, R. A. Locarnini, T.D. O'Brien, and H.E. Garcia, 2002: *World Ocean Atlas 2001, Vol. 2: Salinity*. S. Levitus, Ed., NOAA Atlas NESDIS 50, U.S. Gov. Printing Office, Washington, D.C., 165 pp.

Boyer, T. P., S. Levitus, H. E. Garcia, R. A. Locarnini, C. Stephens, and J.I. Antonov, 2004. Objective Analyses of Annual, Seasonal, and Monthly Temperature and Salinity for the World Ocean on a ¼ degree Grid. *International J. of Climatology*, 25, 931-945.

Boyer, T. P., J .I. Antonov, H. E. Garcia, D. R. Johnson, R.A. Locarnini, A.V. Mishonov, M.T. Pitcher, O.K. Baranova, and I.V. Smolyar, 2006. *World Ocean Database 2005.* S. Levitus, Ed., NOAA Atlas NESDIS 60, U.S. Gov. Printing Office, Washington, D.C., 190 pp.

Broecker, W. S. and T. H. Peng, 1982. *Tracers in the Sea*, Eldigio Press, Palisades, N.Y., 690 pp.

Carpenter, J. H., 1965. The Chesapeake Bay Institute technique for the Winkler dissolved oxygen titration, *Limnol. Oceanogr.*, 10, 141-143.

Conkright, M., S. Levitus, and T. Boyer, 1994: *World Ocean Atlas 1994, Vol. 1: Nutrients*. NOAA Atlas NESDIS 1, U.S. Gov. Printing Office, Washington, D.C., 150 pp.

Conkright, M. E., T. O' Brien, S. Levitus, T.P. Boyer, J. Antonov, and C. Stephens, 1998a: *World Ocean Atlas 1998 Vol. 10: Nutrients and Chlorophyll of the Atlantic Ocean.* NOAA Atlas NESDIS 36, U.S. Gov. Printing Office, Washington, D.C., 245 pp.

Conkright, M. E., T. D. O' Brien, S. Levitus, T.P. Boyer, J.I. Antonov, and C. Stephens, 1998b: *World Ocean Atlas 1998 Vol. 11: Nutrients and Chlorophyll of the Pacific Ocean.* NOAA Atlas NESDIS 37, U.S. U.S. Gov. Printing Office, Washington, D.C., 245 pp.

Conkright, M. E., T. D. O' Brien, S. Levitus, T.P. Boyer, J.I. Antonov, and C. Stephens, 1998c: *World Ocean Atlas 1998 Vol. 12: Nutrients and Chlorophyll of the Indian Ocean.* NOAA Atlas NESDIS 38, U.S. Gov. Printing Office, Washington, D.C., 245 pp.

Conkright, M. E., H. E. Garcia, T. D. O'Brien, R.A. Locarnini, T.P. Boyer, C. Stephens, and J.I. Antonov, 2002: *World Ocean Atlas 2001, Vol. 4: Nutrients*. S. Levitus, Ed., NOAA Atlas NESDIS 52, U.S. Gov. Printing Office, Washington, D.C., 392 pp.

Cressman, G. P., 1959. An operational objective analysis scheme. *Mon. Wea. Rev.*, 87, 329-340.

Culberson, C. H. and S. L. Huang, 1987. Automated amperometric oxygen titration, *Deep-Sea Res.*, 34, 875 880.

Culberson, C. H., G. Knapp, M. C. Stalcup, R.T. Williams, and F. Zemlyak, 1991. A comparison of methods for the determination of dissolved oxygen in seawater, Report No. WHPO 91-2, WOCE Hydrographic Program Office, Woods Hole Oceanographic Institution,

Woods Hole, Mass., U.S.A.

Daley, R., 1991. *Atmospheric Data Analysis*. Cambridge University Press, Cambridge, 457 pp.

Deutsch, C., S. Emerson, and L. Thompson, 2005. Fingerprints of climate change in North Pacific oxygen. *Geophys. Res. Lett.*, 32, doi:10.1029/2005GL023190.

Dickson, A. G., 1994. Determination of dissolved oxygen in sea water by Winkler titration. WOCE Hydrographic Program, Operations and Methods Manual, Woods Hole, Mass., U.S.A., Unpublished manuscript.

England, M. H., 1992. On the formation of Antarctic Intermediate and Bottom Water in Ocean general circulation models. *J. Phys. Oceanogr.,* 22, 918-926.

Emerson S., C. Stump, B. Johnson, and D. M. Karl (2002), In-situ determination of oxygen and nitrogen dynamics in the upper ocean, *Deep-Sea Res.*, 49, 941-952.

ETOPO5, 1988. Data Announcements 88-MGG-02, Digital relief of the Surface of the Earth. NOAA, National Geophysical Data Center, Boulder, CO.

Gandin, L. S., 1963. *Objective Analysis of Meteorological fields*. Gidrometeorol Izdat, Leningrad (translation by Israel program for Scientific Translations, Jerusalem, 1966, 242 pp.

Garcia, H. E. and L. I. Gordon, 1992. Oxygen solubility in seawater: Better fitting equations. *Limnol. Oceanogr.*, 37, 1307-1312.

Garcia, H. E., A. Cruzado, L. I. Gordon, and J. Escanez, 1998. Decadal-scale chemical variability in the subtropical North Atlantic deduced from nutrient and oxygen data. *J. Geophys. Res.*, 103, 2817–2830

Garcia, H. E. and R. E. Keeling, 2001. On the global oxygen anomaly and air-sea flux. *J. Geophys. Res*., 106, 31155-31166.

Garcia, H. E., T. P. Boyer, S. Levitus, R.A. Locarnini, and J.I. Antonov, 2005a. Climatological annual cycle of upper ocean oxygen content, *Geophys. Res. Lett.*, 32, doi:10.1029/2004GL021745.

Garcia, H. E., T. P. Boyer, S. Levitus, R.A. Locarnini, and J.I. Antonov, 2005b. On the variability of dissolved oxygen and apparent oxygen utilization content for the upper world ocean: 1955 to 1998. *Geophys. Res. Lett.*, doi:10.1029/2004GL021745.

Garcia H. E., R. A. Locarnini, T. P. Boyer, and J.I. Antonov, 2006a. *World Ocean Atlas 2005: Vol. 4: Nutrients (phosphate, nitrate, silicate)*, S. Levitus, Ed., NOAA Atlas NESDIS 64, U.S. Gov. Printing Office, Washington, D.C., 395 pp.

Garcia, H. E., R. A. Locarnini, T. P. Boyer, and J. I. Antonov, 2010a. World Ocean Atlas 2009, Volume 4: Nutrients (phosphate, nitrate, silicate). S. Levitus, Ed. NOAA Atlas NESDIS 71, U.S. Gov. Printing Office, Washington, D.C., 398 pp.

Garcia, H. E., J.I. Antonov, O. K. Baranova, T.P. Boyer, D.R. Johnson, R.A. Locarnini, A.V. Mishonov, D.; Seidov, M. Zweng, and I.V. Smolyar, 2010b. Chapter 2: OSD-Ocean Station Data, Low-resolution CTD, Low resolution XCTD, and Plankton Tows, In: Boyer *et al.* (2009).

Hofmann M. and H-J. Schellnhuber, 2009. Oceanic acidification affects marine carbon pump and triggers extended marine oxygen holes. *Proc. U.S. Natl. Acad. Sci.*, 106: 3017-3022.

IOC, 1992a. Summary report of the IGOSS task team on quality control for automated systems and addendum to the summary report. *IOC/INF-888*, 1992.

IOC, 1992b. Summary report of the IGOSS task team on quality control for

automated systems and addendum to the summary report. *IOC/INF-888-append.*, 1992.

IOC, 1998. *Global Temperature-Salinity Profile Programme (GTSPP) – Overview and Future*. IOC Technical Series, 49, Intergovernmental Oceanographic Commission, Paris, 12 pp.

Ito, T., M. Follows, and E. A. Boyle, 2004. Is AOU a good measure of respiration in the oceans? *Geophys. Res. Lett.*, 31, doi:10.1029/2004GL020900

JPOTS (Joint Panel on Oceanographic Tables and Standards) Editorial Panel, 1991. Processing of Oceanographic Station Data. UNESCO, Paris, 138 pp.

Knapp, G. P., M. C. Stalcup, and R. J. Stanley, 1990. Automated oxygen titration and salinity determination, Woods Hole Oceanographic Institution, WHOI Ref. No. 90-35.

Johnson, D. R., T. P. Boyer, H. E. Garcia, R. A. Locarnini, O. K. Baranova, and M. M. Zweng, 2009. *World Ocean Database 2009*. S. Levitus, Ed., NODC Internal Report 20, U.S. Gov. Printing Office, Washington, D.C., 175 pp.

Keeling, R. and H. Garcia, 2002. The change in oceanic O_2 inventory associated with recent global warming, *Proc. U.S. Natl. Acad. Sci.*, 99:7848-7853.

Körtzinger, A., J. Schimanski, U. Send, and D. Wallace, 2004. The ocean takes a deep breath, *Science,* 306, 1337.

Körtzinger, A., J. Schimanski and U. Send, 2005. High Quality Oxygen Measurements from Profiling Floats: A Promising New Technique, *J. of Atmos. and Oceanic Tech.*, 22, doi: 10.1175/JTECH1701.1.

Levitus, S., 1982. *Climatological Atlas of the World Ocean,* NOAA Professional Paper No. 13, U.S. Gov. Printing Office, 173 pp.

Levitus, S., and T. P. Boyer, 1994a: *World Ocean Atlas 1994, Vol. 2: Oxygen*. NOAA Atlas NESDIS 2, U.S. Gov. Printing Office, Washington, D.C., 186 pp.

Levitus, S., and T. Boyer, 1994b: *World Ocean Atlas 1994, Vol. 4: Temperature*. NOAA Atlas NESDIS 4, U.S. Gov. Printing Office, Washington, D.C., 117 pp.

Levitus, S., R. Burgett, and T. P. Boyer, 1994: *World Ocean Atlas 1994, Vol. 3: Salinity*. NOAA Atlas NESDIS 3, U.S. Gov. Printing Office, Washington, D.C., 99 pp.

Levitus, S., S. Sato, C. Maillard, N. Mikhailov, P. Caldwell, H. Dooley, 2005, *Building Ocean Profile-Plankton Databases for Climate and Ecosystem Research*, NOAA Technical Report NESDIS 117, U.S. Gov. Printing Office, Washington, D.C., 29 pp.

Locarnini, R. A., A. V. Mishonov, J. I. Antonov, T. P. Boyer, and H. E. Garcia, 2010. World Ocean Atlas 2009, Volume 1: Temperature. S. Levitus, Ed., NOAA Atlas NESDIS 68, U.S. Gov. Printing Office, Washington, D.C., 184 pp.

Locarnini, R. A., T. D. O'Brien, H. E. Garcia, J.I. Antonov, T.P. Boyer, M.E. Conkright, and C. Stephens, 2002: *World Ocean Atlas 2001, Vol. 3: Oxygen*. S. Levitus, Ed., NOAA Atlas NESDIS 51, U.S. Gov. Printing Office, Washington, D.C., 286 pp.

Locarnini, R. A., A. V. Mishonov, J. I. Antonov, T. P. Boyer, and H. E. Garcia, 2006: *World Ocean Atlas 2005, Vol. 1: Temperature*. S. Levitus, Ed., NOAA Atlas NESDIS 61, U.S. Gov. Printing Office, Washington, D.C. 182 pp.

Matear, R. J. and A. C. Hirst, 2003, Long-term changes in dissolved oxygen concentrations in the ocean caused by protracted global warming. *Glob. Biogeochem. Cycles*, 17(4), 1125,

doi:10.1029/2002GB001997.

O' Brien, T. D., S. Levitus, T. P. Boyer, M.E. Conkright, J.I. Antonov, and C. Stephens, 1998a: *World Ocean Atlas 1998 Vol. 7: Oxygen of the Atlantic Ocean*. NOAA Atlas NESDIS 33, U.S. Gov. Printing Office, Washington, D.C., 234 pp.

O' Brien, T. D., S. Levitus, T. P. Boyer, M. E. Conkright, J. I. Antonov, and C. Stephens, 1998b: *World Ocean Atlas 1998 Vol. 8: Oxygen of the Pacific Ocean.* NOAA Atlas NESDIS 34, U.S. Gov. Printing Office, Washington, D.C., 234 pp.

O' Brien, T. D., S. Levitus, T. P. Boyer, M. E. Conkright, J.I. Antonov, and C. Stephens, 1998c: *World Ocean Atlas 1998 Vol. 9: Oxygen of the Indian Ocean.* NOAA Atlas NESDIS 35, U.S. Gov. Printing Office, Washington, D.C., 234 pp.

Rabiner, L. R., M. R. Sambur, and C. E. Schmidt, 1975. *Applications of a nonlinear smoothing algorithm to speech processing, IEEE Trans. on Acoustics, Speech and Signal Processing*, 23, 552-557.

Redfield A., B. Ketchum, and F. Richards, 1963. The influence of organisms on the composition of sea water, *In The Sea*, Vol. 2, pages 224-228, N. Hill, Ed., Interscience, New York.

Reiniger, R. F. and C. F. Ross, 1968. A method of interpolation with application to oceanographic data. *Deep-Sea Res.*, 9, 185-193.

Riebesell U., A. Körtzinger, and A. Oschlies, 2009. Sensitivities of marine carbon fluxes to ocean change. *Proc. U.S. Natl. Acad. Sci*., 106:20602-20609.

Sasaki, Y., 1960. An objective analysis for determining initial conditions for the primitive equations. Ref. 60-1 6T, Atmospheric Research Lab., Univ. of Oklahoma Research Institute, Norman, 23 pp.

Seaman, R. S., 1983. Objective Analysis accuracies of statistical interpolation and successive correction schemes. *Australian Meteor. Mag.*, 31, 225-240.

Shaffer G., S. M. Olsen, and J. O. P. Pedersen, 2009. Long-term pcean oxygen depletion in response to carbon dioxide emissions from fossil fuels. *Nature* geoscience, DOI:10.1038/NGEO420.

Shuman, F. G., 1957. Numerical methods in weather prediction: II. Smoothing and filtering. *Mon. Wea. Rev.*, 85, 357-361.

Smith, D. R. and F. Leslie, 1984. Error determination of a successive correction type objective analysis scheme. *J Atm. and Oceanic Tech.*, 1, 121-130.

Smith, D. R., M. E. Pumphry, and J. T. Snow, 1986. A comparison of errors in objectively analyzed fields for uniform and nonuniform station distribution, *J. Atm. Oceanic Tech.*, 3, 84-97.

Stephens, C., J. I. Antonov, T. P. Boyer, M. E. Conkright, R. A. Locarnini, T. D. O' Brien, and H. E. Garcia, 2002: *World Ocean Atlas 2001, Vol. 1: Temperature*. S. Levitus, Ed., NOAA Atlas NESDIS 49, U.S. Gov. Printing Office, Washington**,** D.C., 167 pp.

Stramma, L., G. C. Johnson, J. Sprintall, and V. Mohrholz, 2008. Expanding Oxygen-Minimum Zones in the Tropical Oceans. *Science*, 320(5876):655–658. DOI: 10.1126/science.115384.

Sverdrup, H. U., M. W. Johnson, and R. H. Fleming, 1942. *The Oceans: Their physics, chemistry, and general biology.* Prentice Hall, 1060 pp.

Thiebaux, H. J. and M. A. Pedder, 1987. *Spatial Objective Analysis: with applications in atmospheric science*. Academic Press, 299 pp.

Tukey, J.W., 1974. Nonlinear (nonsuperposable) methods for smoothing data, in *"Cong. Rec."*, 1974

EASCON, 673 pp.

Winkler, L. W., 1888, Die Bestimmung des in Wasser gelösten Sauerstoffen. Berichte der Deutschen Chemischen Gesellschaft, 21, 2843–2855.

Wessel, P., and W. H. F. Smith., 1998, New, improved version of Generic Mapping Tools released, *EOS Trans. Amer. Geophys. U.*, 79, 579.

Table 1. Descriptions of climatologies for dissolved oxygen (O_2), Apparent Oxygen Utilization (AOU), and oxygen saturation (O_2^S) in WOA09. The climatologies have been calculated based on bottle data (OSD) from WOD09. The standard depth levels are shown in Table 2.

Oceanographic Variable	Depths for Annual Climatology	Depths for Seasonal Climatology	Depths for Monthly Climatology
O_2, AOU, and O_2^S	0-5500 m (33 levels)	0-5500 m (33 levels)	0-1500 m (24 levels)

Table 2. Acceptable distances (m) for defining interior and exterior values used in the Reiniger and Ross (1968) scheme for interpolating observed level data to standard levels.

Standard Level number	Standard depths (m)	Acceptable distances (m) for interior values	Acceptable distances (m) for exterior values
1	0	5	200
2	10	50	200
3	20	50	200
4	30	50	200
5	50	50	200
6	75	50	200
7	100	50	200
8	125	50	200
9	150	50	200
10	200	50	200
11	250	100	200
12	300	100	200
13	400	100	200
14	500	100	400
15	600	100	400
16	700	100	400
17	800	100	400
18	900	200	400
19	1000	200	400
20	1100	200	400
21	1200	200	400
22	1300	200	1000
23	1400	200	1000
24	1500	200	1000
25	1750	200	1000
26	2000	1000	1000
27	2500	1000	1000
28	3000	1000	1000
29	3500	1000	1000
30	4000	1000	1000
31	4500	1000	1000
32	5000	1000	1000
33	5500	1000	1000

Table 3. Response function of the objective analysis scheme as a function of wavelength for WOA09 and earlier analyses. Response function is normalized to 1.0.

Wavelength*	Levitus (1982)	WOA94	WOA98, 01, 05, 09
360ΔX	1.000	0.999	1.000
180ΔX	1.000	0.997	0.999
120ΔX	1.000	0.994	0.999
90ΔX	1.000	0.989	0.998
72ΔX	1.000	0.983	0.997
60ΔX	1.000	0.976	0.995
45ΔX	1.000	0.957	0.992
40ΔX	0.999	0.946	0.990
36ΔX	0.999	0.934	0.987
30ΔX	0.996	0.907	0.981
24ΔX	0.983	0.857	0.969
20ΔX	0.955	0.801	0.952
18ΔX	0.923	0.759	0.937
15ΔX	0.828	0.671	0.898
12ΔX	0.626	0.532	0.813
10ΔX	0.417	0.397	0.698
9ΔX	0.299	0.315	0.611
8ΔX	0.186	0.226	0.500
6ΔX	3.75×10^{-2}	0.059	0.229
5ΔX	1.34×10^{-2}	0.019	0.105
4ΔX	1.32×10^{-3}	2.23×10^{-3}	2.75×10^{-2}
3ΔX	2.51×10^{-3}	1.90×10^{-4}	5.41×10^{-3}
2ΔX	5.61×10^{-7}	5.30×10^{-7}	1.36×10^{-6}

*For ΔX = 111 km, the meridional separation at the Equator.

Table 4. Basins defined for objective analysis and the shallowest standard depth level for which each basin is defined.

#	Basin	Standard Depth Level	#	Basin	Standard Depth Level
1	Atlantic Ocean	1*	30	North American Basin	29
2	Pacific Ocean	1*	31	West European Basin	29
3	Indian Ocean	1*	32	Southeast Indian Basin	29
4	Mediterranean Sea	1*	33	Coral Sea	29
5	Baltic Sea	1	34	East Indian Basin	29
6	Black Sea	1	35	Central Indian Basin	29
7	Red Sea	1	36	Southwest Atlantic Basin	29
8	Persian Gulf	1	37	Southeast Atlantic Basin	29
9	Hudson Bay	1	38	Southeast Pacific Basin	29
10	Southern Ocean	1*	39	Guatemala Basin	29
11	Arctic Ocean	1	40	East Caroline Basin	30
12	Sea of Japan	1	41	Marianas Basin	30
13	Kara Sea	8	42	Philippine Sea	30
14	Sulu Sea	10	43	Arabian Sea	30
15	Baffin Bay	14	44	Chile Basin	30
16	East Mediterranean	16	45	Somali Basin	30
17	West Mediterranean	19	46	Mascarene Basin	30
18	Sea of Okhotsk	19	47	Crozet Basin	30
19	Banda Sea	23	48	Guinea Basin	30
20	Caribbean Sea	23	49	Brazil Basin	31
21	Andaman Basin	25	50	Argentine Basin	31
22	North Caribbean	26	51	Tasman Sea	30
23	Gulf of Mexico	26	52	Atlantic Indian Basin	31
24	Beaufort Sea	28	53	Caspian Sea	1
25	South China Sea	28	54	Sulu Sea II	14
26	Barents Sea	28	55	Venezuela Basin	14
27	Celebes Sea	25	56	Bay of Bengal	1*
28	Aleutian Basin	28	57	Java Sea	6
29	Fiji Basin	29	58	East Indian Atlantic Basin	32

Basins marked with a "" can interact with adjacent basins in the objective analysis.

Table 5. Statistical fields calculated as part of WOA09 ("√"denotes field was calculated and is publicly available).

Statistical field	One-degree Field Calculated	Five-degree Statisctics calculated
Objectively analyzed climatology	√	
Statistical mean	√	√
Number of observations	√	√
Seasonal (monthly) climatology minus annual climatology	√	
Standard deviation from statistical mean	√	√
Standard error of the statistical mean	√	√
Statistical mean minus objectively analyzed climatology	√	
Number of mean values within radius of influence	√	

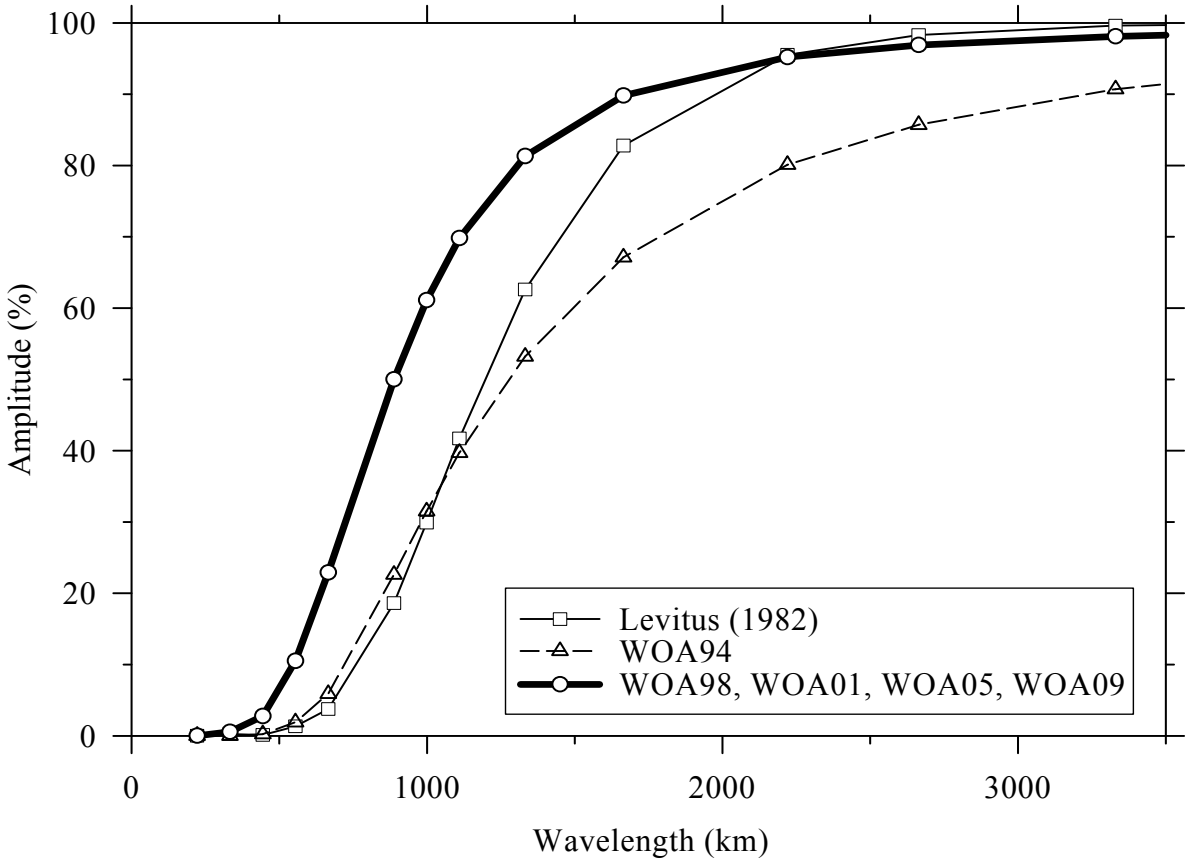

Figure 1. Response function of the WOA09, WOA05, WOA01, WOA98, WOA94, and Levitus (1982) objective analysis schemes.

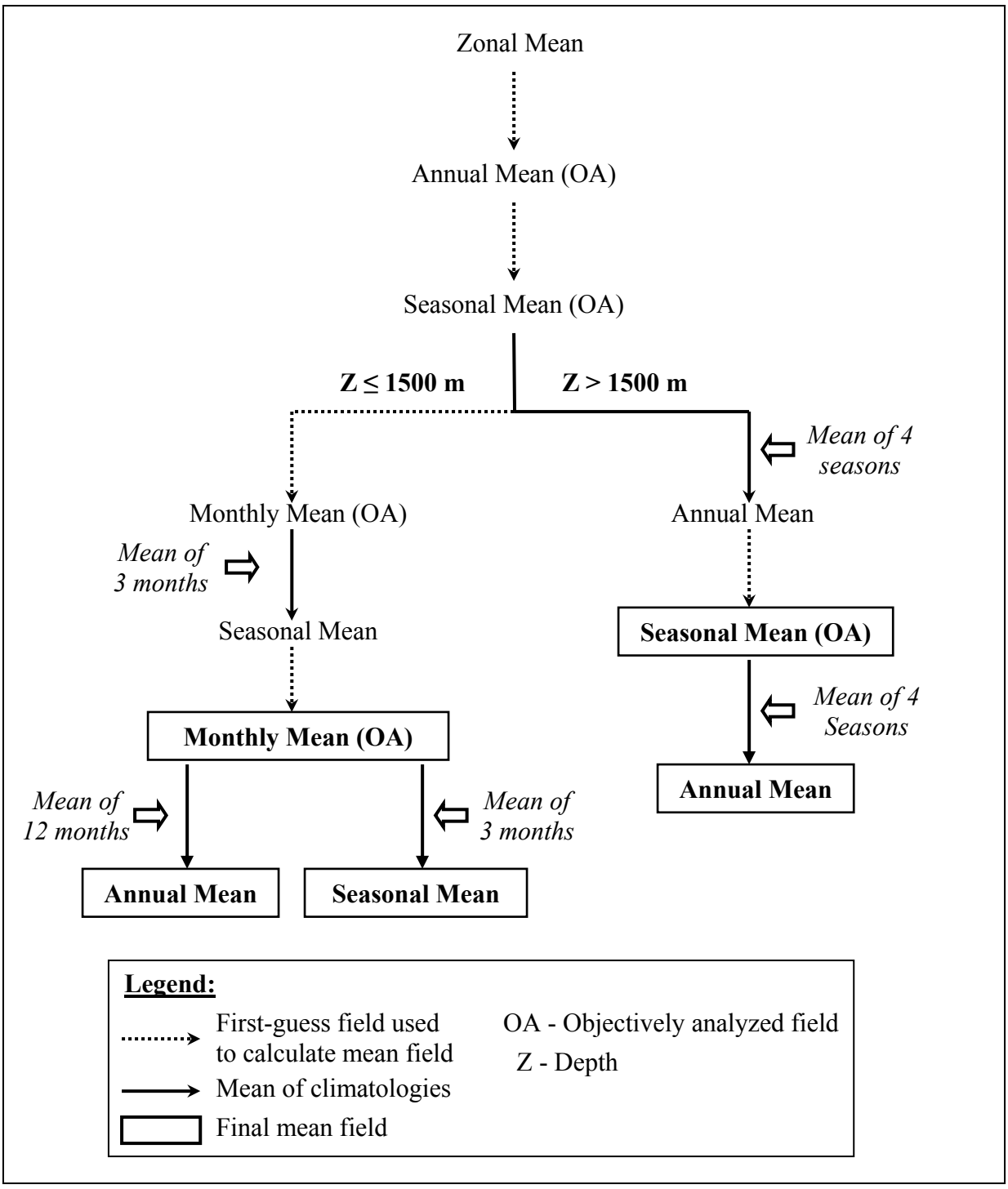

Figure 2. Scheme used in computing annual, seasonal, and monthly objectively analyzed means for dissolved oxygen, Apparent Oxygen Utilization (AOU), and oxygen saturation (O_2^S).

8. APPENDICES

8.1 Appendix A: Maps of the annual number of observations and distribution of dissolved oxygen (O_2) at selected depth levels (Pages 27 to 50).

8.2 Appendix B: Maps of the seasonal (winter, summer, fall, spring) number of observations, seasonal distribution of dissolved oxygen (O_2), and seasonal minus annual distribution of O_2 at selected depth levels (Pages 51 to 90).

8.3 Appendix C: Maps of the monthly number of observations, monthly distribution of dissolved oxygen (O_2), and monthly minus annual distribution of O_2 at selected depth levels (pages 91 to 150).

8.4 Appendix D: Maps of the annual distribution of Apparent Oxygen Utilization (AOU) at selected depth levels (Pages 150 to 166).

8.5 Appendix E: Maps of the seasonal (winter, summer, fall, spring) distribution of Apparent Oxygen Utilization (AOU) and seasonal minus annual distribution of AOU at selected depth levels (Pages 167 to 198).

8.6 Appendix F: Maps of the monthly distribution of Apparent Oxygen Utilization (AOU) and monthly minus annual distribution of AOU at selected depth levels (Pages 199 to 246).

8.7 Appendix G: Maps of the annual distribution of oxygen saturation (O_2^S) at selected depth levels (Pages 247 to 262).

8.8 Appendix H: Maps of the seasonal (winter, summer, fall, spring) distribution of oxygen saturation (O_2^S), and seasonal minus annual distribution of O_2^S at selected depth levels (Pages 263 to 294).

8.9 Appendix I: Maps of the monthly distribution of oxygen saturation (O_2^S), and monthly minus annual distribution of O_2^S at selected depth levels (Pages 295 to 342).

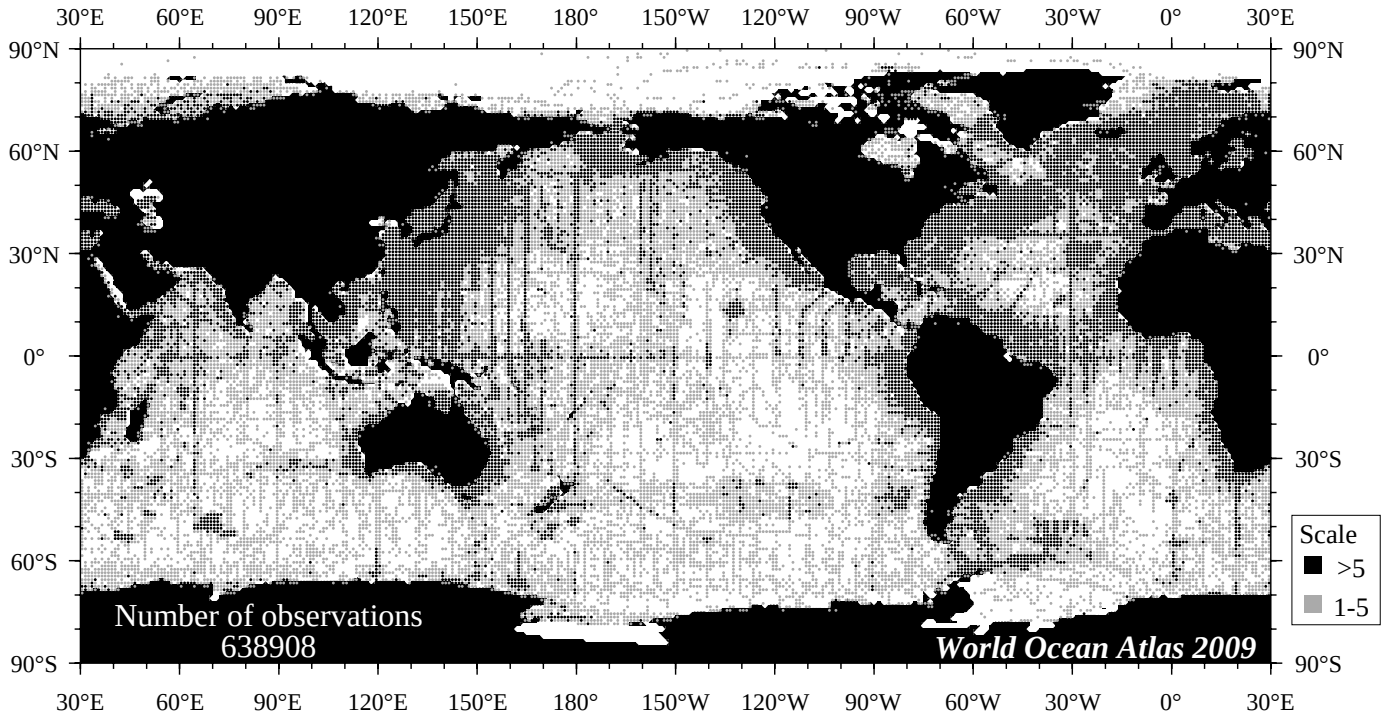

Fig A1 Annual oxygen observations at the surface.

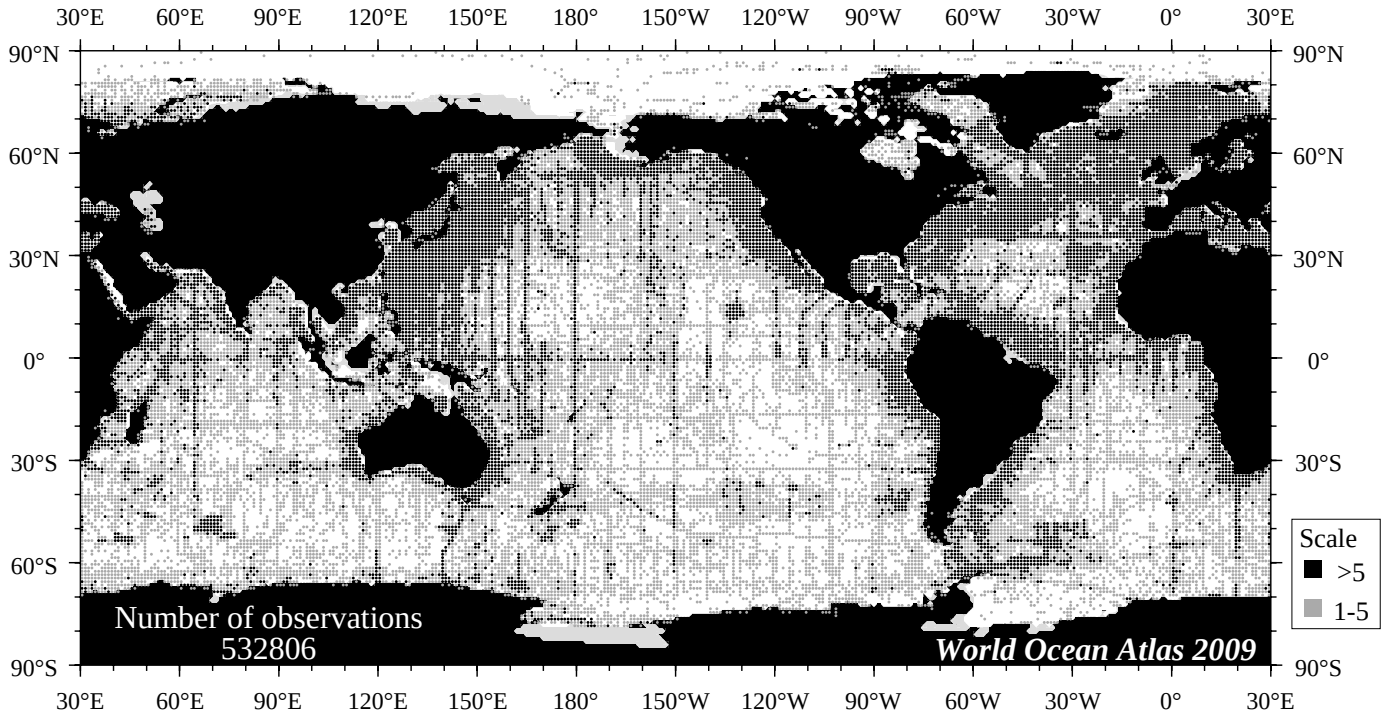

Fig A2 Annual oxygen observations at 50 m. depth.

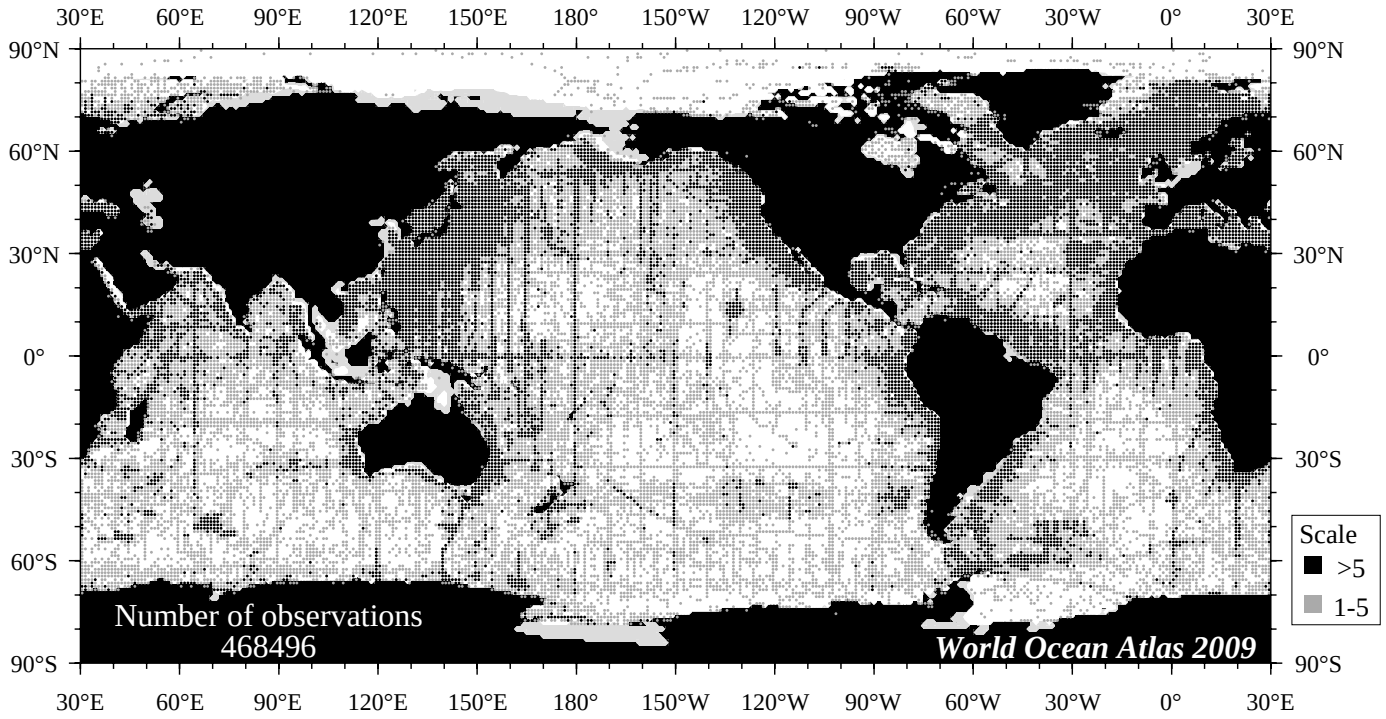

Fig A3 Annual oxygen observations at 75 m. depth.

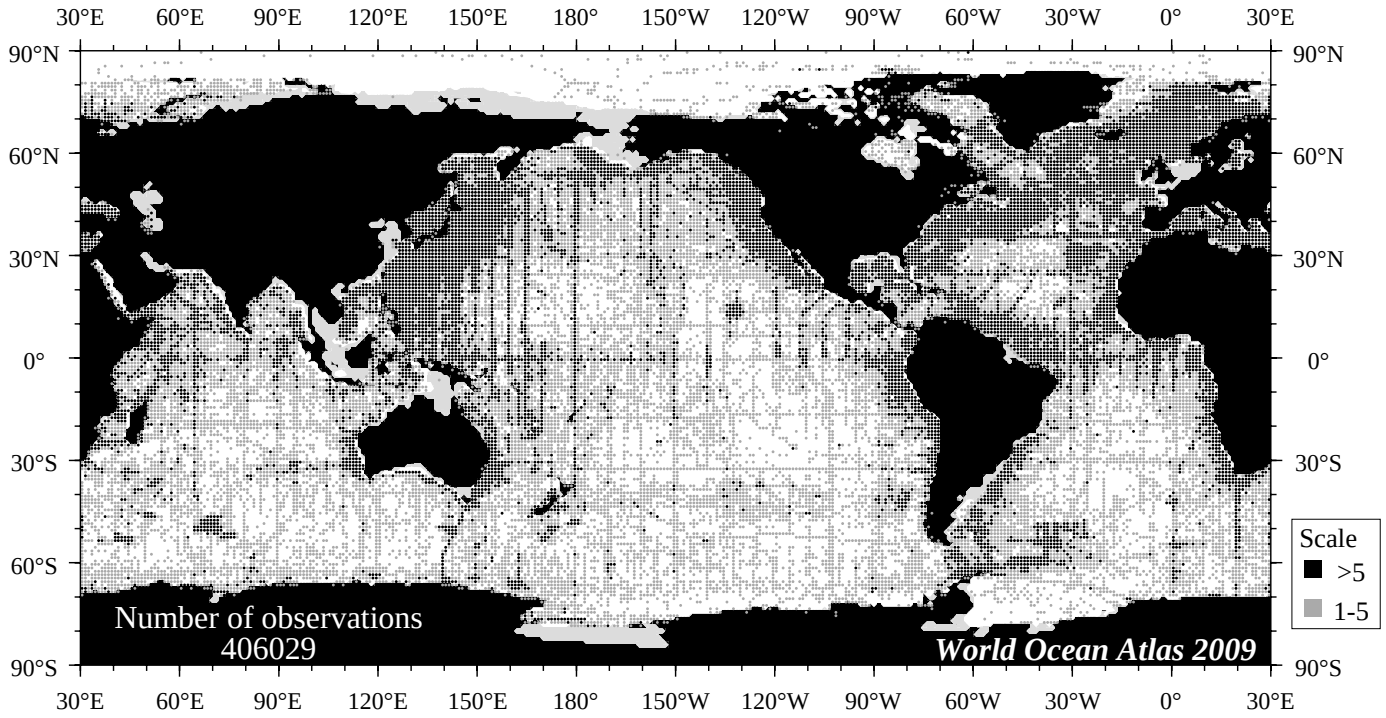

Fig A4 Annual oxygen observations at 100 m. depth.

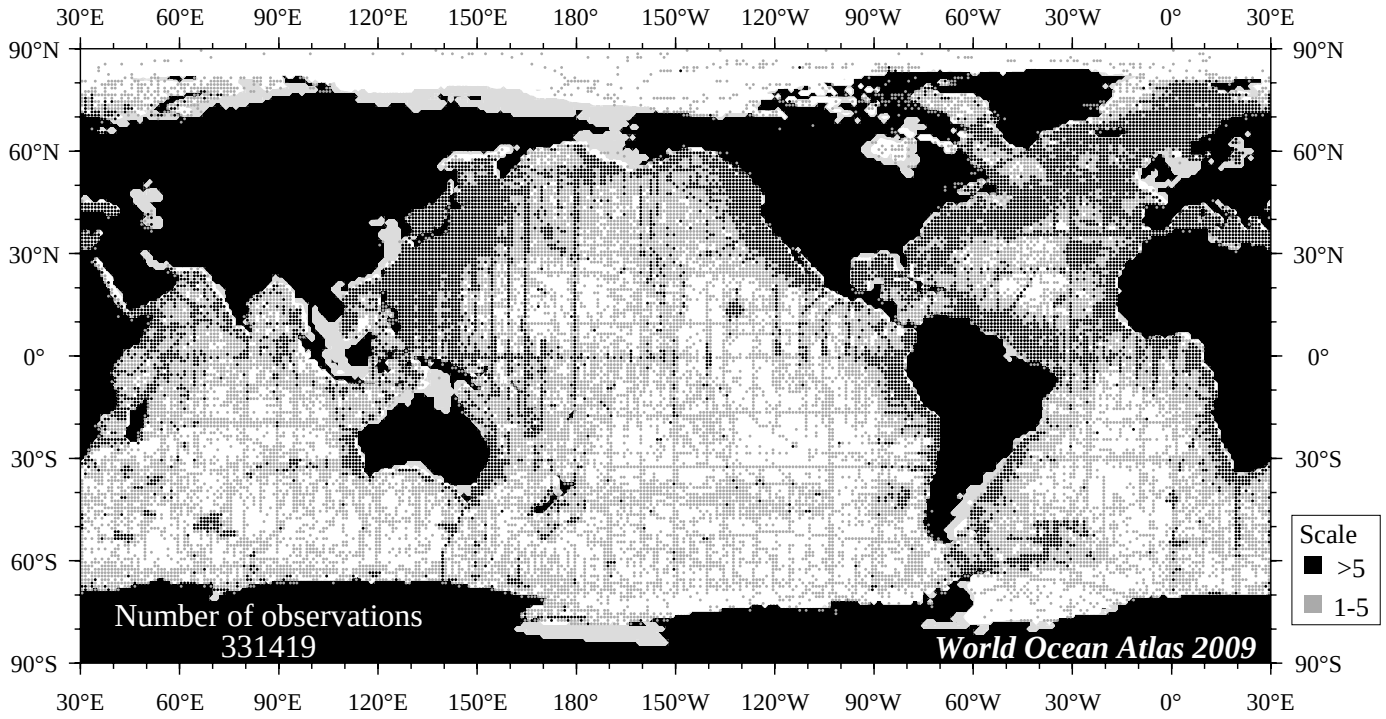

Fig A5 Annual oxygen observations at 150 m. depth.

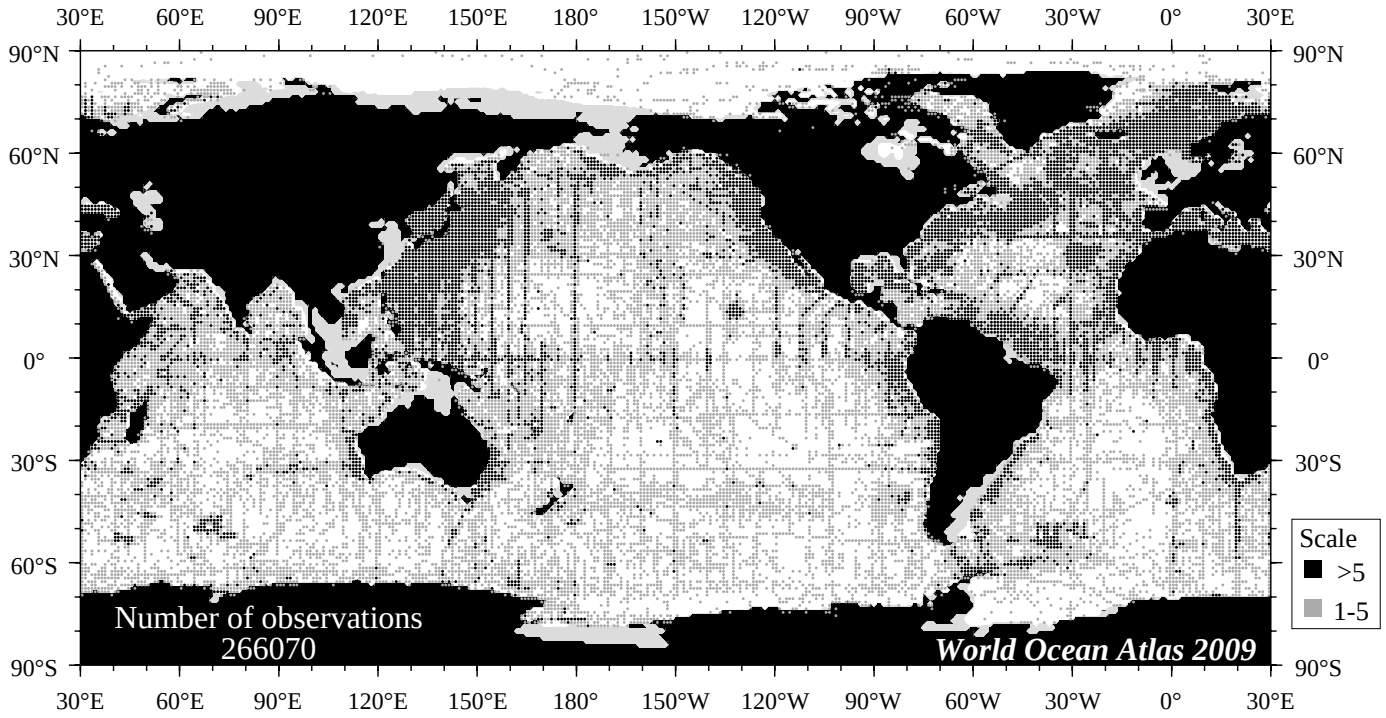

Fig A6 Annual oxygen observations at 200 m. depth.

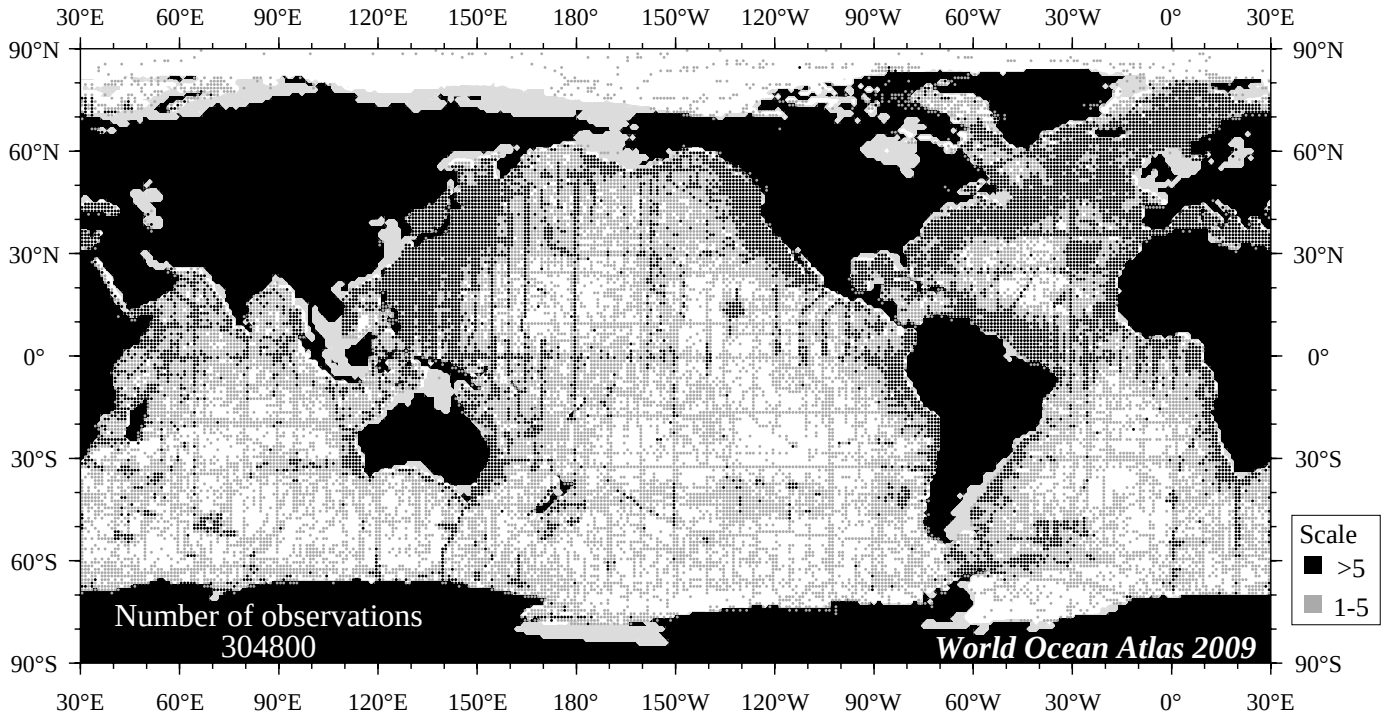

Fig A7 Annual oxygen observations at 250 m. depth.

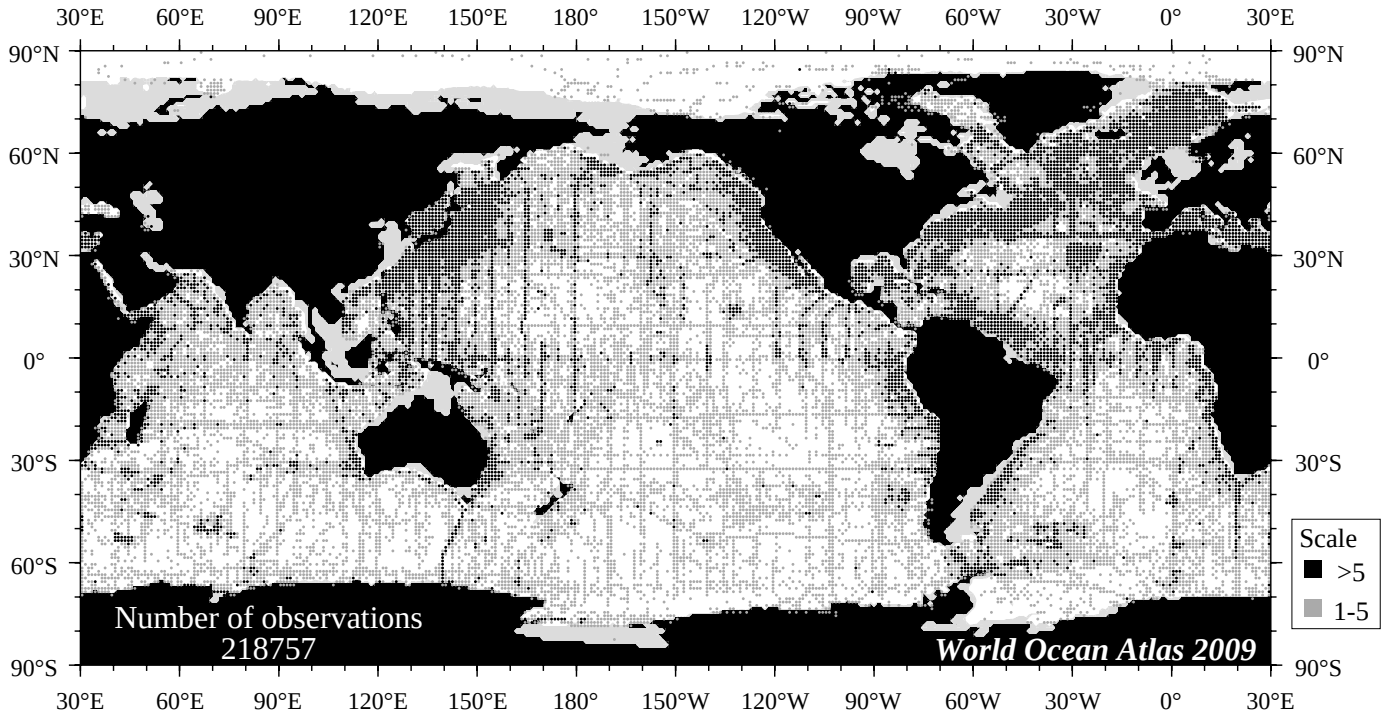

Fig A8 Annual oxygen observations at 400 m. depth.

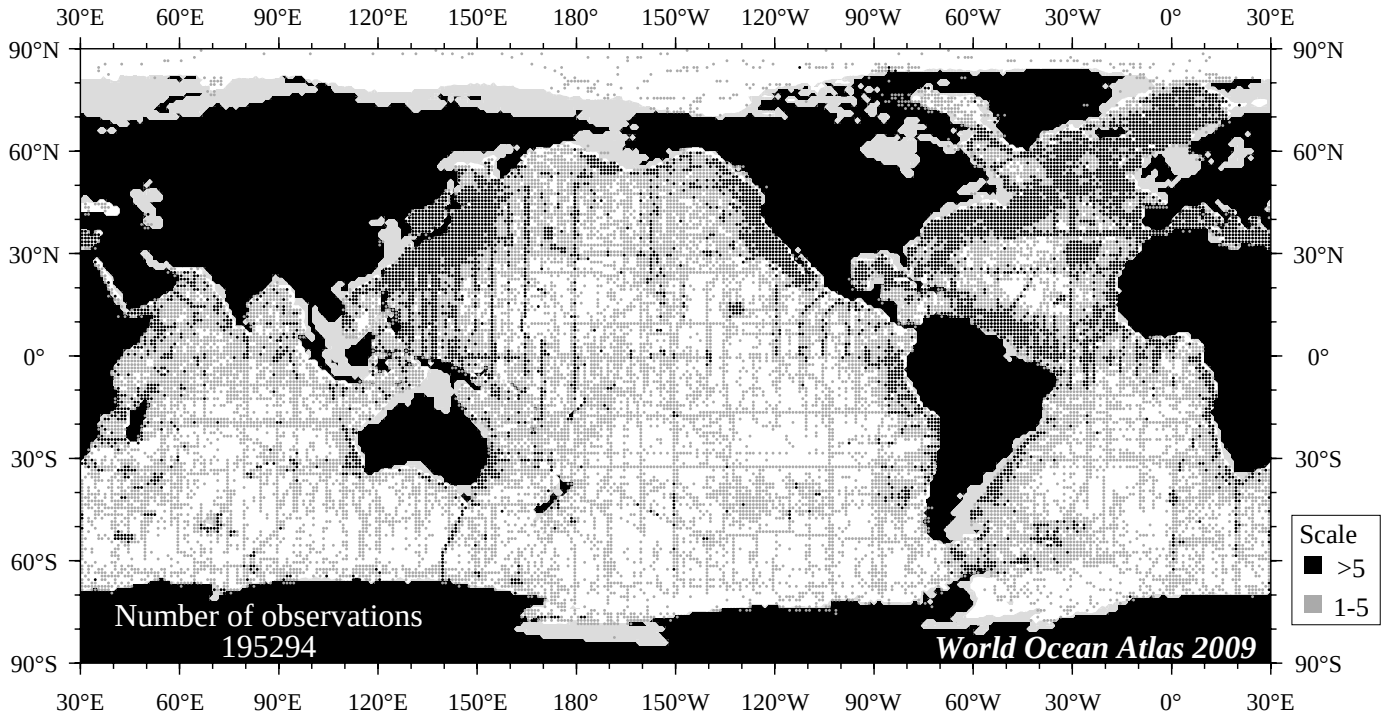

Fig A9 Annual oxygen observations at 500 m. depth.

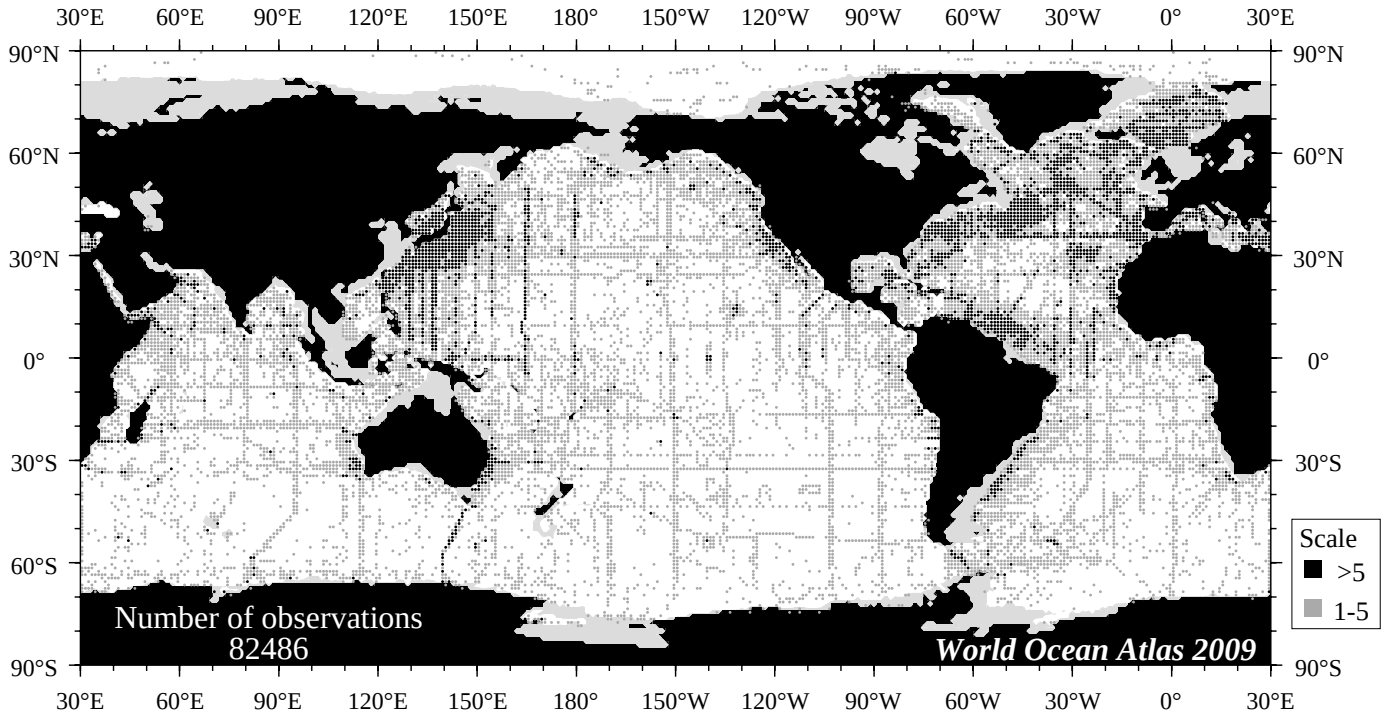

Fig A10 Annual oxygen observations at 700 m. depth.

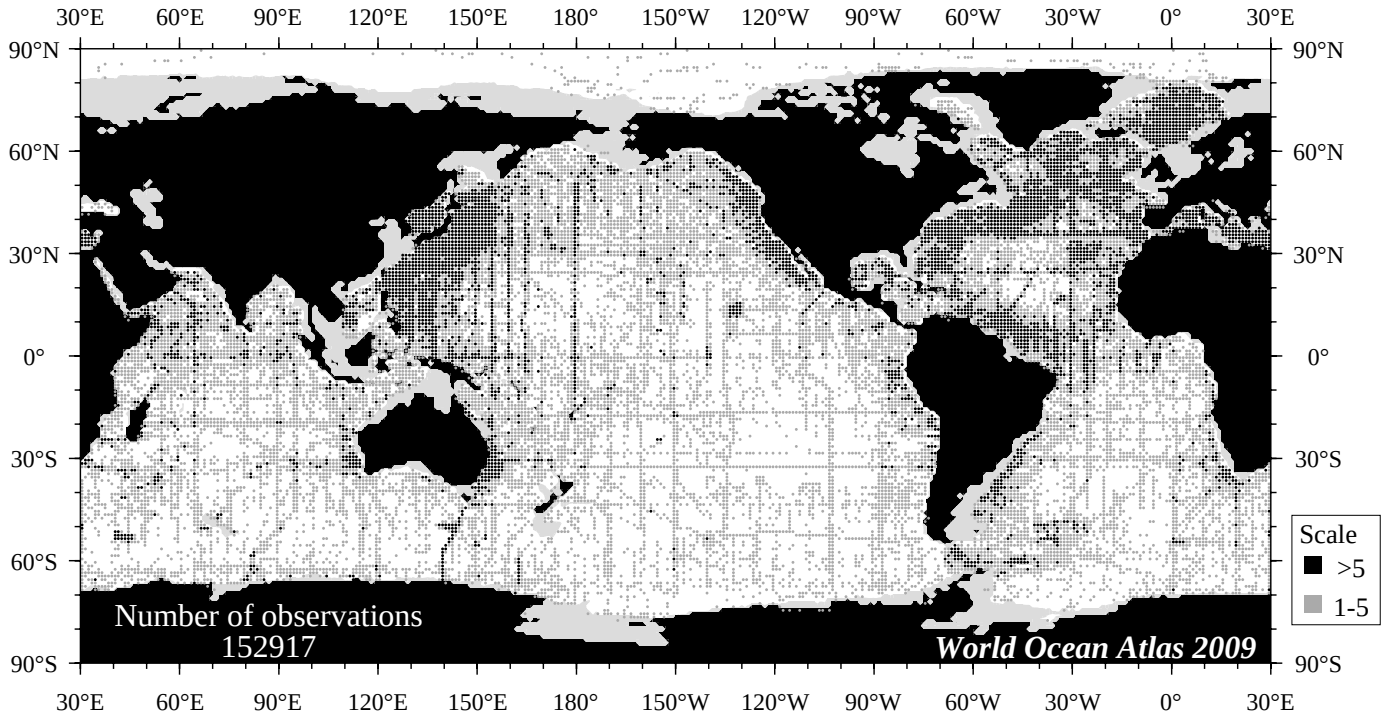

Fig A11 Annual oxygen observations at 1000 m. depth.

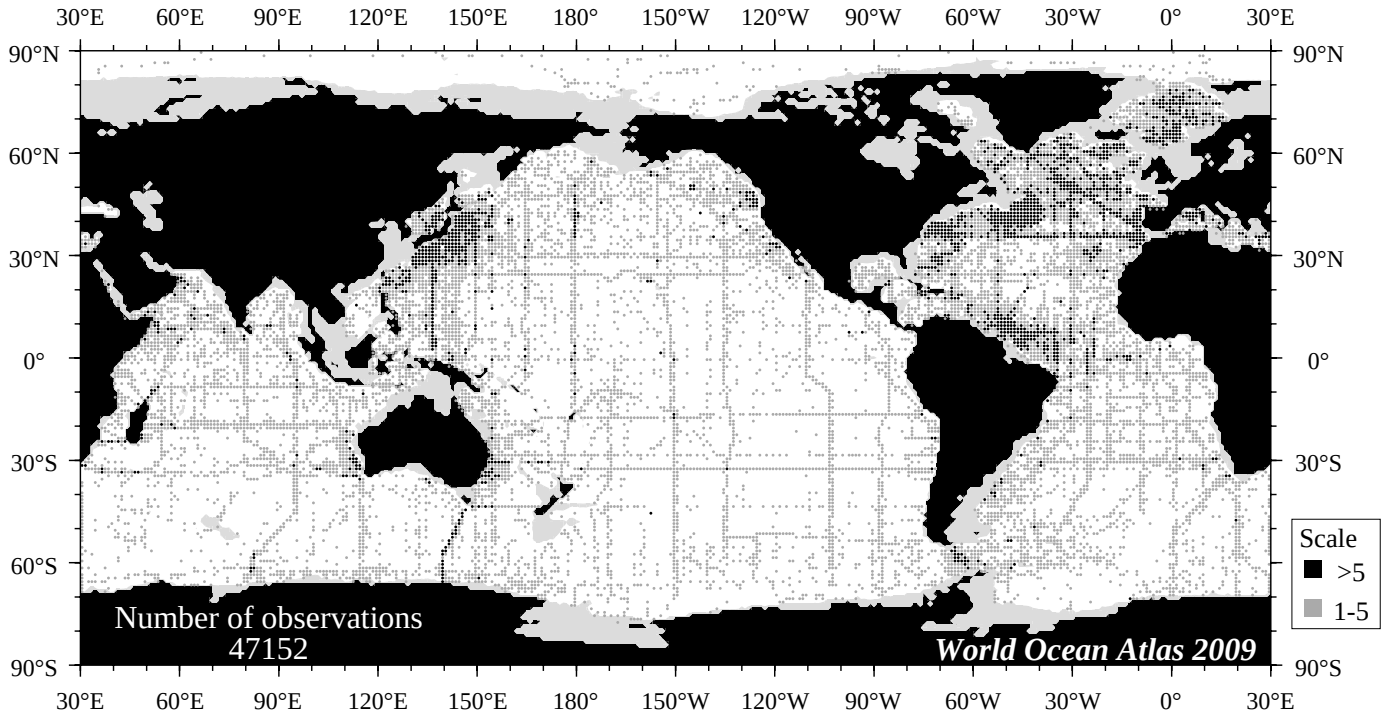

Fig A12 Annual oxygen observations at 1500 m. depth.

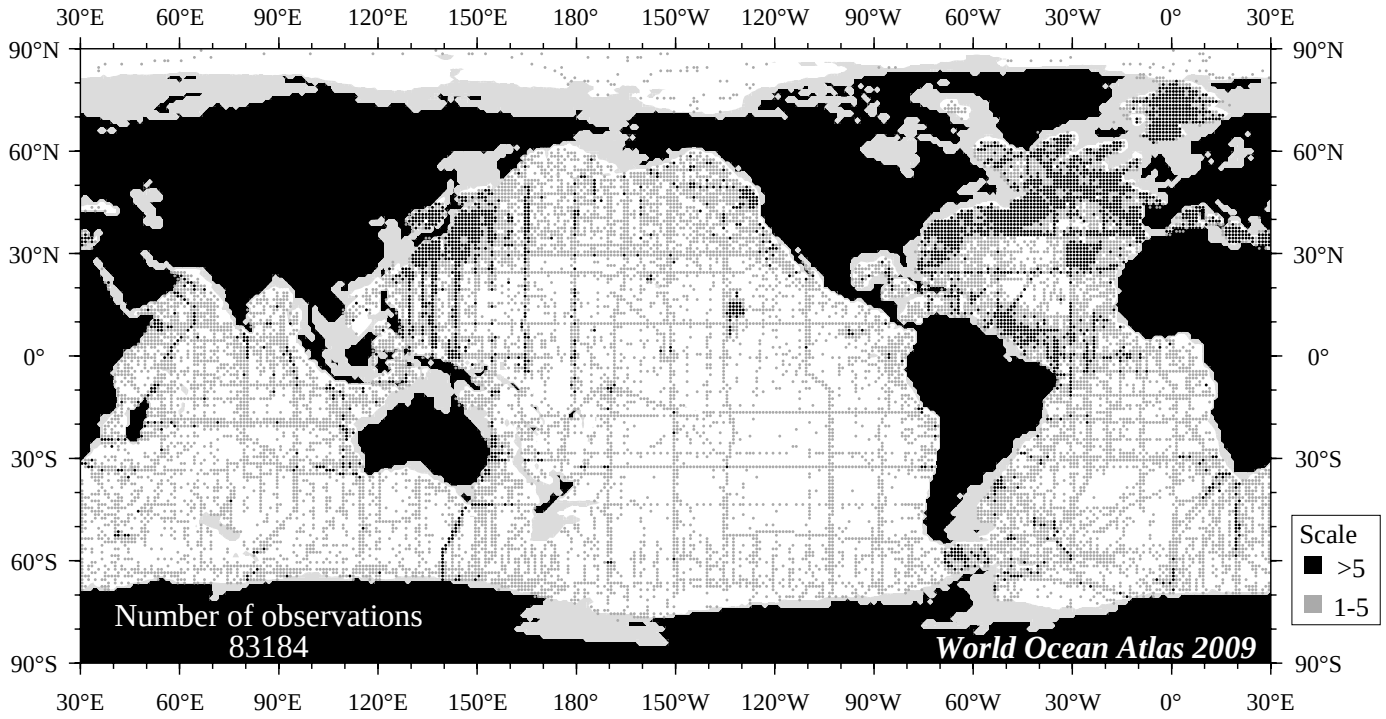

Fig A13 Annual oxygen observations at 2000 m. depth.

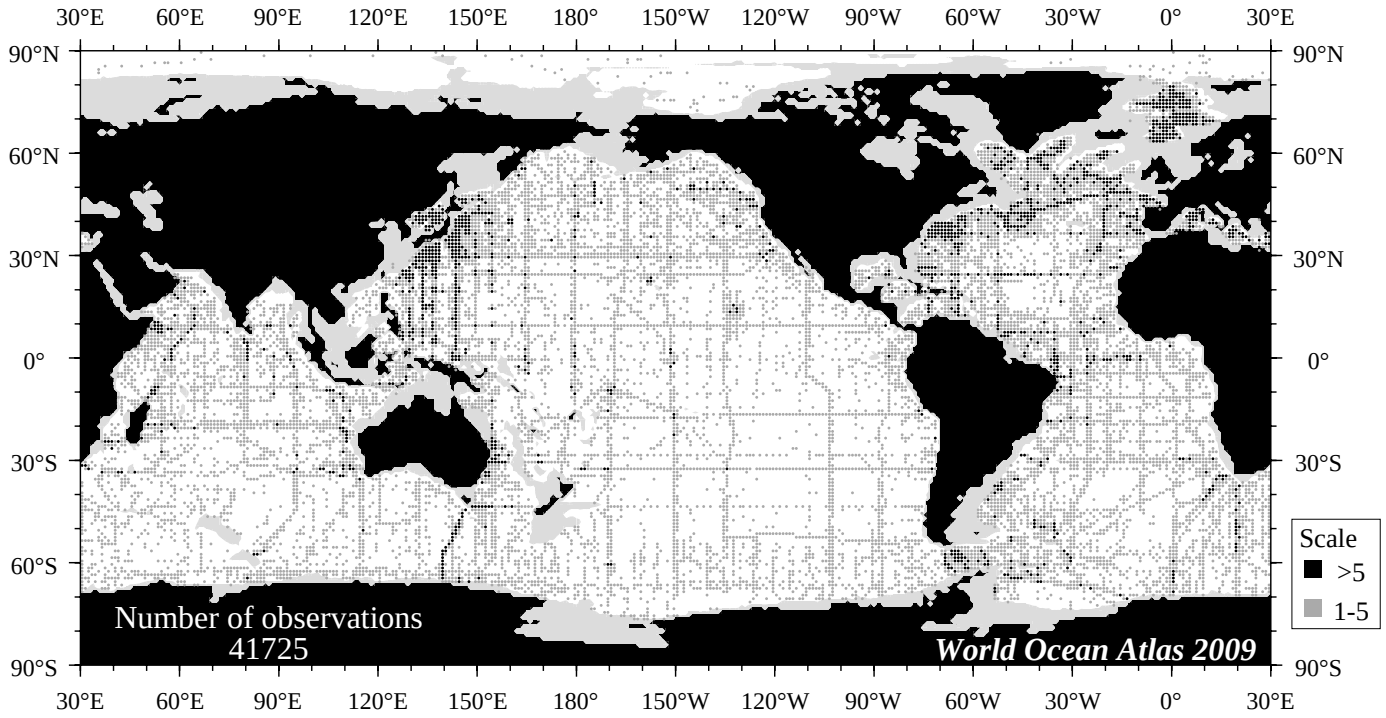

Fig A14 Annual oxygen observations at 2500 m. depth.

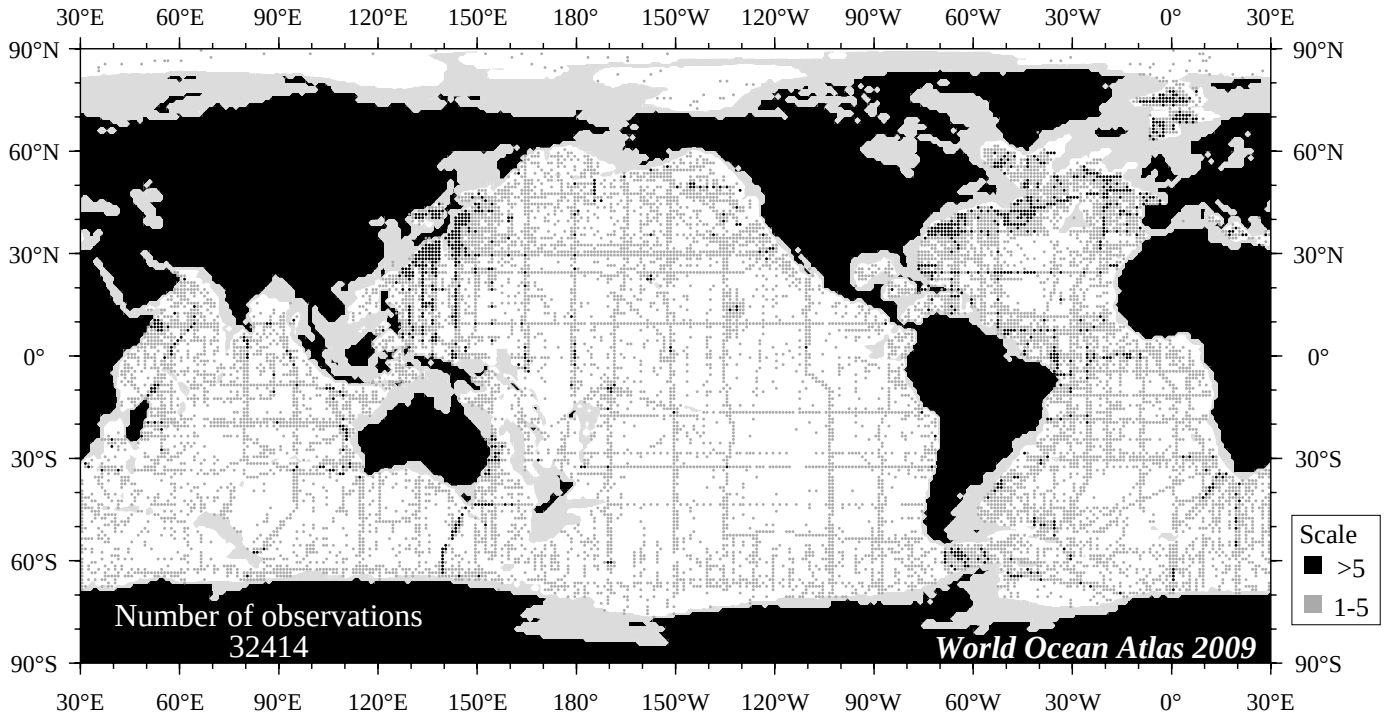

Fig A15 Annual oxygen observations at 3000 m. depth.

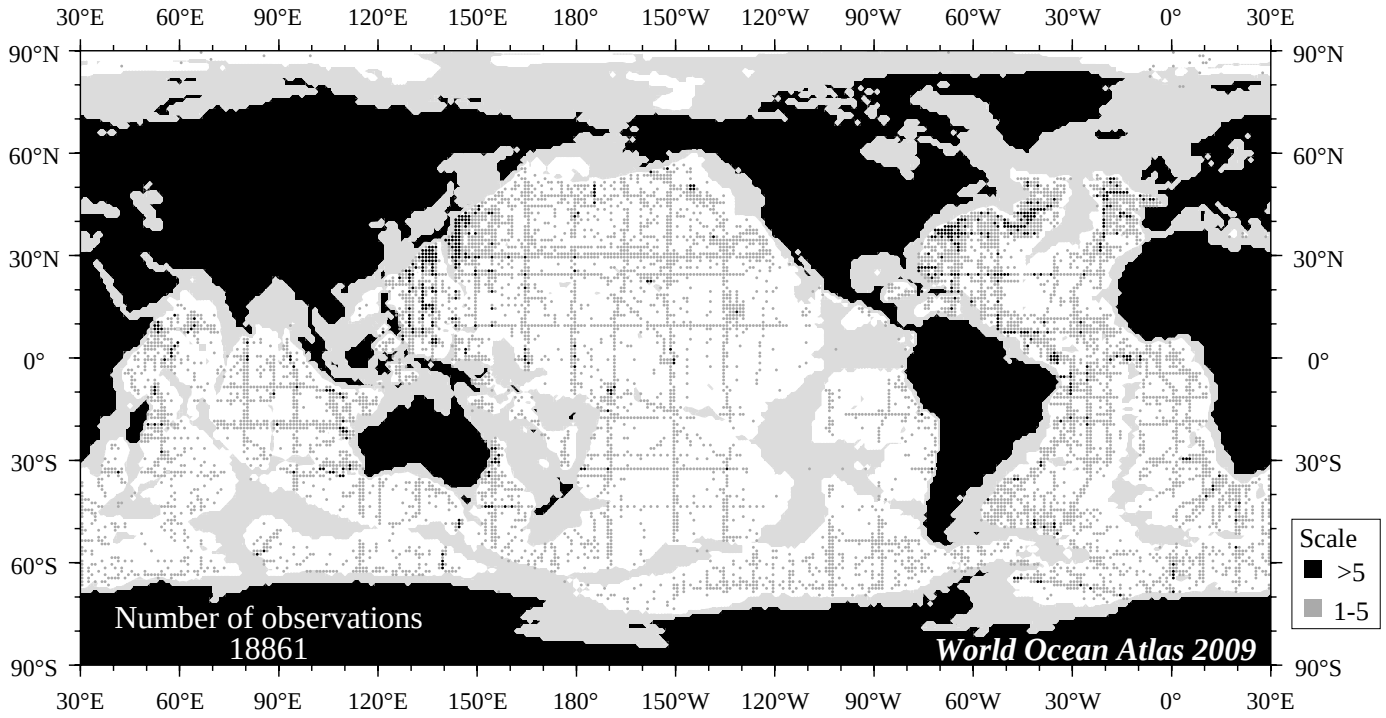

Fig A16 Annual oxygen observations at 4000 m. depth.

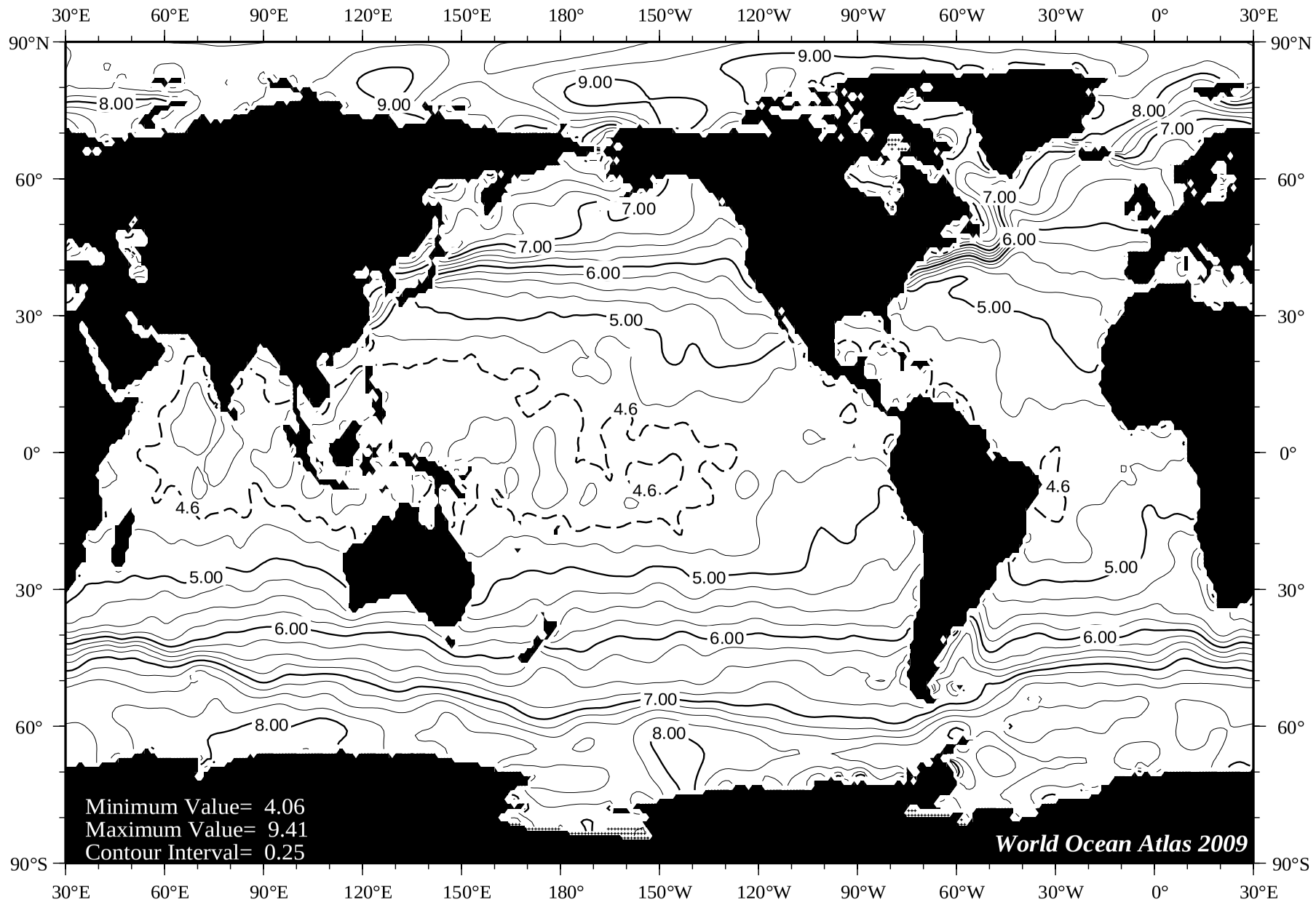

Fig A17 Annual oxygen [ml/l] at the surface.

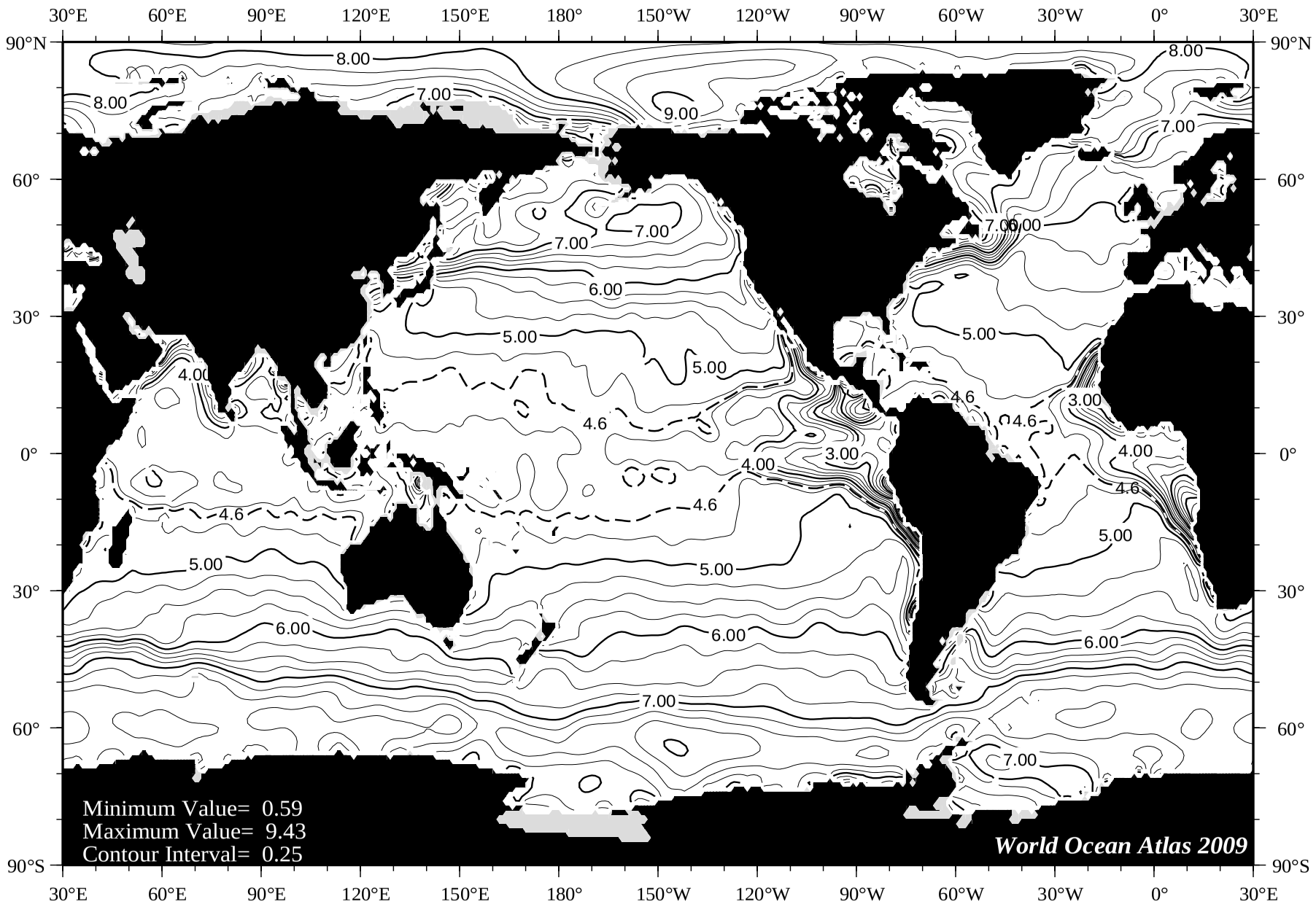

Fig A18 Annual oxygen [ml/l] at 50 m. depth.

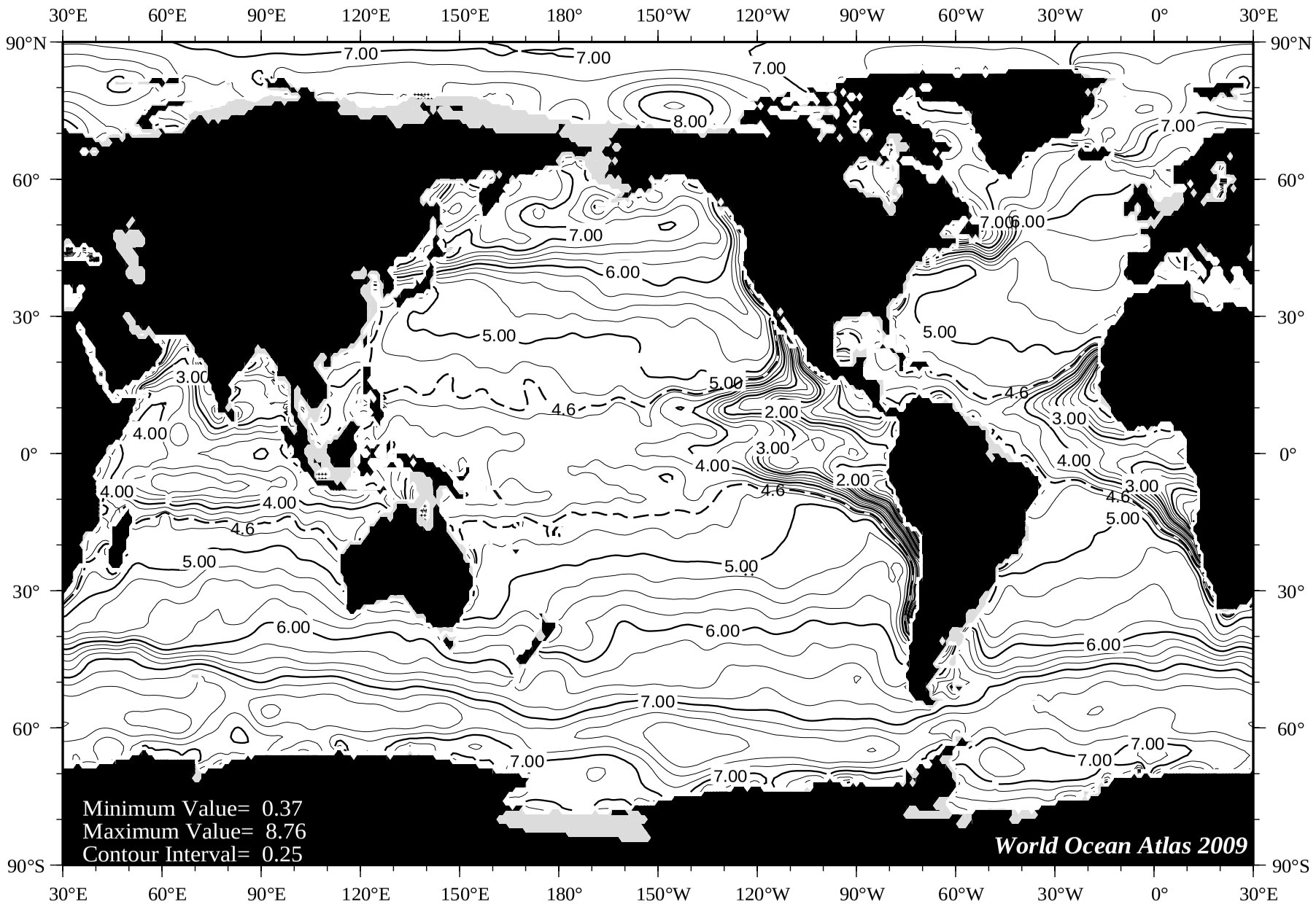

Fig A19 Annual oxygen [ml/l] at 75 m. depth.

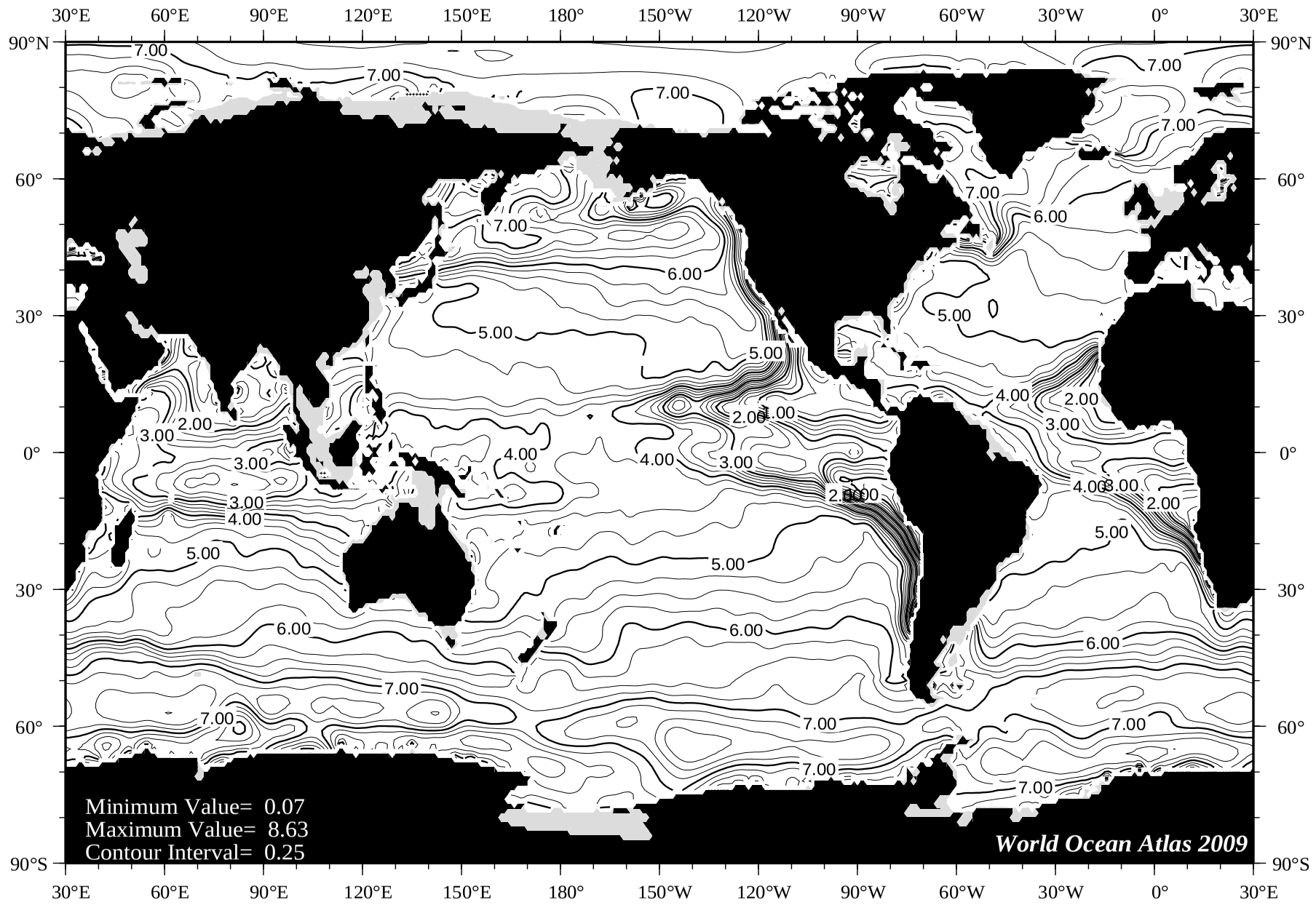

Fig A20 Annual oxygen [ml/l] at 100 m. depth.

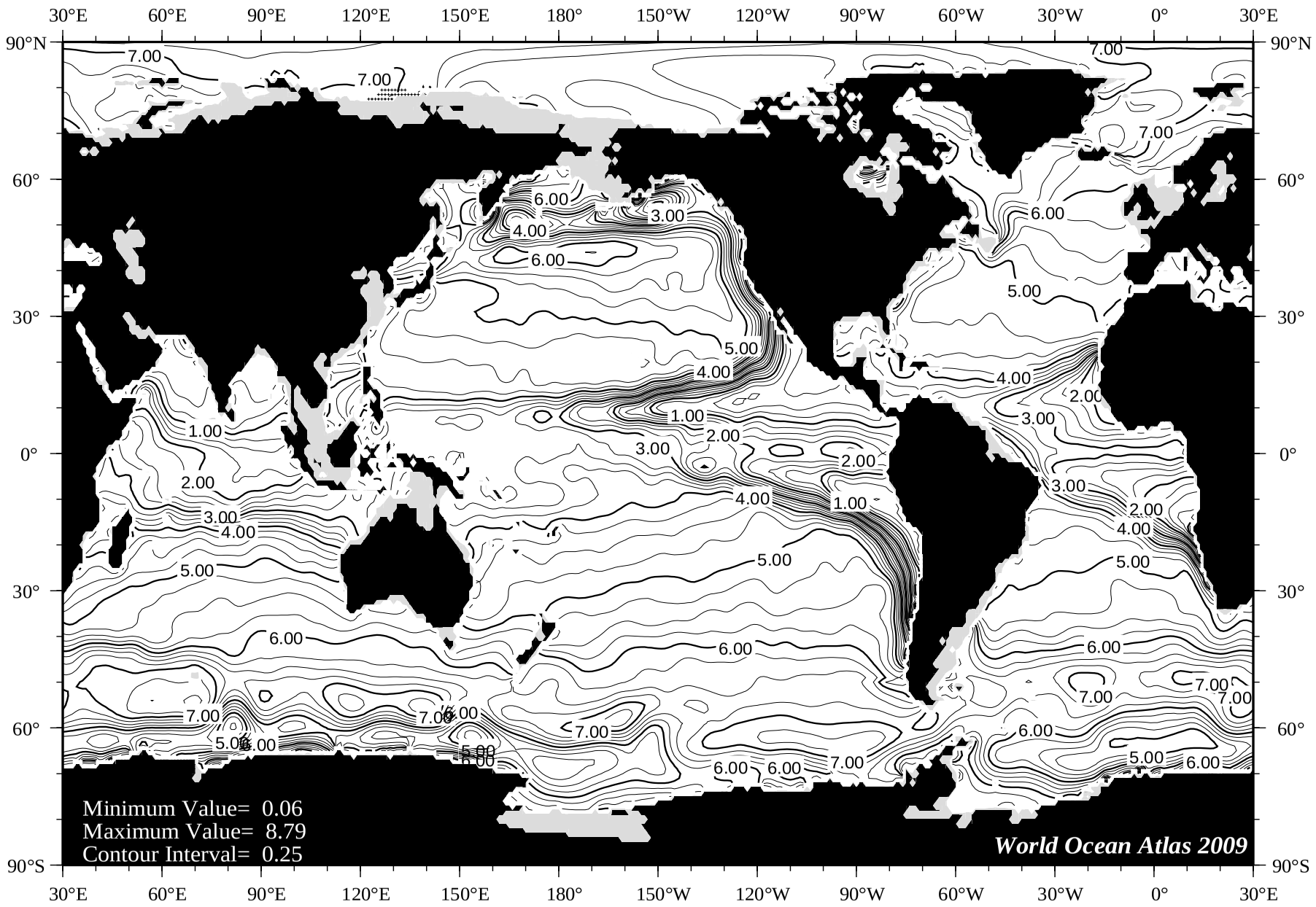

Fig A21 Annual oxygen [ml/l] at 150 m. depth.

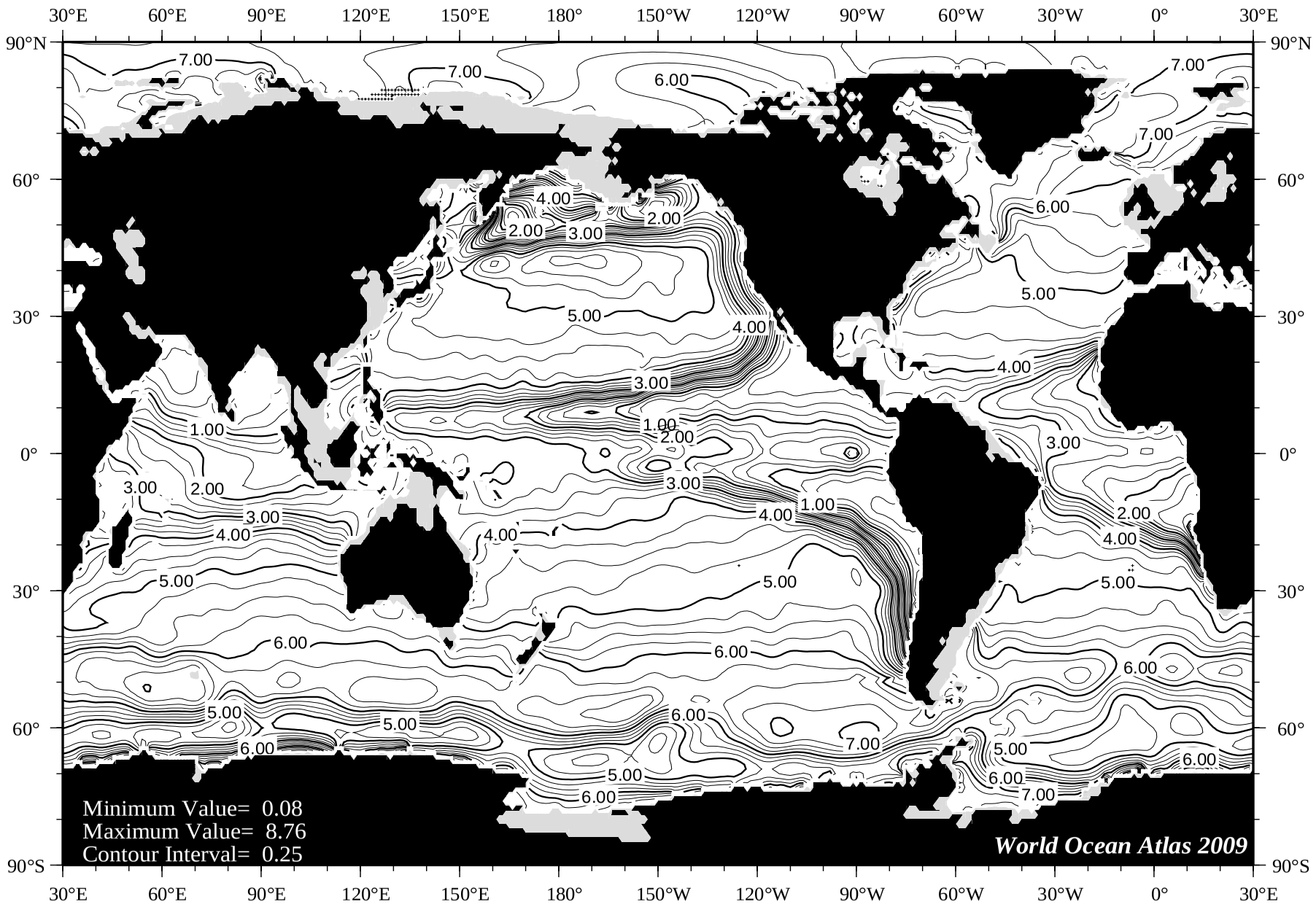

Fig A22 Annual oxygen [ml/l] at 200 m. depth.

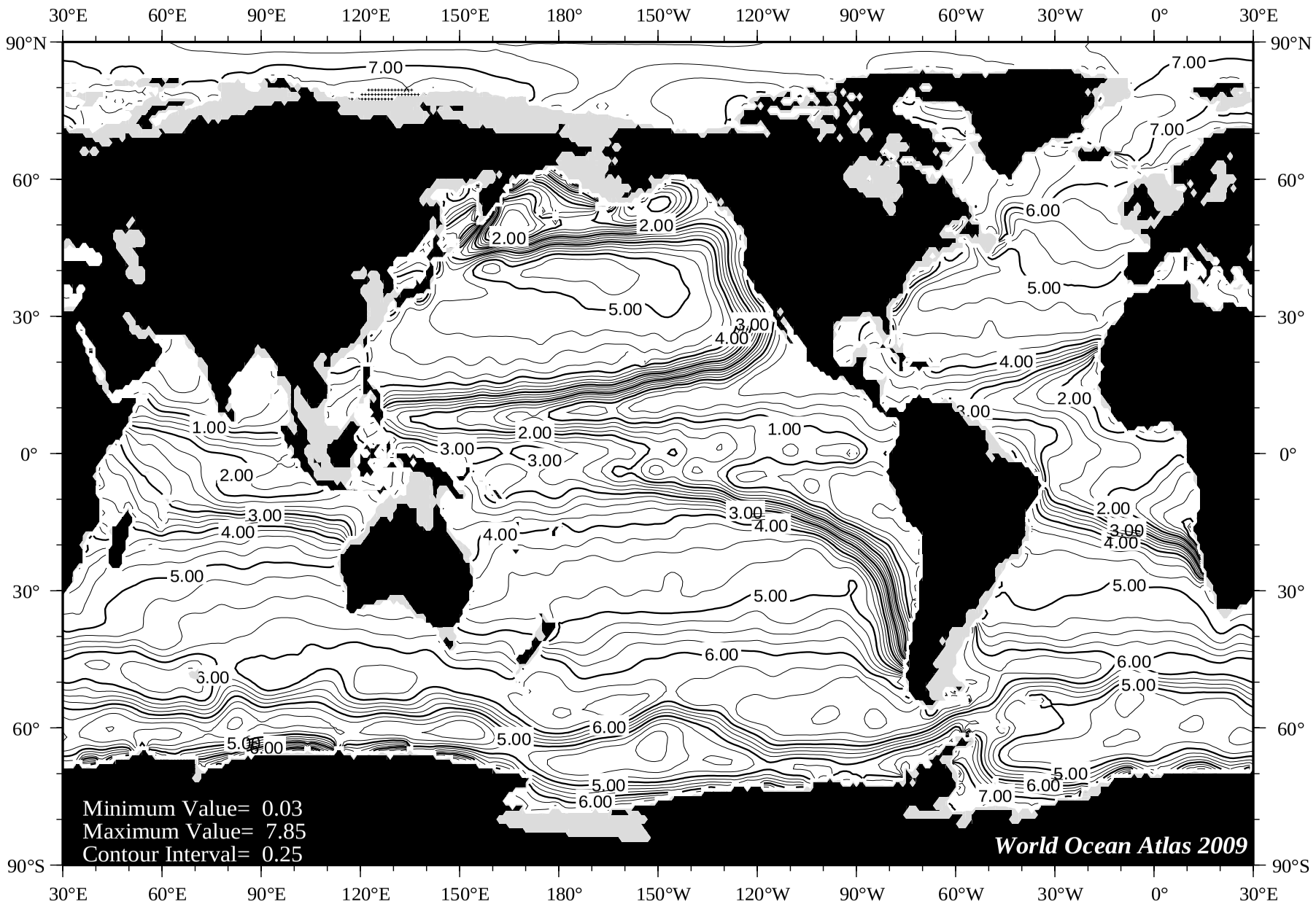

Fig A23 Annual oxygen [ml/l] at 250 m. depth.

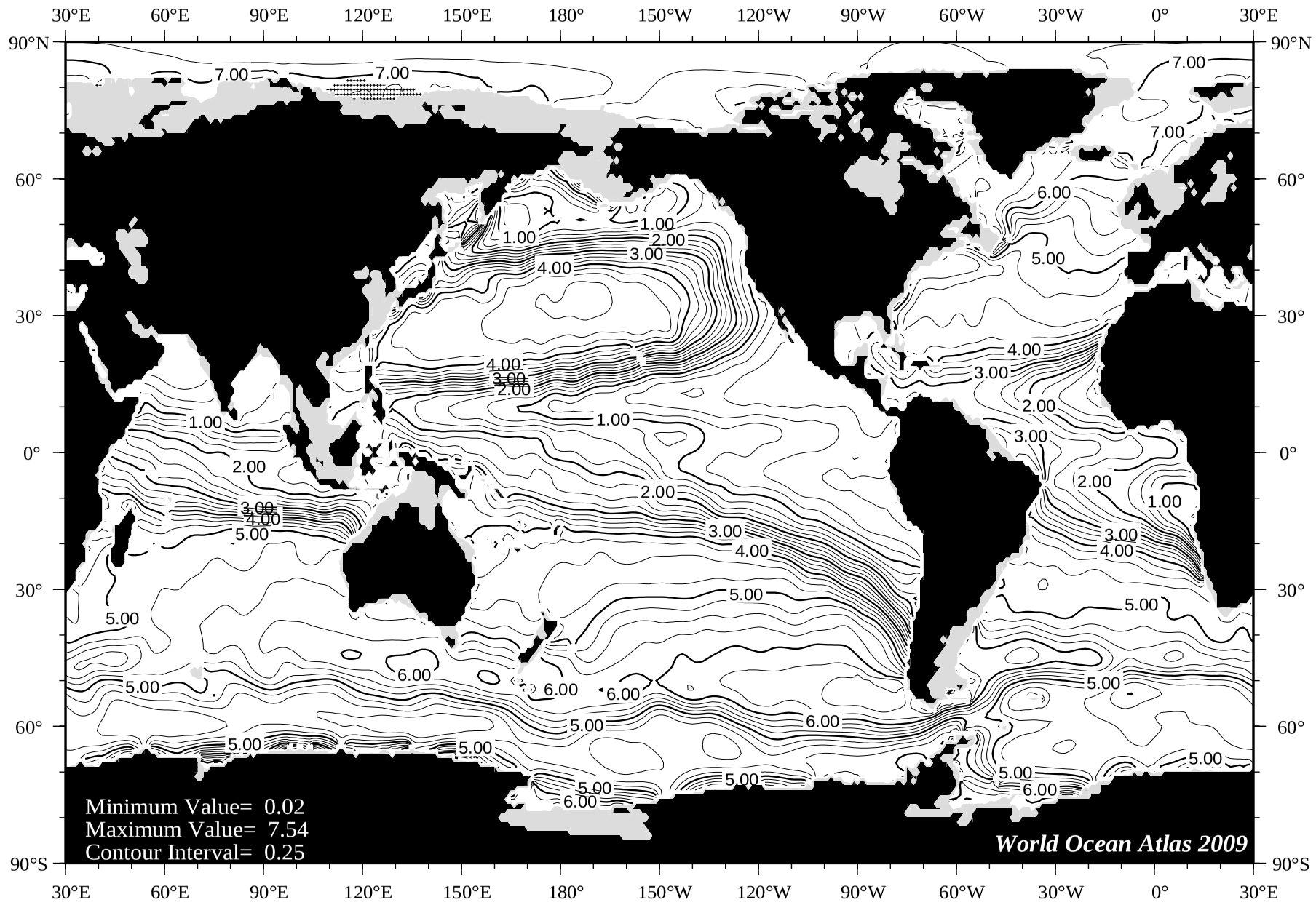

Fig A24 Annual oxygen [ml/l] at 400 m. depth.

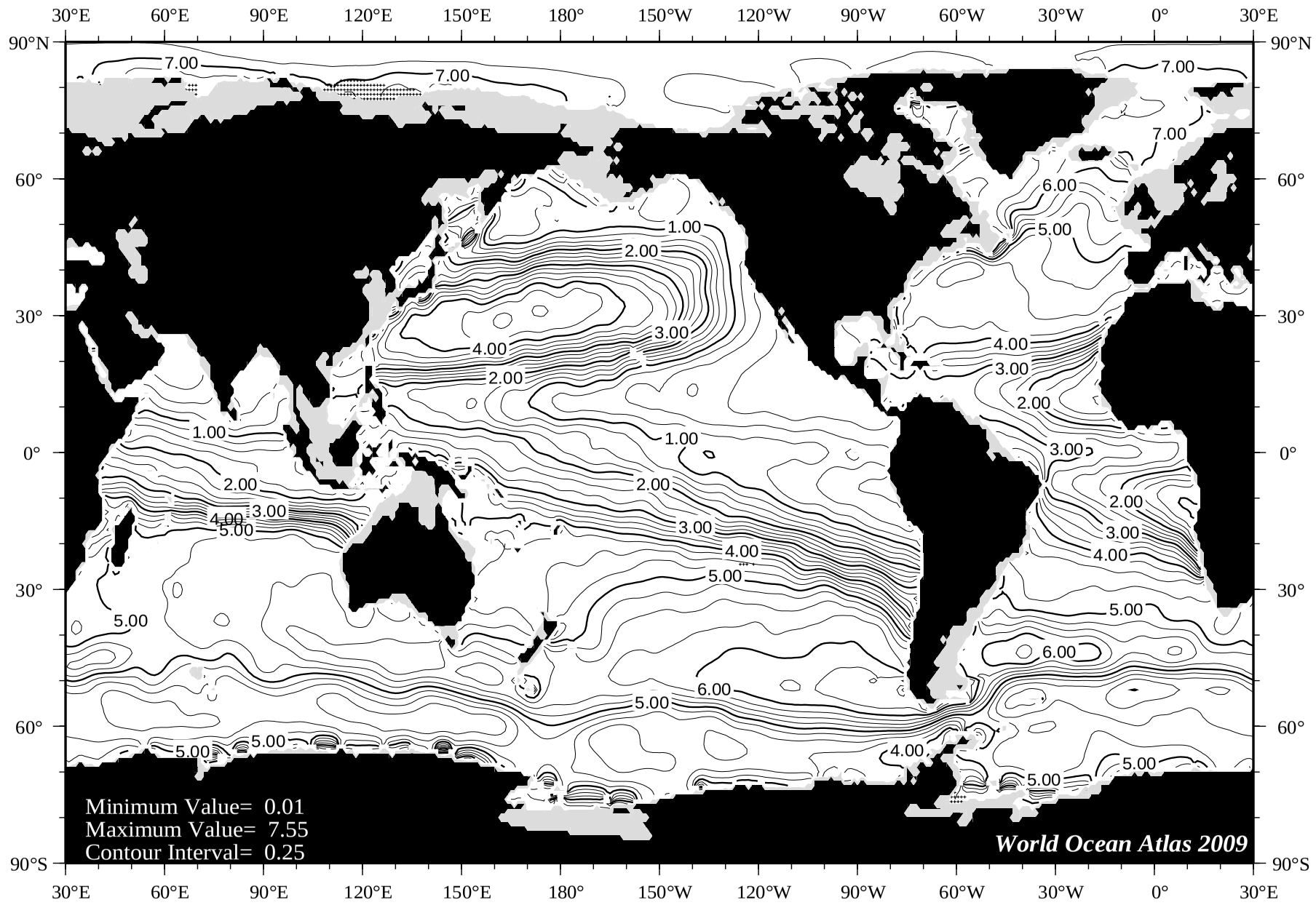

Fig A25 Annual oxygen [ml/l] at 500 m. depth.

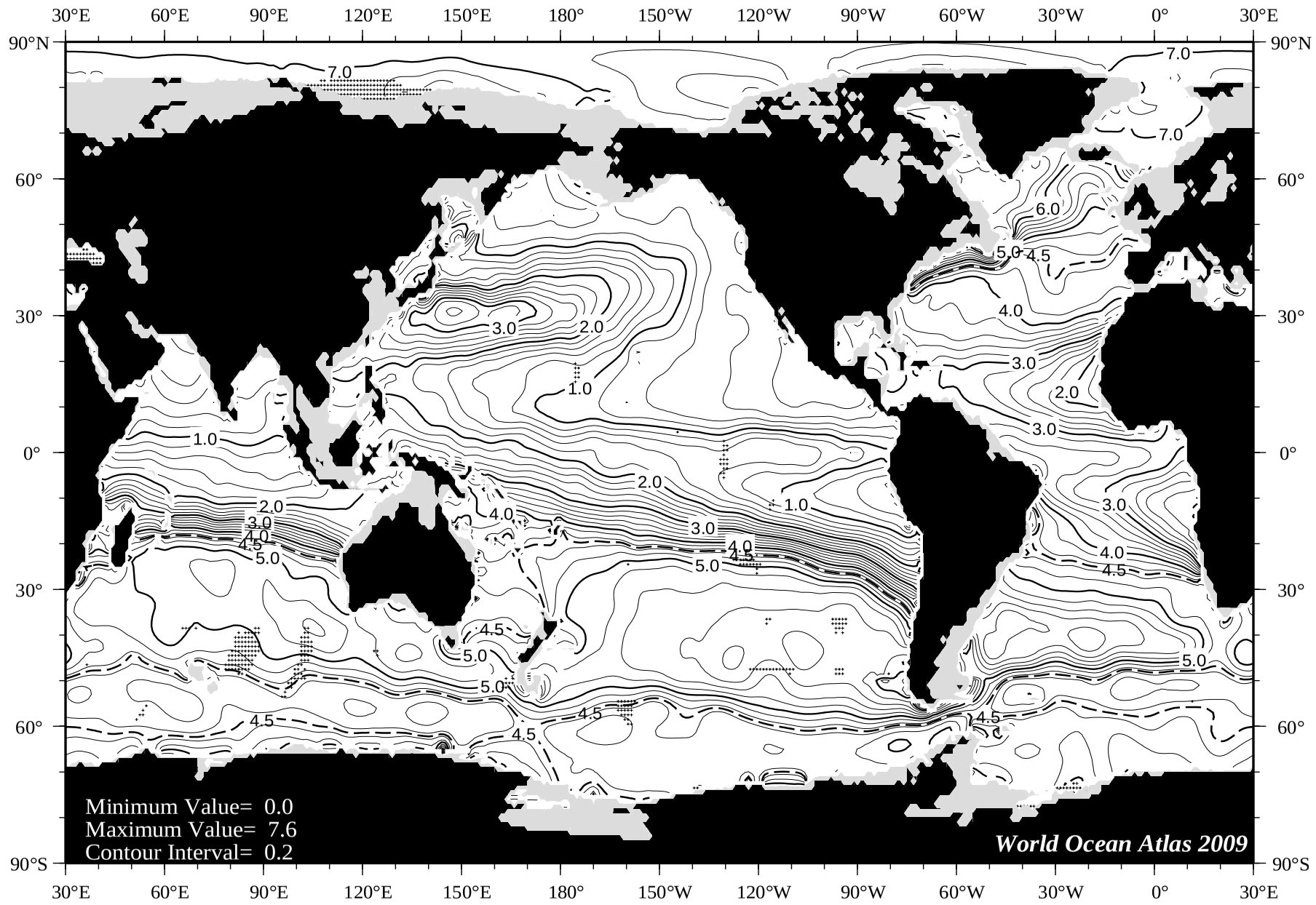

Fig A26 Annual oxygen [ml/l] at 700 m. depth.

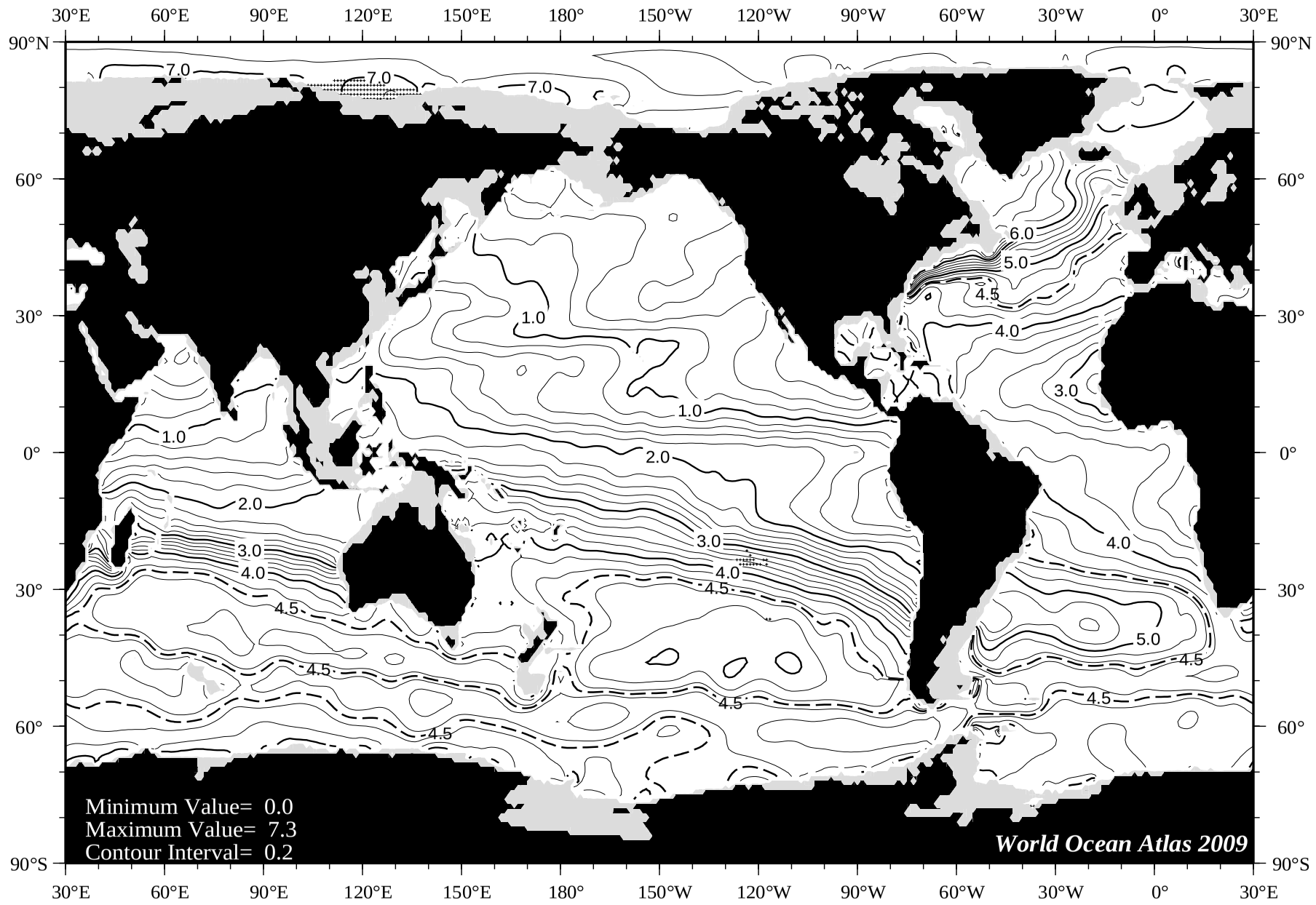

Fig A27 Annual oxygen [ml/l] at 1000 m. depth.

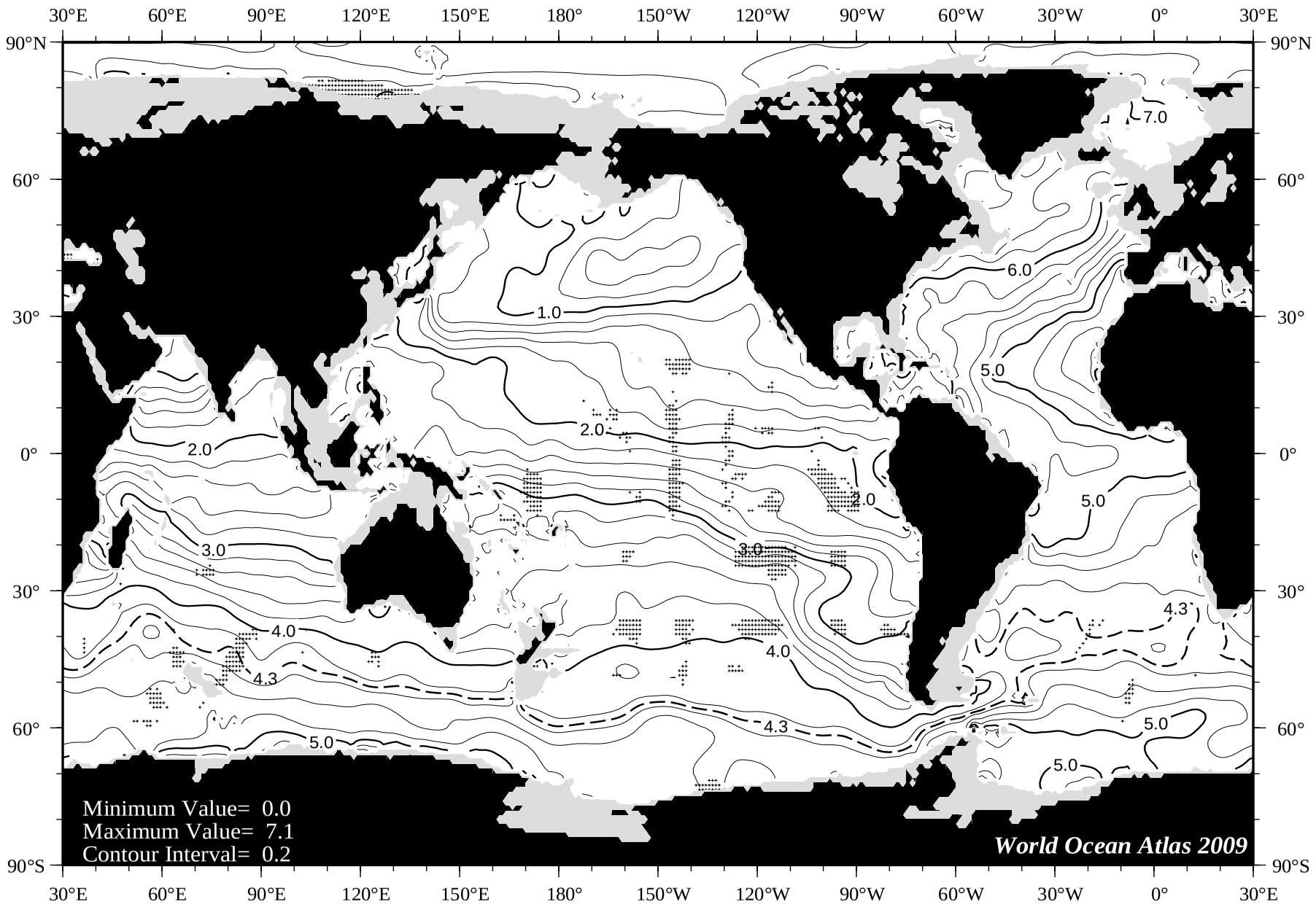

Fig A28 Annual oxygen [ml/l] at 1500 m. depth.

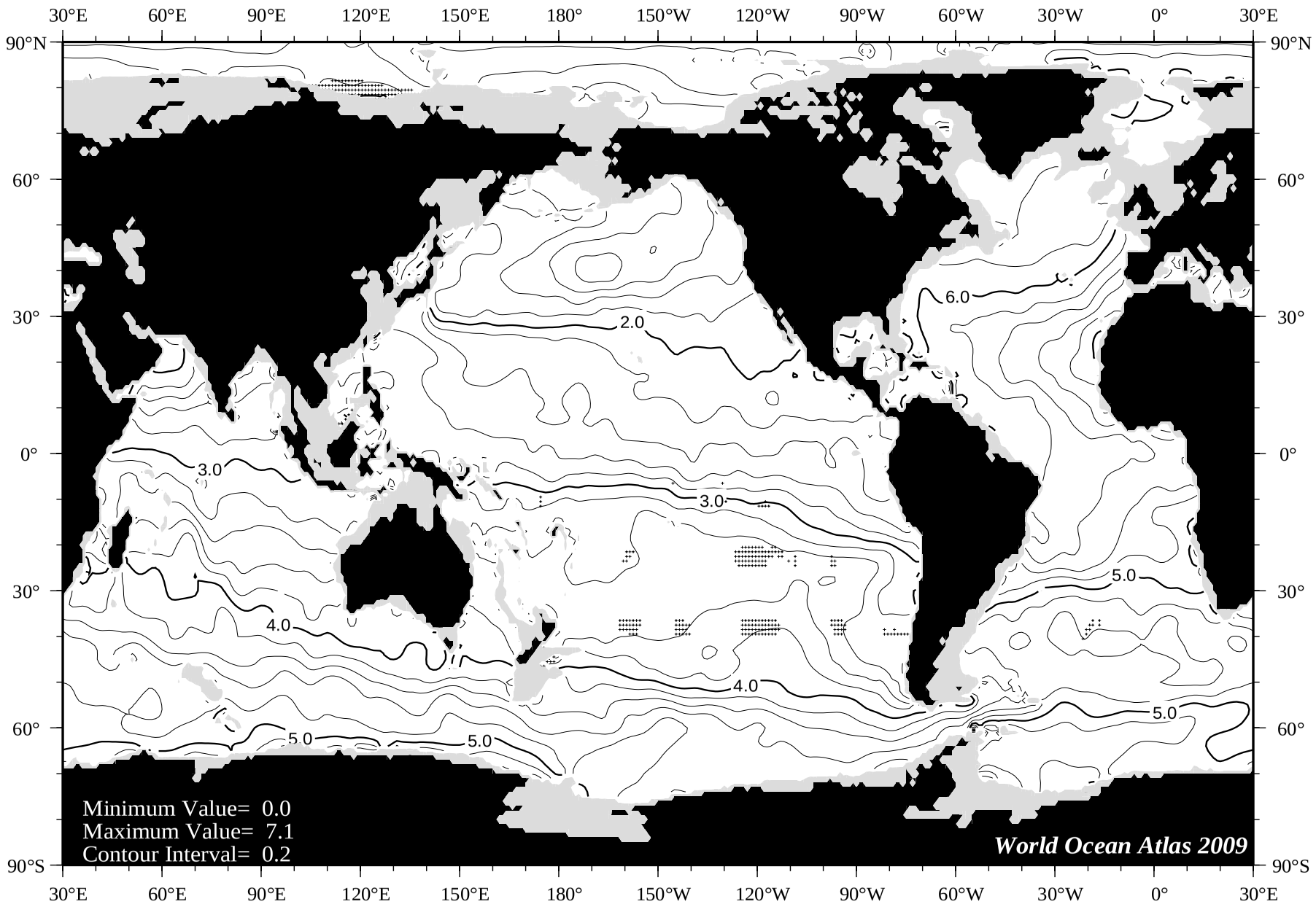

Fig A29 Annual oxygen [ml/l] at 2000 m. depth.

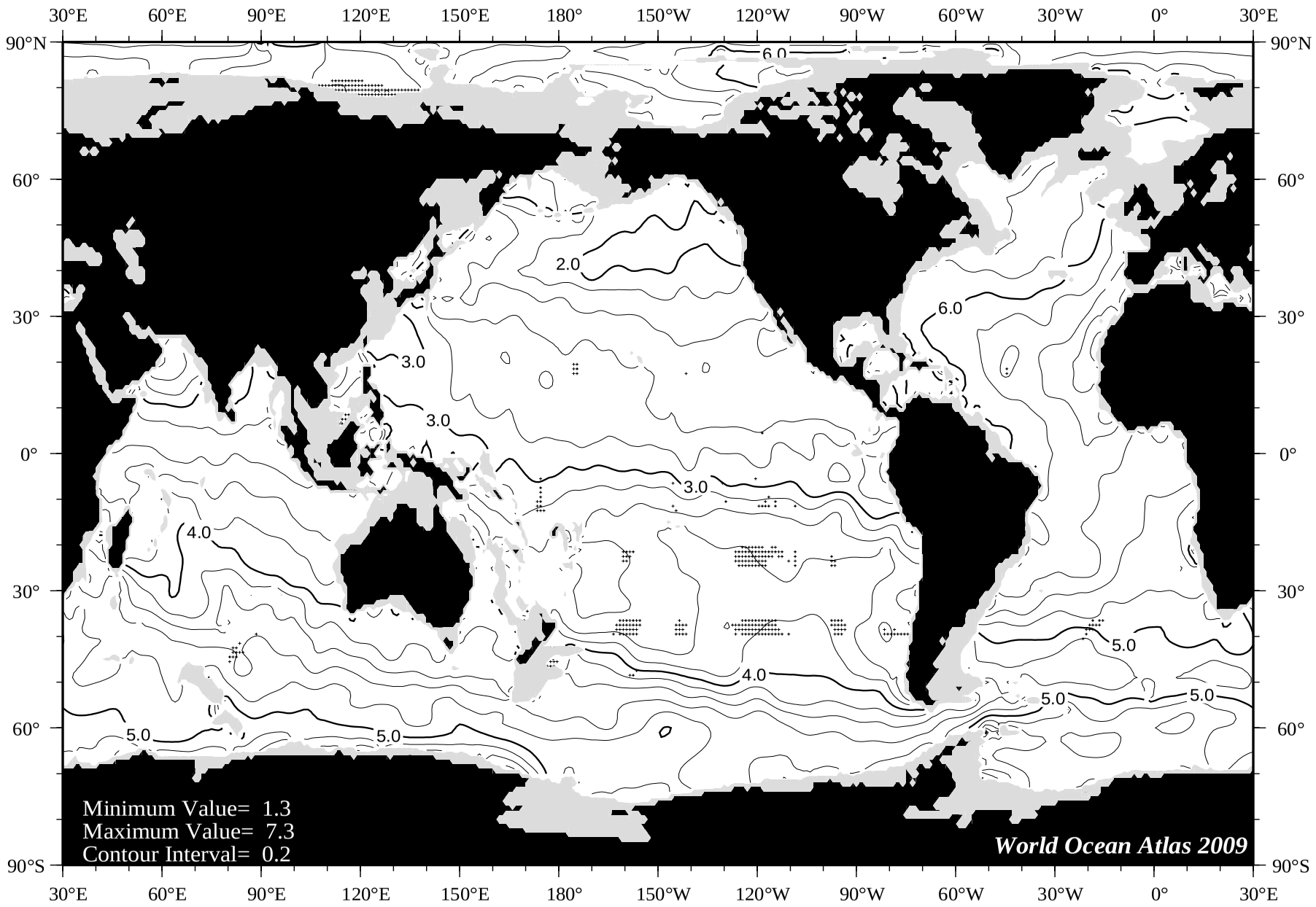

Fig A30 Annual oxygen [ml/l] at 2500 m. depth.

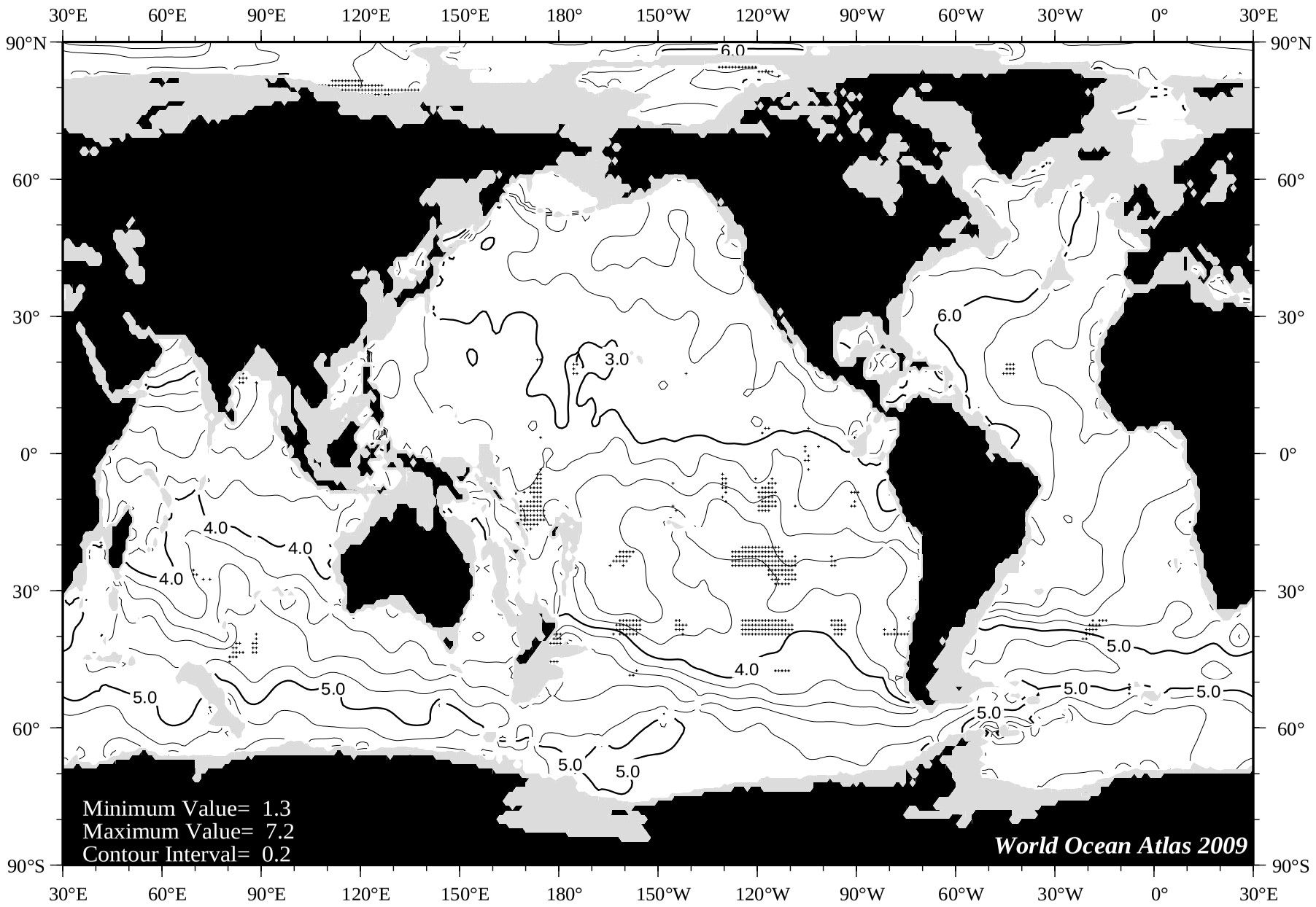

Fig A31 Annual oxygen [ml/l] at 3000 m. depth.

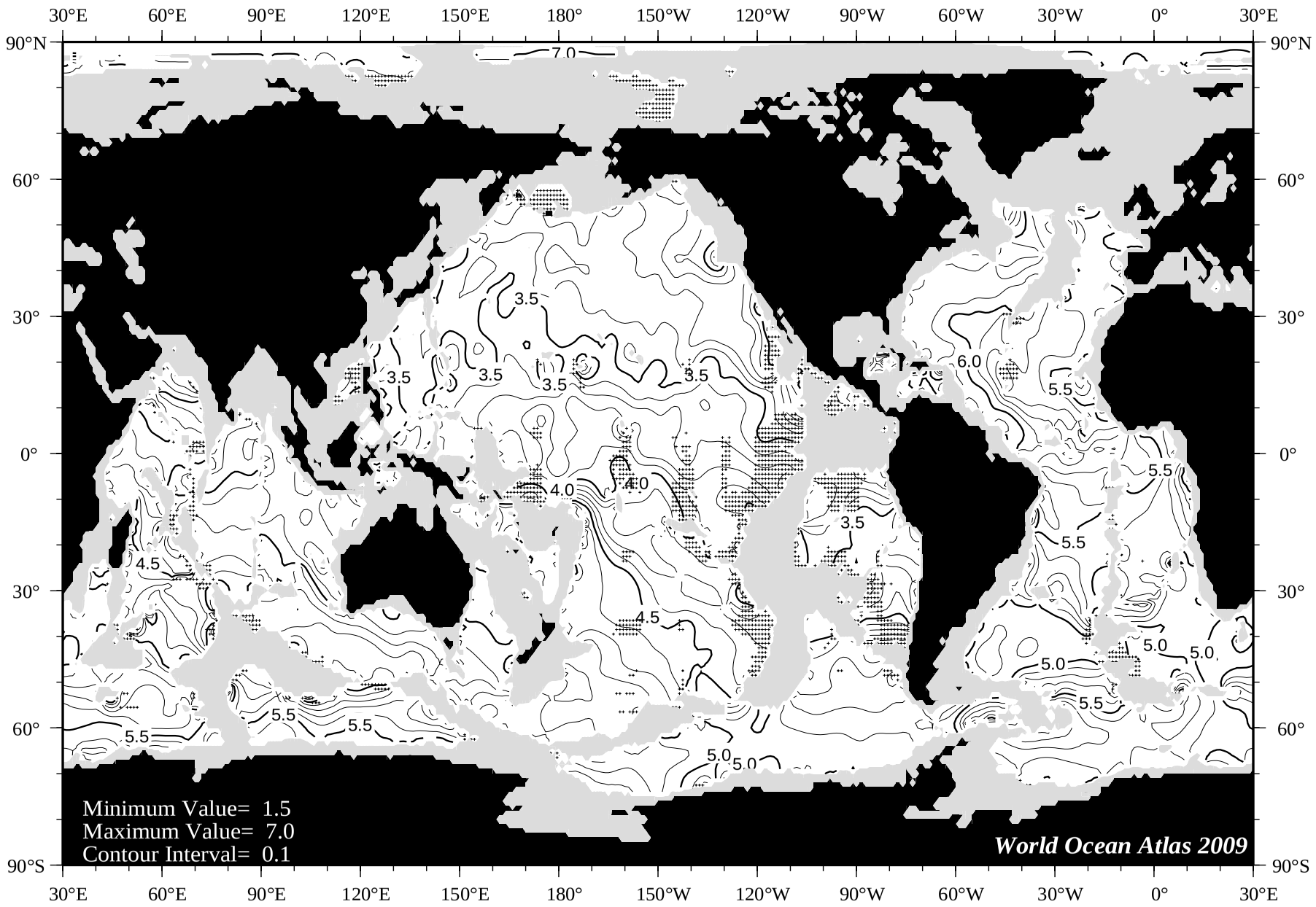

Fig A32 Annual oxygen [ml/l] at 4000 m. depth.

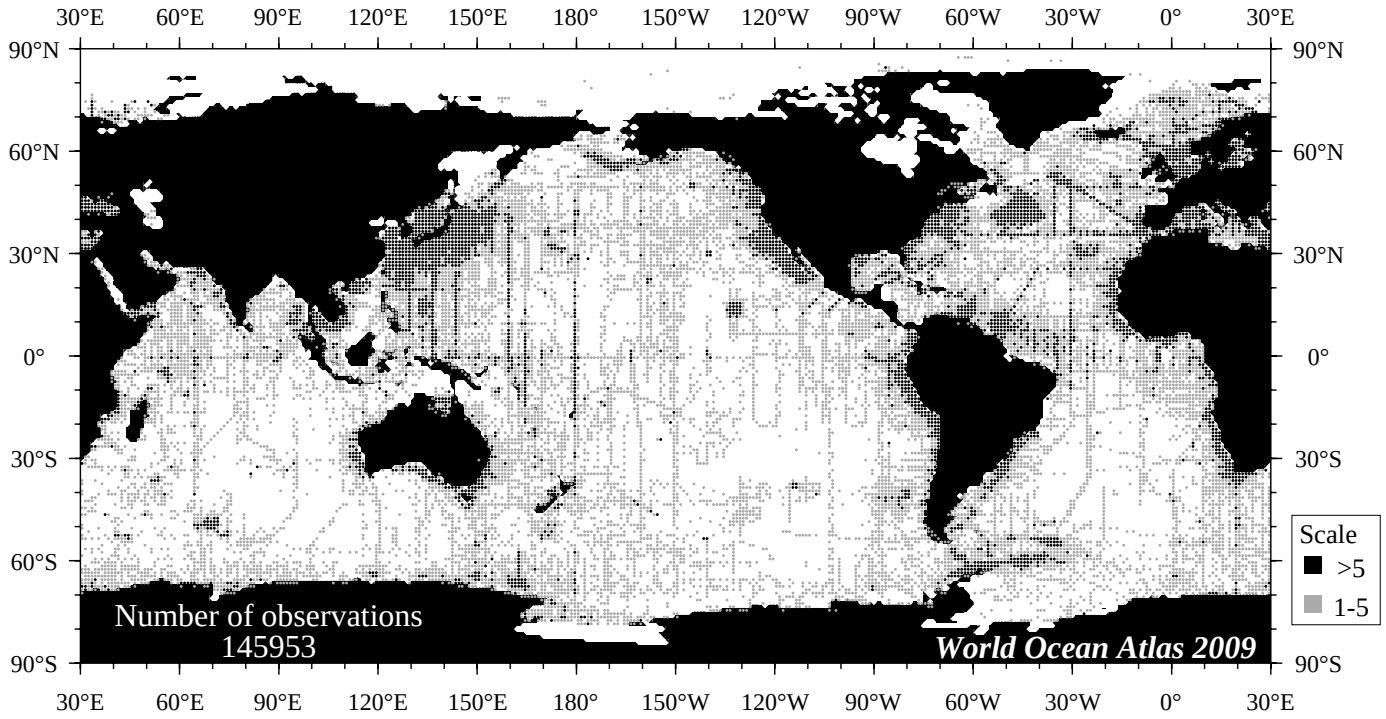

Fig B1 Winter (Jan.-Mar.) oxygen observations at the surface.

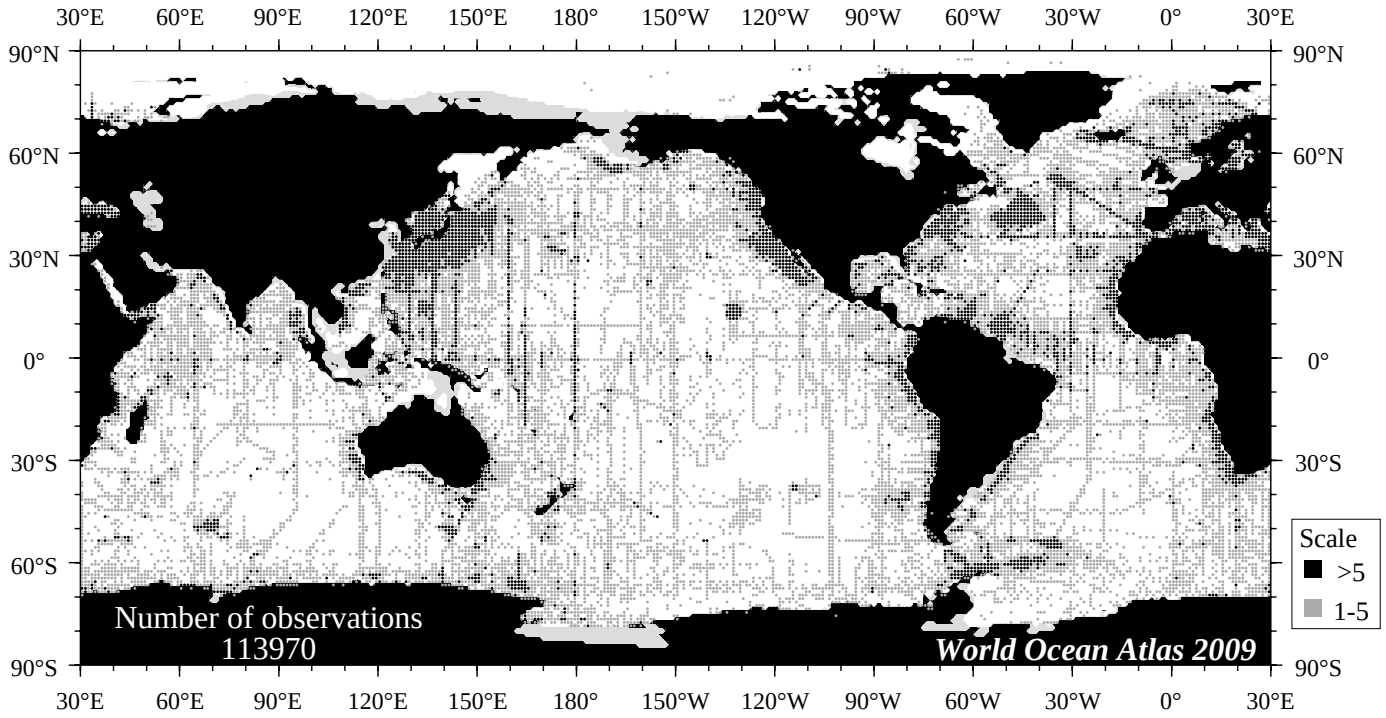

Fig B2 Winter (Jan.-Mar.) oxygen observations at 75 m. depth.

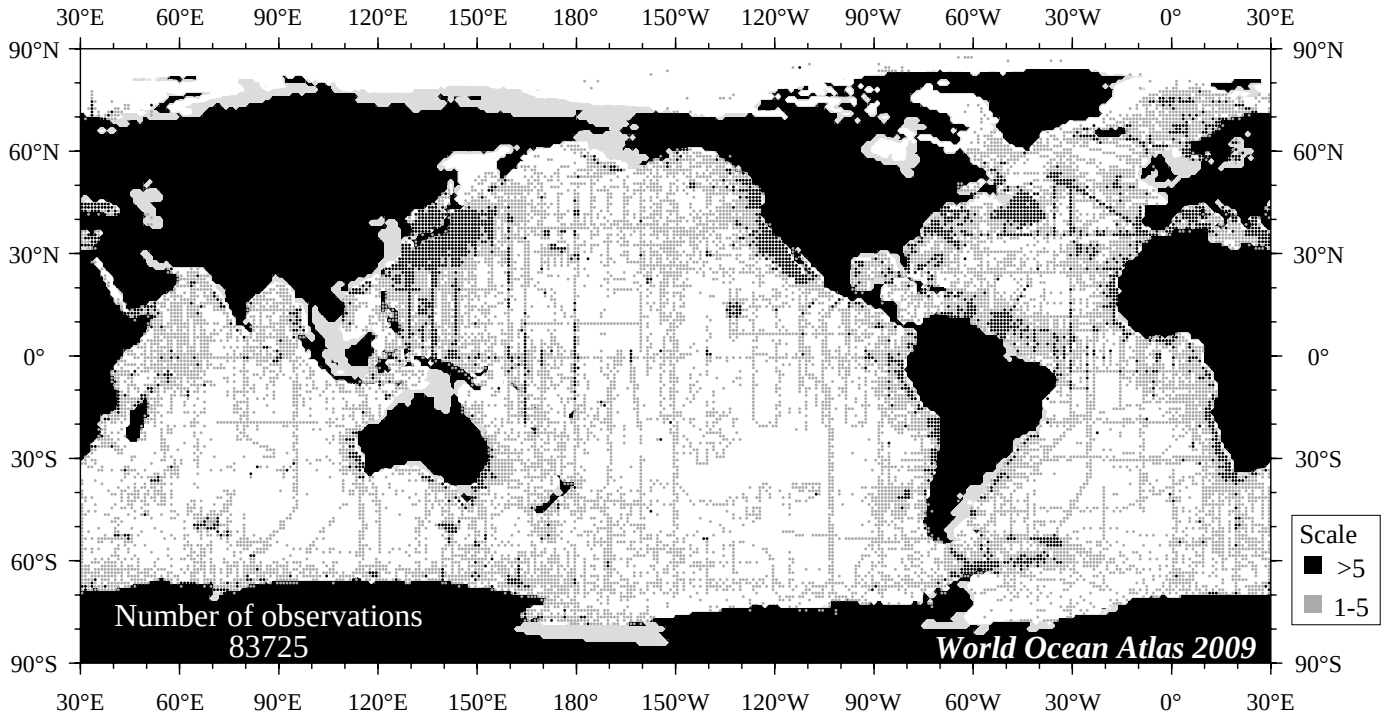

Fig B3 Winter (Jan.-Mar.) oxygen observations at 150 m. depth.

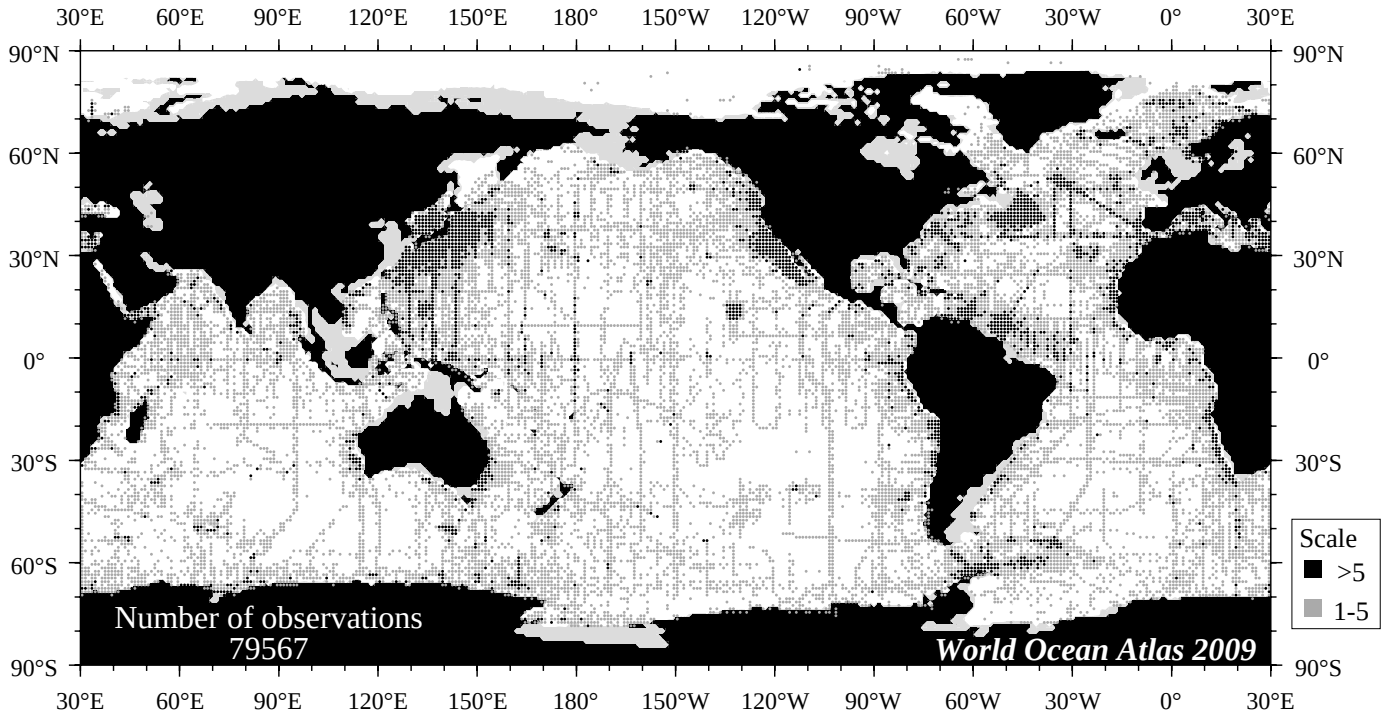

Fig B4 Winter (Jan.-Mar.) oxygen observations at 250 m. depth.

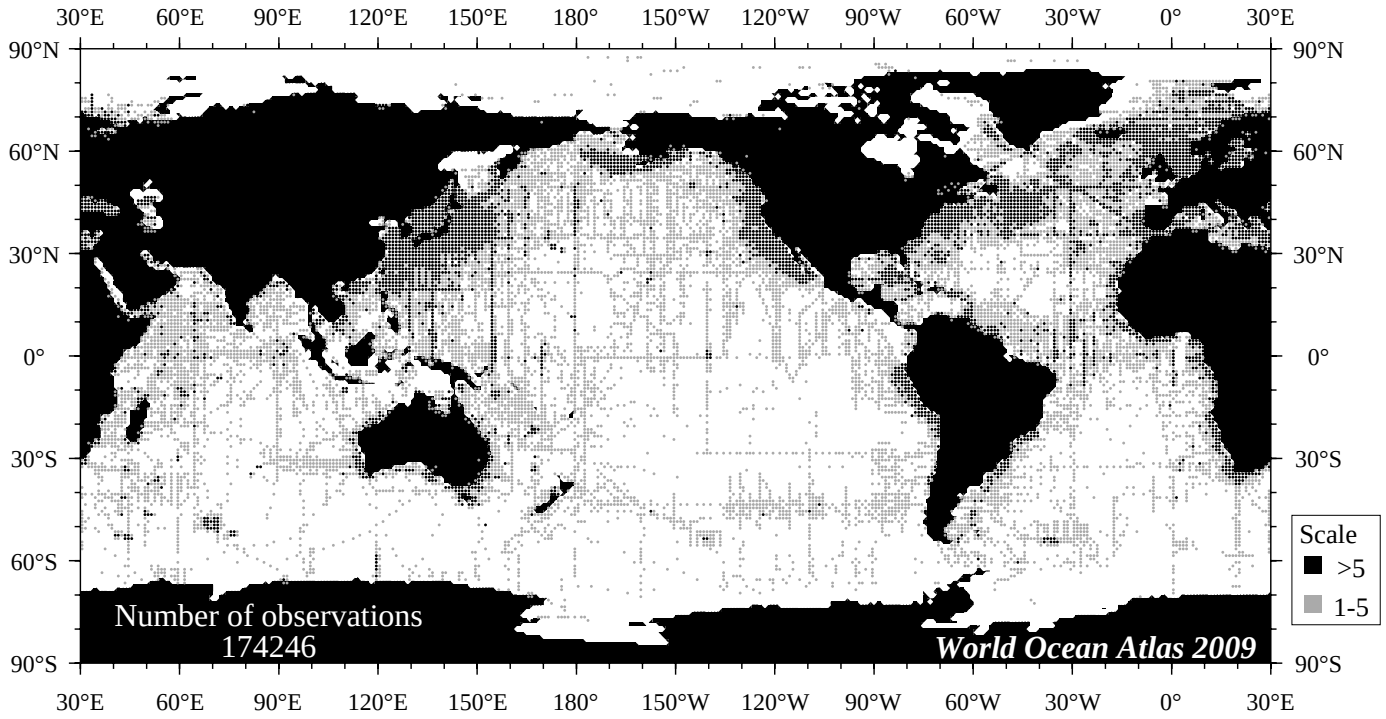

Fig B5 Spring (Apr.-Jun.) oxygen observations at the surface.

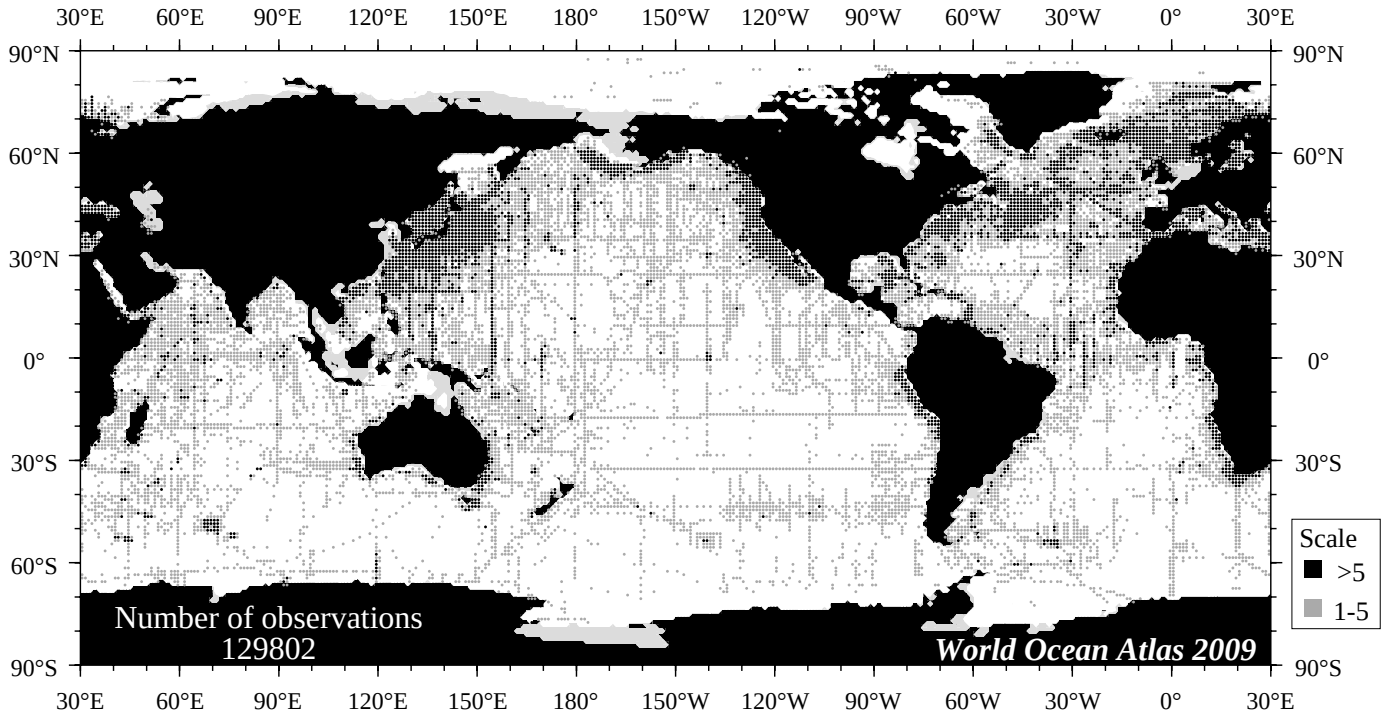

Fig B6 Spring (Apr.-Jun.) oxygen observations at 75 m. depth.

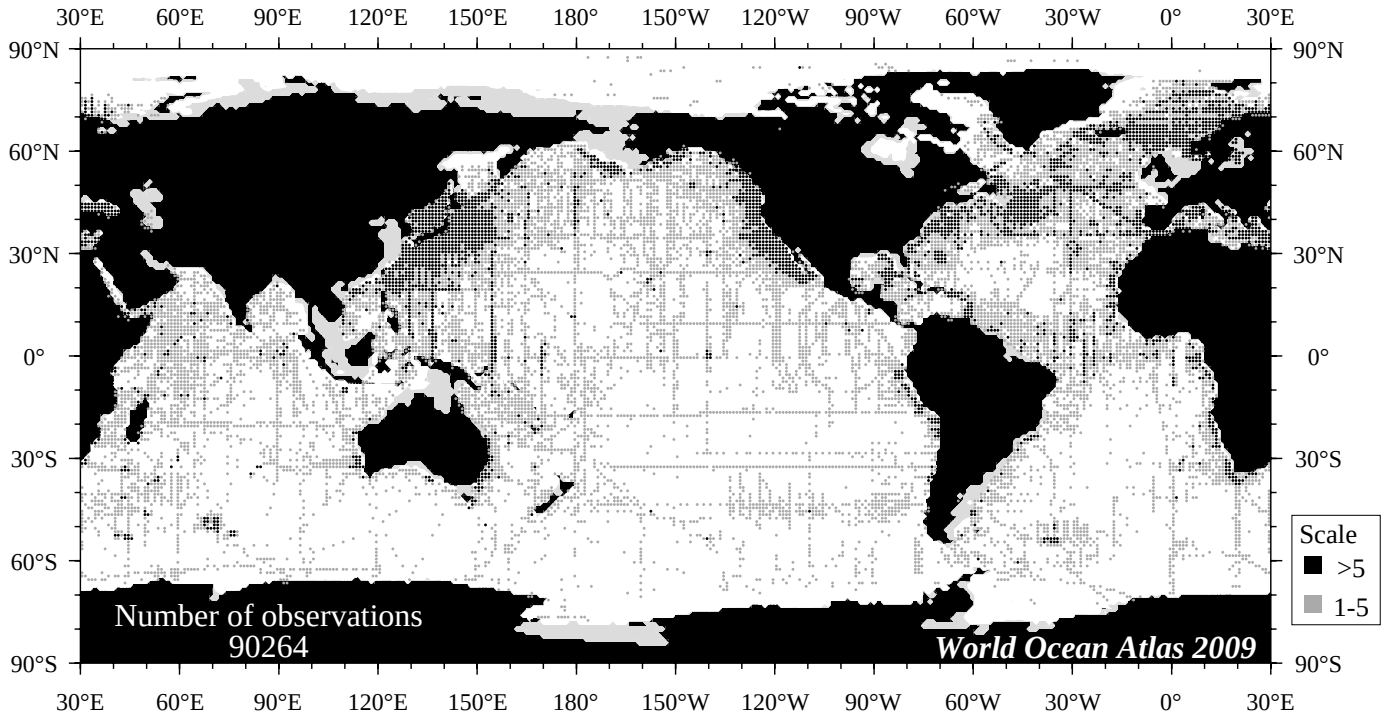

Fig B7 Spring (Apr.-Jun.) oxygen observations at 150 m. depth.

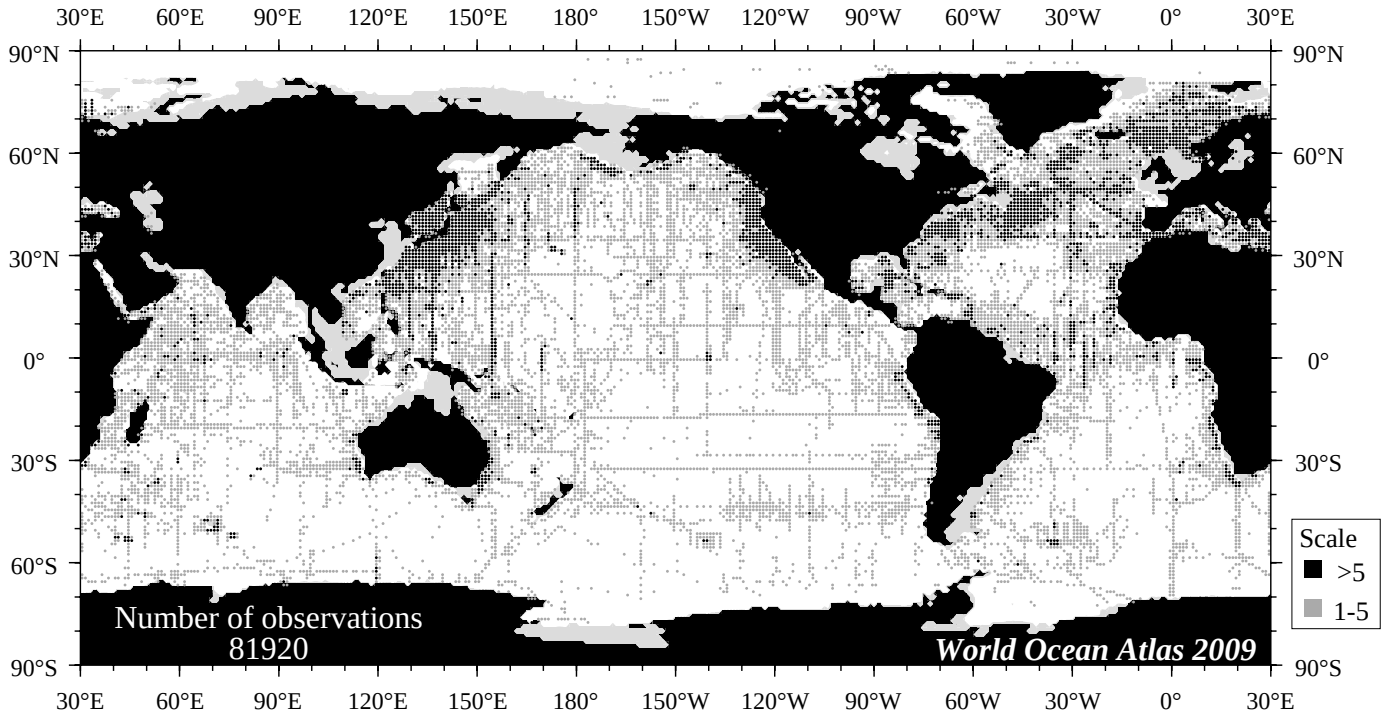

Fig B8 Spring (Apr.-Jun.) oxygen observations at 250 m. depth.

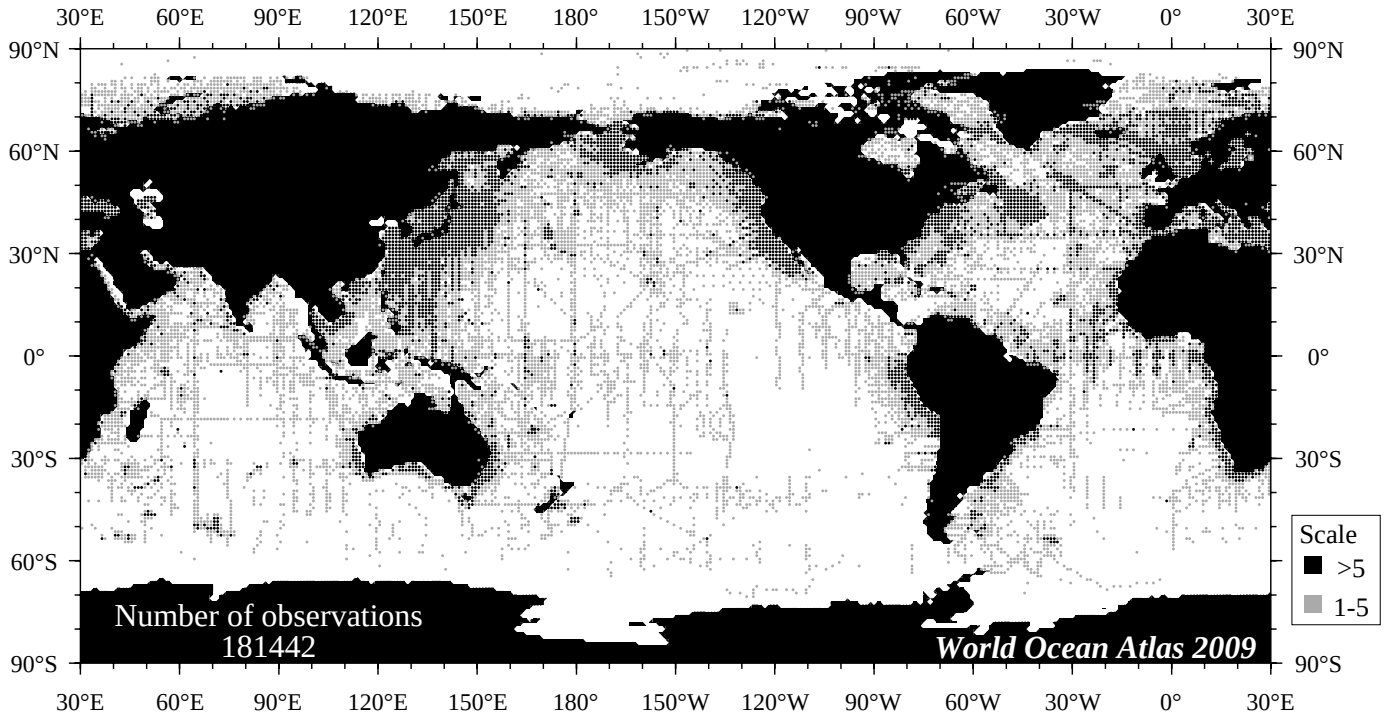

Fig B9 Summer (Jul.-Sep.) oxygen observations at the surface.

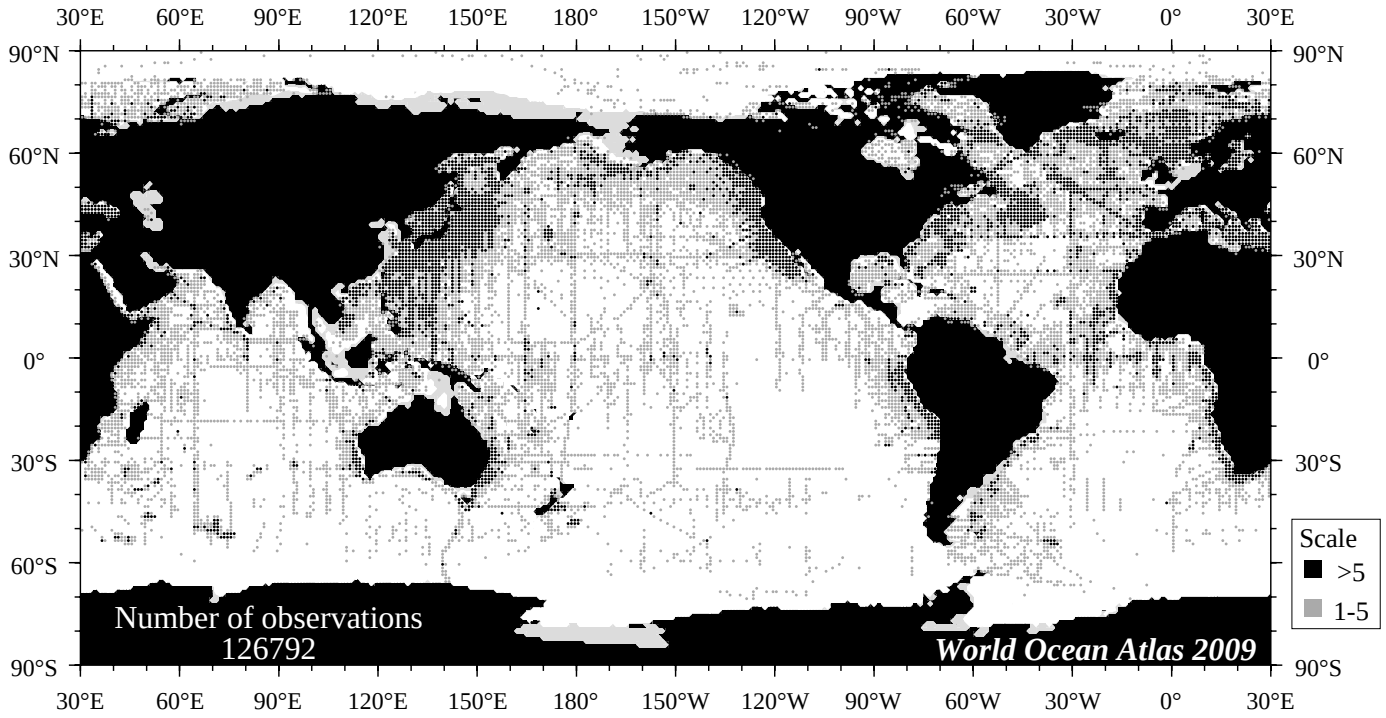

Fig B10 Summer (Jul.-Sep.) oxygen observations at 75 m. depth.

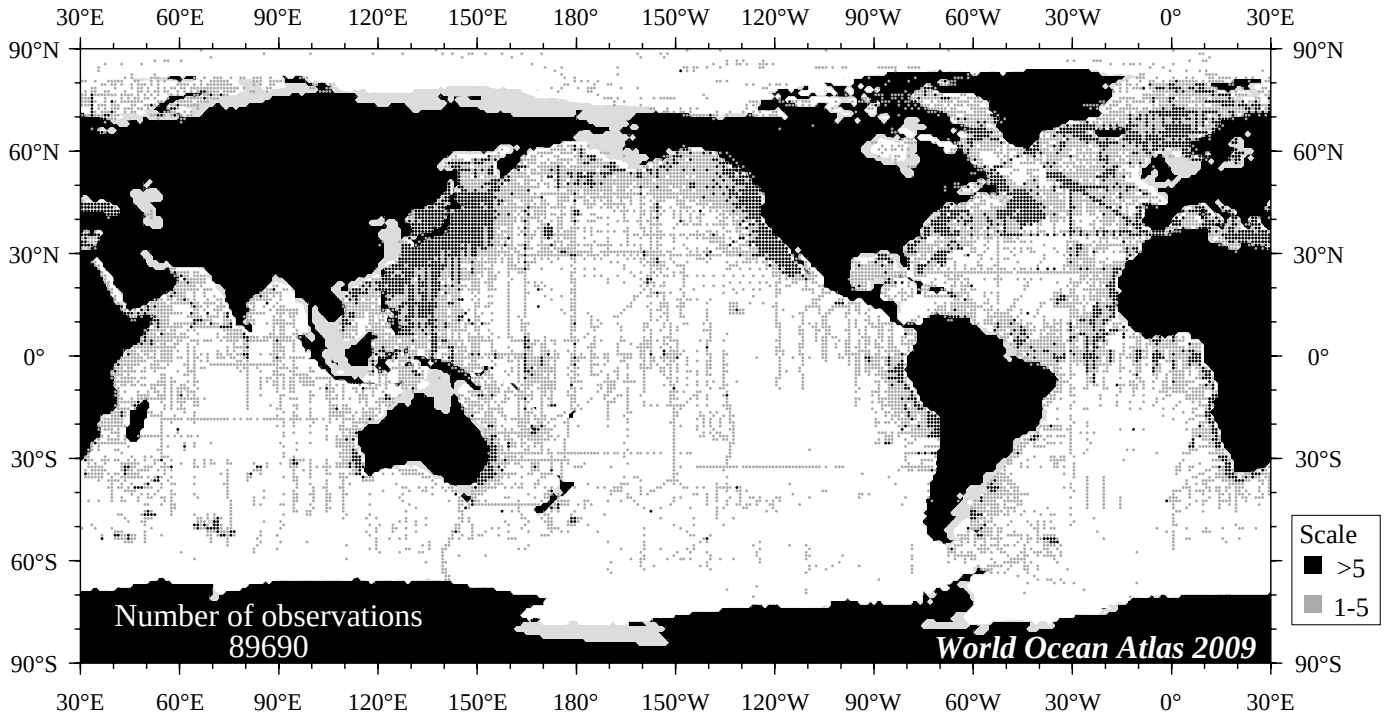

Fig B11 Summer (Jul.-Sep.) oxygen observations at 150 m. depth.

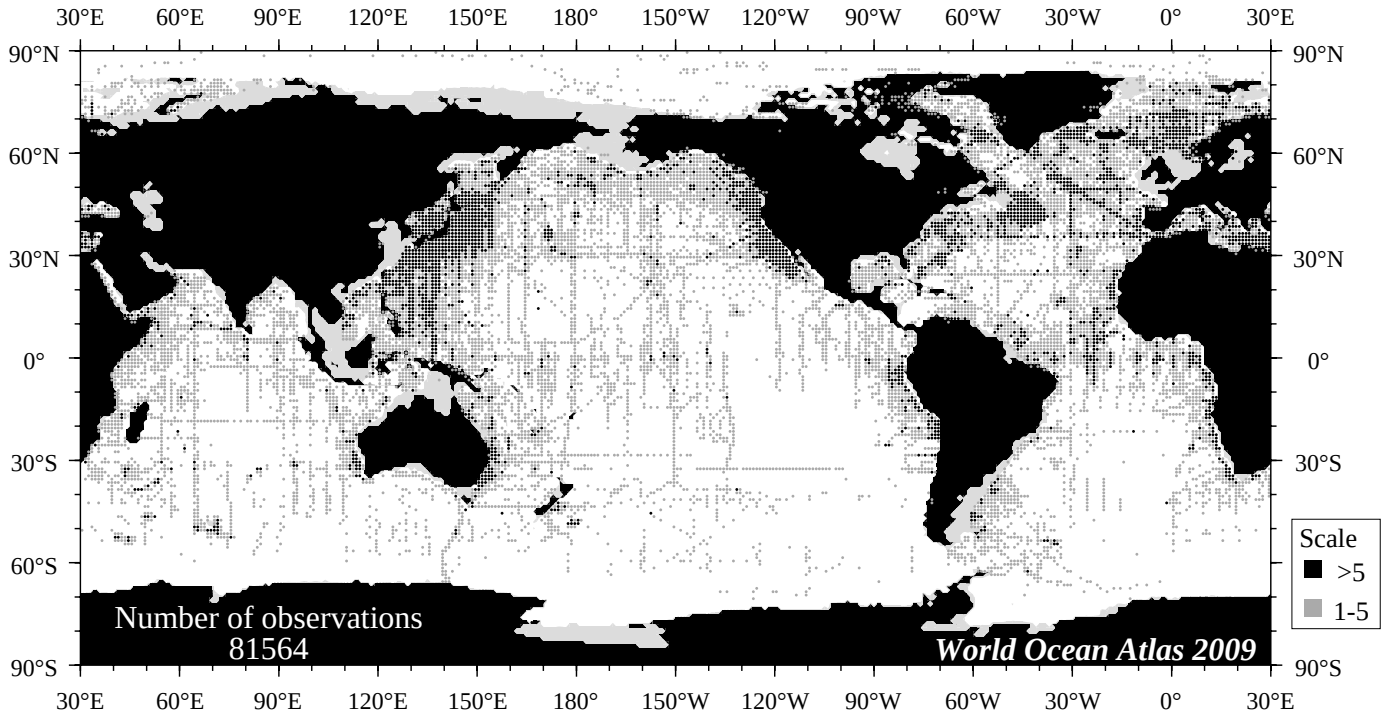

Fig B12 Summer (Jul.-Sep.) oxygen observations at 250 m. depth.

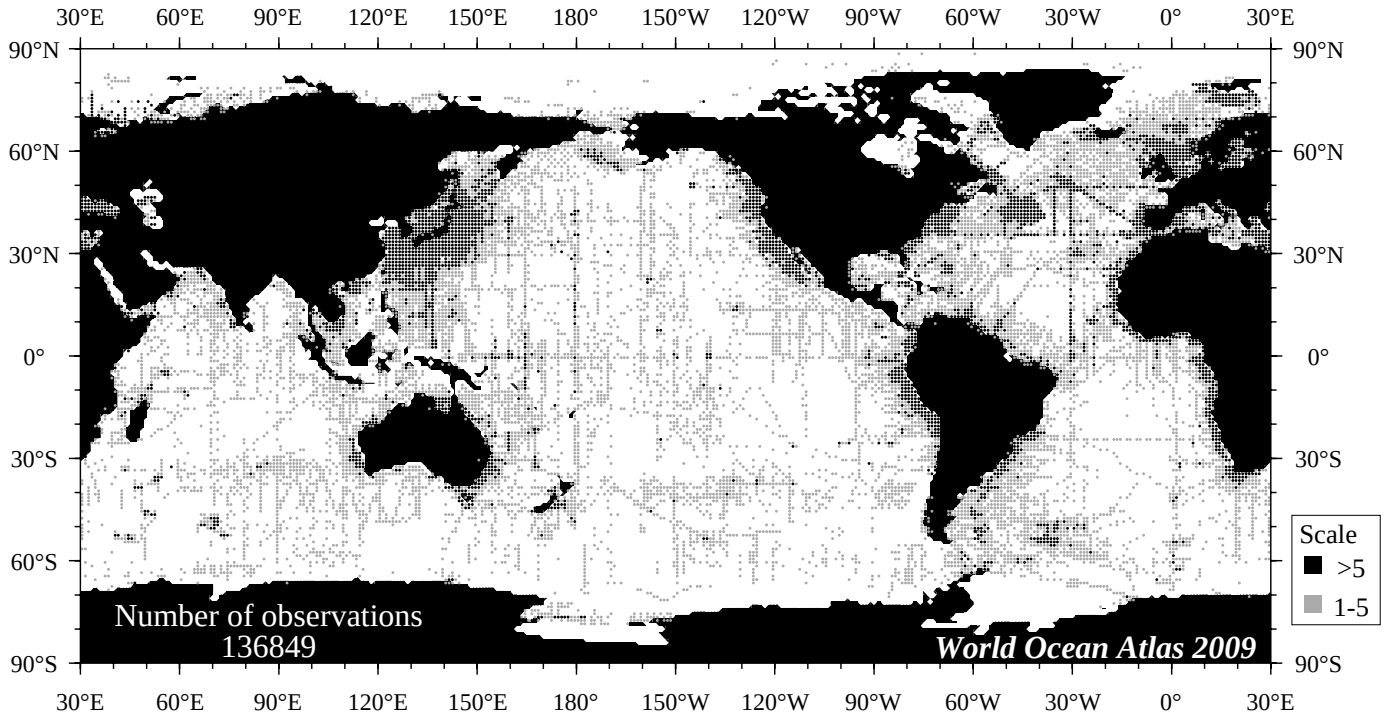

Fig B13 Fall (Oct.-Dec.) oxygen observations at the surface.

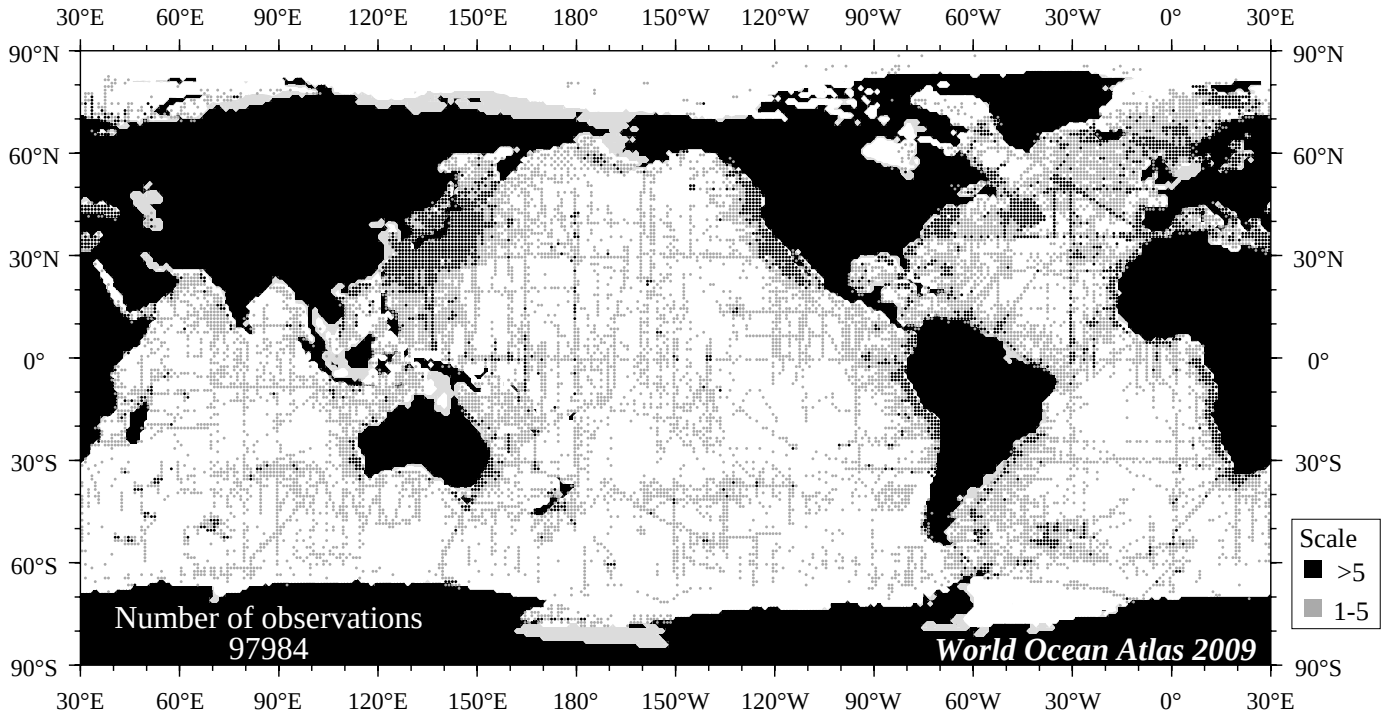

Fig B14 Fall (Oct.-Dec.) oxygen observations at 75 m. depth.

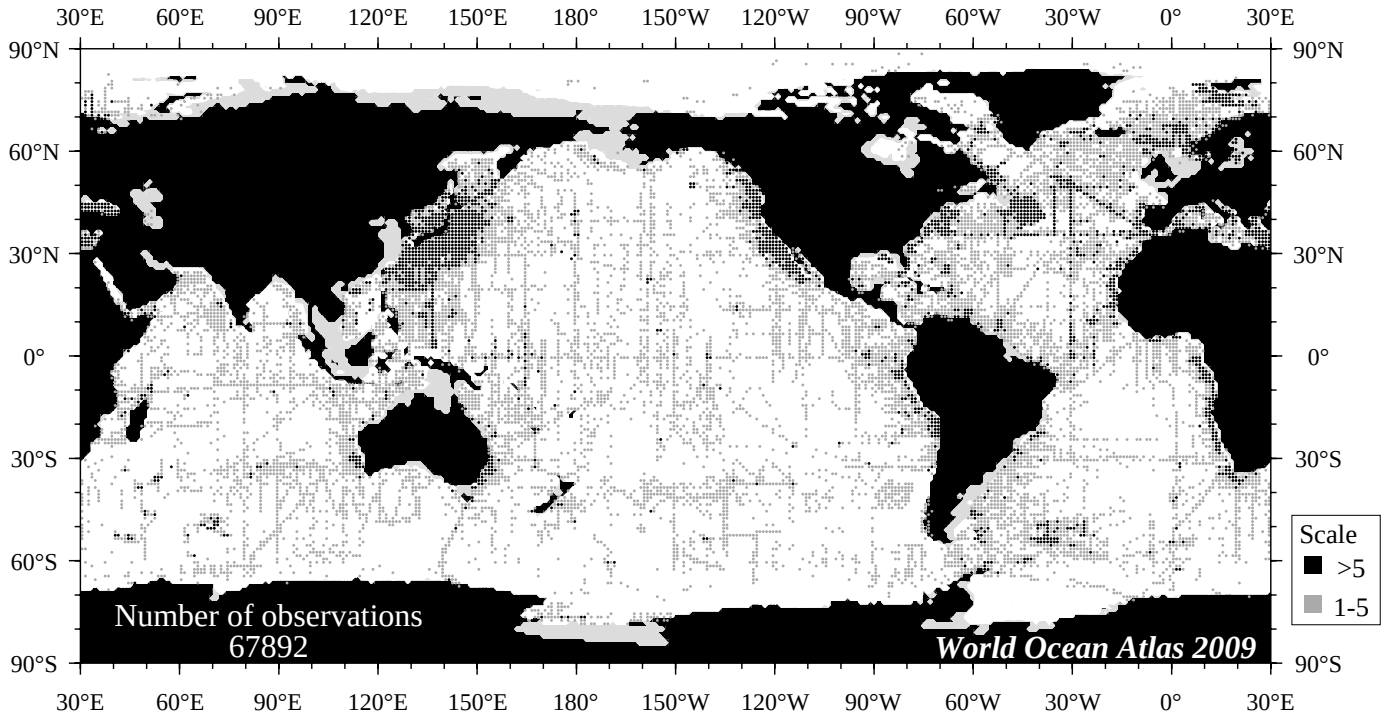

Fig B15 Fall (Oct.-Dec.) oxygen observations at 150 m. depth.

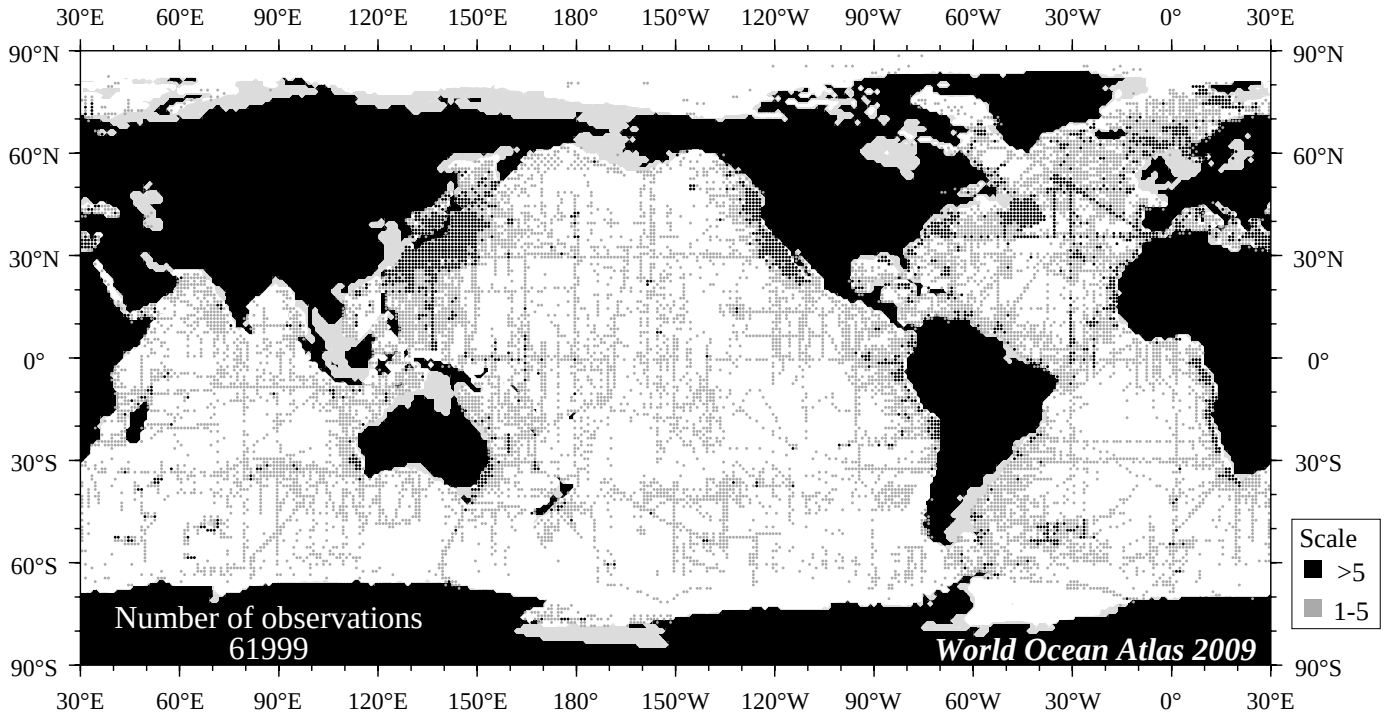

Fig B16 Fall (Oct.-Dec.) oxygen observations at 250 m. depth.

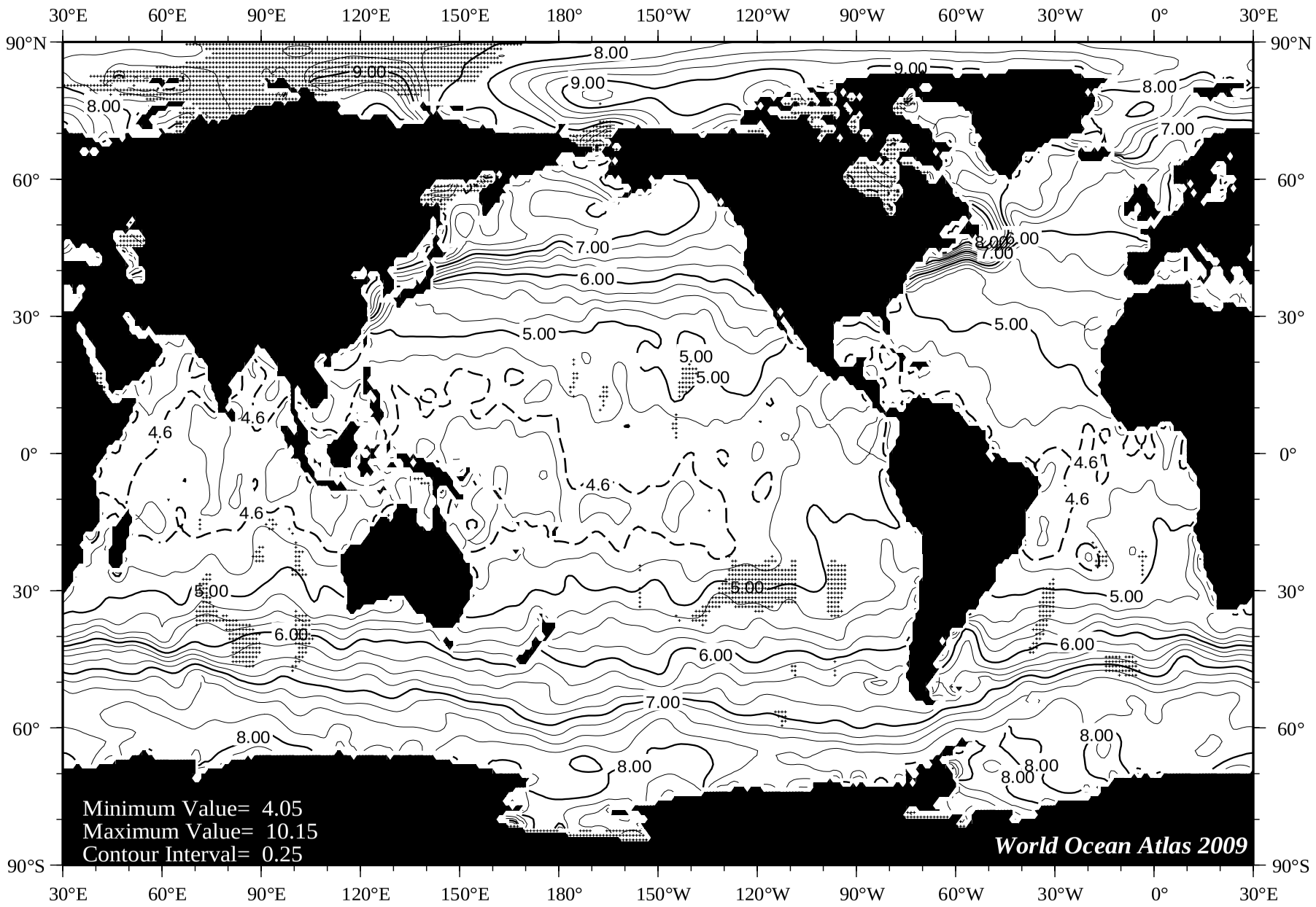

Fig B17 Winter (Jan.-Mar.) oxygen [ml/l] at the surface.

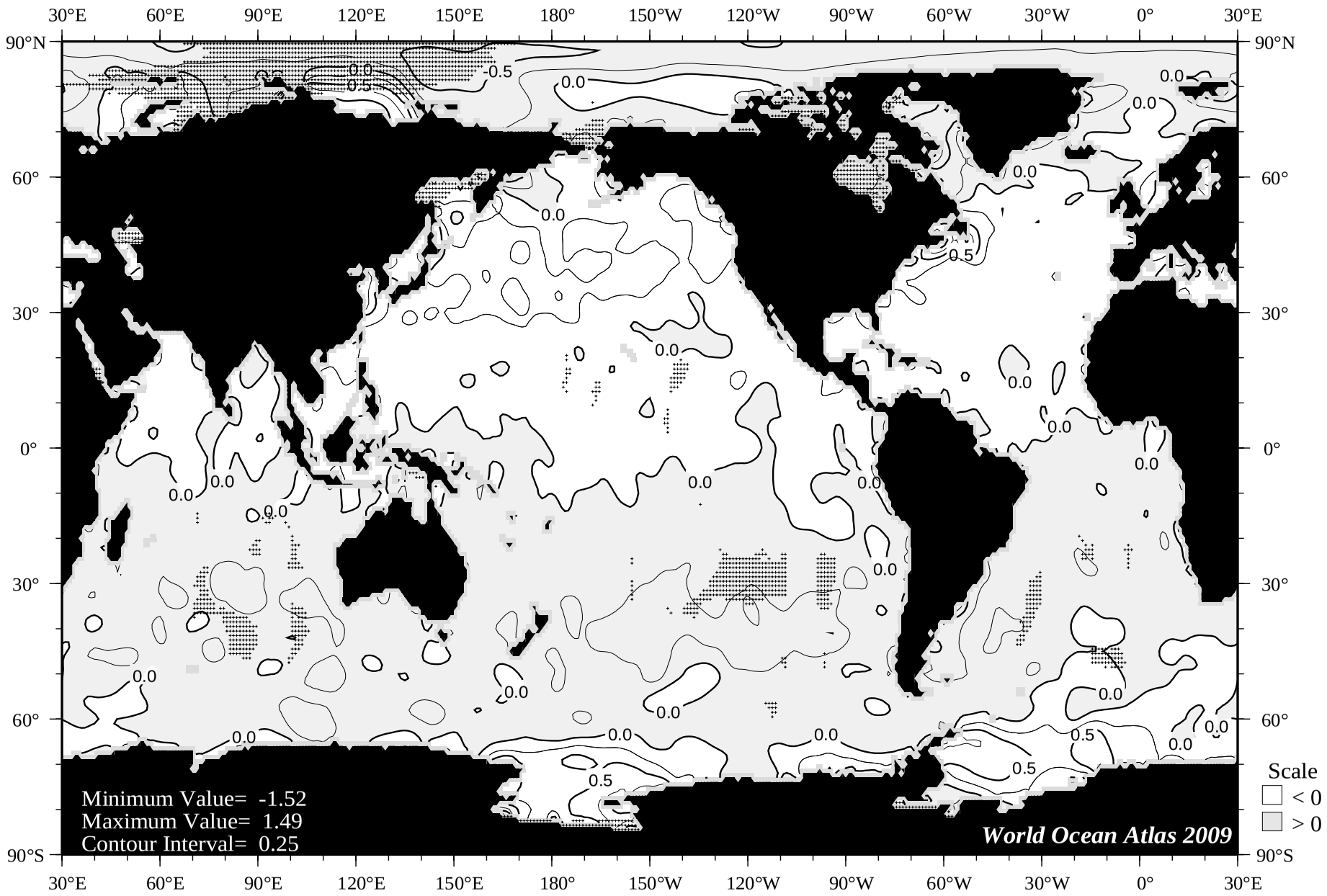

Fig B18 Winter (Jan.-Mar.) minus annual oxygen [ml/l] at the surface.

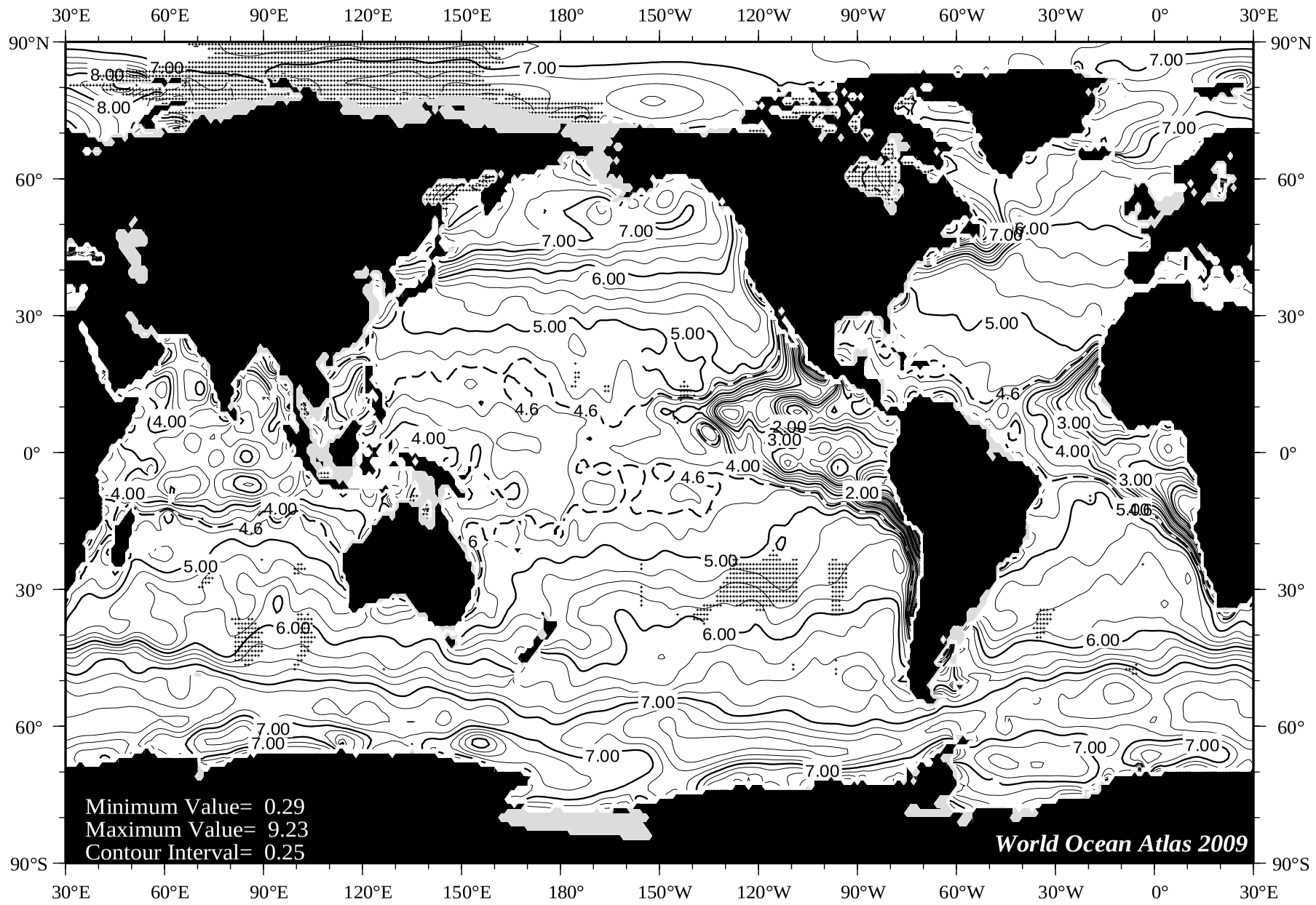

Fig B19 Winter (Jan.-Mar.) oxygen [ml/l] at 75 m. depth.

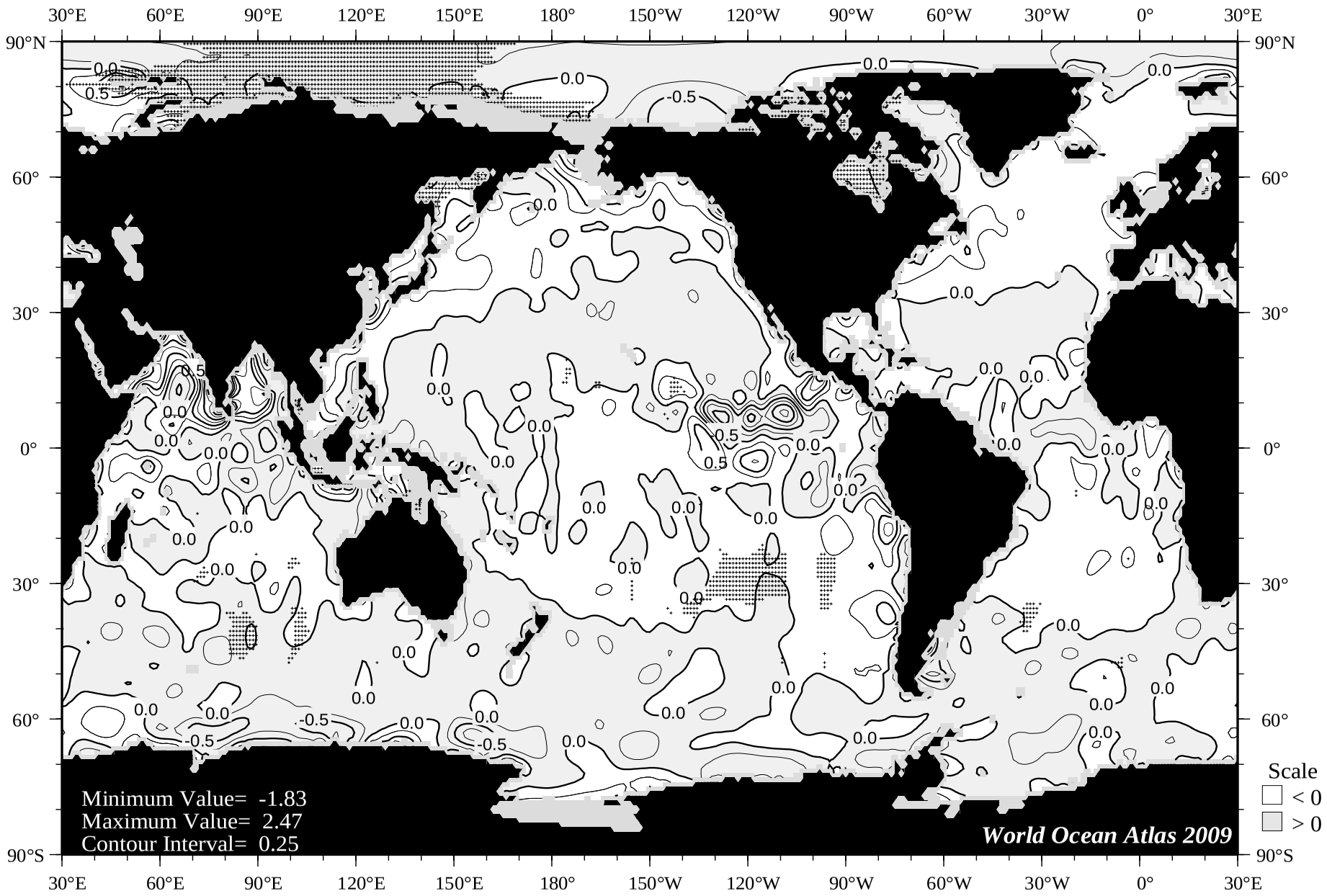

Fig B20 Winter (Jan.-Mar.) minus annual oxygen [ml/l] at 75 m. depth.

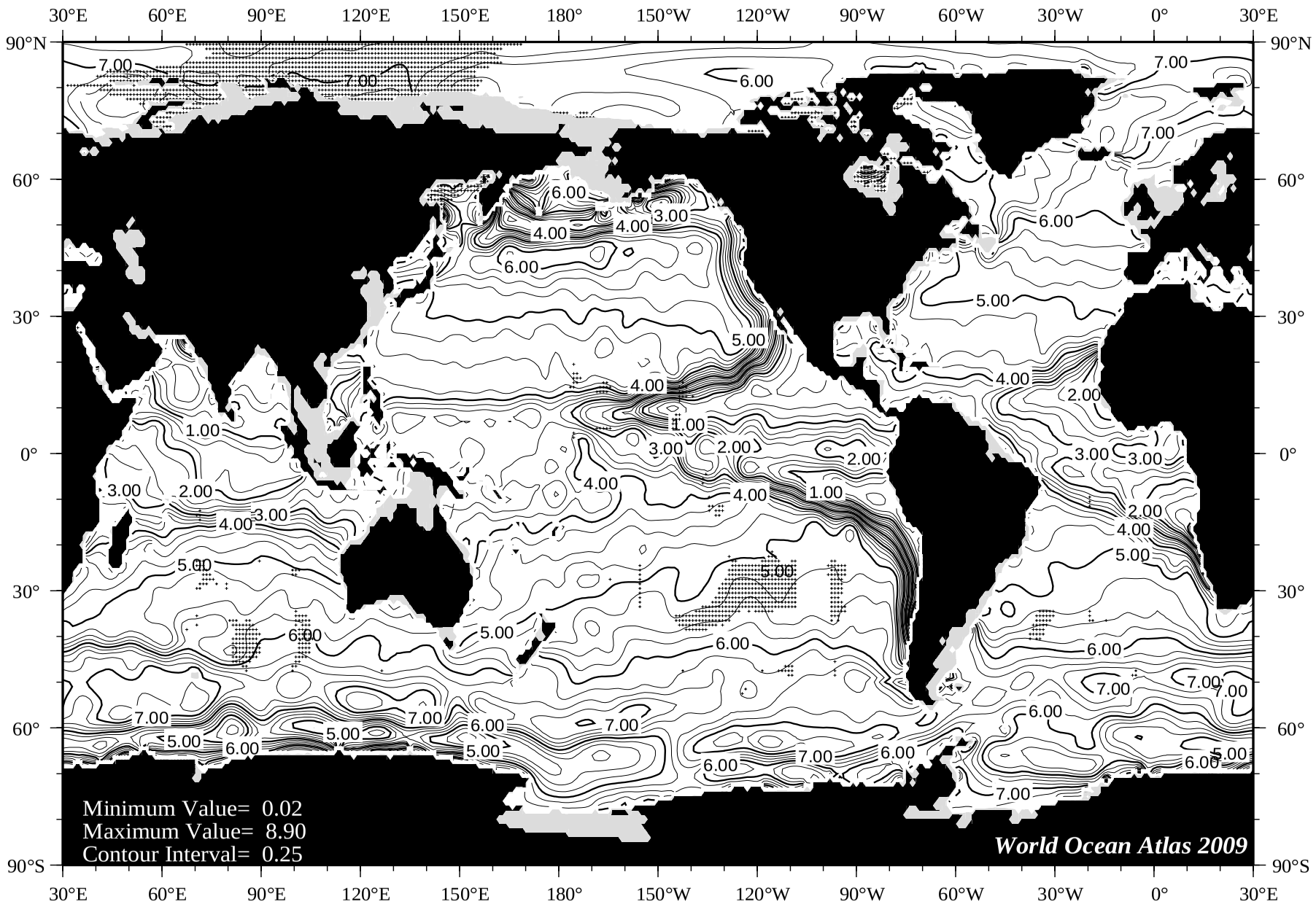

Fig B21 Winter (Jan.-Mar.) oxygen [ml/l] at 150 m. depth.

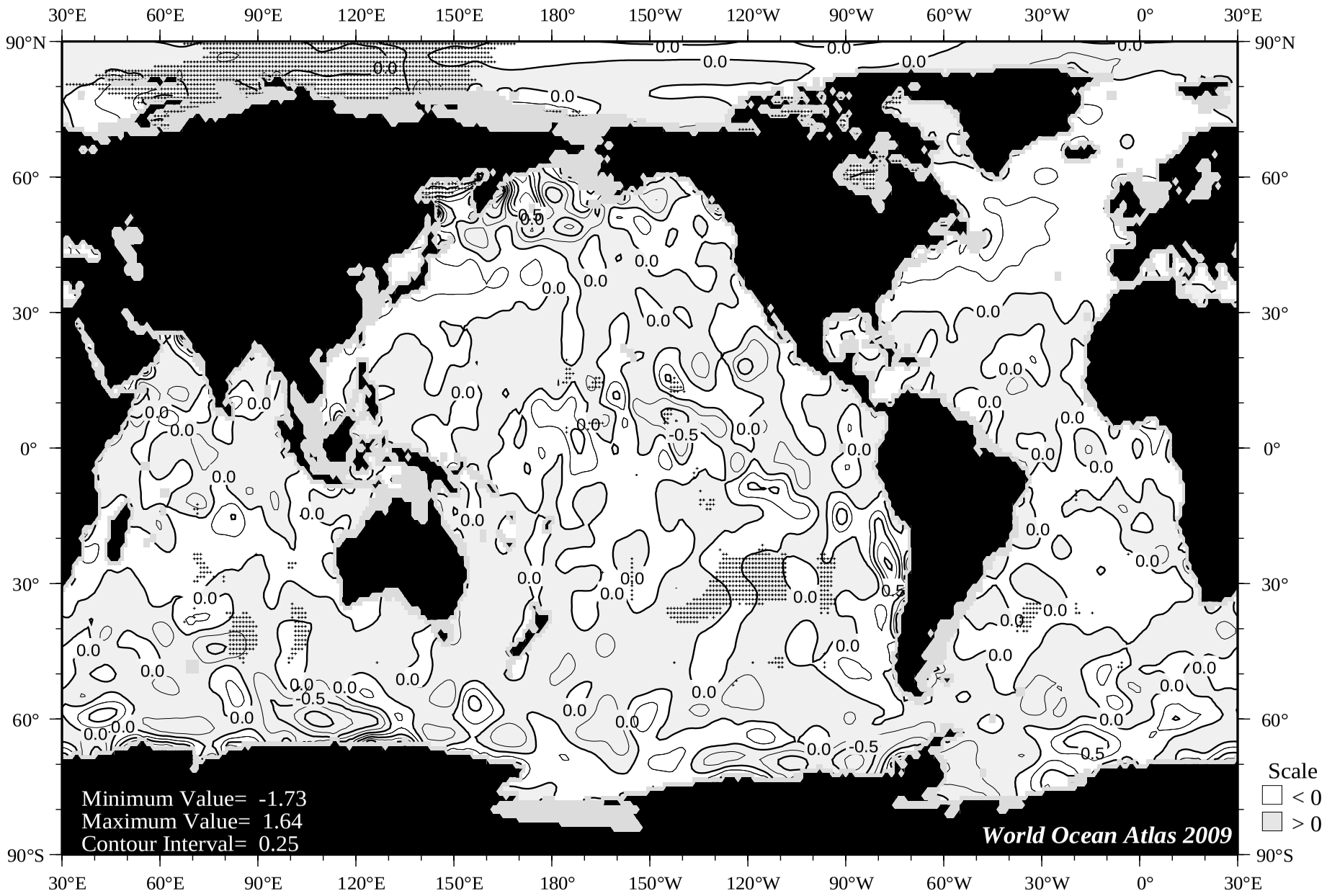

Fig B22 Winter (Jan.-Mar.) minus annual oxygen [ml/l] at 150 m. depth.

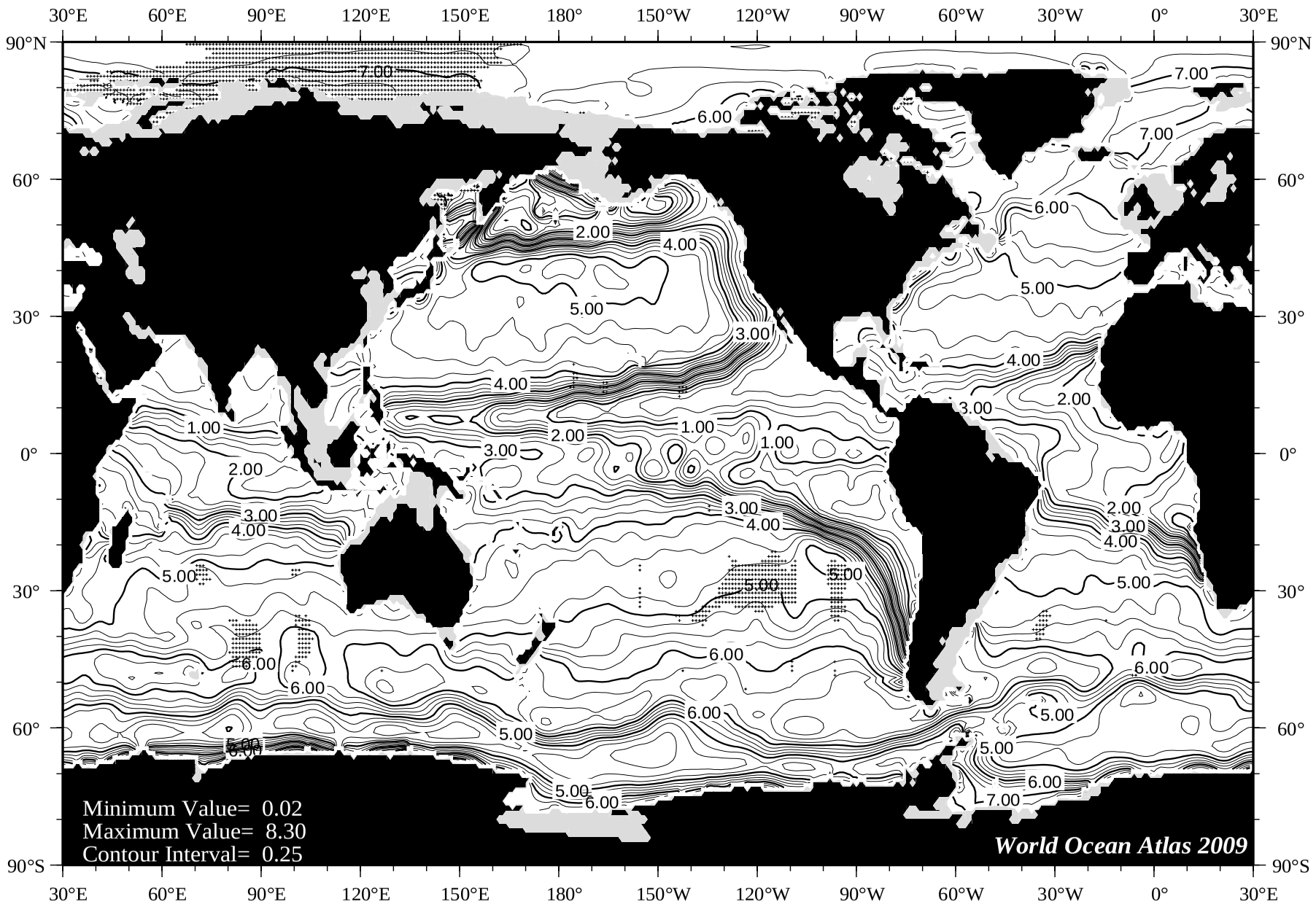

Fig B23 Winter (Jan.-Mar.) oxygen [ml/l] at 250 m. depth.

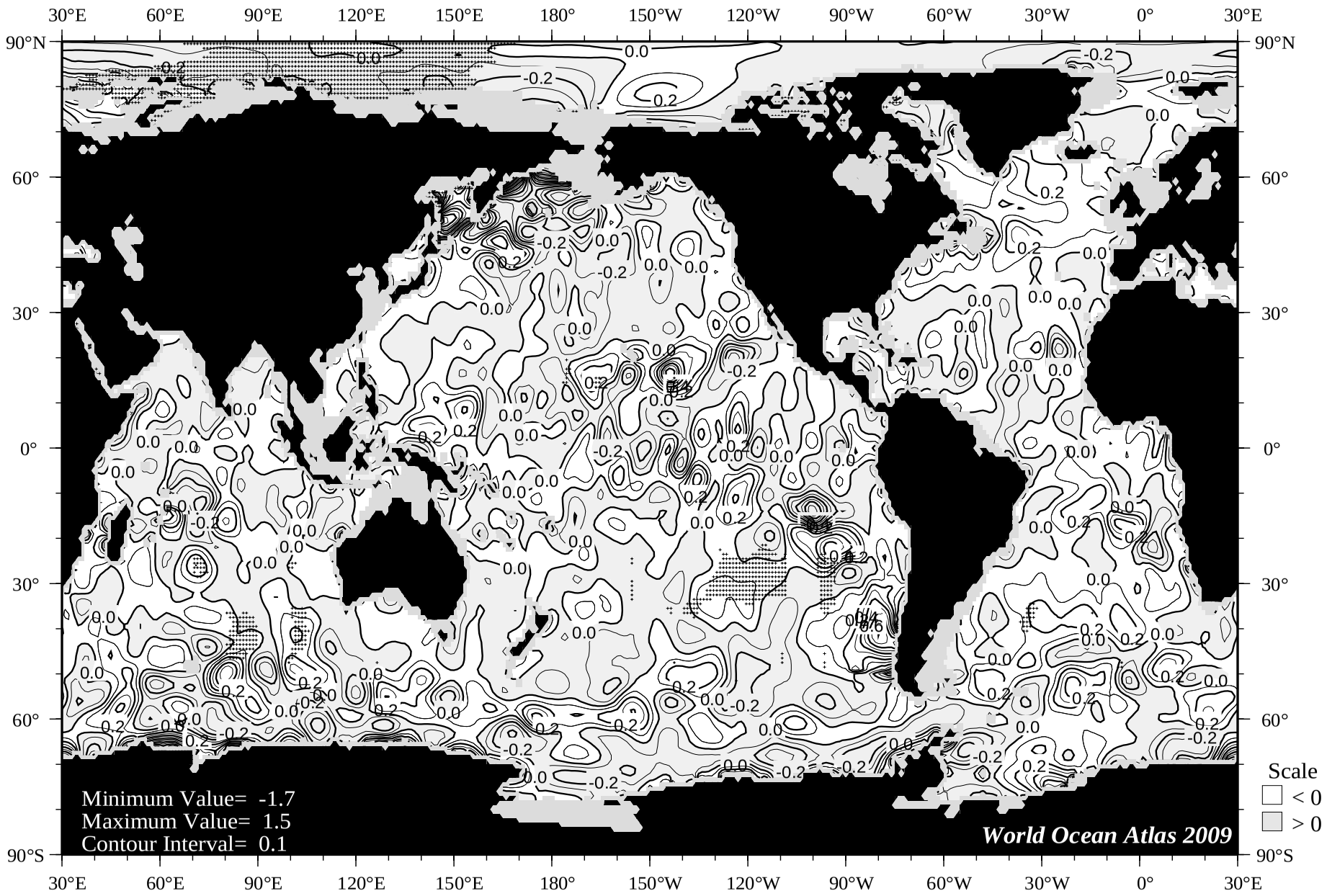

Fig B24 Winter (Jan.-Mar.) minus annual oxygen [ml/l] at 250 m. depth.

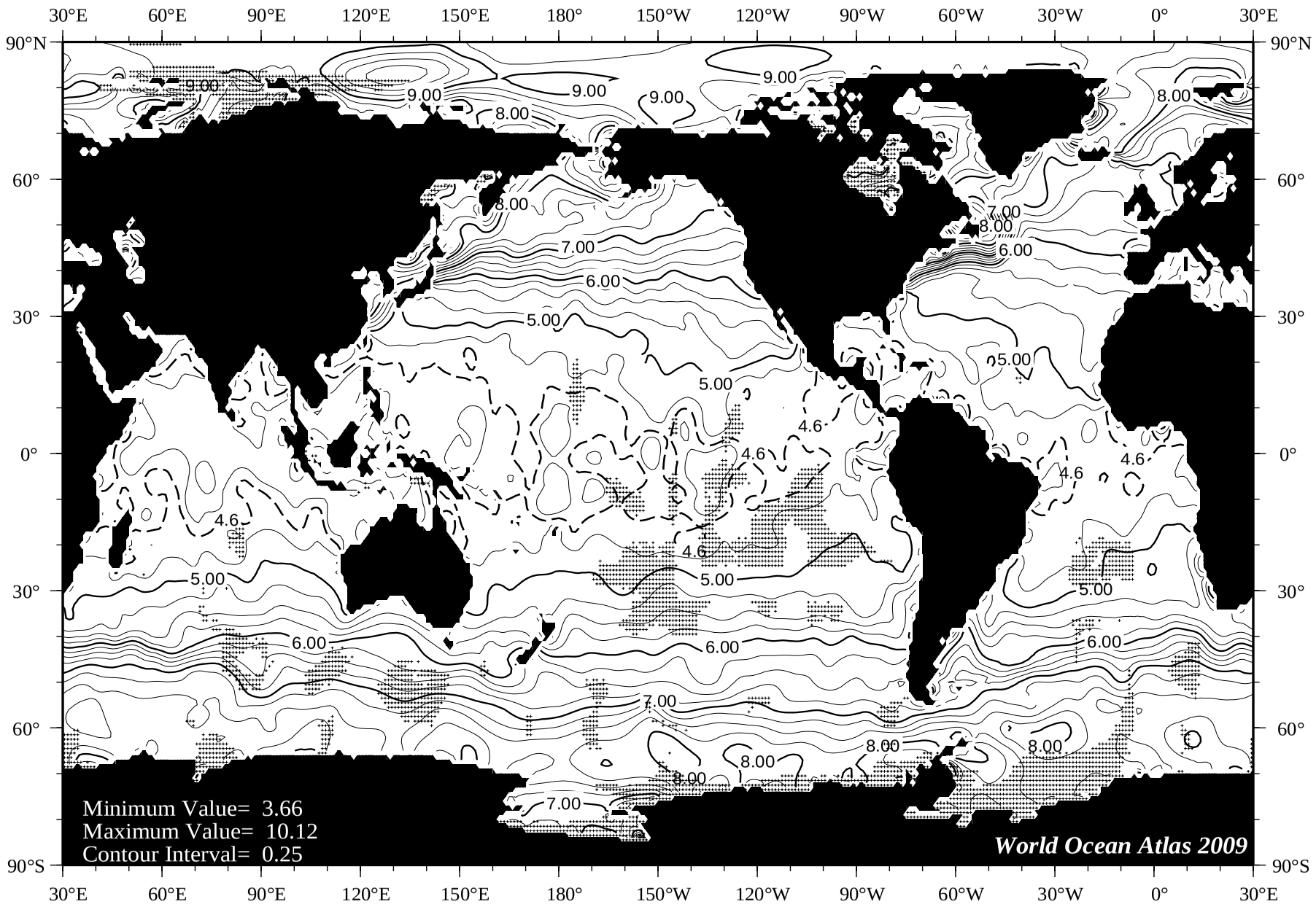

Fig B25 Spring (Apr.-Jun.) oxygen [ml/l] at the surface.

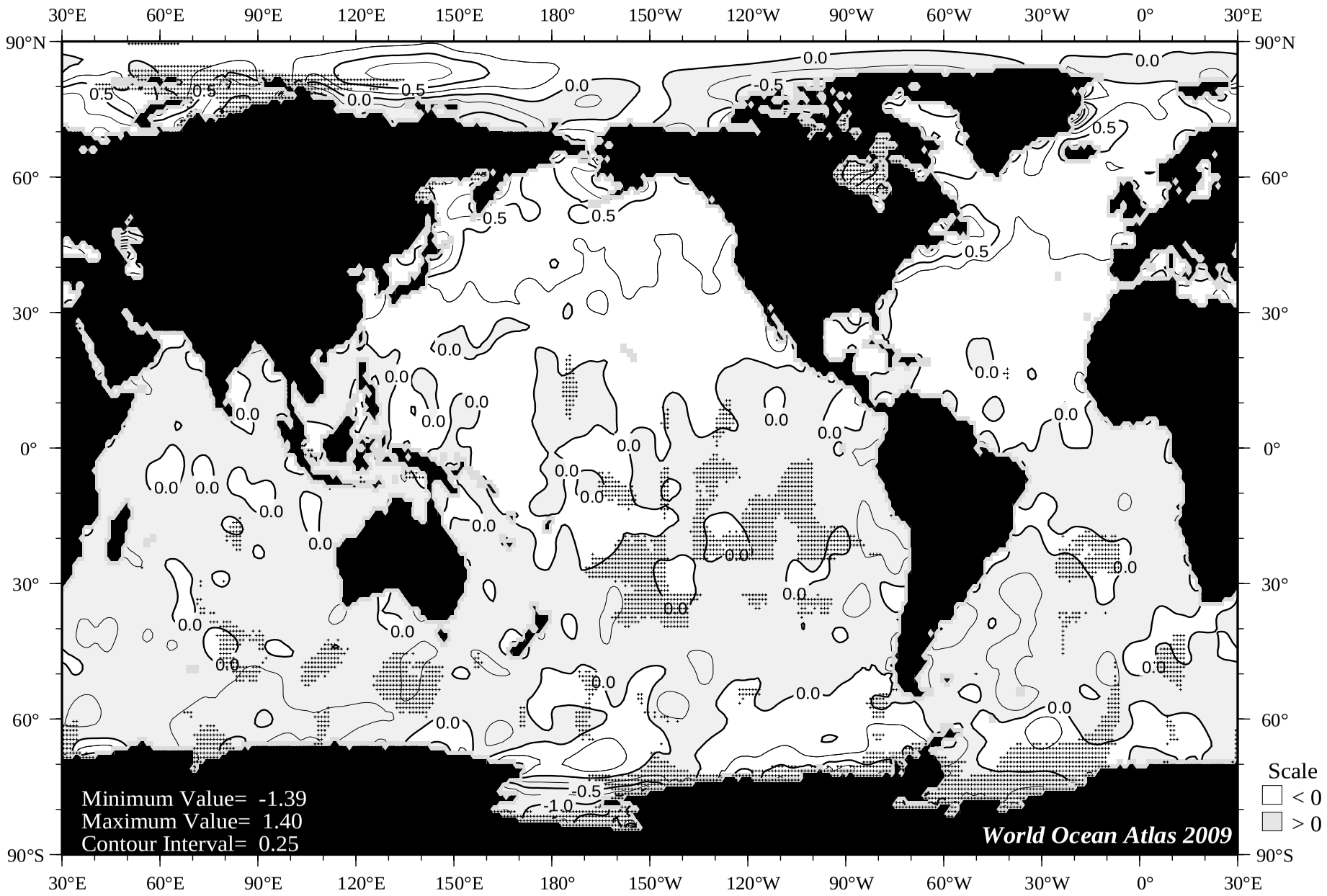

Fig B26 Spring (Apr.-Jun.) minus annual oxygen [ml/l] at the surface.

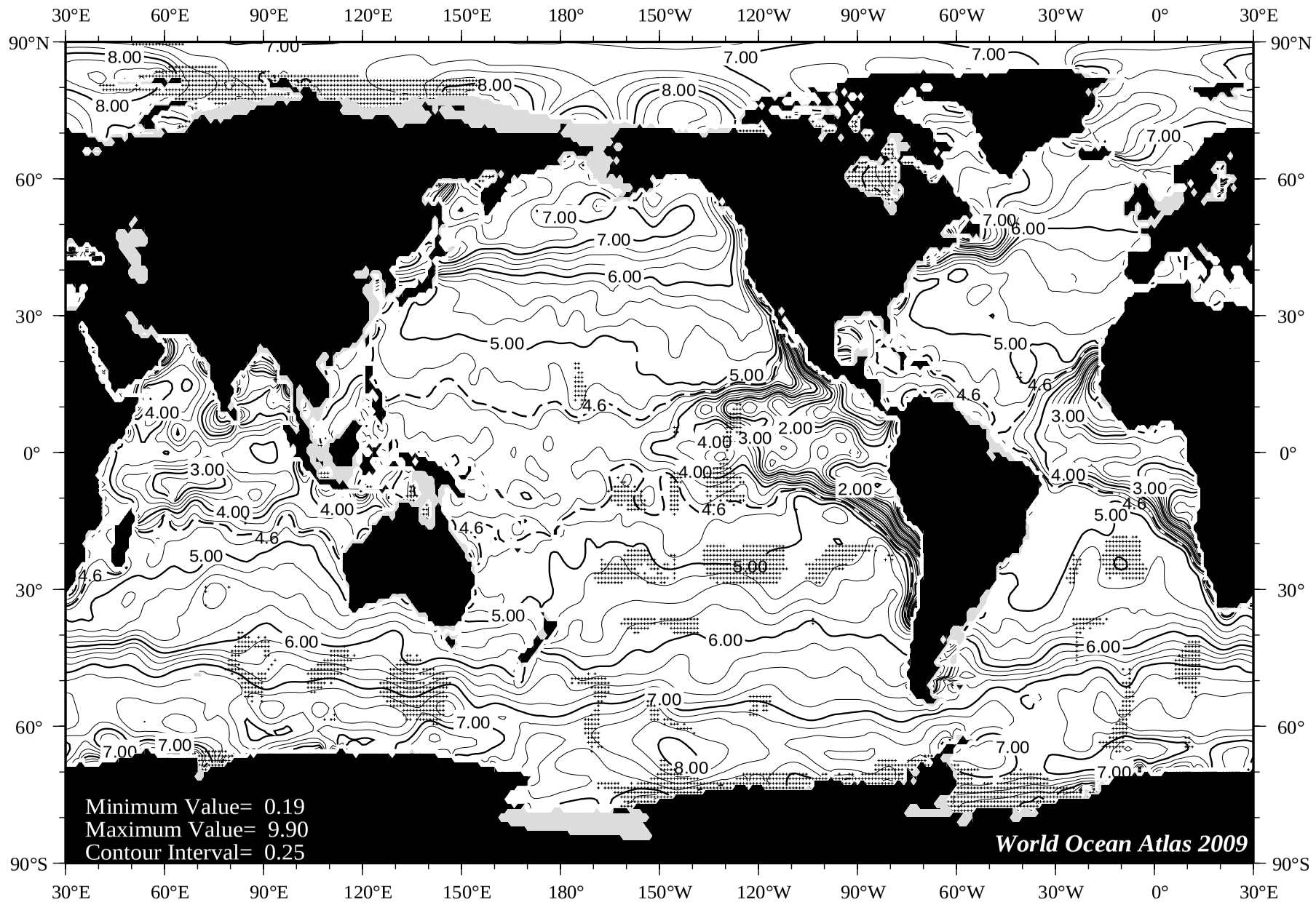

Fig B27 Spring (Apr.-Jun.) oxygen [ml/l] at 75 m. depth.

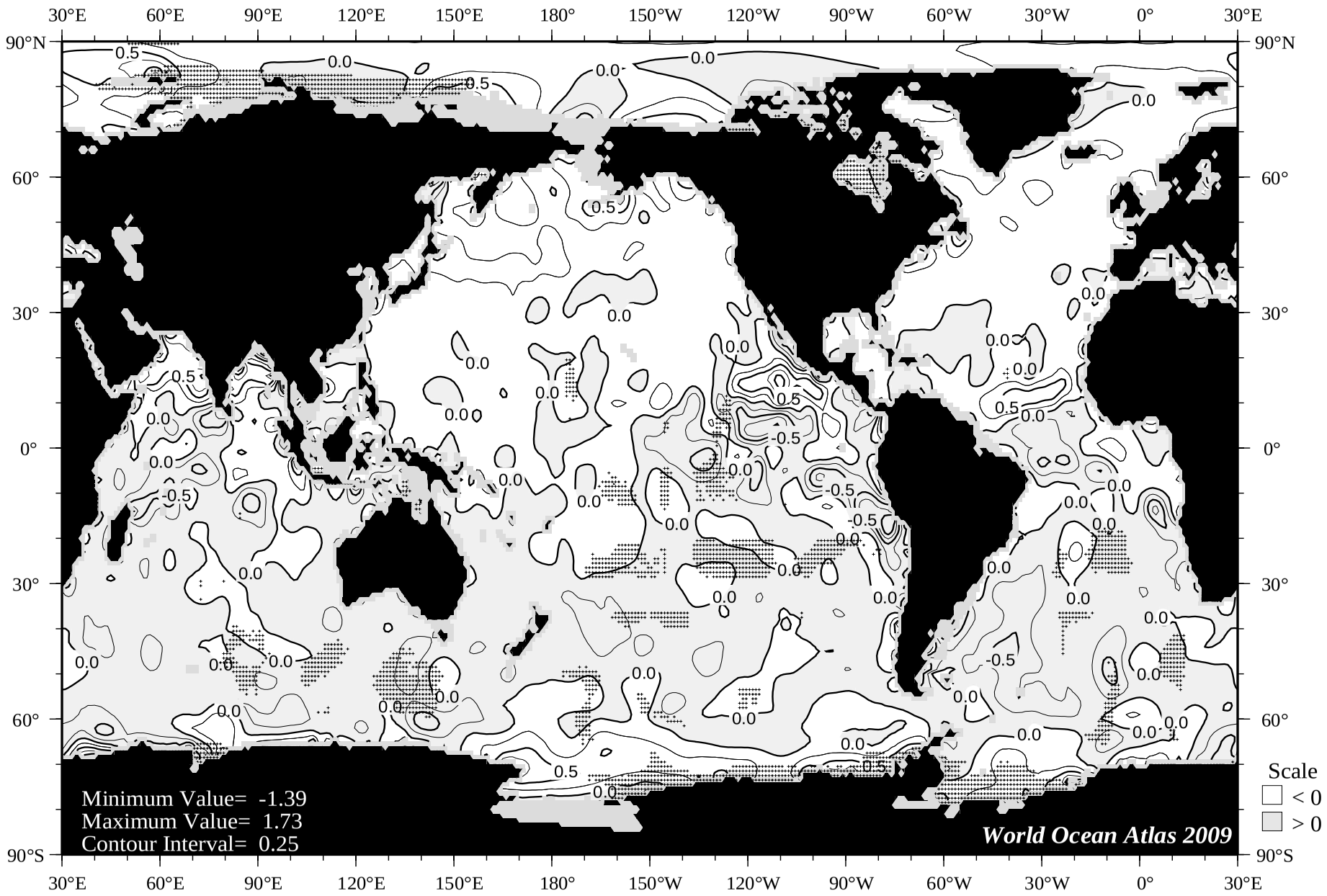

Fig B28 Spring (Apr.-Jun.) minus annual oxygen [ml/l] at 75 m. depth.

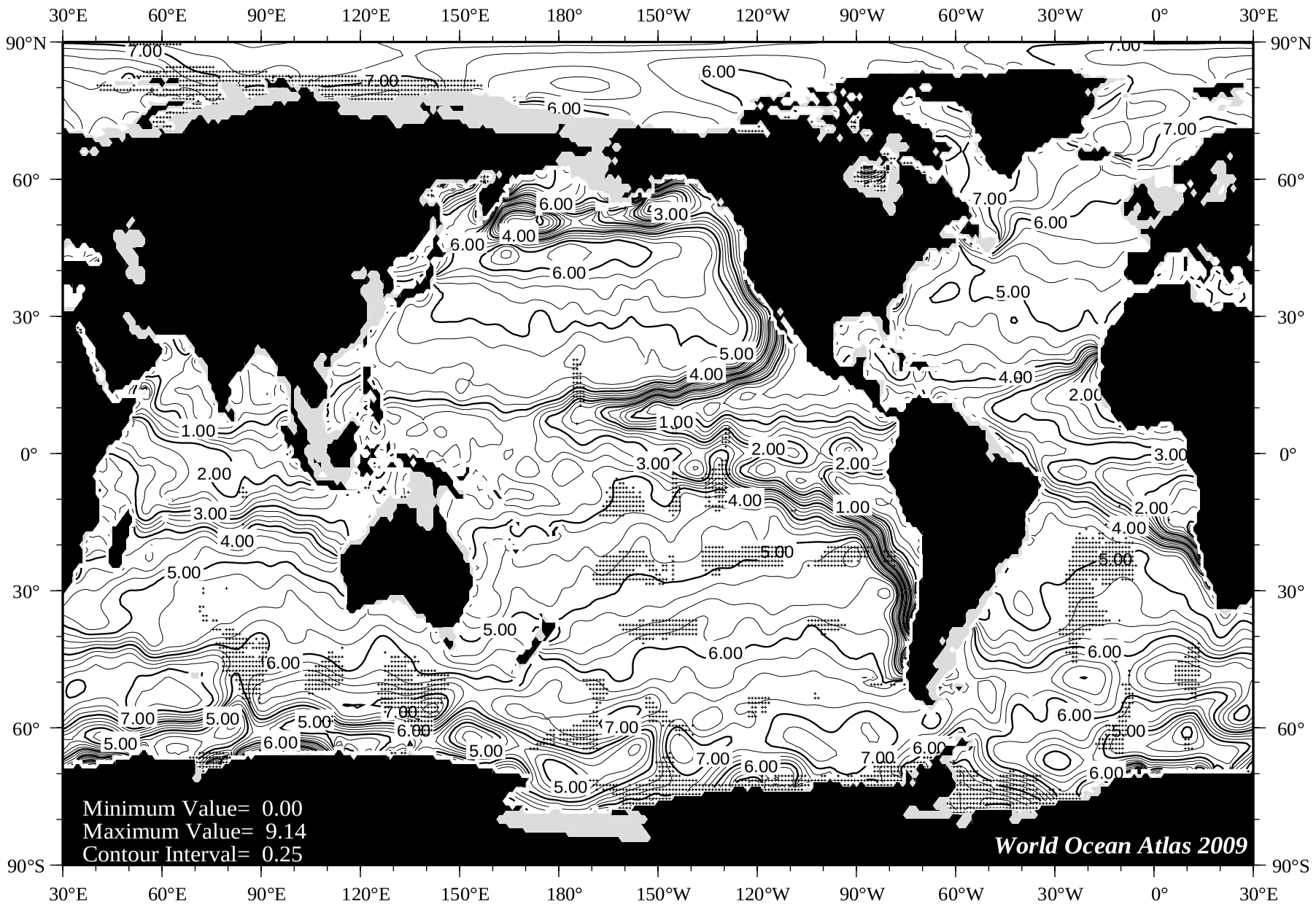

Fig B29 Spring (Apr.-Jun.) oxygen [ml/l] at 150 m. depth.

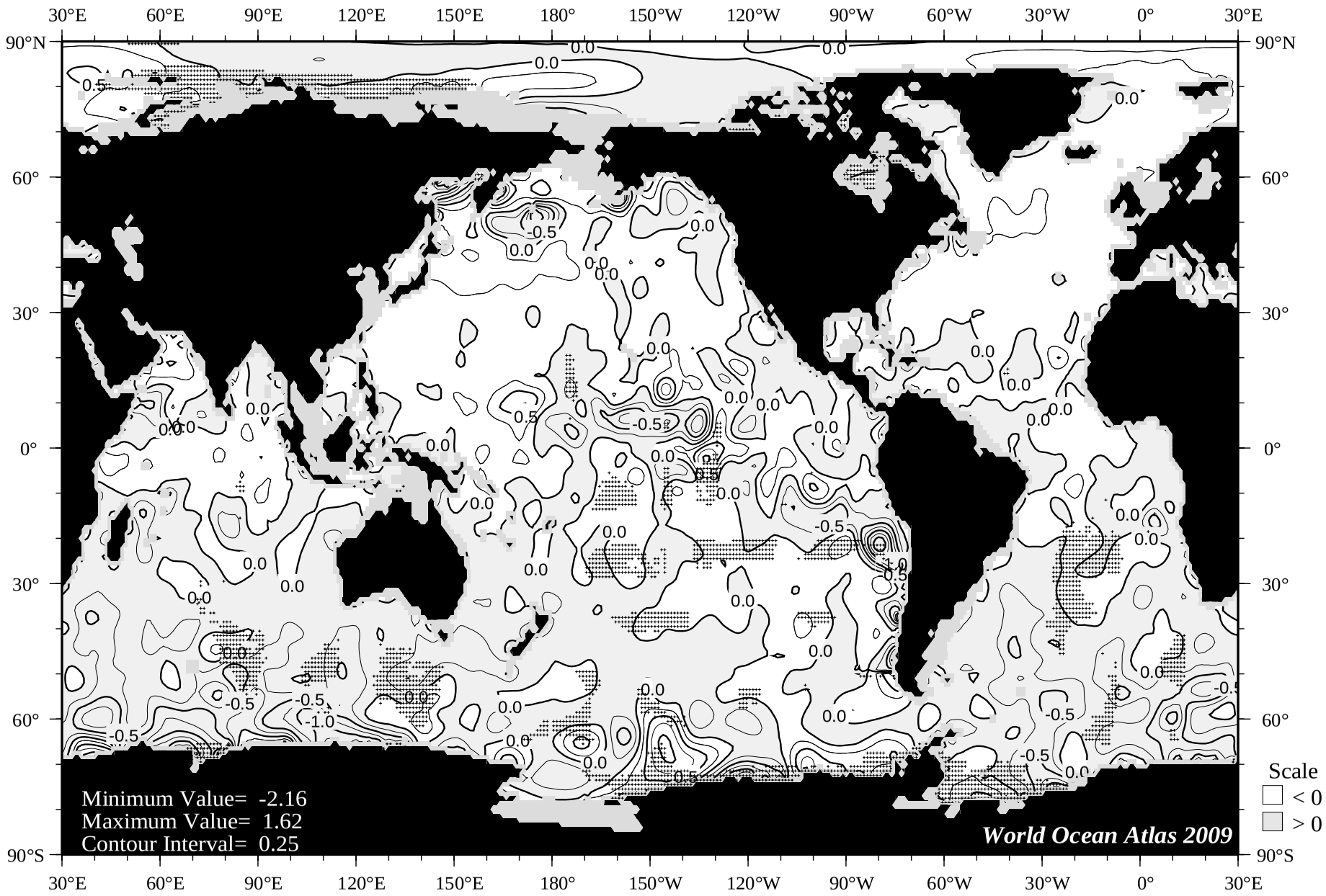

Fig B30 Spring (Apr.-Jun.) minus annual oxygen [ml/l] at 150 m. depth.

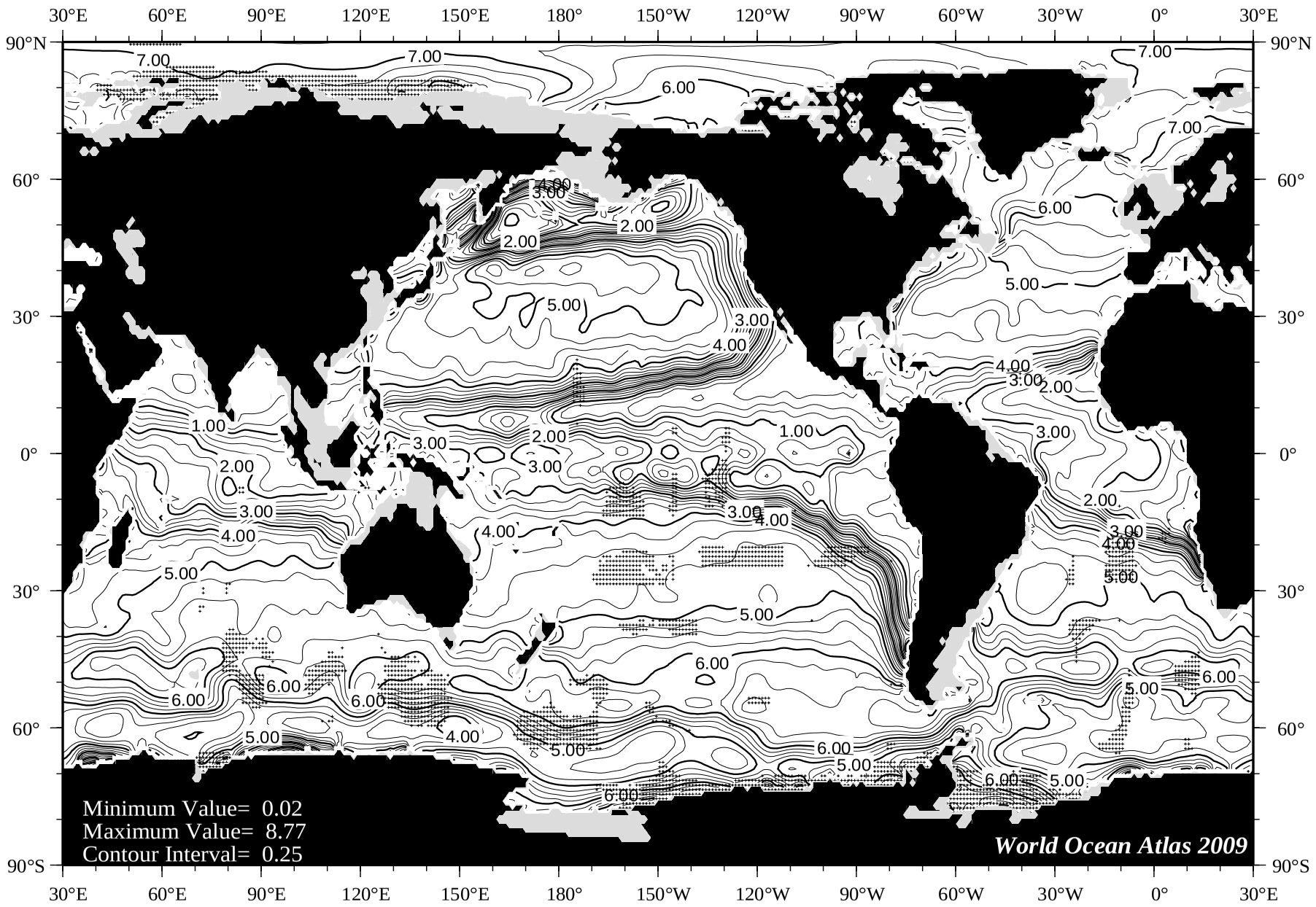

Fig B31 Spring (Apr.-Jun.) oxygen [ml/l] at 250 m. depth.

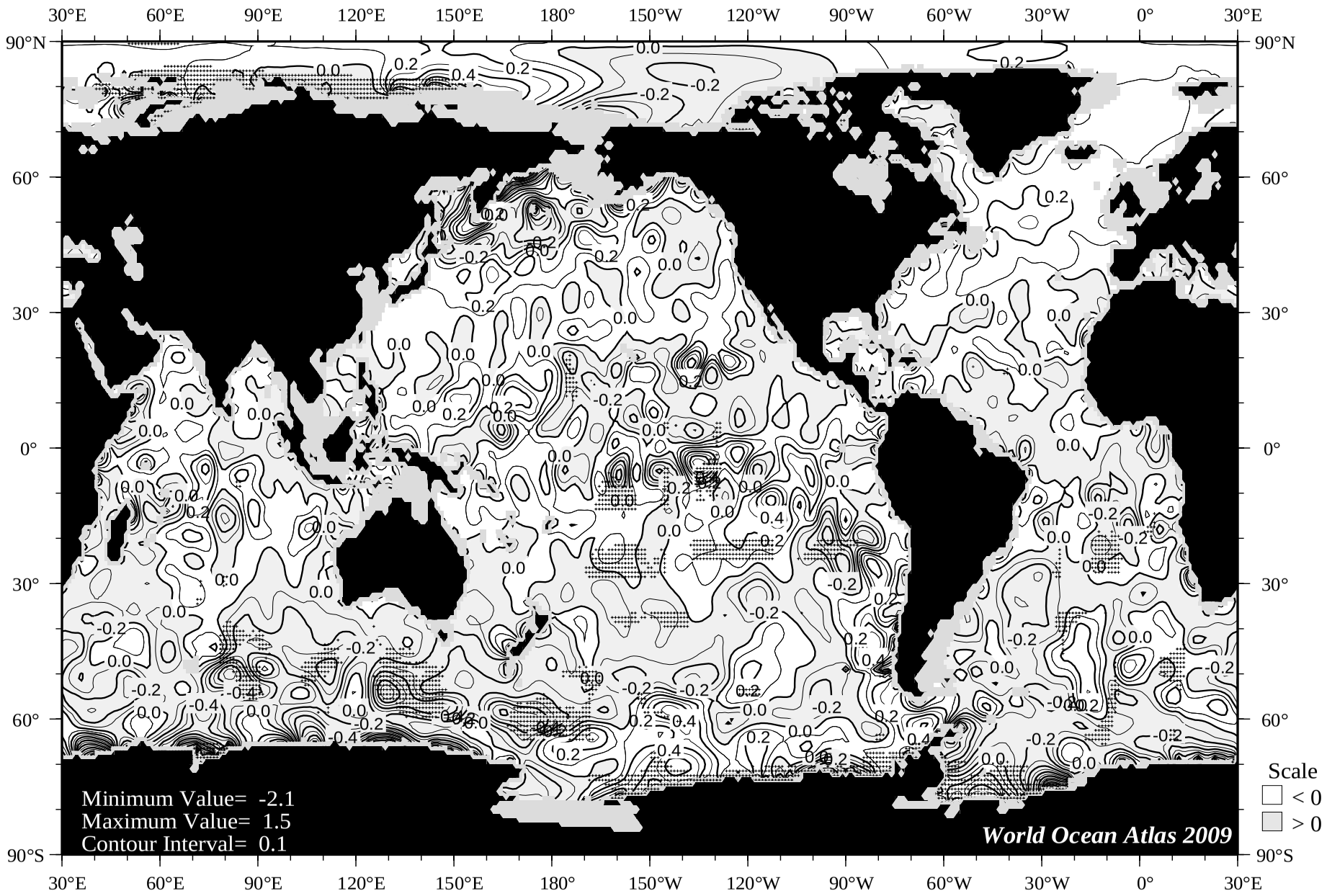

Fig B32 Spring (Apr.-Jun.) minus annual oxygen [ml/l] at 250 m. depth.

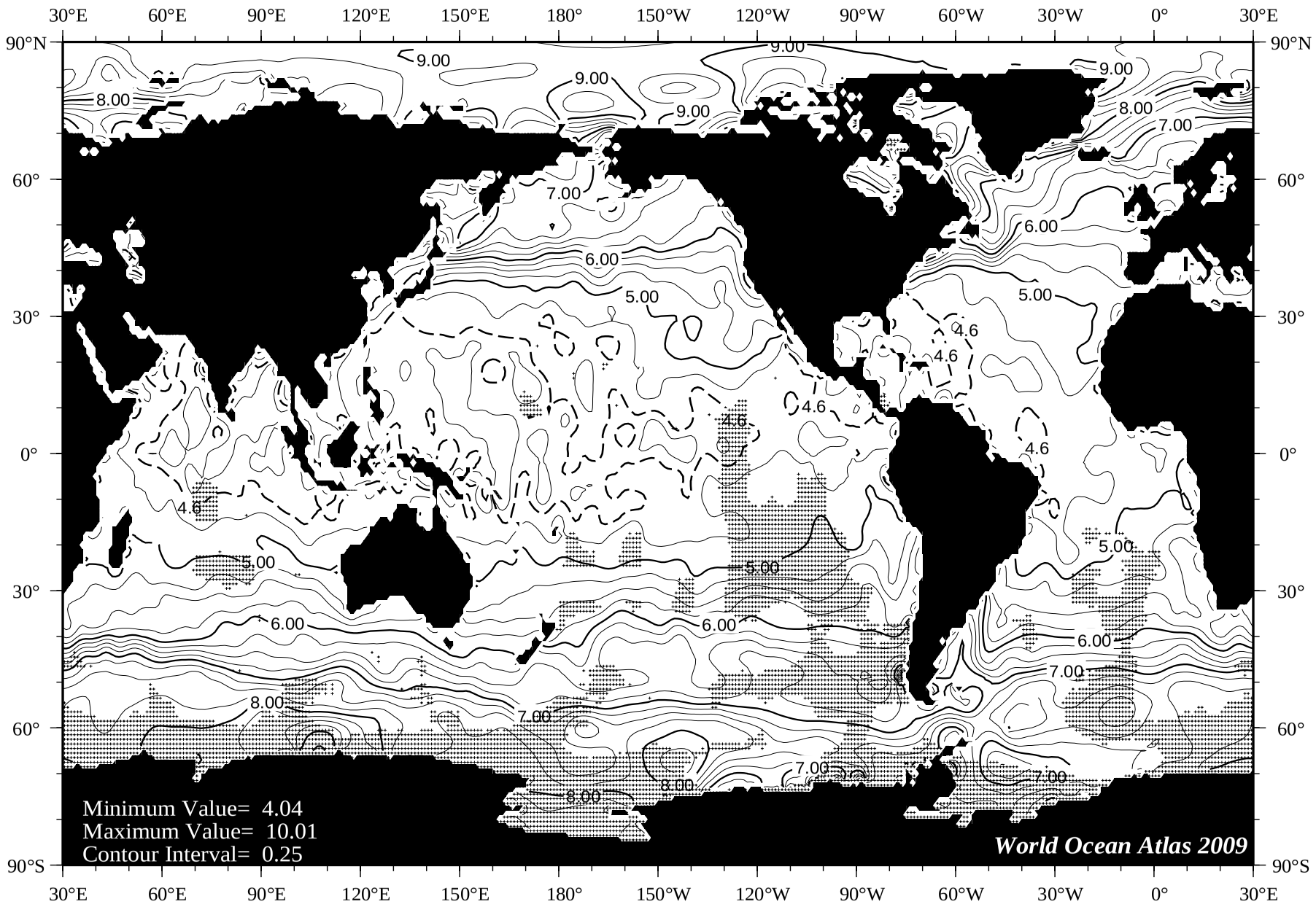

Fig B33 Summer (Jul.-Sep.) oxygen [ml/l] at the surface.

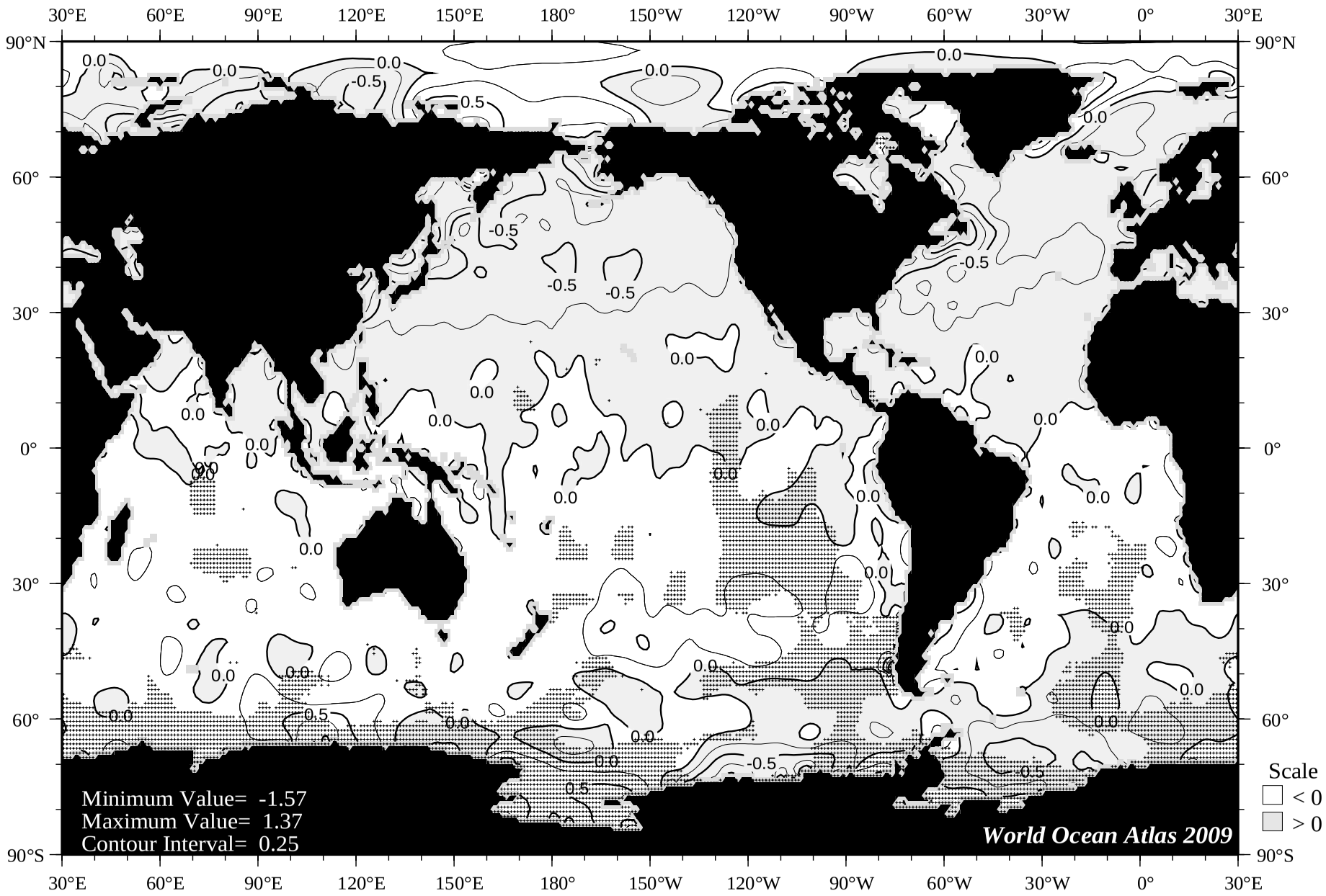

Fig B34 Summer (Jul.-Sep.) minus annual oxygen [ml/l] at the surface.

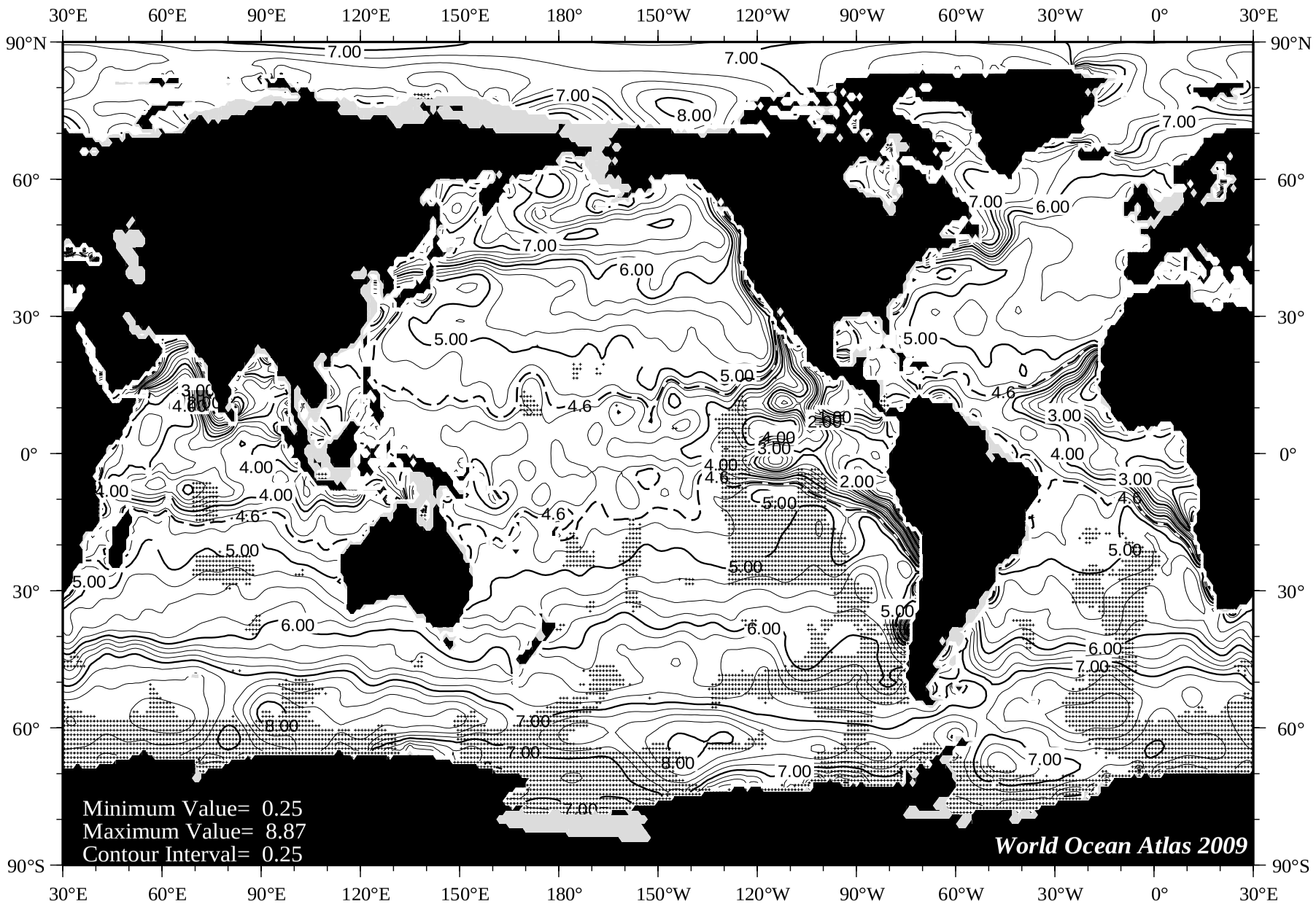

Fig B35 Summer (Jul.-Sep.) oxygen [ml/l] at 75 m. depth.

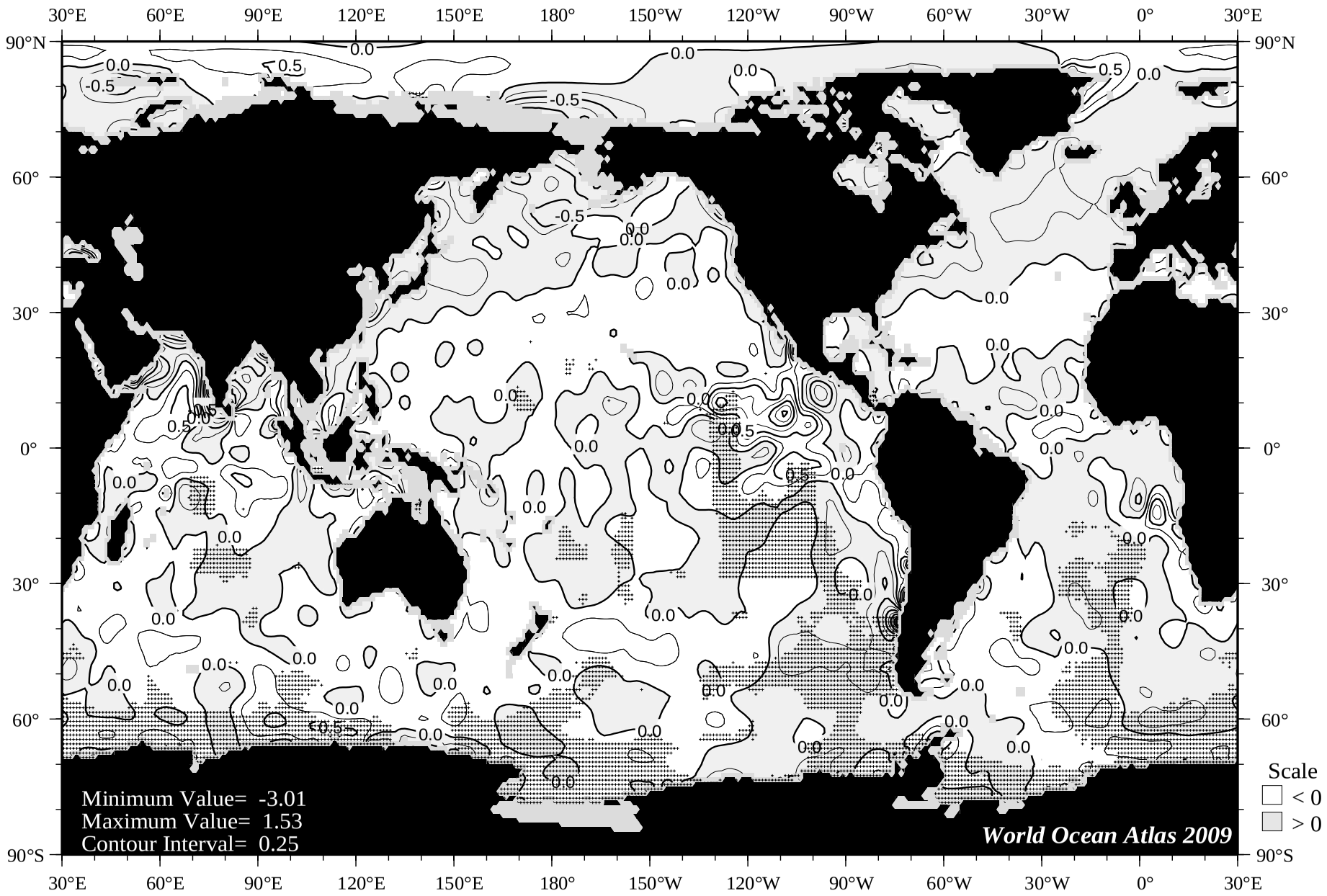

Fig B36 Summer (Jul.-Sep.) minus annual oxygen [ml/l] at 75 m. depth.

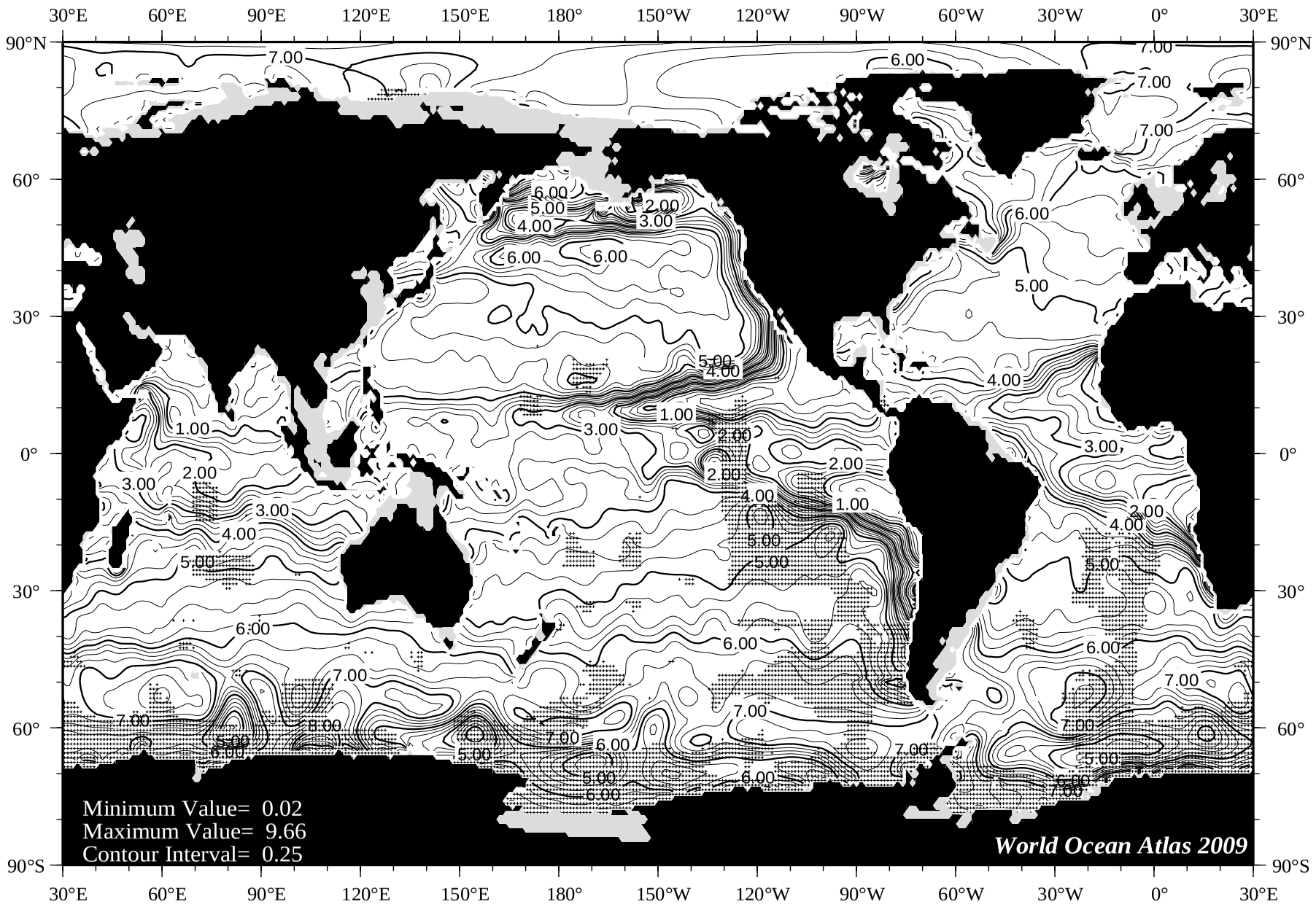

Fig B37 Summer (Jul.-Sep.) oxygen [ml/l] at 150 m. depth.

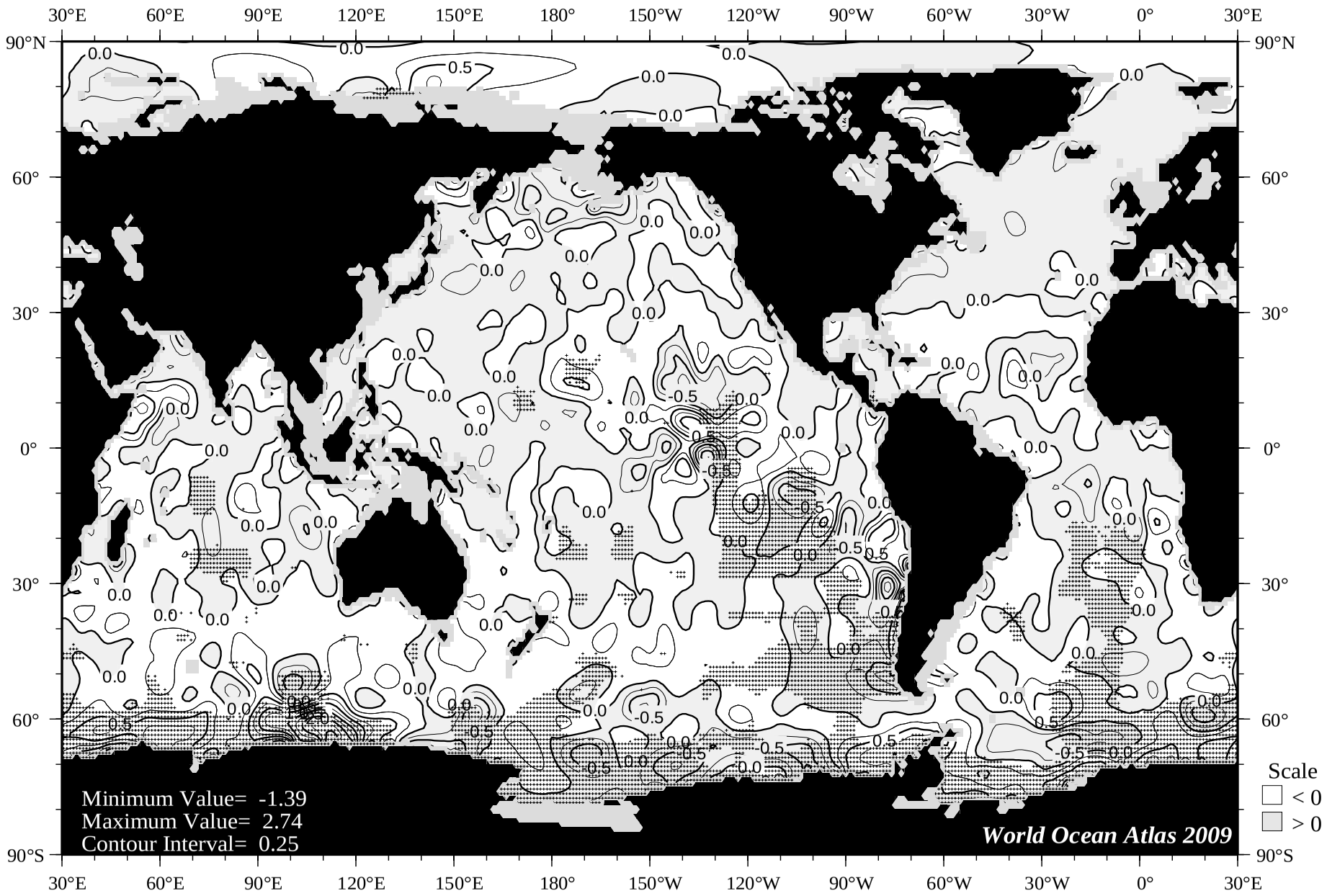

Fig B38 Summer (Jul.-Sep.) minus annual oxygen [ml/l] at 150 m. depth.

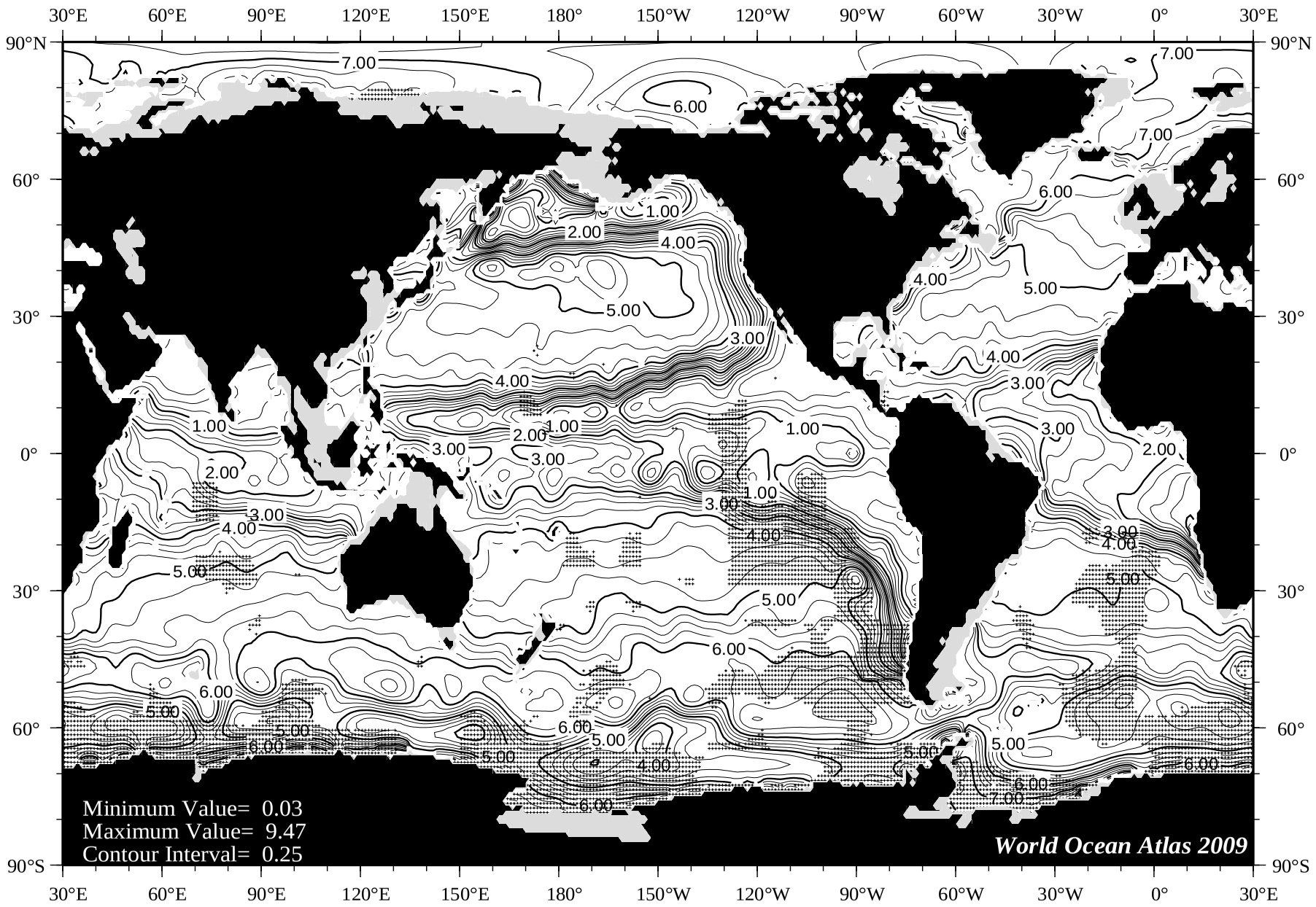

Fig B39 Summer (Jul.-Sep.) oxygen [ml/l] at 250 m. depth.

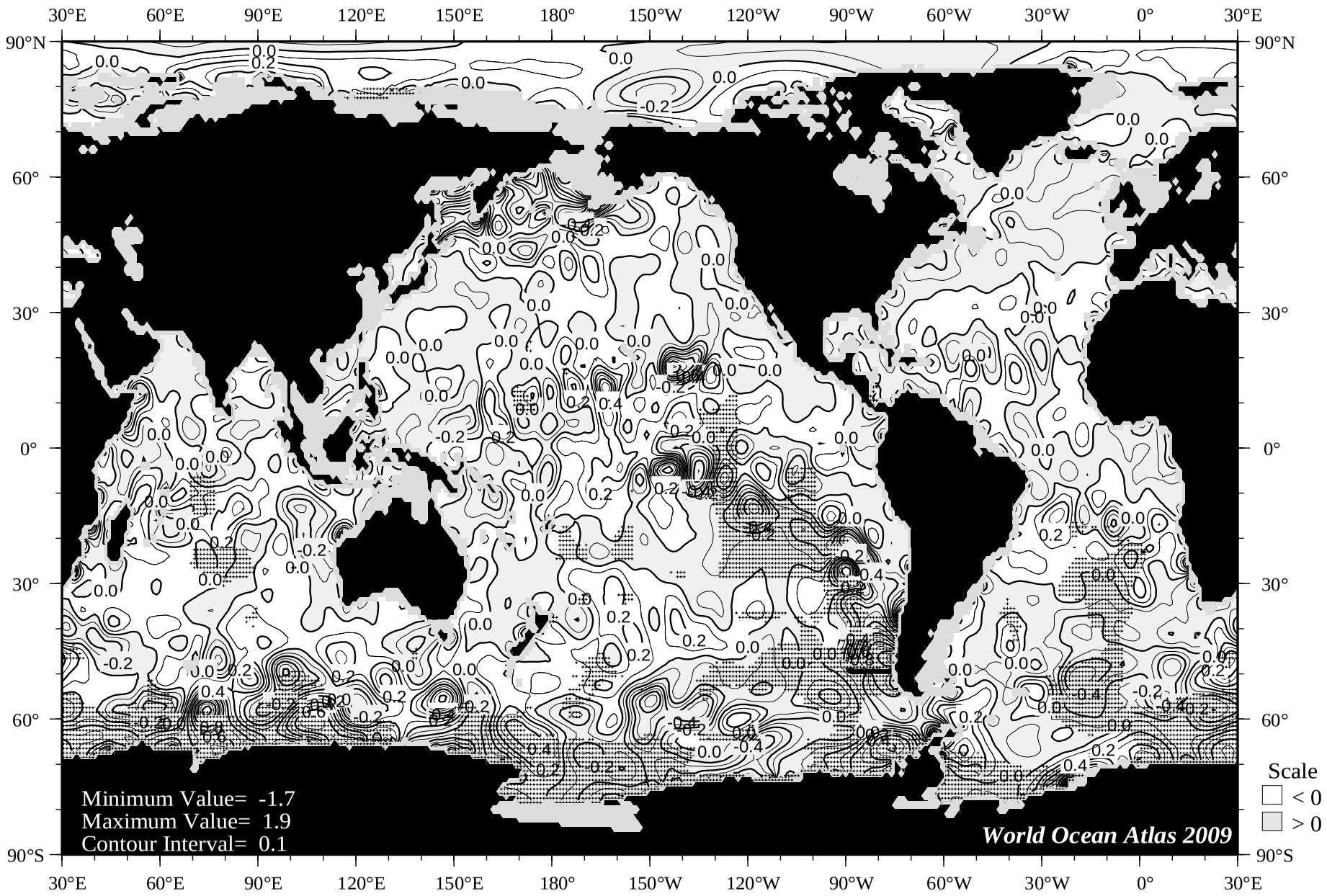

Fig B40 Summer (Jul.-Sep.) minus annual oxygen [ml/l] at 250 m. depth.

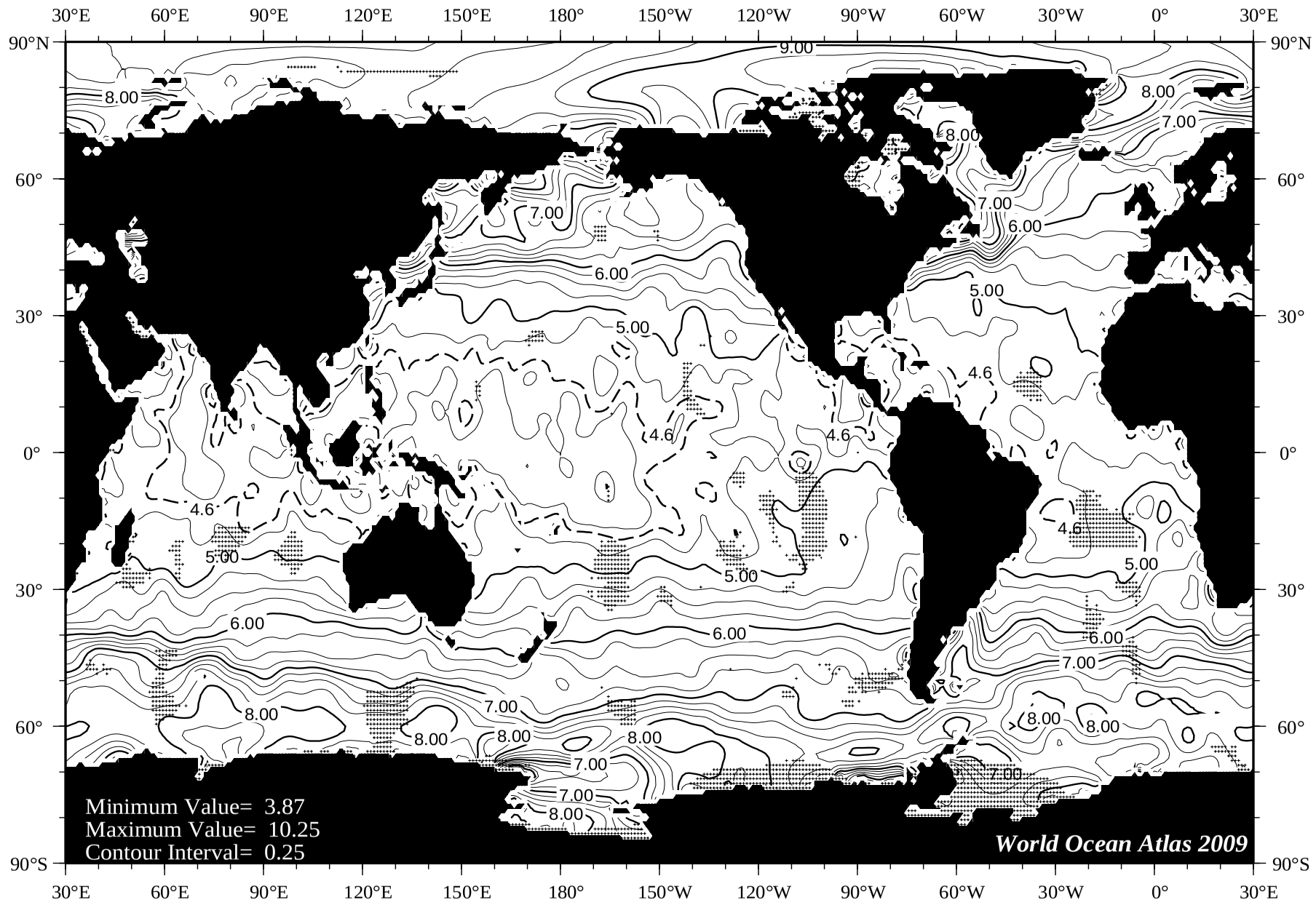

Fig B41 Fall (Oct.-Dec.) oxygen [ml/l] at the surface.

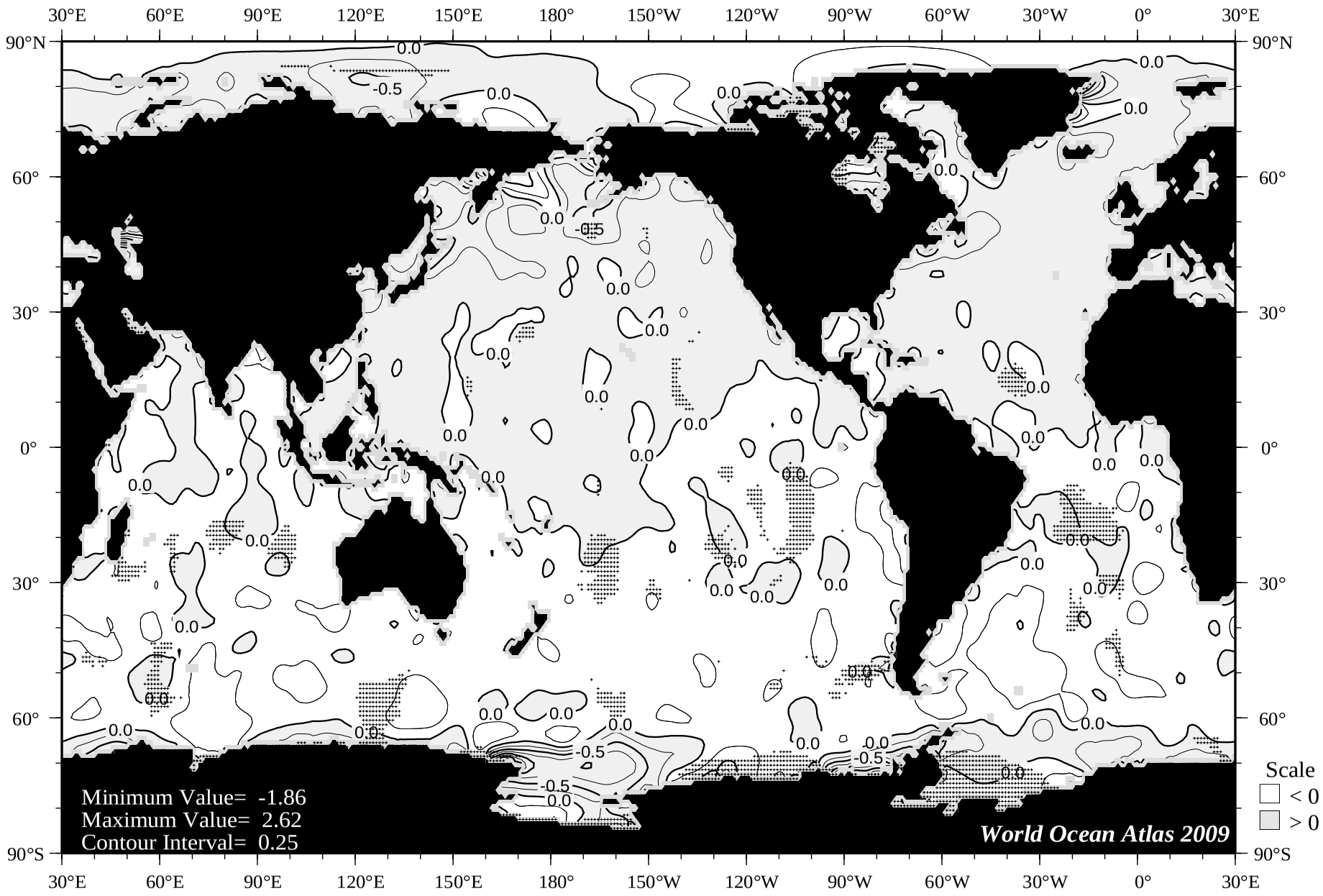

Fig B42 Fall (Oct.-Dec.) minus annual oxygen [ml/l] at the surface.

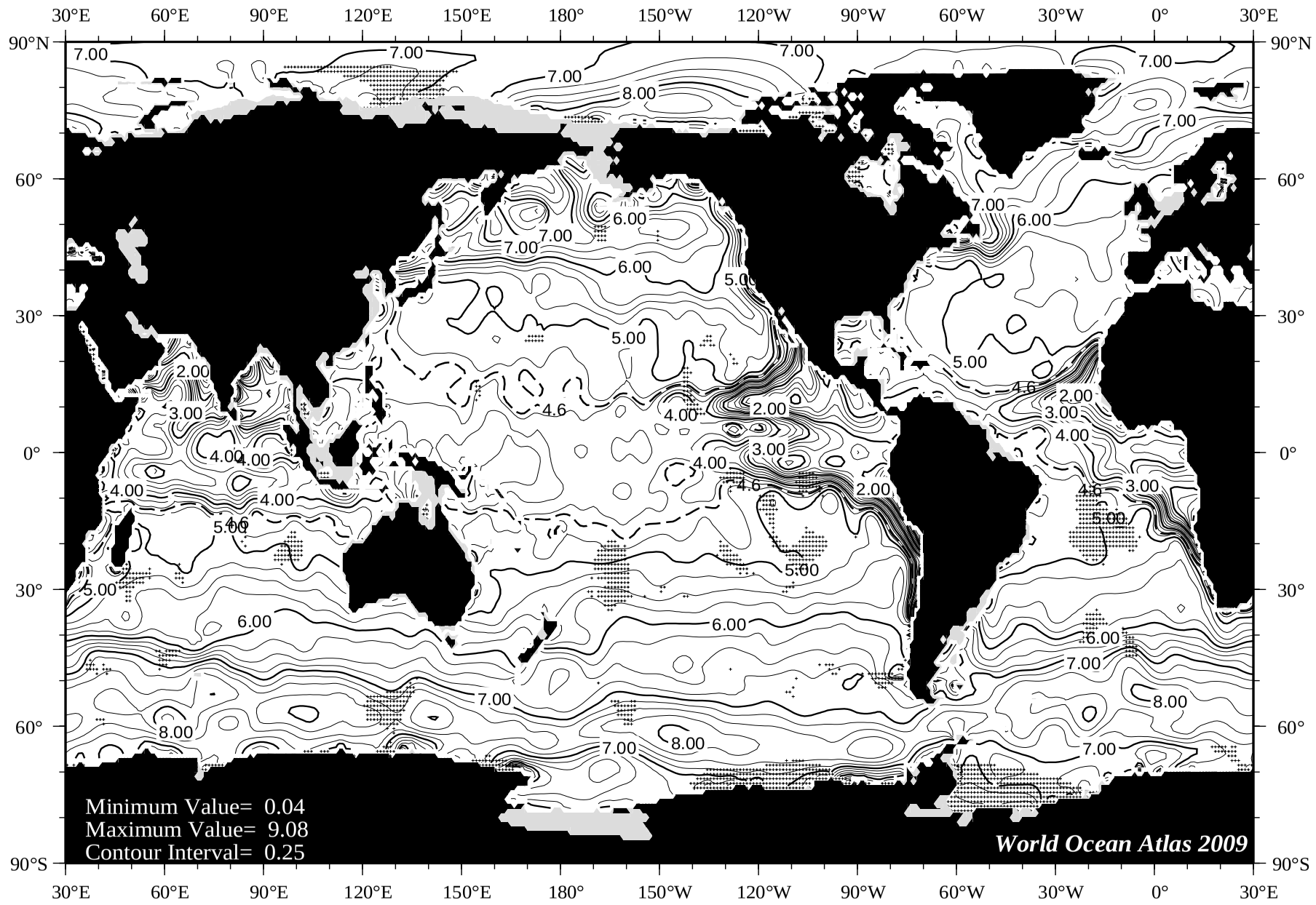

Fig B43 Fall (Oct.-Dec.) oxygen [ml/l] at 75 m. depth.

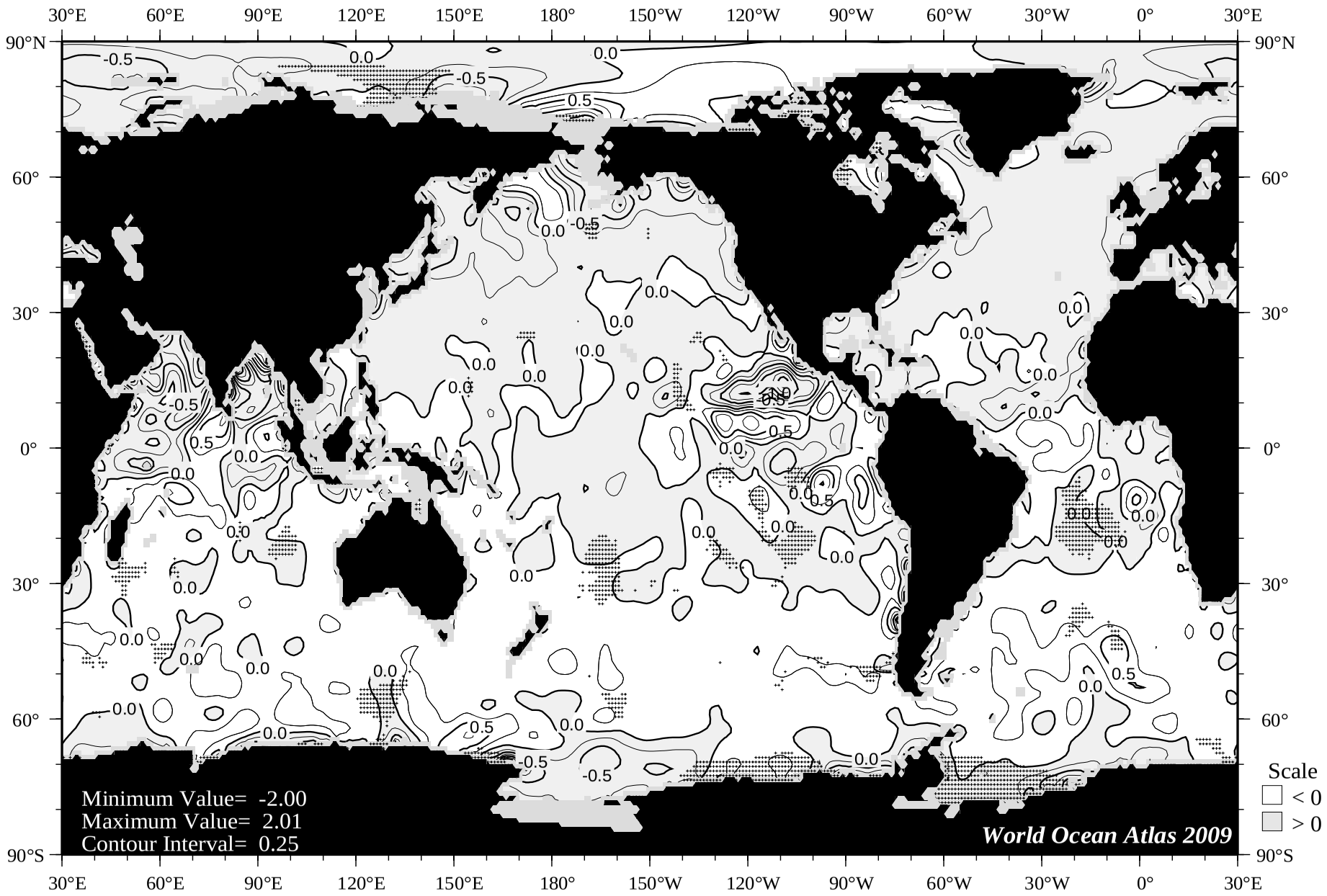

Fig B44 Fall (Oct.-Dec.) minus annual oxygen [ml/l] at 75 m. depth.

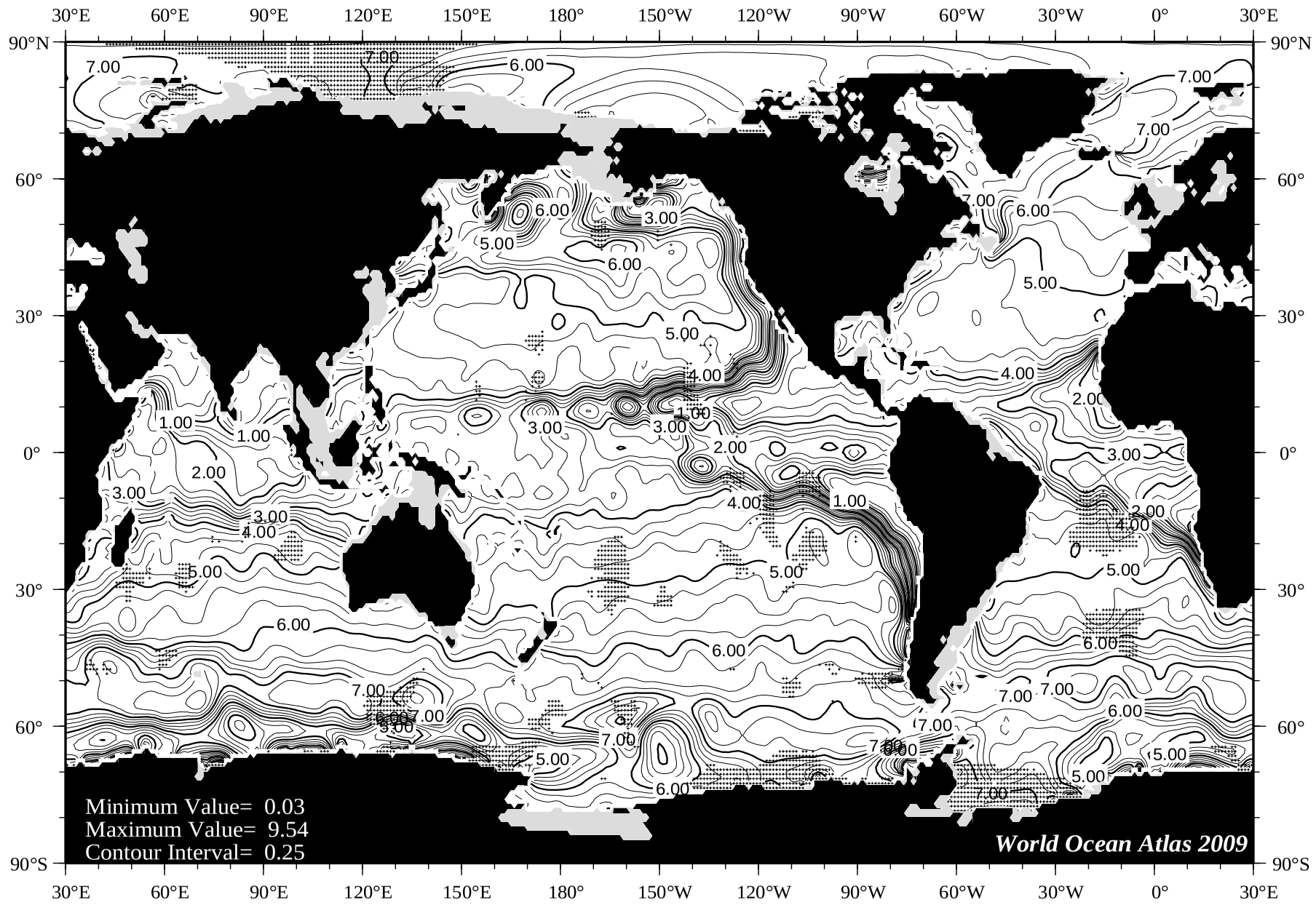

Fig B45 Fall (Oct.-Dec.) oxygen [ml/l] at 150 m. depth.

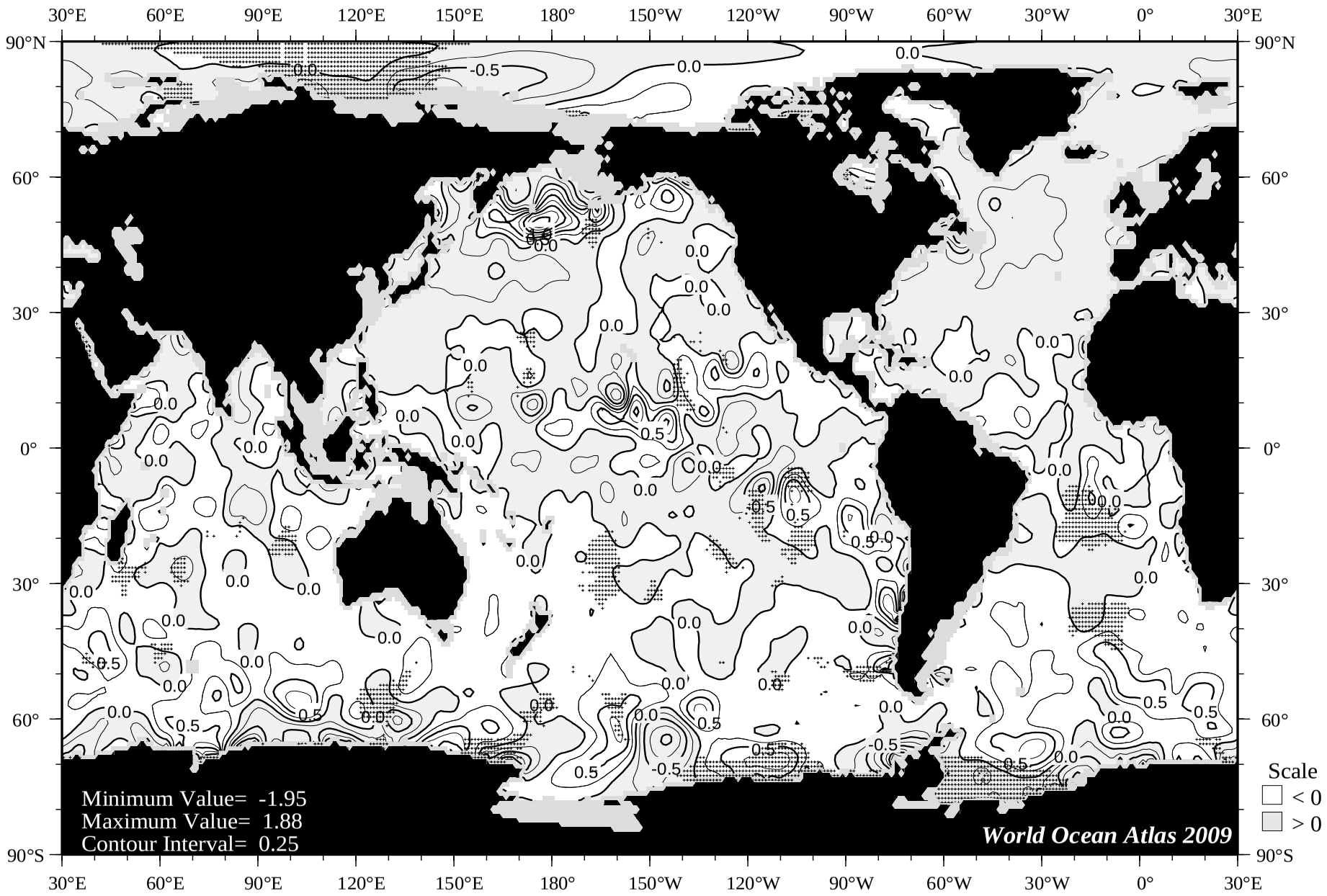

Fig B46 Fall (Oct.-Dec.) minus annual oxygen [ml/l] at 150 m. depth.

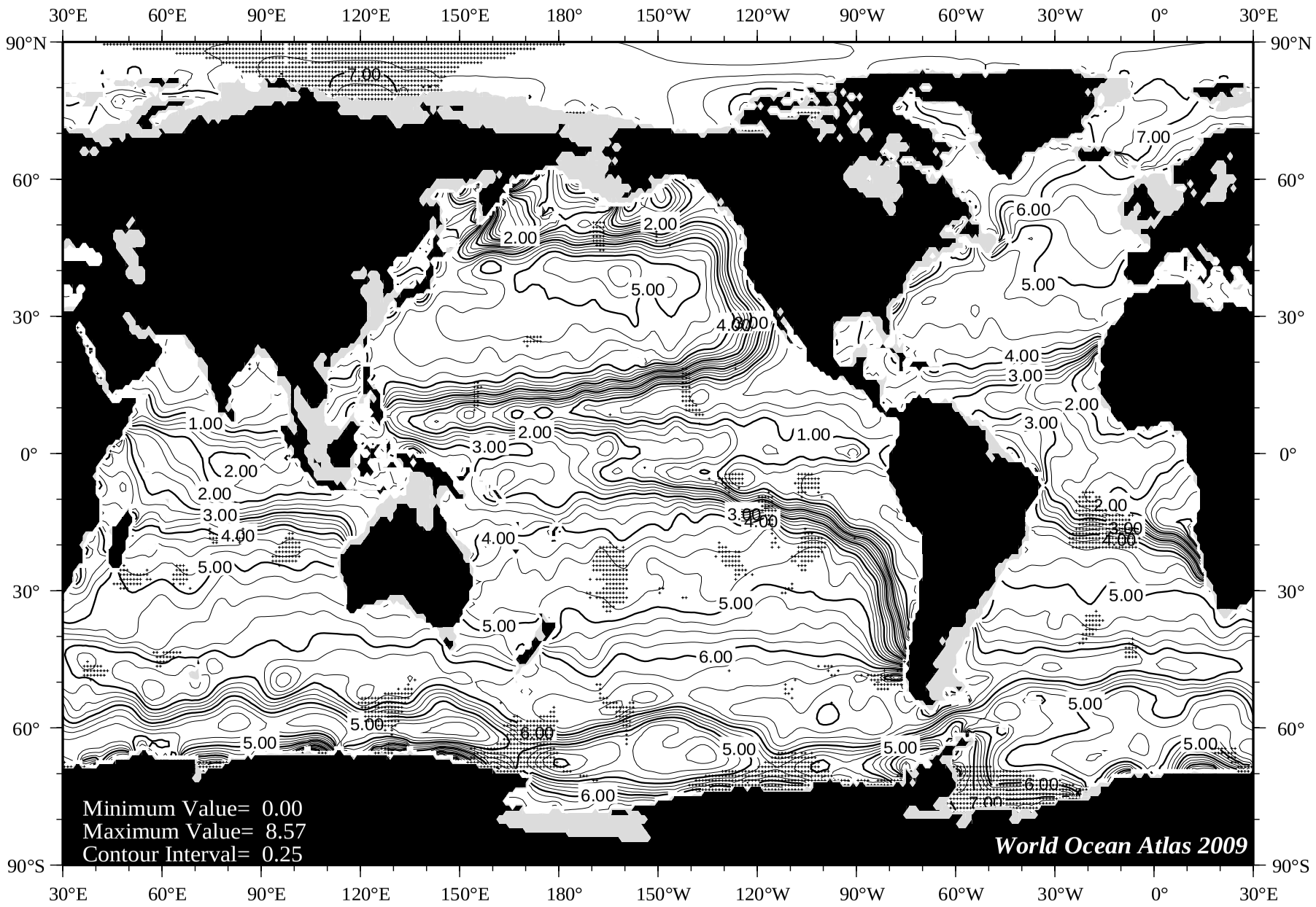

Fig B47 Fall (Oct.-Dec.) oxygen [ml/l] at 250 m. depth.

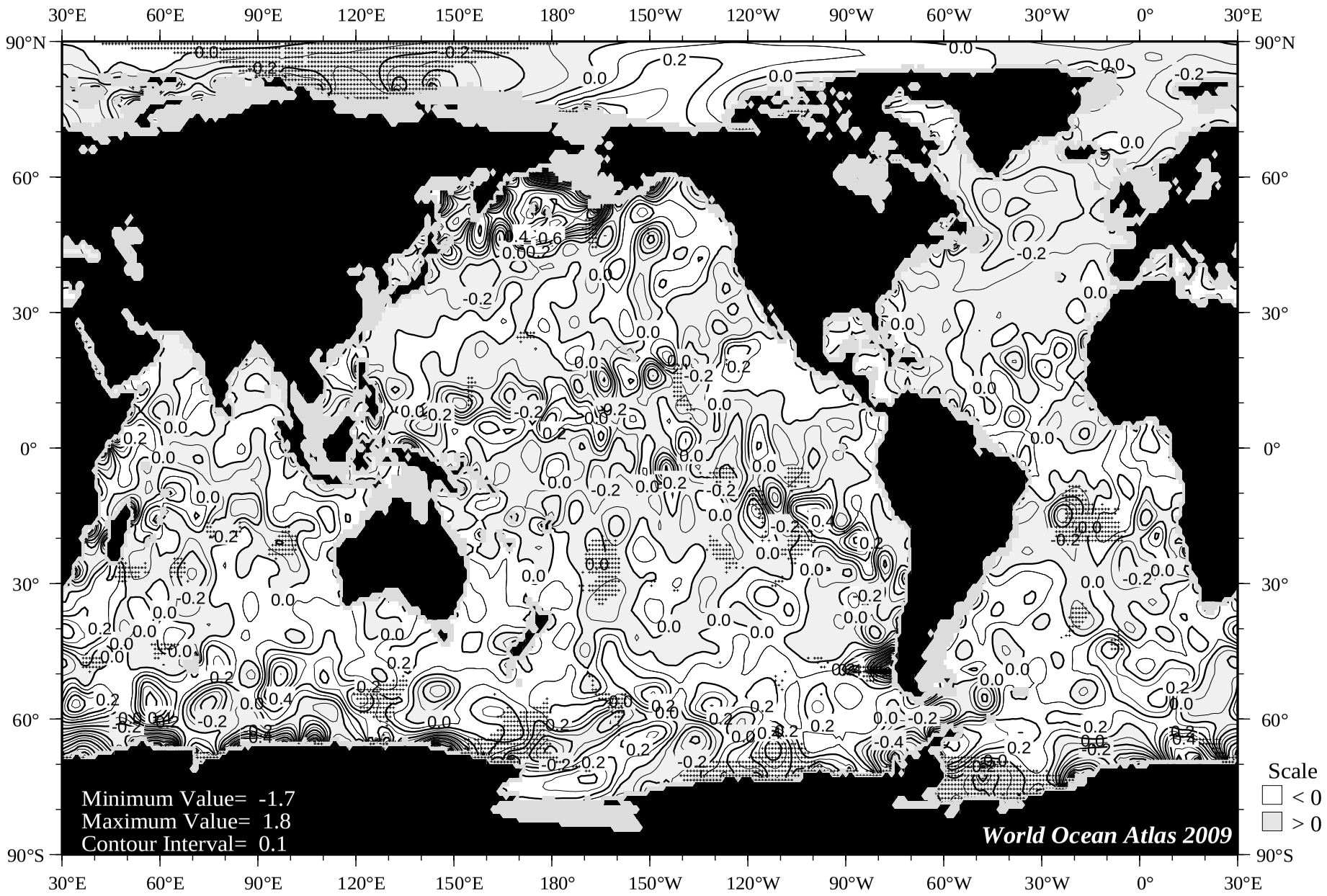

Fig B48 Fall (Oct.-Dec.) minus annual oxygen [ml/l] at 250 m. depth.

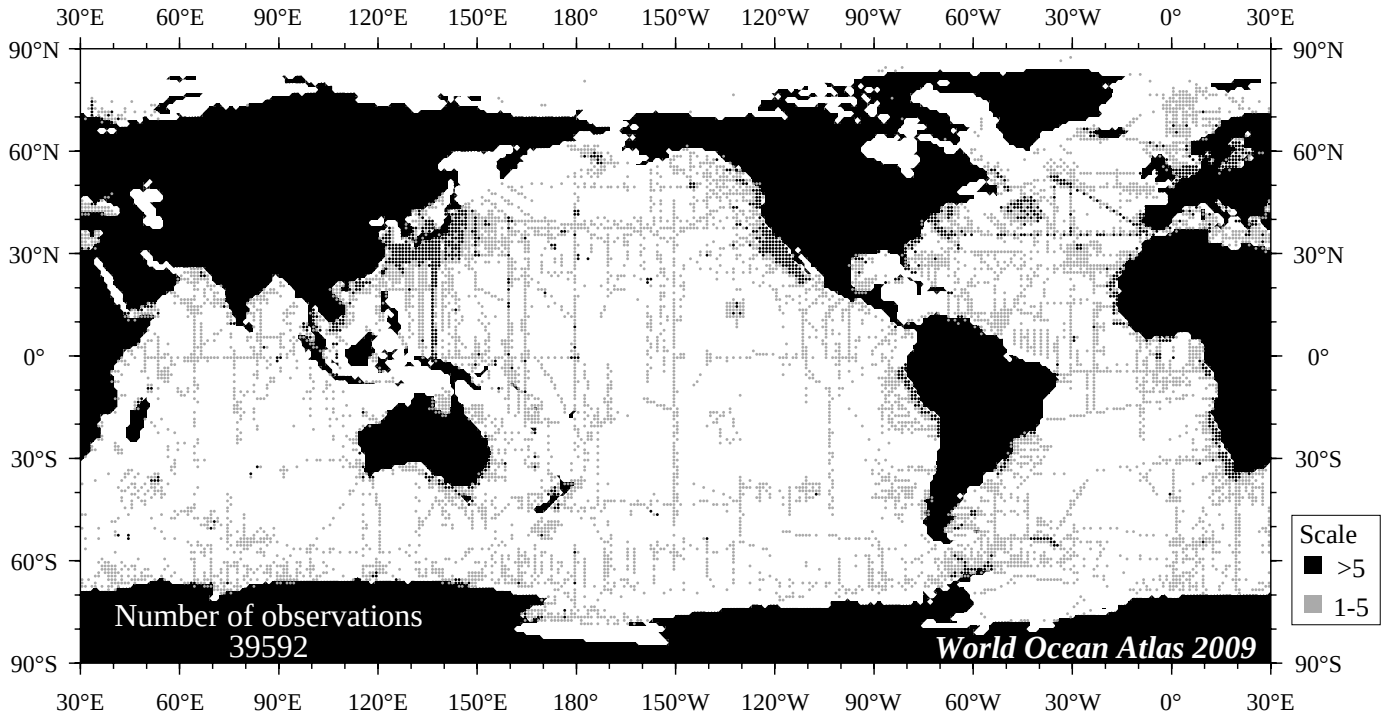

Fig C1 January oxygen observations at the surface.

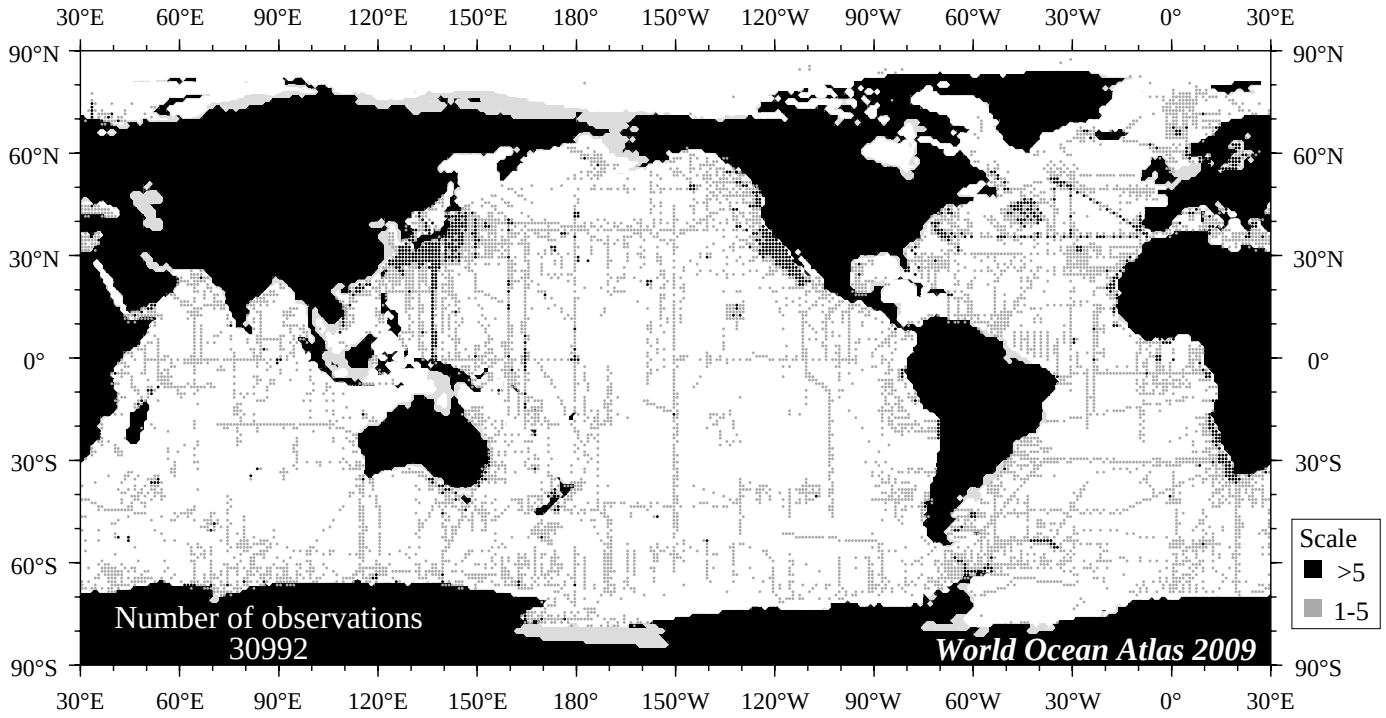

Fig C2 January oxygen observations at 75 m. depth.

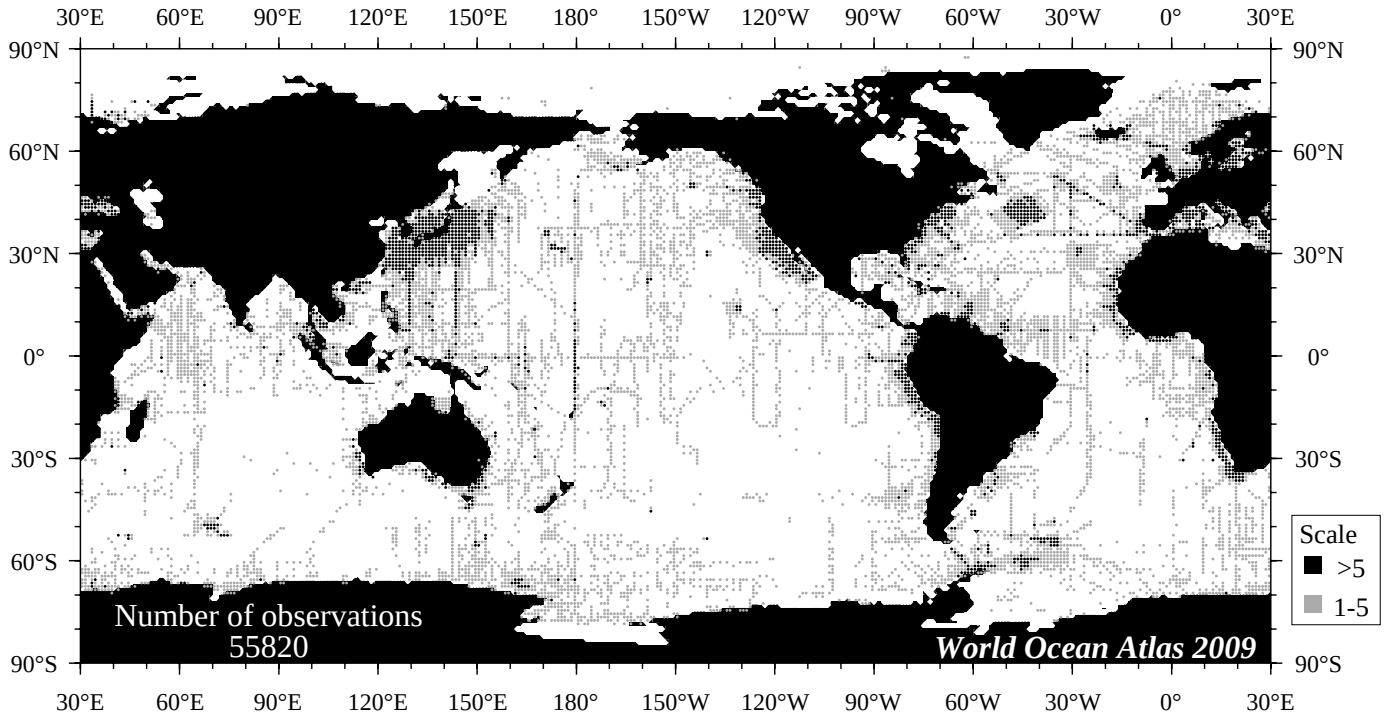

Fig C3 February oxygen observations at the surface.

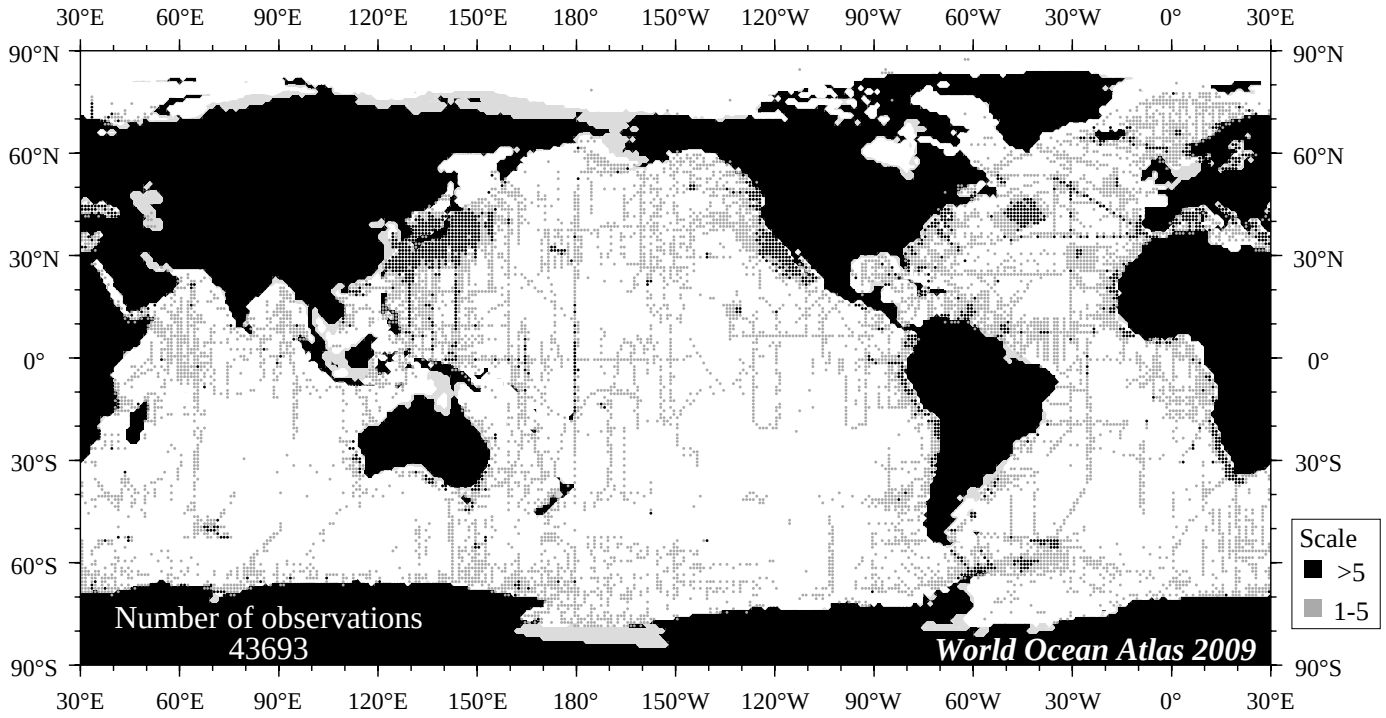

Fig C4 February oxygen observations at 75 m. depth.

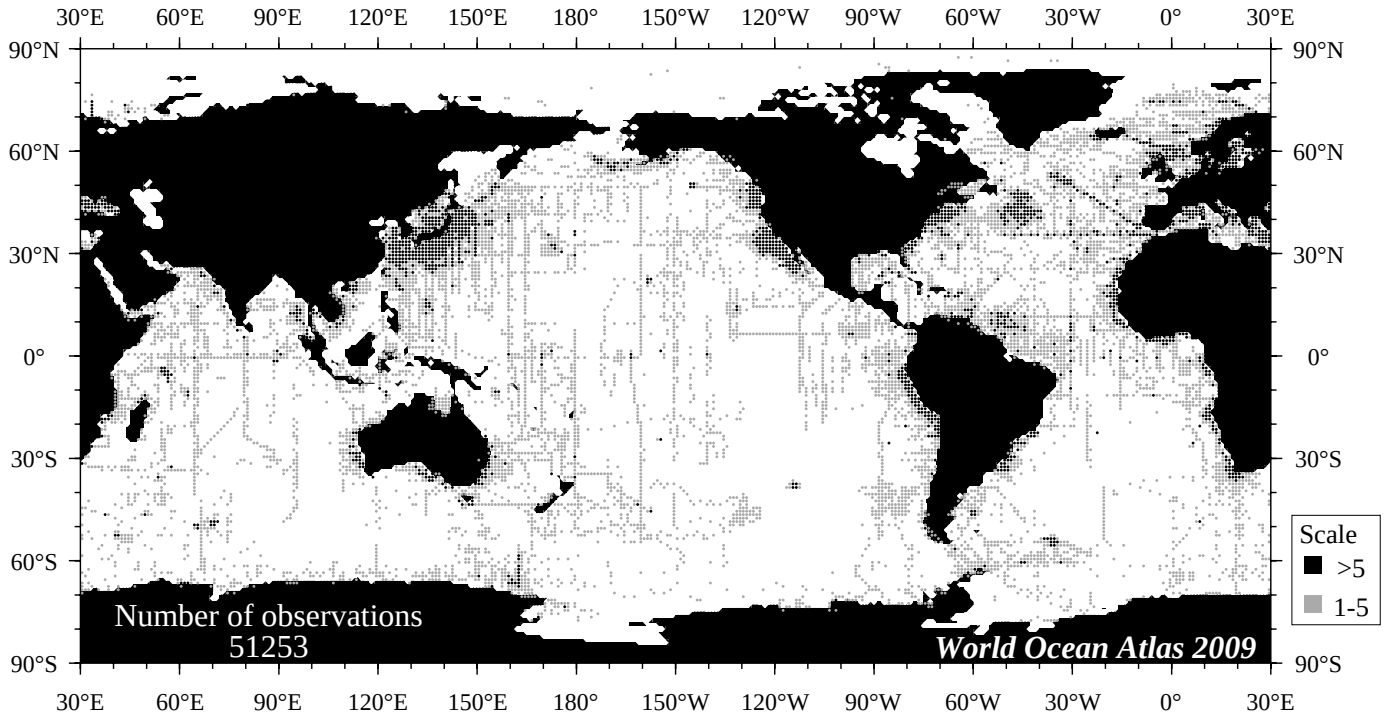

Fig C5 March oxygen observations at the surface.

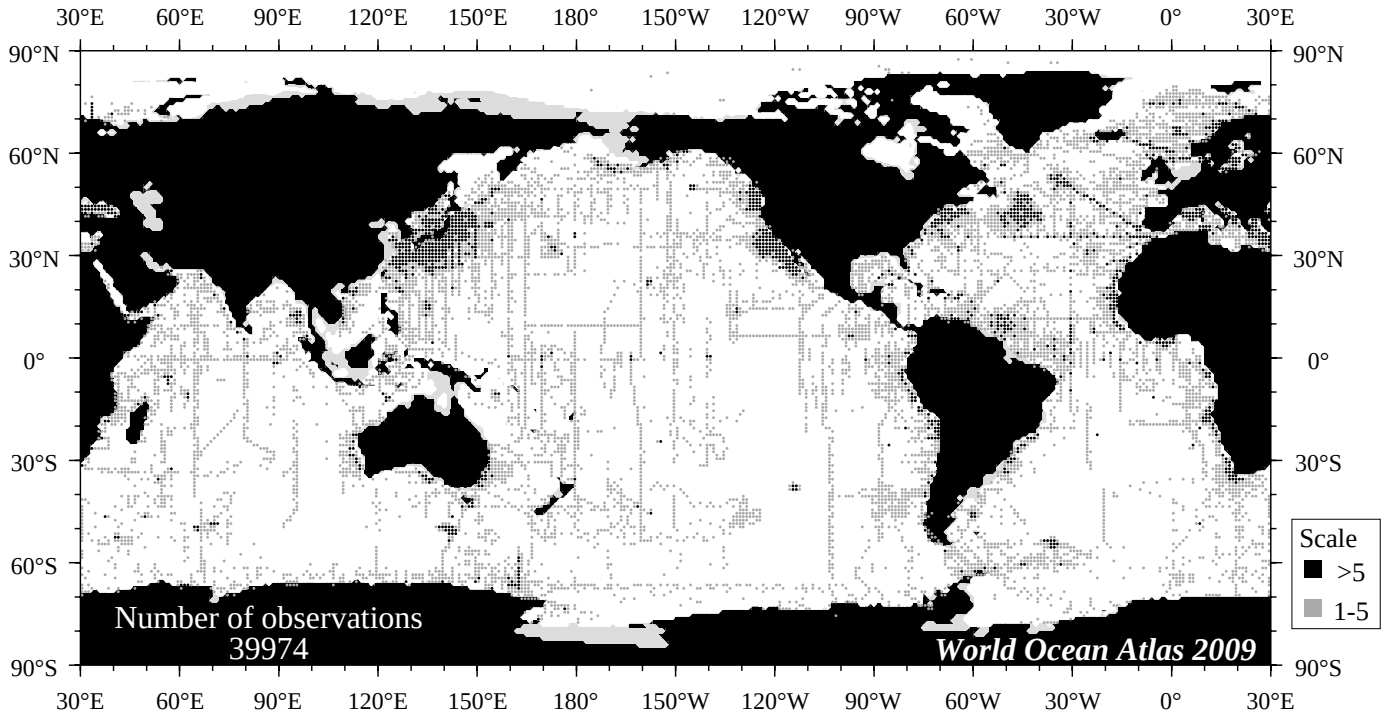

Fig C6 March oxygen observations at 75 m. depth.

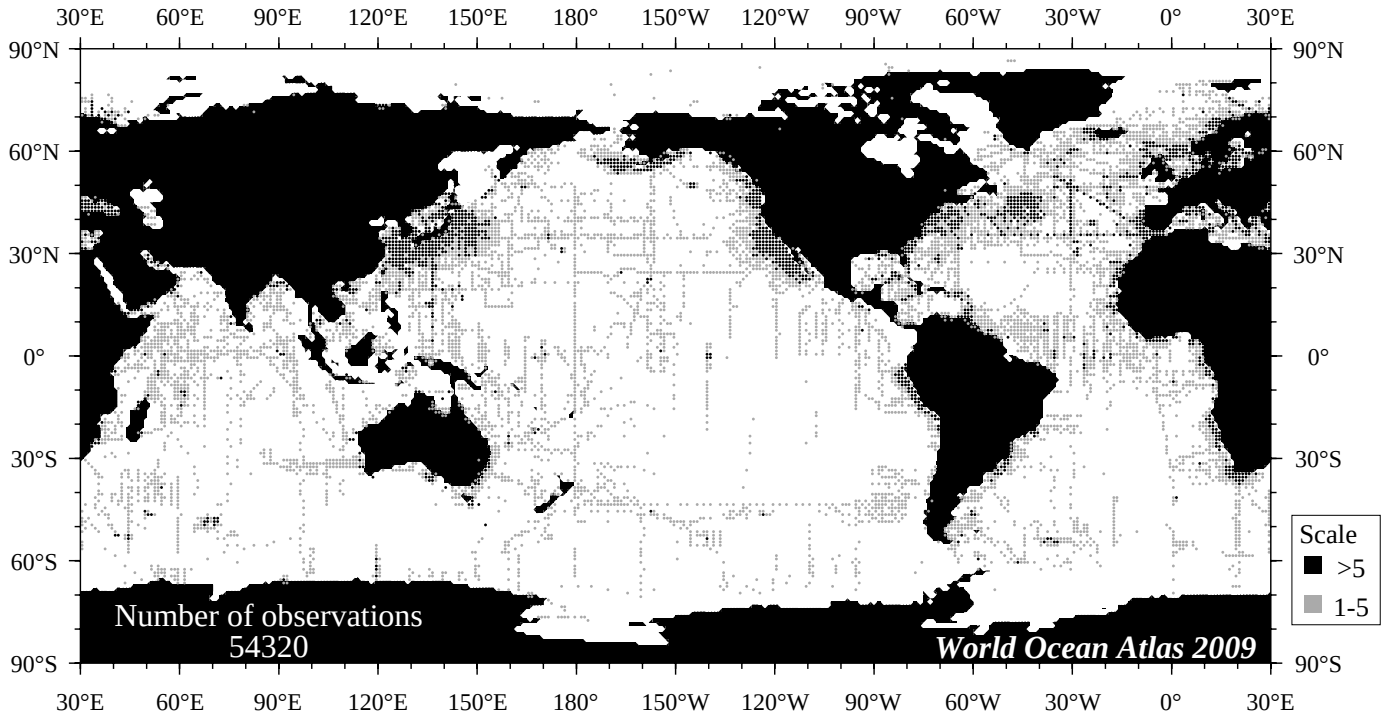

Fig C7 April oxygen observations at the surface.

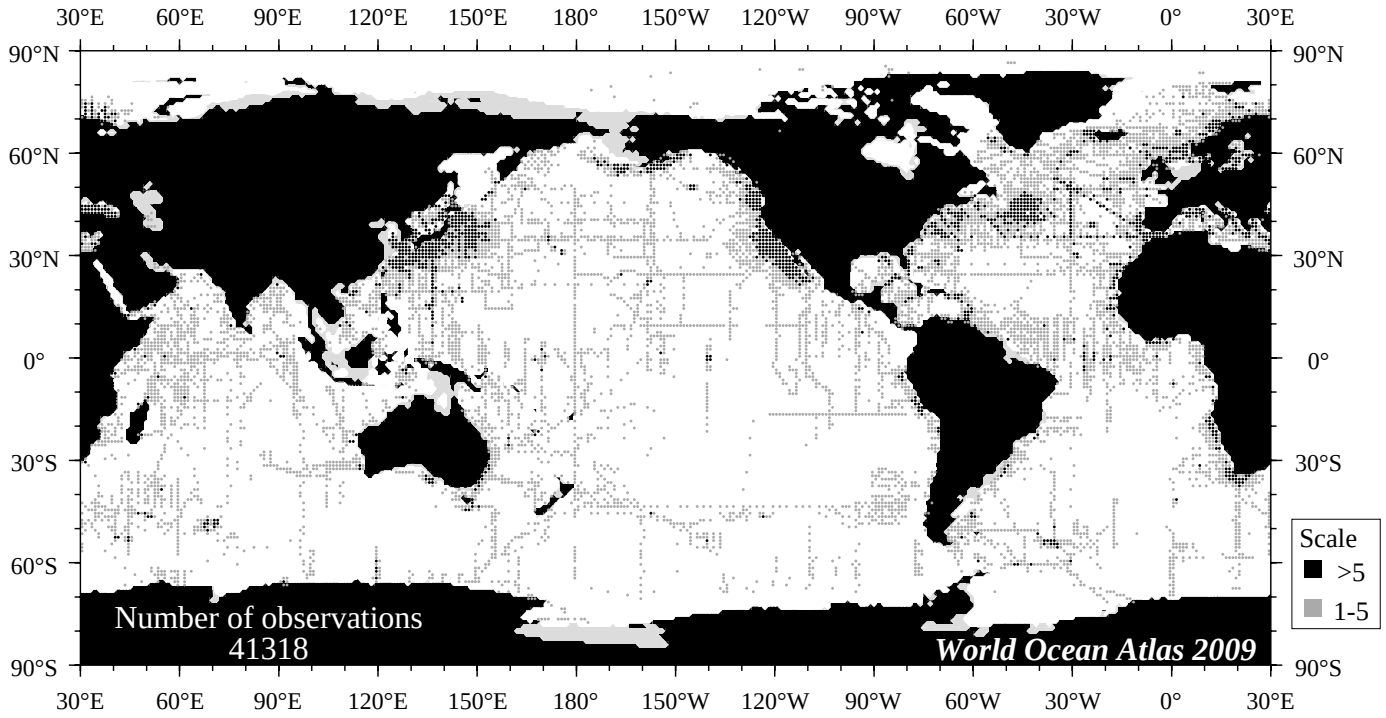

Fig C8 April oxygen observations at 75 m. depth.

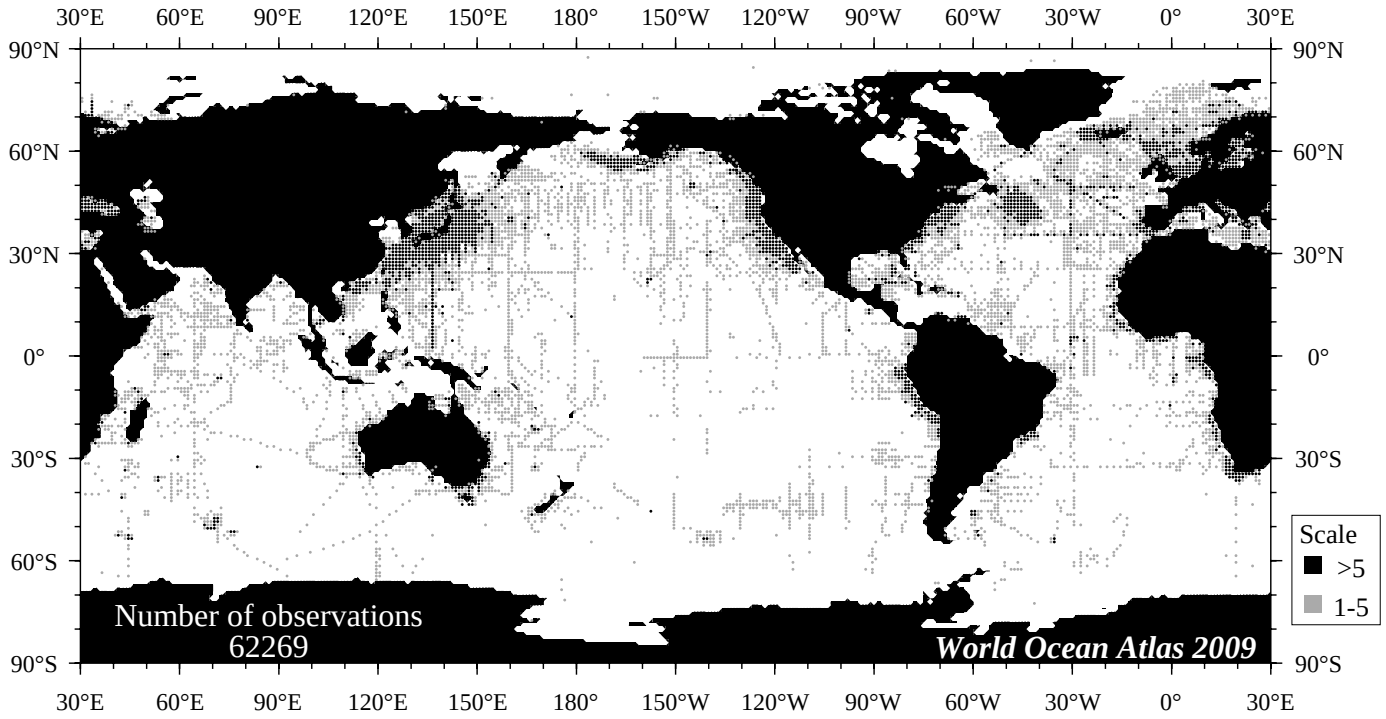

Fig C9 May oxygen observations at the surface.

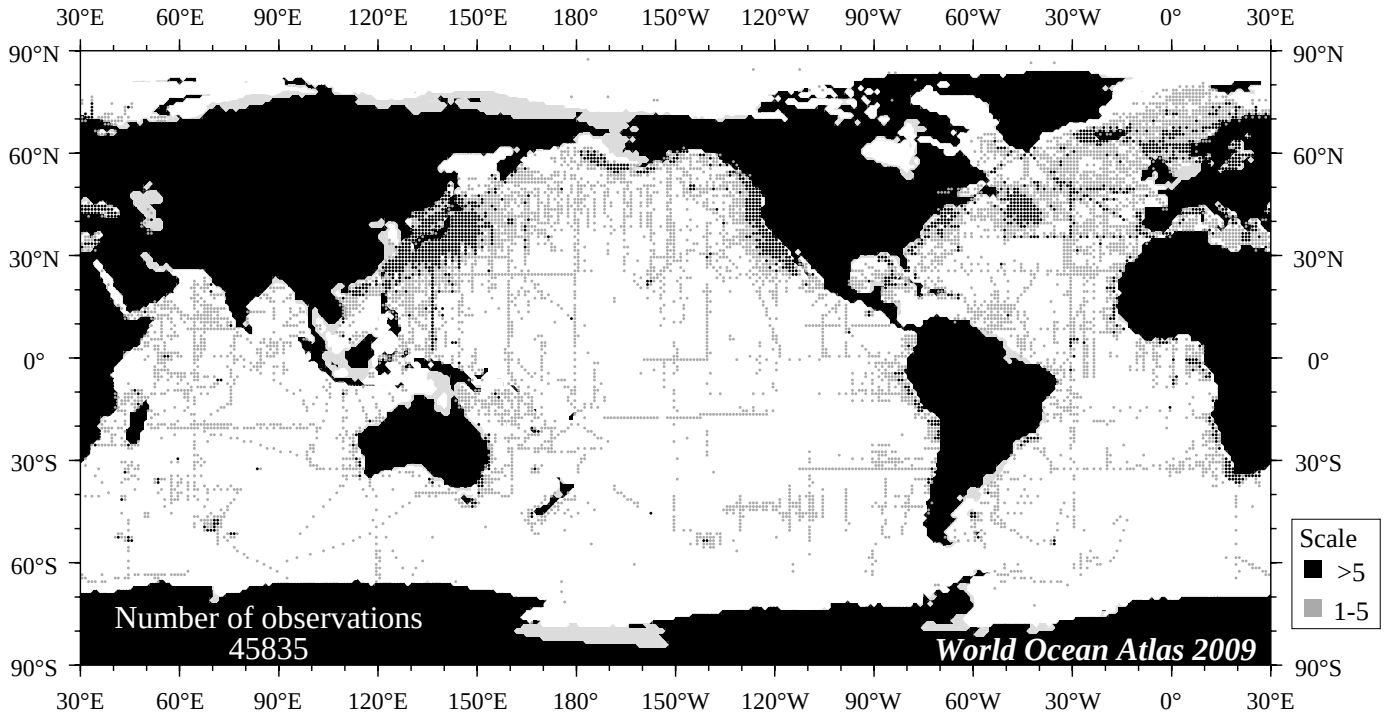

Fig C10 May oxygen observations at 75 m. depth.

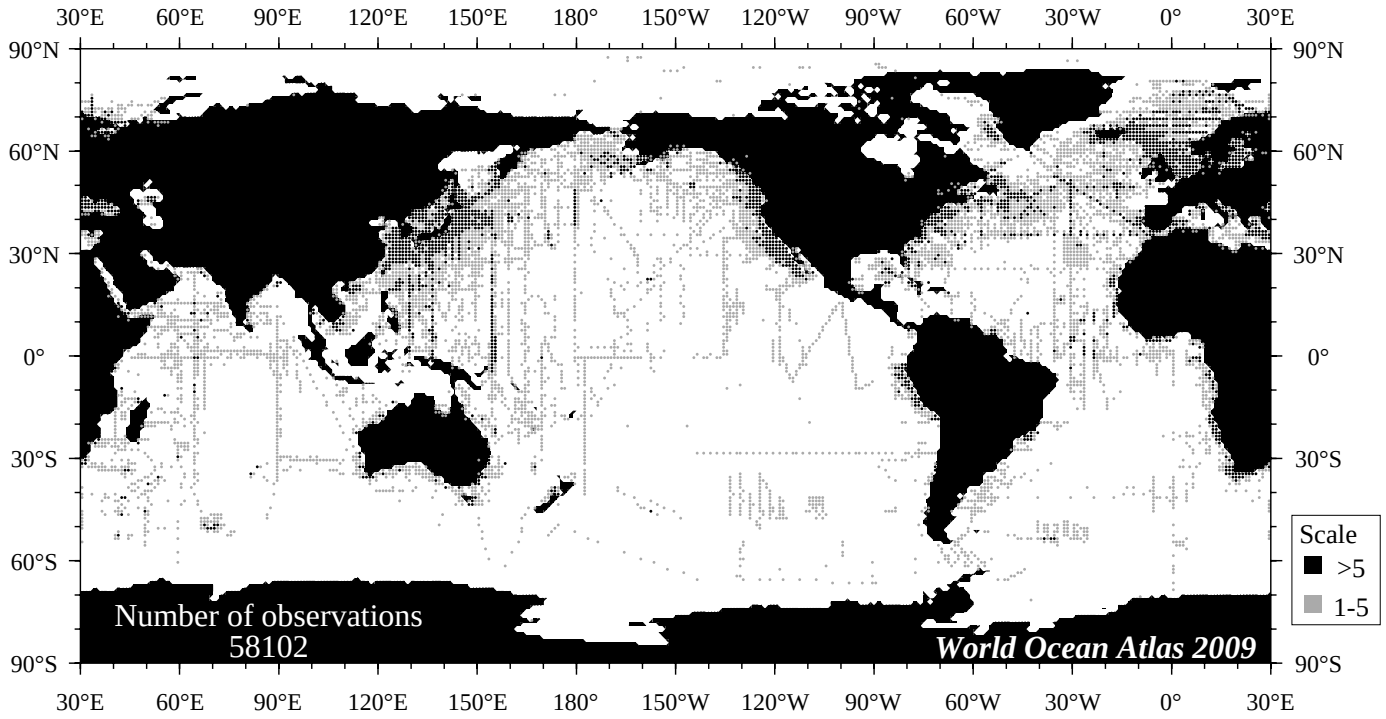

Fig C11 June oxygen observations at the surface.

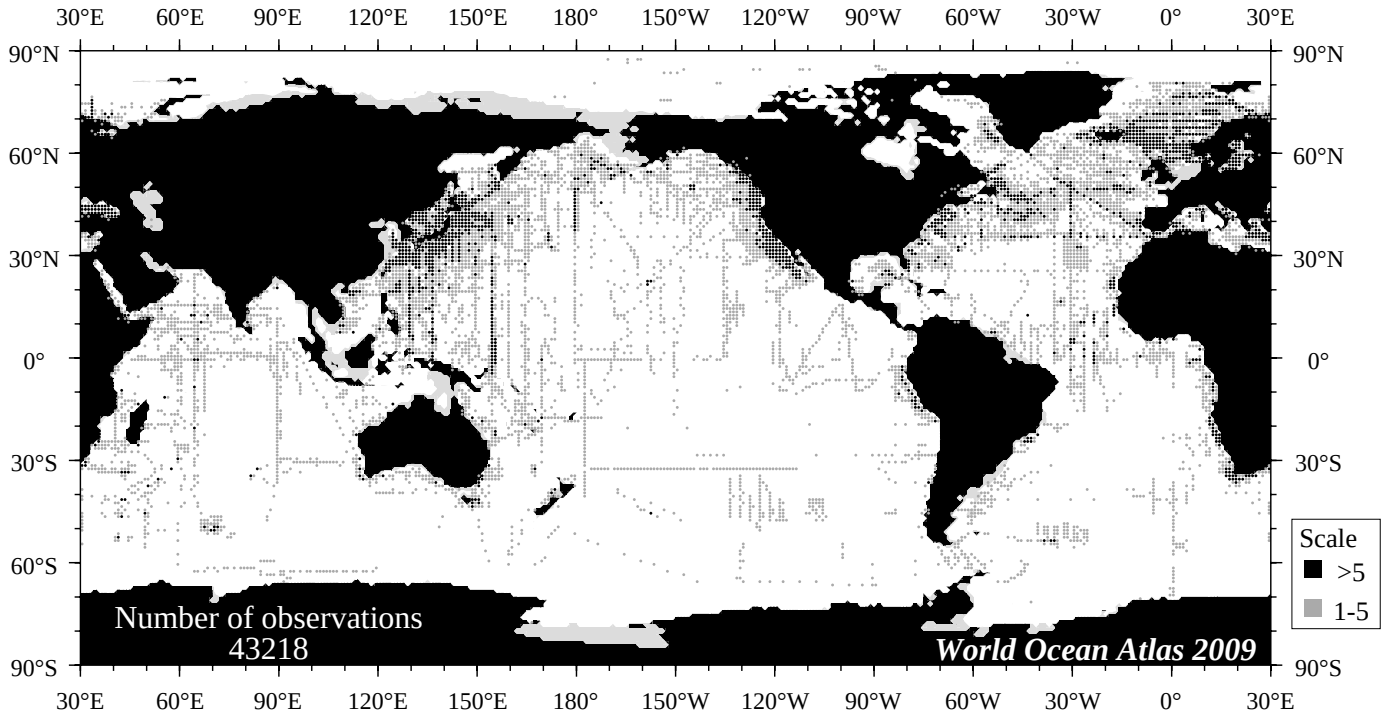

Fig C12 June oxygen observations at 75 m. depth.

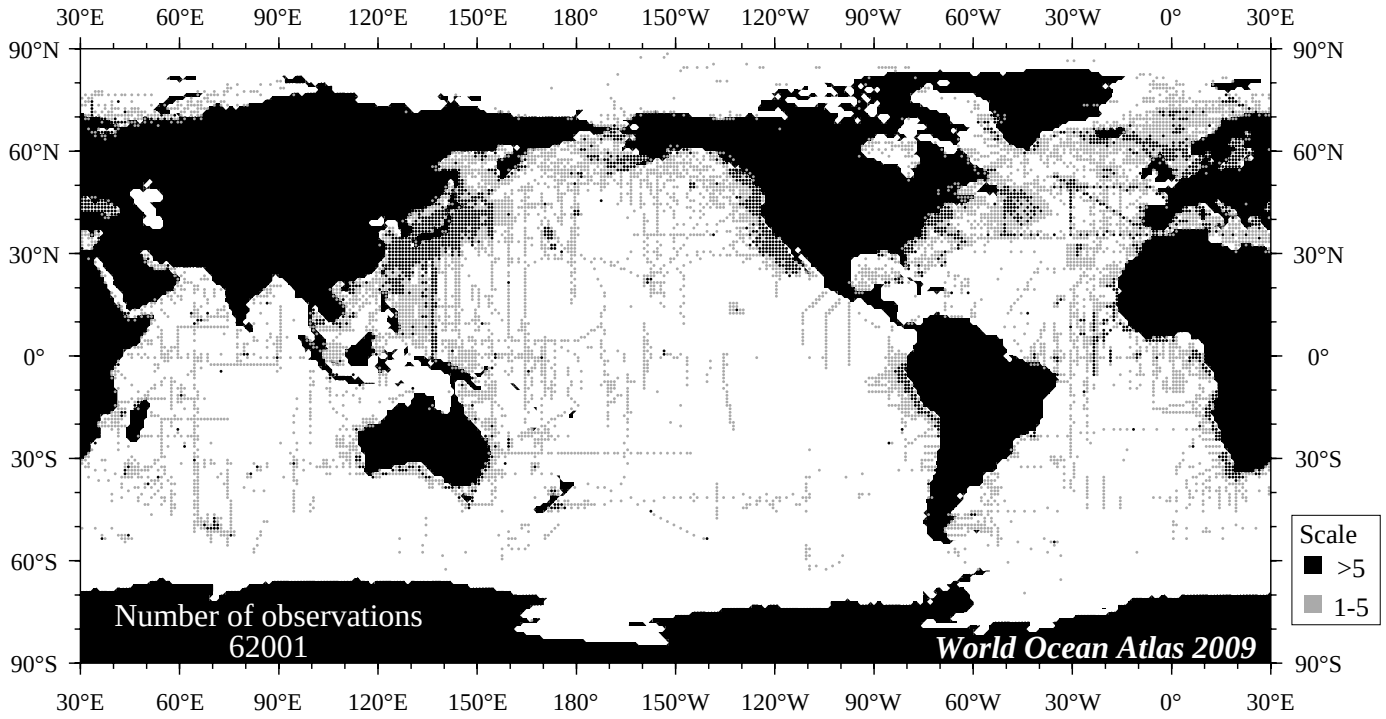

Fig C13 July oxygen observations at the surface.

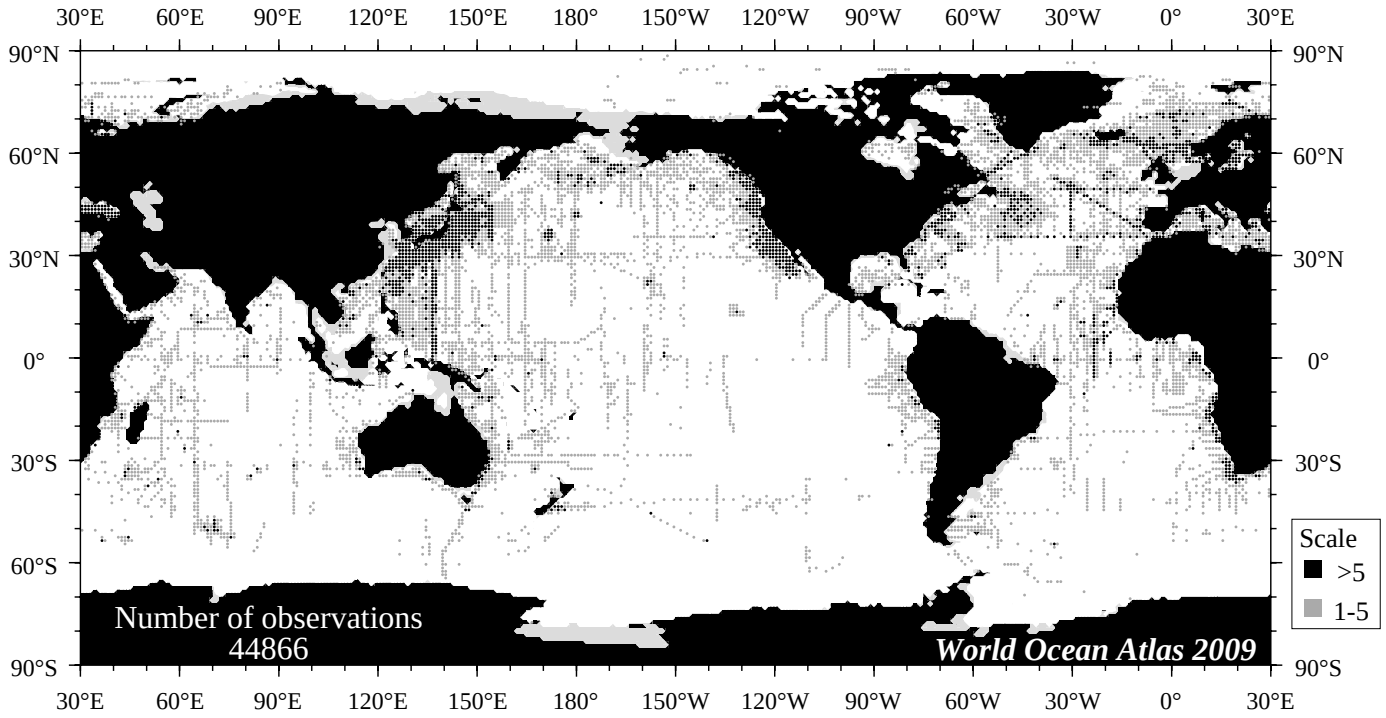

Fig C14 July oxygen observations at 75 m. depth.

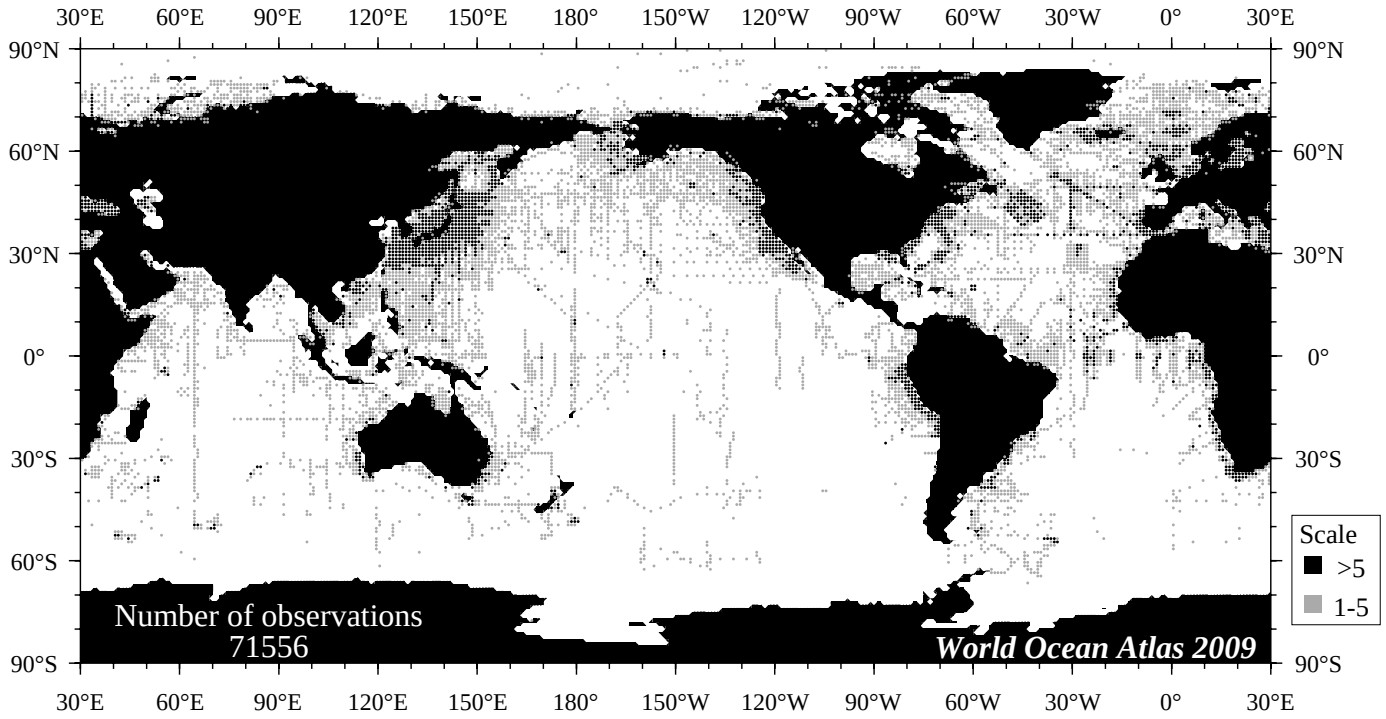

Fig C15 August oxygen observations at the surface.

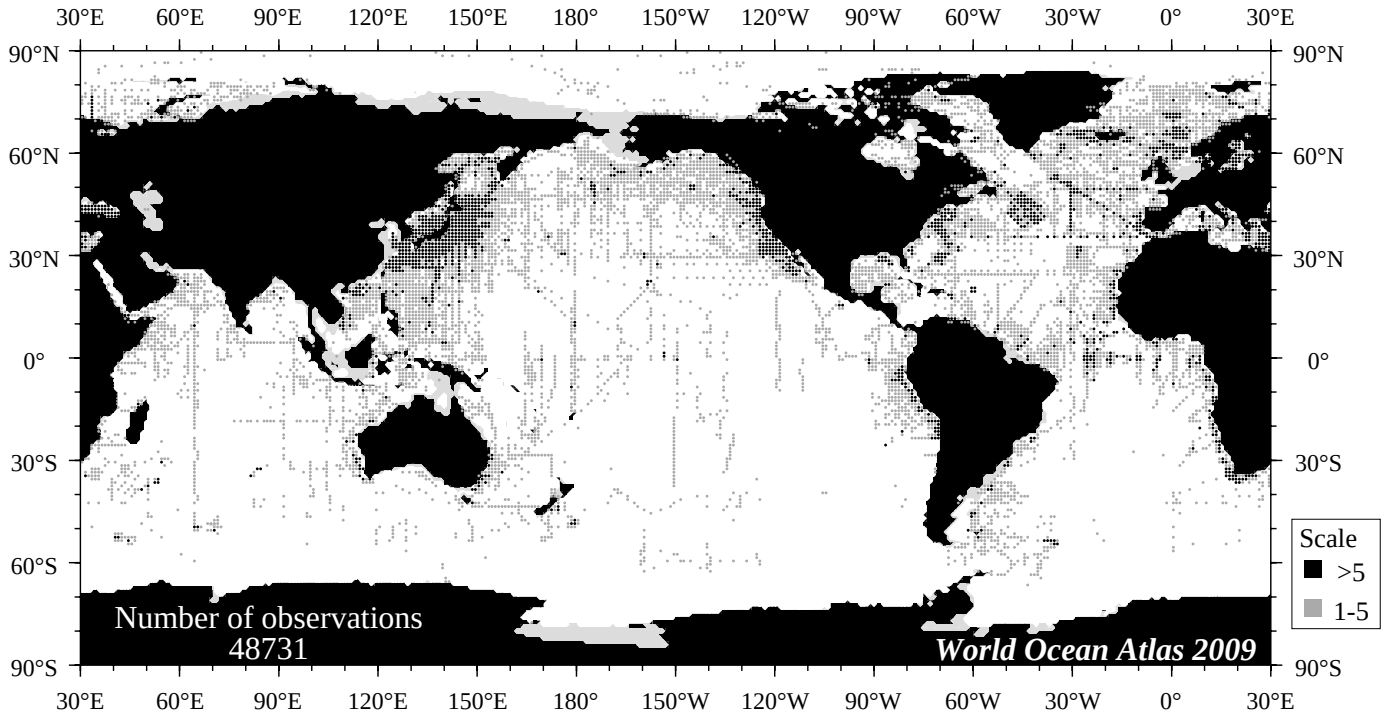

Fig C16 August oxygen observations at 75 m. depth.

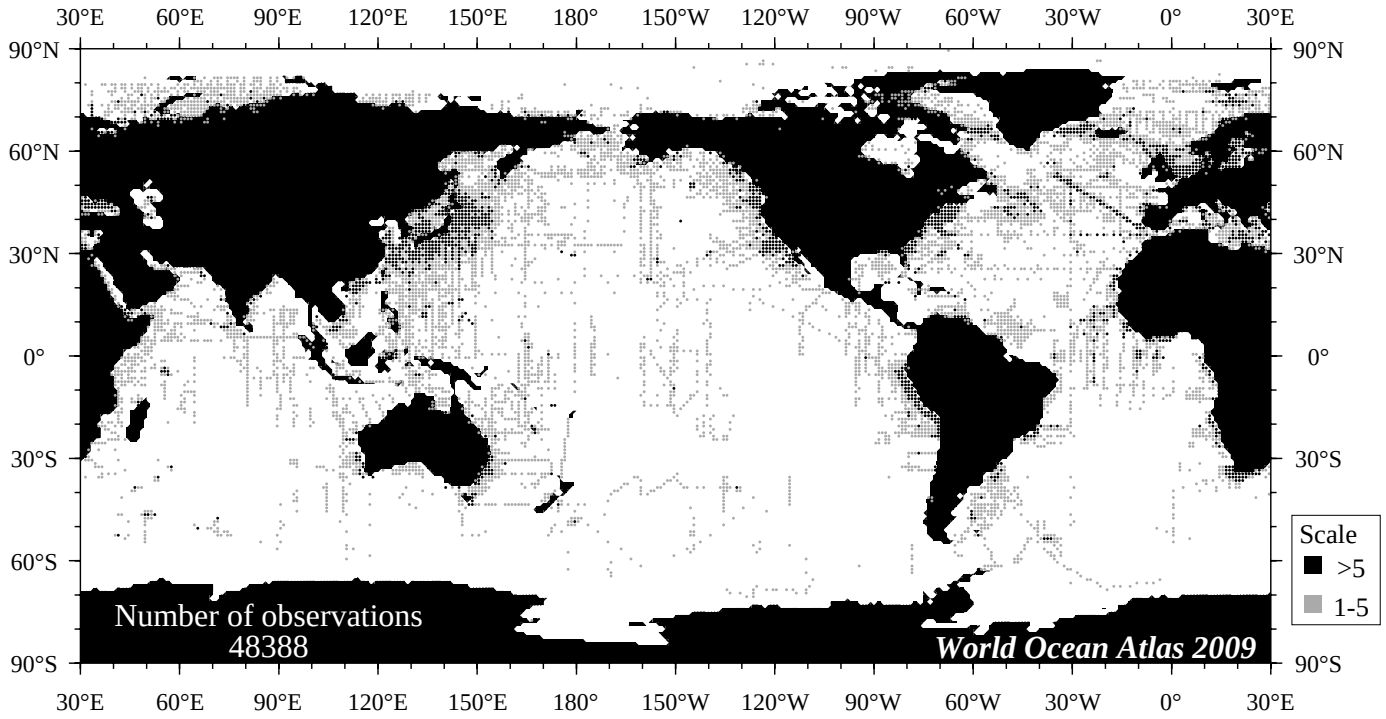

Fig C17 September oxygen observations at the surface.

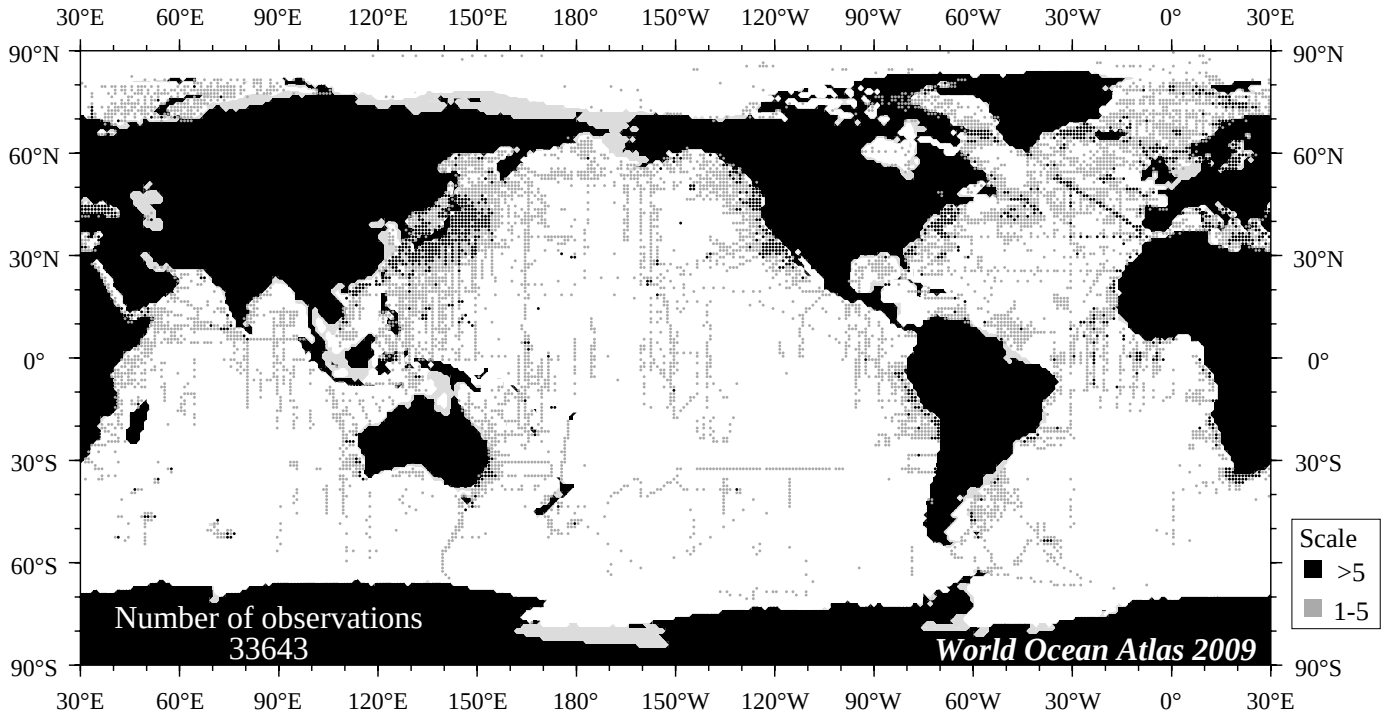

Fig C18 September oxygen observations at 75 m. depth.

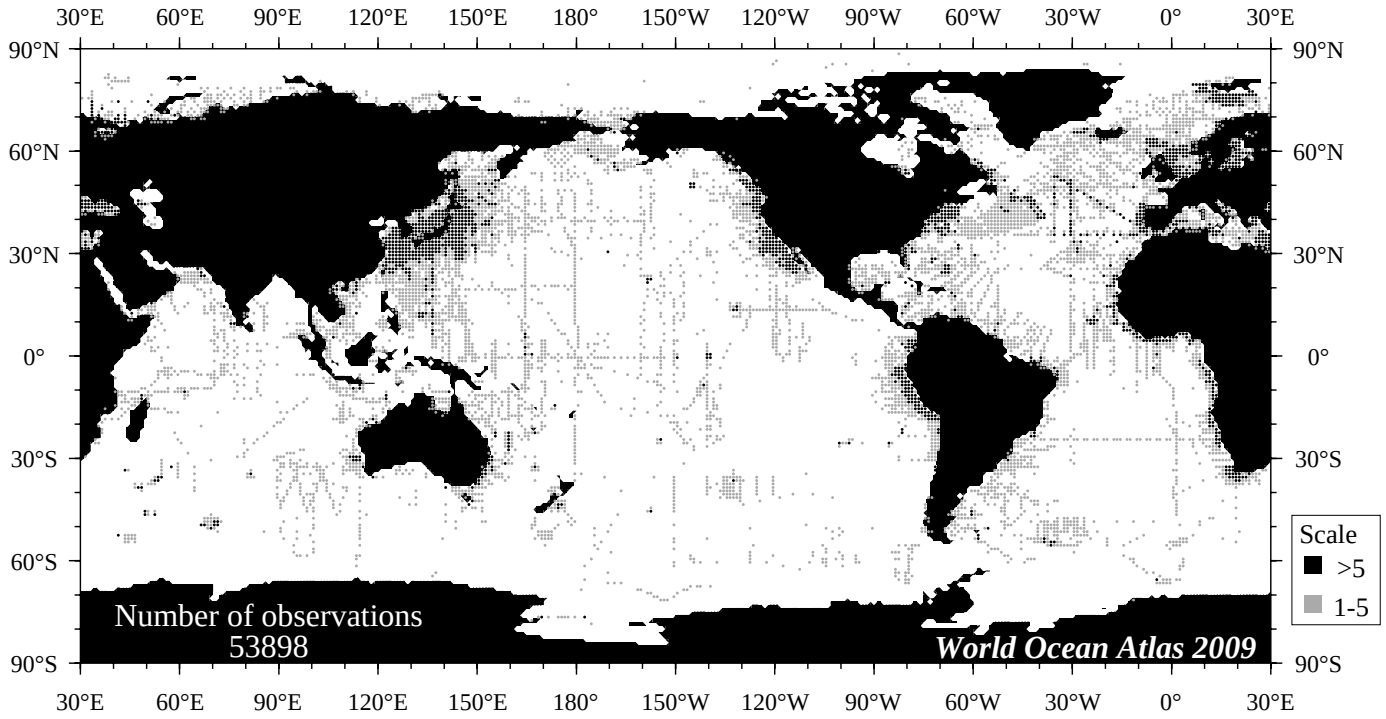

Fig C19 October oxygen observations at the surface.

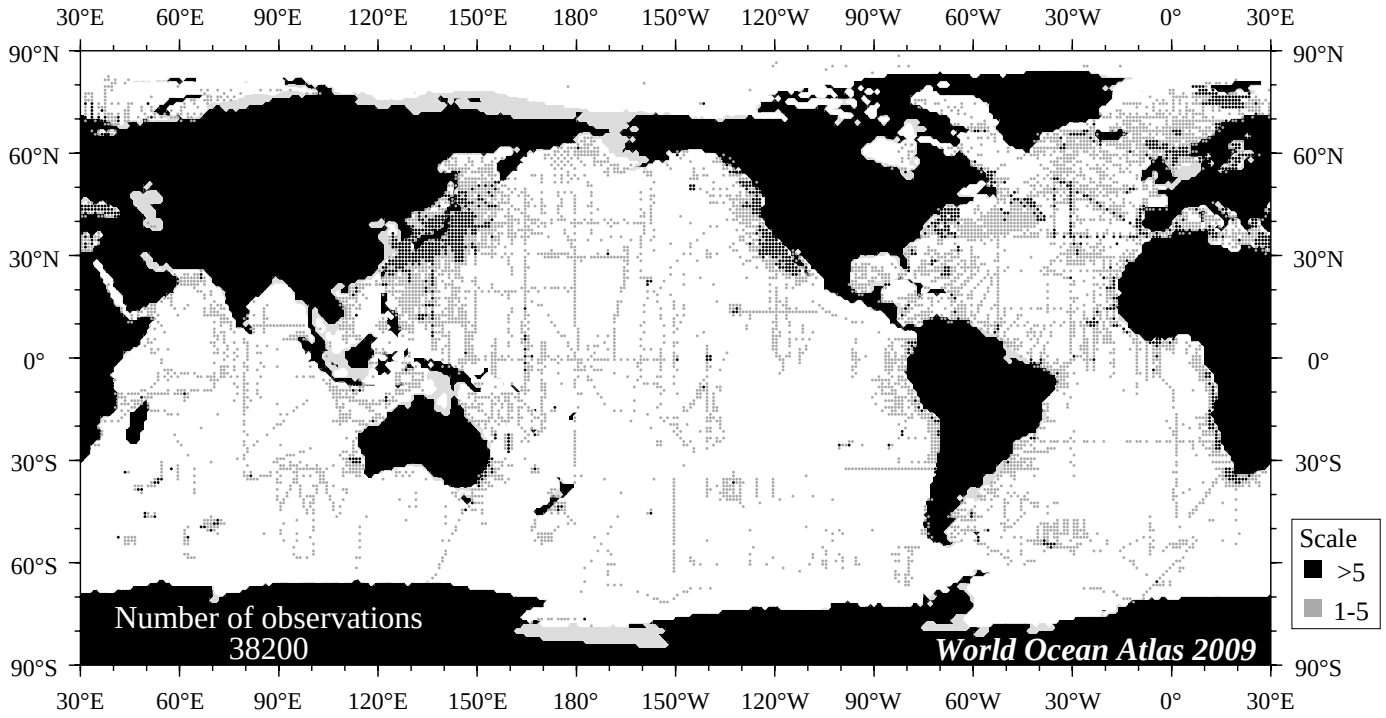

Fig C20 October oxygen observations at 75 m. depth.

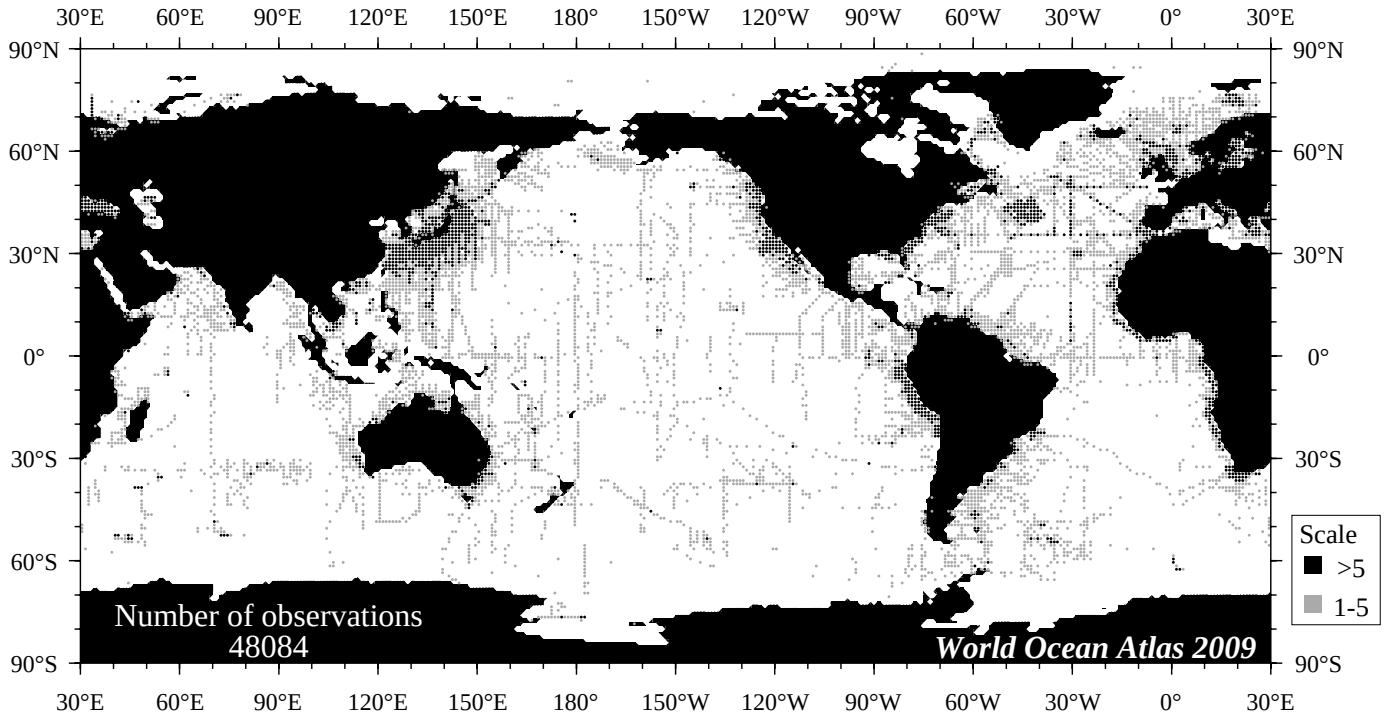

Fig C21 November oxygen observations at the surface.

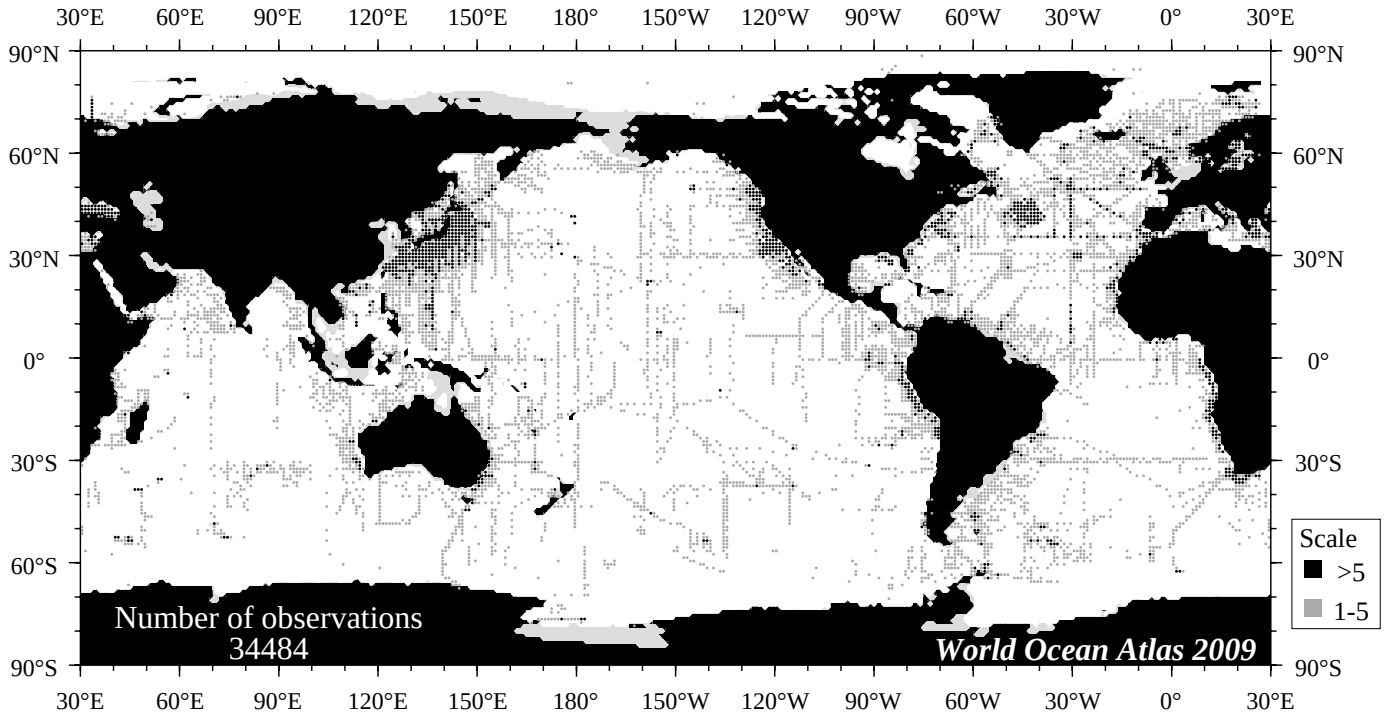

Fig C22 November oxygen observations at 75 m. depth.

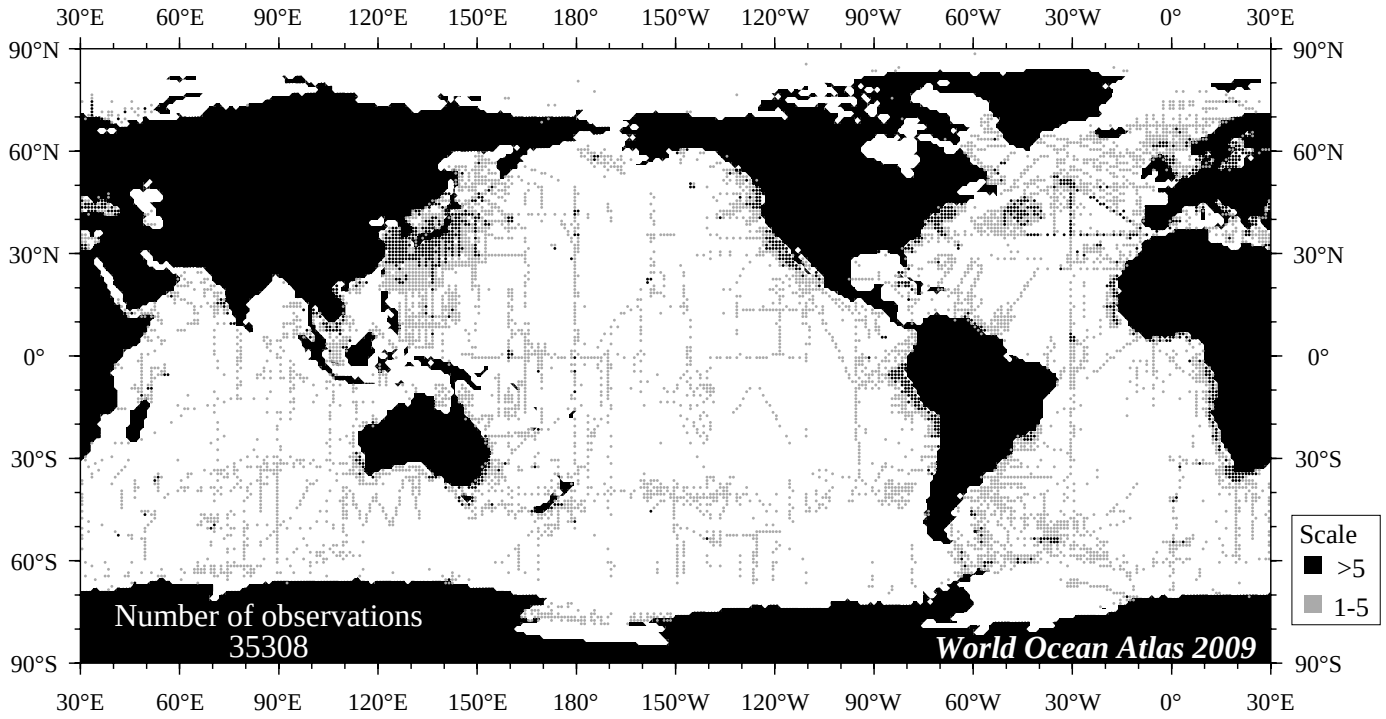

Fig C23 December oxygen observations at the surface.

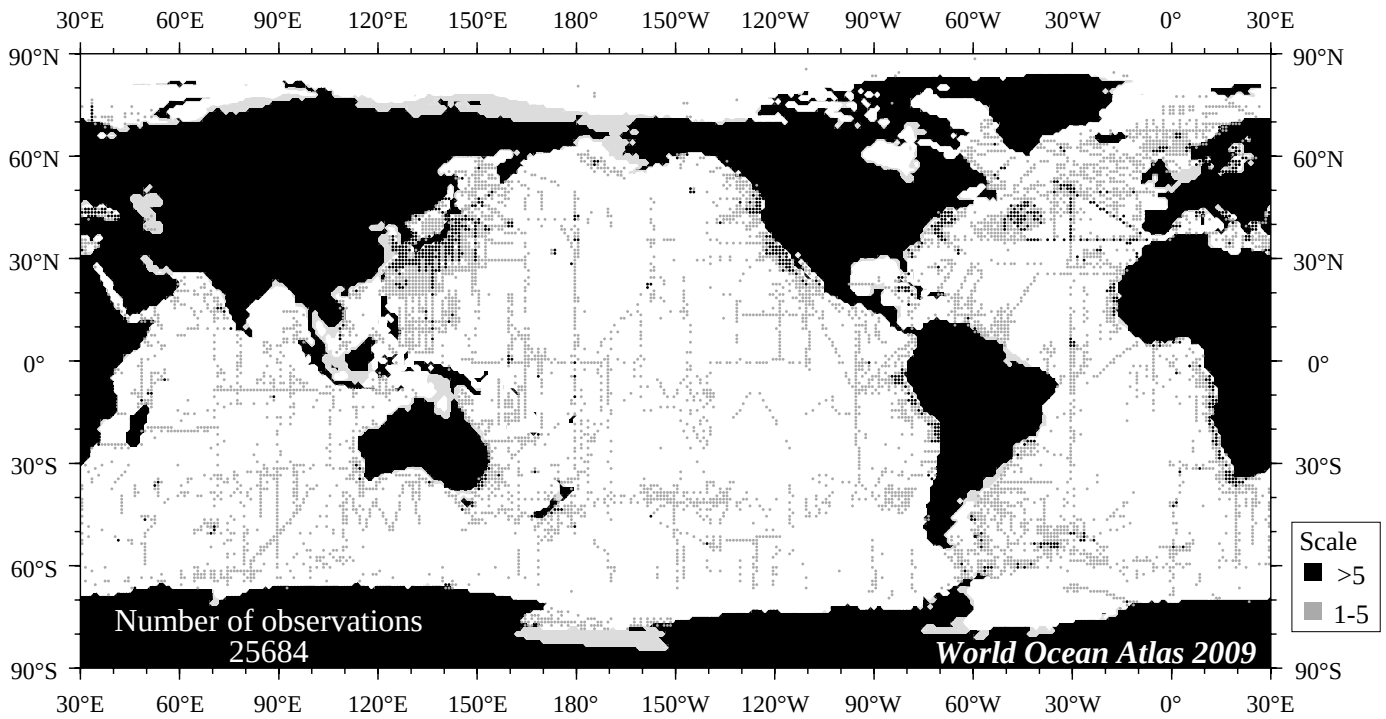

Fig C24 December oxygen observations at 75 m. depth.

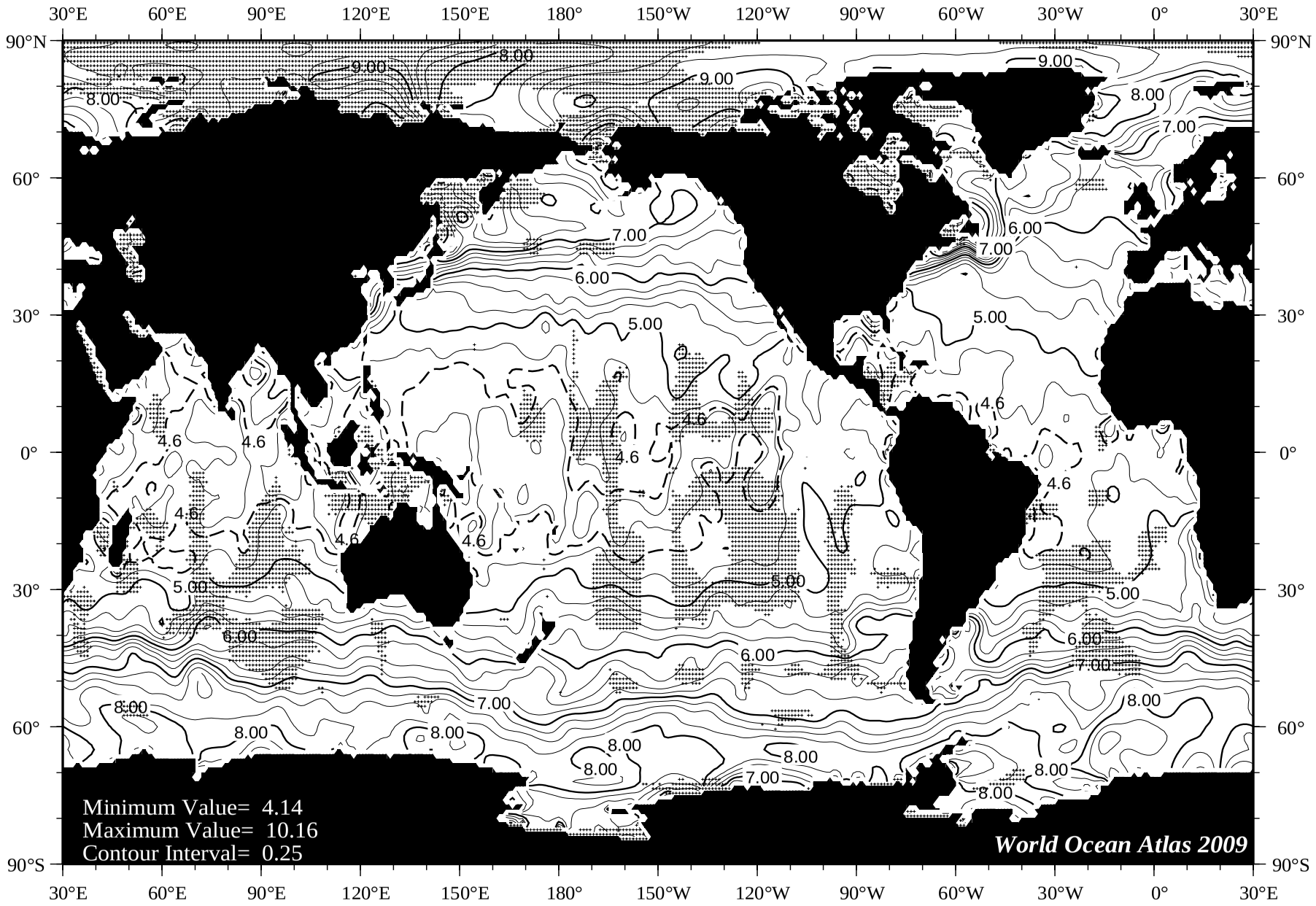

Fig C25 January mean oxygen [ml/l] at the surface.

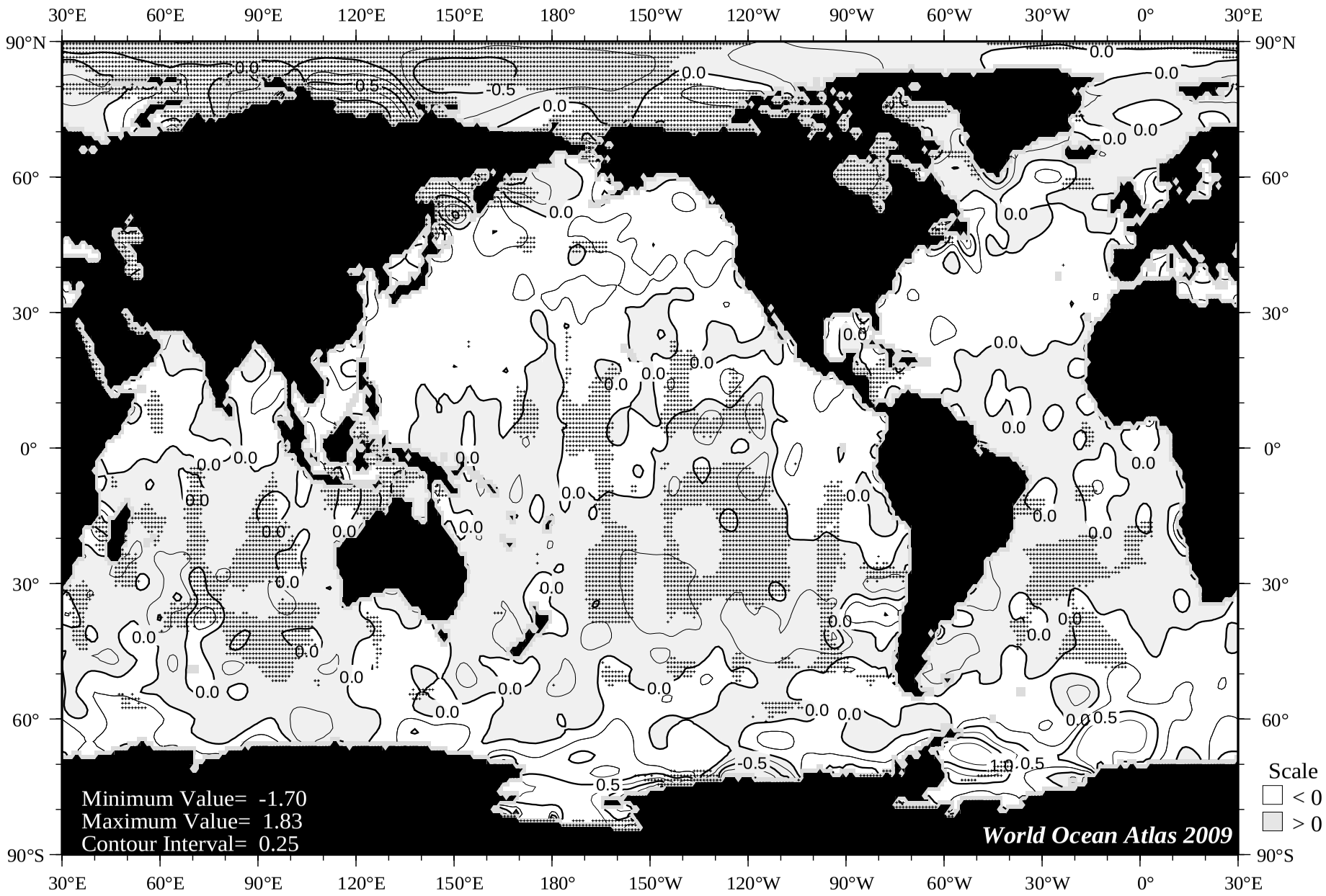

Fig C26 January minus annual oxygen [ml/l] at the surface.

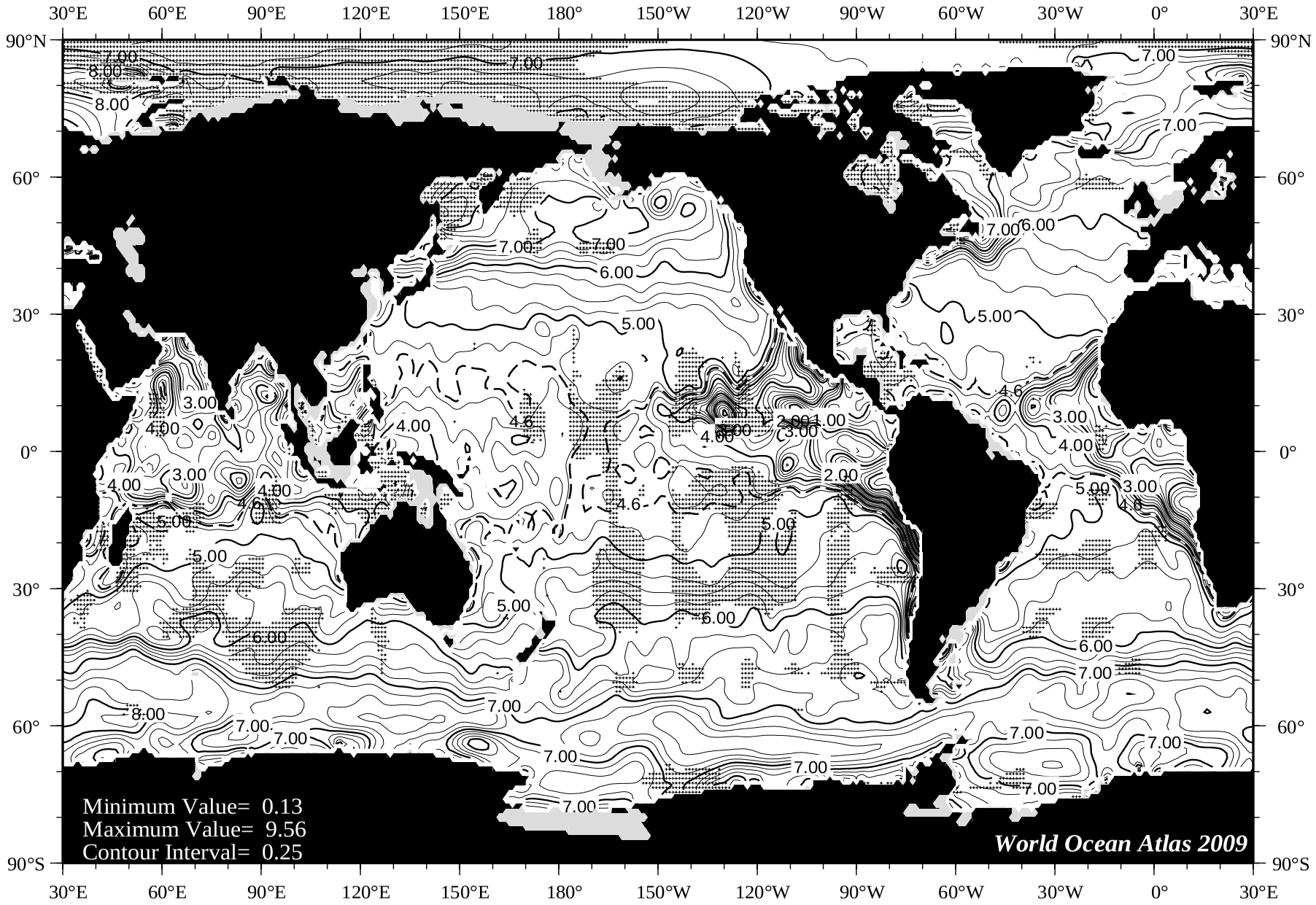

Fig C27 January mean oxygen [ml/l] at 75 m. depth.

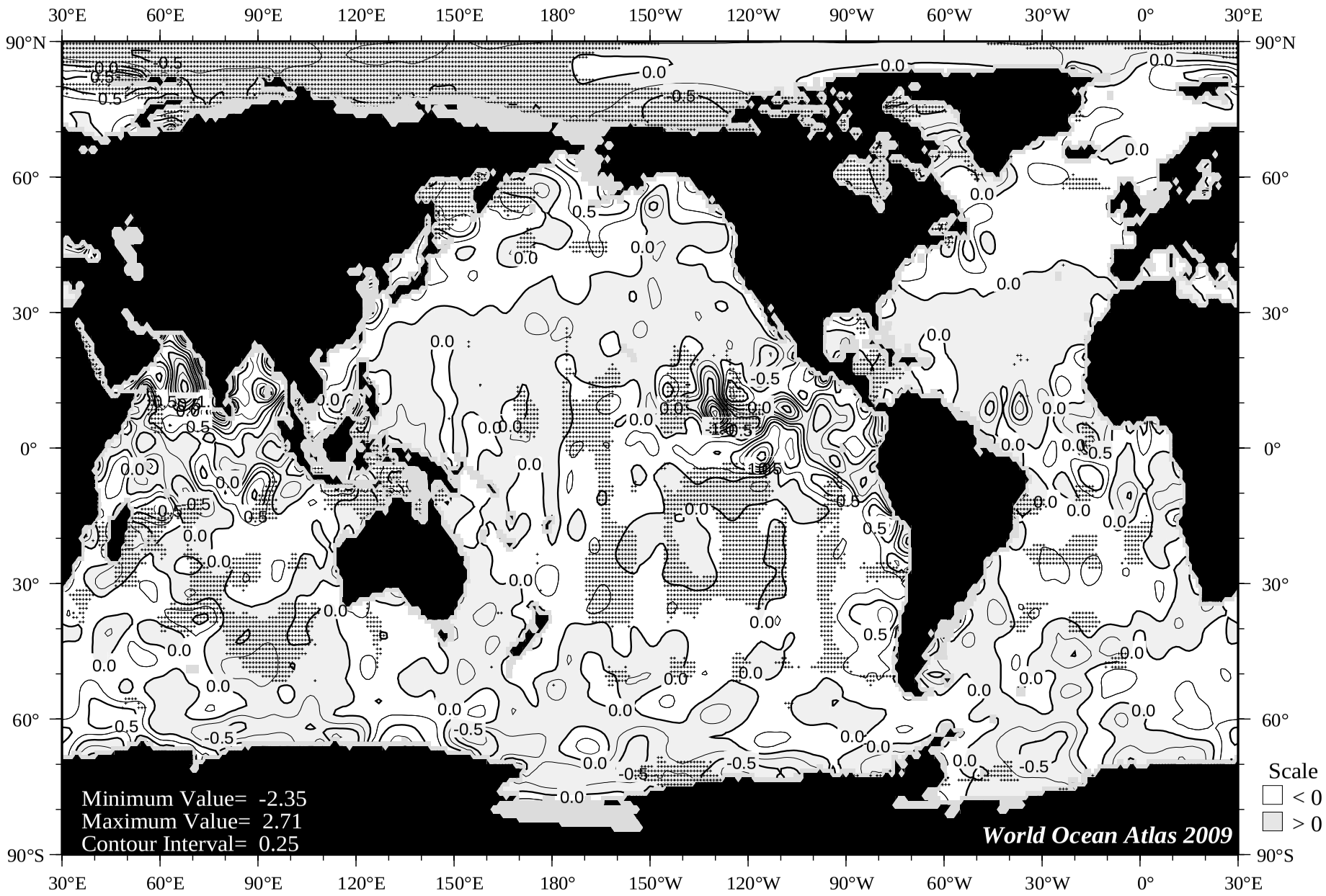

Fig C28 January minus annual oxygen [ml/l] at 75 m. depth.

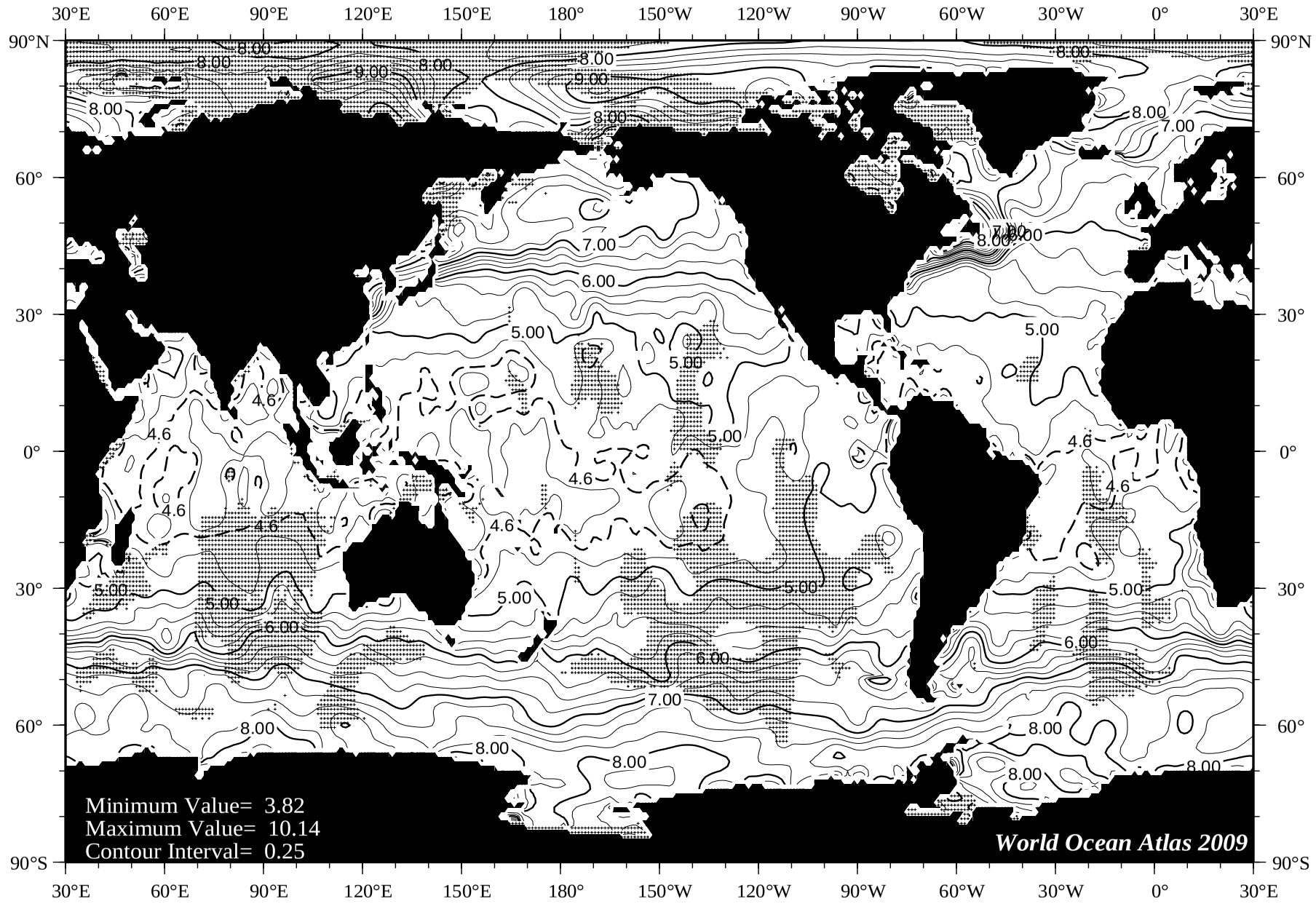

Fig C29 February mean oxygen [ml/l] at the surface.

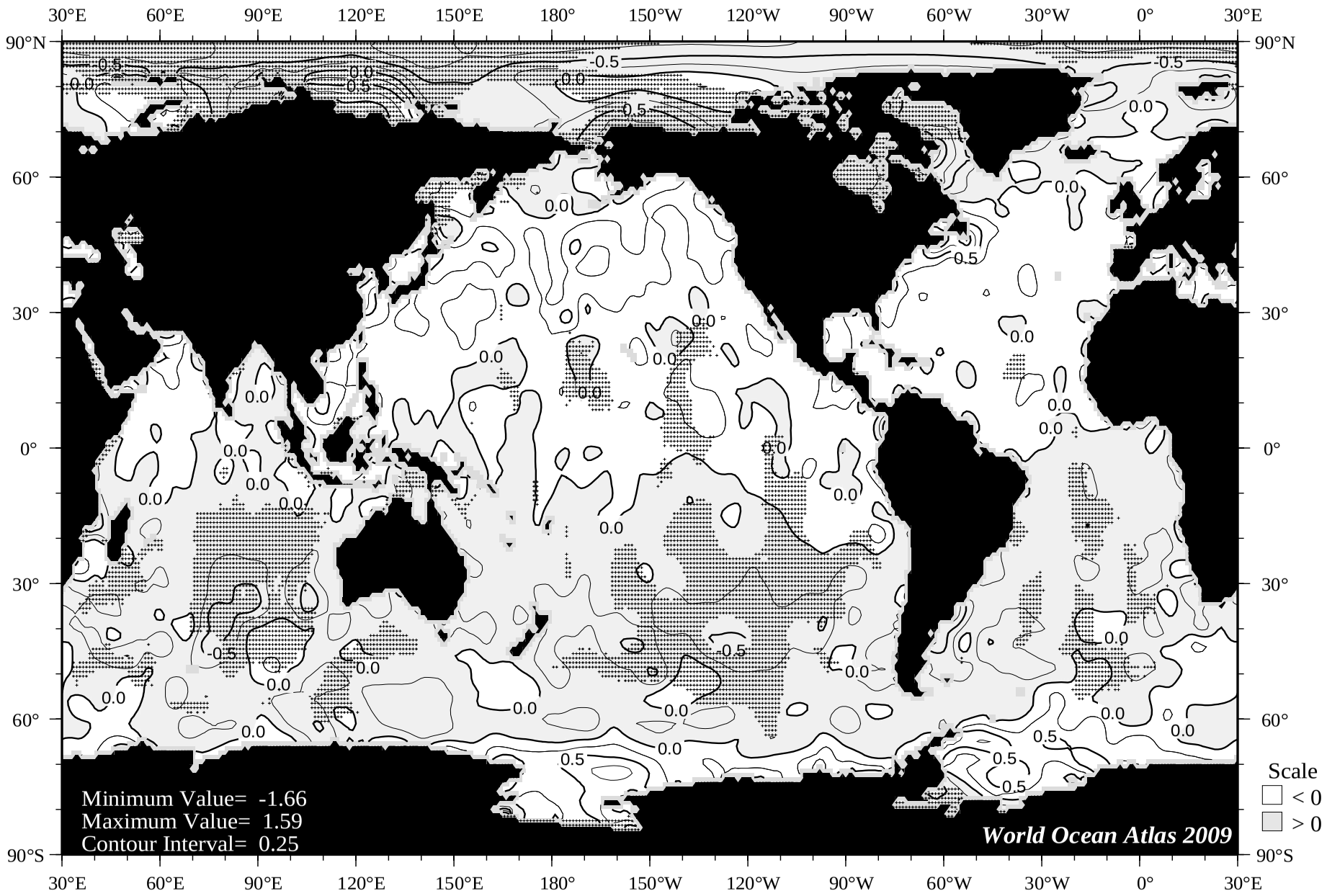

Fig C30 February minus annual oxygen [ml/l] at the surface.

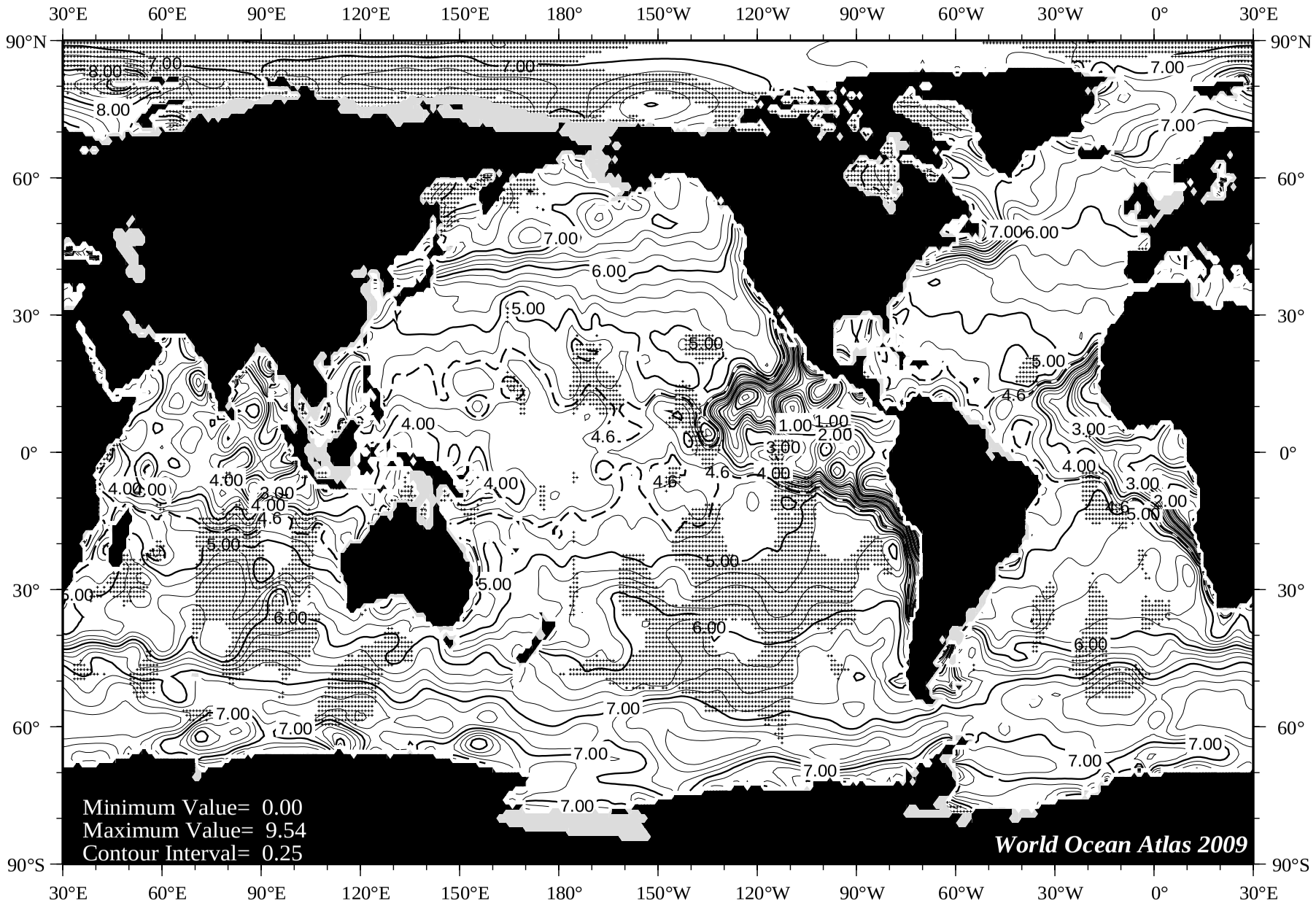

Fig C31 February mean oxygen [ml/l] at 75 m. depth.

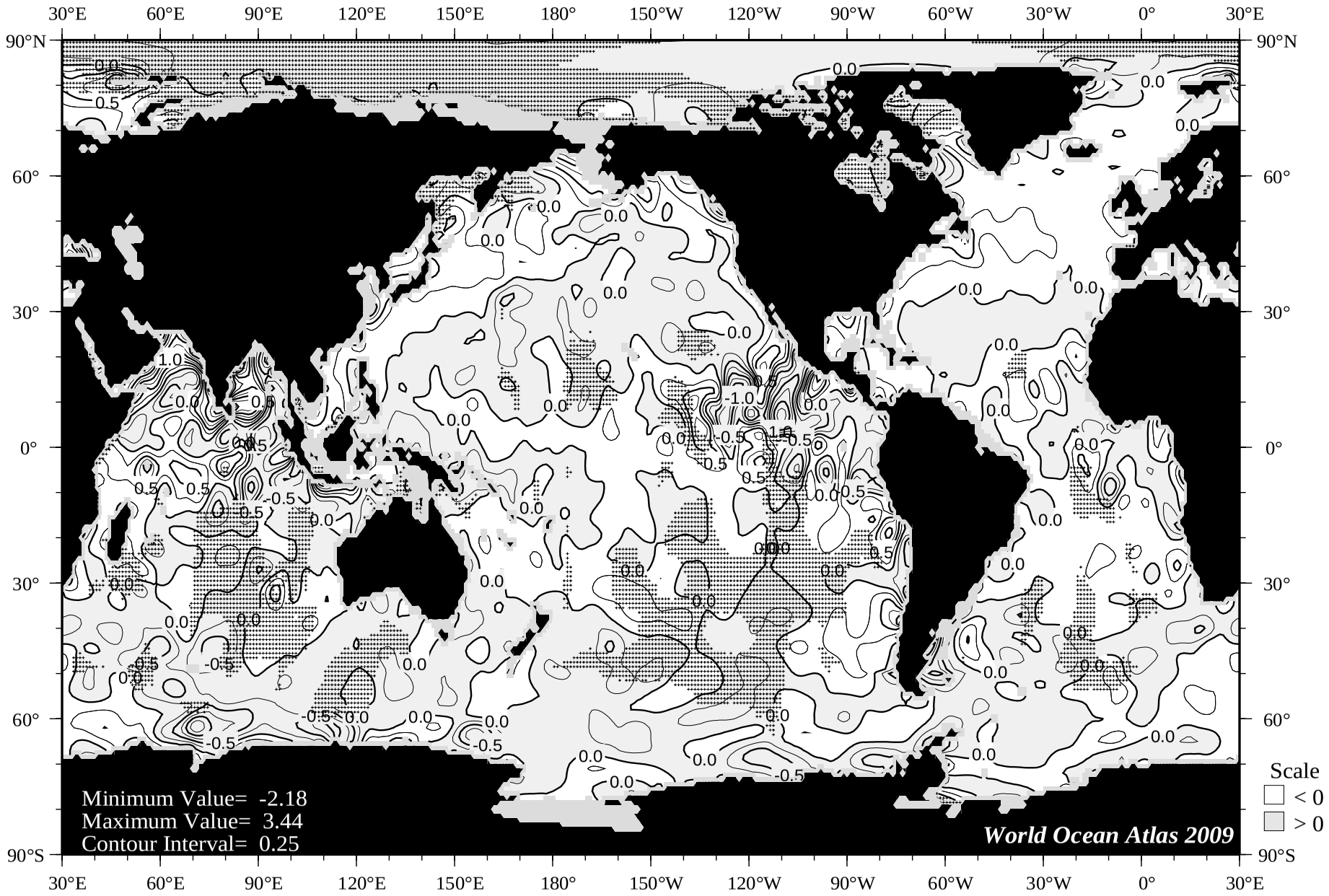

Fig C32 February minus annual oxygen [ml/l] at 75 m. depth.

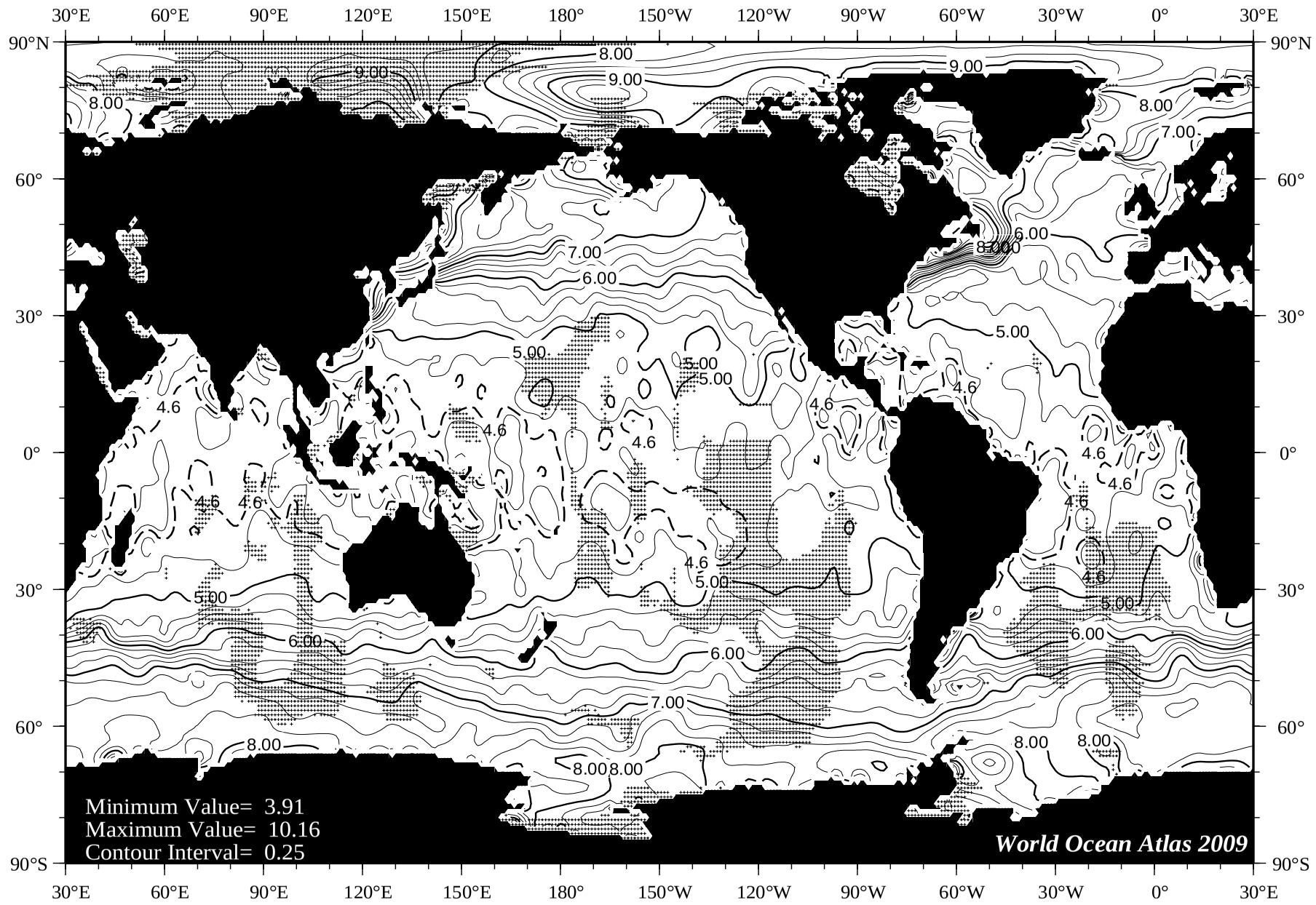

Fig C33 March mean oxygen [ml/l] at the surface.

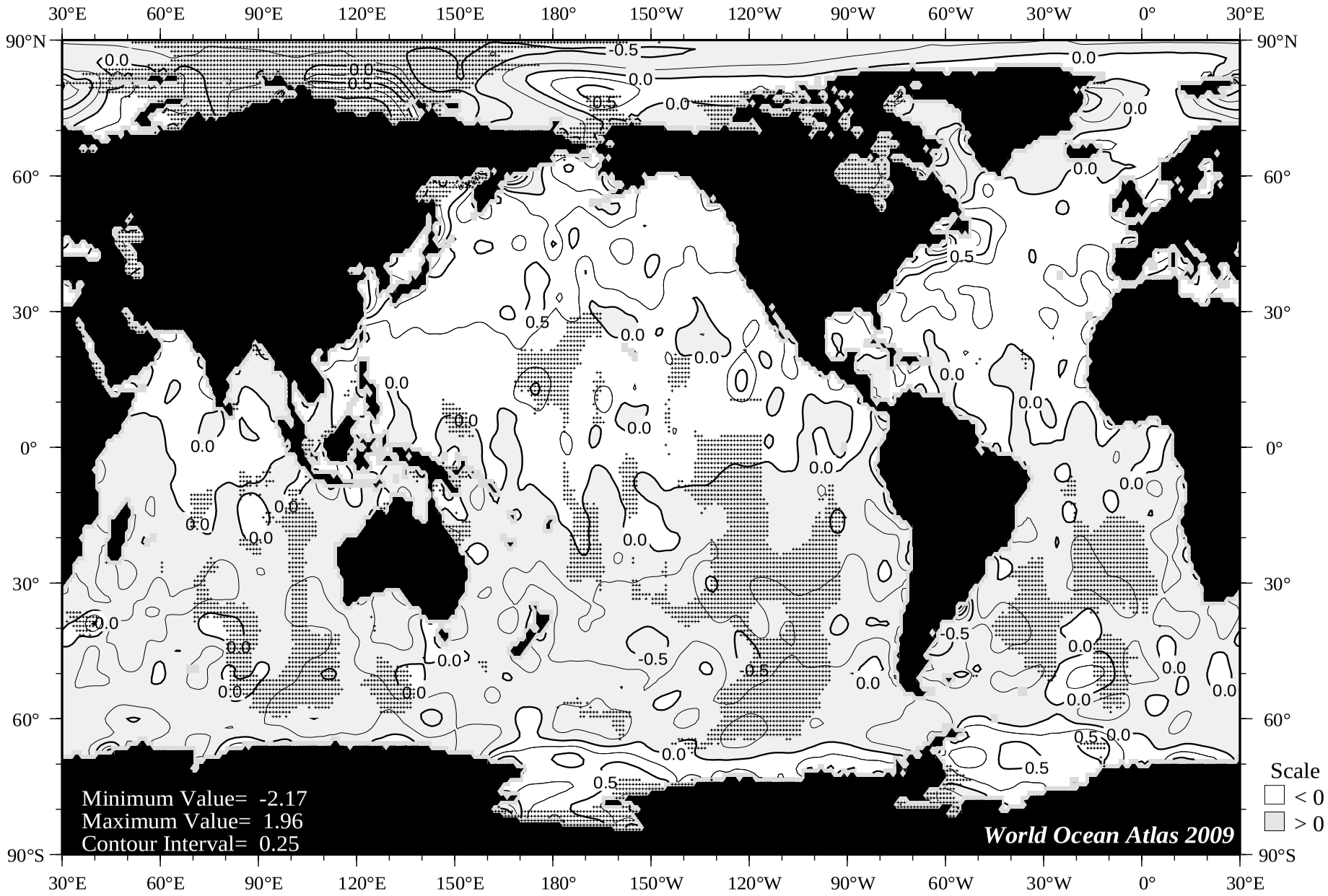

Fig C34 March minus annual oxygen [ml/l] at the surface.

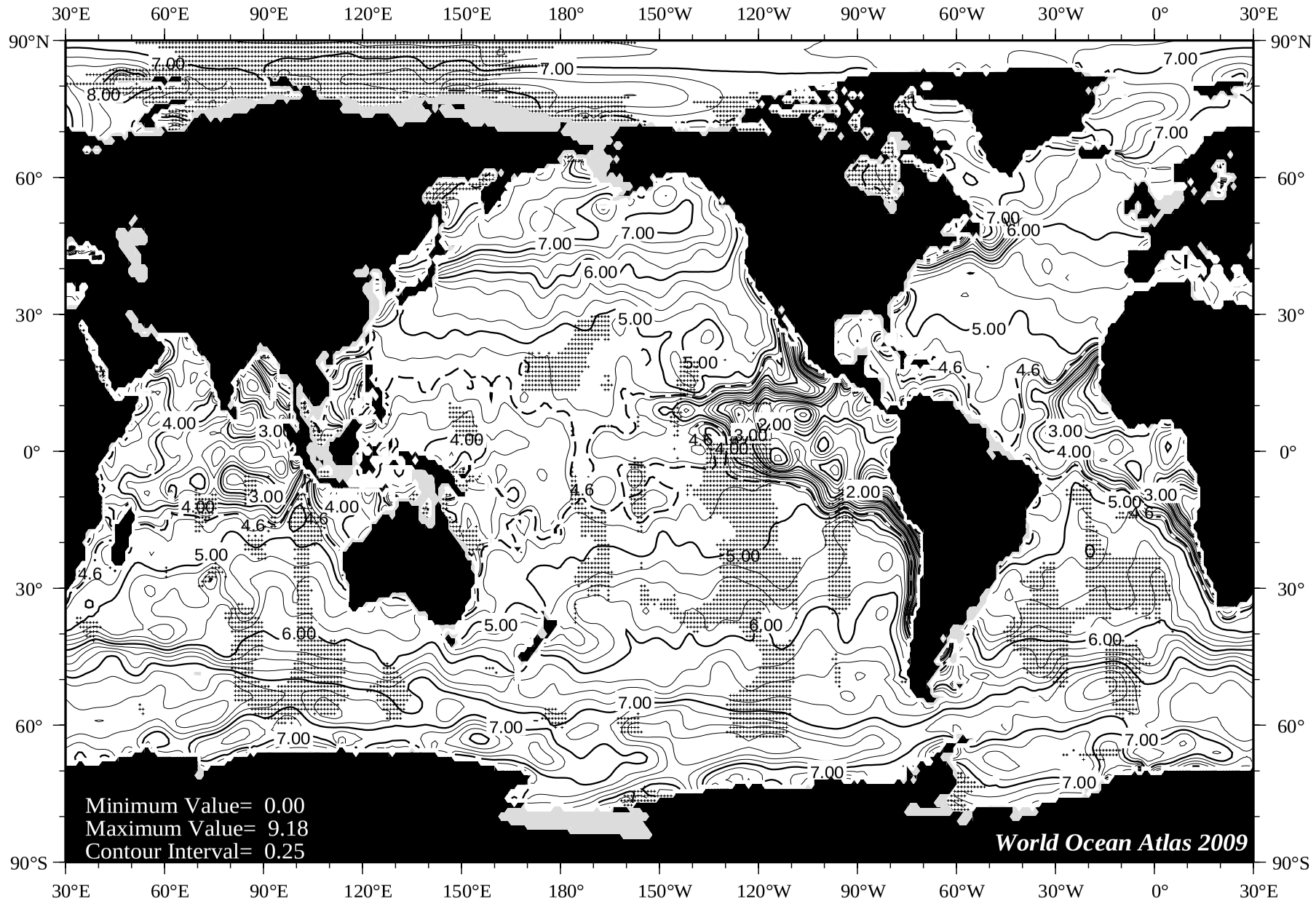

Fig C35 March mean oxygen [ml/l] at 75 m. depth.

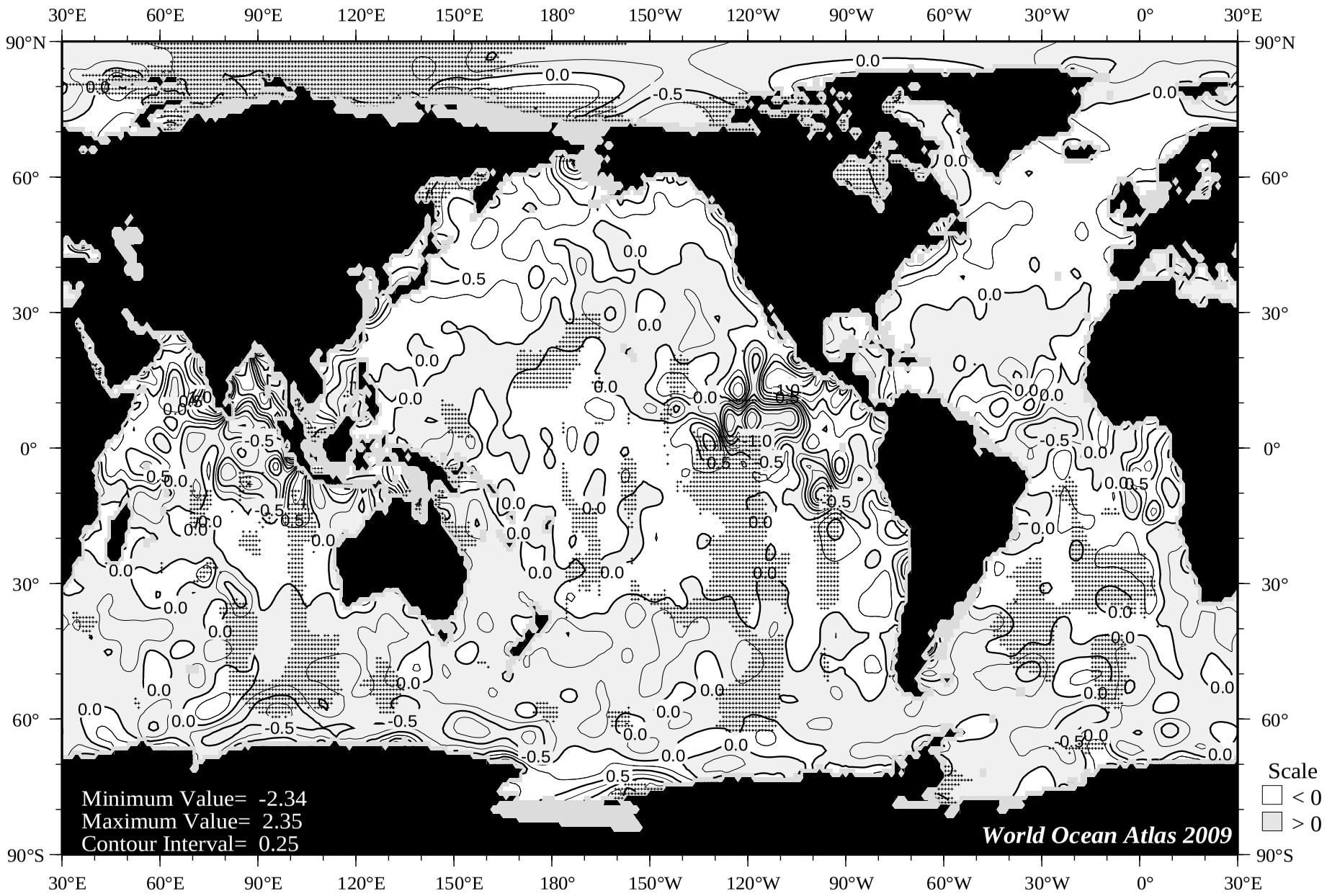

Fig C36 March minus annual oxygen [ml/l] at 75 m. depth.

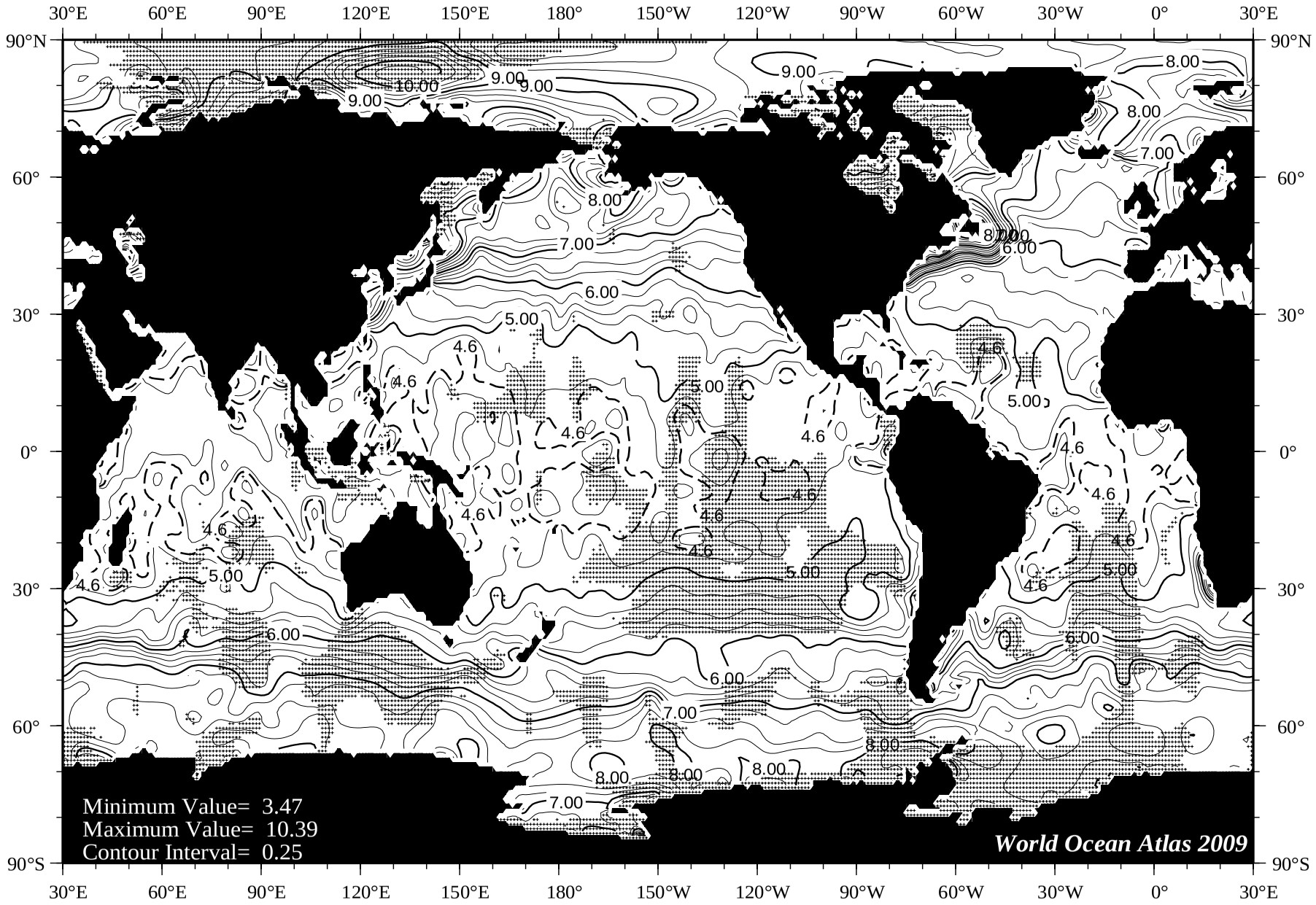

Fig C37 April mean oxygen [ml/l] at the surface.

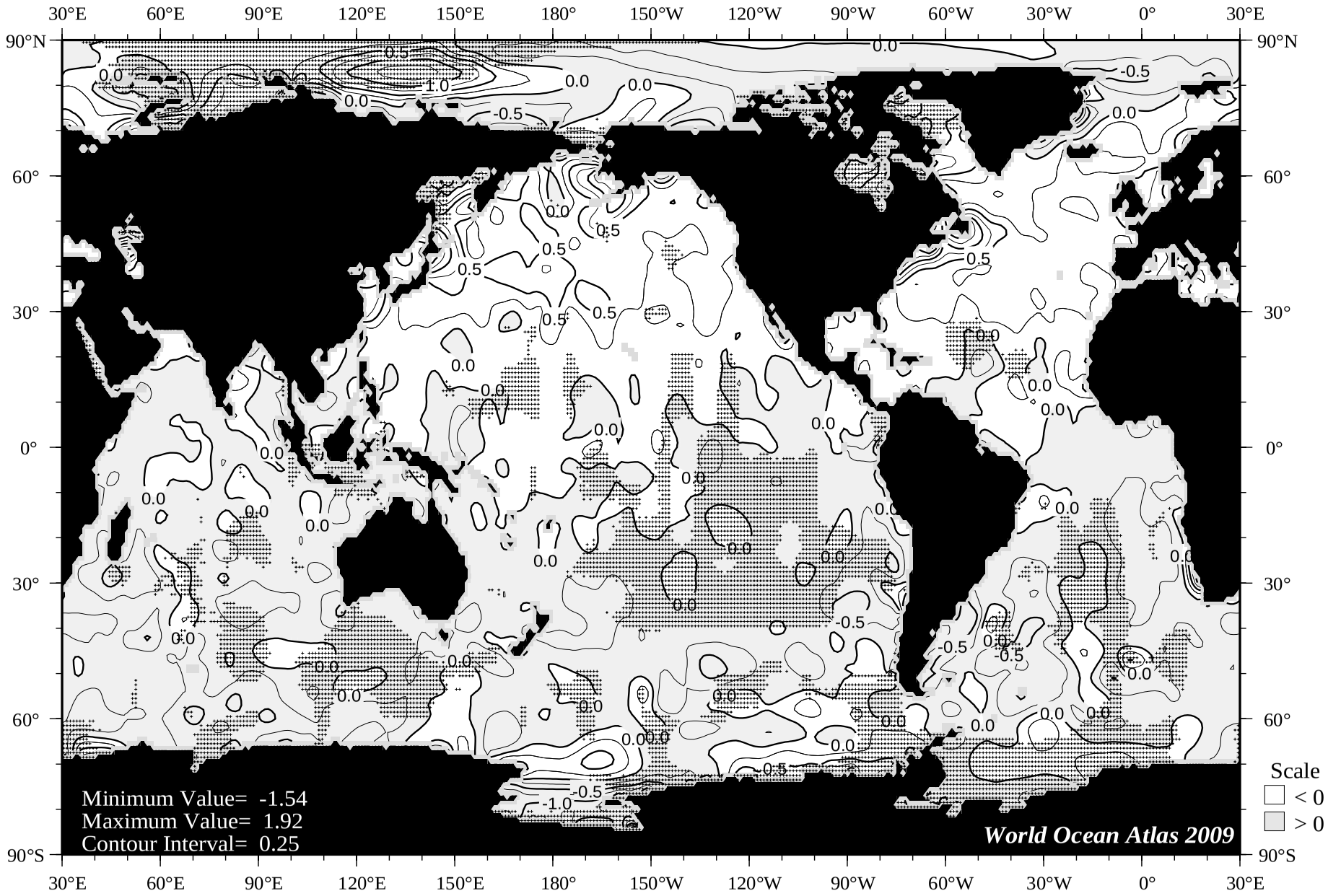

Fig C38 April minus annual oxygen [ml/l] at the surface.

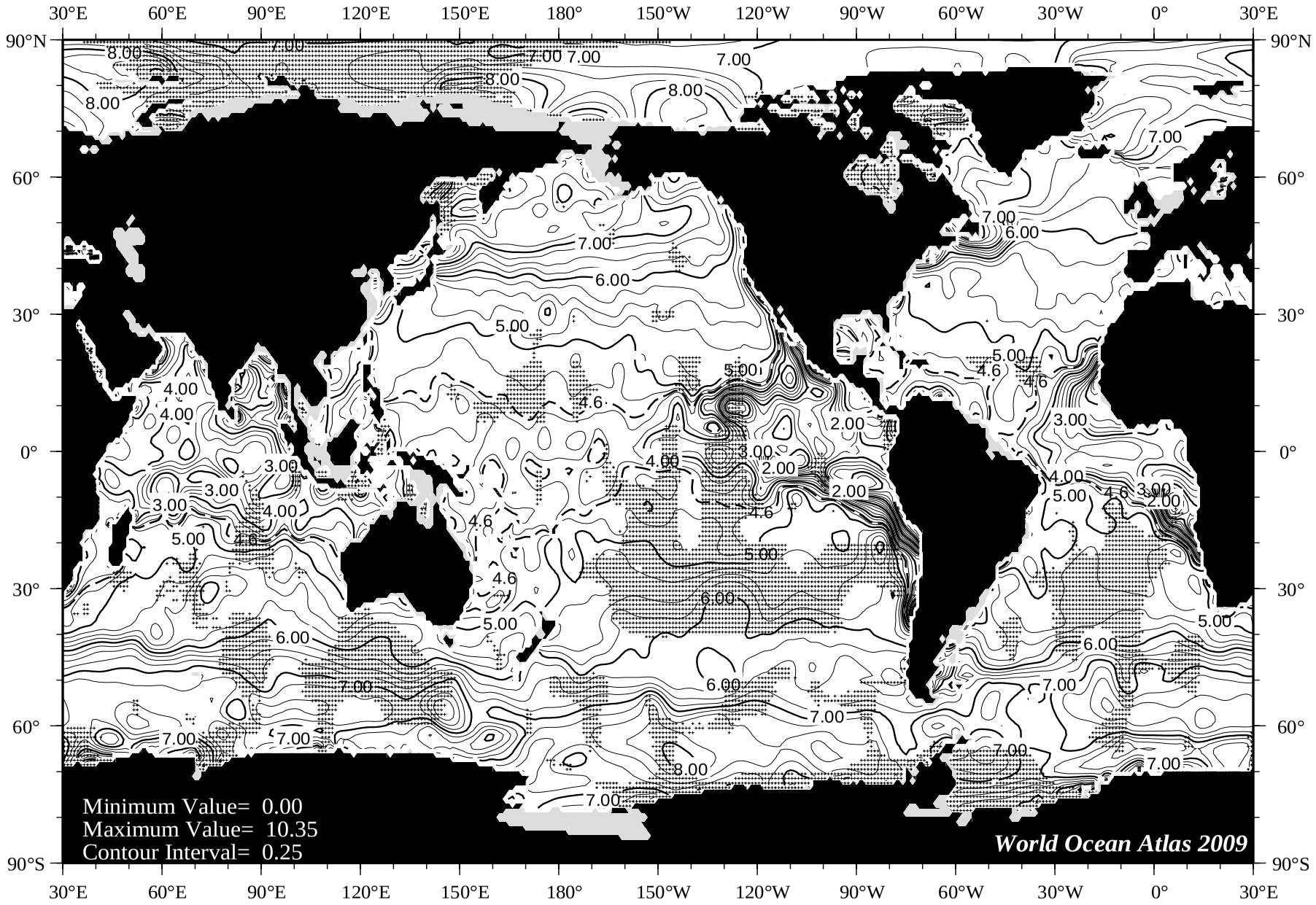

Fig C39 April mean oxygen [ml/l] at 75 m. depth.

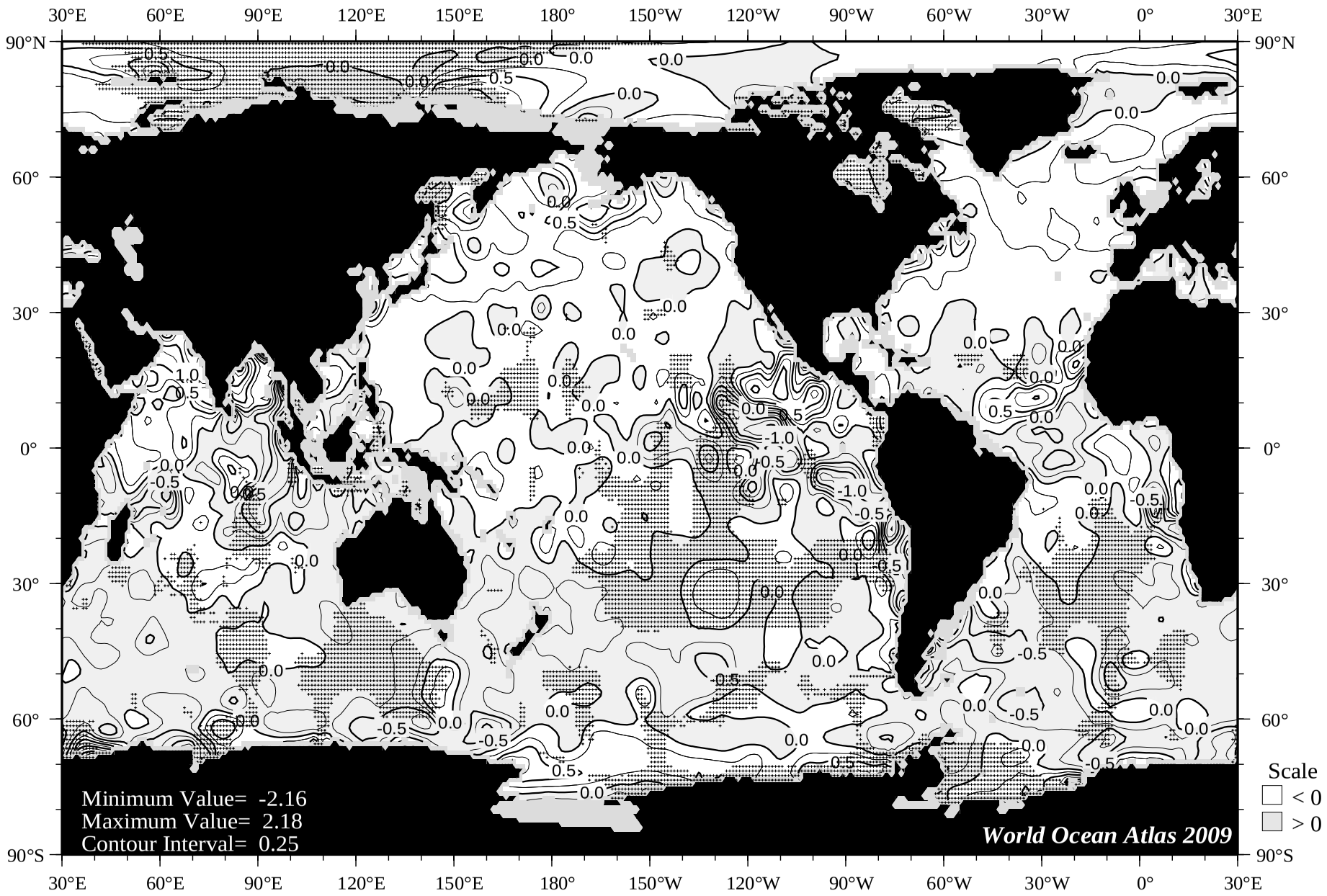

Fig C40 April minus annual oxygen [ml/l] at 75 m. depth.

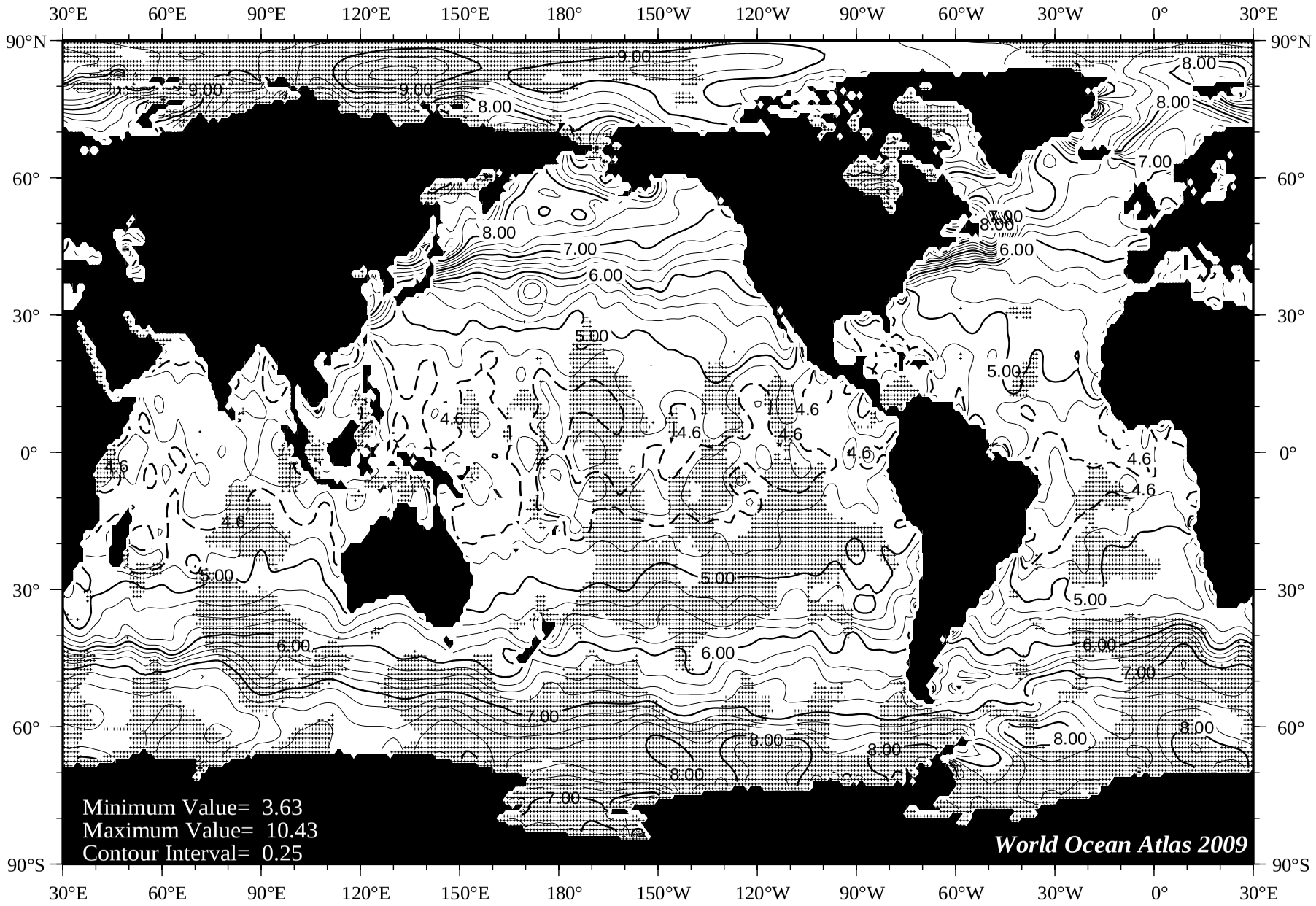

Fig C41 May mean oxygen [ml/l] at the surface.

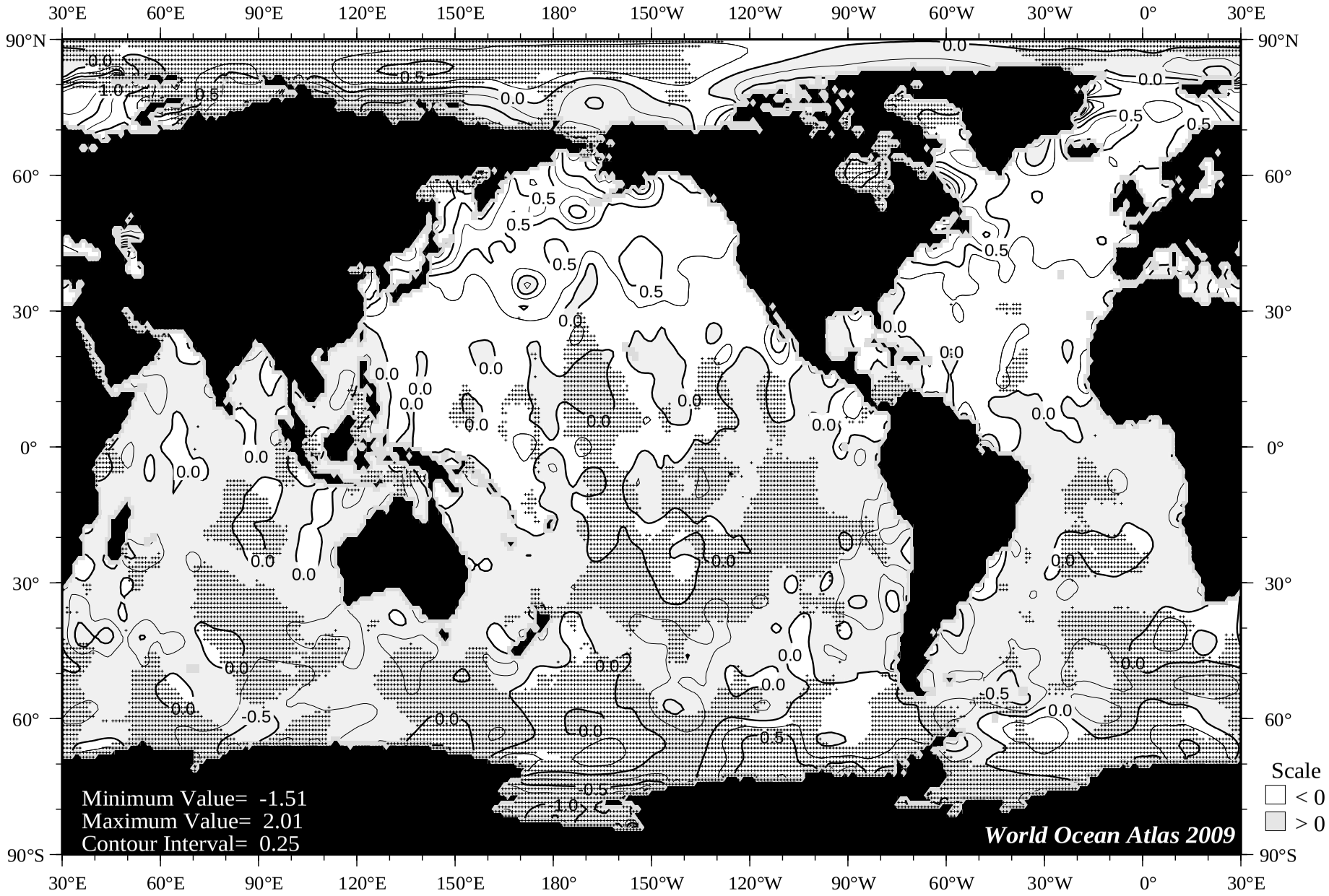

Fig C42 May minus annual oxygen [ml/l] at the surface.

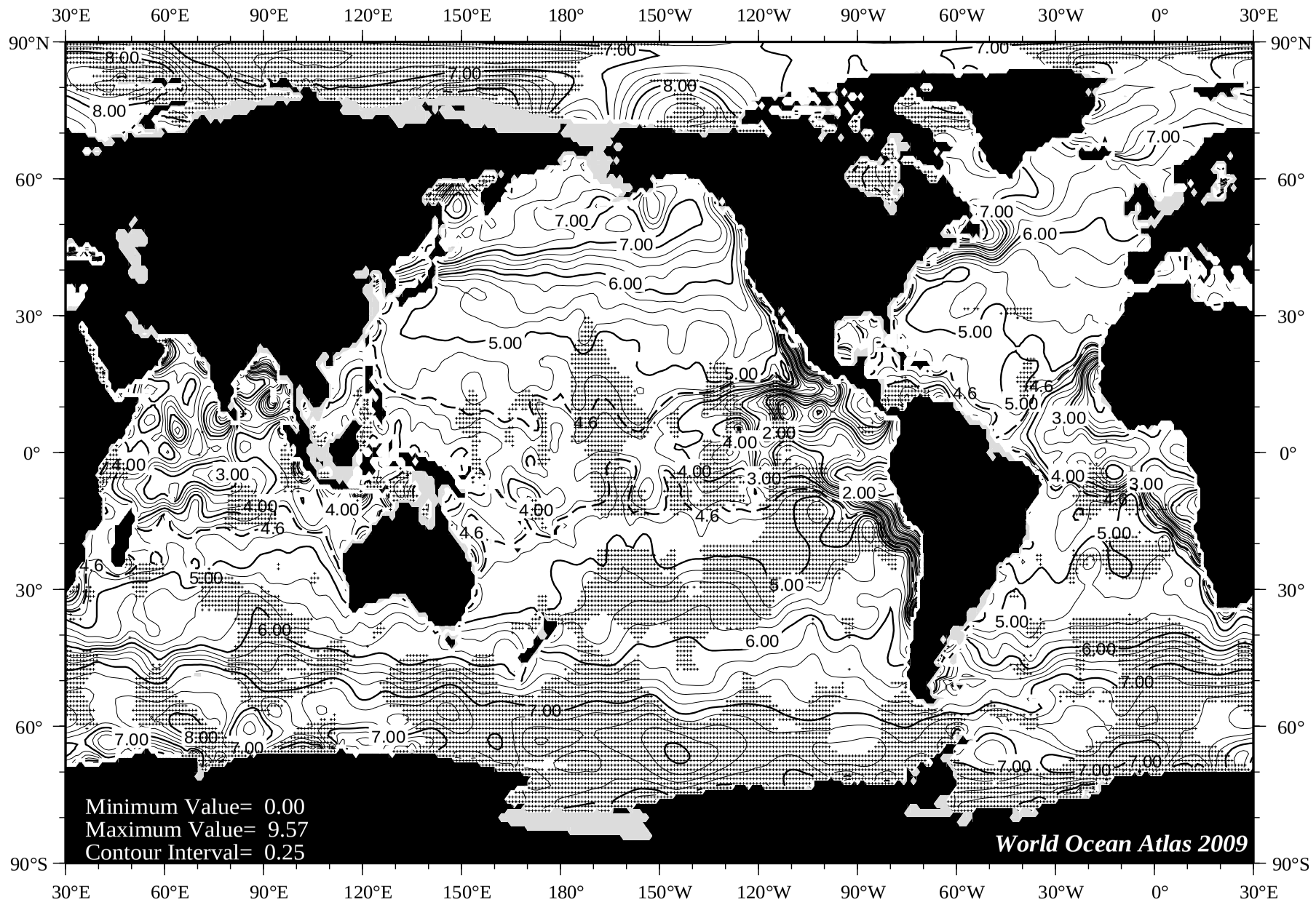

Fig C43 May mean oxygen [ml/l] at 75 m. depth.

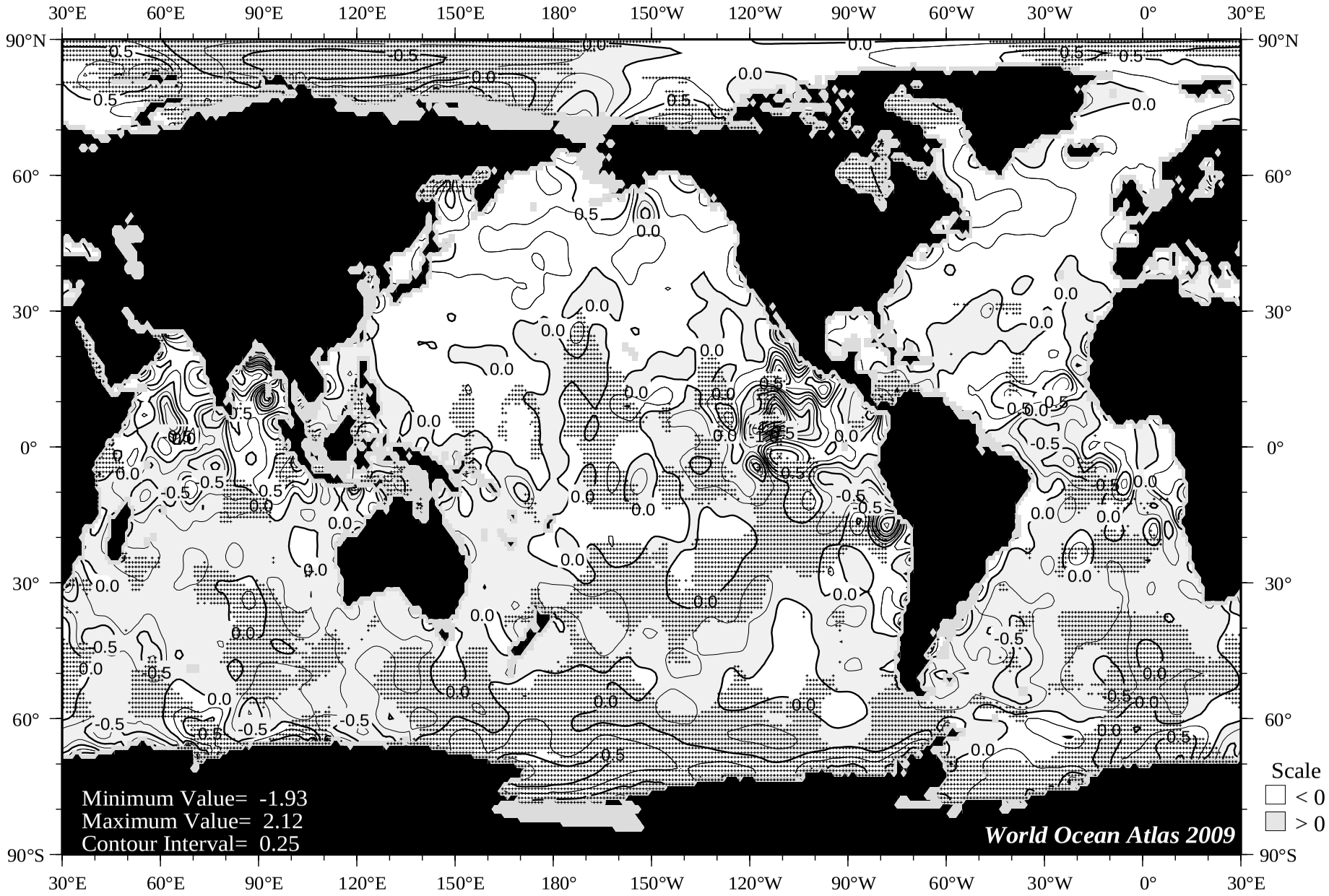

Fig C44 May minus annual oxygen [ml/l] at 75 m. depth.

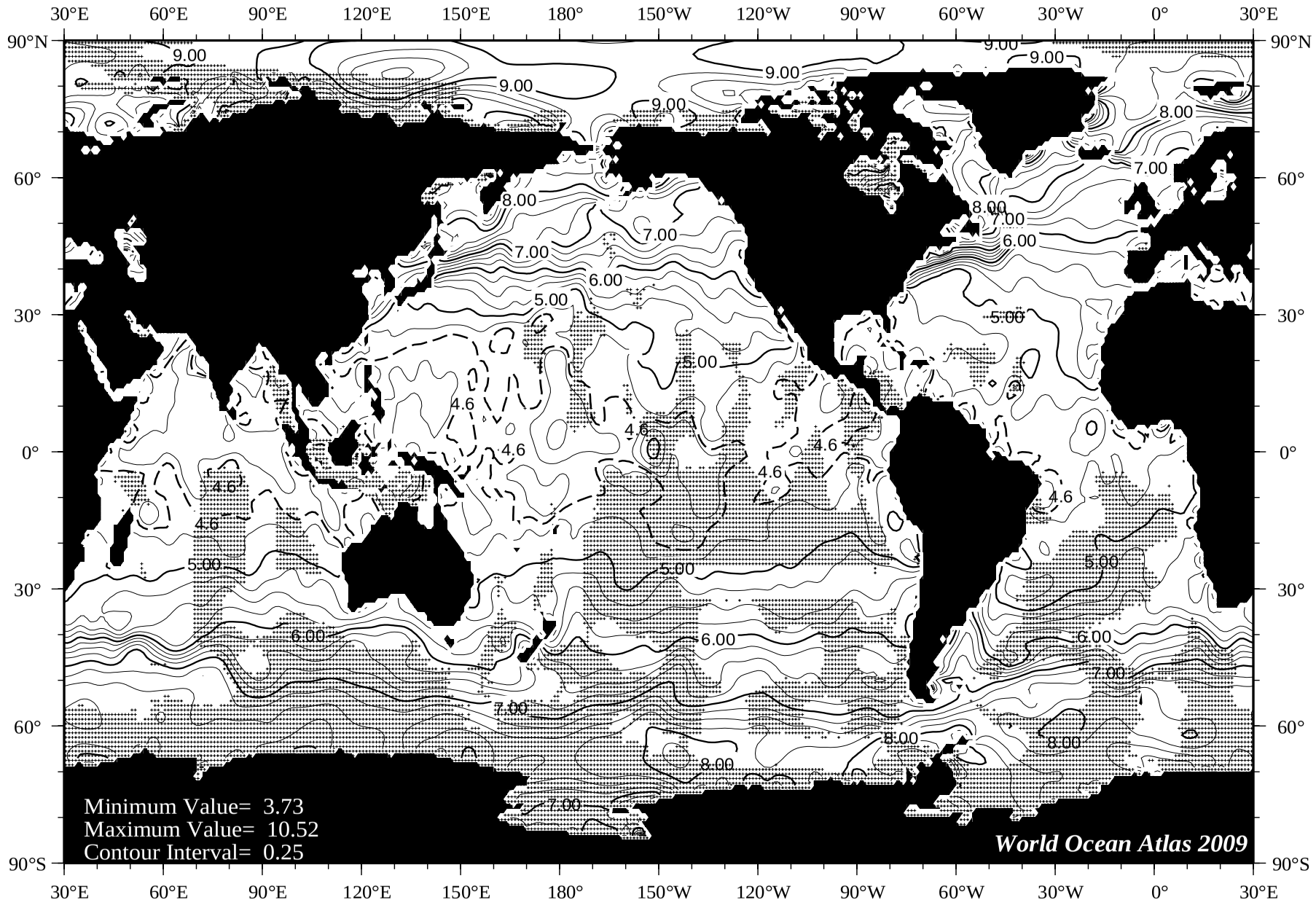

Fig C45 June mean oxygen [ml/l] at the surface.

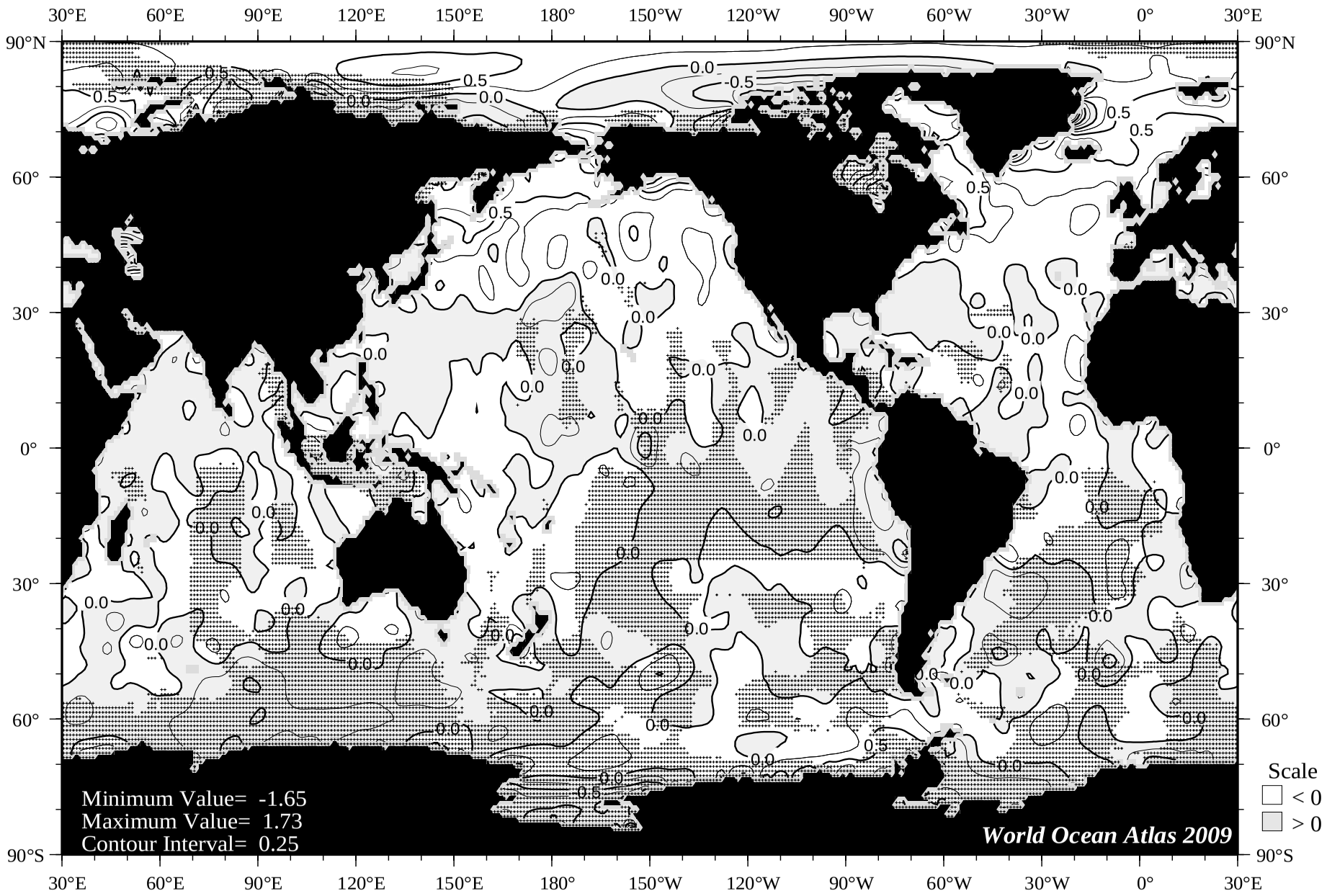

Fig C46 June minus annual oxygen [ml/l] at the surface.

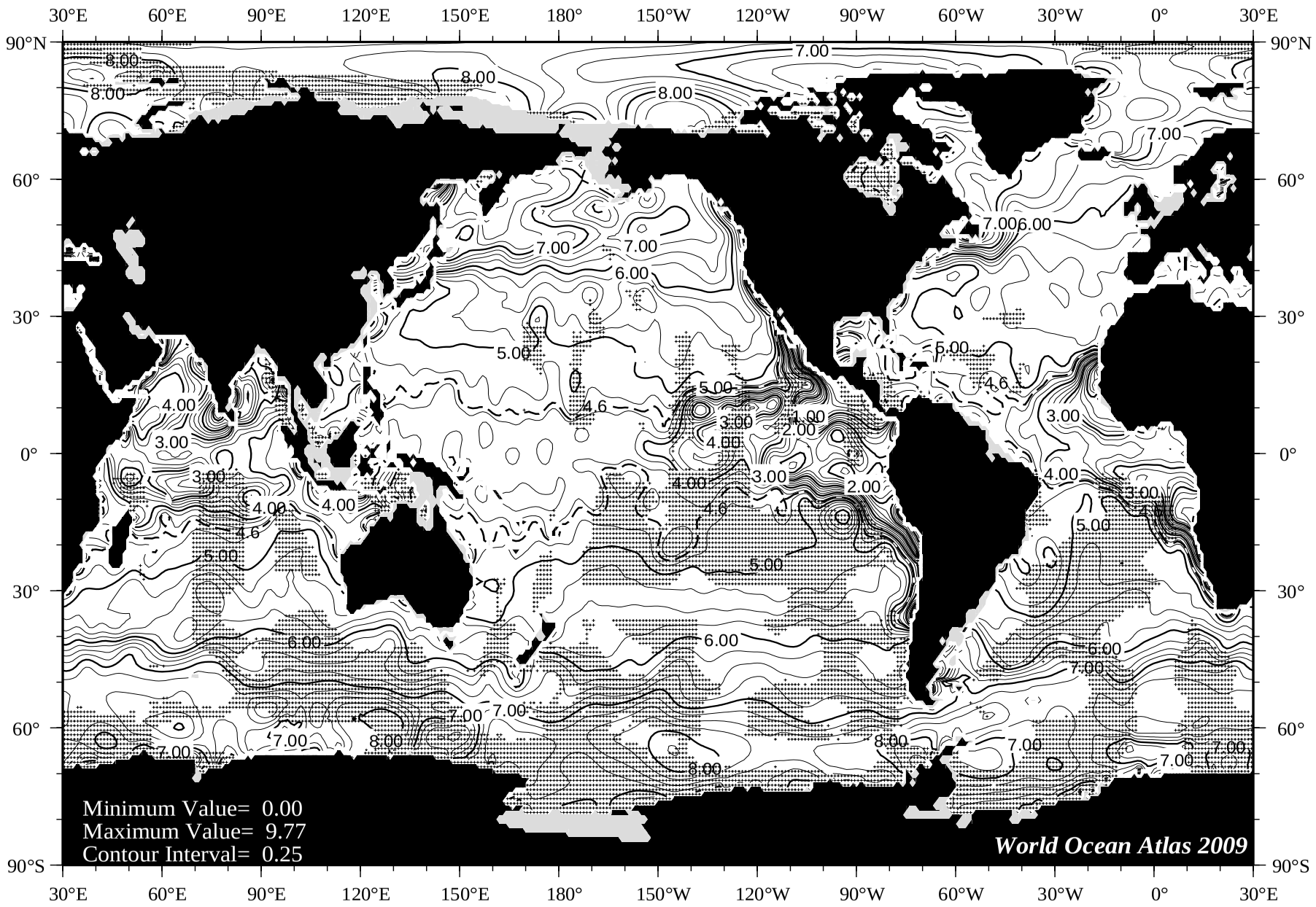

Fig C47 June mean oxygen [ml/l] at 75 m. depth.

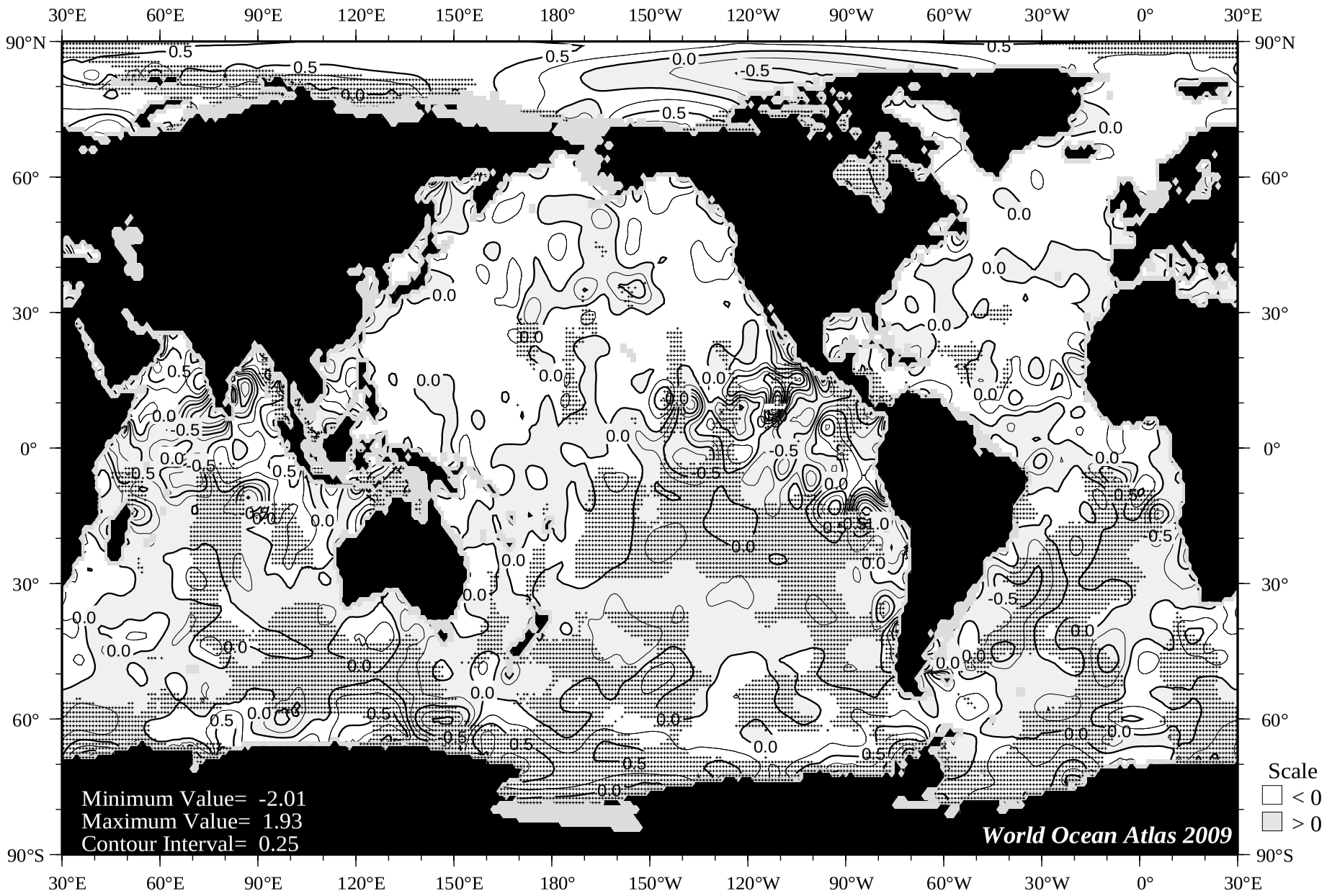

Fig C48 June minus annual oxygen [ml/l] at 75 m. depth.

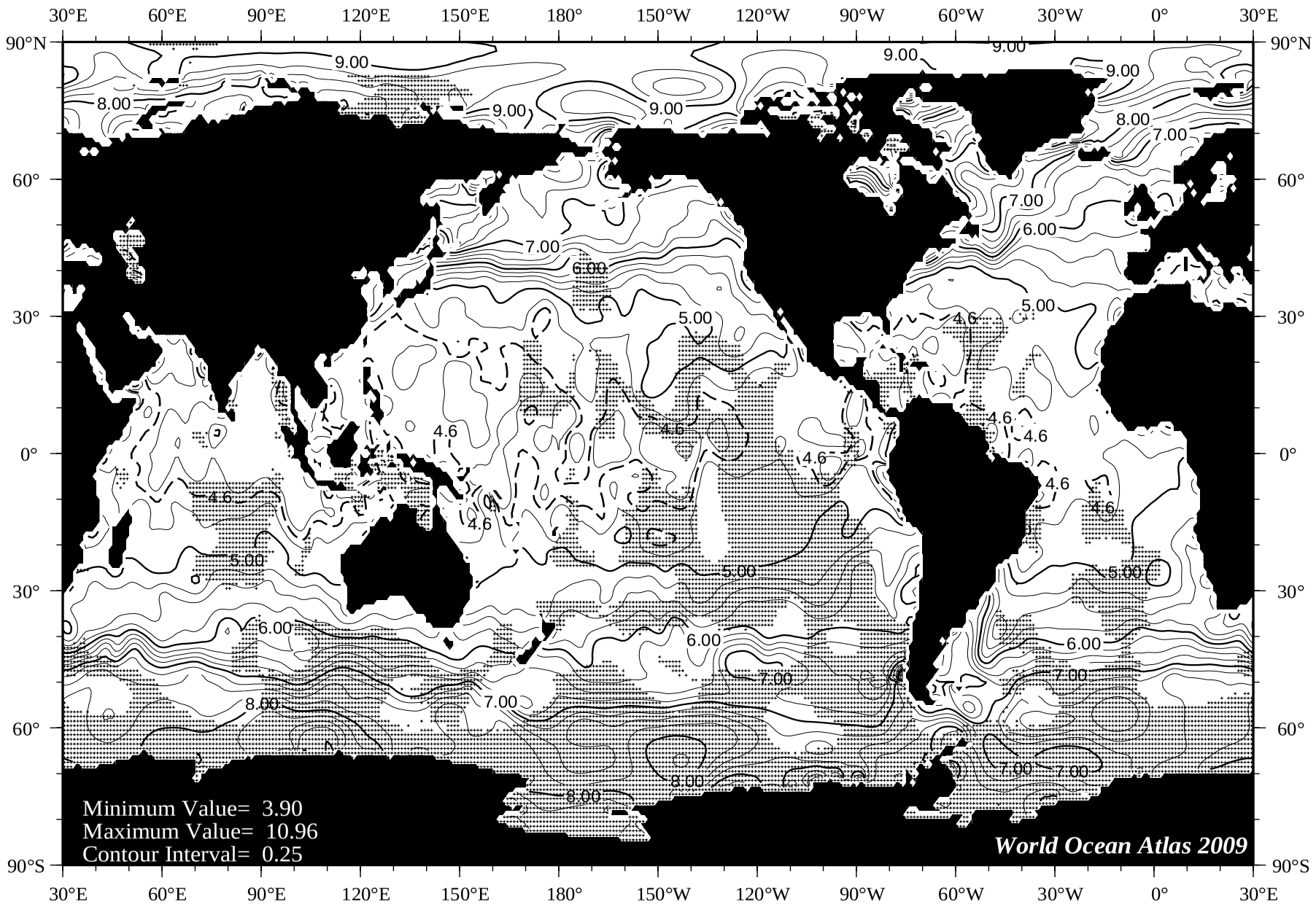

Fig C49 July mean oxygen [ml/l] at the surface.

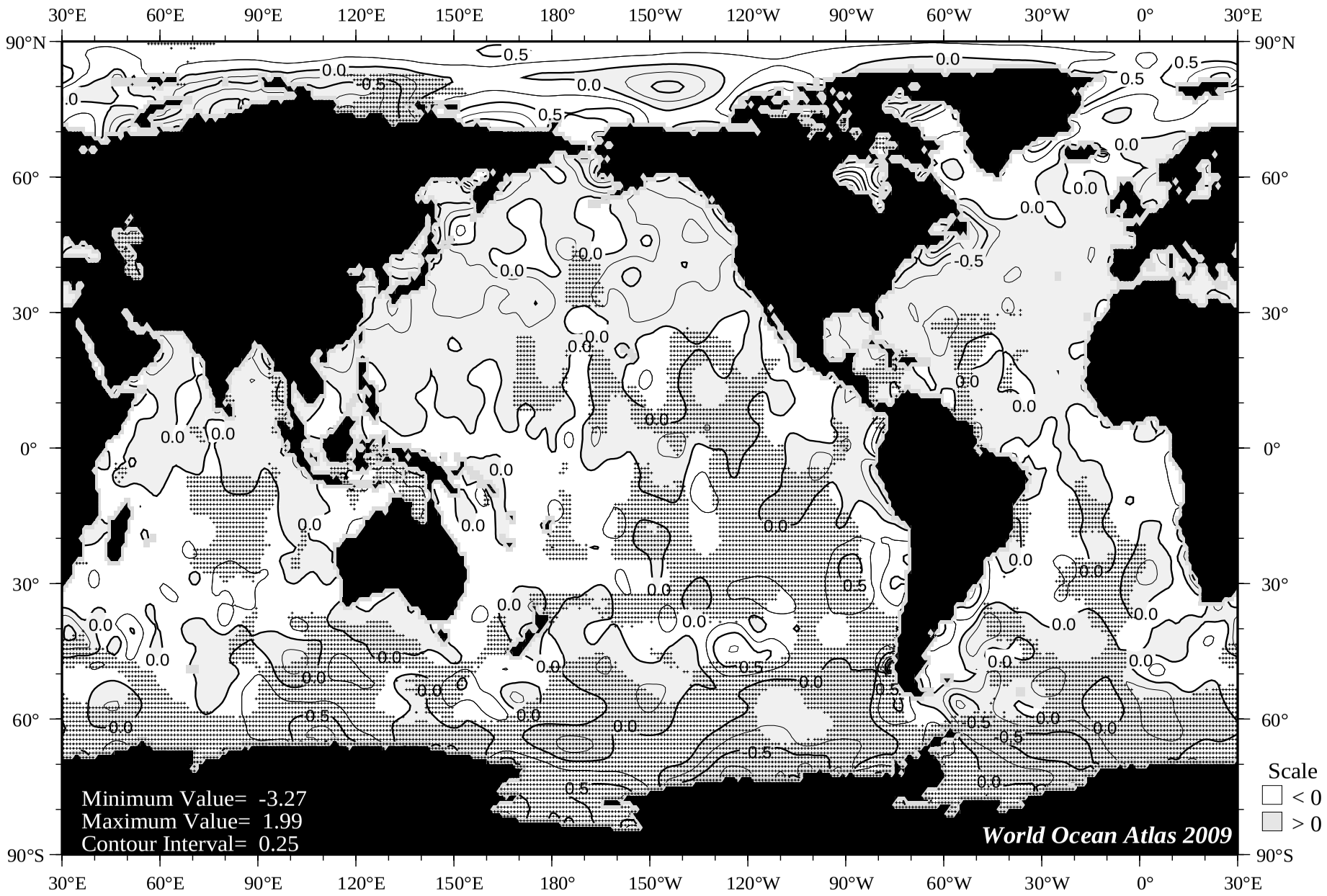

Fig C50 July minus annual oxygen [ml/l] at the surface.

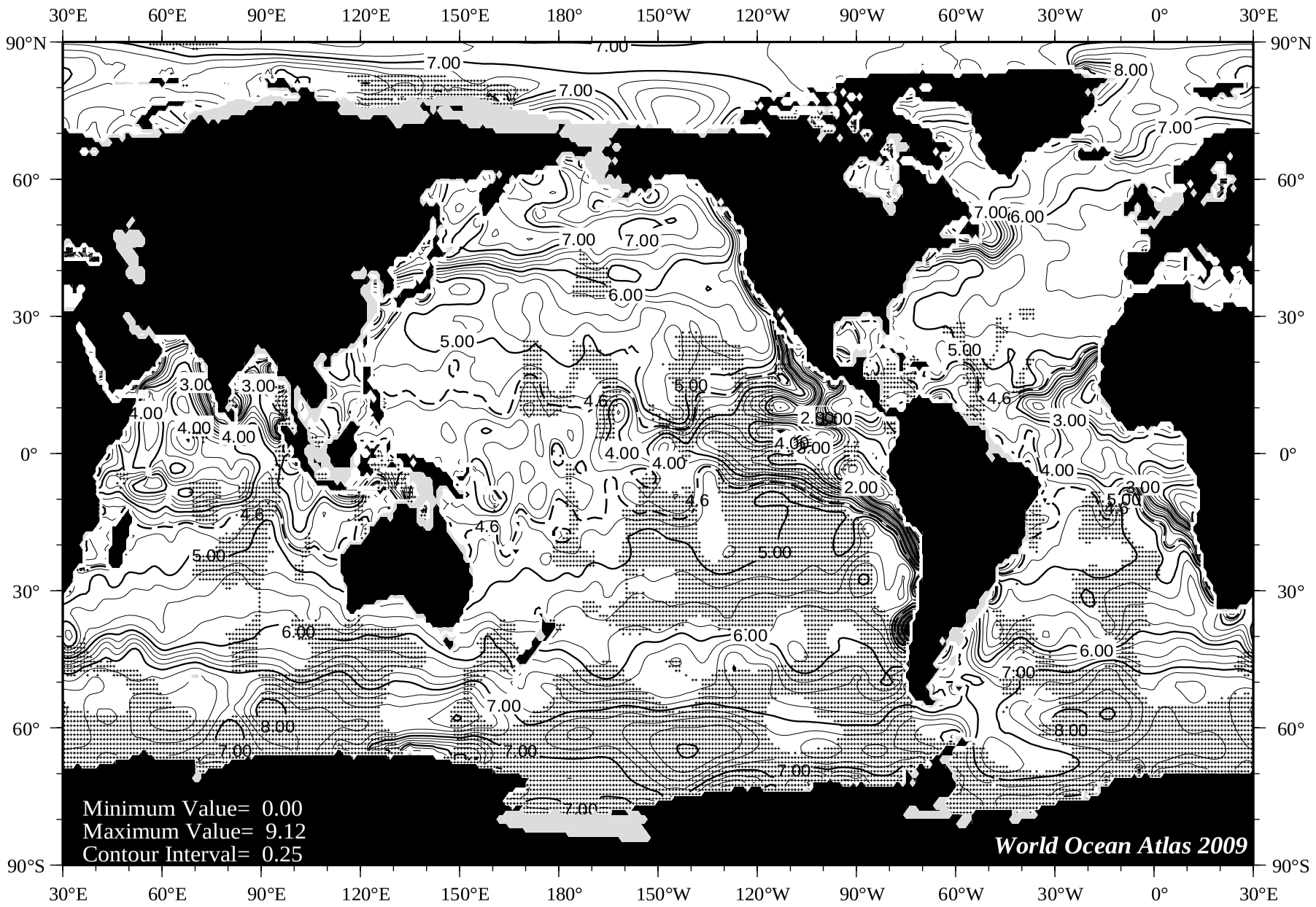

Fig C51 July mean oxygen [ml/l] at 75 m. depth.

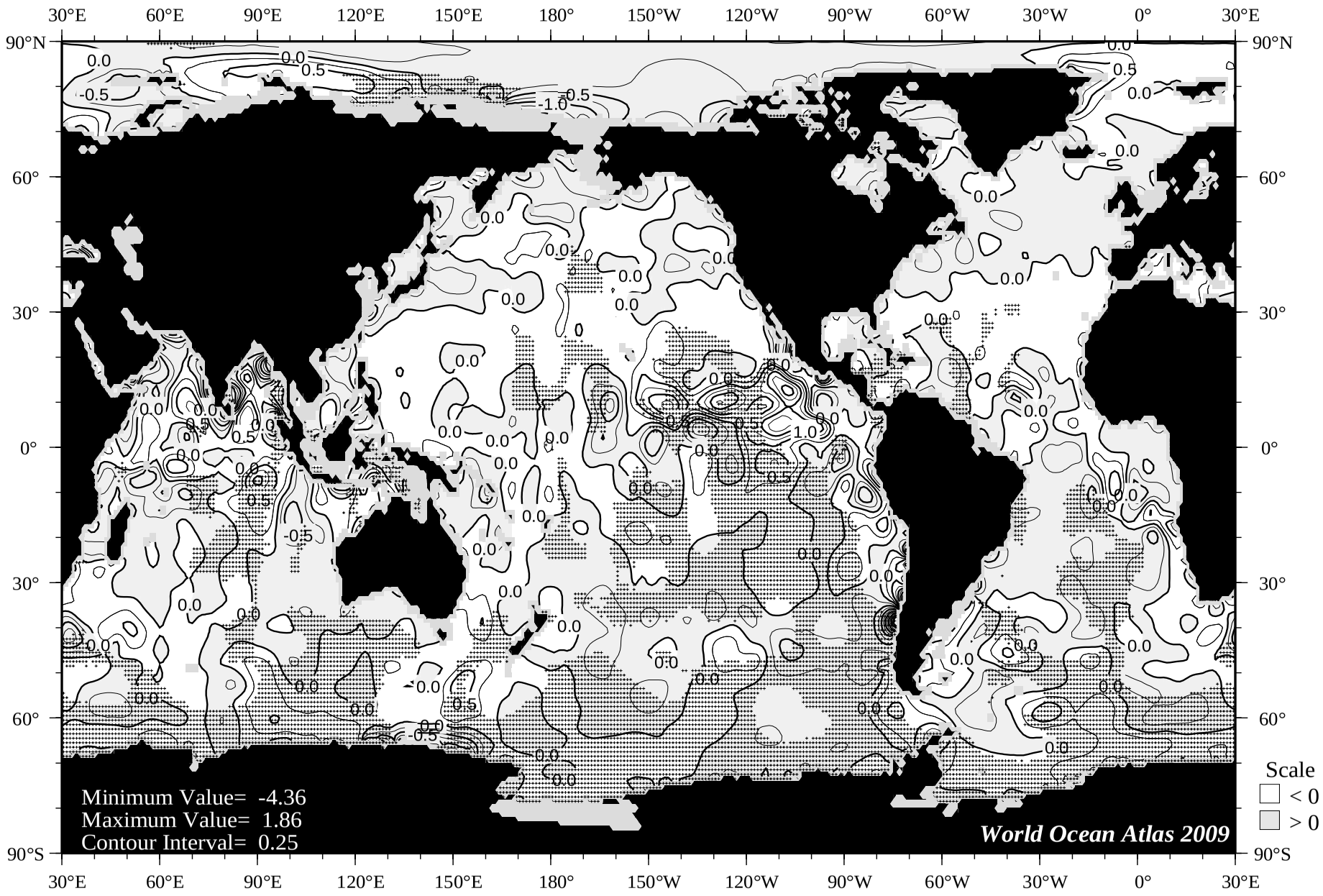

Fig C52 July minus annual oxygen [ml/l] at 75 m. depth.

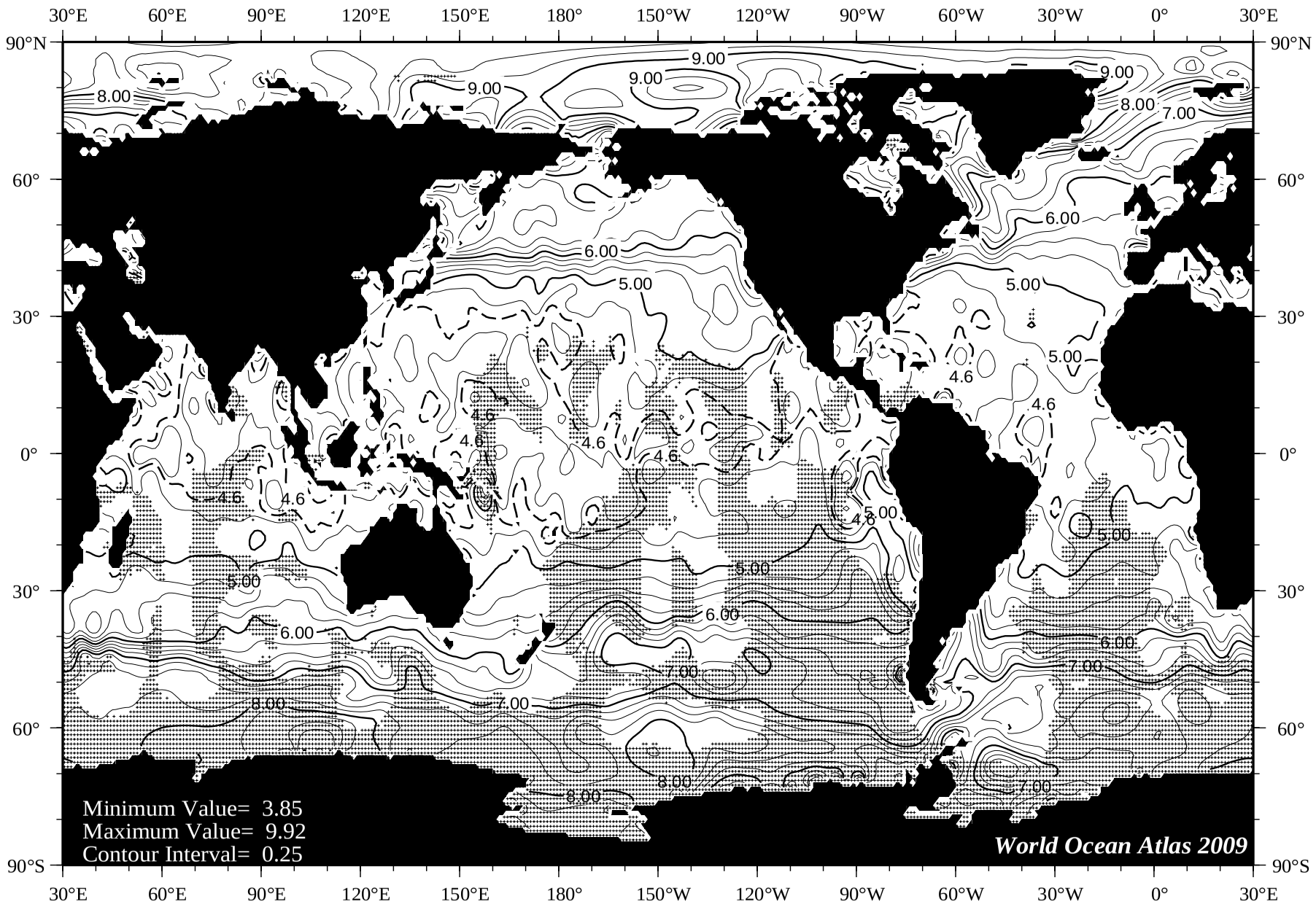

Fig C53 August mean oxygen [ml/l] at the surface.

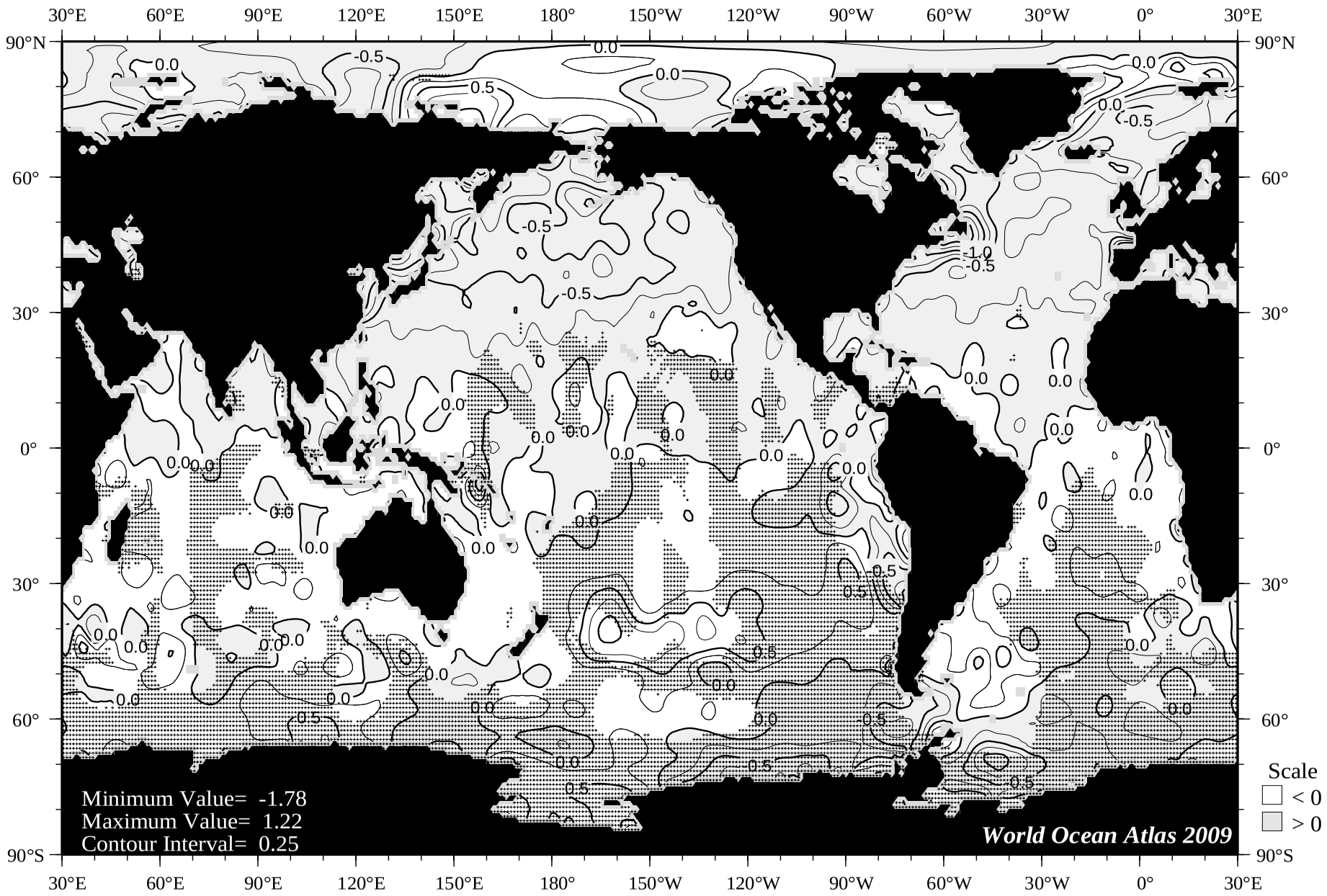

Fig C54 August minus annual oxygen [ml/l] at the surface.

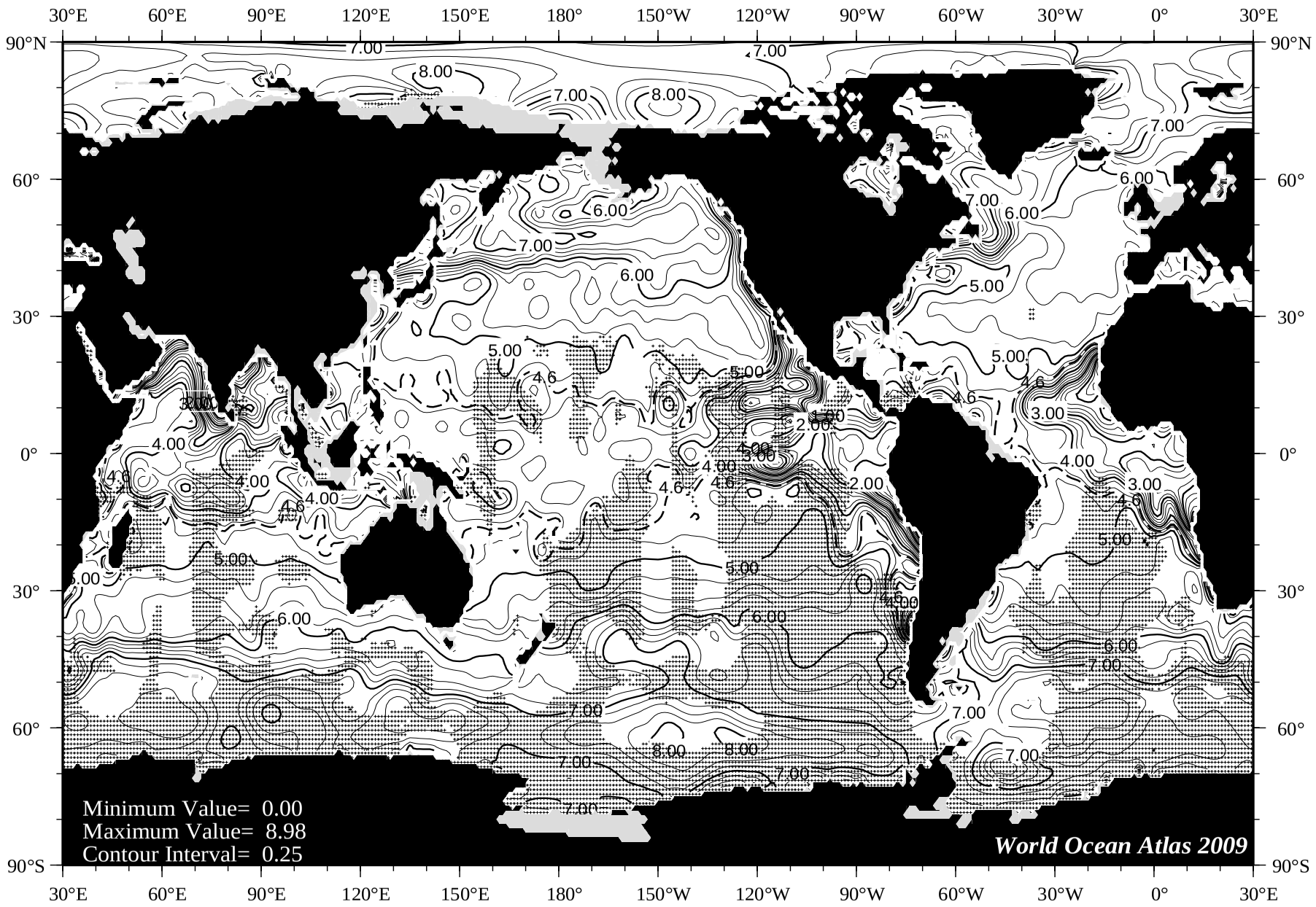

Fig C55 August mean oxygen [ml/l] at 75 m. depth.

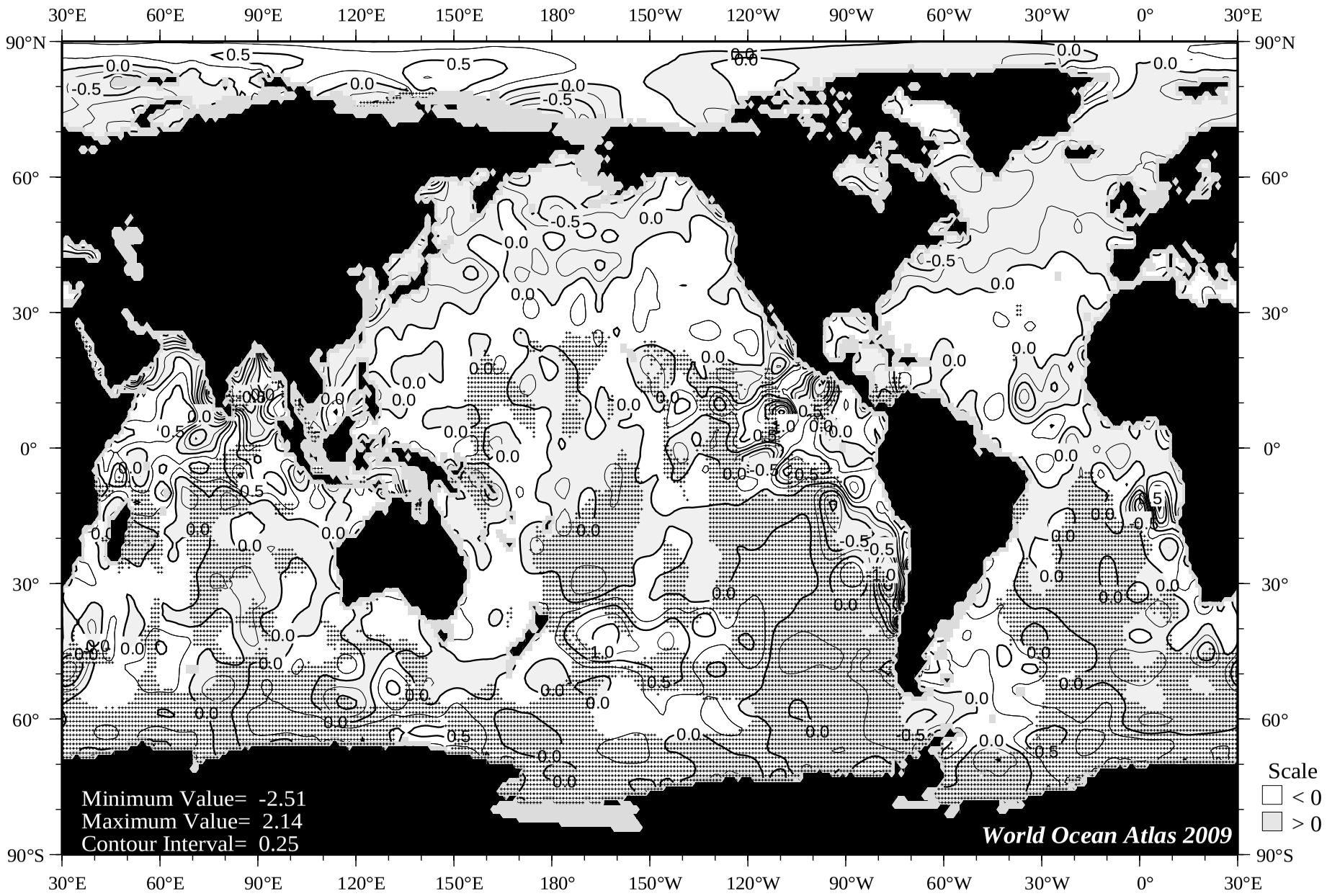

Fig C56 August minus annual oxygen [ml/l] at 75 m. depth.

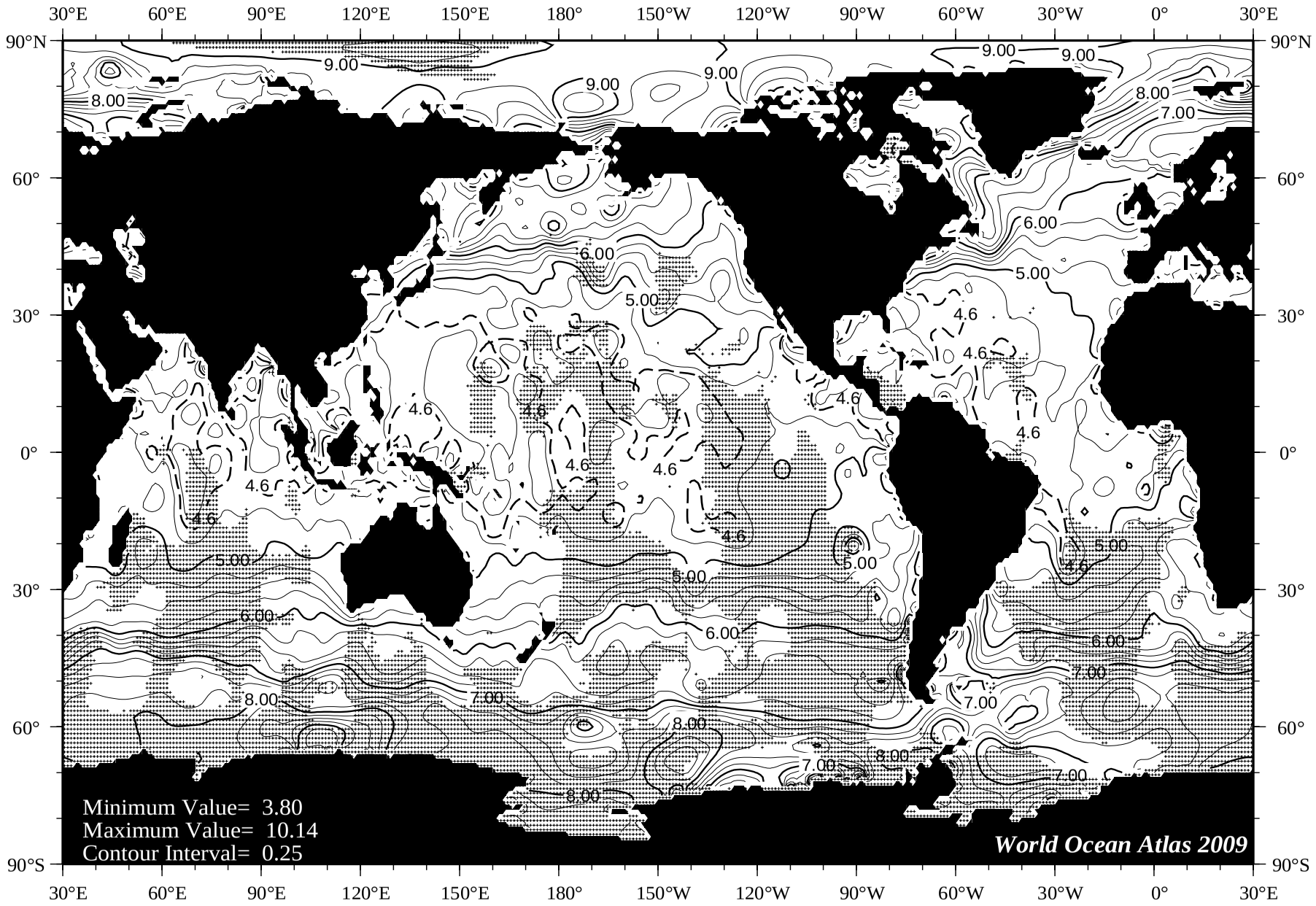

Fig C57 September mean oxygen [ml/l] at the surface.

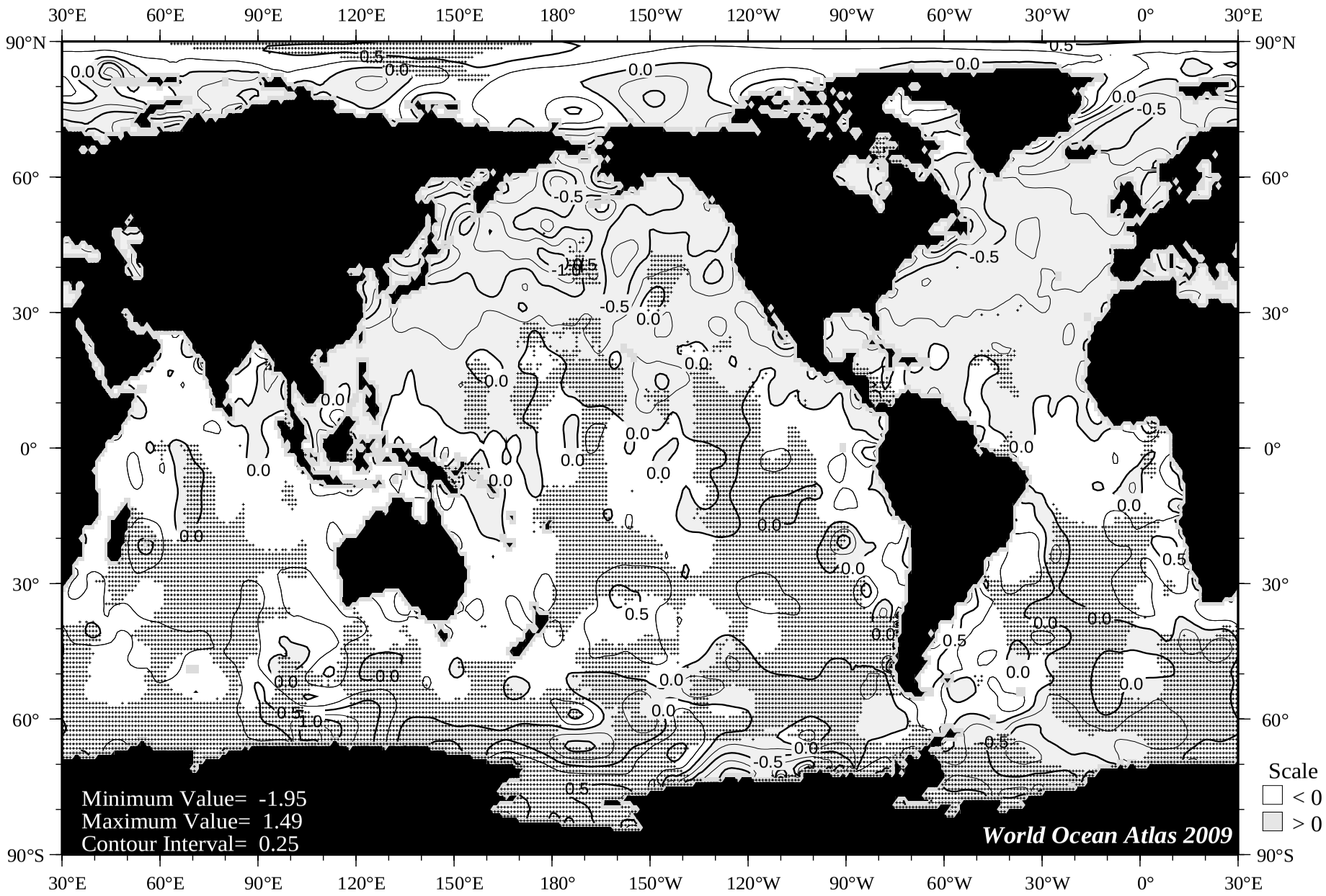

Fig C58 September minus annual oxygen [ml/l] at the surface.

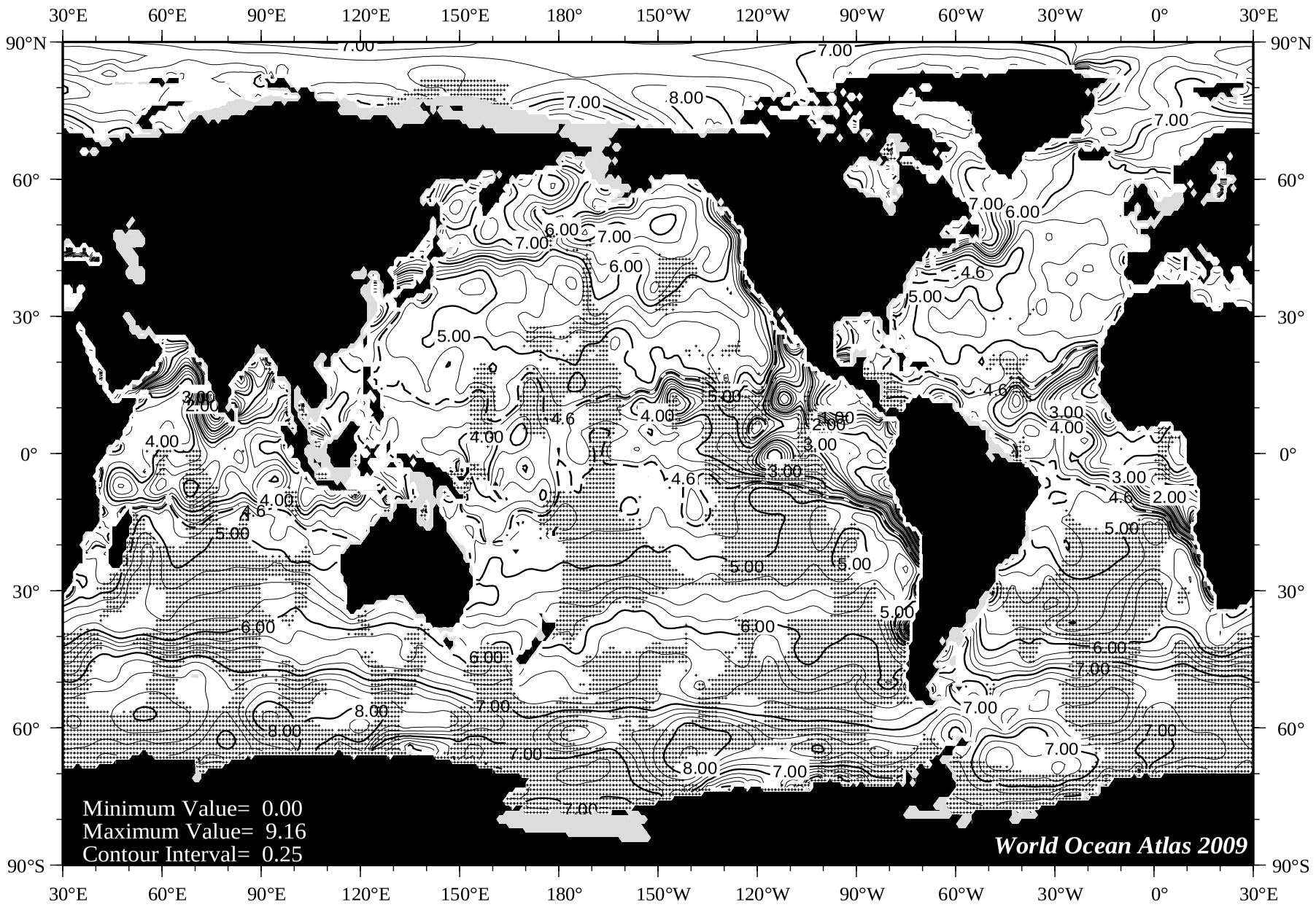

Fig C59 September mean oxygen [ml/l] at 75 m. depth.

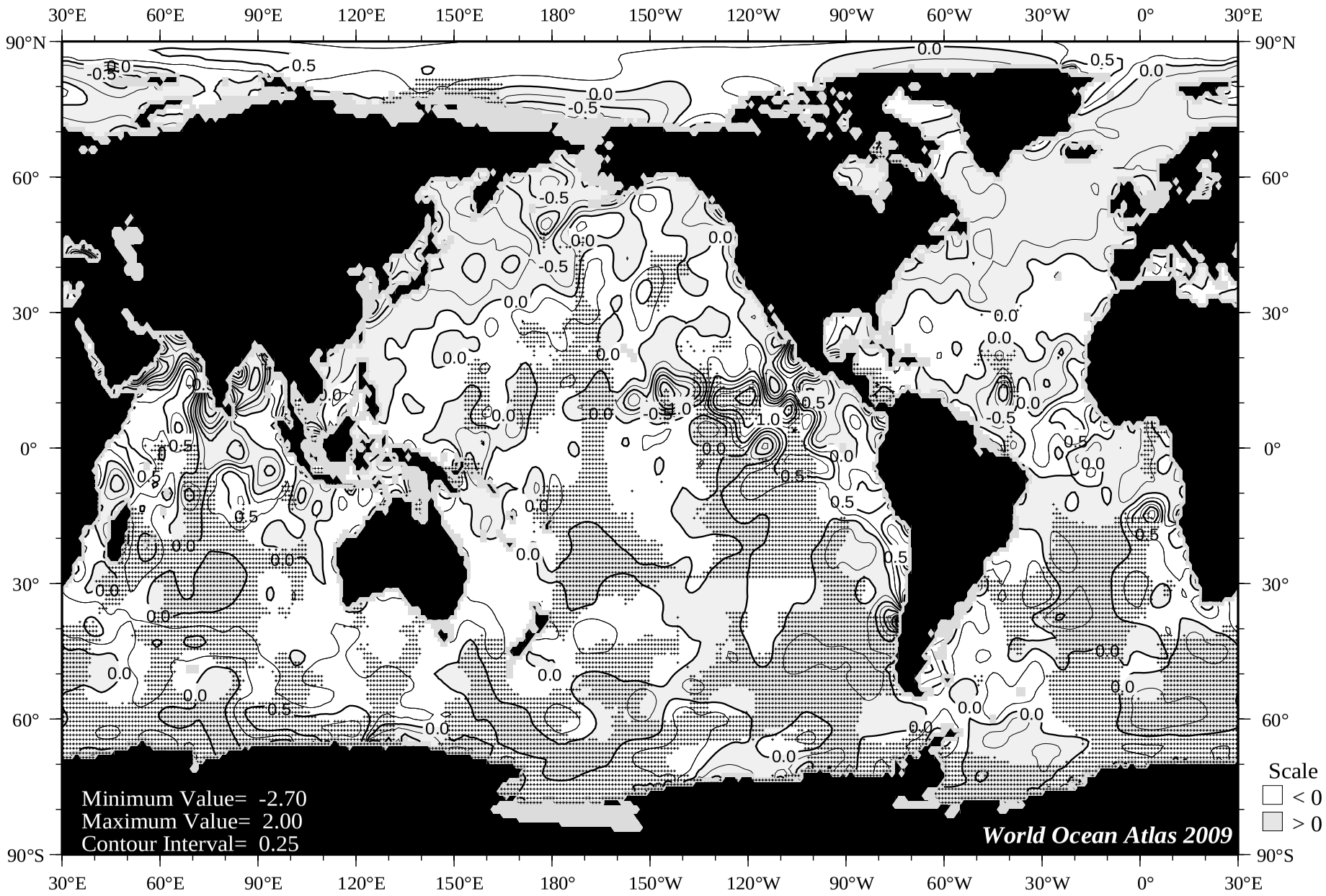

Fig C60 September minus annual oxygen [ml/l] at 75 m. depth.

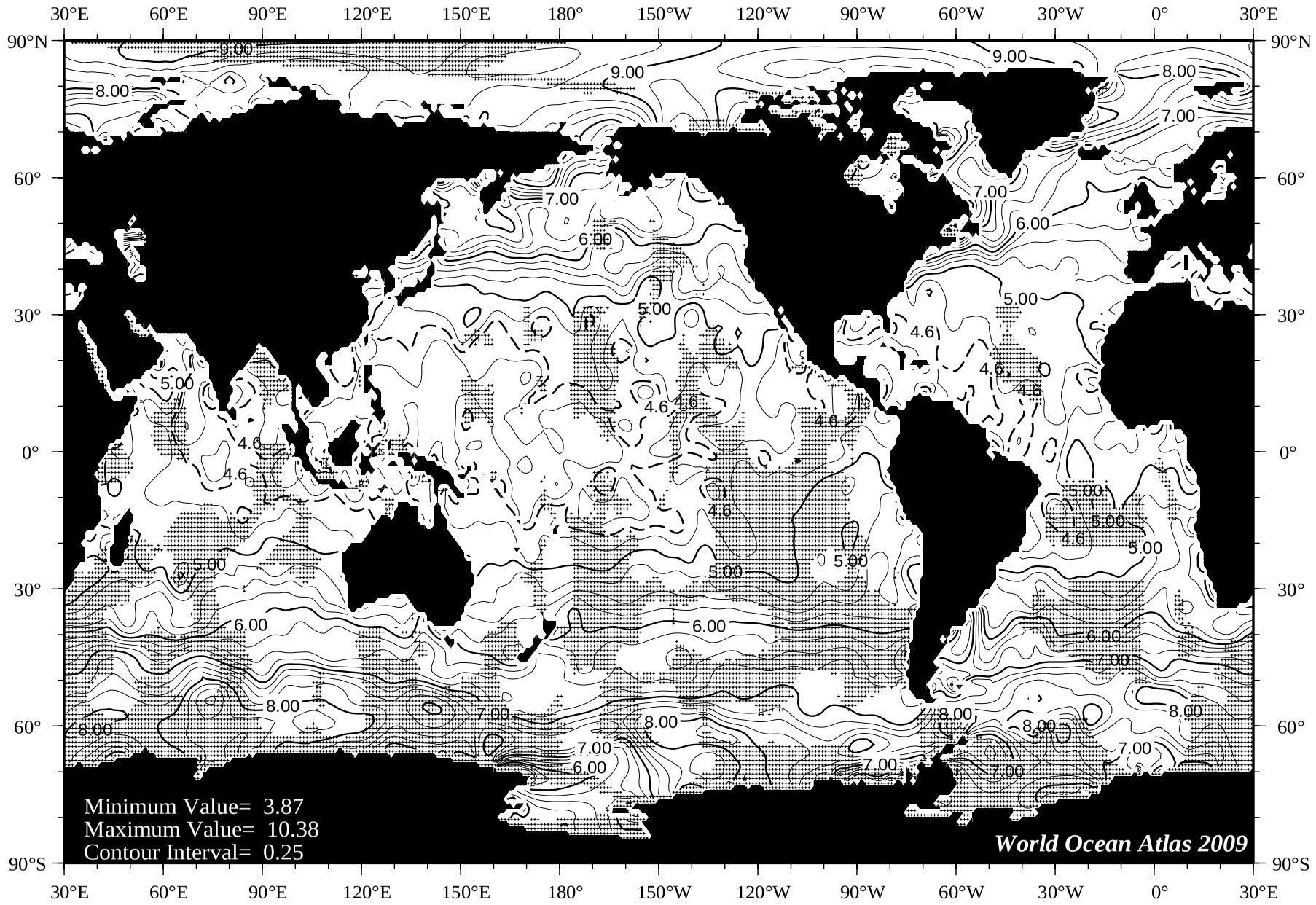

Fig C61 October mean oxygen [ml/l] at the surface.

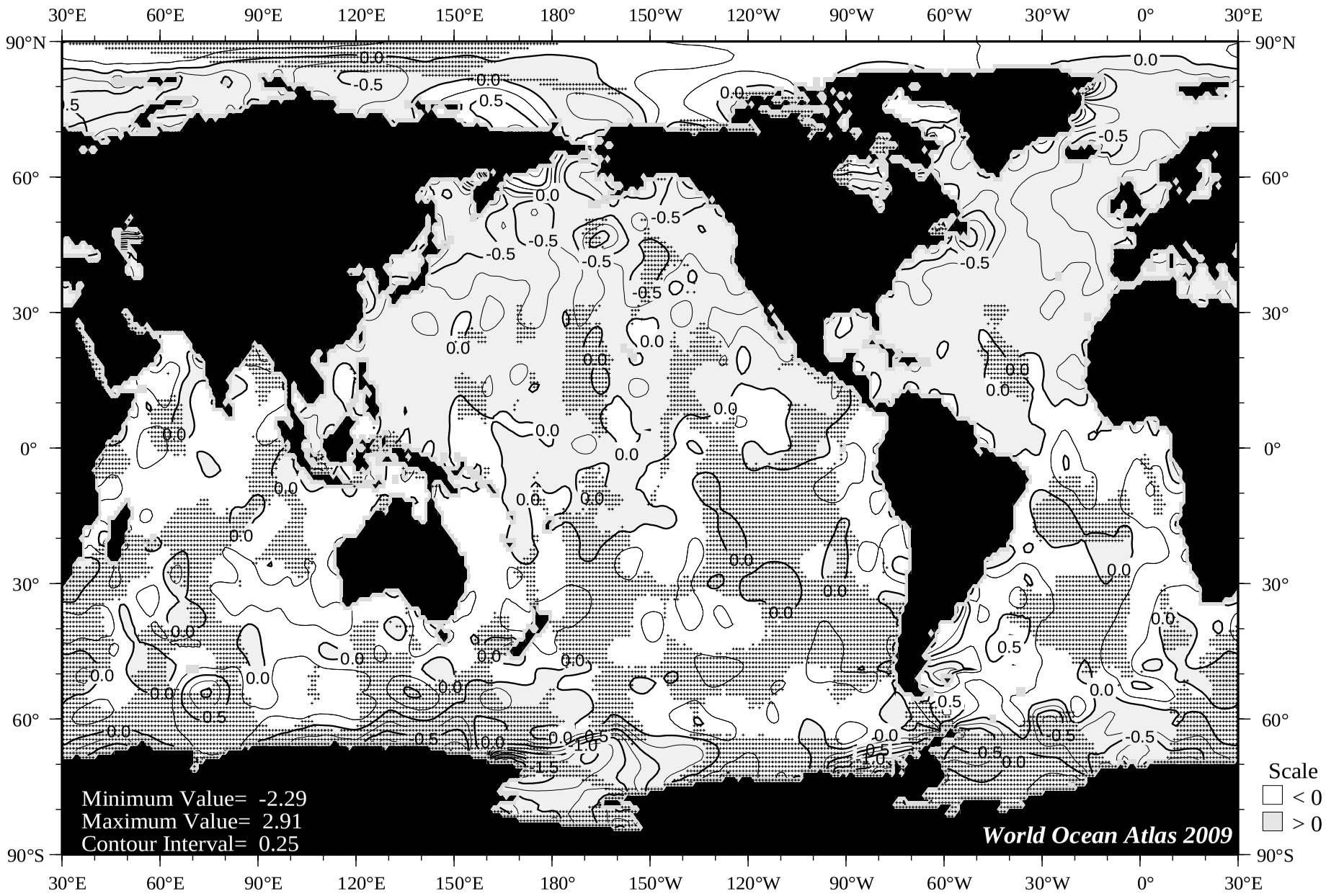

Fig C62 October minus annual oxygen [ml/l] at the surface.

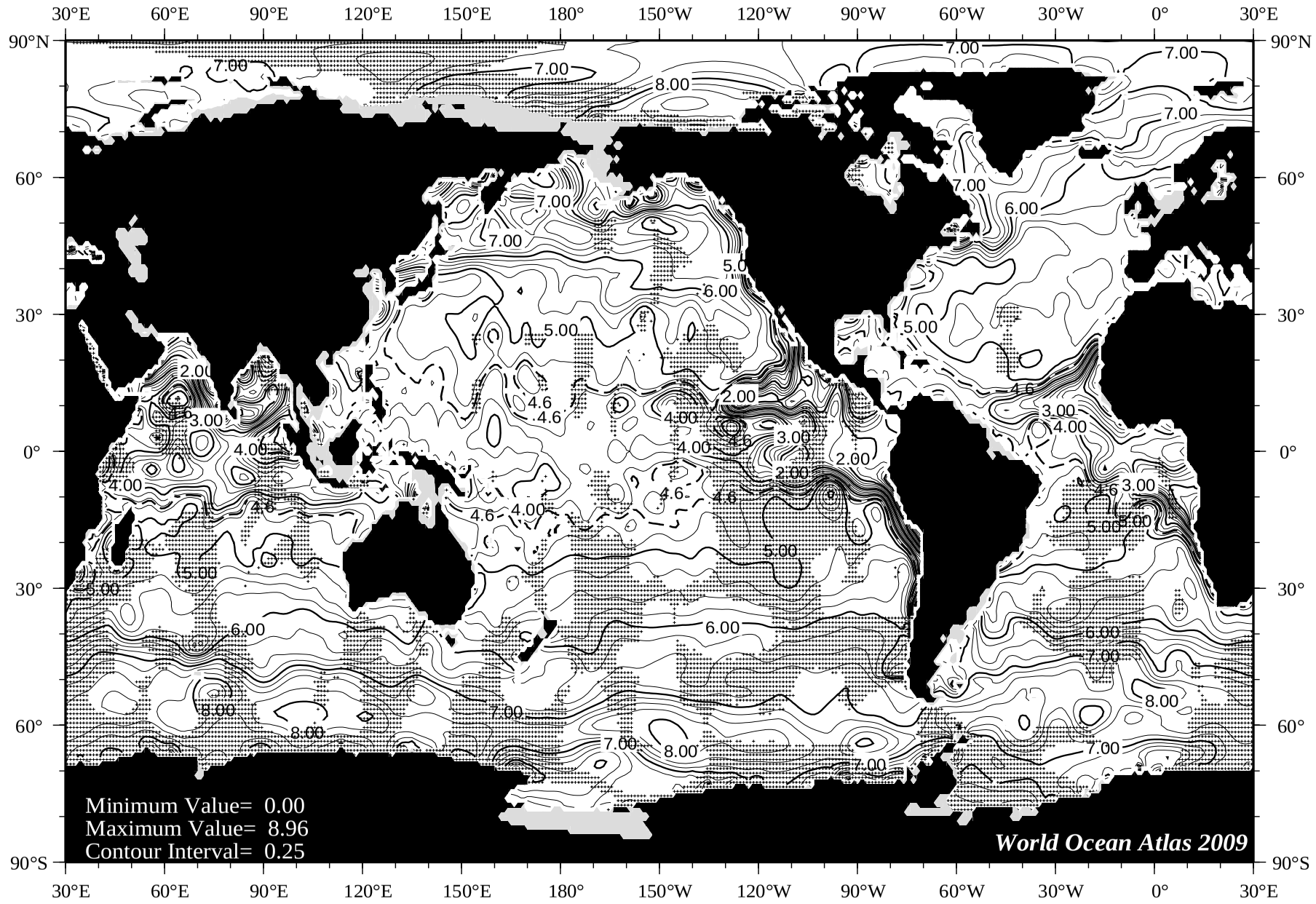

Fig C63 October mean oxygen [ml/l] at 75 m. depth.

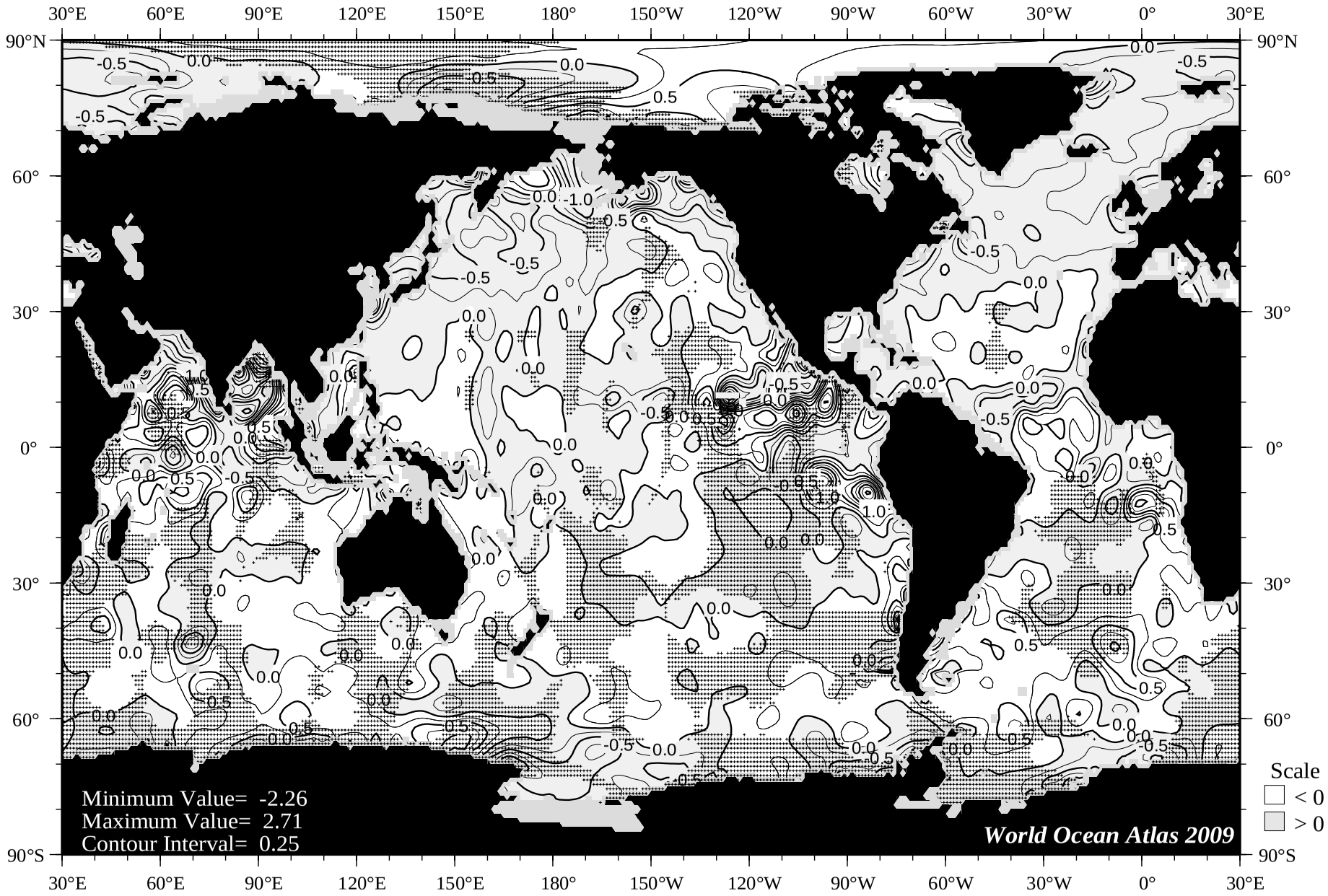

Fig C64 October minus annual oxygen [ml/l] at 75 m. depth.

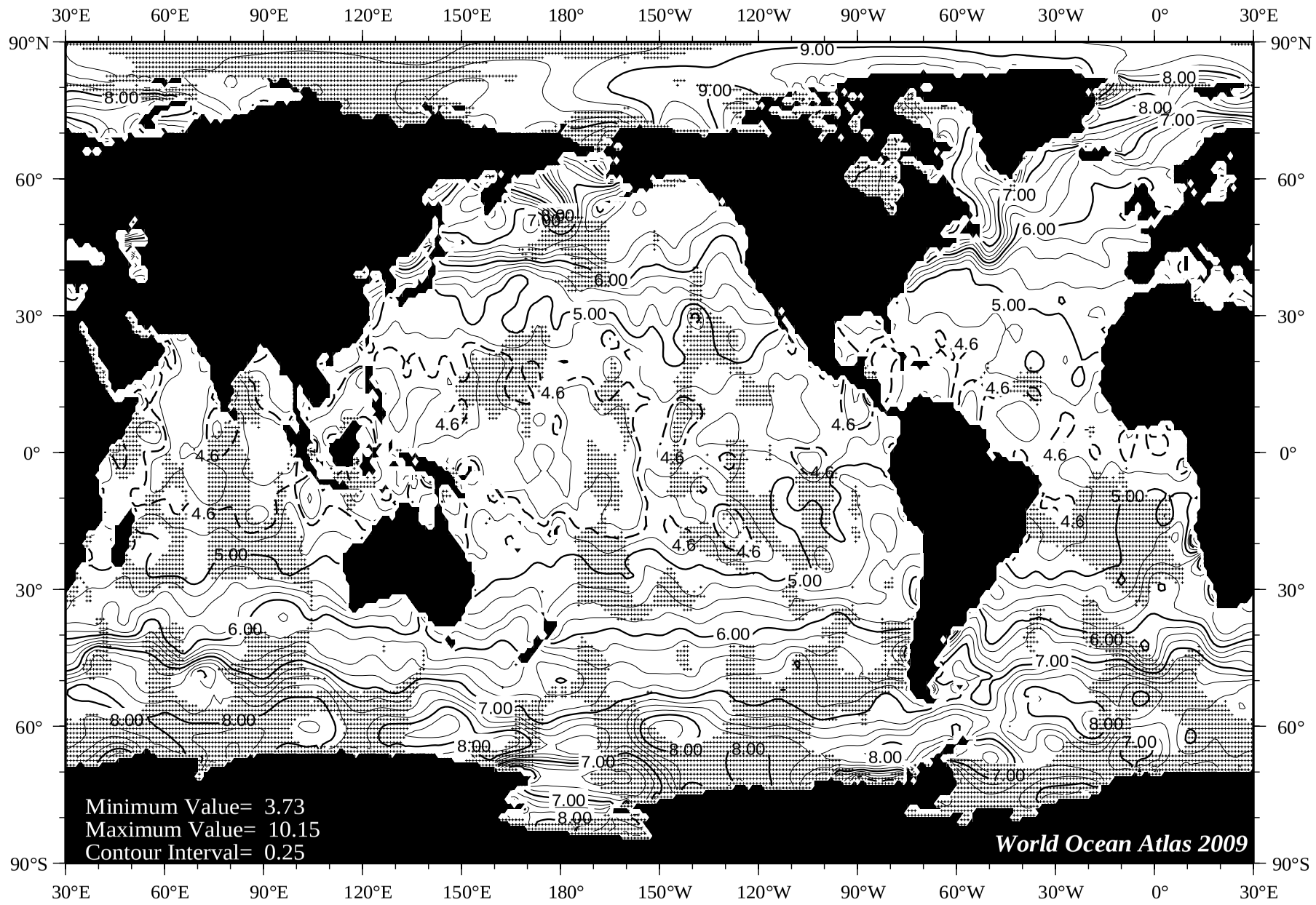

Fig C65 November mean oxygen [ml/l] at the surface.

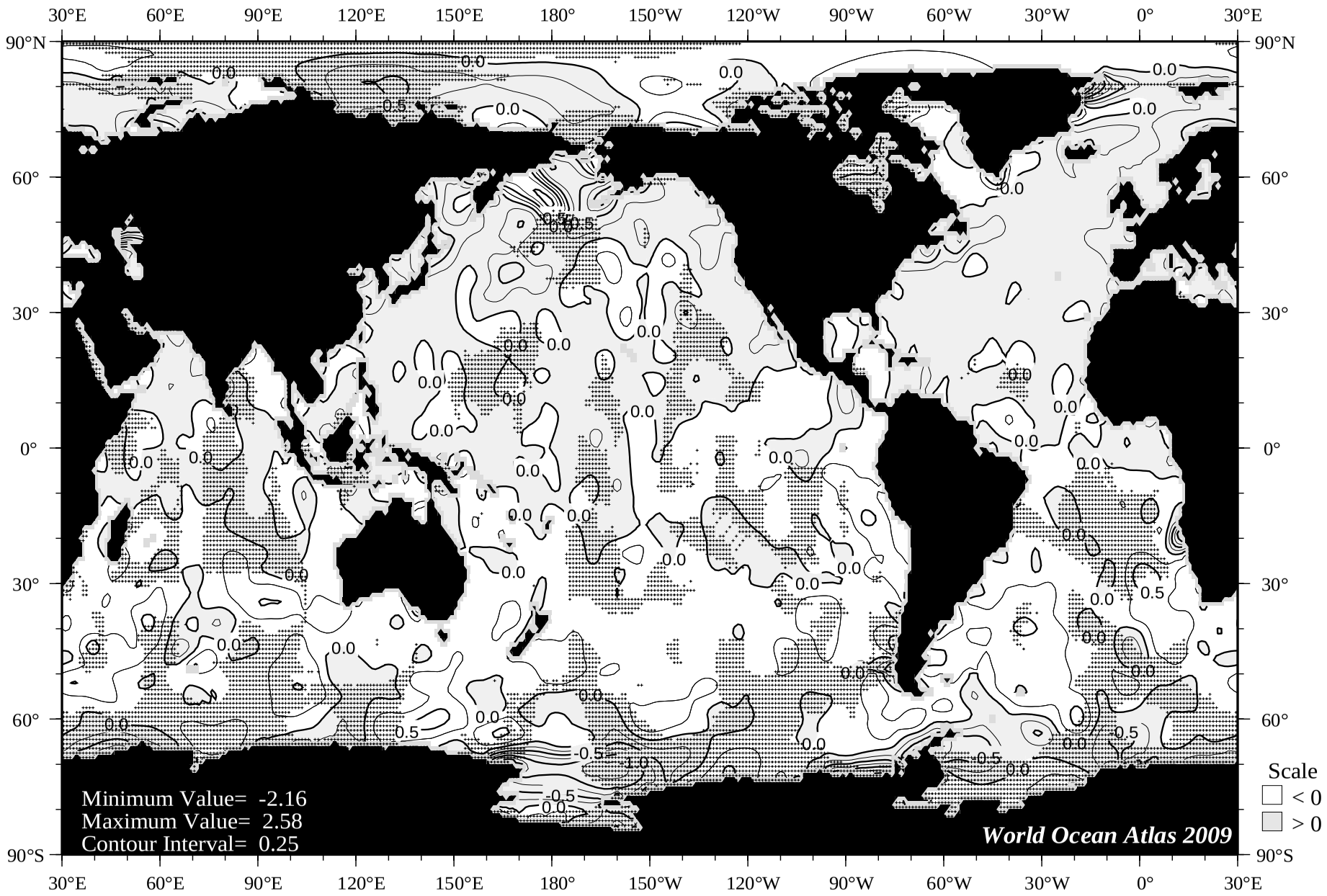

Fig C66 November minus annual oxygen [ml/l] at the surface.

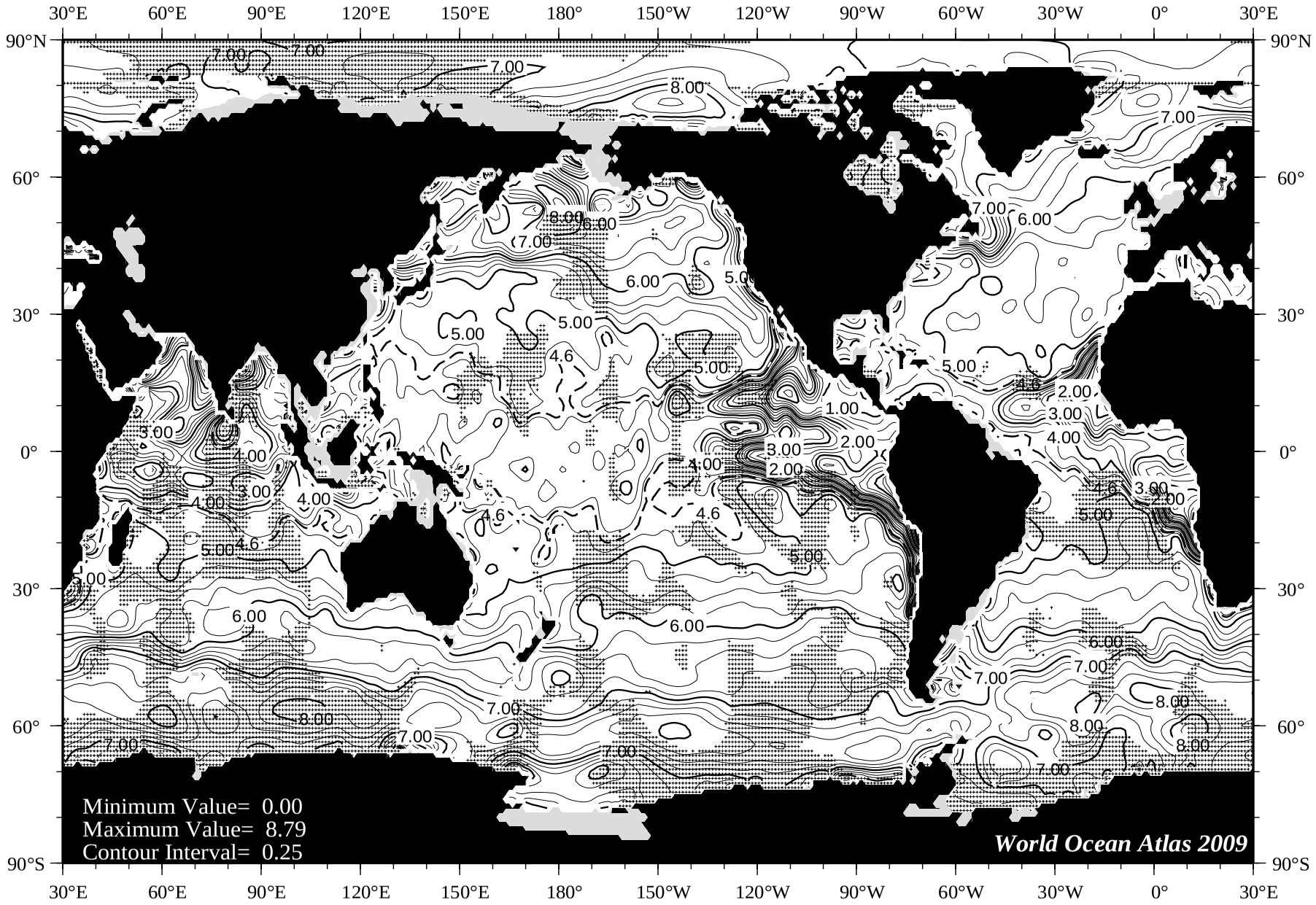

Fig C67 November mean oxygen [ml/l] at 75 m. depth.

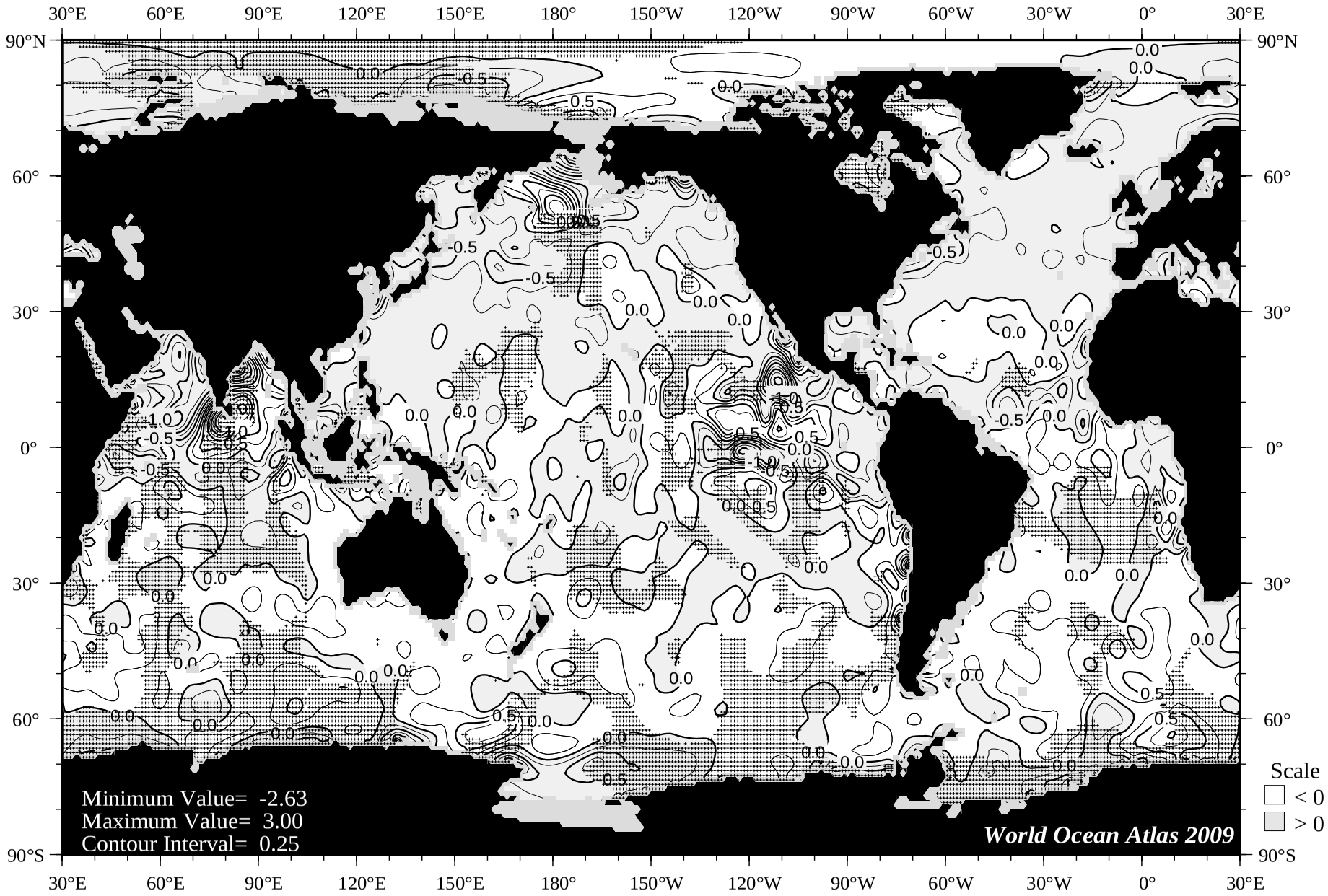

Fig C68 November minus annual oxygen [ml/l] at 75 m. depth.

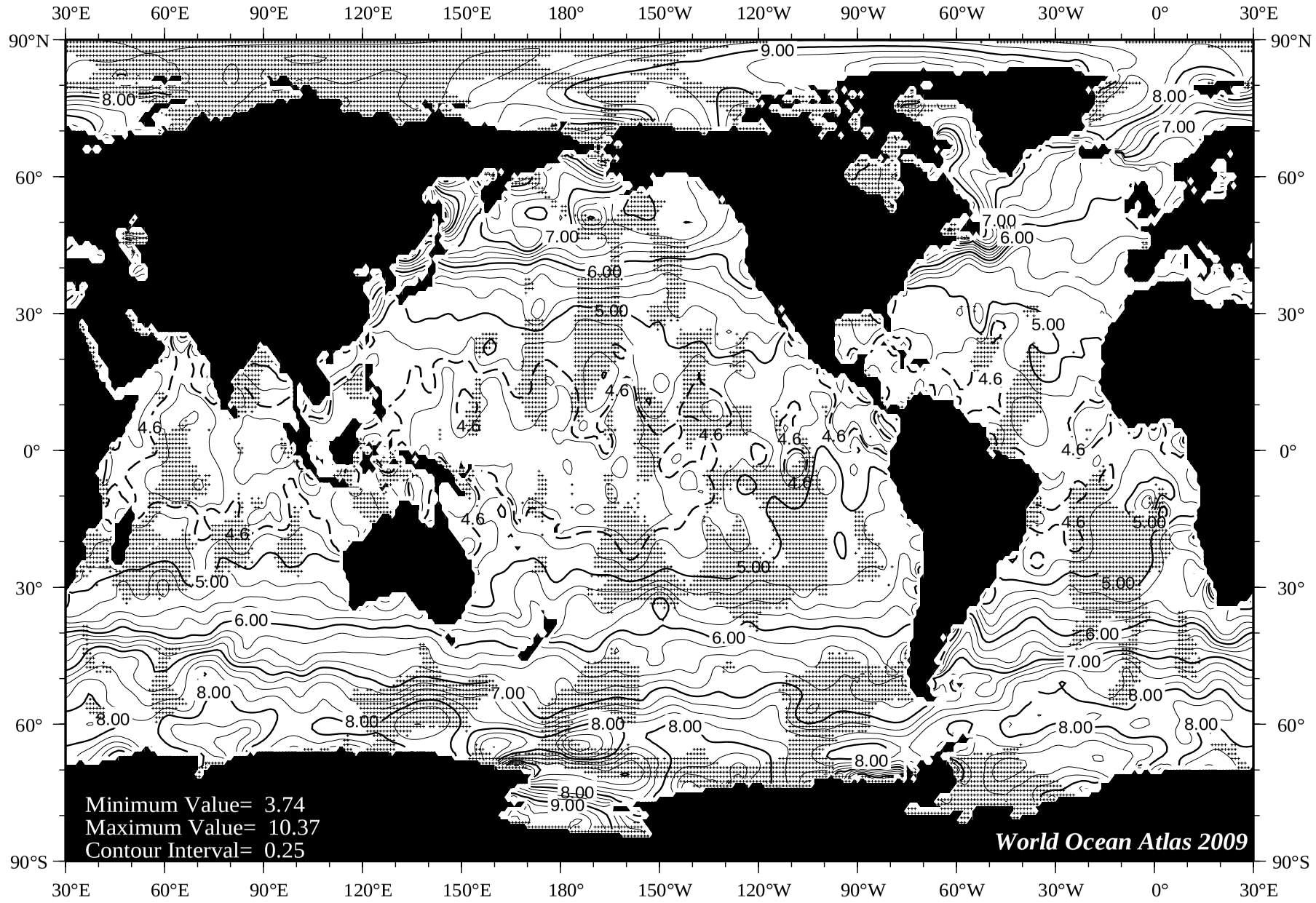

Fig C69 December mean oxygen [ml/l] at the surface.

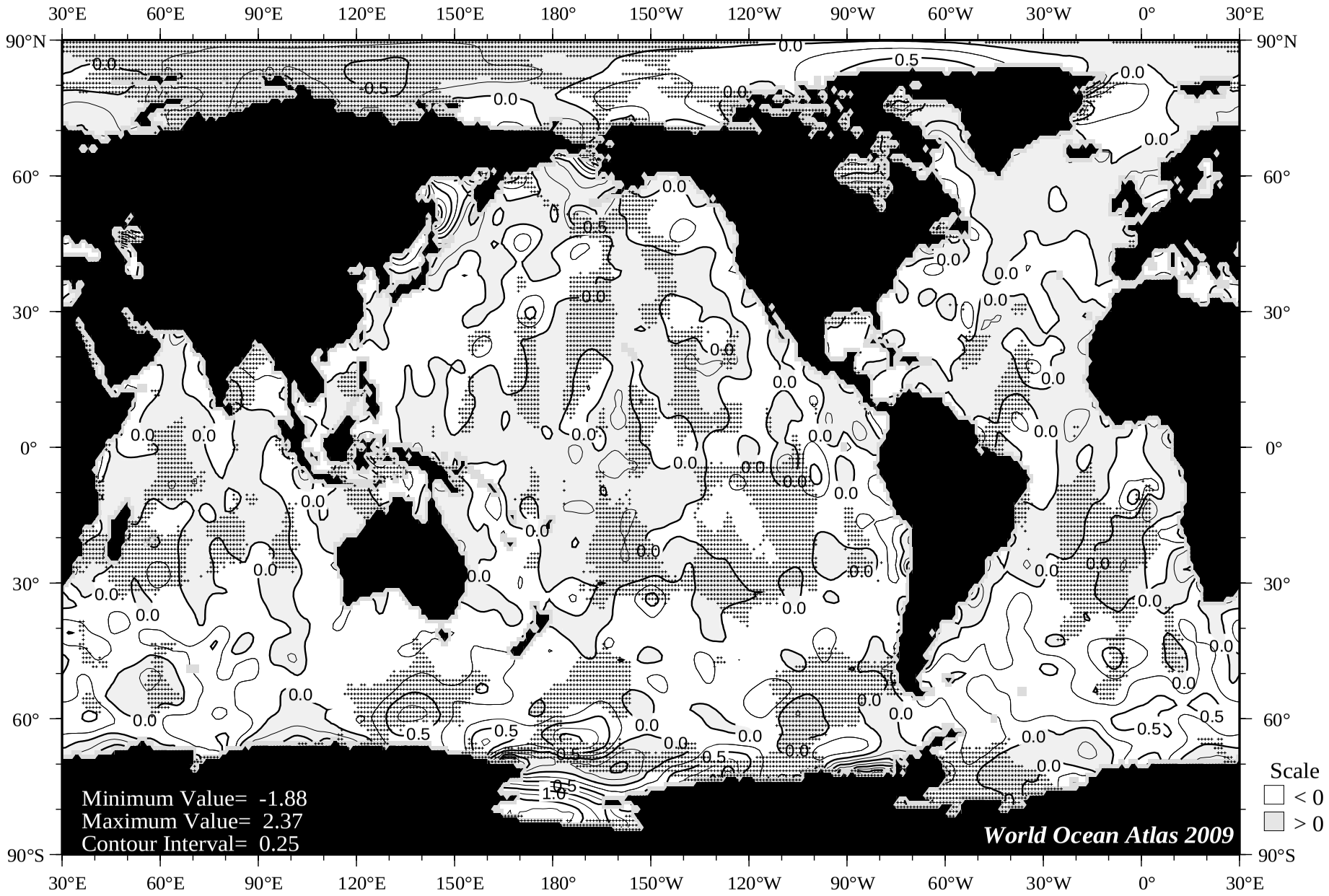

Fig C70 December minus annual oxygen [ml/l] at the surface.

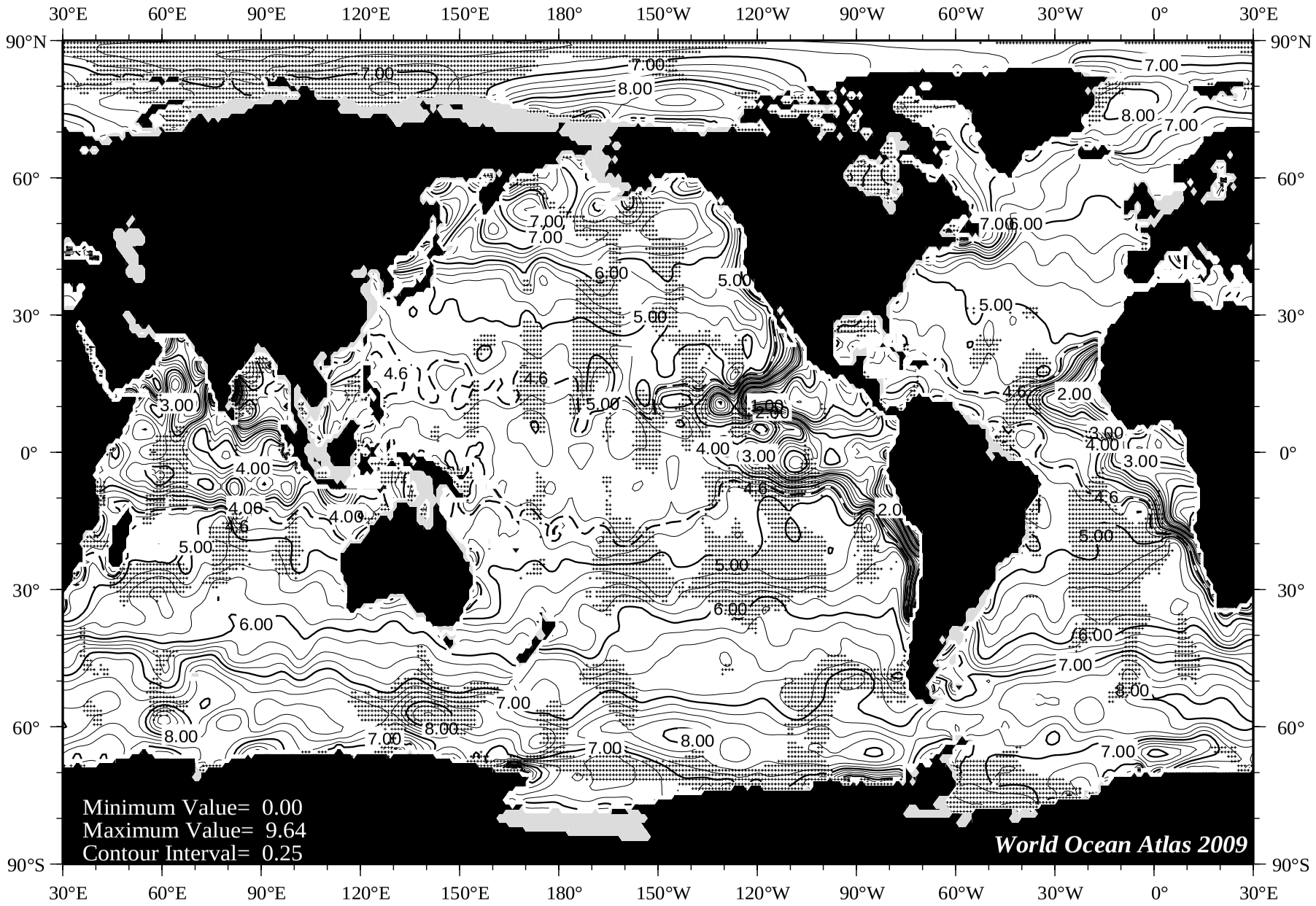

Fig C71 December mean oxygen [ml/l] at 75 m. depth.

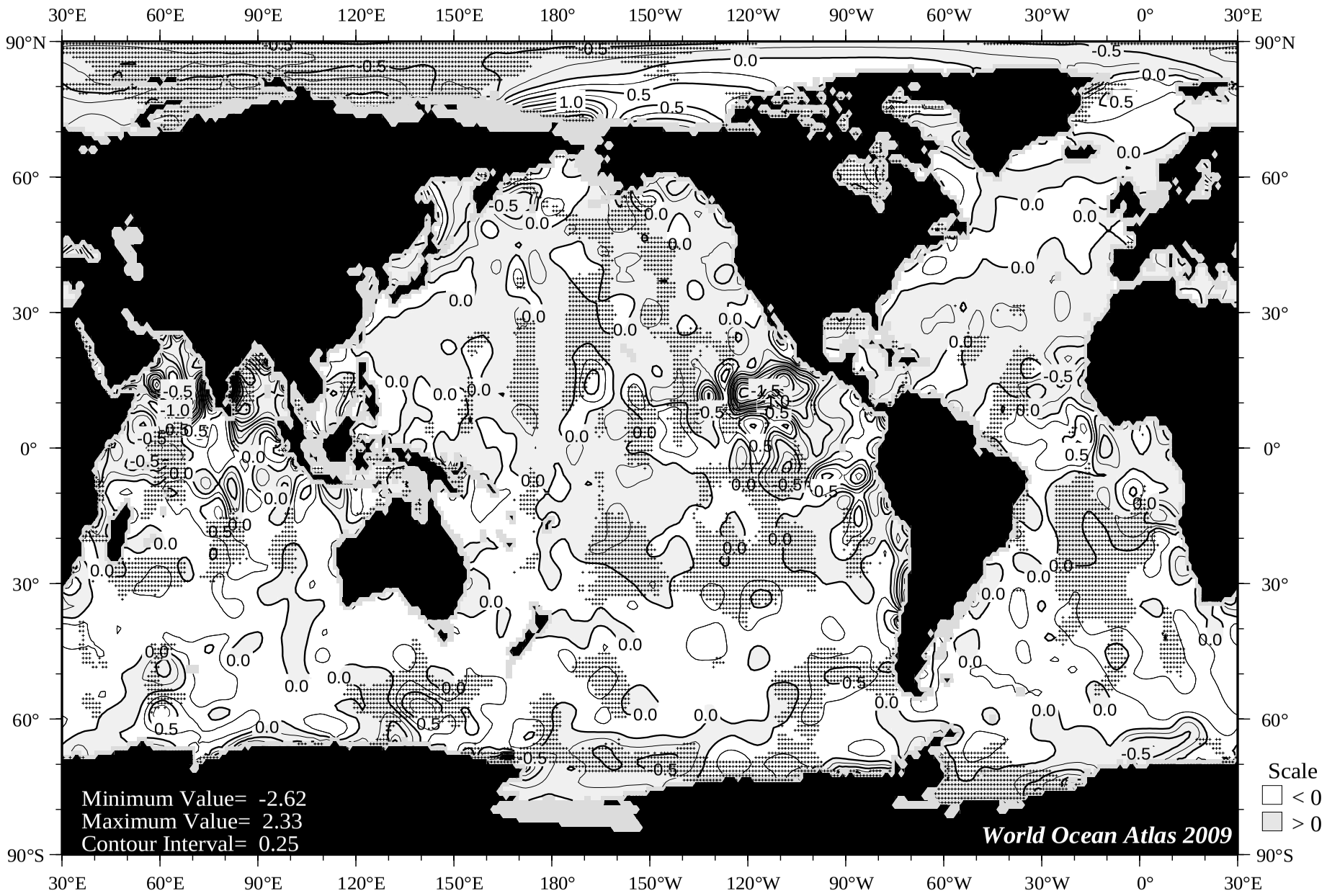

Fig C72 December minus annual oxygen [ml/l] at 75 m. depth.

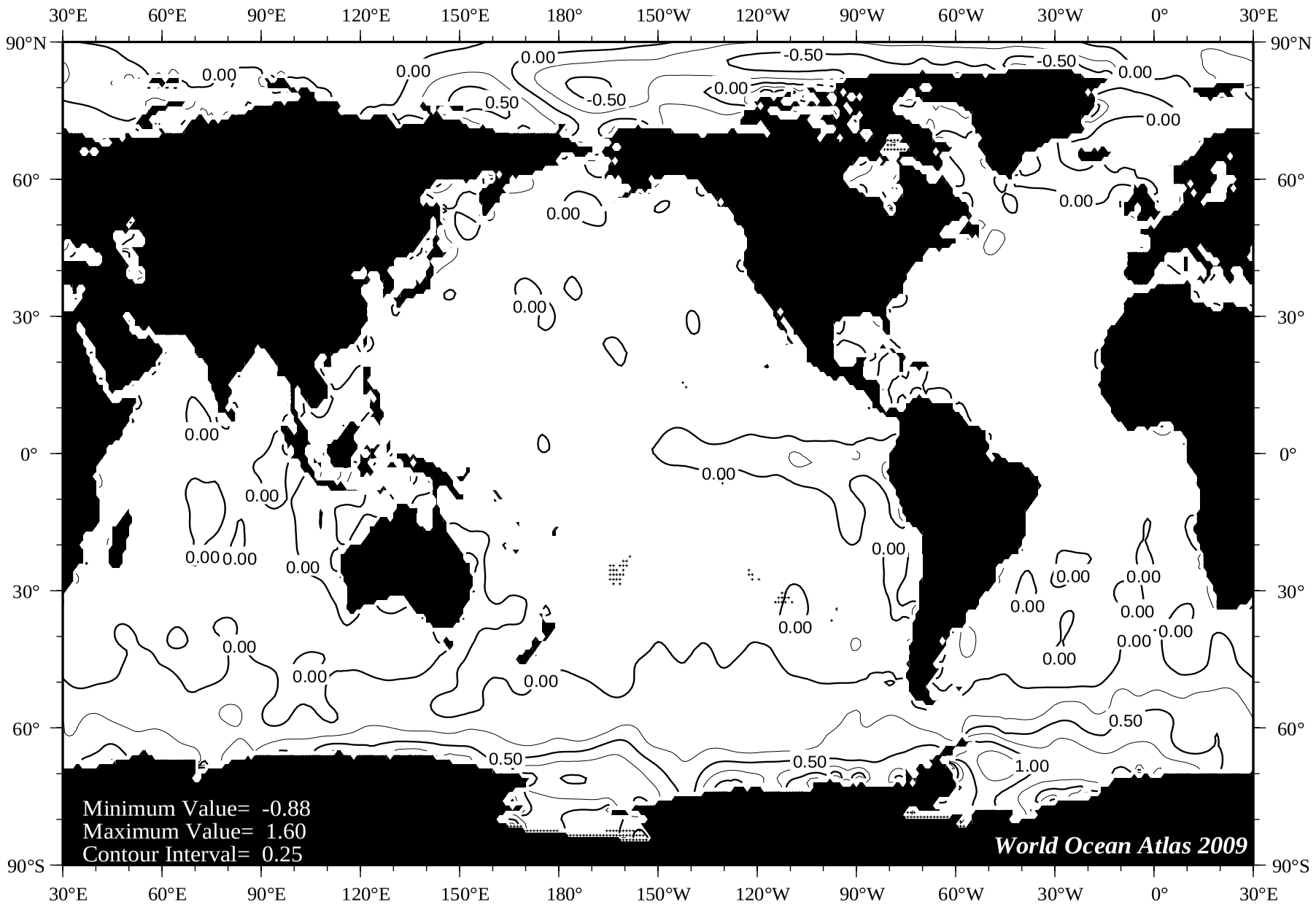

Fig D1 Annual apparent oxygen utilization (ml/l) at the surface.

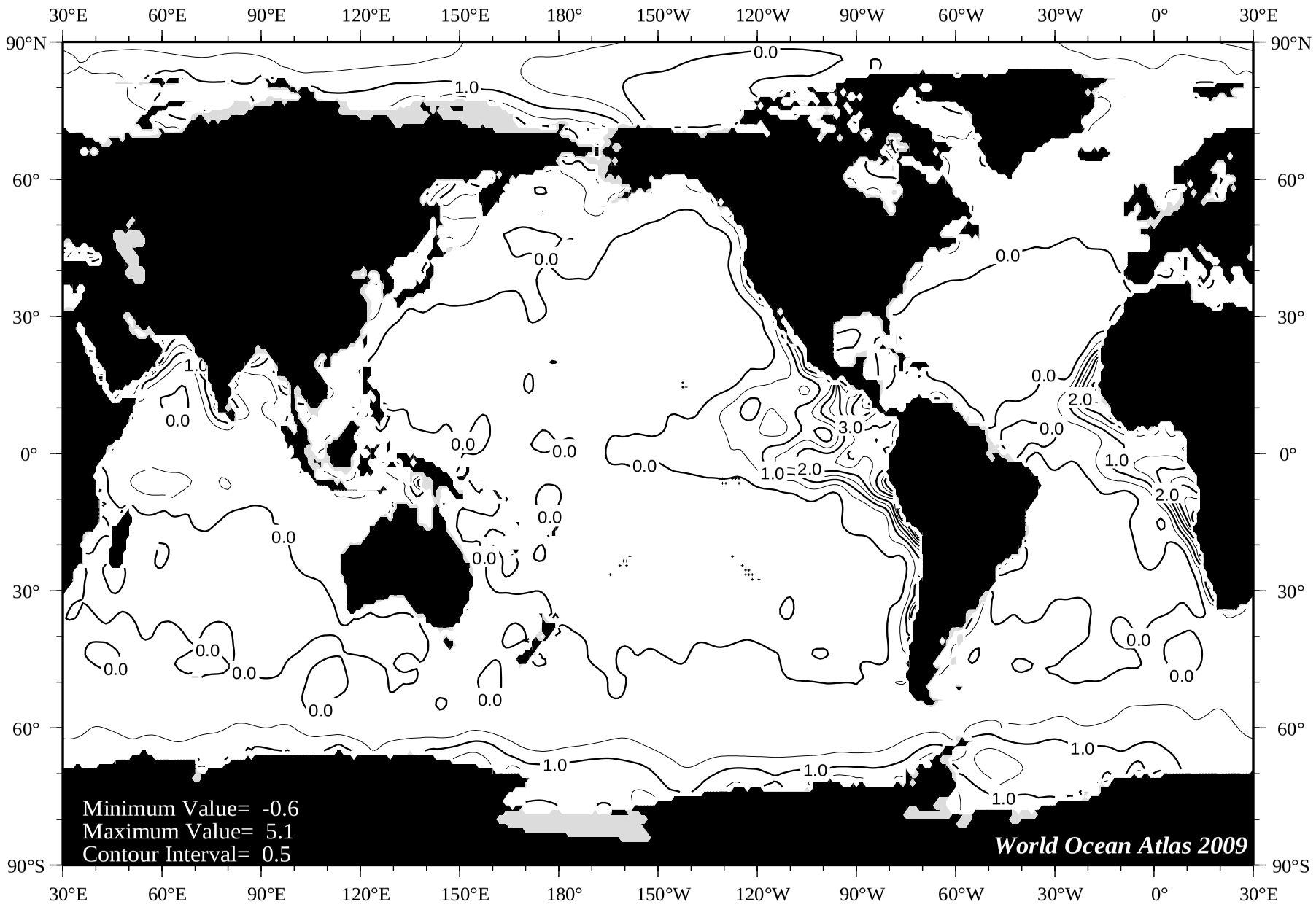

Fig D2 Annual apparent oxygen utilization (ml/l) at 50 m. depth.

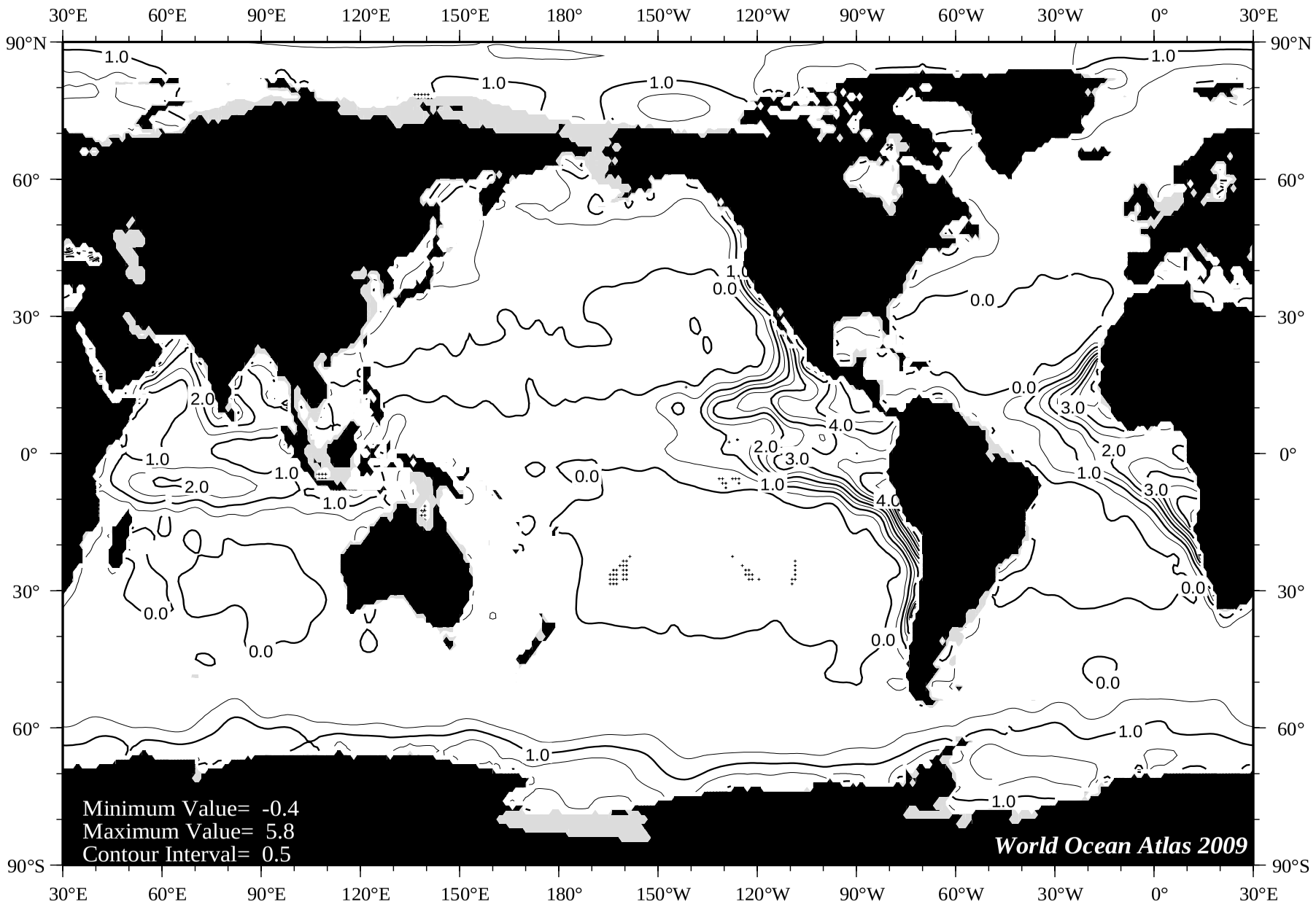

Fig D3 Annual apparent oxygen utilization (ml/l) at 75 m. depth.

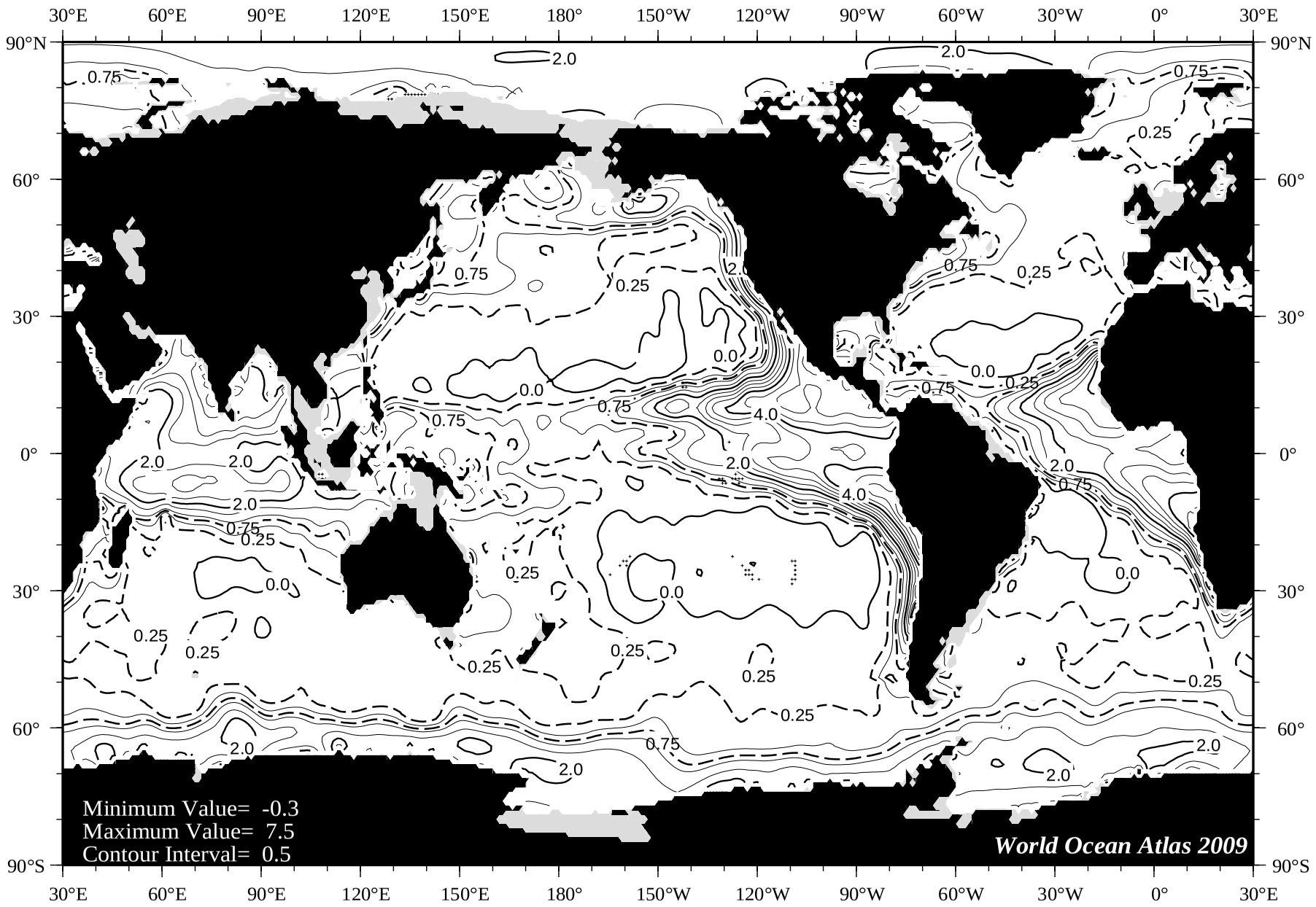

Fig D4 Annual apparent oxygen utilization (ml/l) at 100 m. depth.

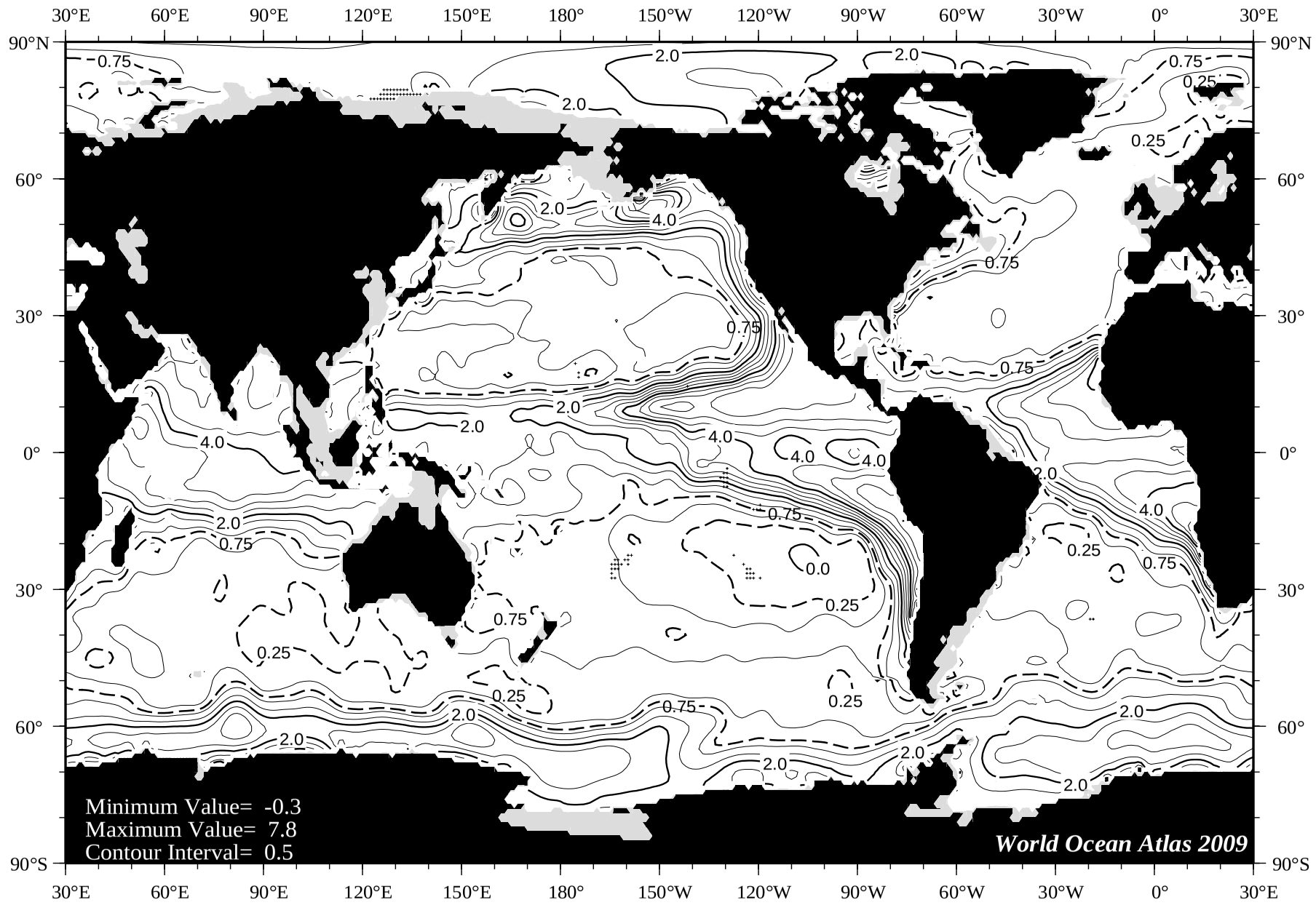

Fig D5 Annual apparent oxygen utilization (ml/l) at 150 m. depth.

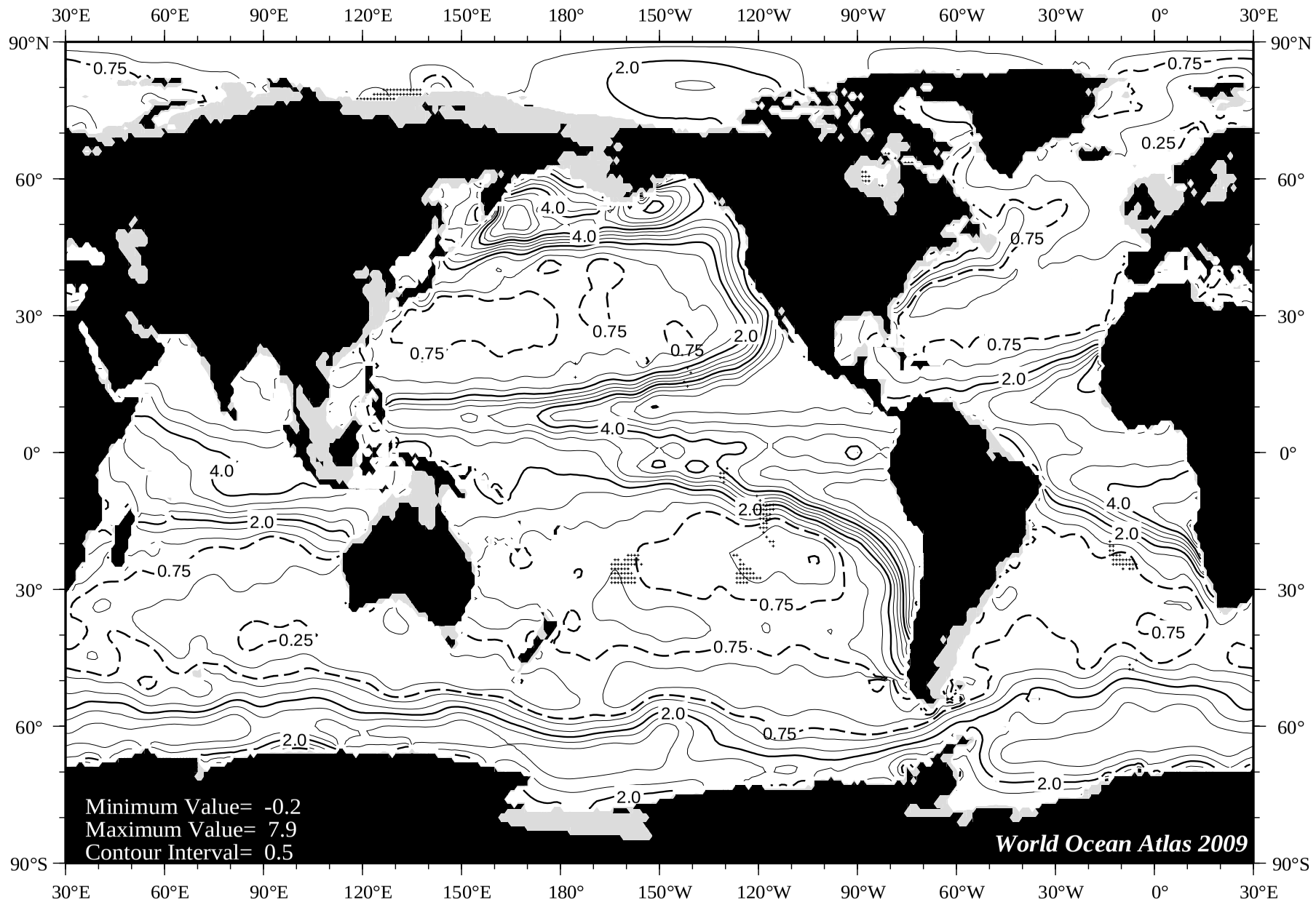

Fig D6 Annual apparent oxygen utilization (ml/l) at 200 m. depth.

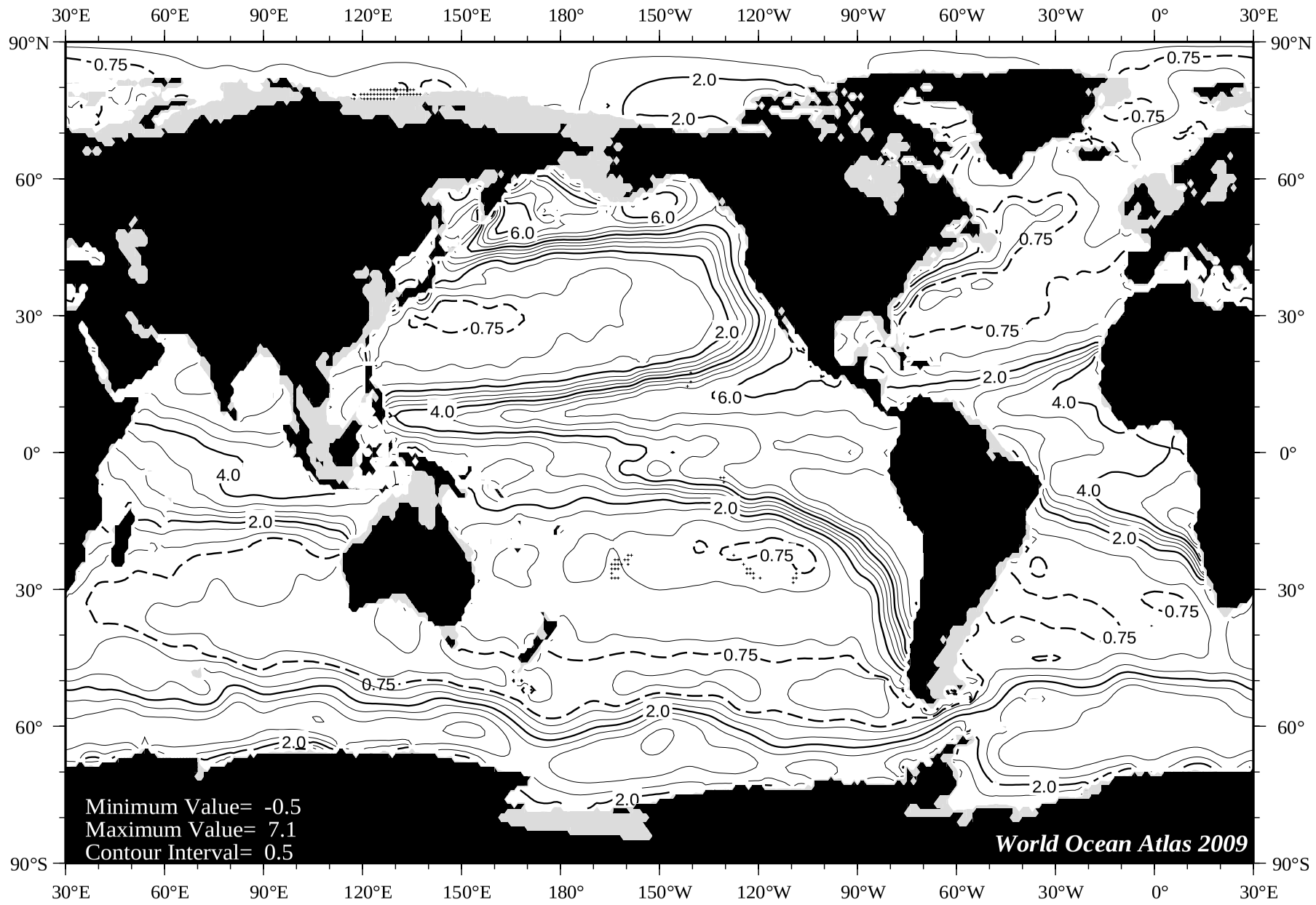

Fig D7 Annual apparent oxygen utilization (ml/l) at 250 m. depth.

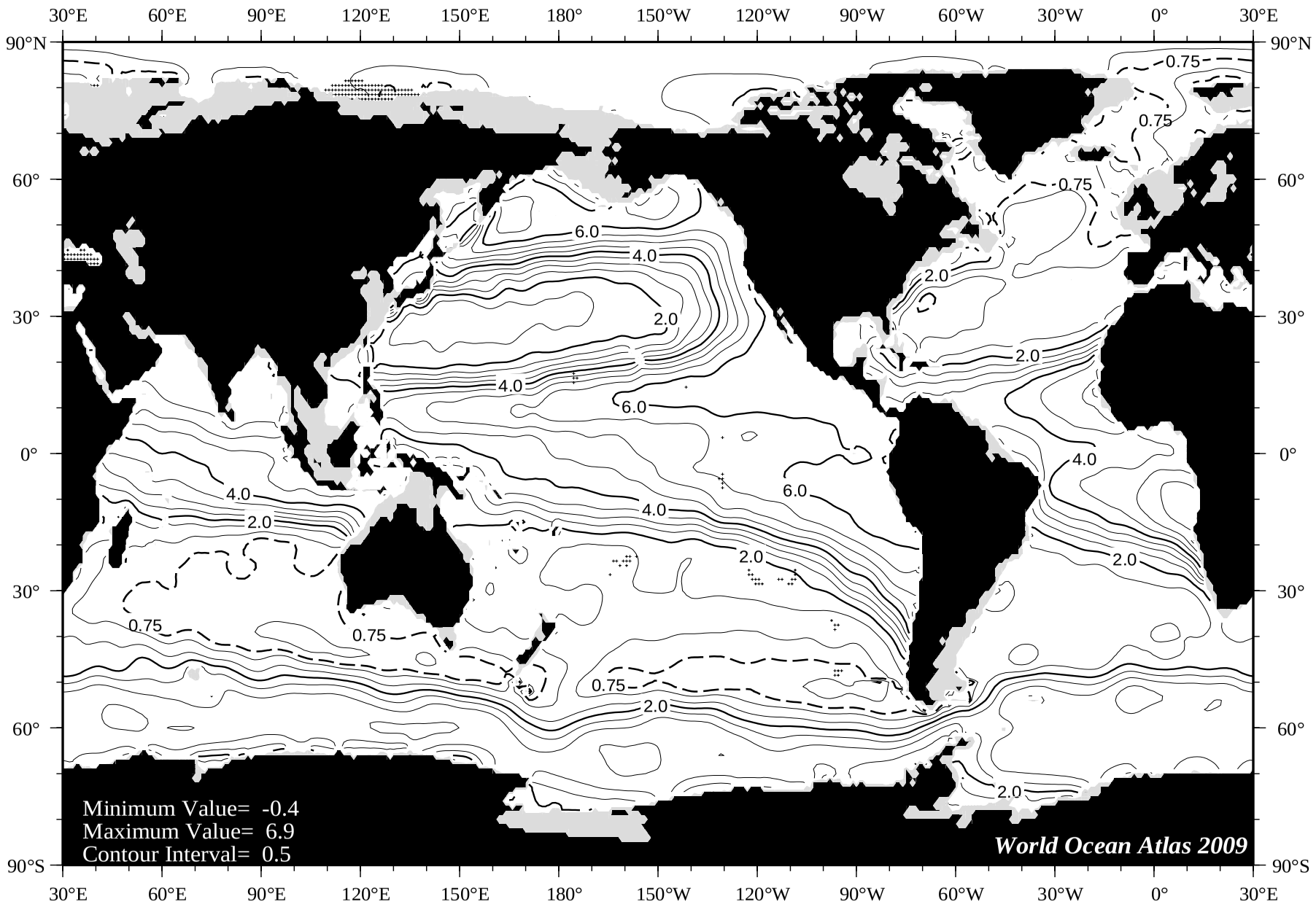

Fig D8 Annual apparent oxygen utilization (ml/l) at 400 m. depth.

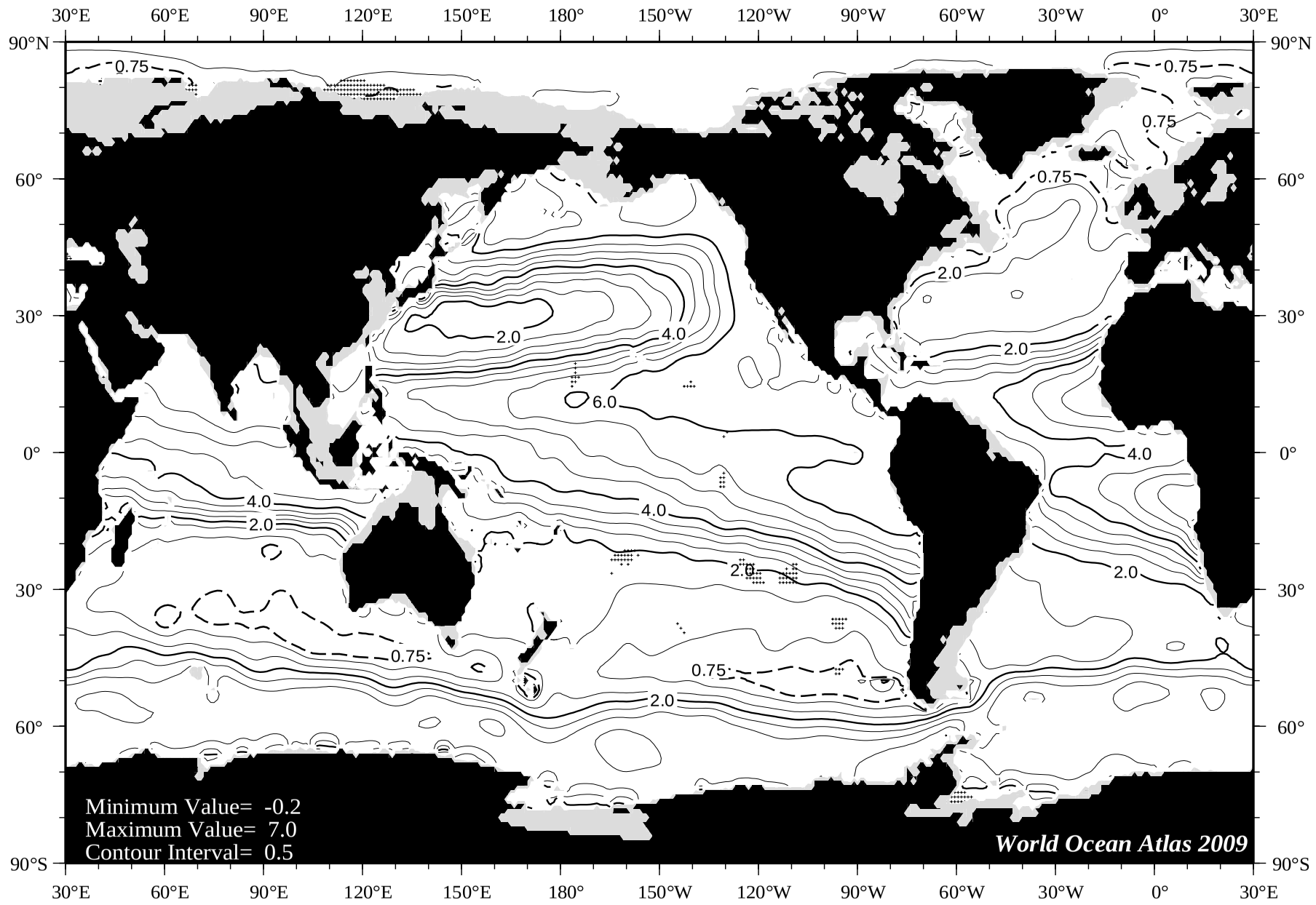

Fig D9 Annual apparent oxygen utilization (ml/l) at 500 m. depth.

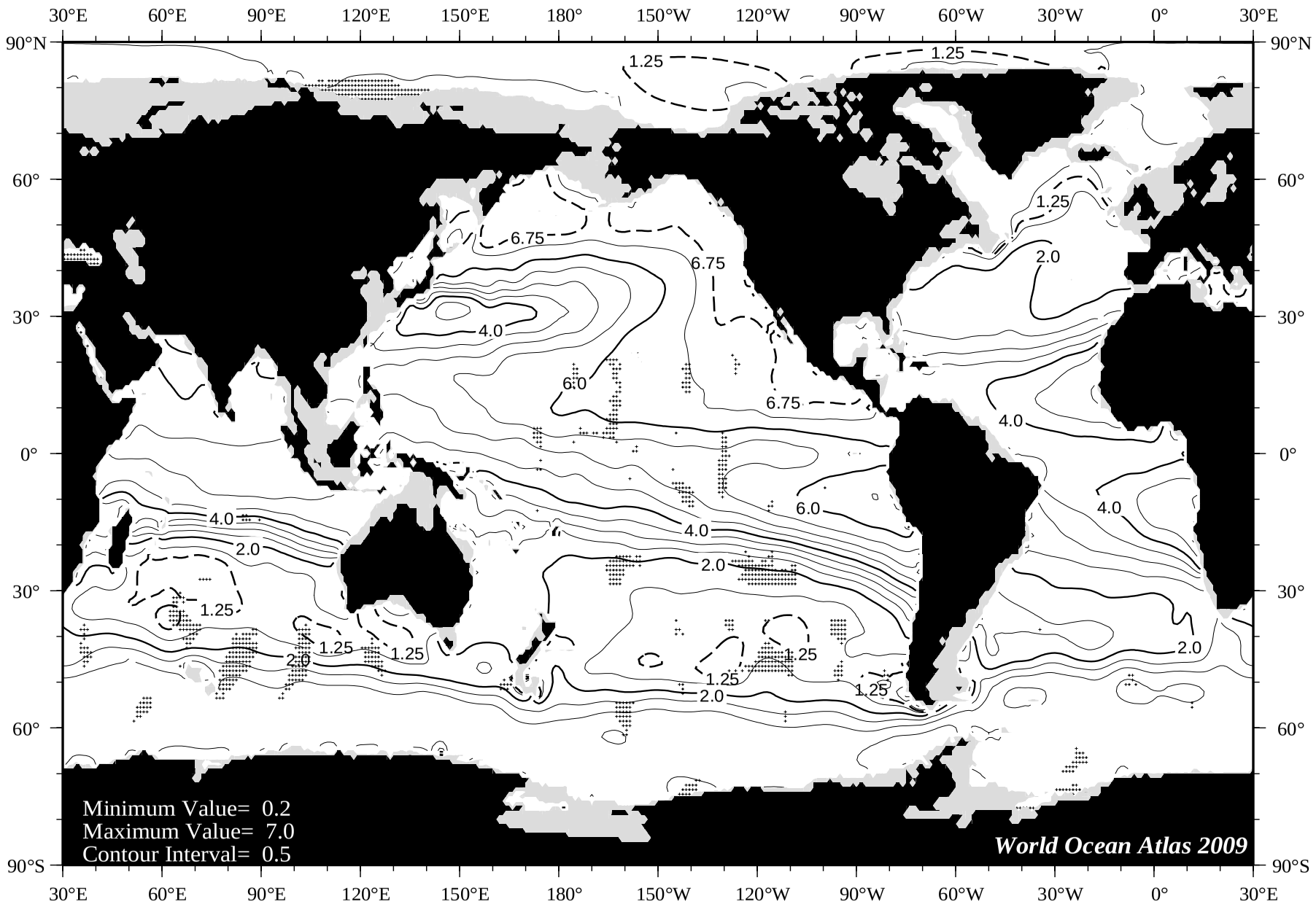

Fig D10 Annual apparent oxygen utilization (ml/l) at 700 m. depth.

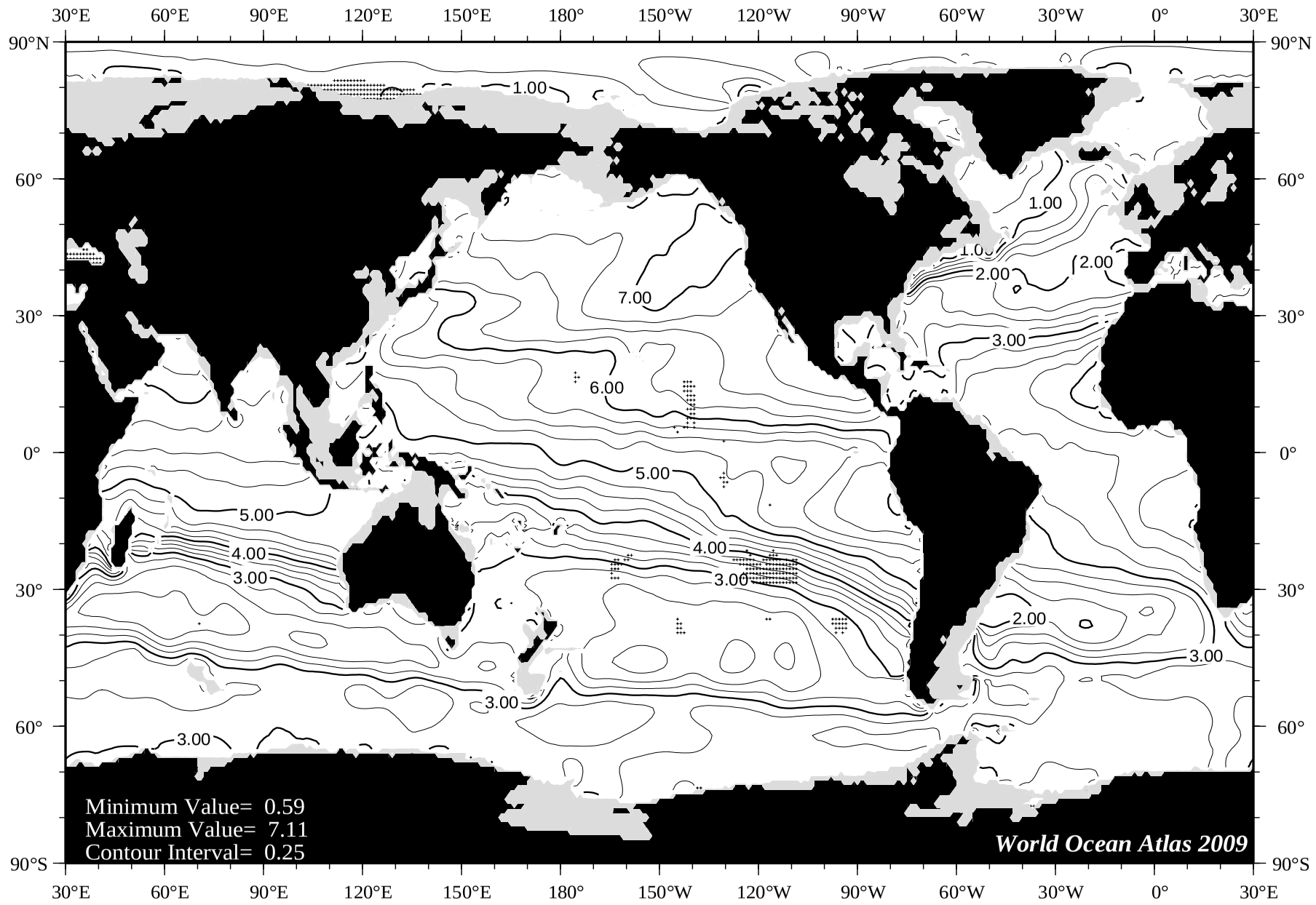

Fig D11 Annual apparent oxygen utilization (ml/l) at 1000 m. depth.

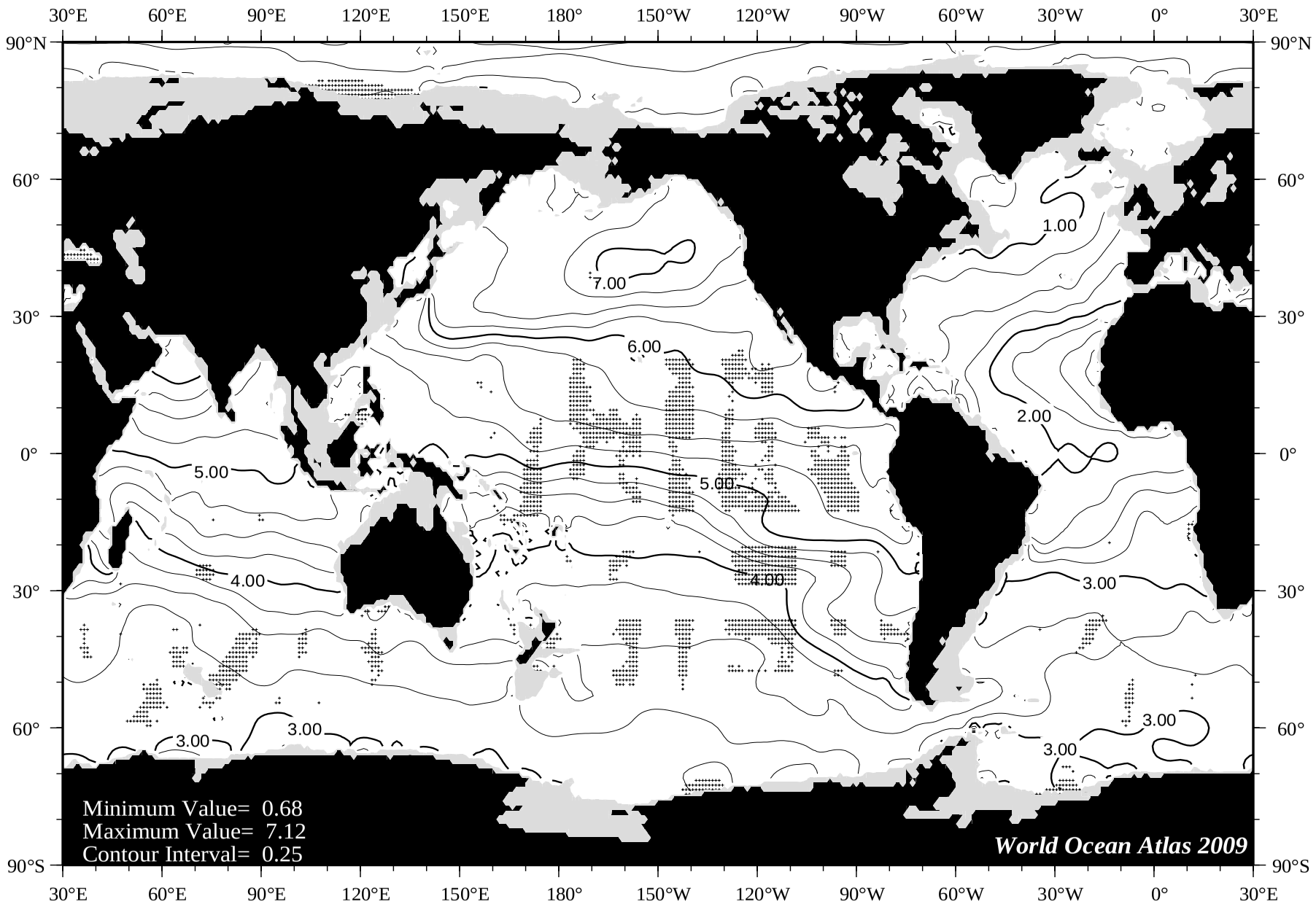

Fig D12 Annual apparent oxygen utilization (ml/l) at 1500 m. depth.

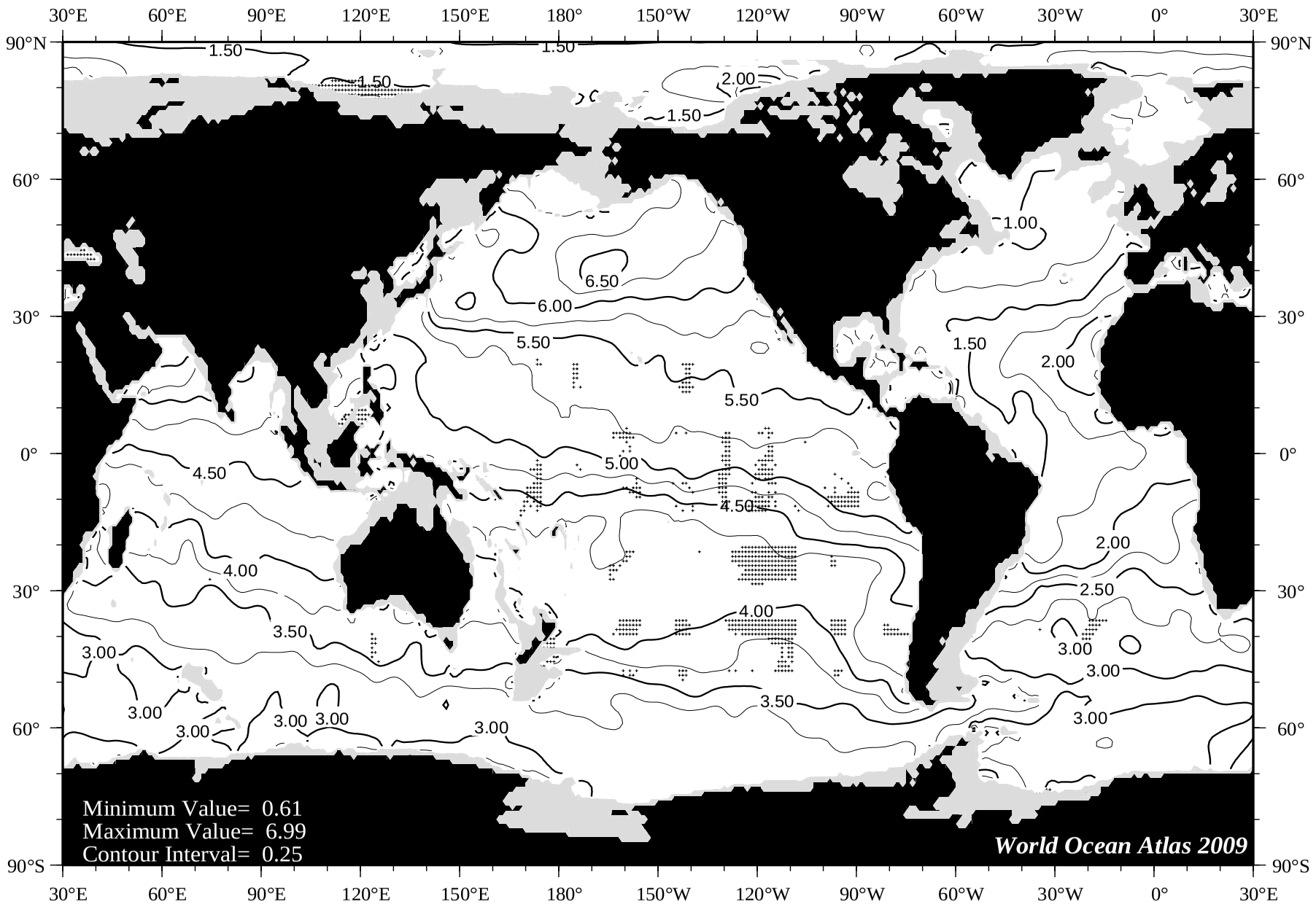

Fig D13 Annual apparent oxygen utilization (ml/l) at 2000 m. depth.

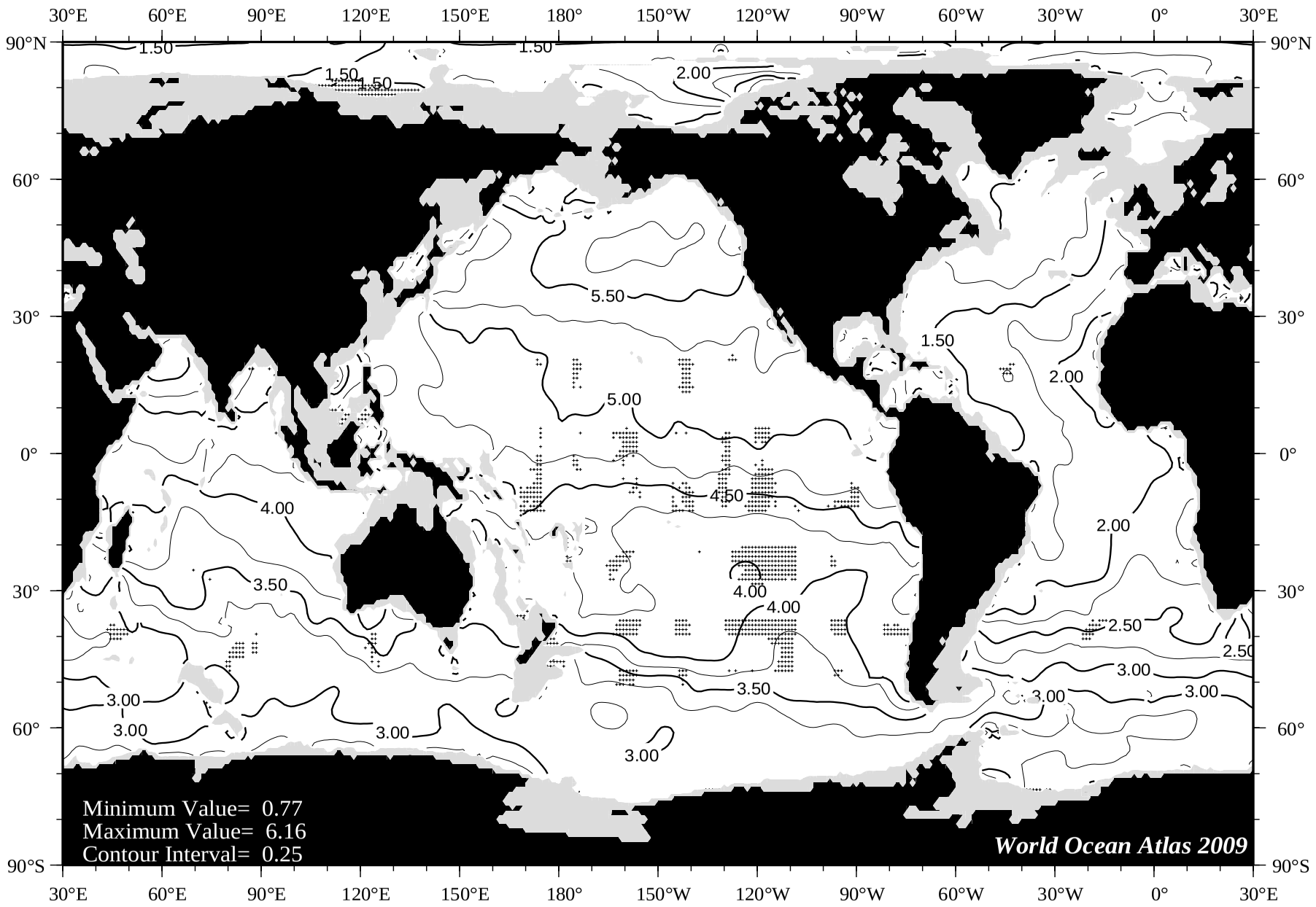

Fig D14 Annual apparent oxygen utilization (ml/l) at 2500 m. depth.

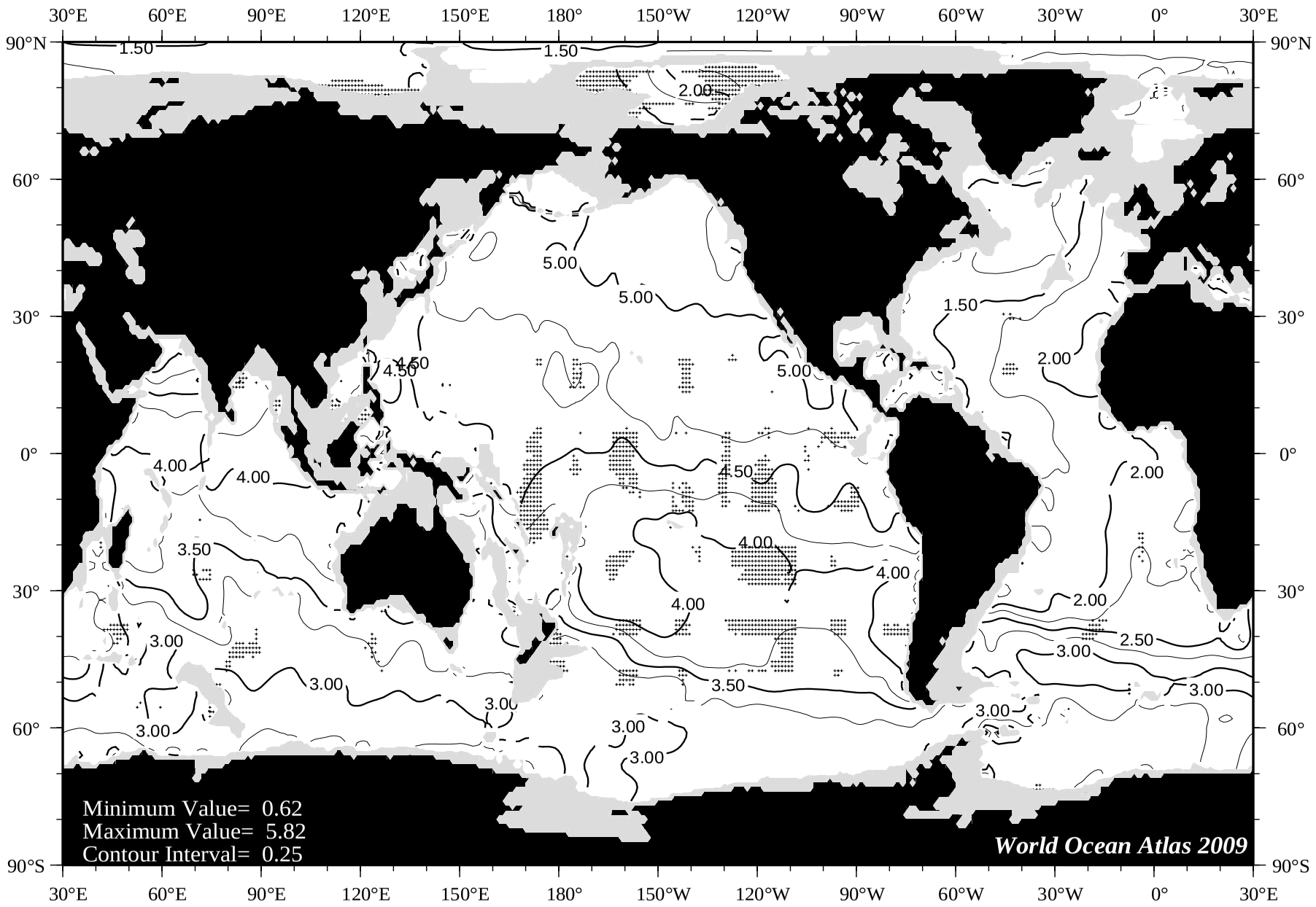

Fig D15 Annual apparent oxygen utilization (ml/l) at 3000 m. depth.

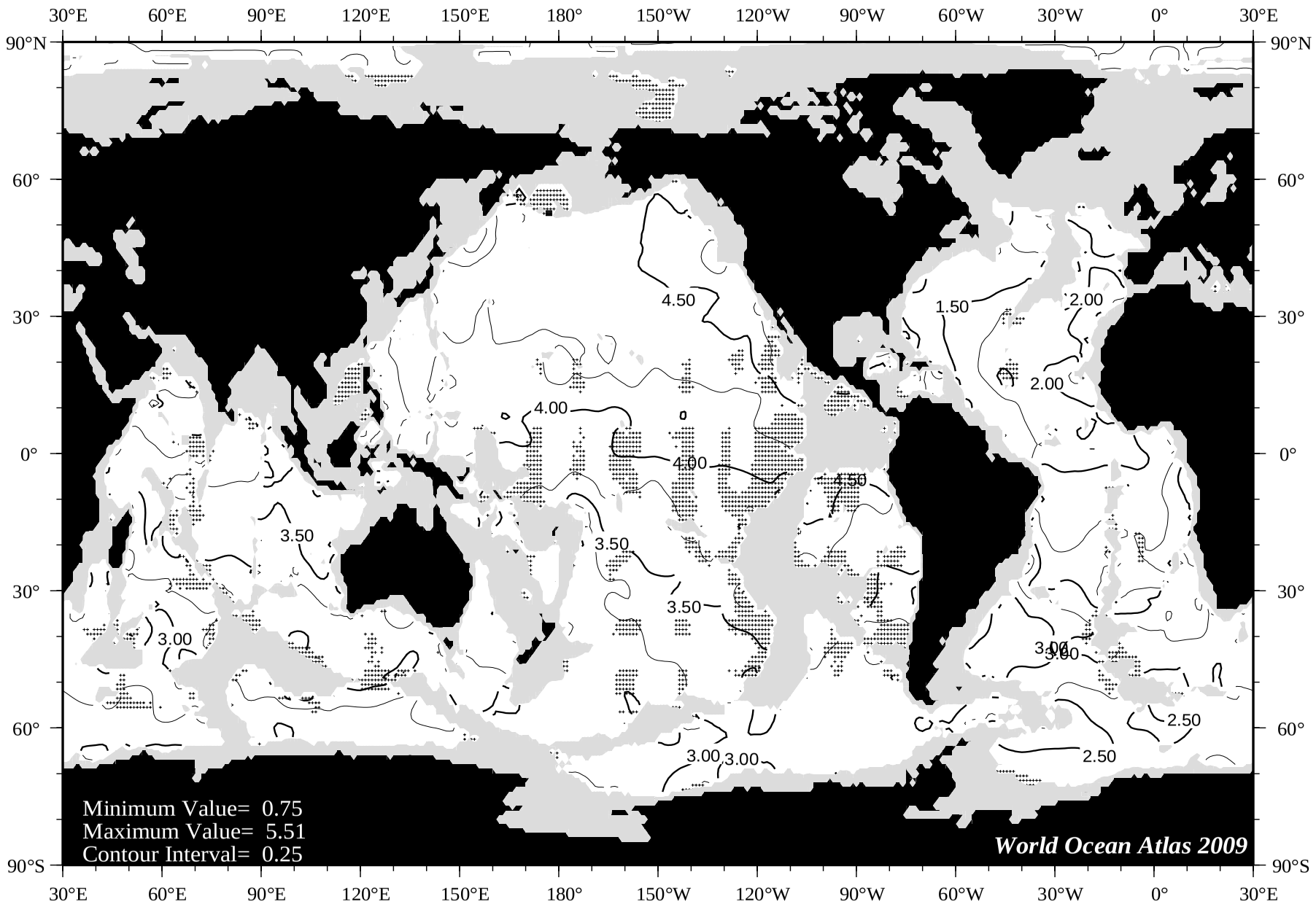

Fig D16 Annual apparent oxygen utilization (ml/l) at 4000 m. depth.

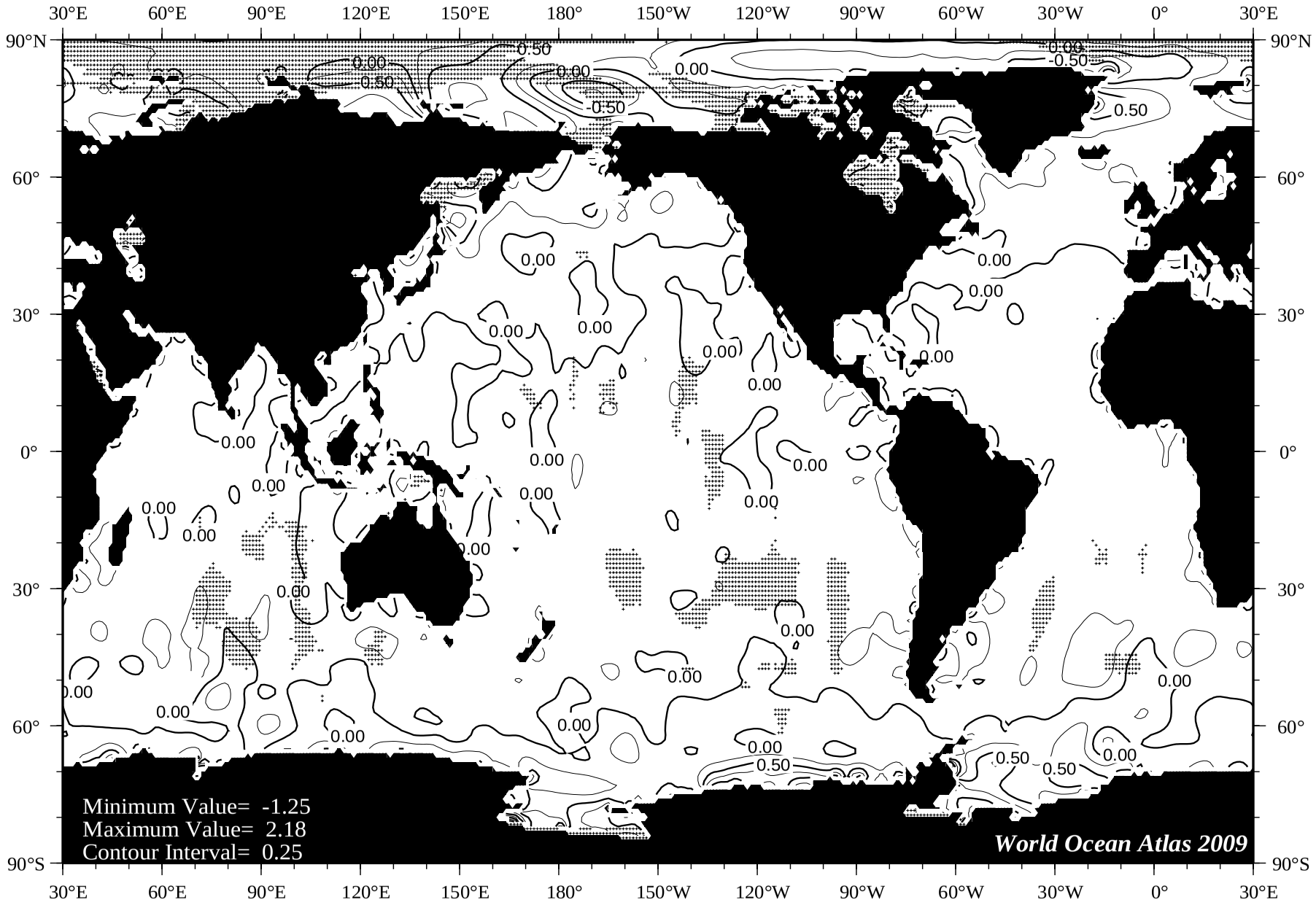

Fig E1 Winter (Jan.-Mar.) apparent oxygen utilization (ml/l) at the surface.

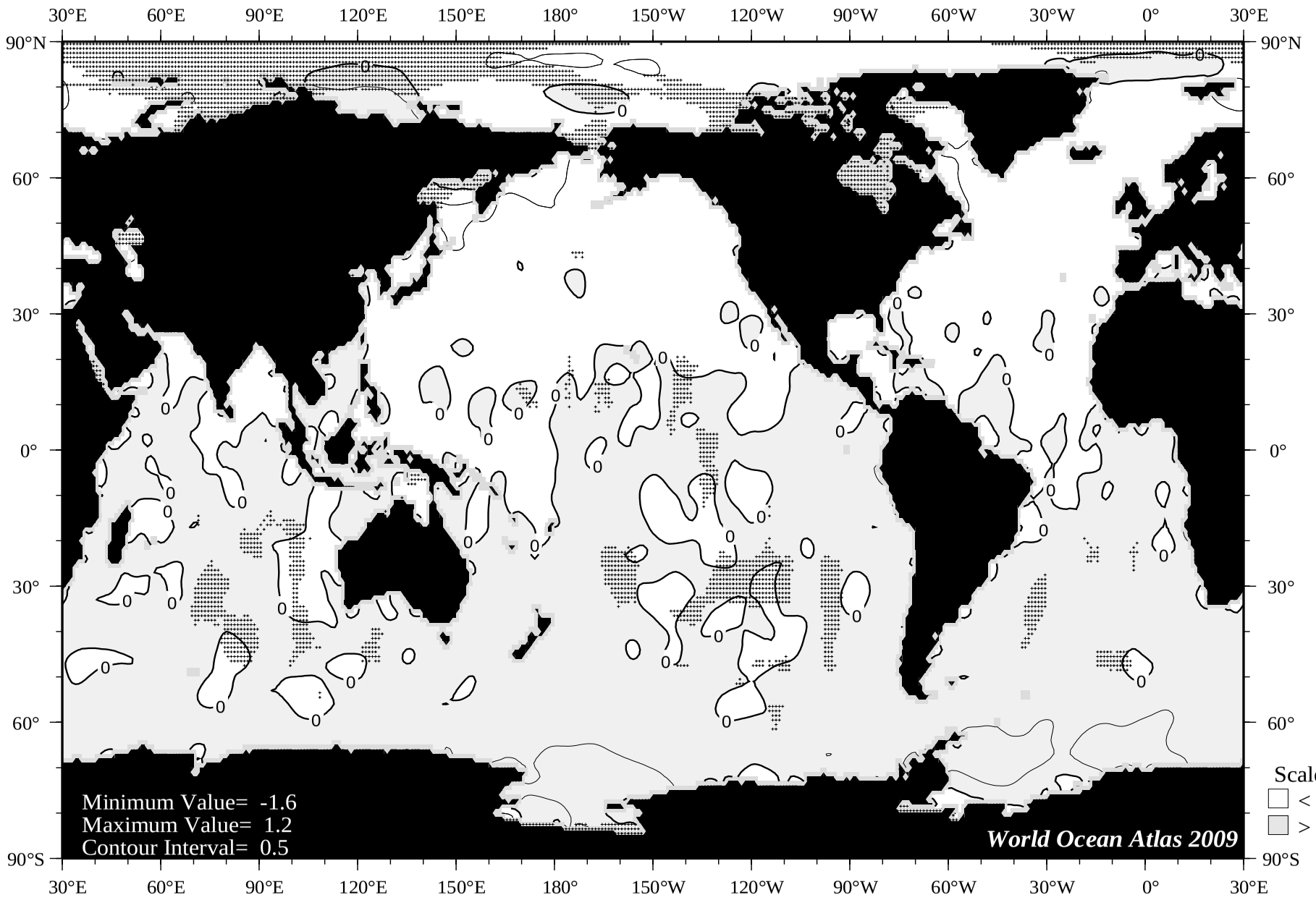

Fig E2 Winter (Jan.-Mar.) minus annual AOU at the surface.

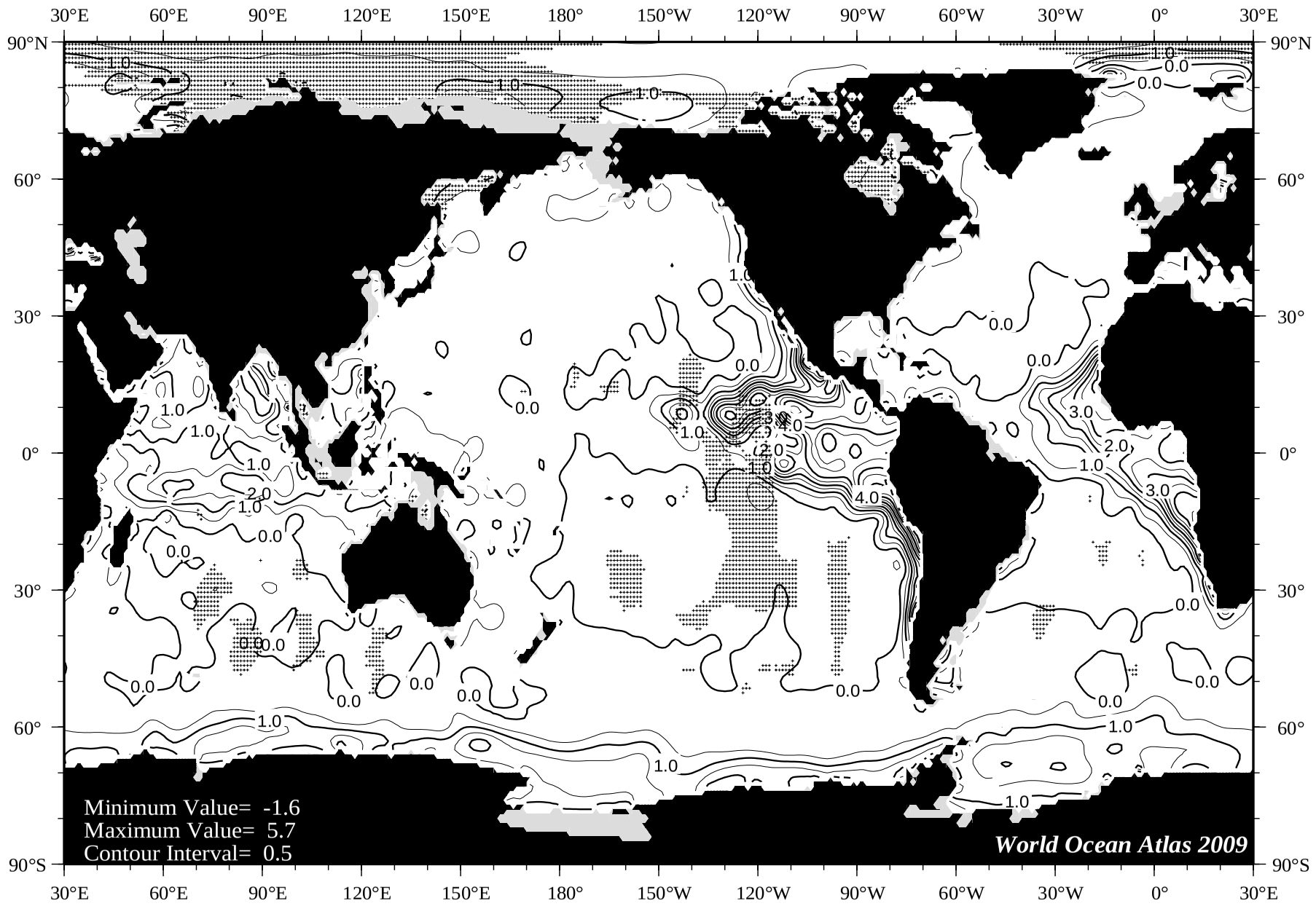

Fig E3 Winter (Jan.-Mar.) apparent oxygen utilization (ml/l) at 75 m. depth.

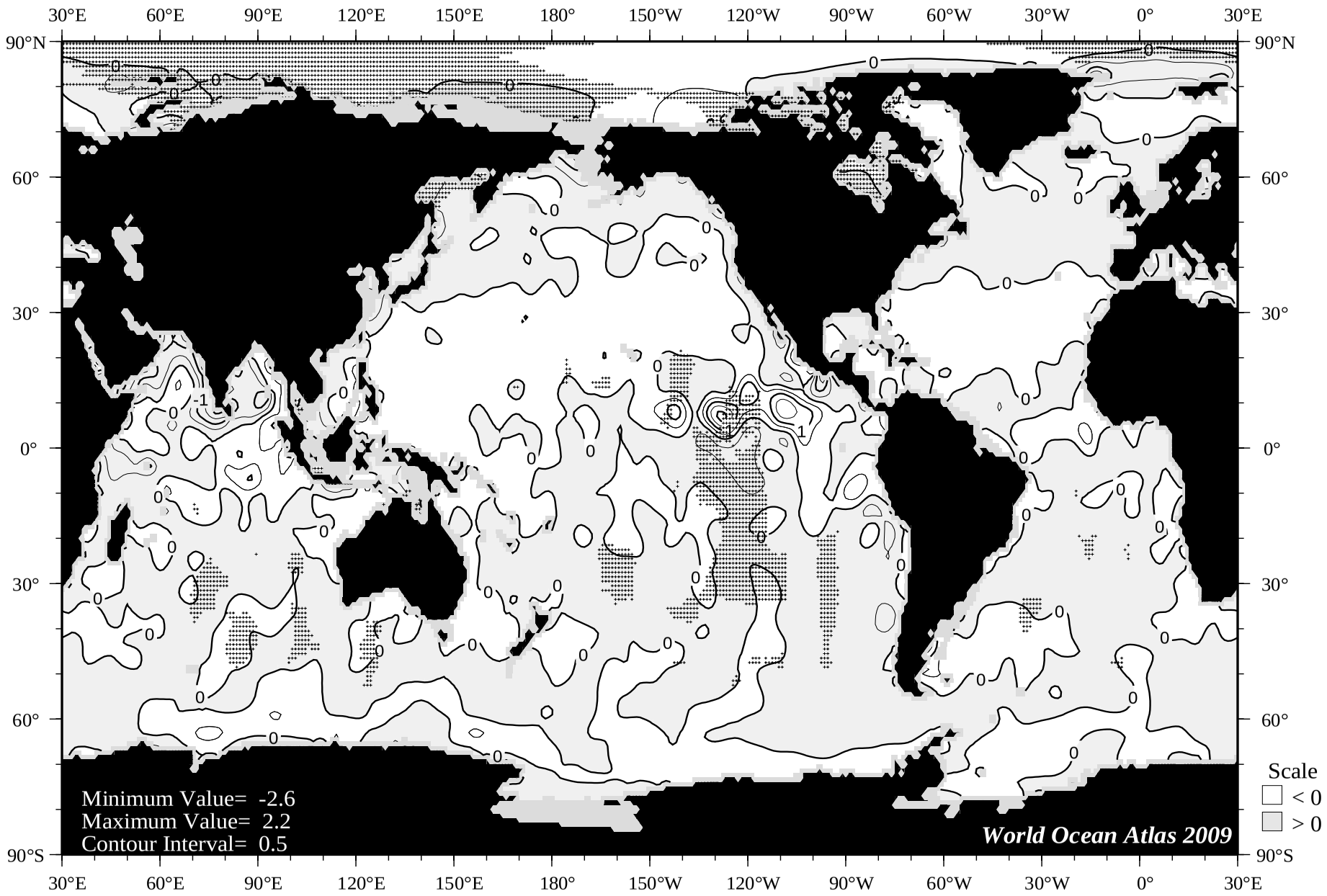

Fig E4 Winter (Jan.-Mar.) minus annual AOU at 75 m. depth.

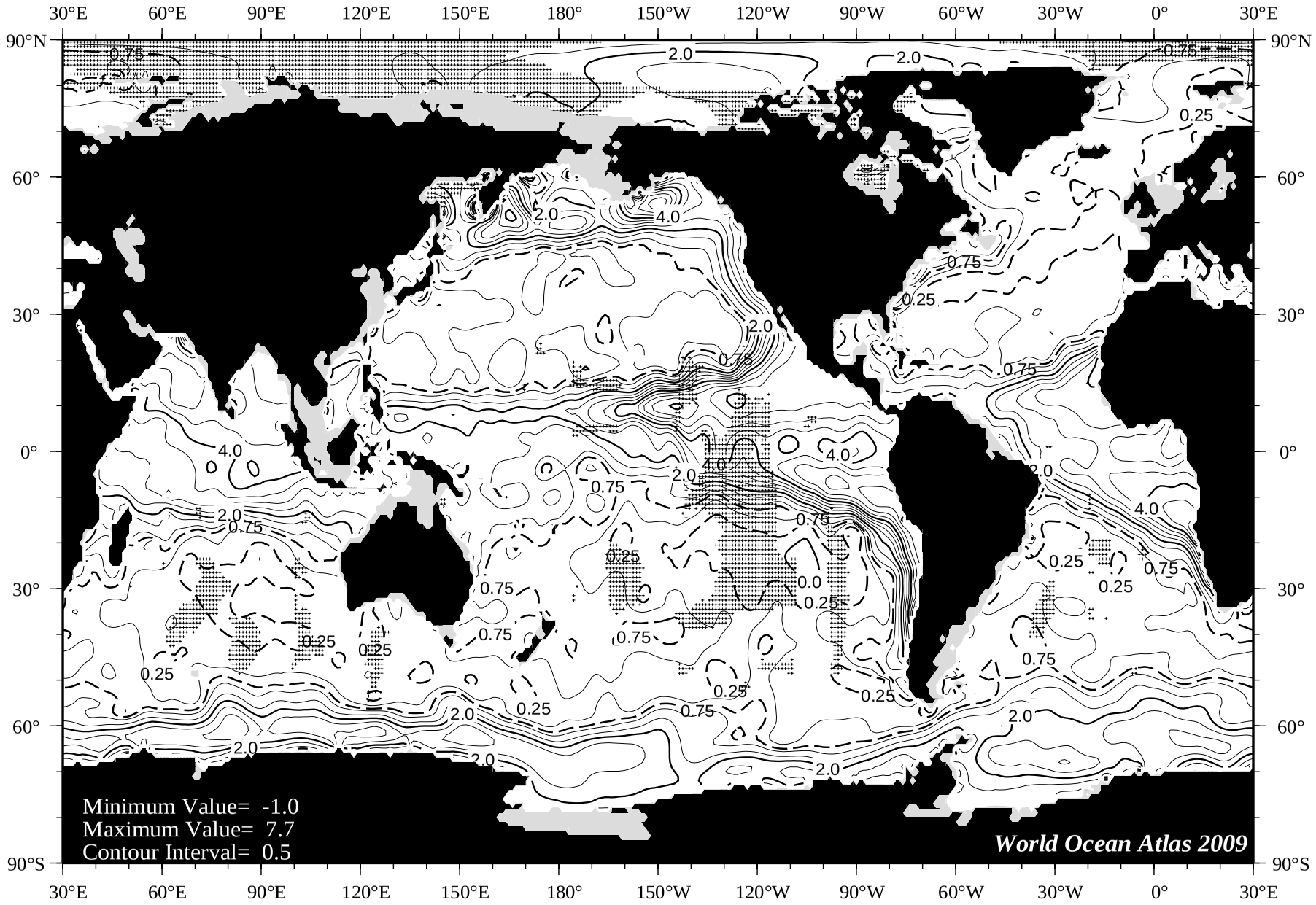

Fig E5 Winter (Jan.-Mar.) apparent oxygen utilization (ml/l) at 150 m. depth.

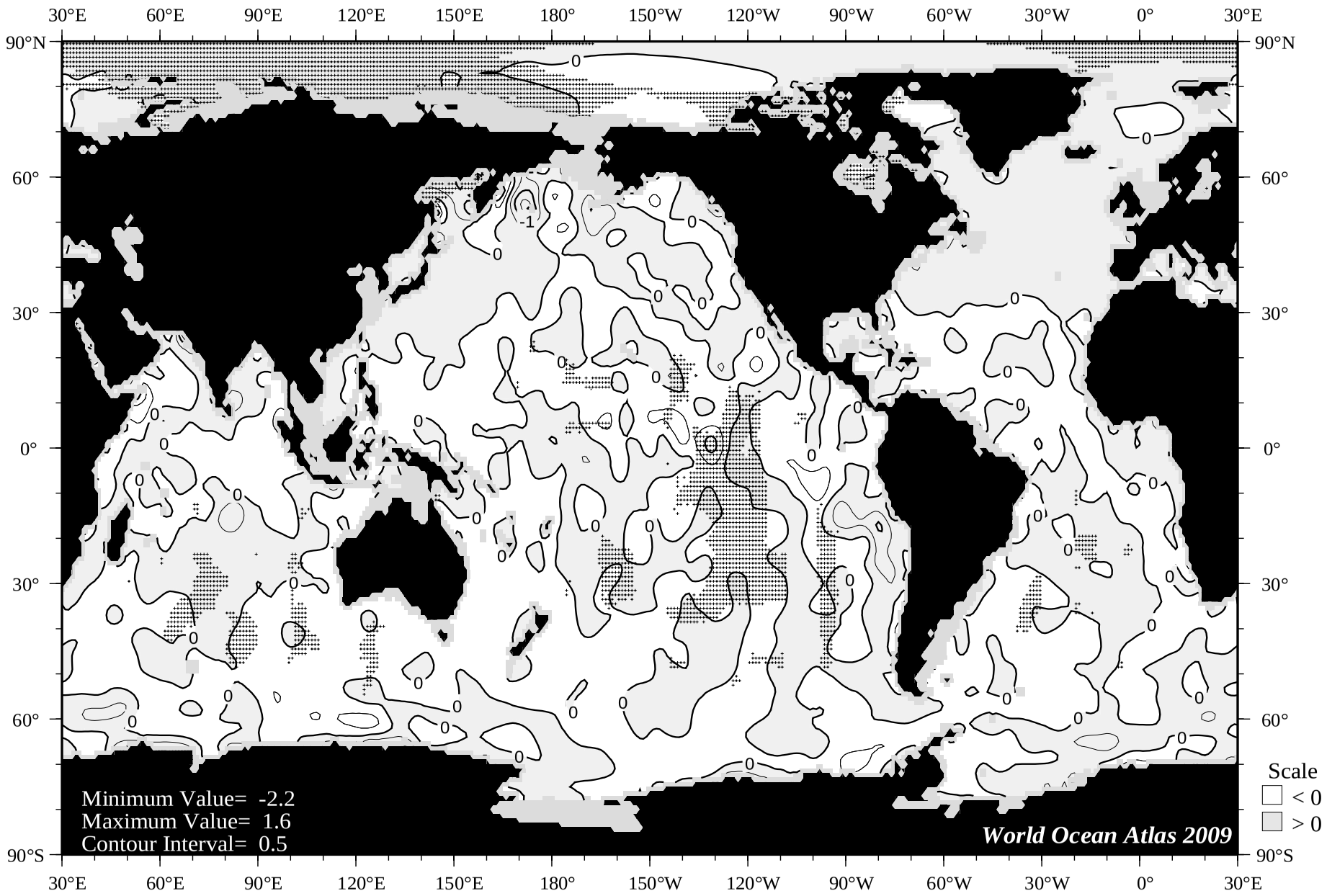

Fig E6 Winter (Jan.-Mar.) minus annual AOU at 150 m. depth.

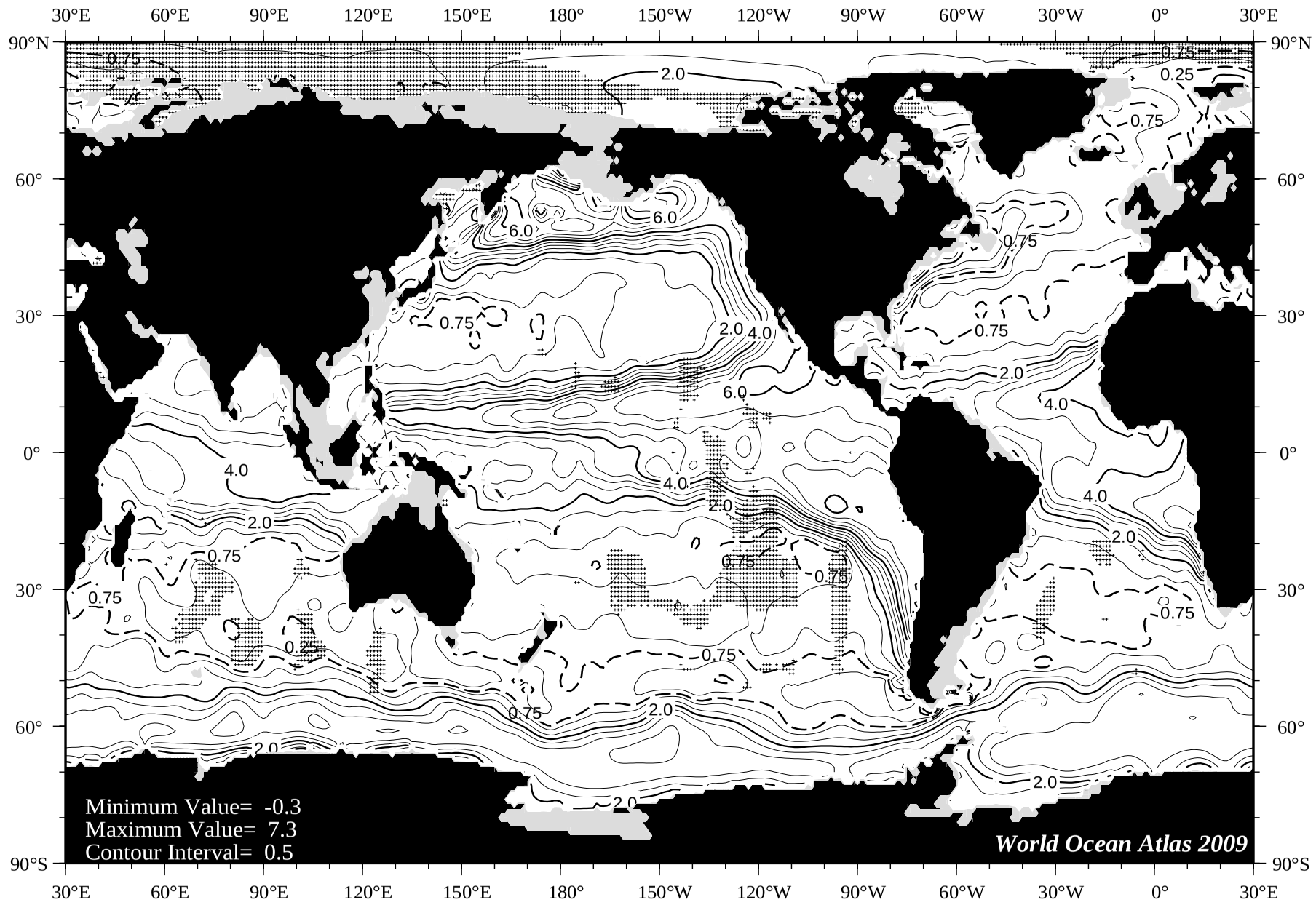

Fig E7 Winter (Jan.-Mar.) apparent oxygen utilization (ml/l) at 250 m. depth.

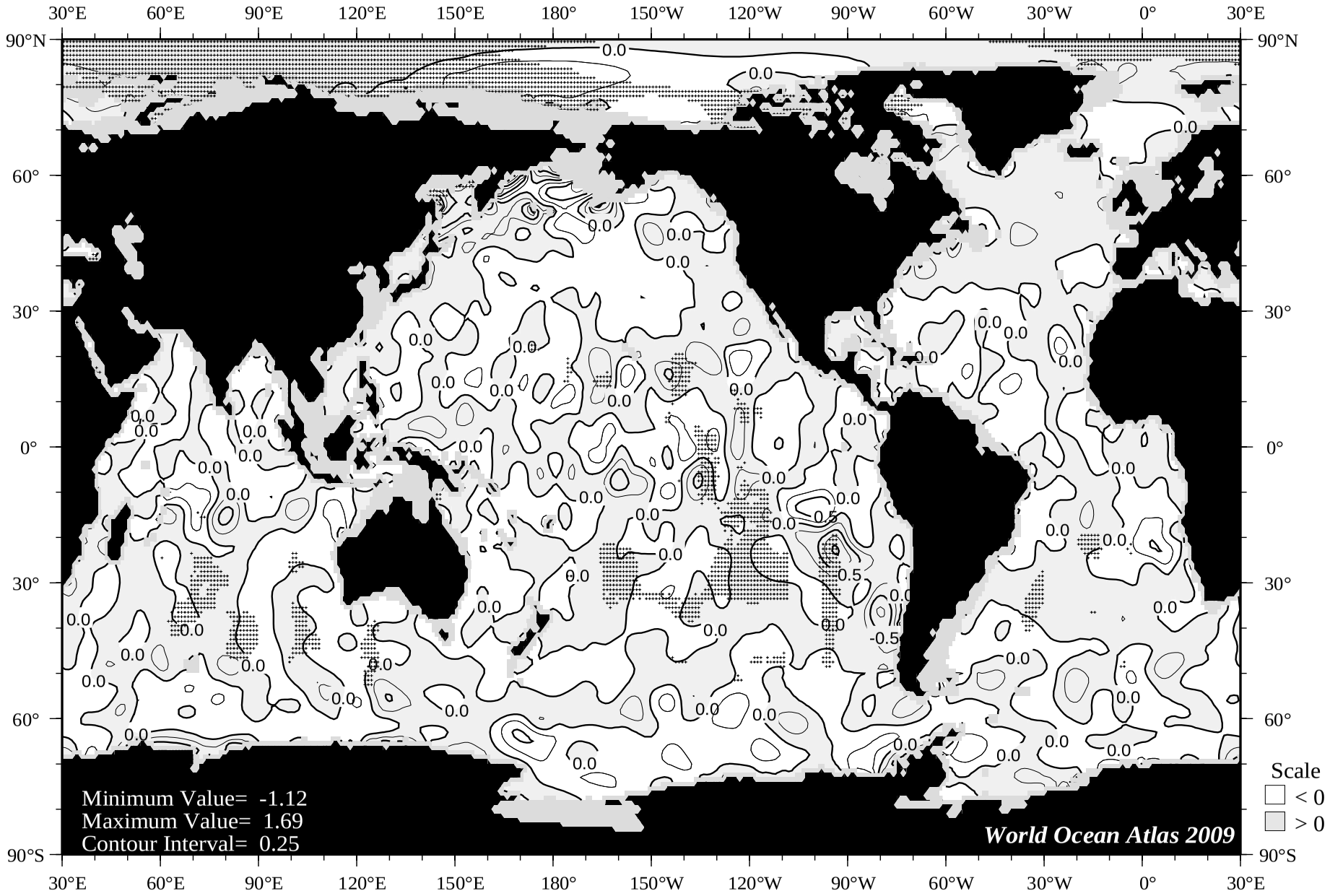

Fig E8 Winter (Jan.-Mar.) minus annual AOU at 250 m. depth.

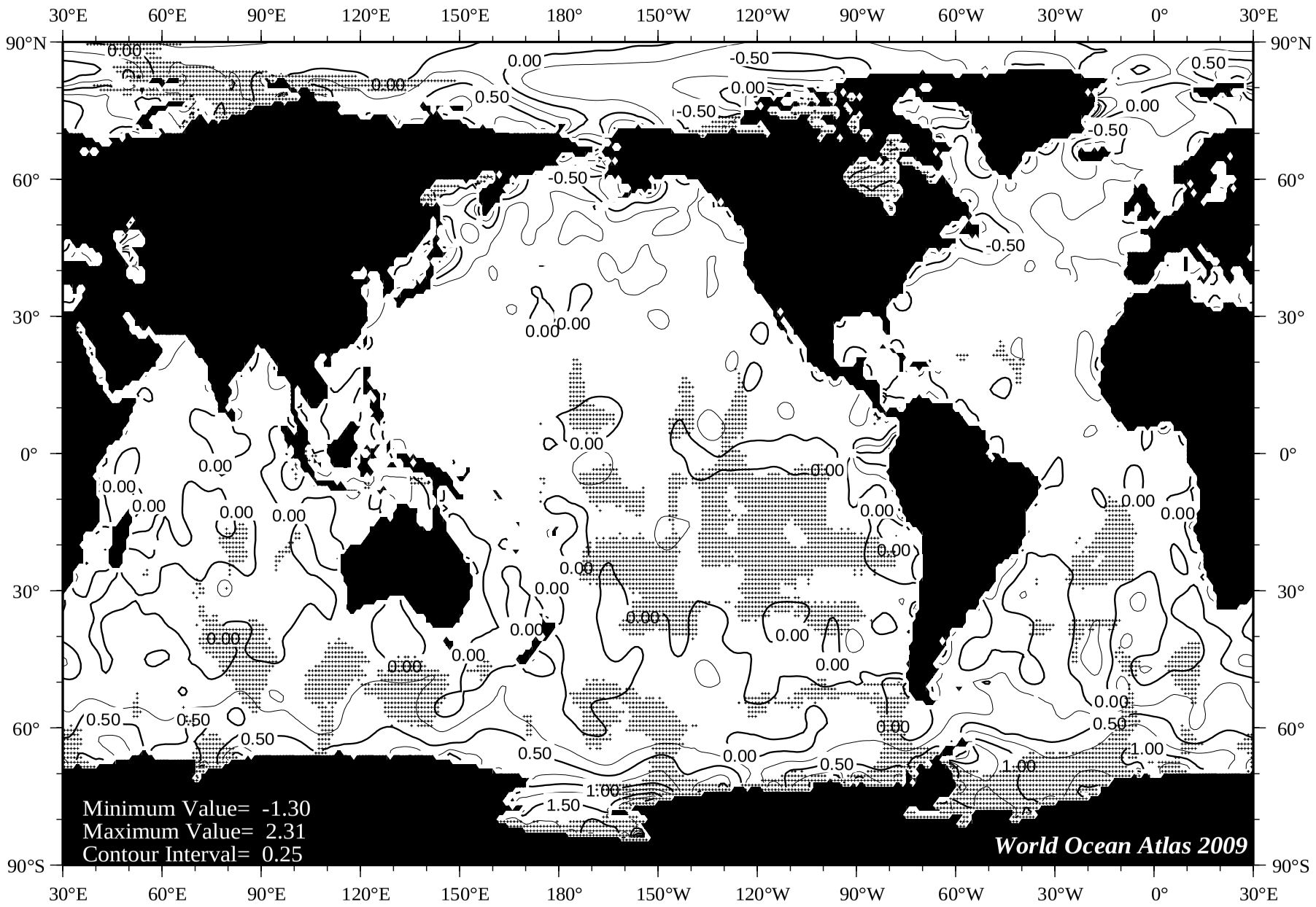

Fig E9 Spring (Apr.-Jun.) apparent oxygen utilization (ml/l) at the surface.

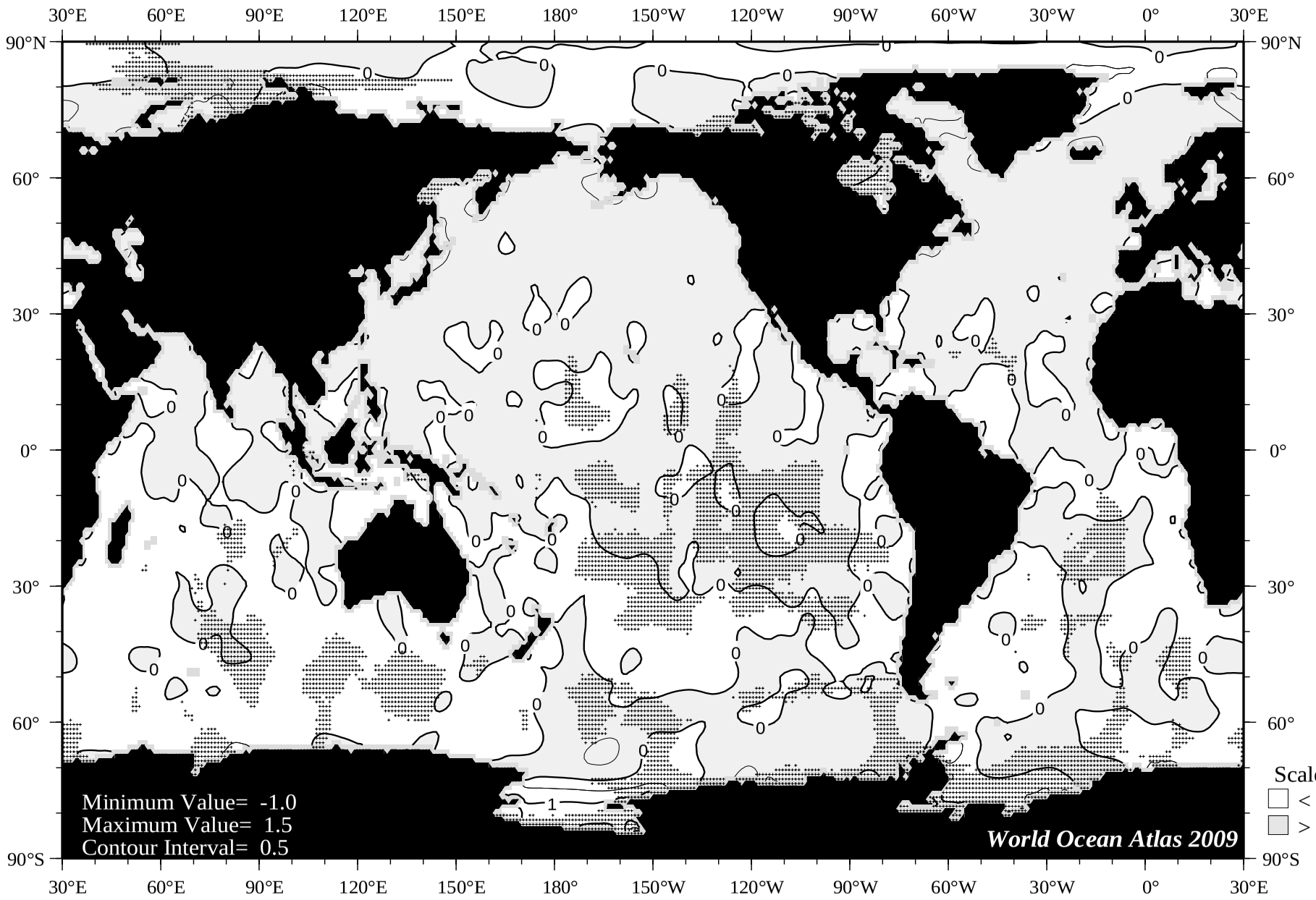

Fig E10 Spring (Apr.-Jun.) minus annual AOU at the surface.

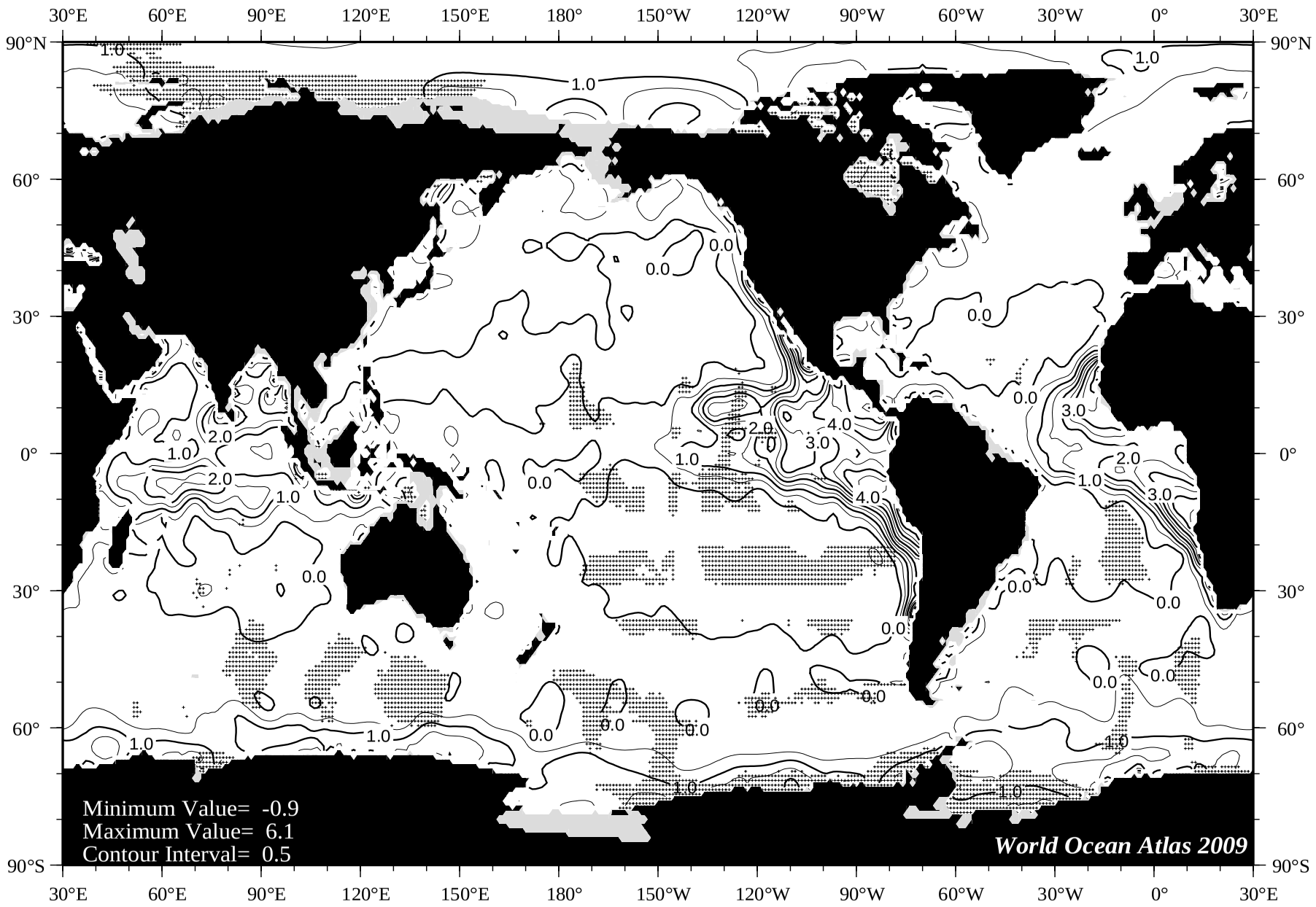

Fig E11 Spring (Apr.-Jun.) apparent oxygen utilization (ml/l) at 75 m. depth.

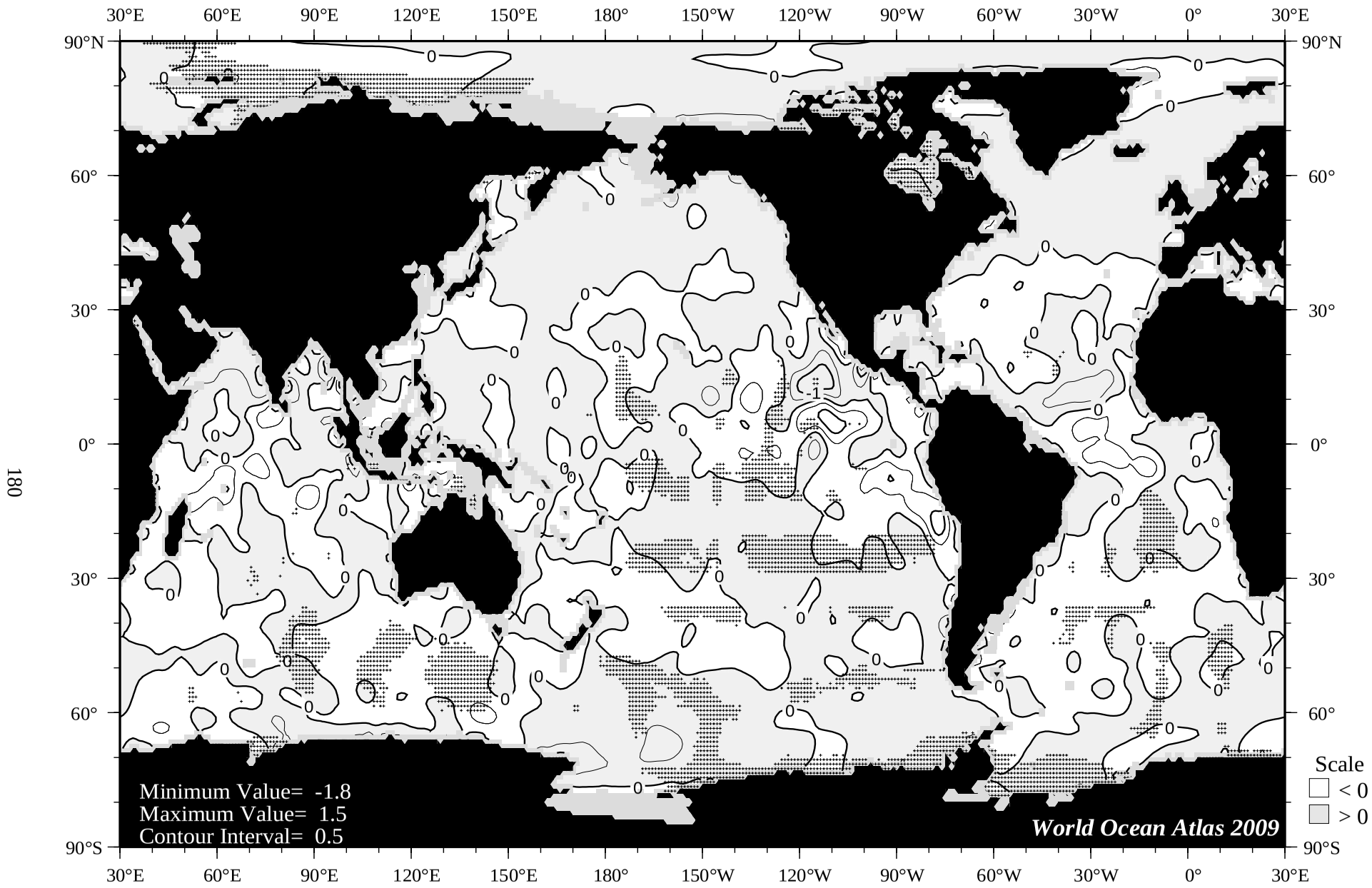

Fig E12 Spring (Apr.-Jun.) minus annual AOU at 75 m. depth.

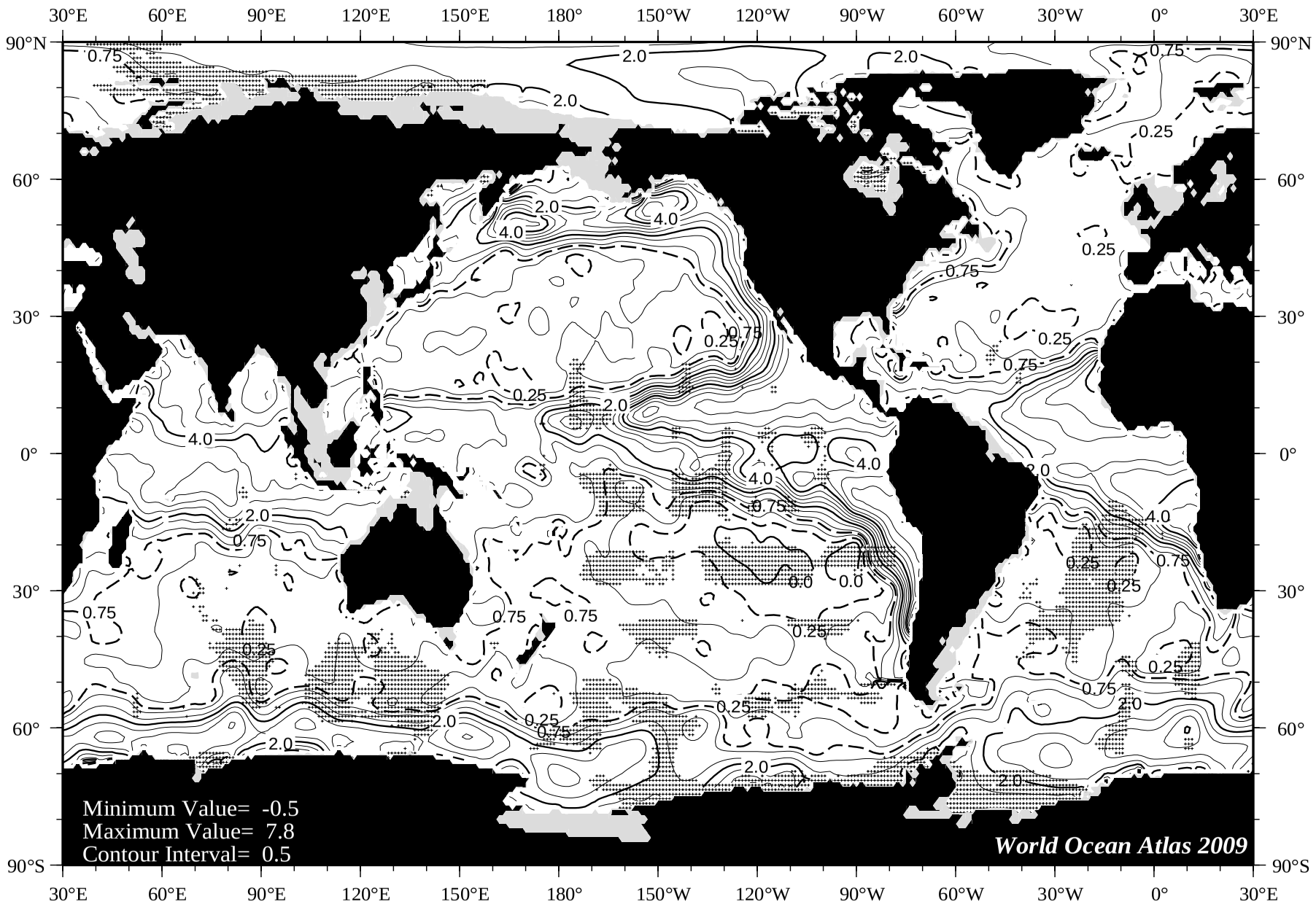

Fig E13 Spring (Apr.-Jun.) apparent oxygen utilization (ml/l) at 150 m. depth.

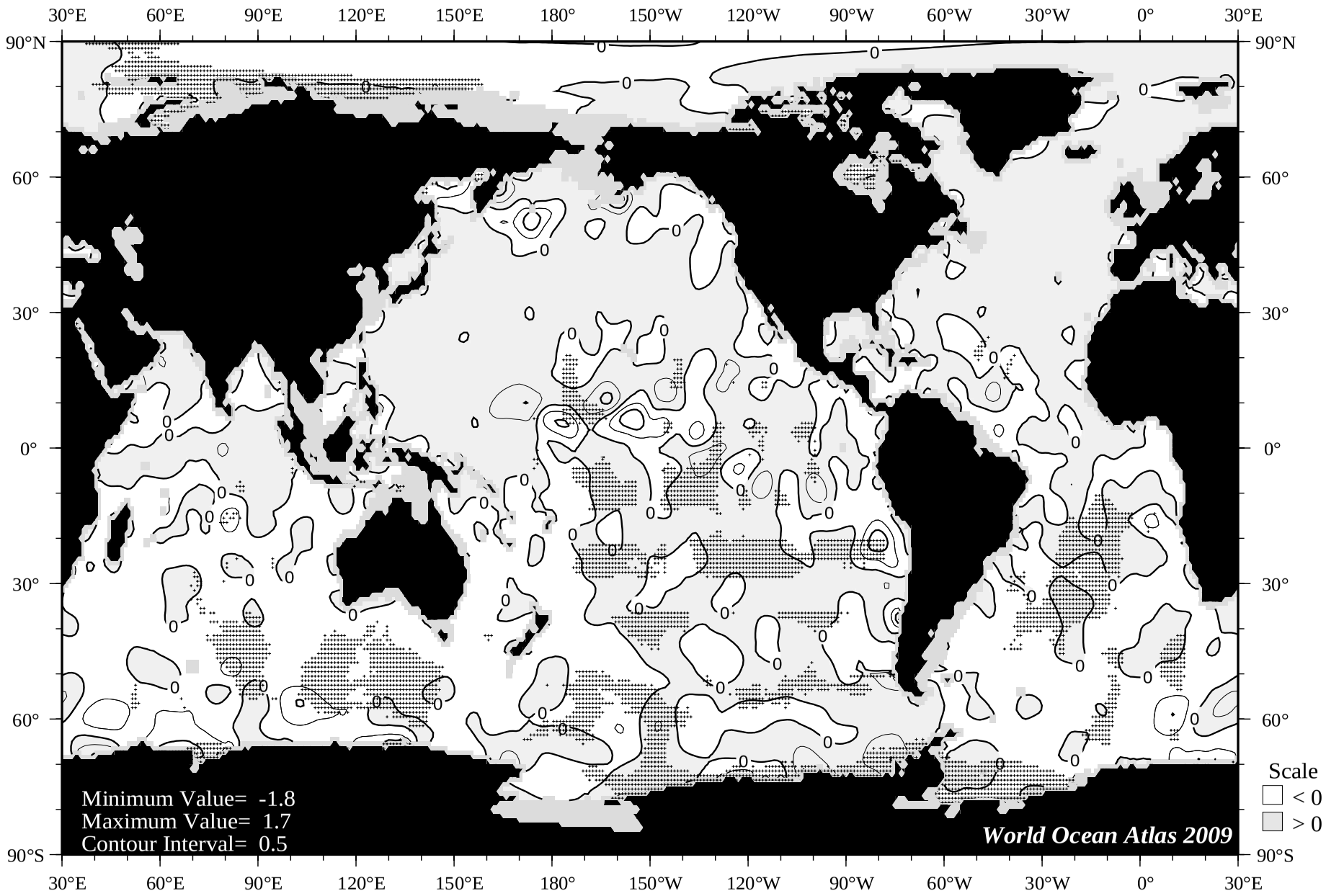

Fig E14 Spring (Apr.-Jun.) minus annual AOU at 150 m. depth.

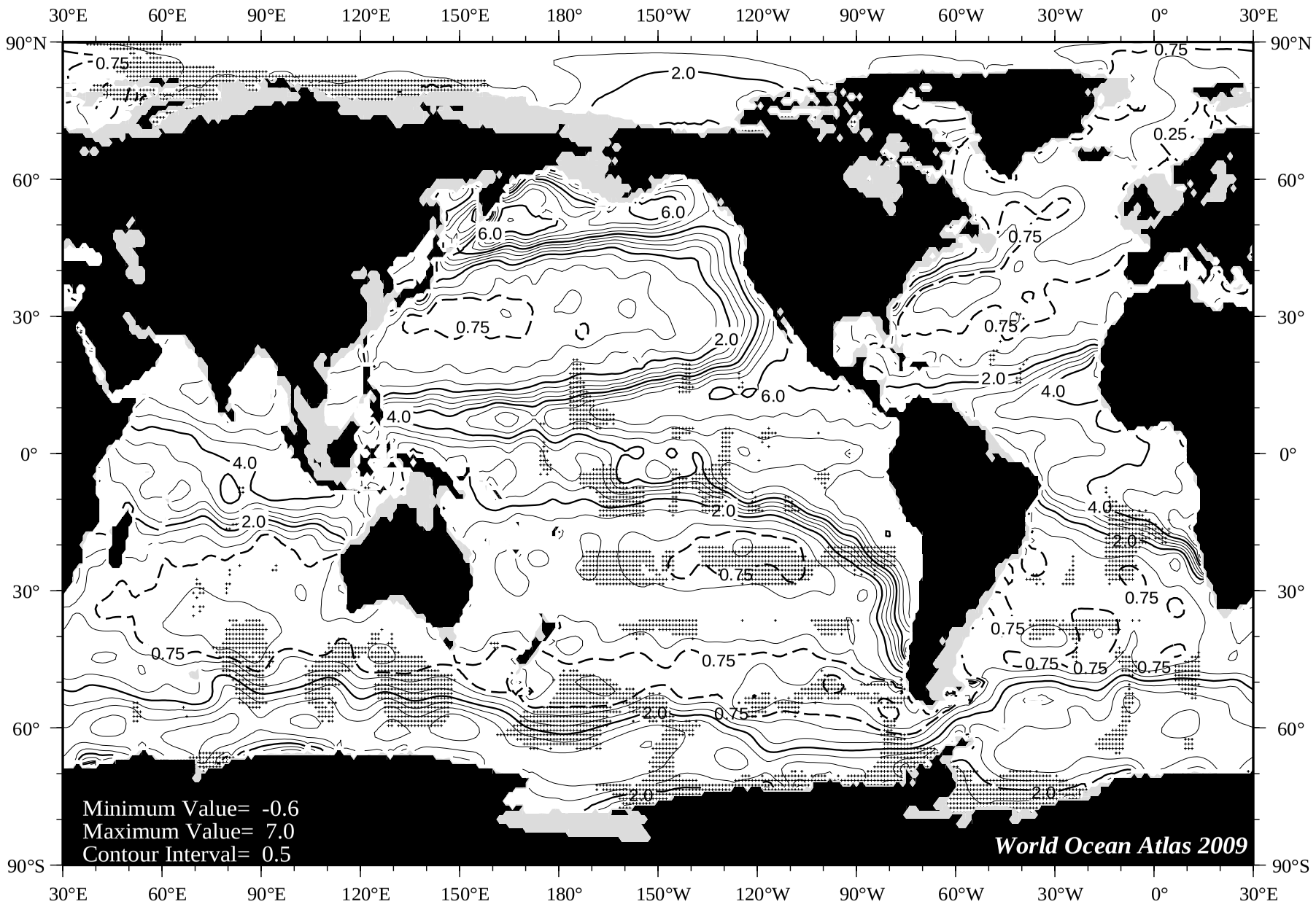

Fig E15 Spring (Apr.-Jun.) apparent oxygen utilization (ml/l) at 250 m. depth.

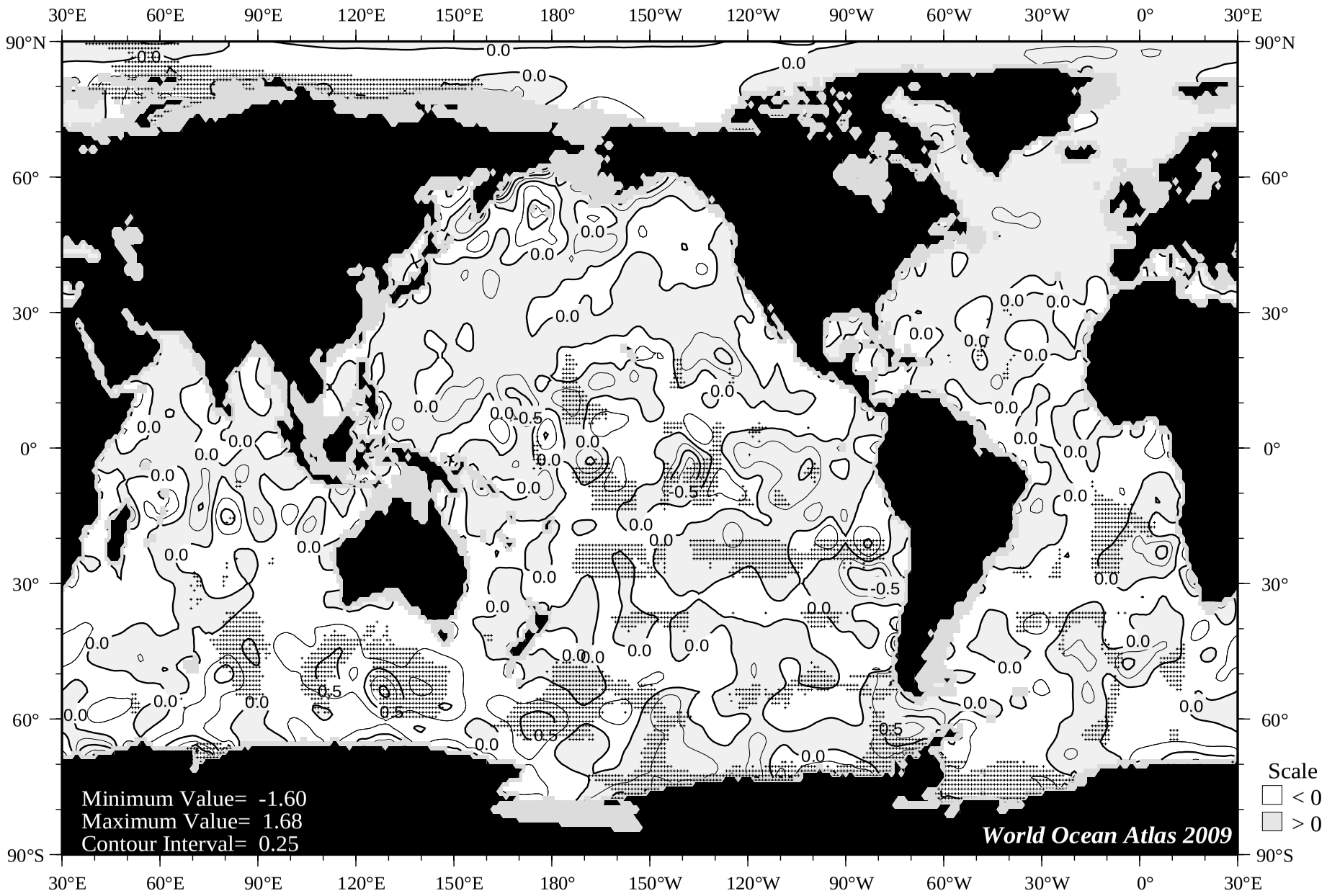

Fig E16 Spring (Apr.-Jun.) minus annual AOU at 250 m. depth.

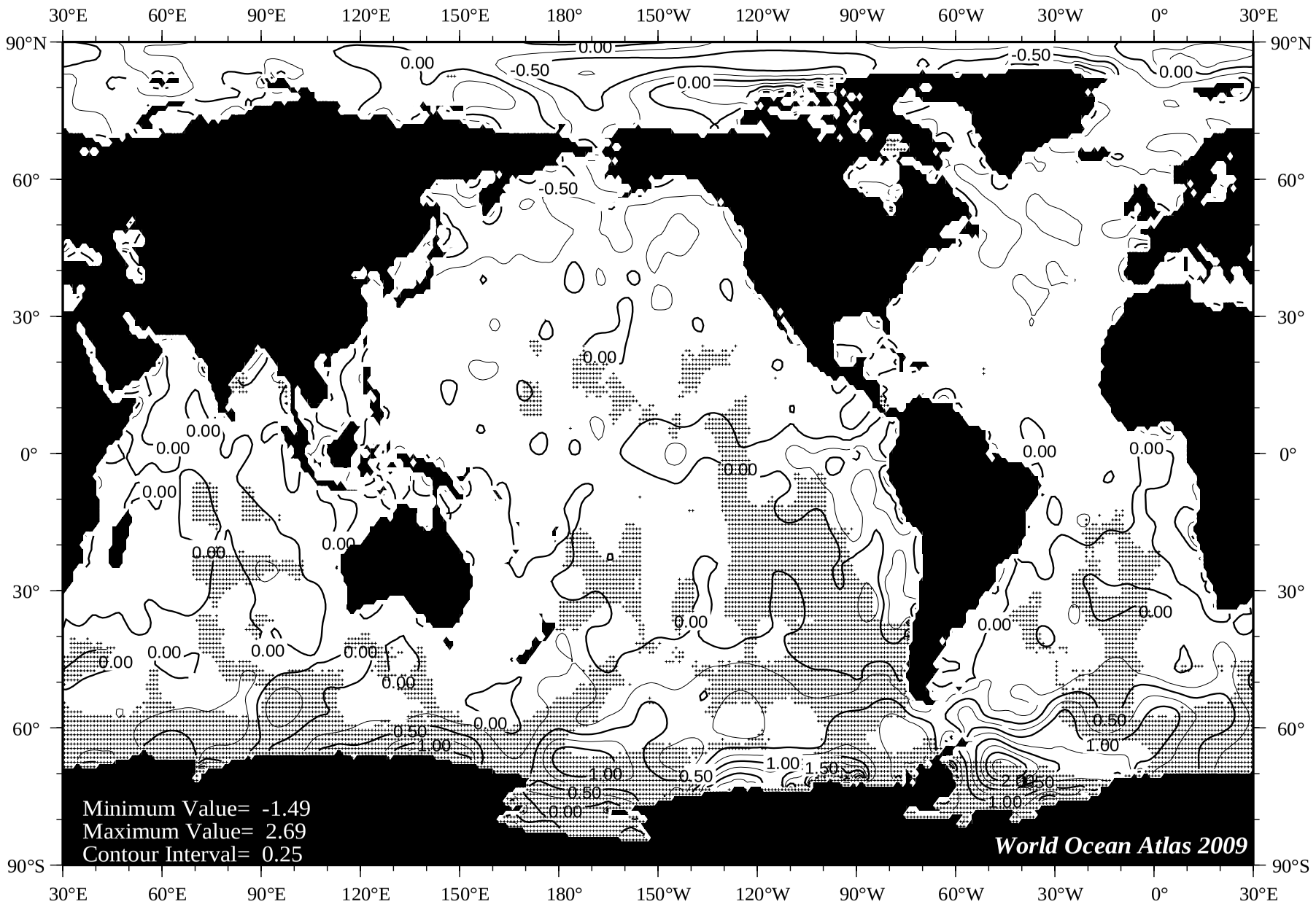

Fig E17 Summer (Jul.-Sep.) apparent oxygen utilization (ml/l) at the surface.

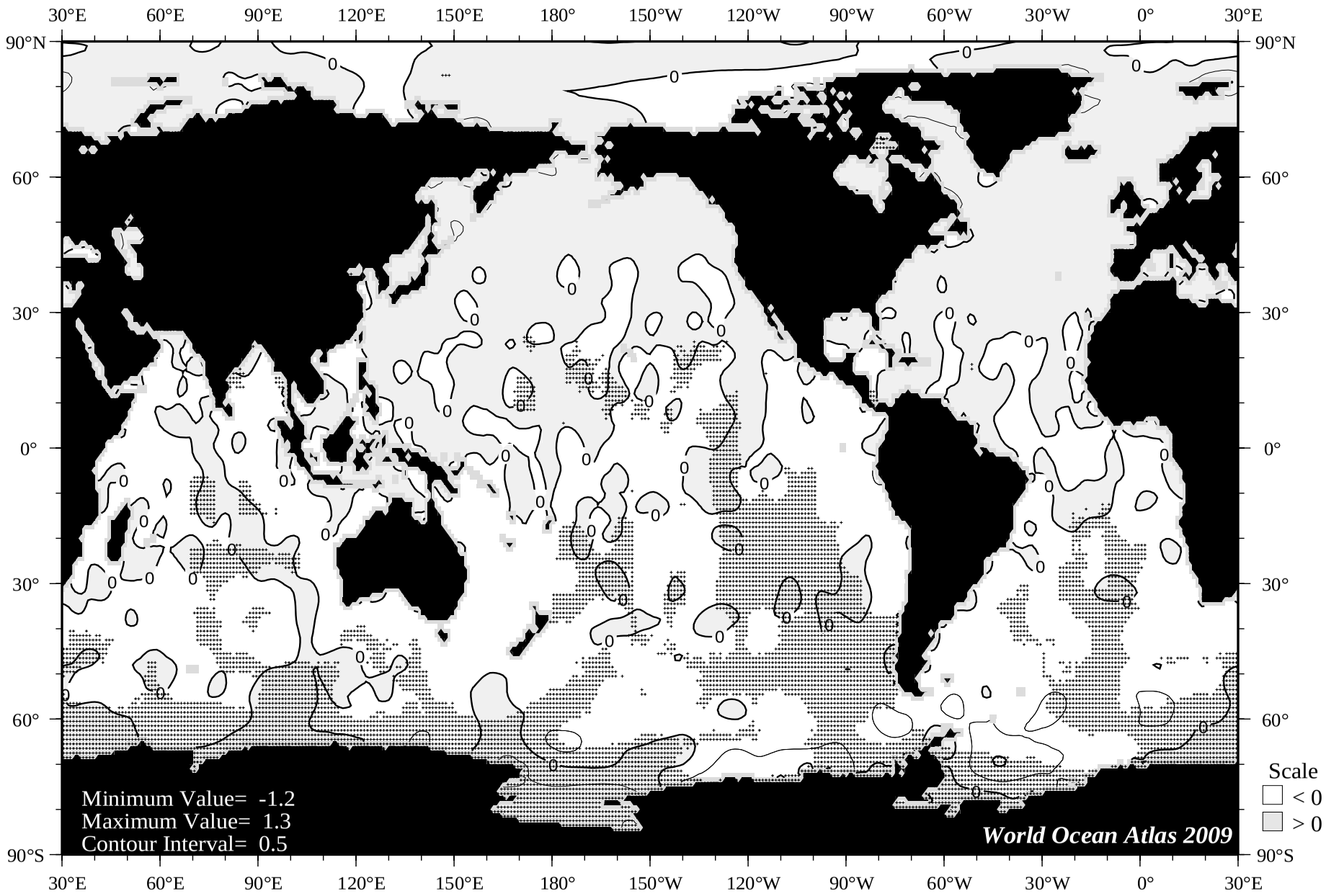

Fig E18 Summer (Jul.-Sep.) minus annual AOU at the surface.

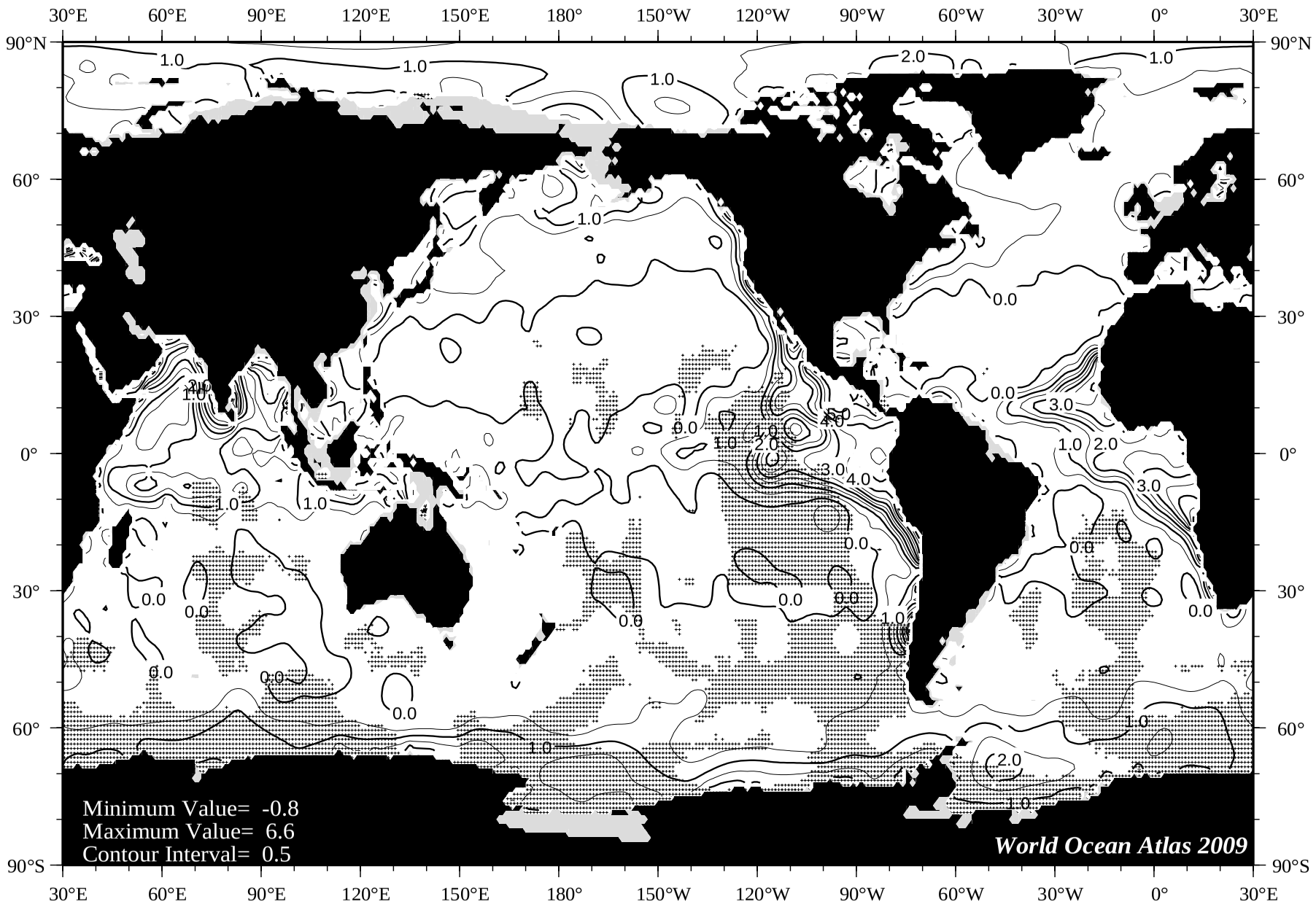

Fig E19 Summer (Jul.-Sep.) apparent oxygen utilization (ml/l) at 75 m. depth.

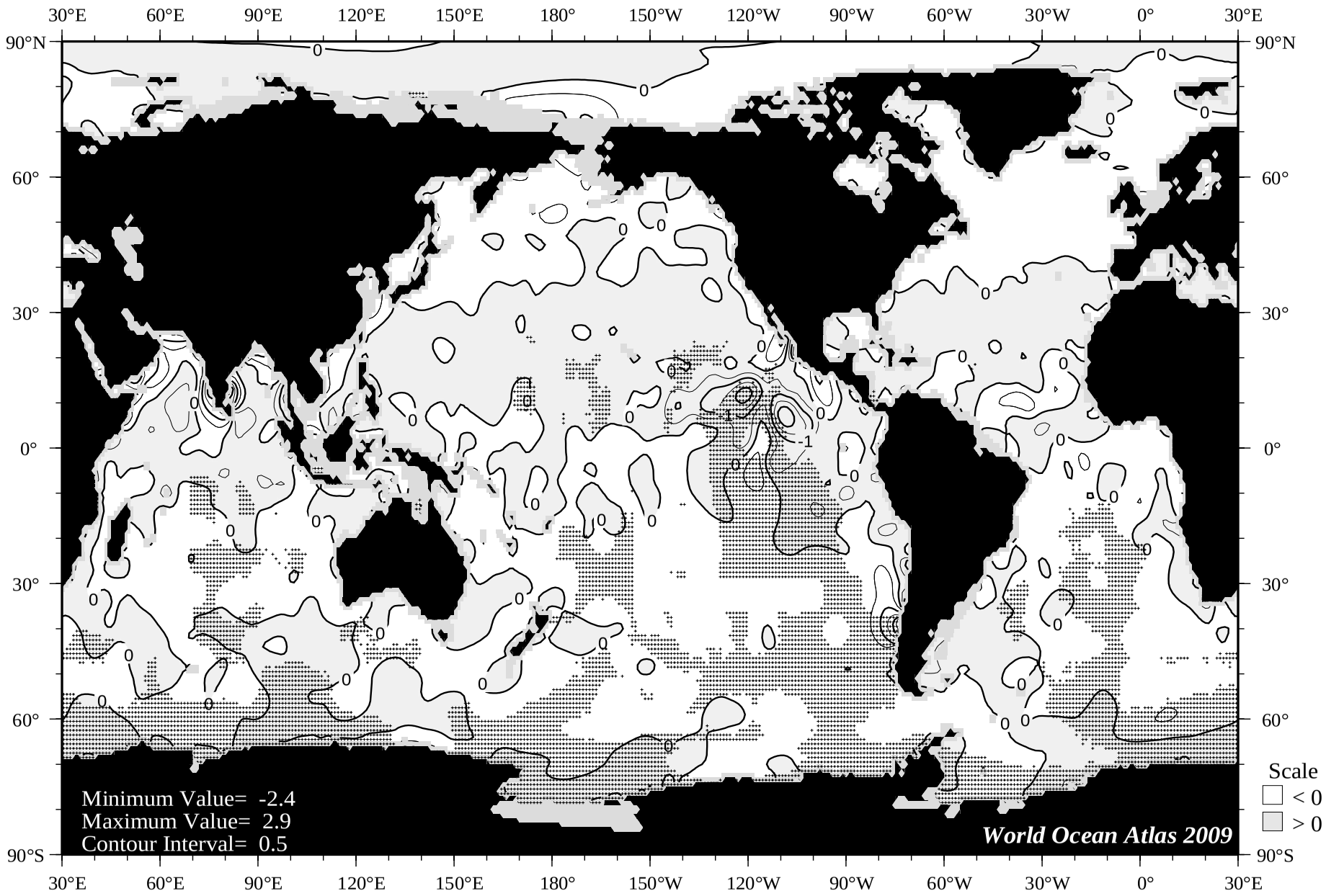

Fig E20 Summer (Jul.-Sep.) minus annual AOU at 75 m. depth.

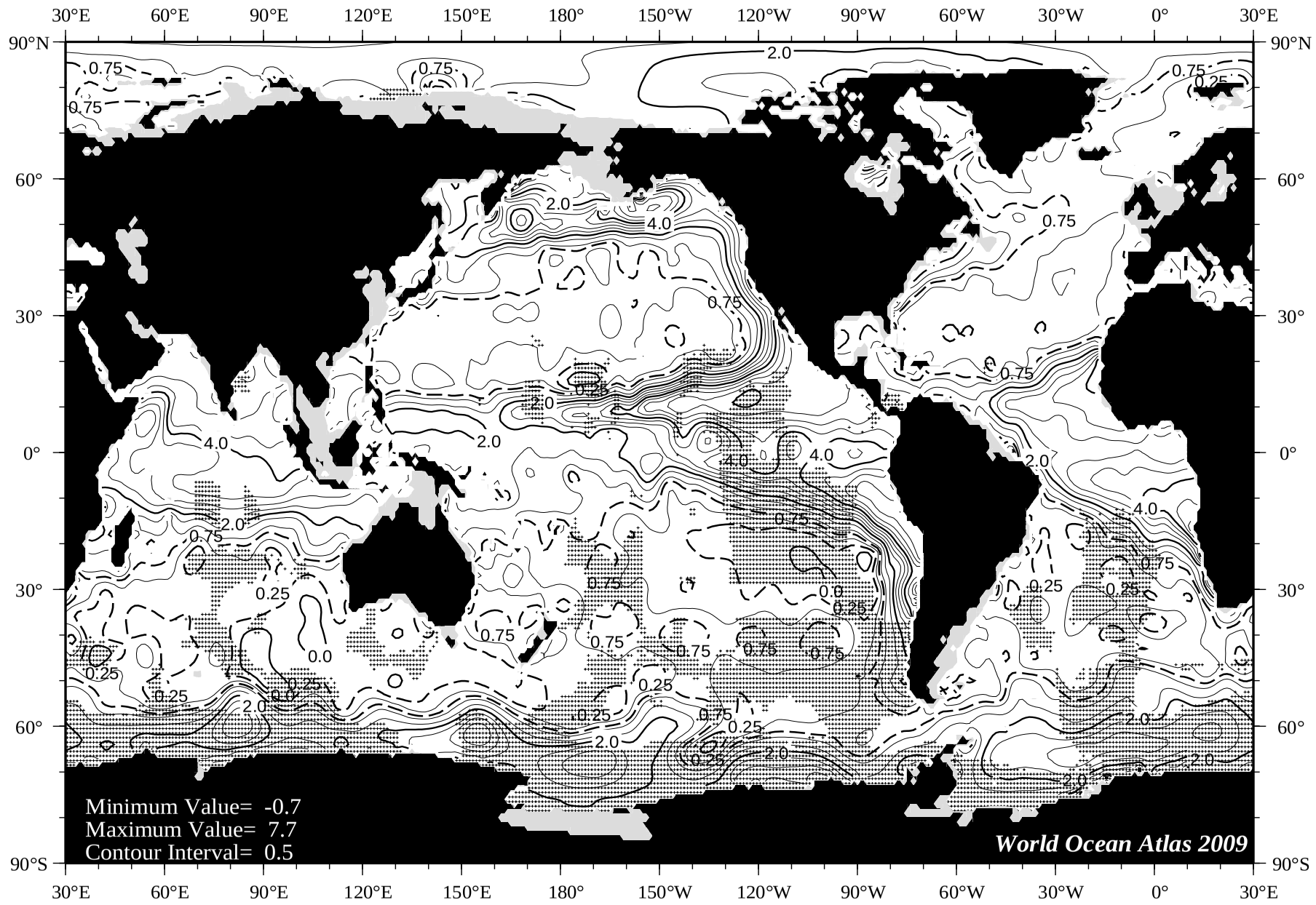

Fig E21 Summer (Jul.-Sep.) apparent oxygen utilization (ml/l) at 150 m. depth.

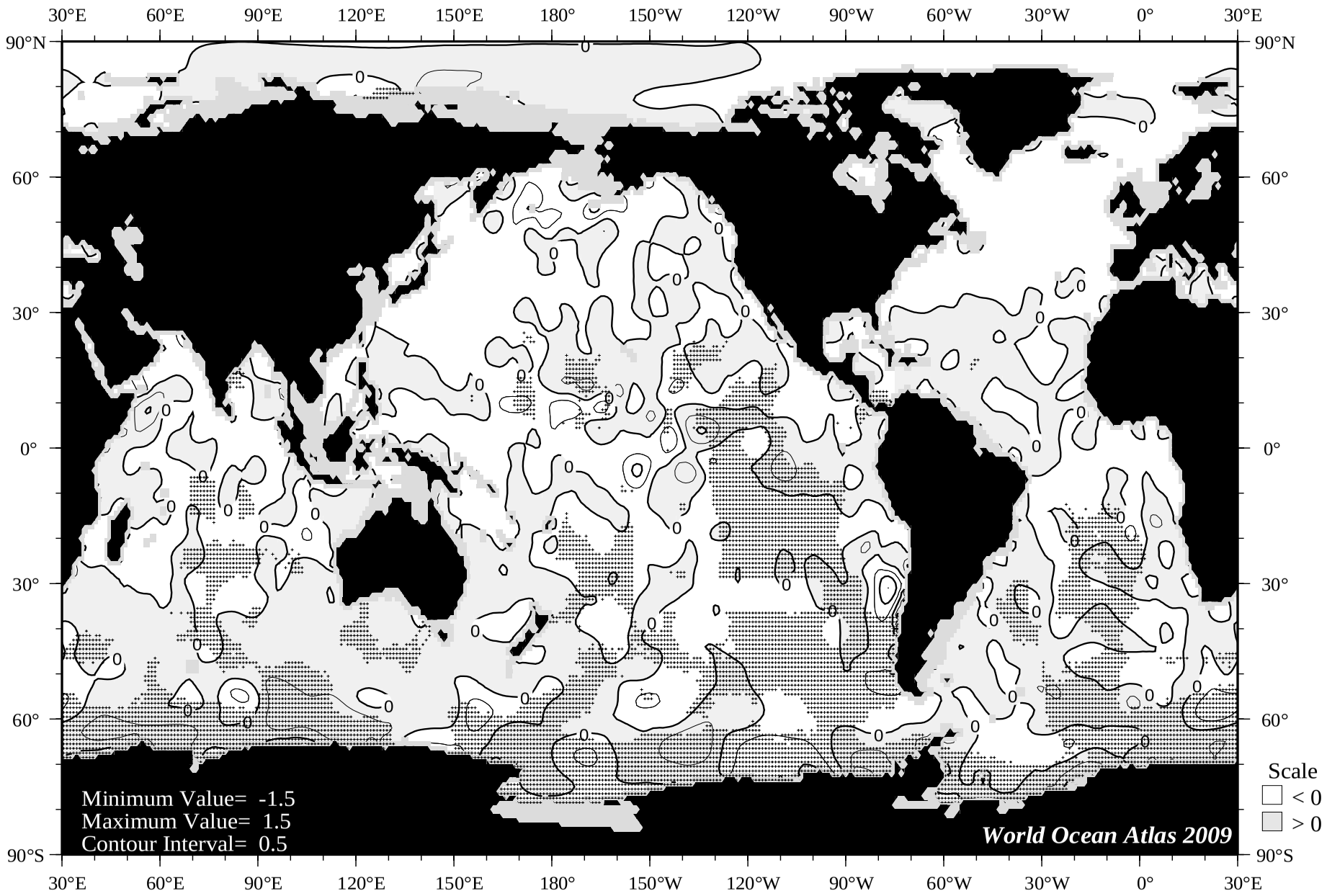

Fig E22 Summer (Jul.-Sep.) minus annual AOU at 150 m. depth.

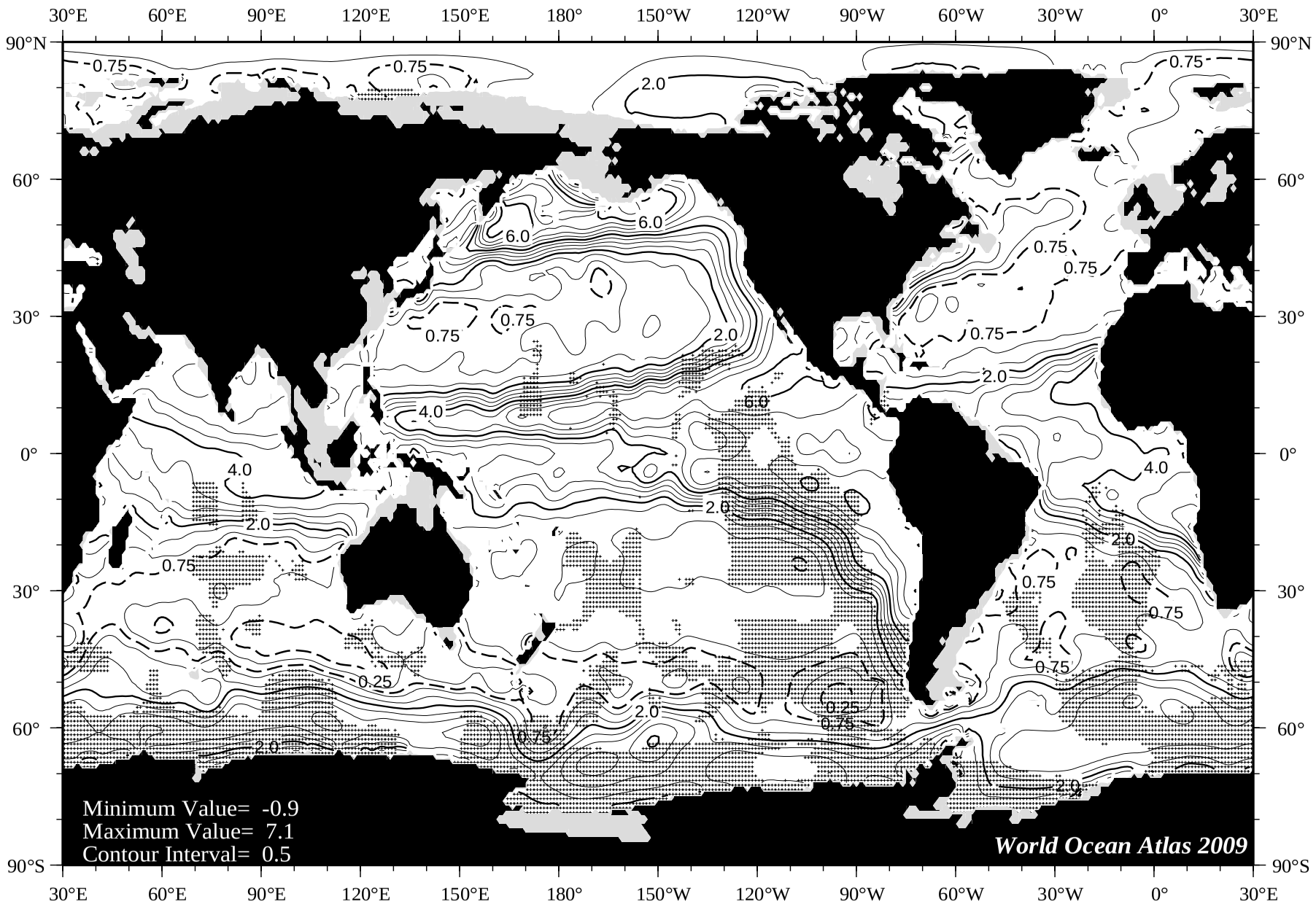

Fig E23 Summer (Jul.-Sep.) apparent oxygen utilization (ml/l) at 250 m. depth.

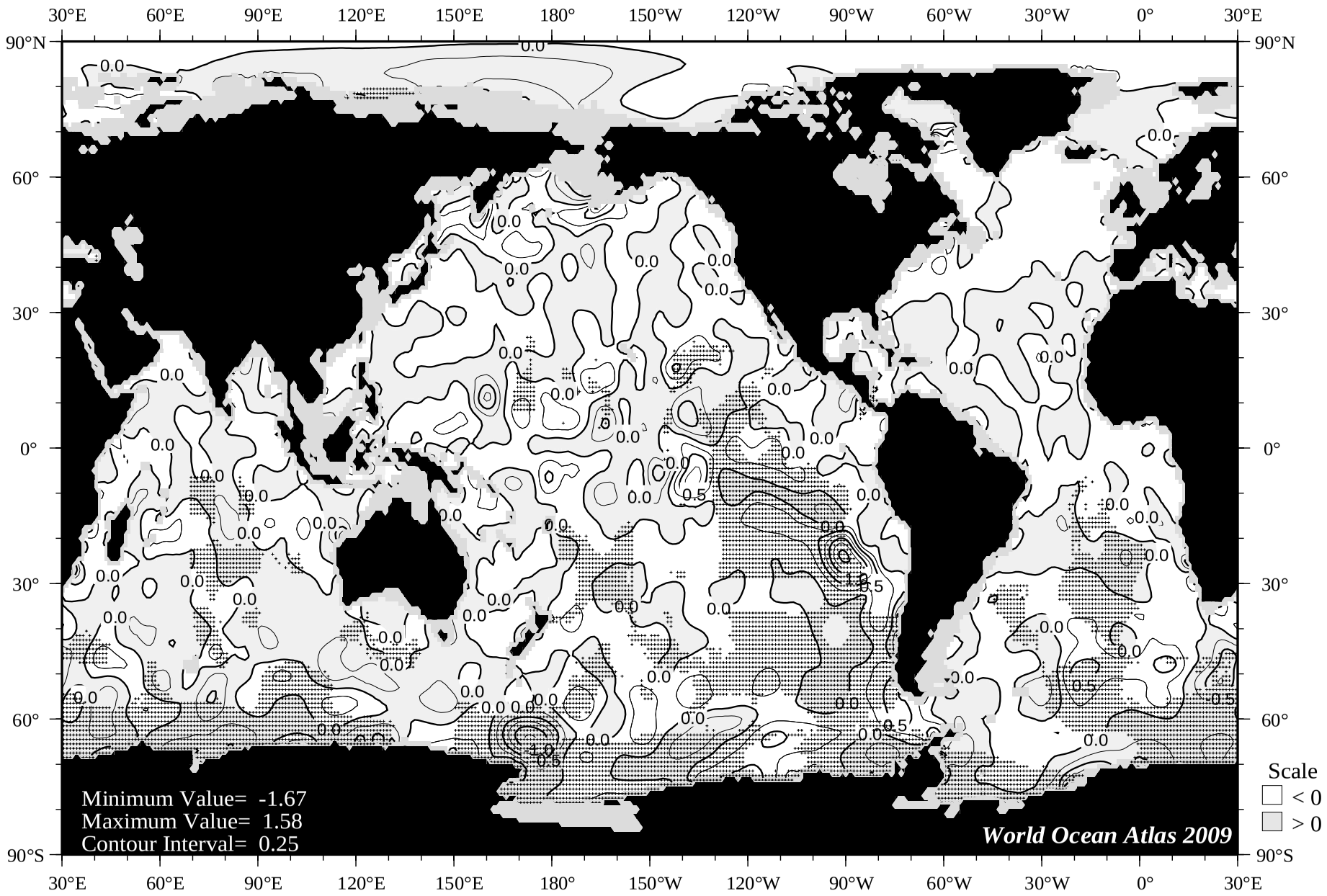

Fig E24 Summer (Jul.-Sep.) minus annual AOU at 250 m. depth.

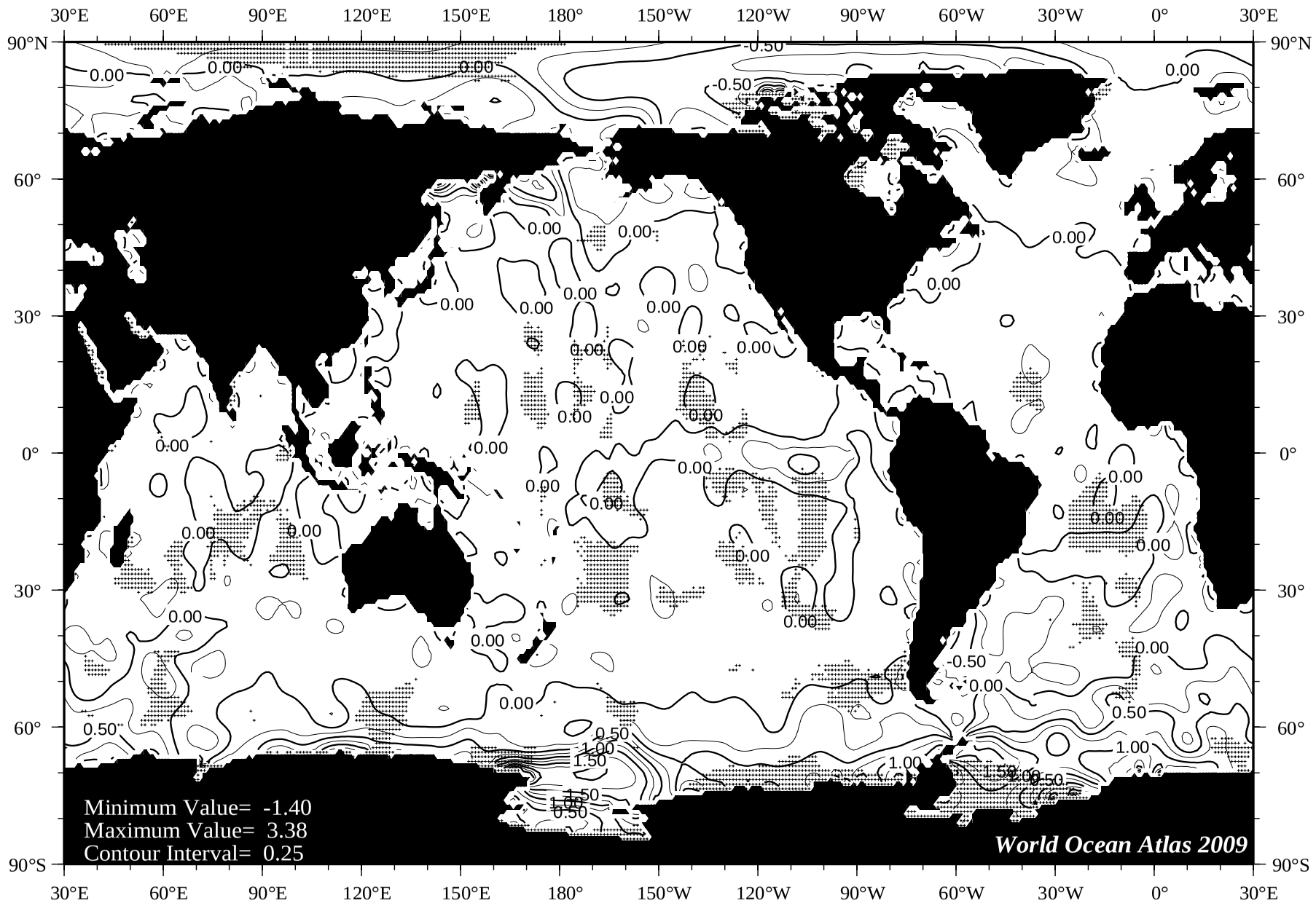

Fig E25 Fall (Oct.-Dec.) apparent oxygen utilization (ml/l) at the surface.

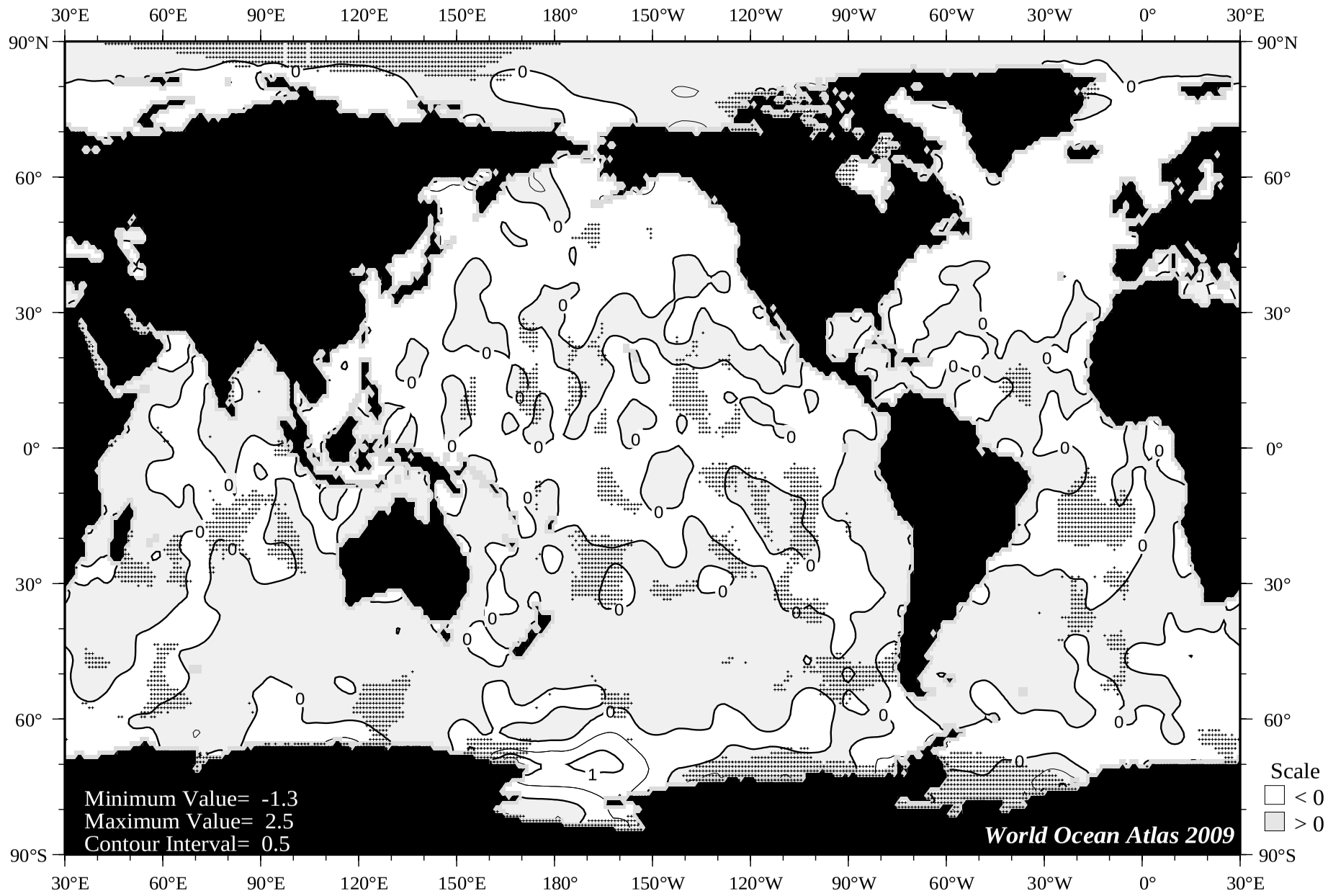

Fig E26 Fall (Oct.-Dec.) minus annual AOU at the surface.

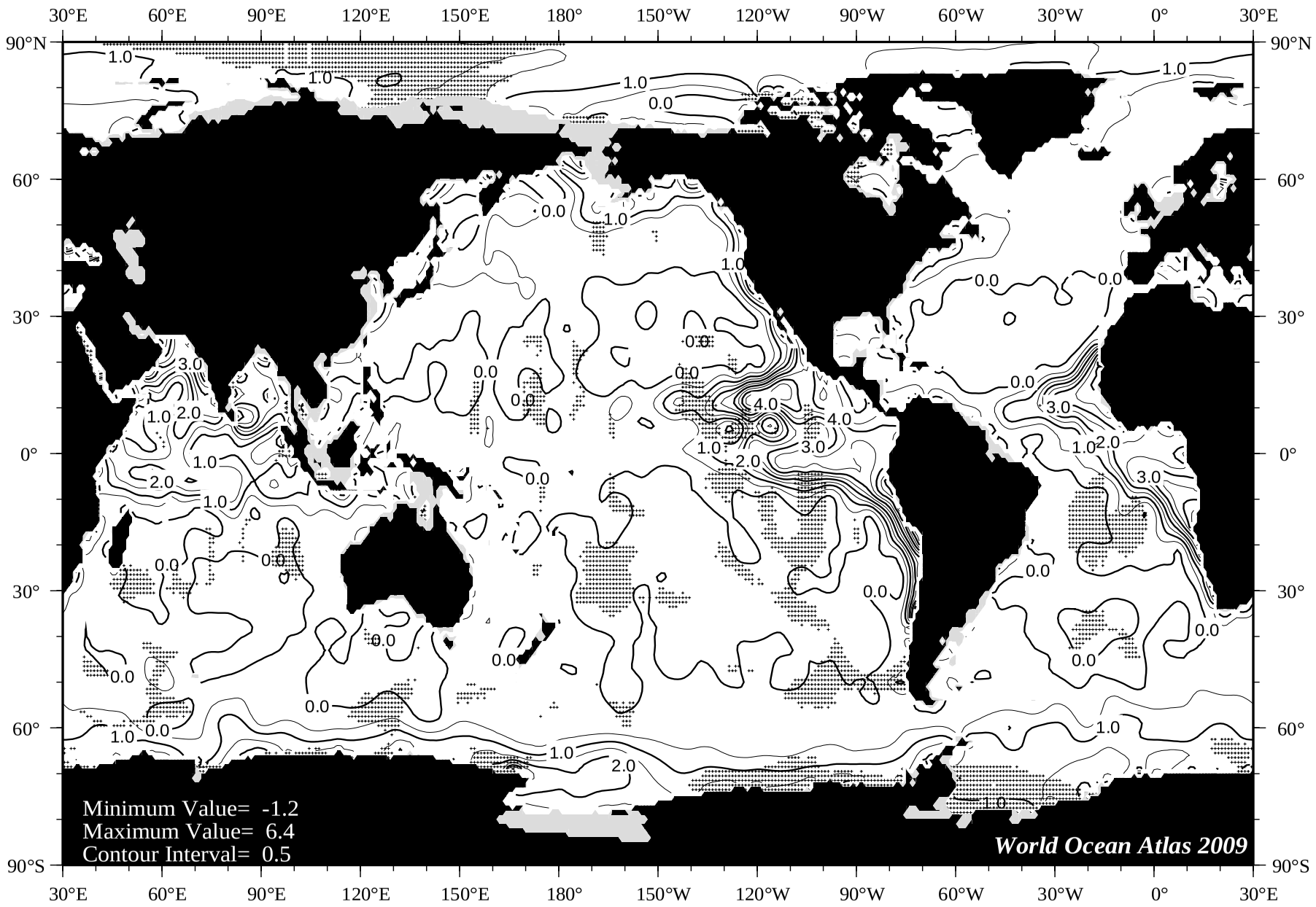

Fig E27 Fall (Oct.-Dec.) apparent oxygen utilization (ml/l) at 75 m. depth.

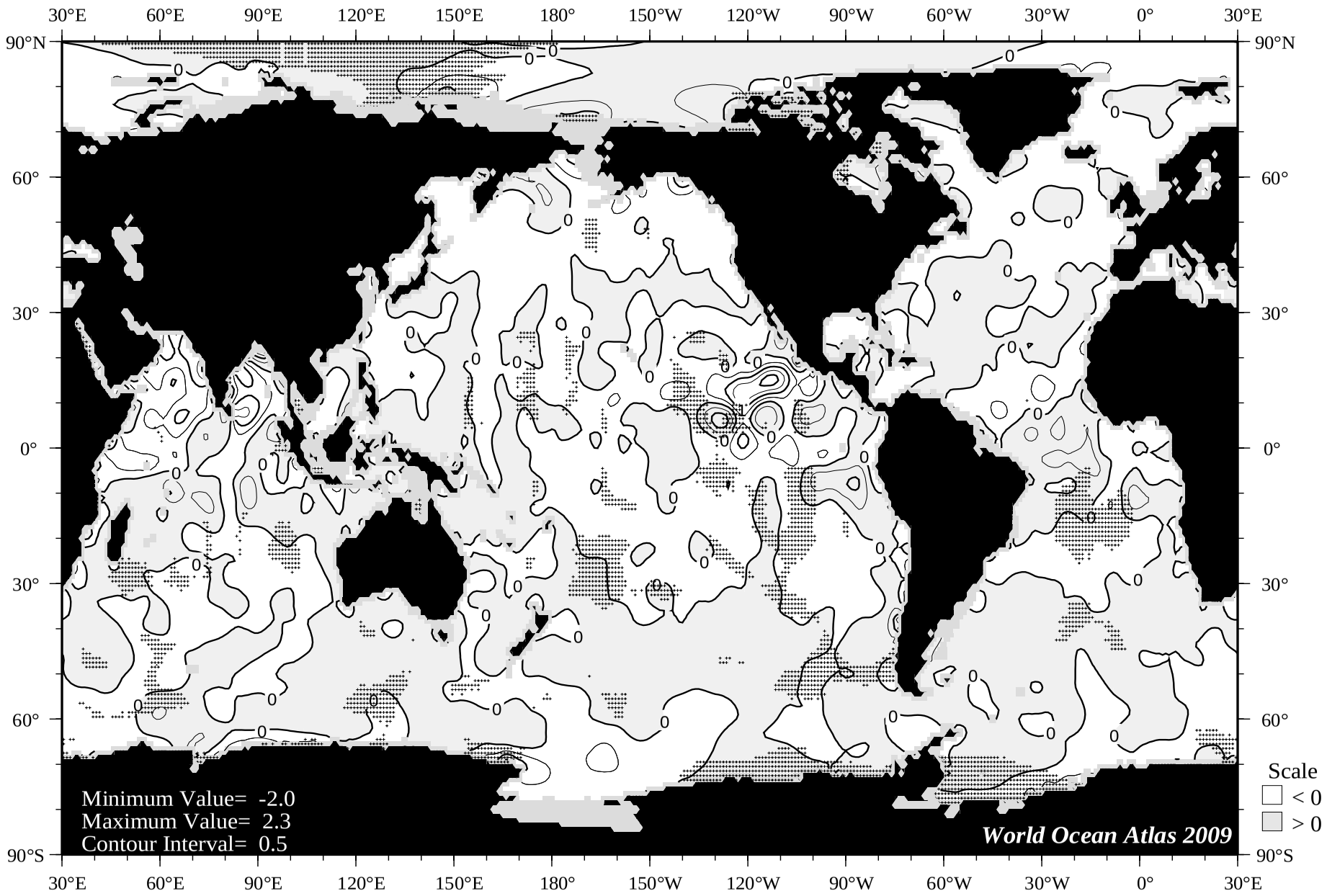

Fig E28 Fall (Oct.-Dec.) minus annual AOU at 75 m. depth.

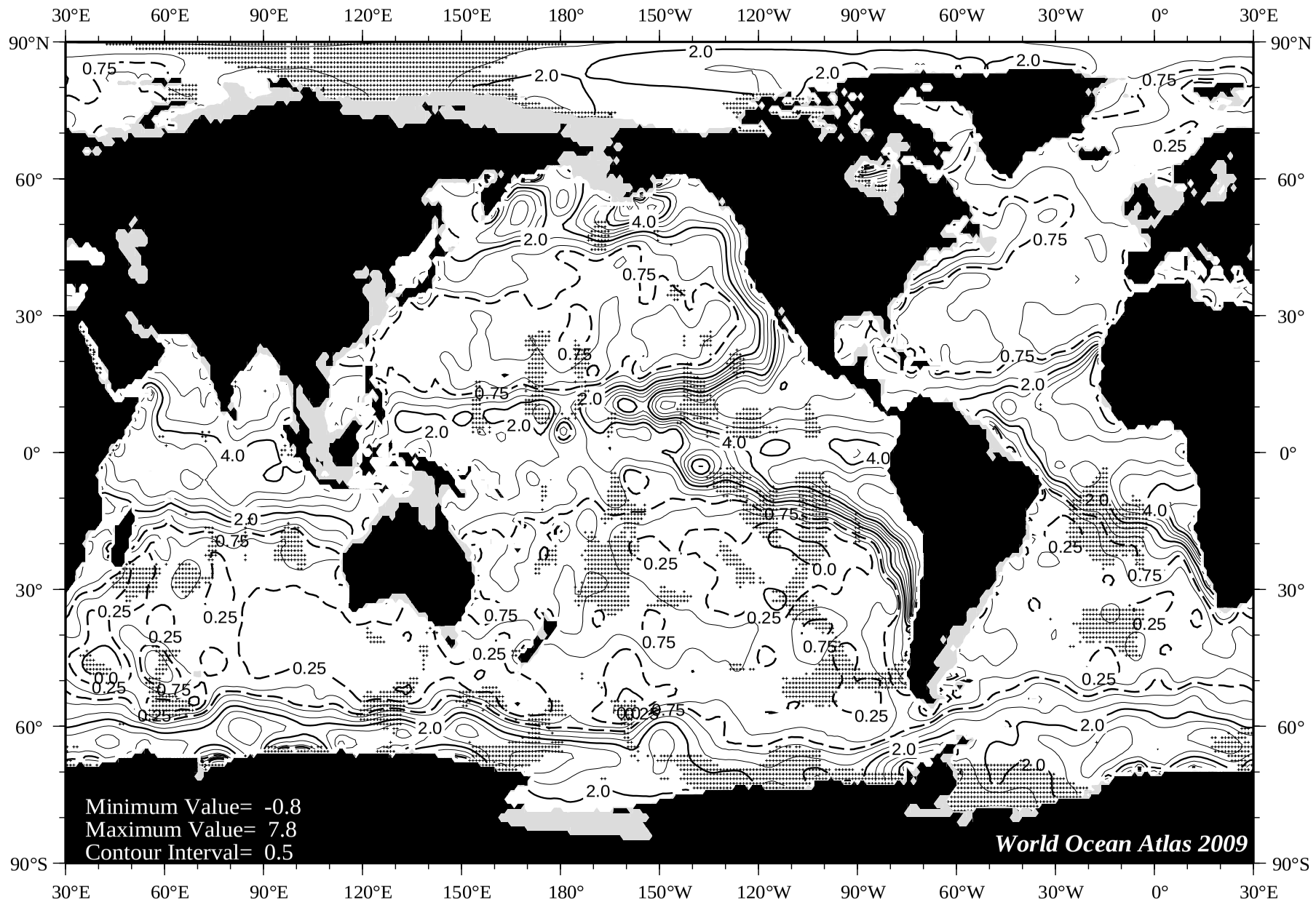

Fig E29 Fall (Oct.-Dec.) apparent oxygen utilization (ml/l) at 150 m. depth.

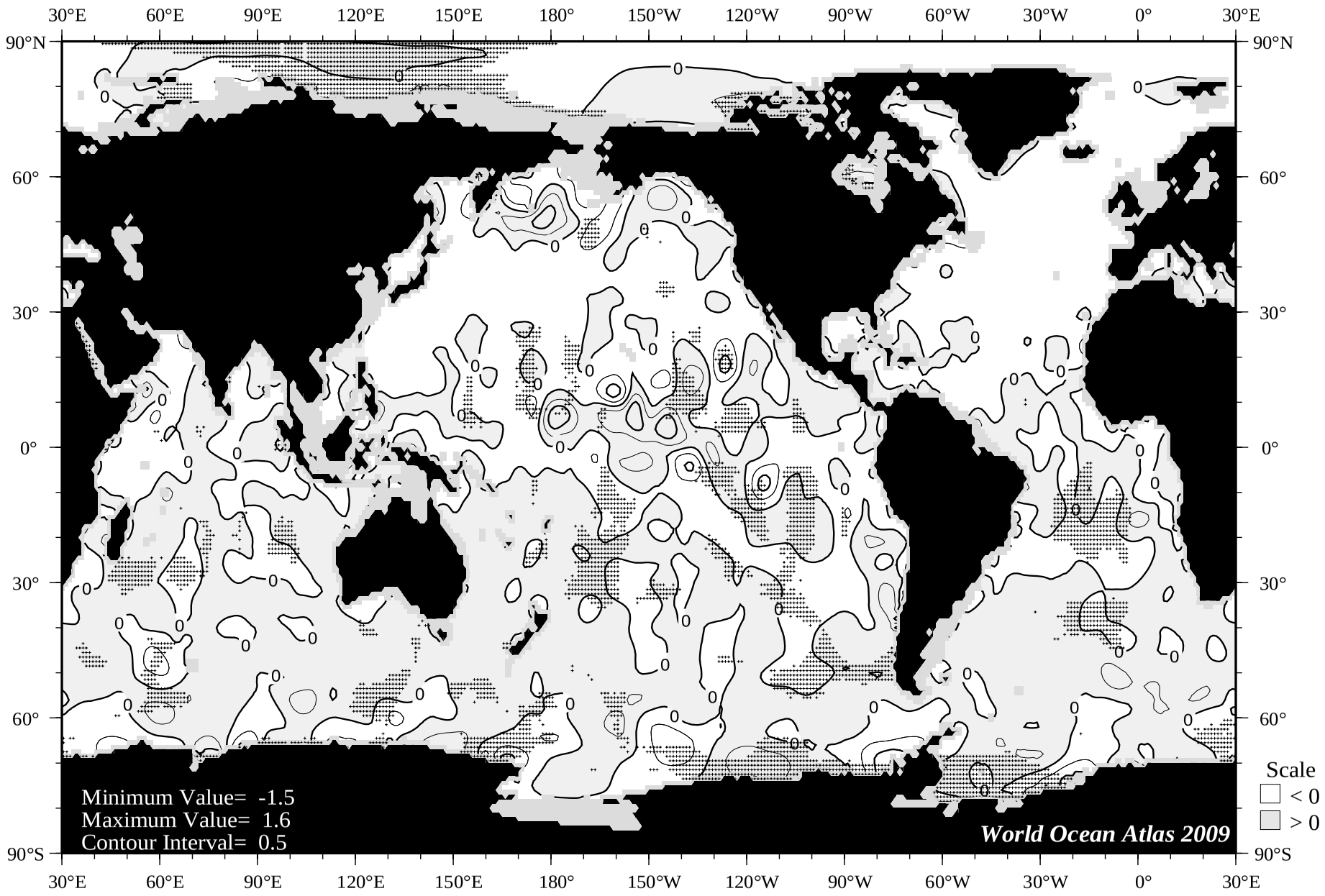

Fig E30 Fall (Oct.-Dec.) minus annual AOU at 150 m. depth.

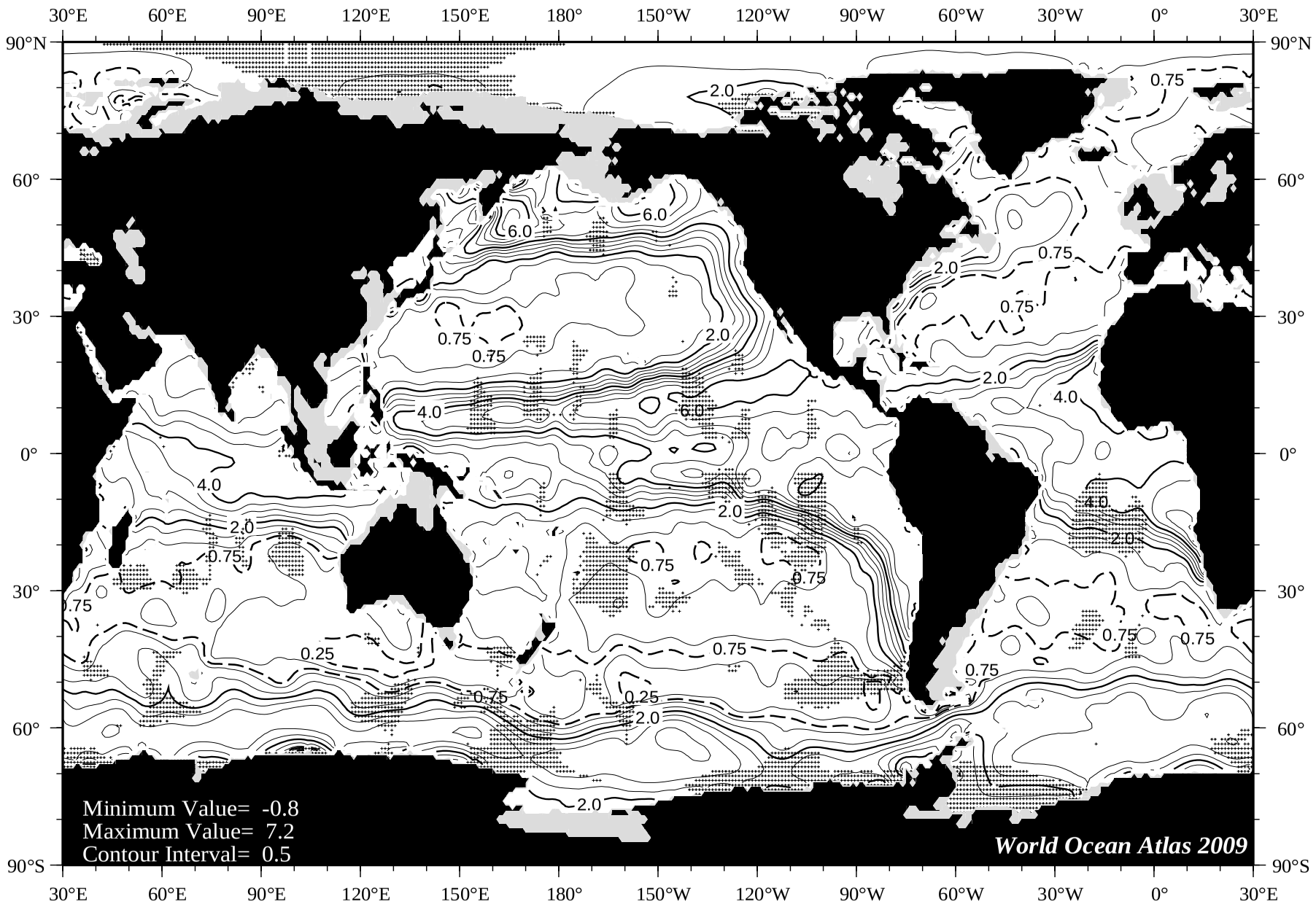

Fig E31 Fall (Oct.-Dec.) apparent oxygen utilization (ml/l) at 250 m. depth.

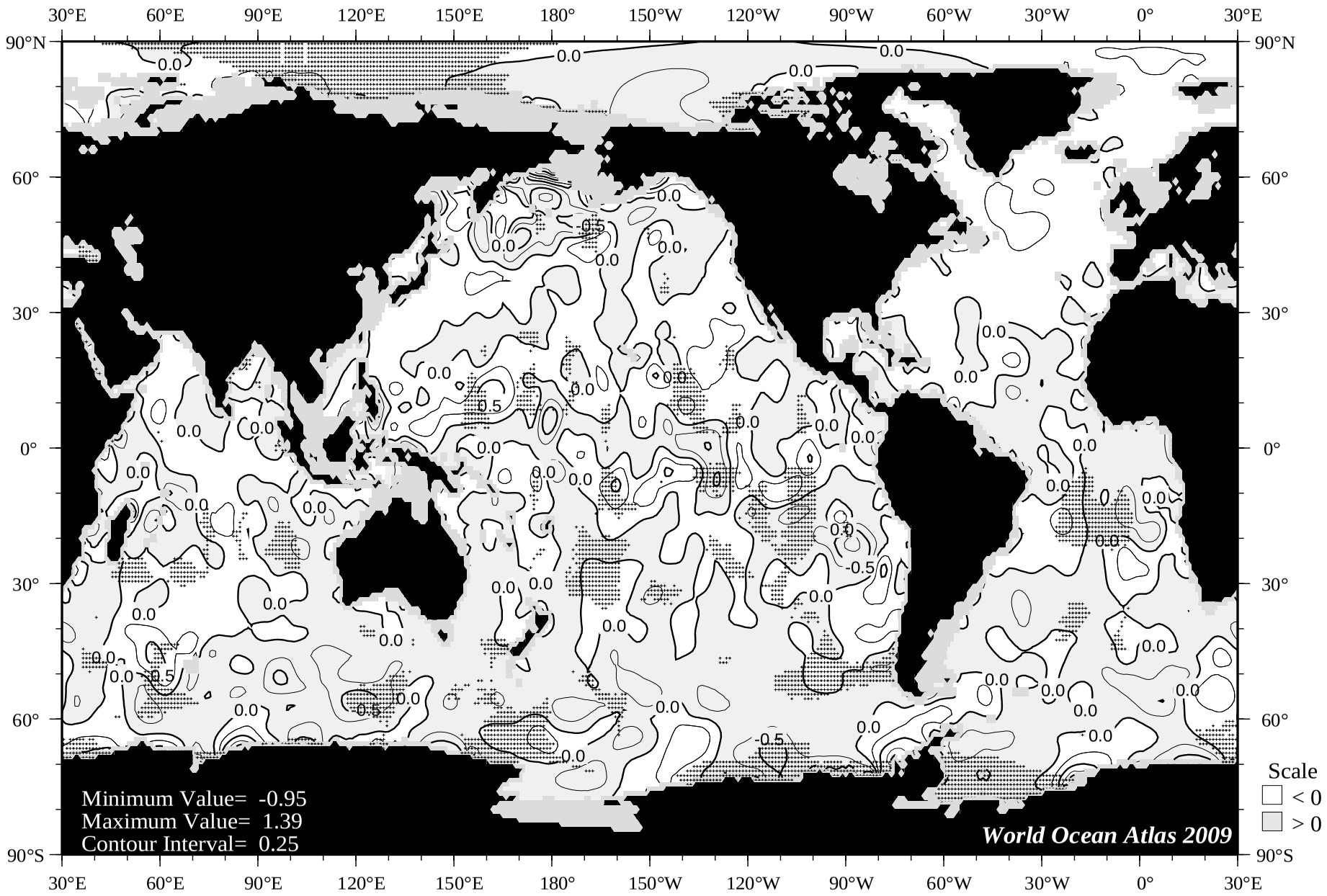

Fig E32 Fall (Oct.-Dec.) minus annual AOU at 250 m. depth.

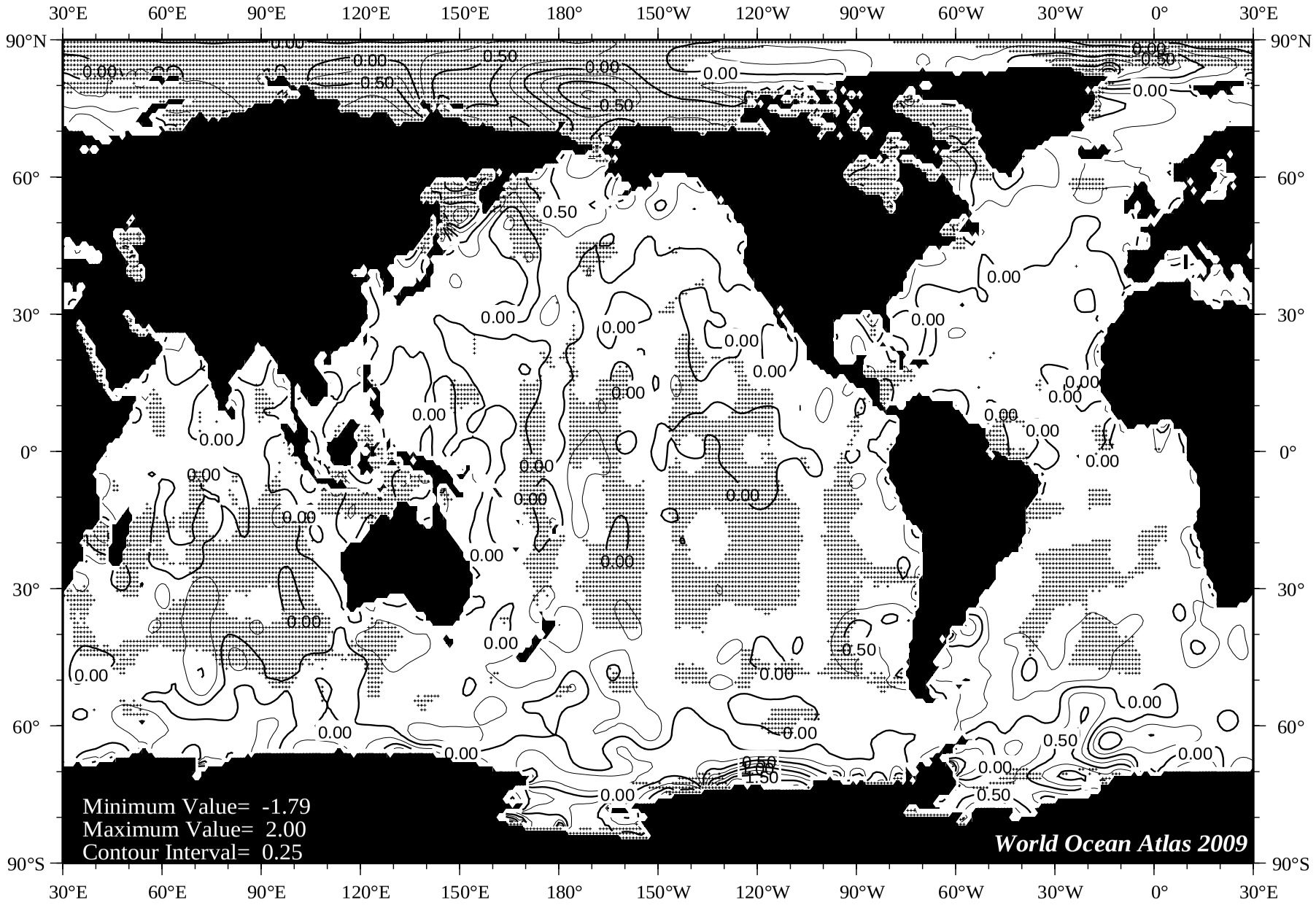

Fig F1 January mean apparent oxygen utilization (ml/l) at the surface.

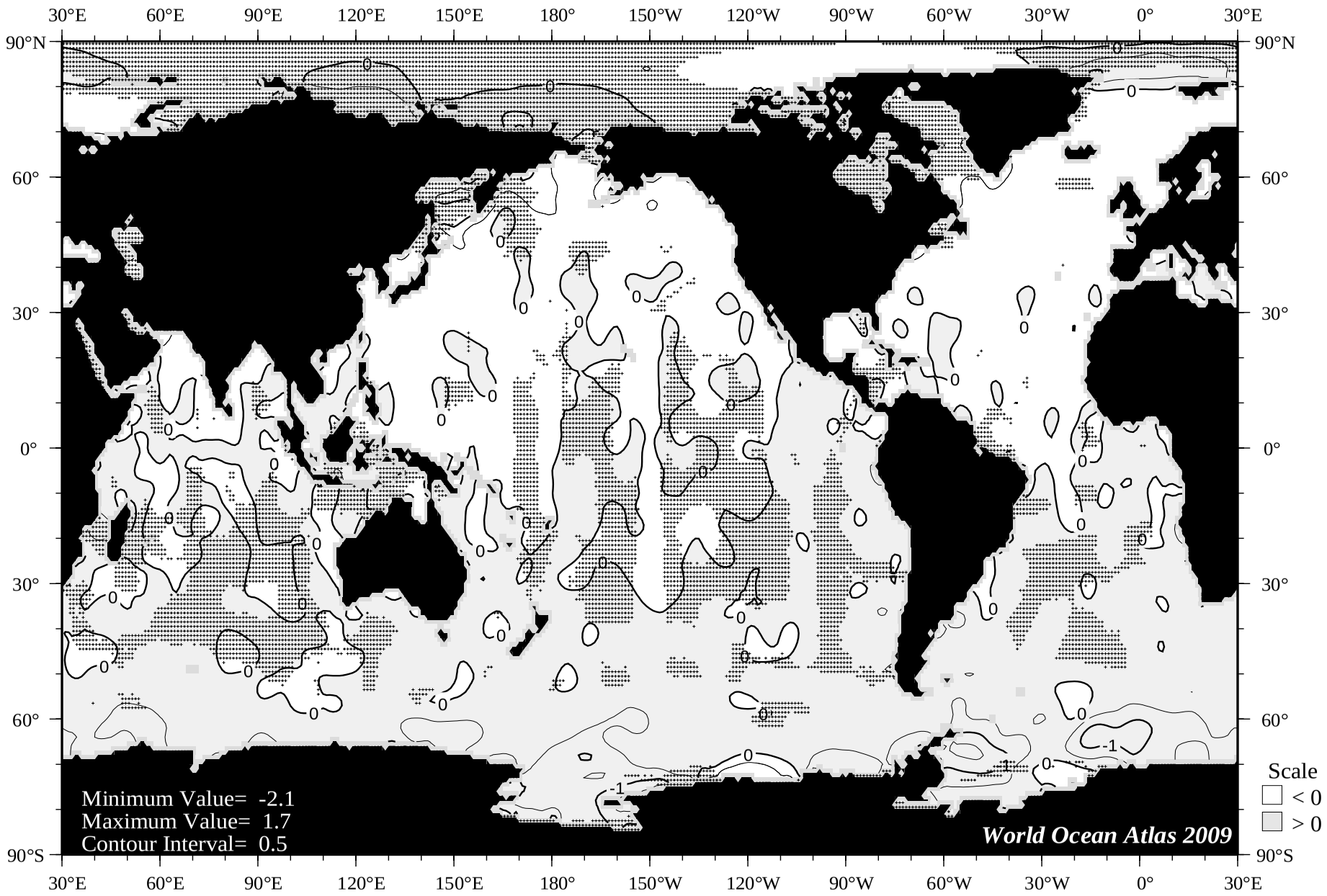

Fig F2 January minus annual AOU at the surface.

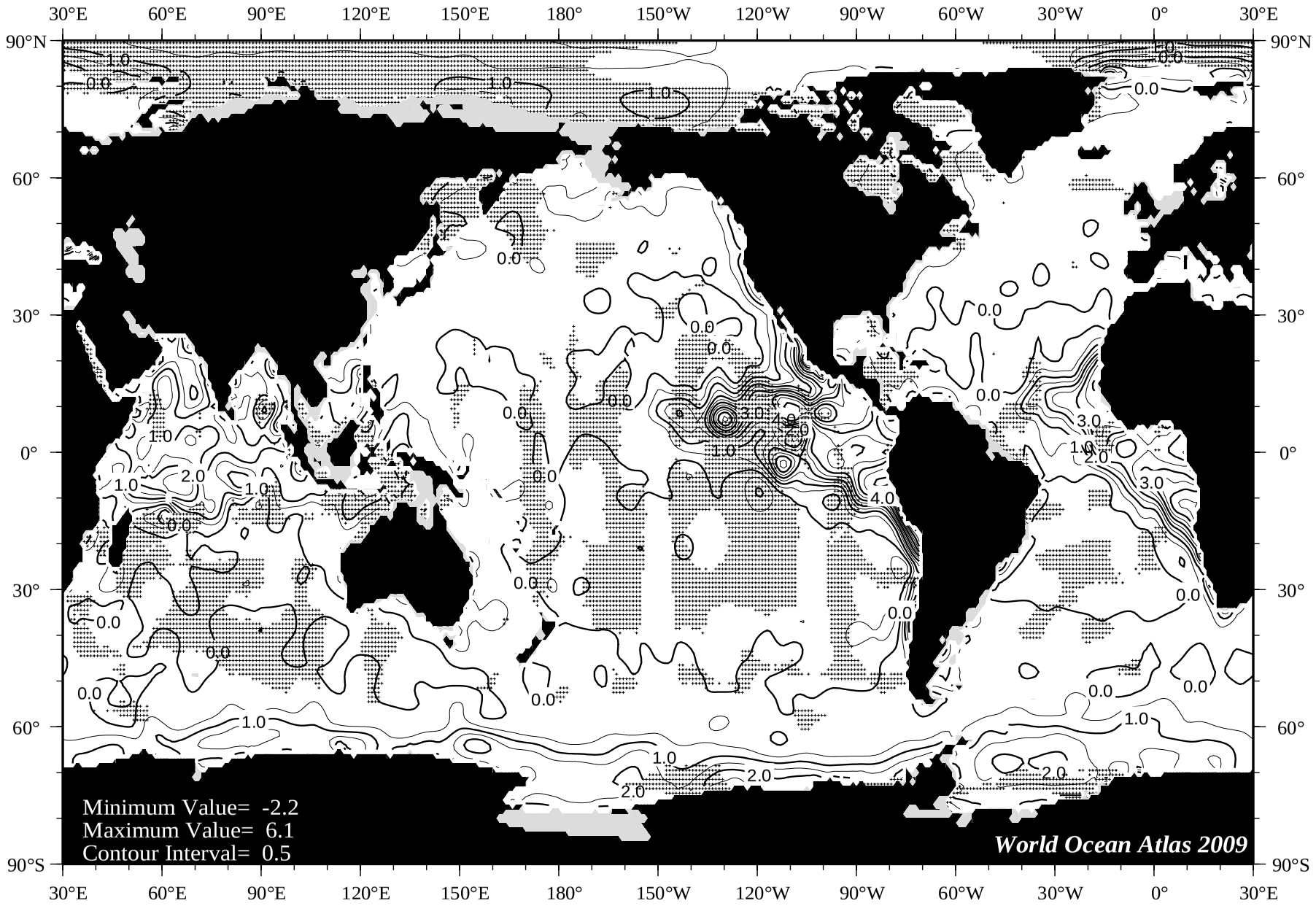

Fig F3 January mean apparent oxygen utilization (ml/l) at 75 m. depth.

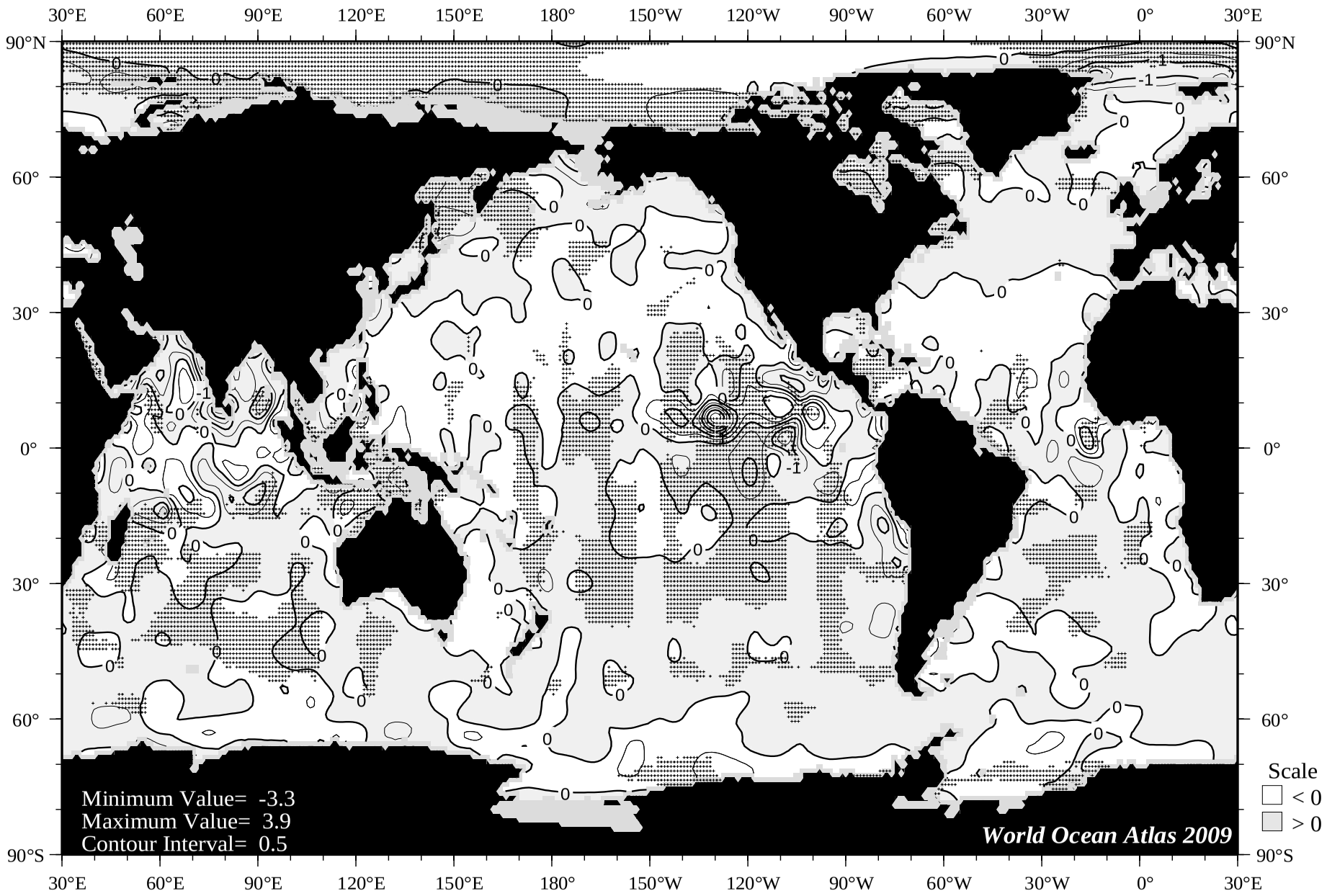

Fig F4 January minus annual AOU at 75 m. depth.

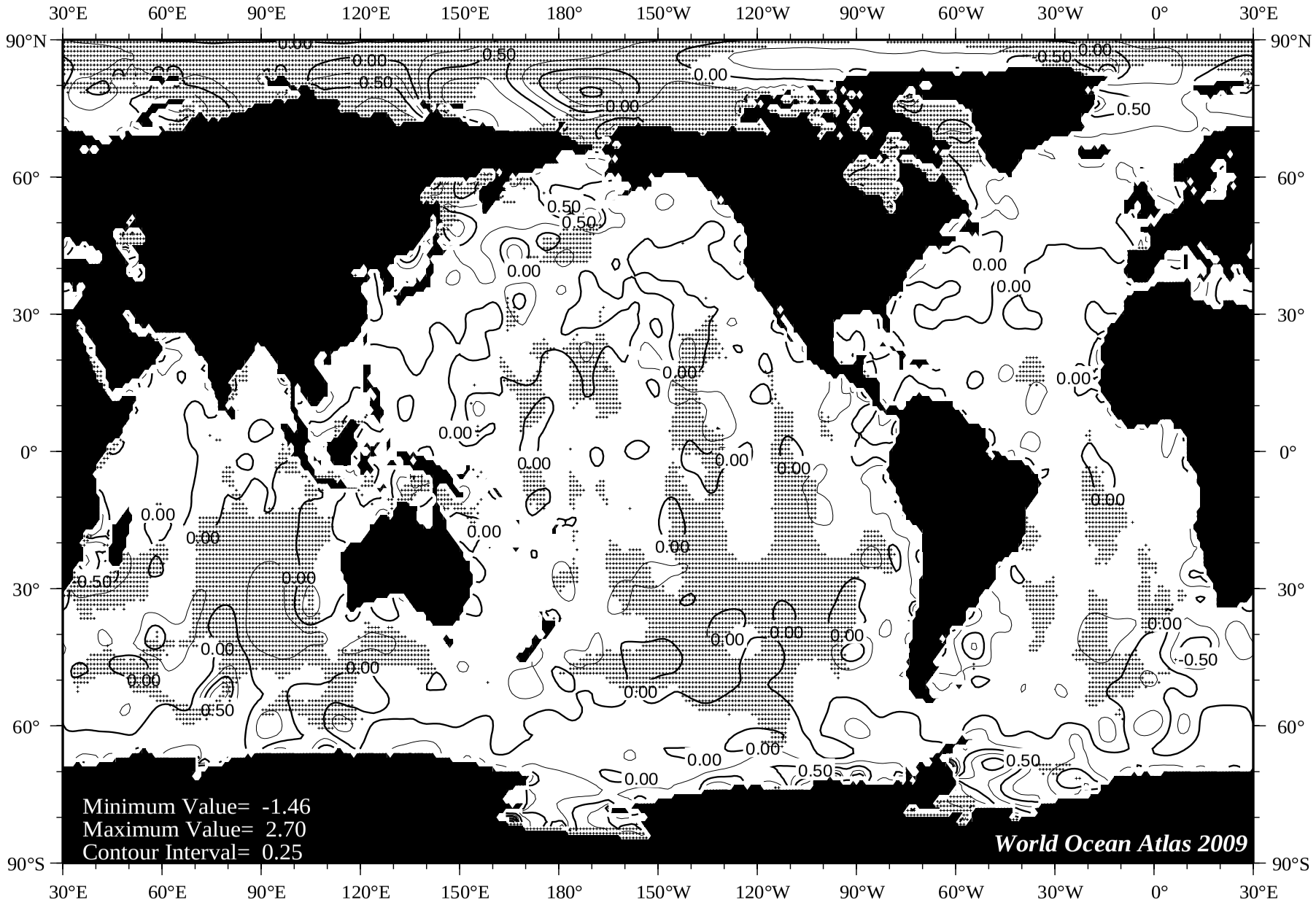

Fig F5 February mean apparent oxygen utilization (ml/l) at the surface.

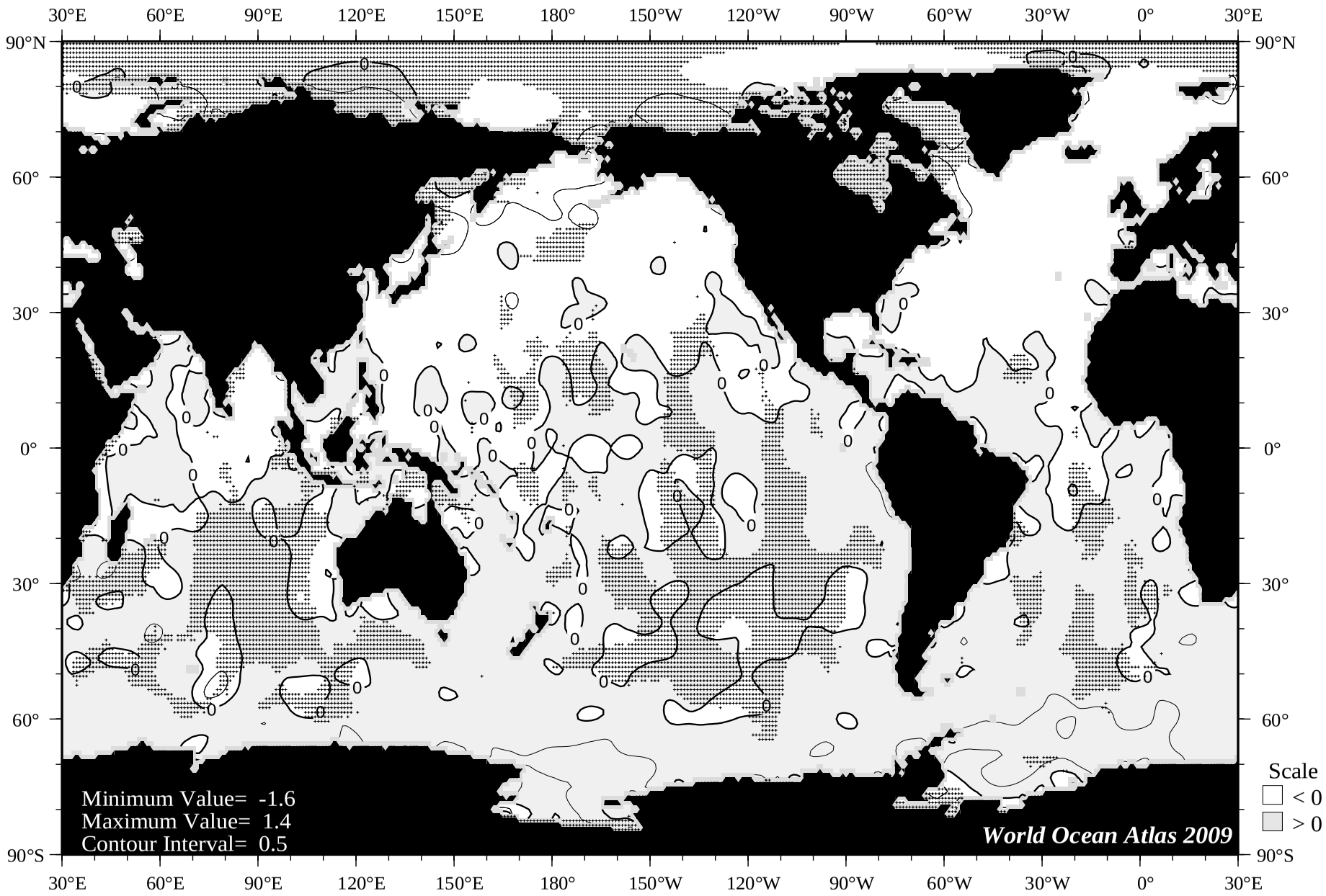

Fig F6 February minus annual AOU at the surface.

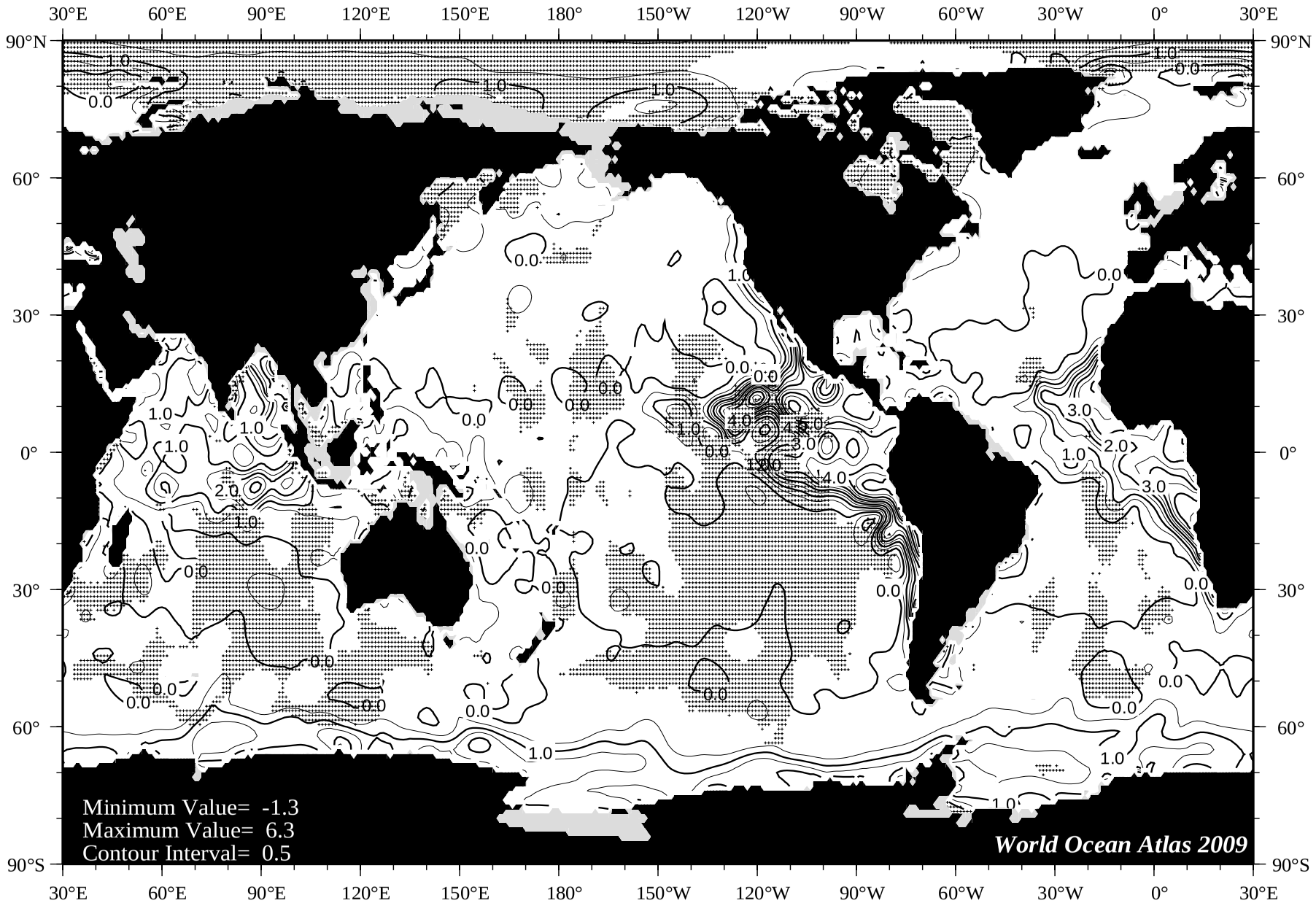

Fig F7 February mean apparent oxygen utilization (ml/l) at 75 m. depth.

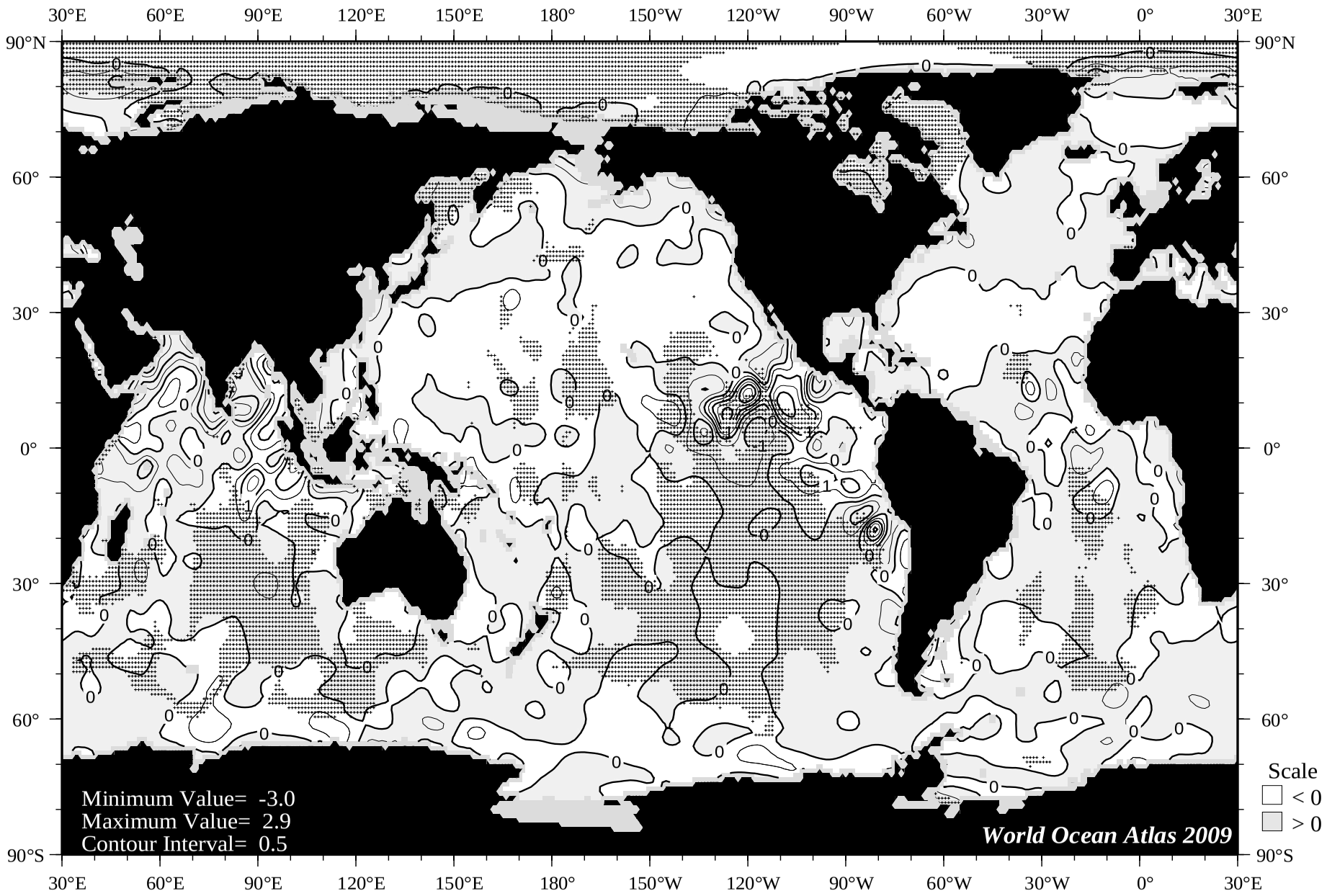

Fig F8 February minus annual AOU at 75 m. depth.

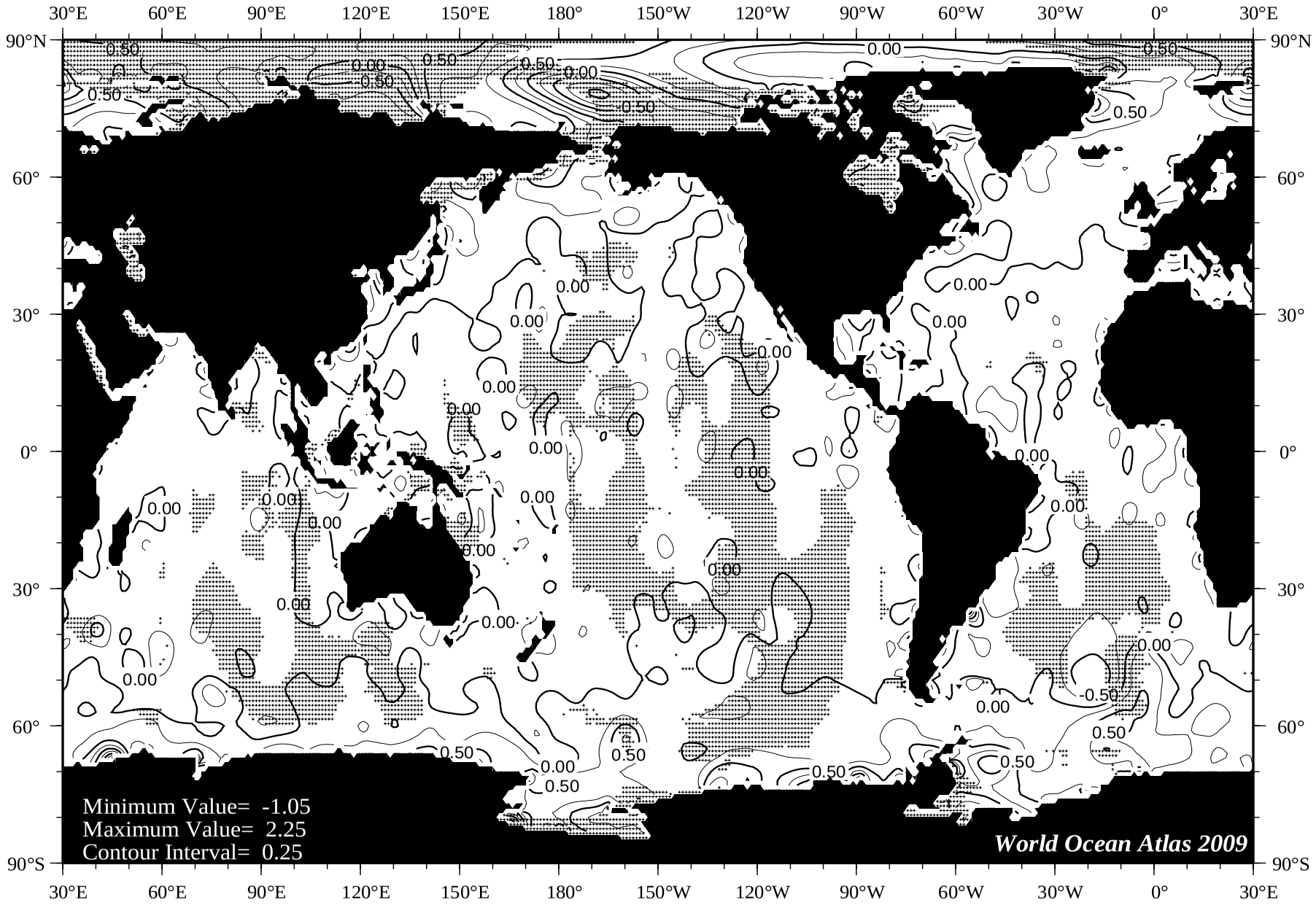

Fig F9 March mean apparent oxygen utilization (ml/l) at the surface.

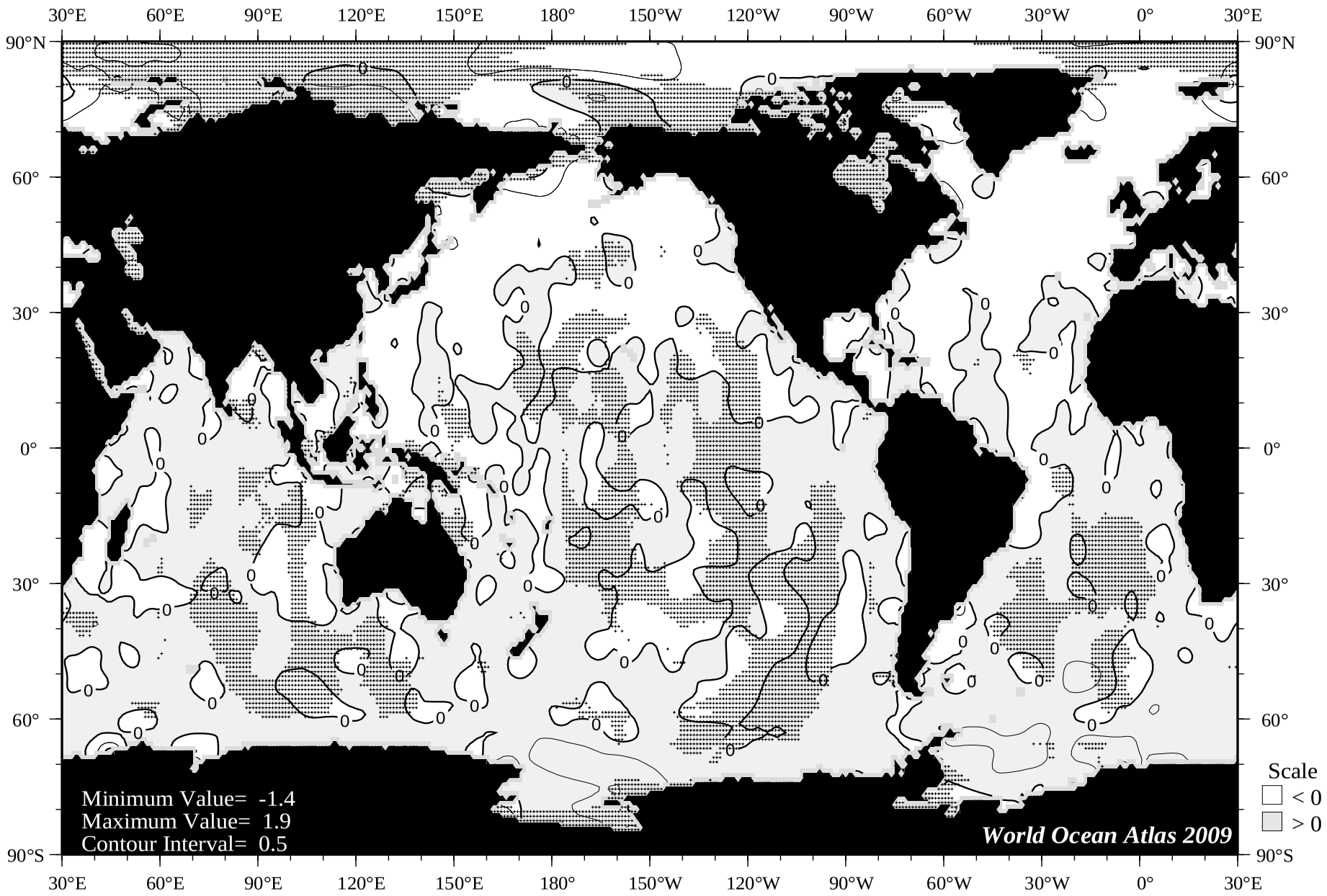

Fig F10 March minus annual AOU at the surface.

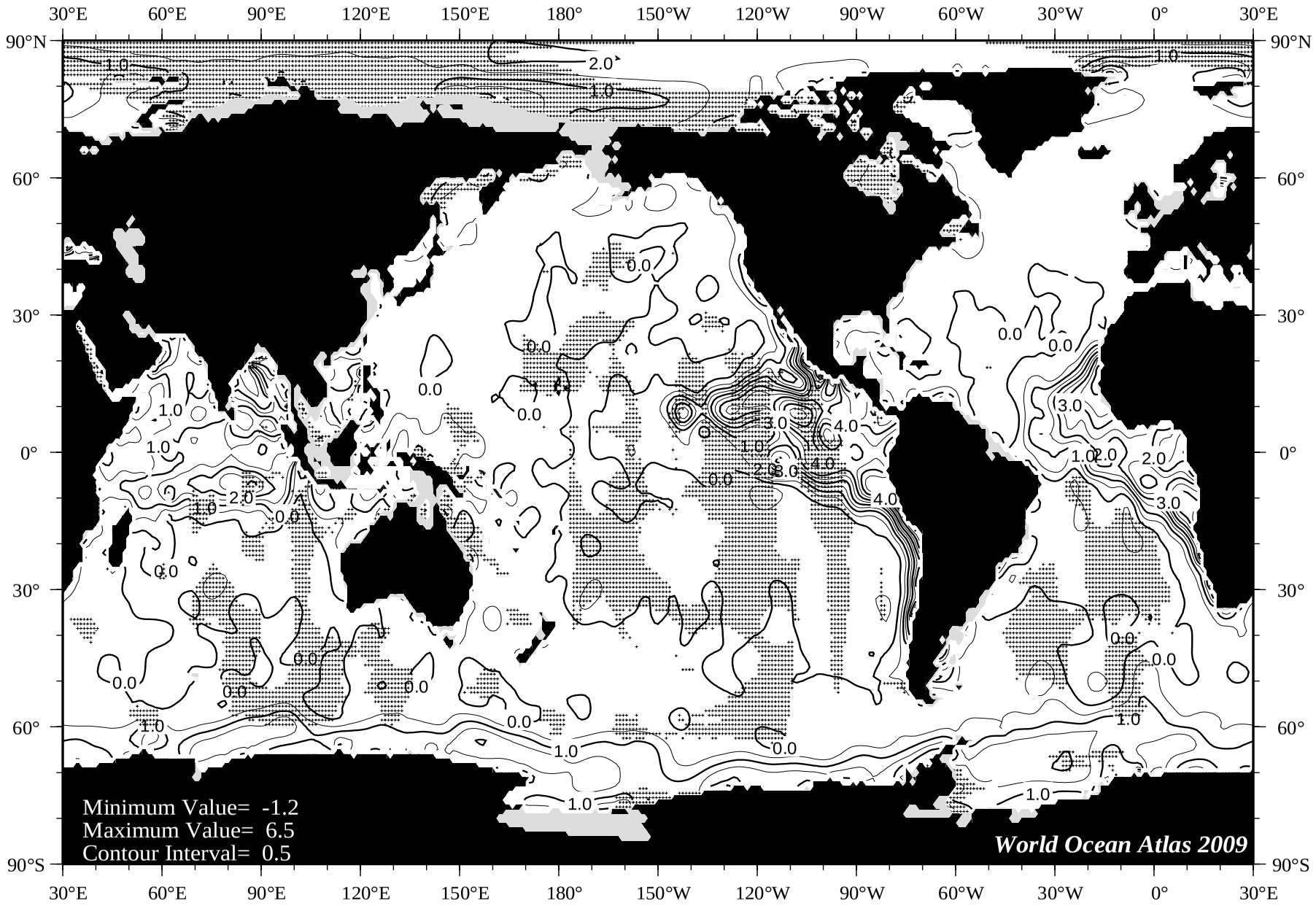

Fig F11 March mean apparent oxygen utilization (ml/l) at 75 m. depth.

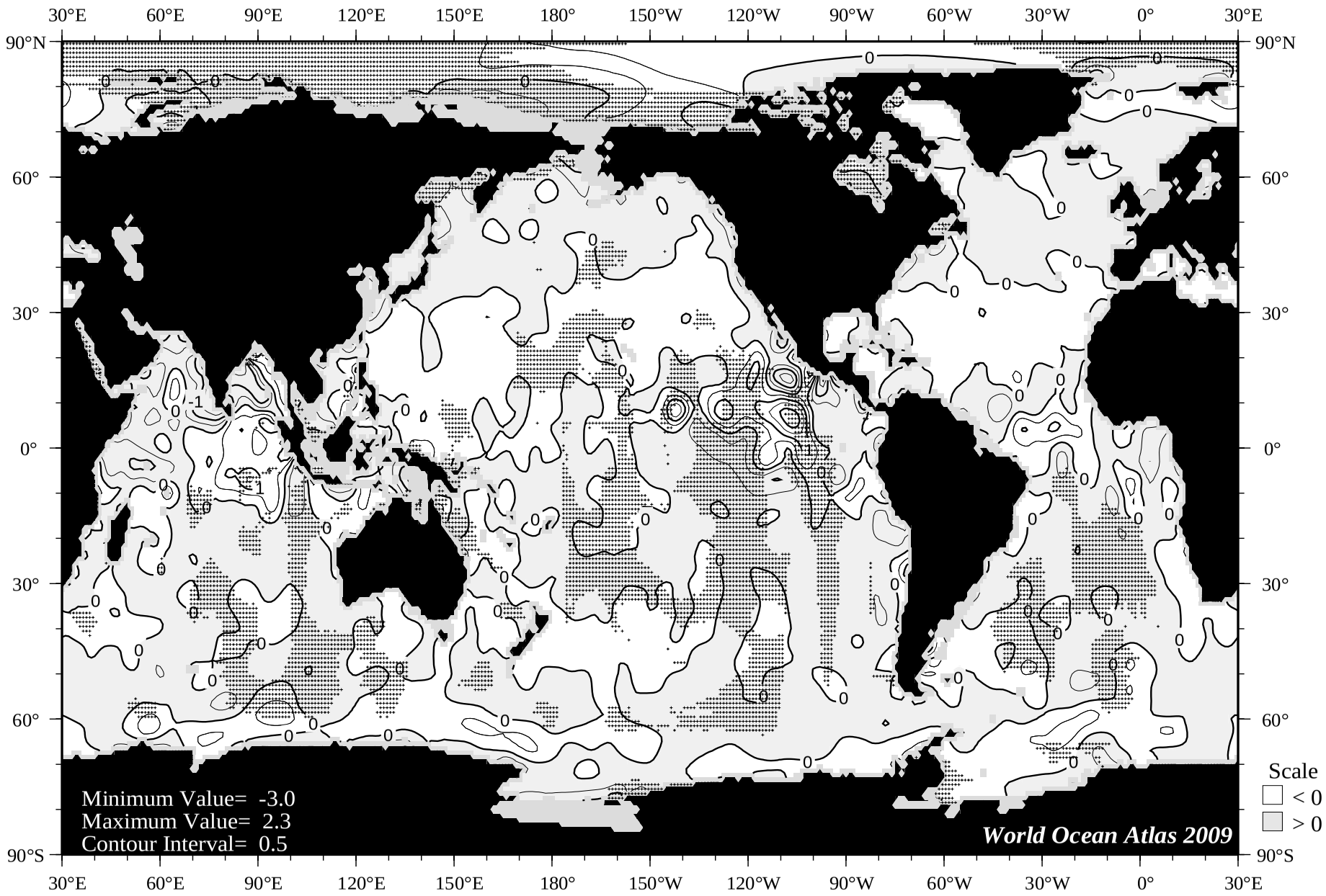

Fig F12 March minus annual AOU at 75 m. depth.

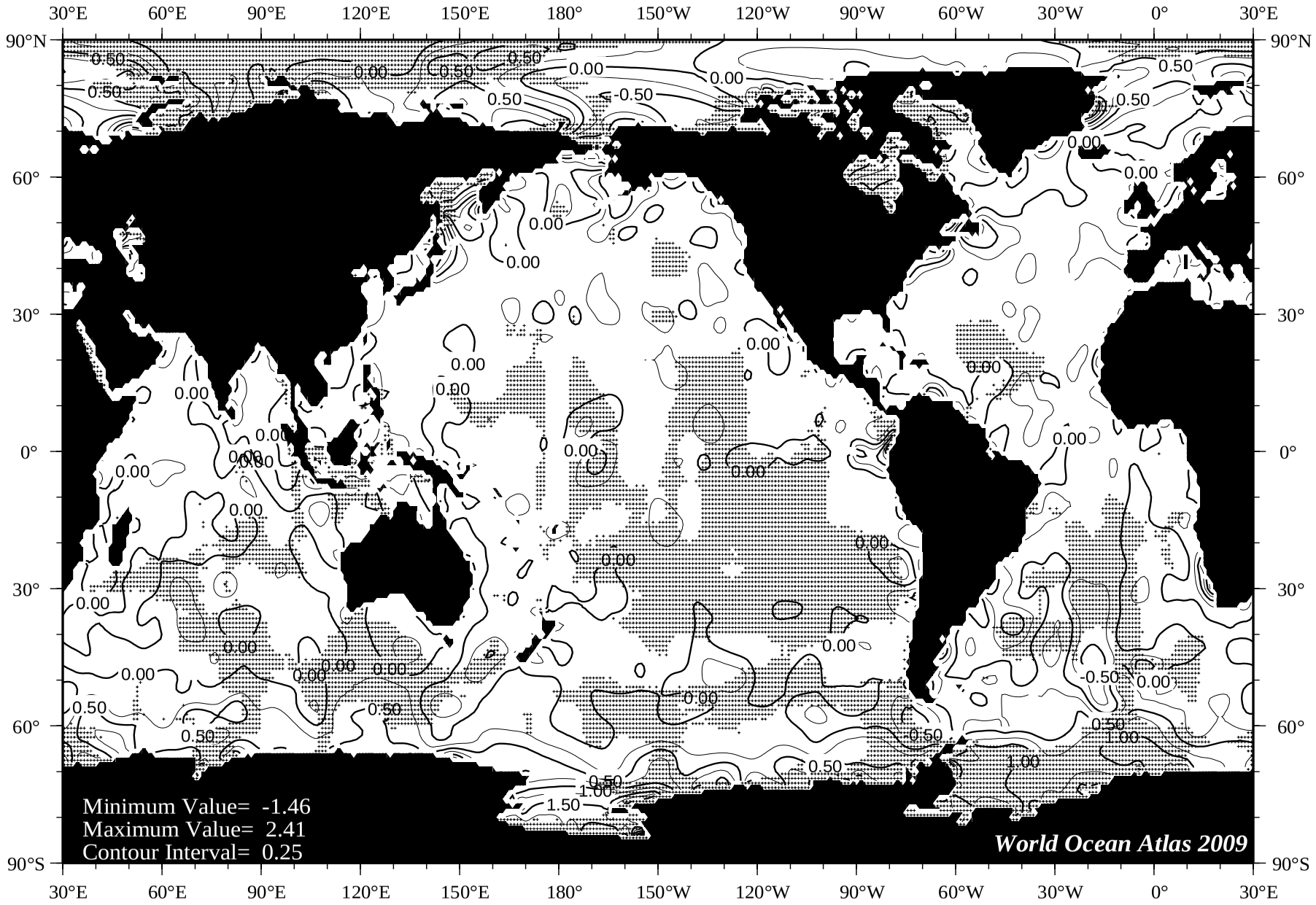

Fig F13 April mean apparent oxygen utilization (ml/l) at the surface.

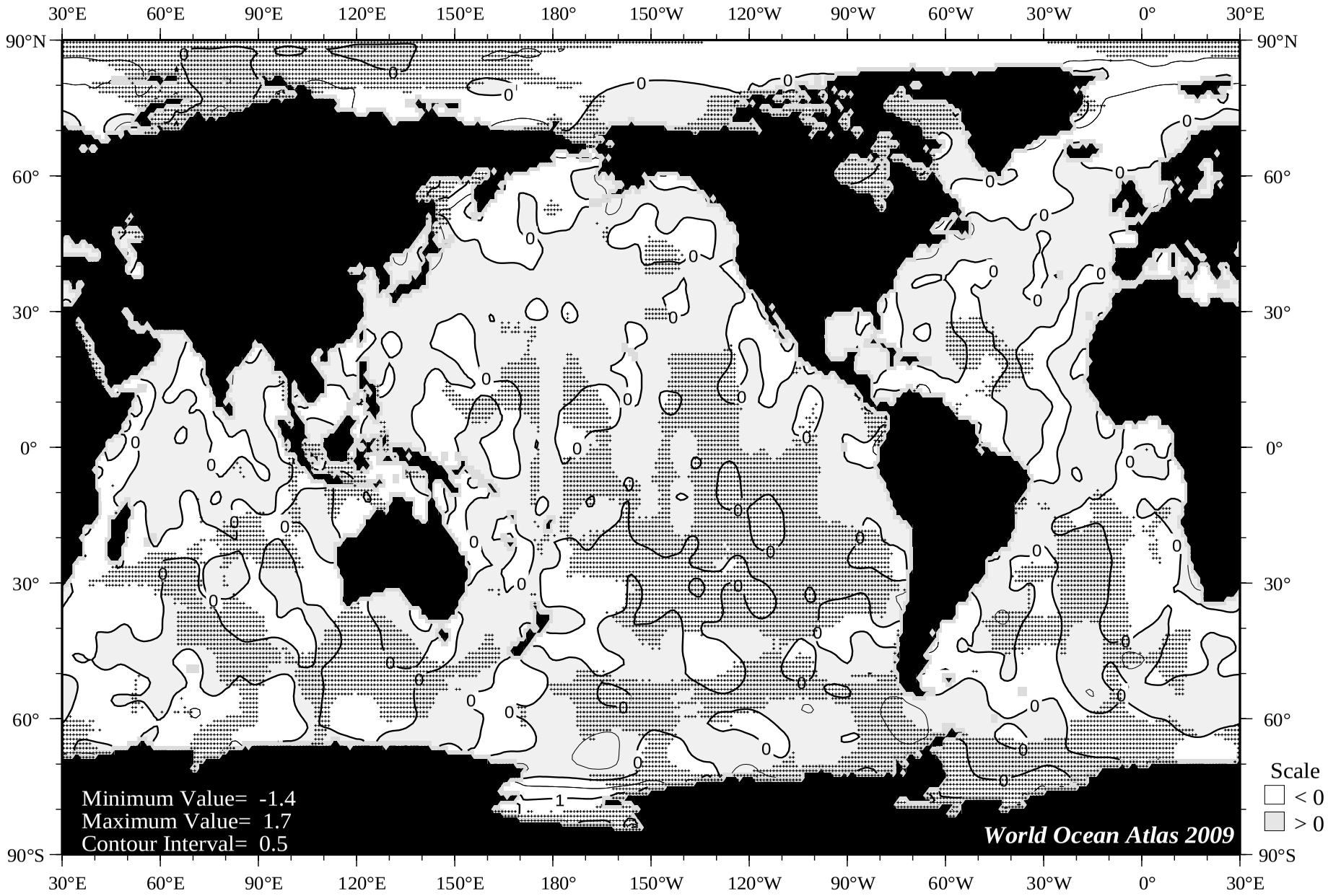

Fig F14 April minus annual AOU at the surface.

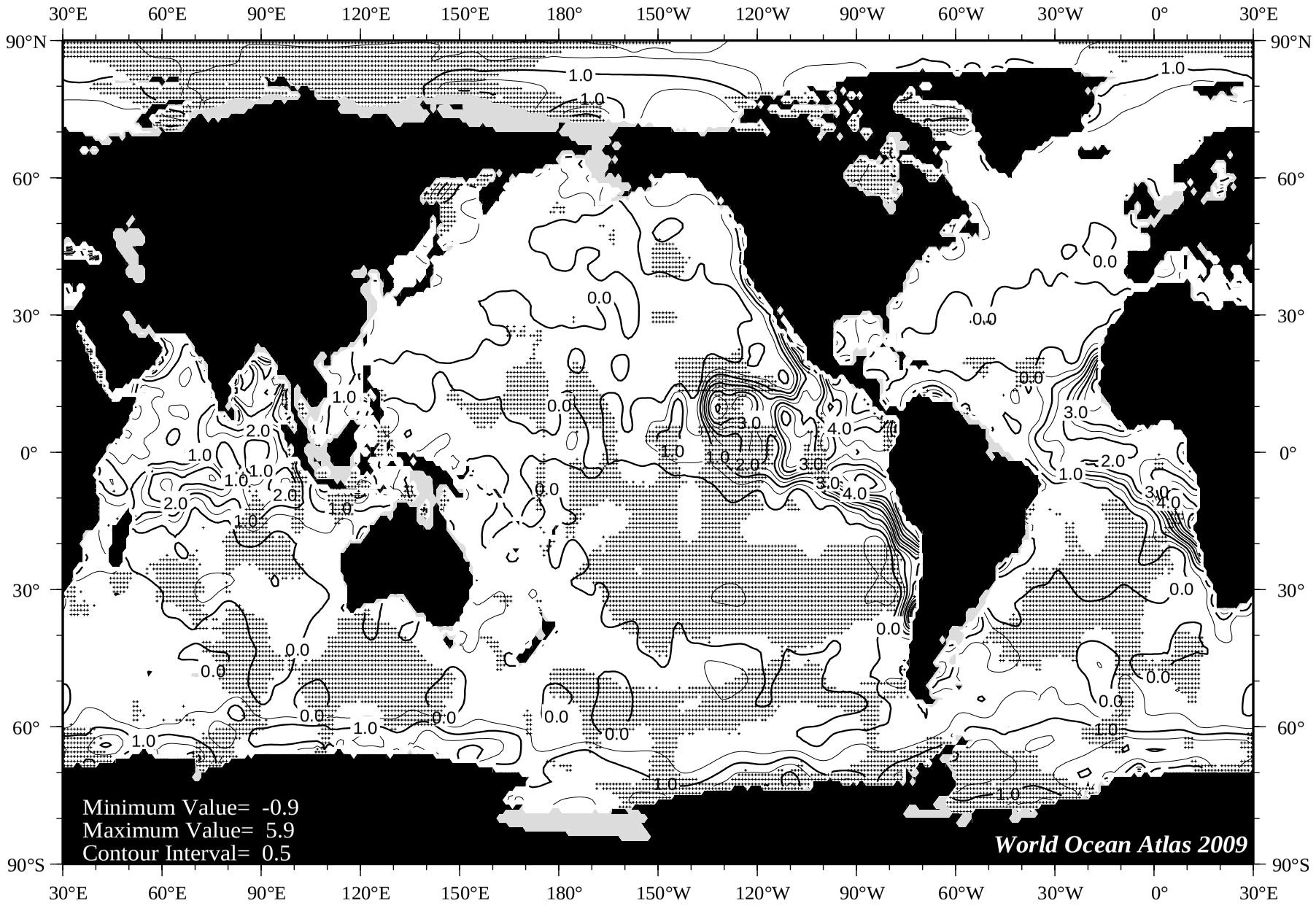

Fig F15 April mean apparent oxygen utilization (ml/l) at 75 m. depth.

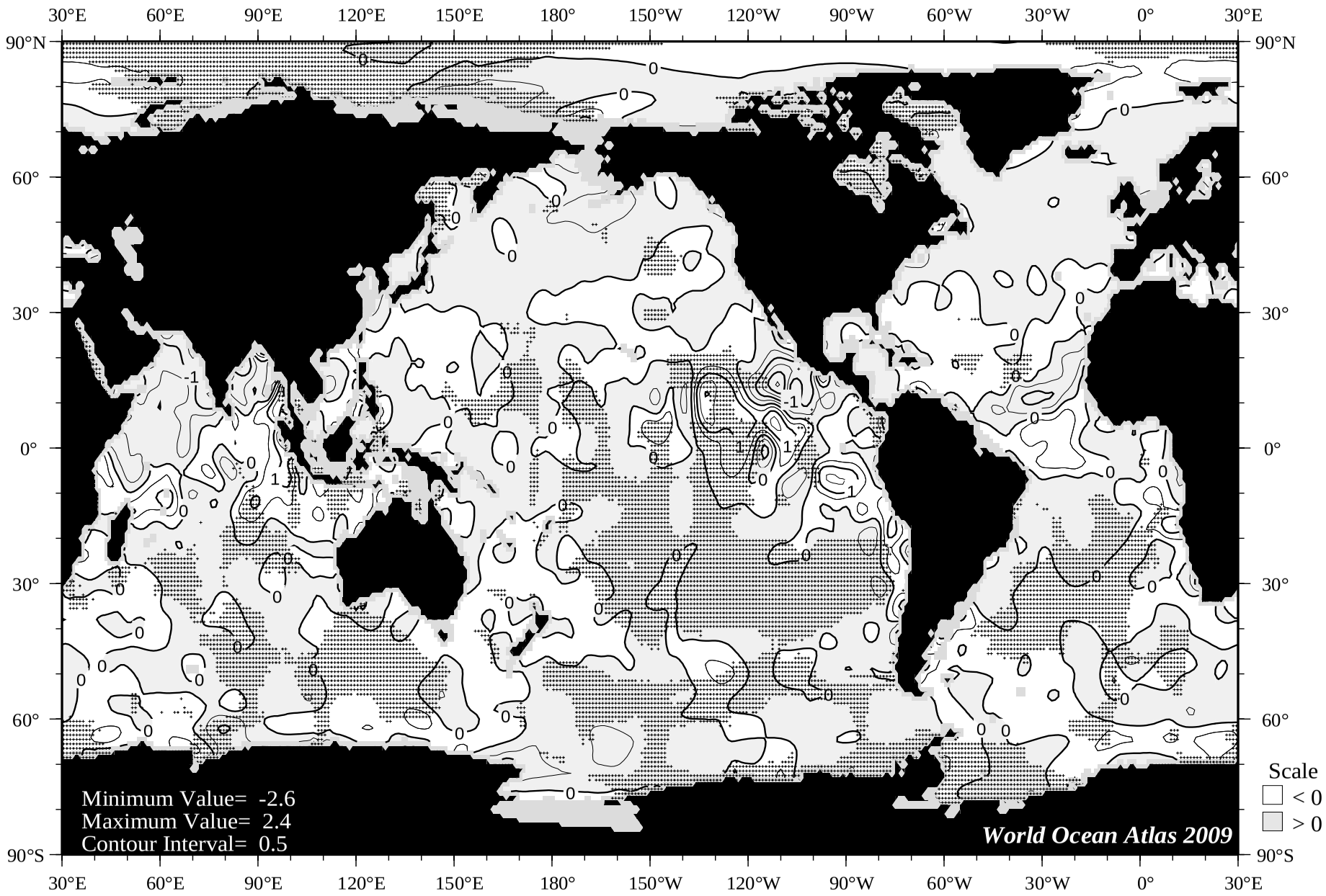

Fig F16 April minus annual AOU at 75 m. depth.

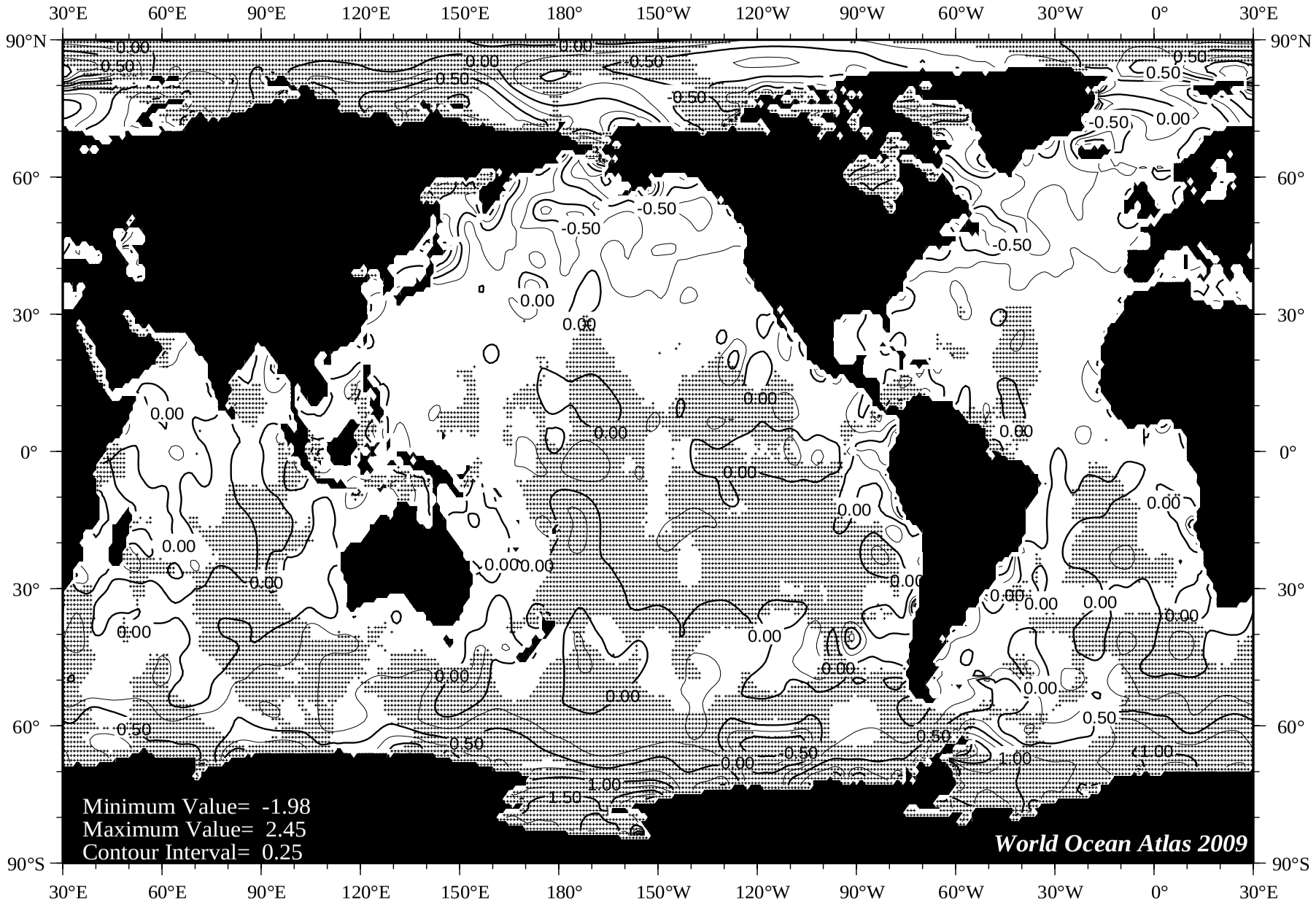

Fig F17 May mean apparent oxygen utilization (ml/l) at the surface.

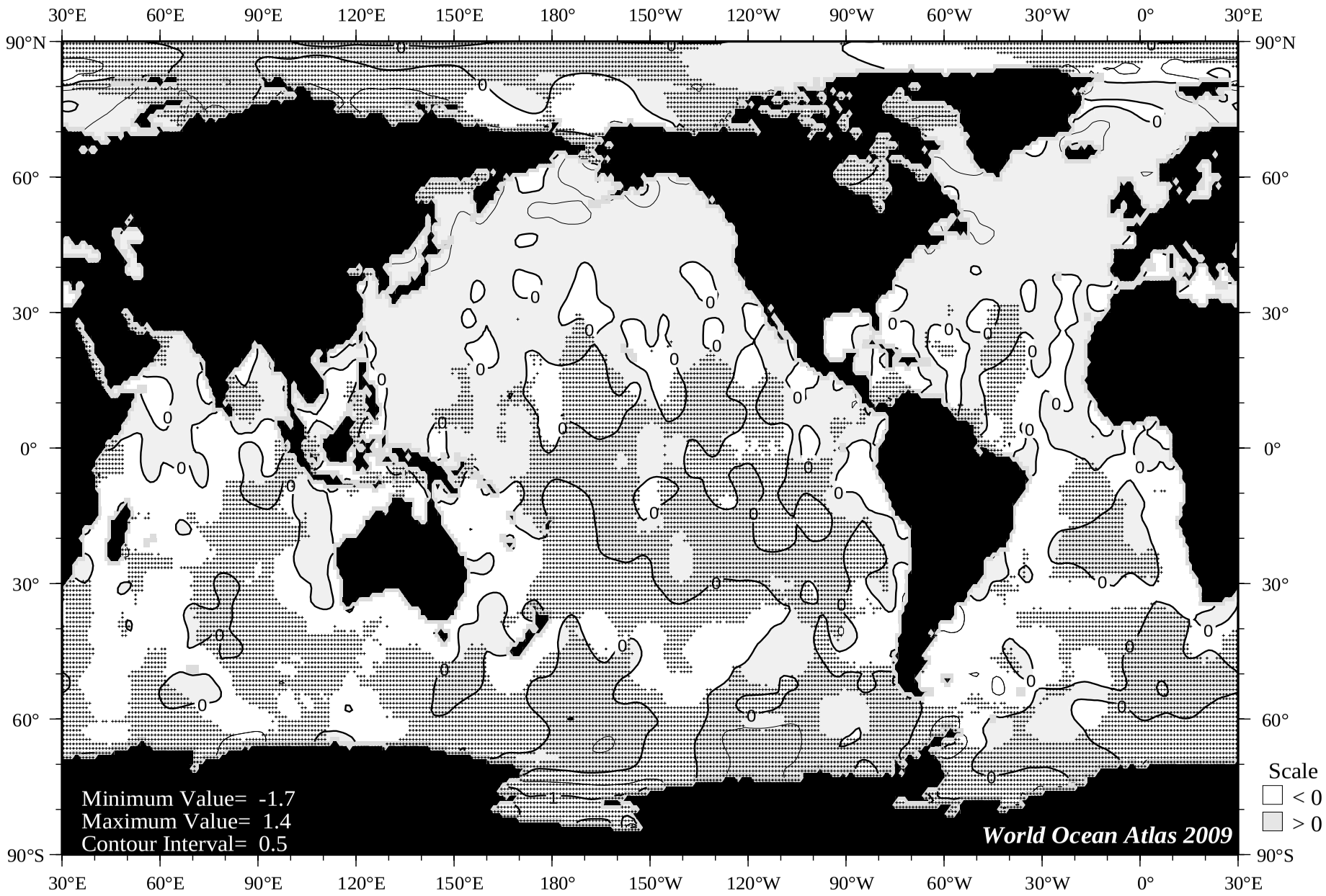

Fig F18 May minus annual AOU at the surface.

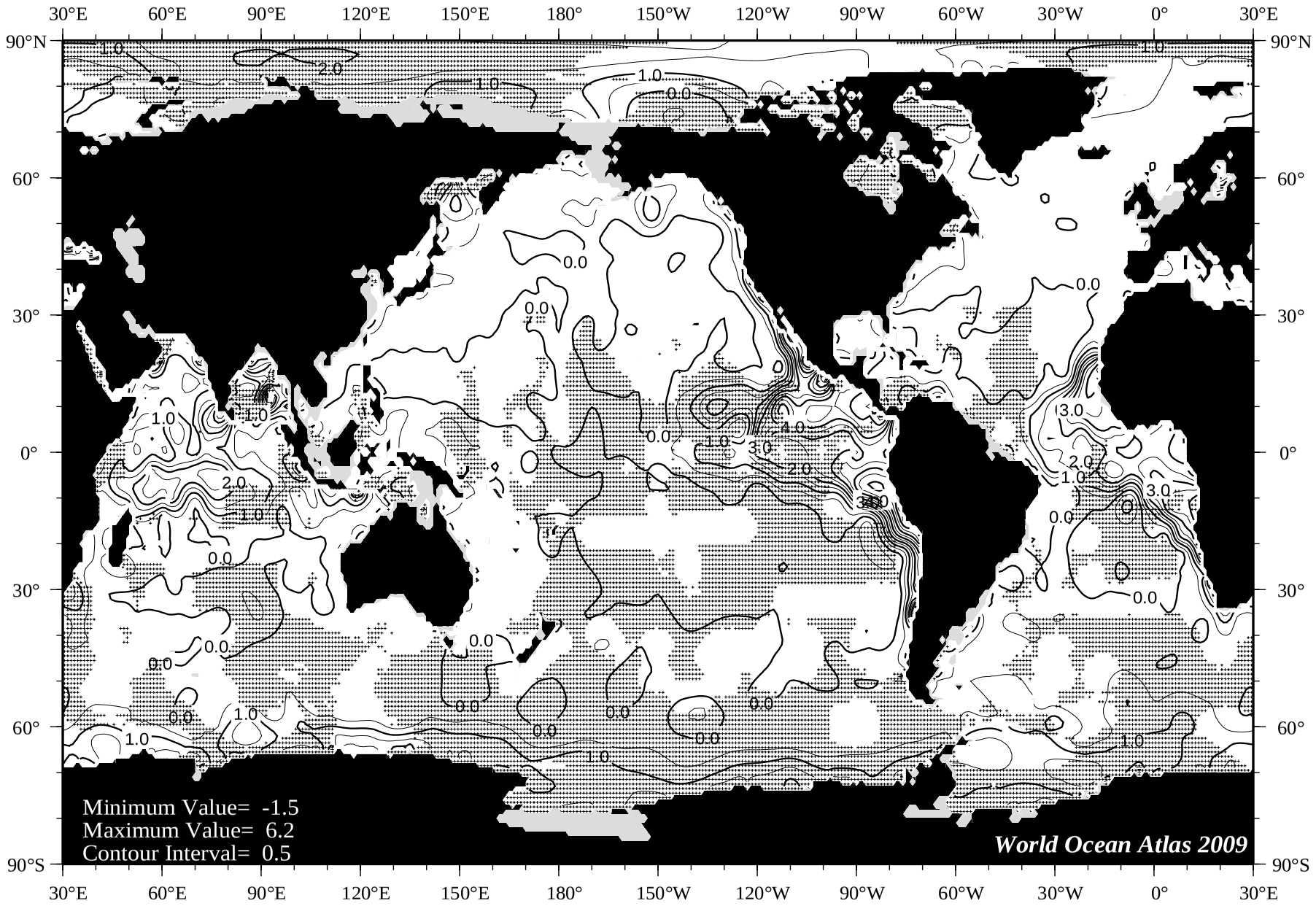

Fig F19 May mean apparent oxygen utilization (ml/l) at 75 m. depth.

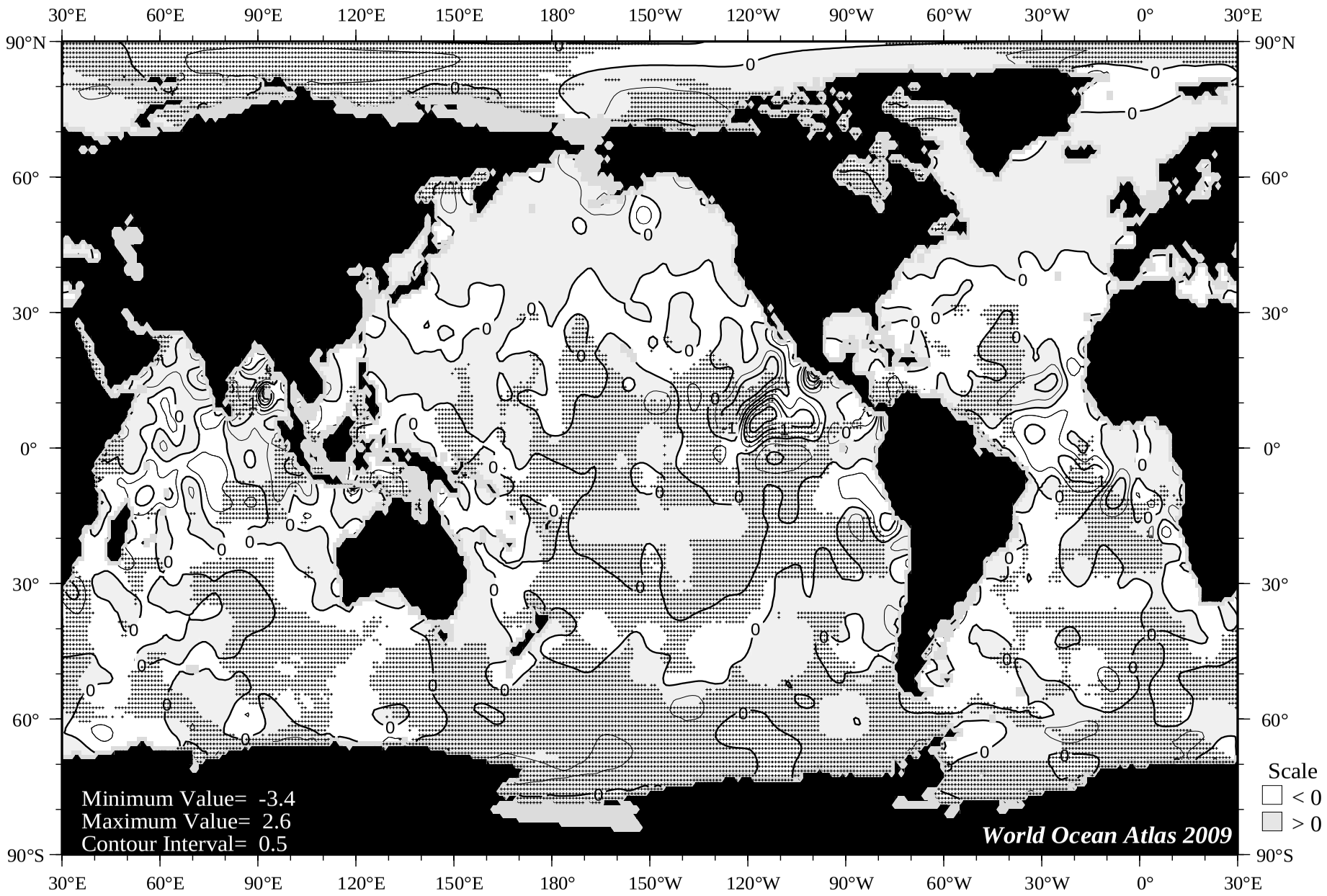

Fig F20 May minus annual AOU at 75 m. depth.

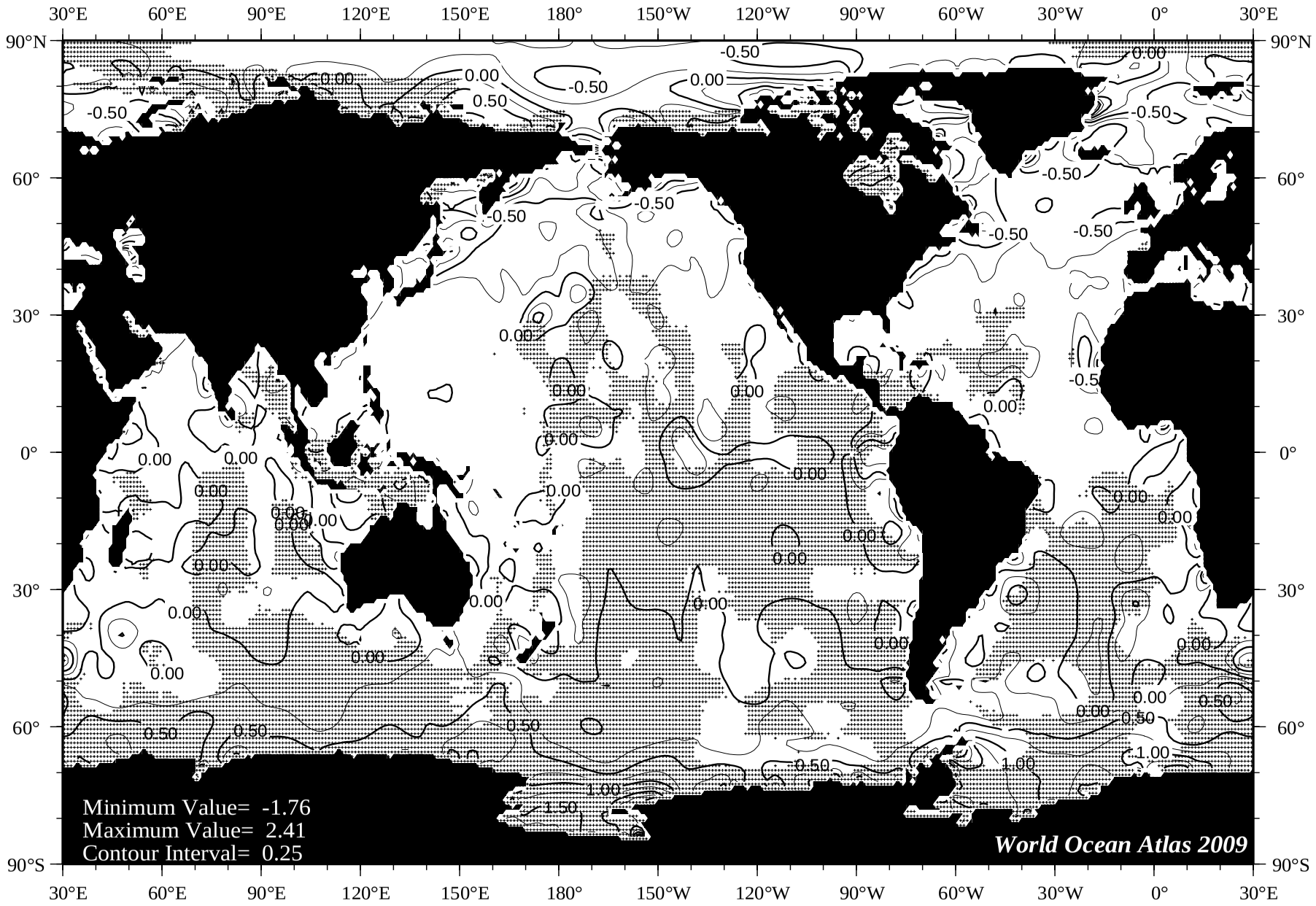

Fig F21 June mean apparent oxygen utilization (ml/l) at the surface.

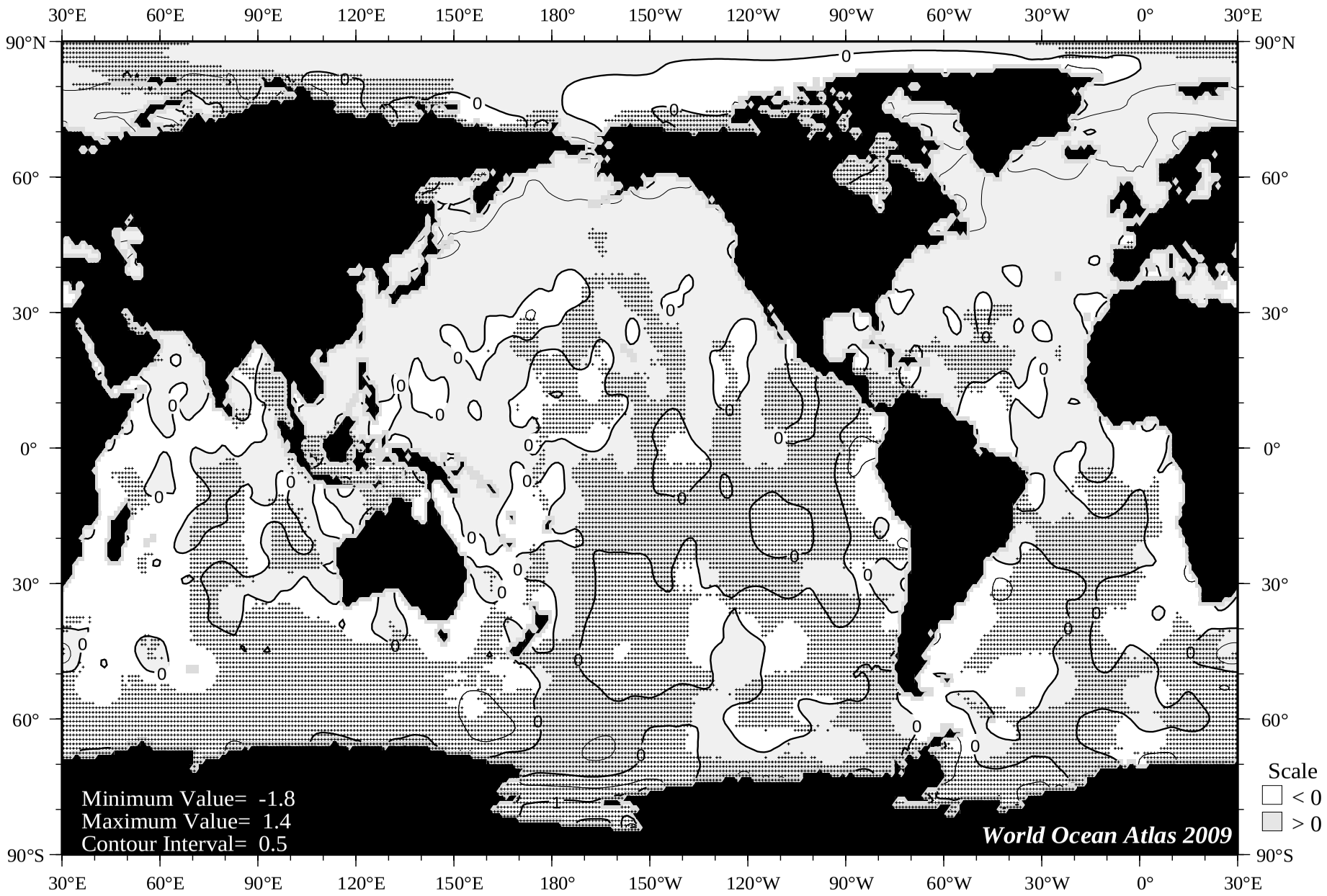

Fig F22 June minus annual AOU at the surface.

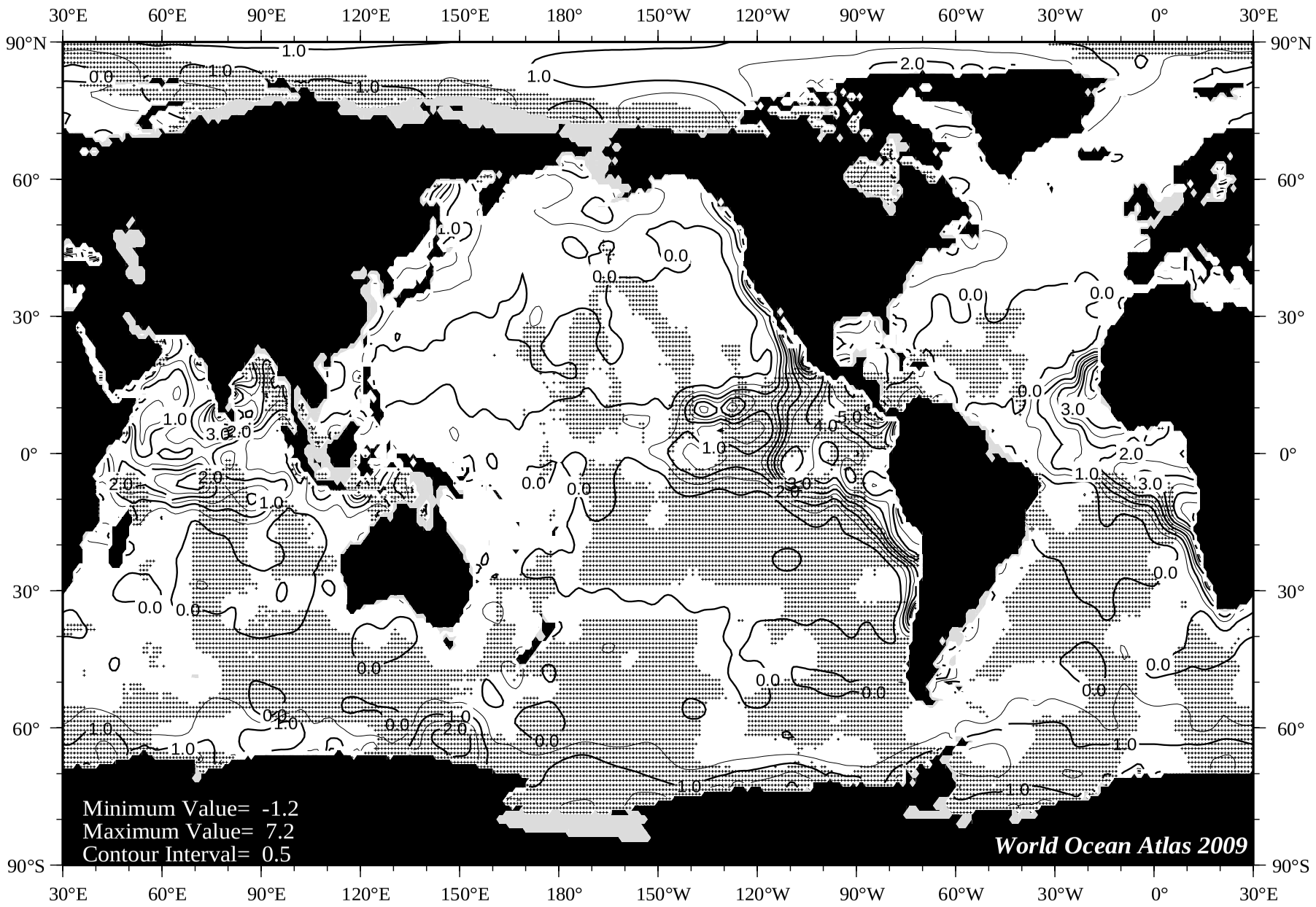

Fig F23 June mean apparent oxygen utilization (ml/l) at 75 m. depth.

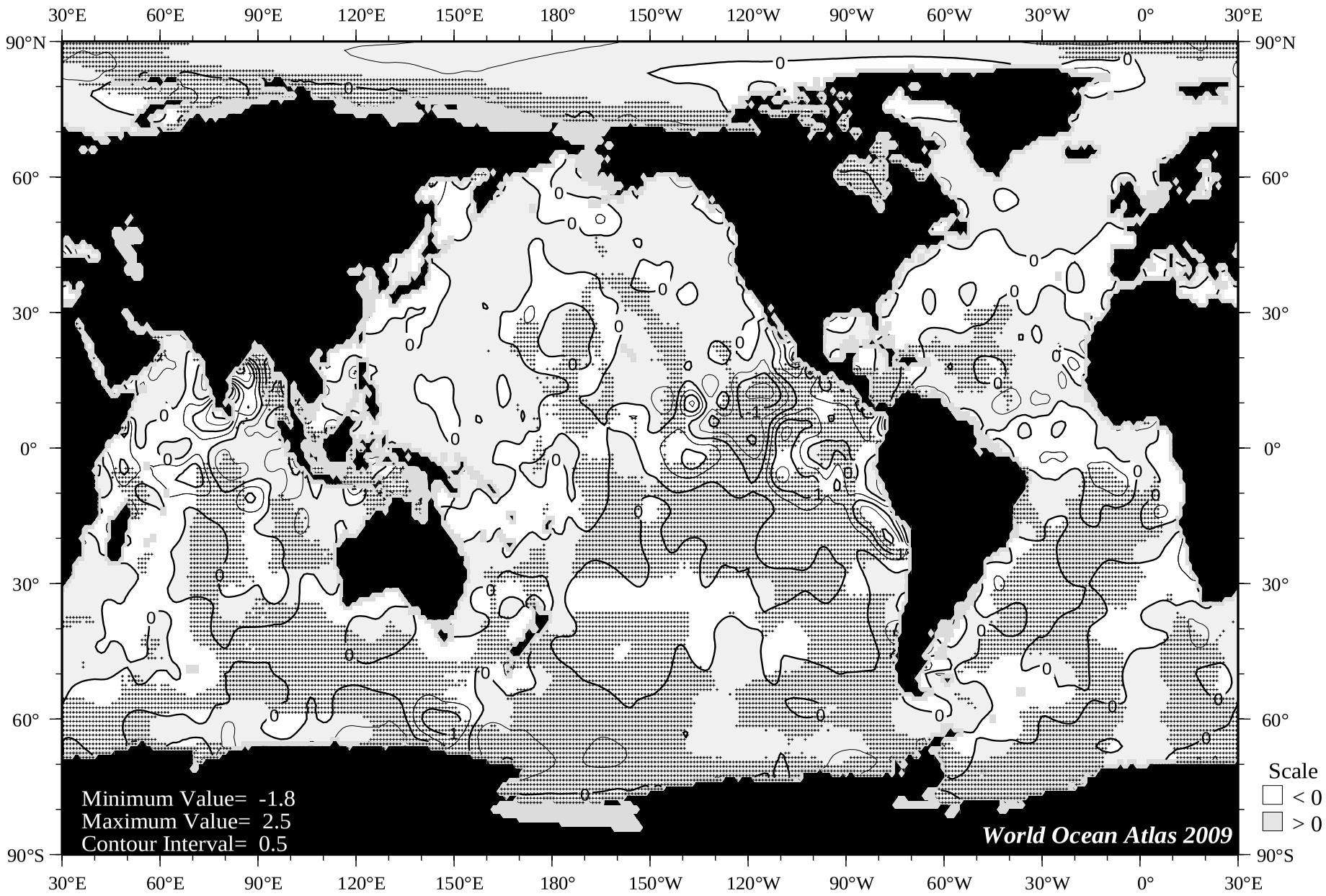

Fig F24 June minus annual AOU at 75 m. depth.

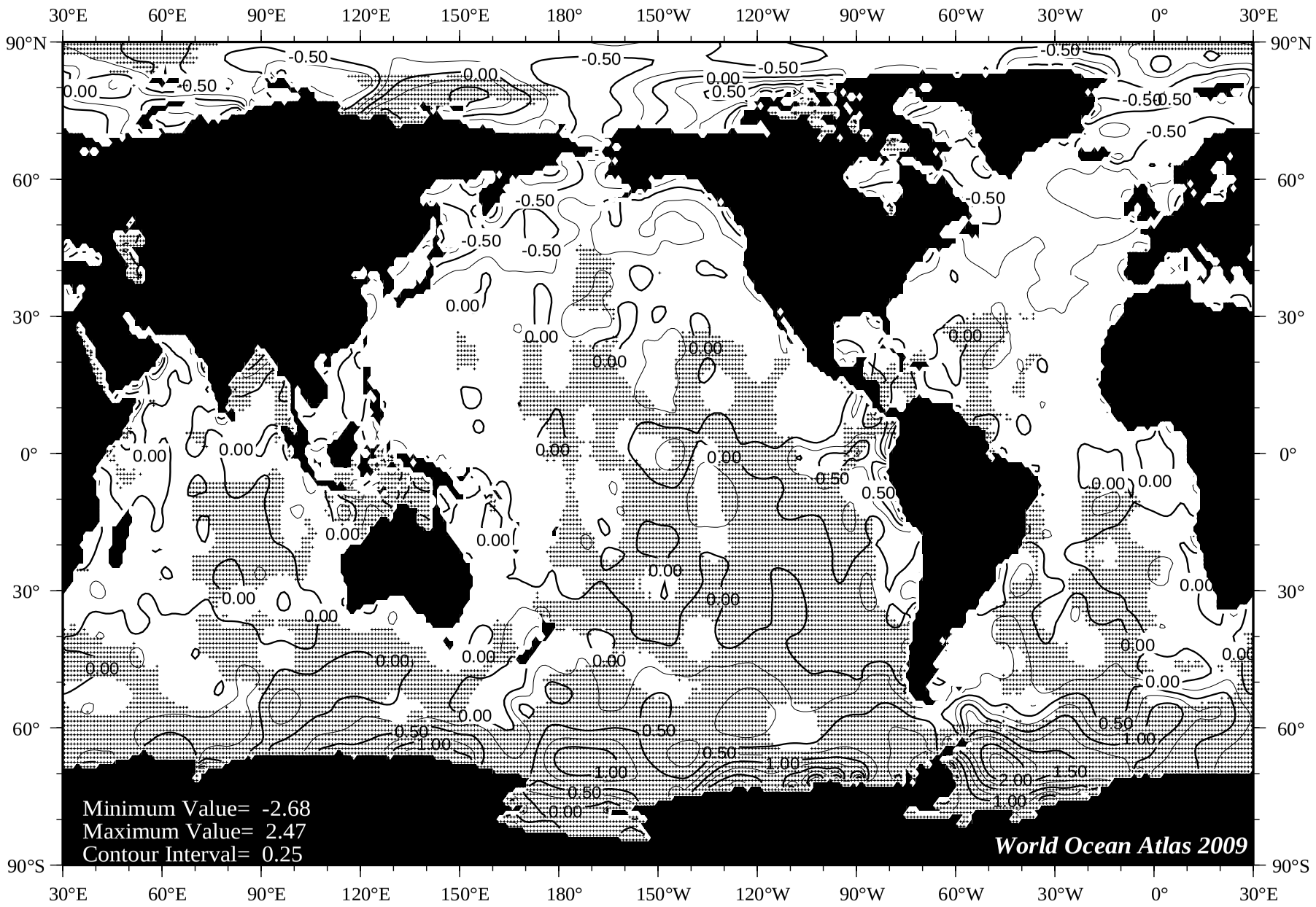

Fig F25 July mean apparent oxygen utilization (ml/l) at the surface.

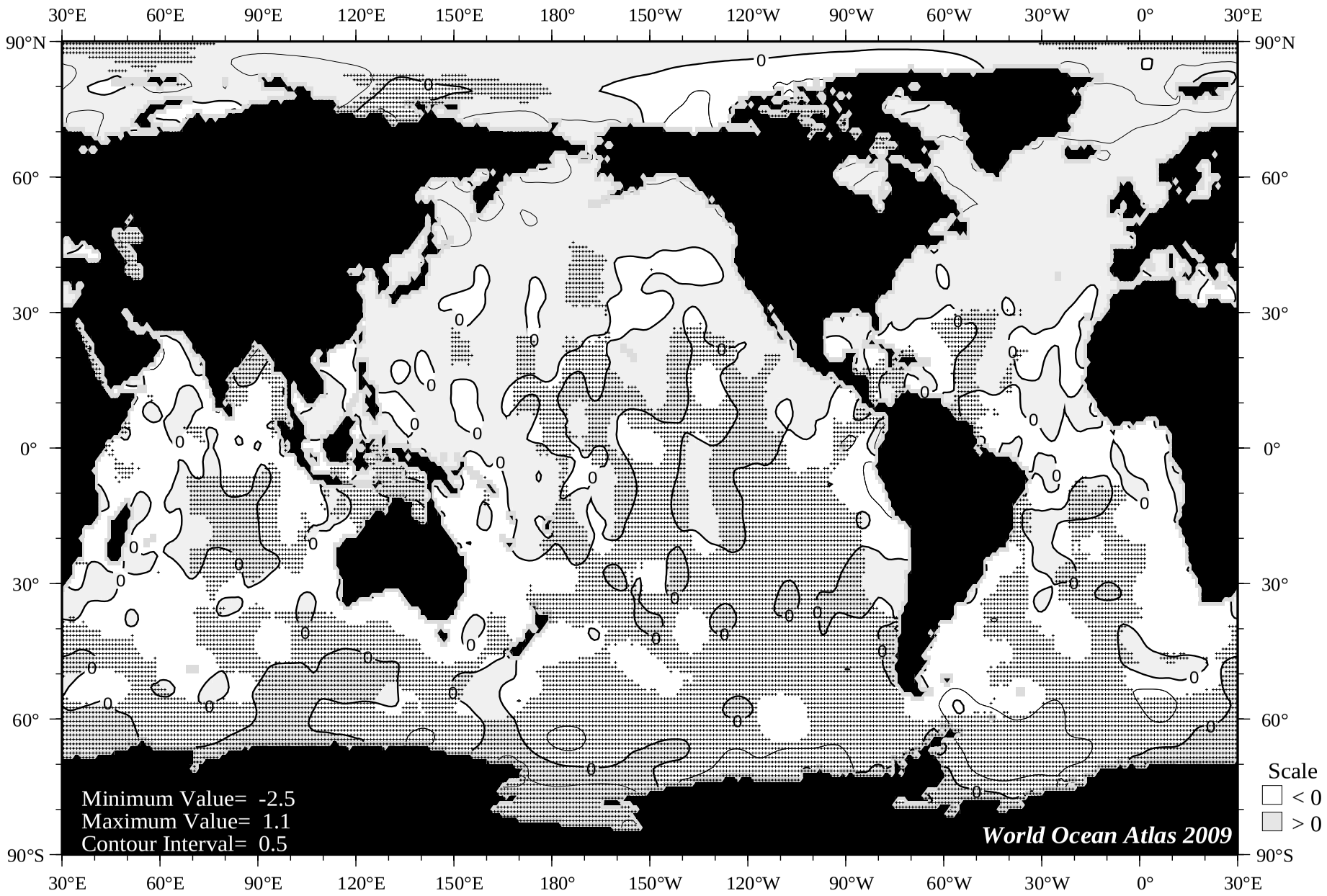

Fig F26 July minus annual AOU at the surface.

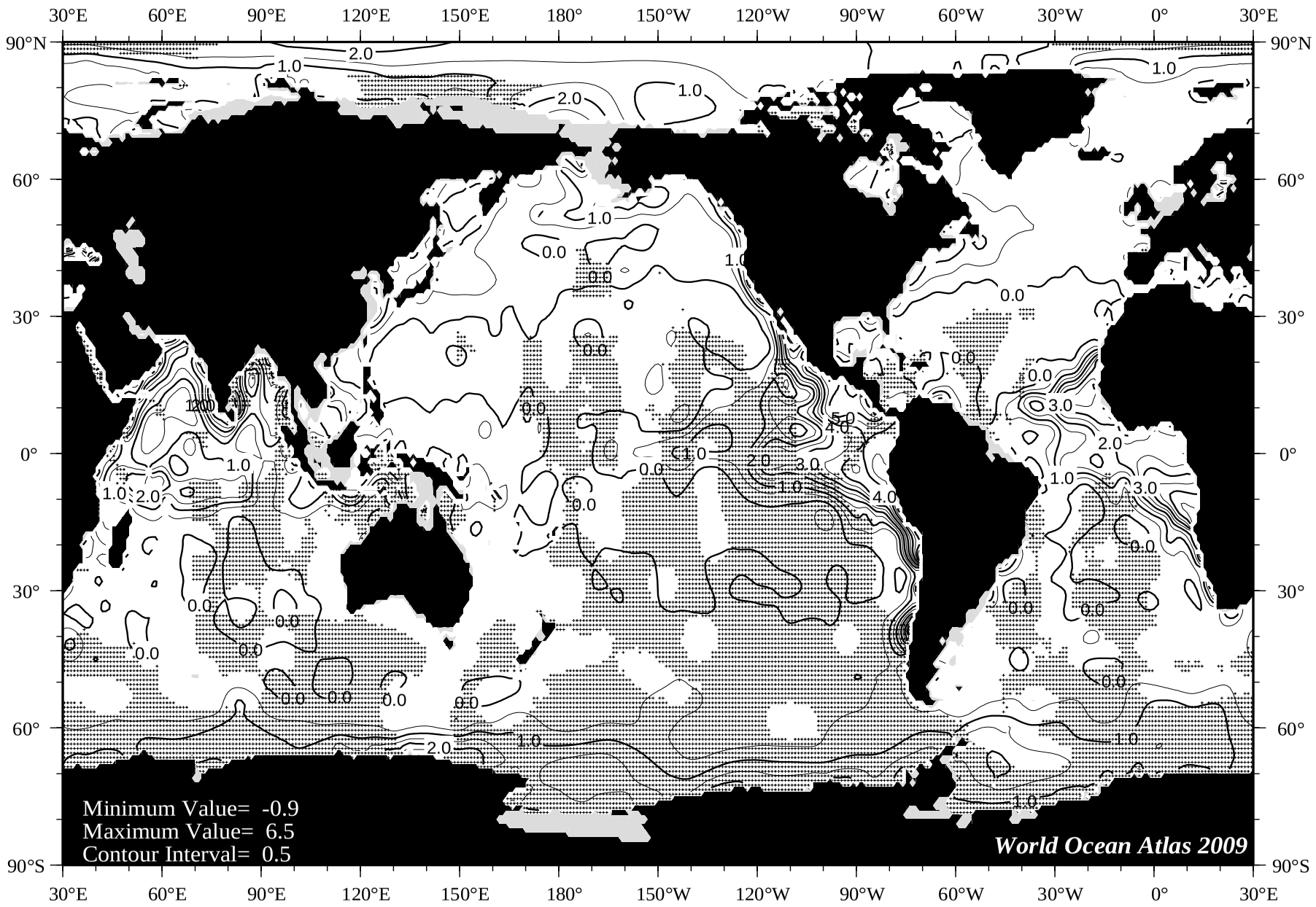

Fig F27 July mean apparent oxygen utilization (ml/l) at 75 m. depth.

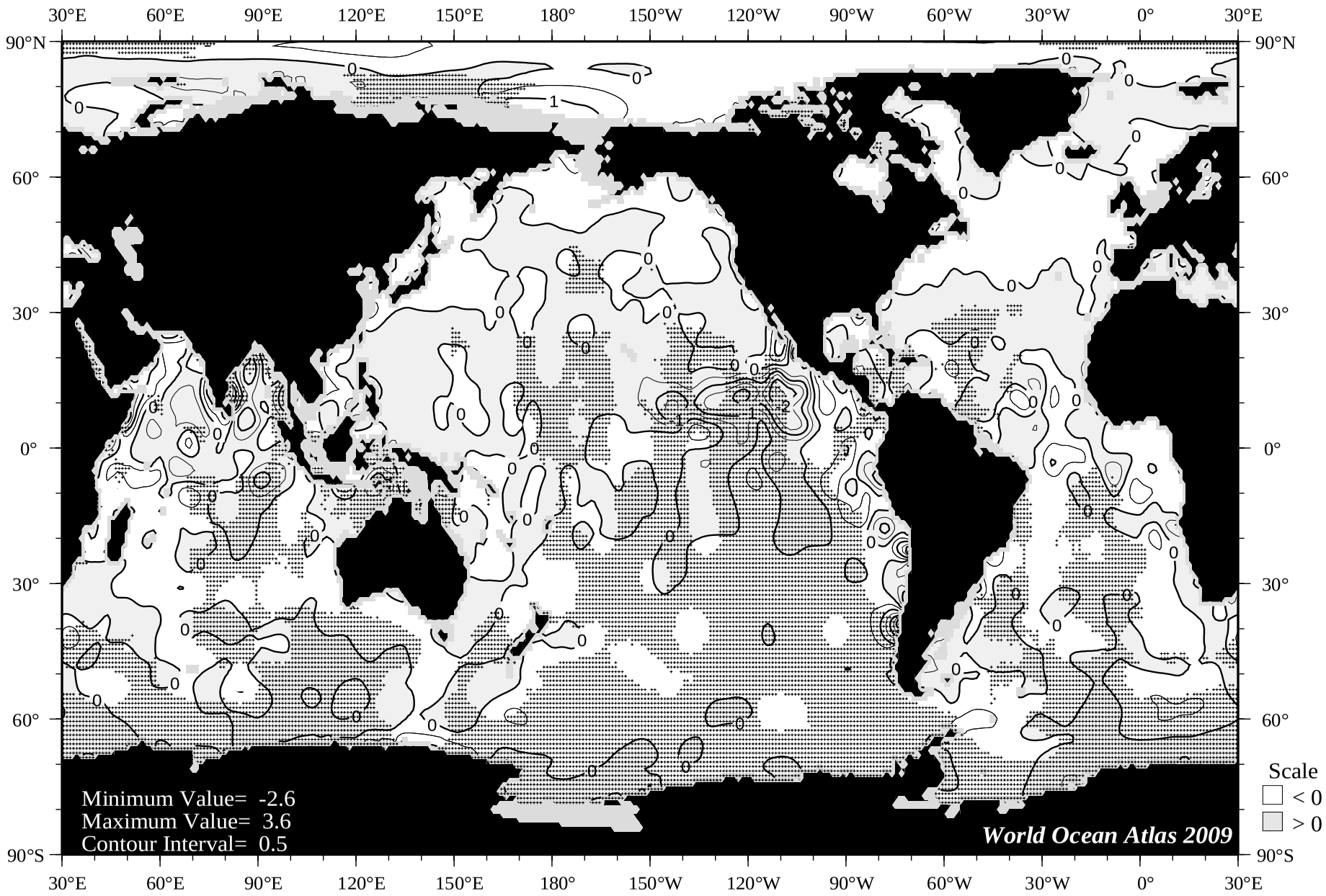

Fig F28 July minus annual AOU at 75 m. depth.

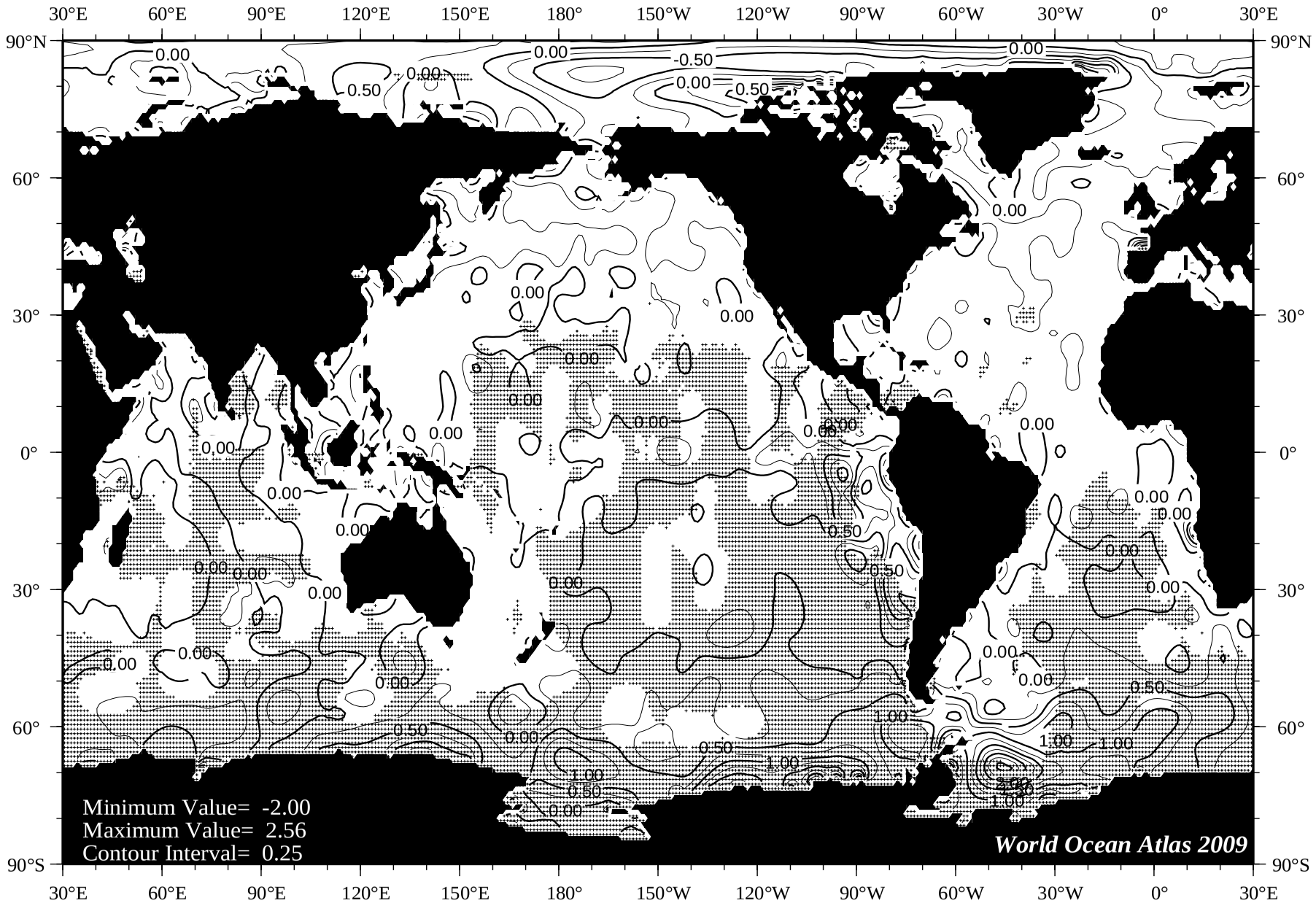

Fig F29 August mean apparent oxygen utilization (ml/l) at the surface.

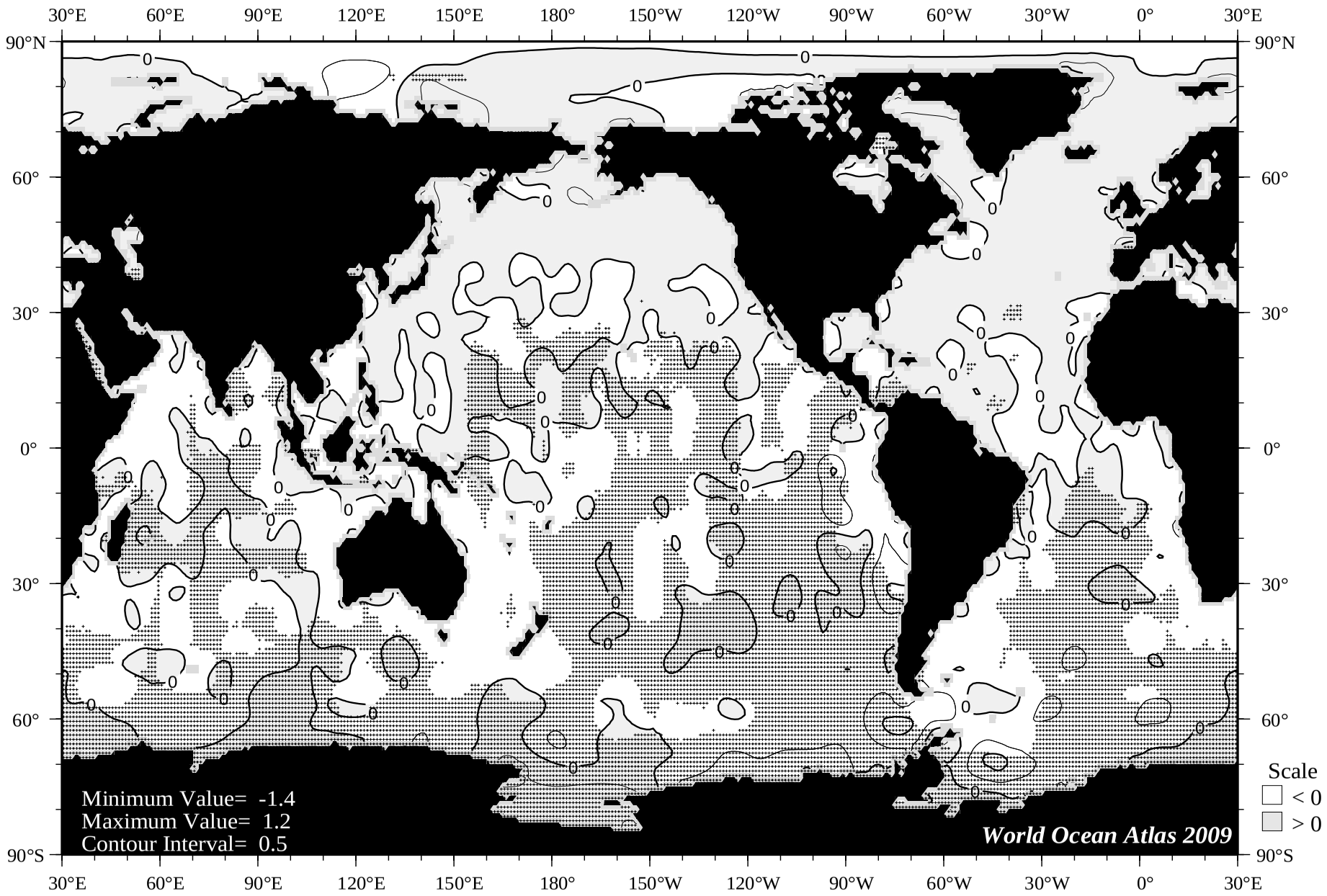

Fig F30 August minus annual AOU at the surface.

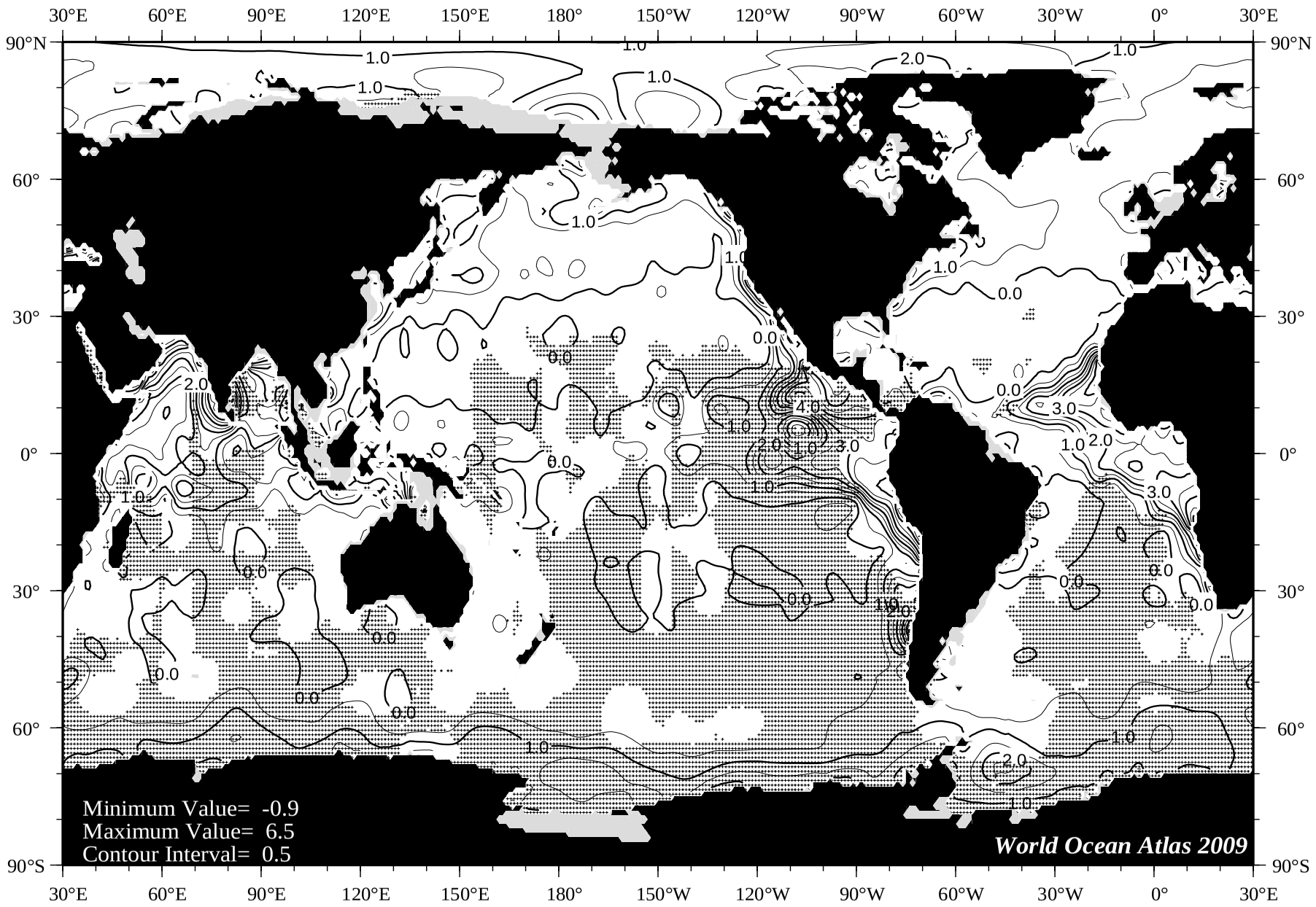

Fig F31 August mean apparent oxygen utilization (ml/l) at 75 m. depth.

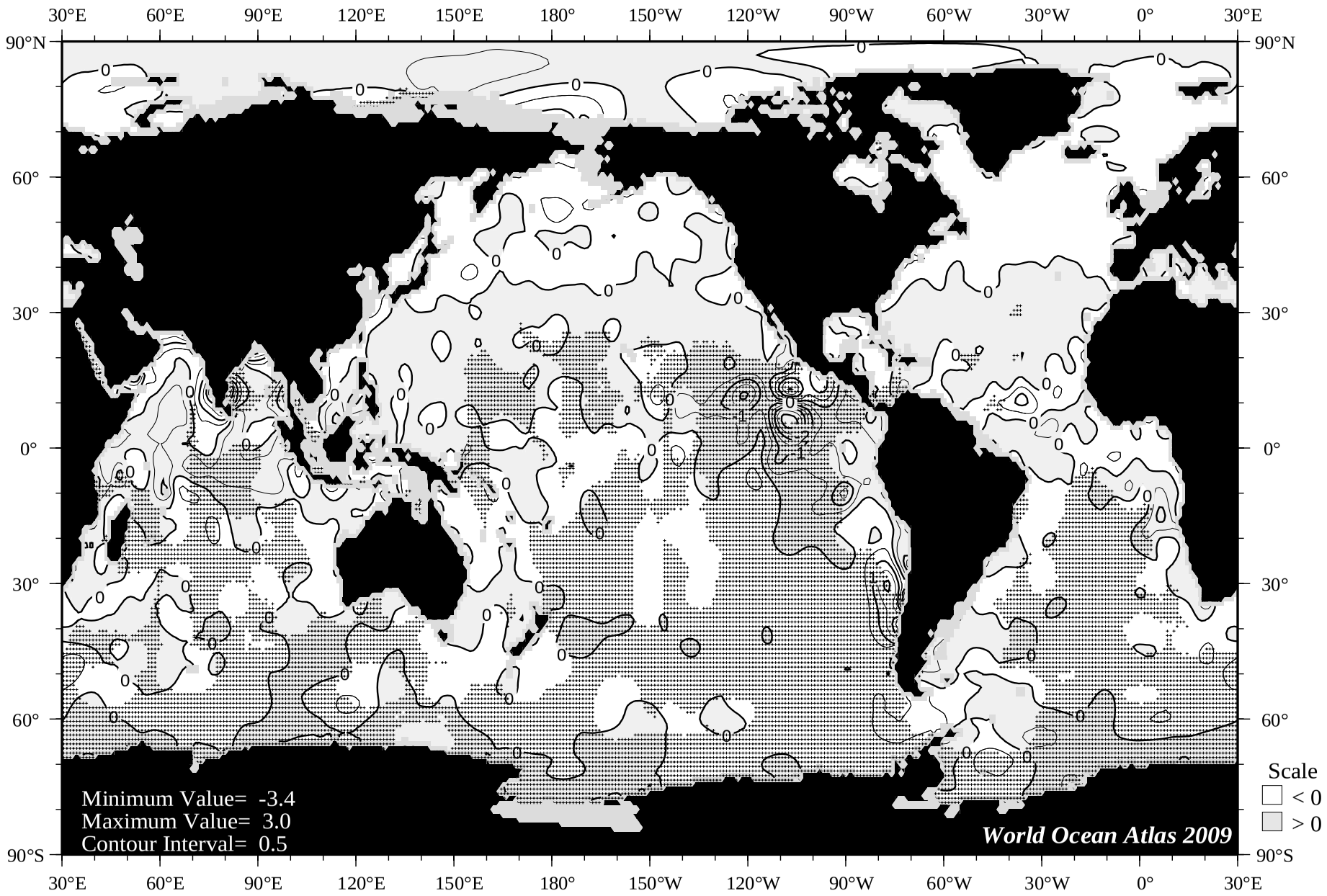

Fig F32 August minus annual AOU at 75 m. depth.

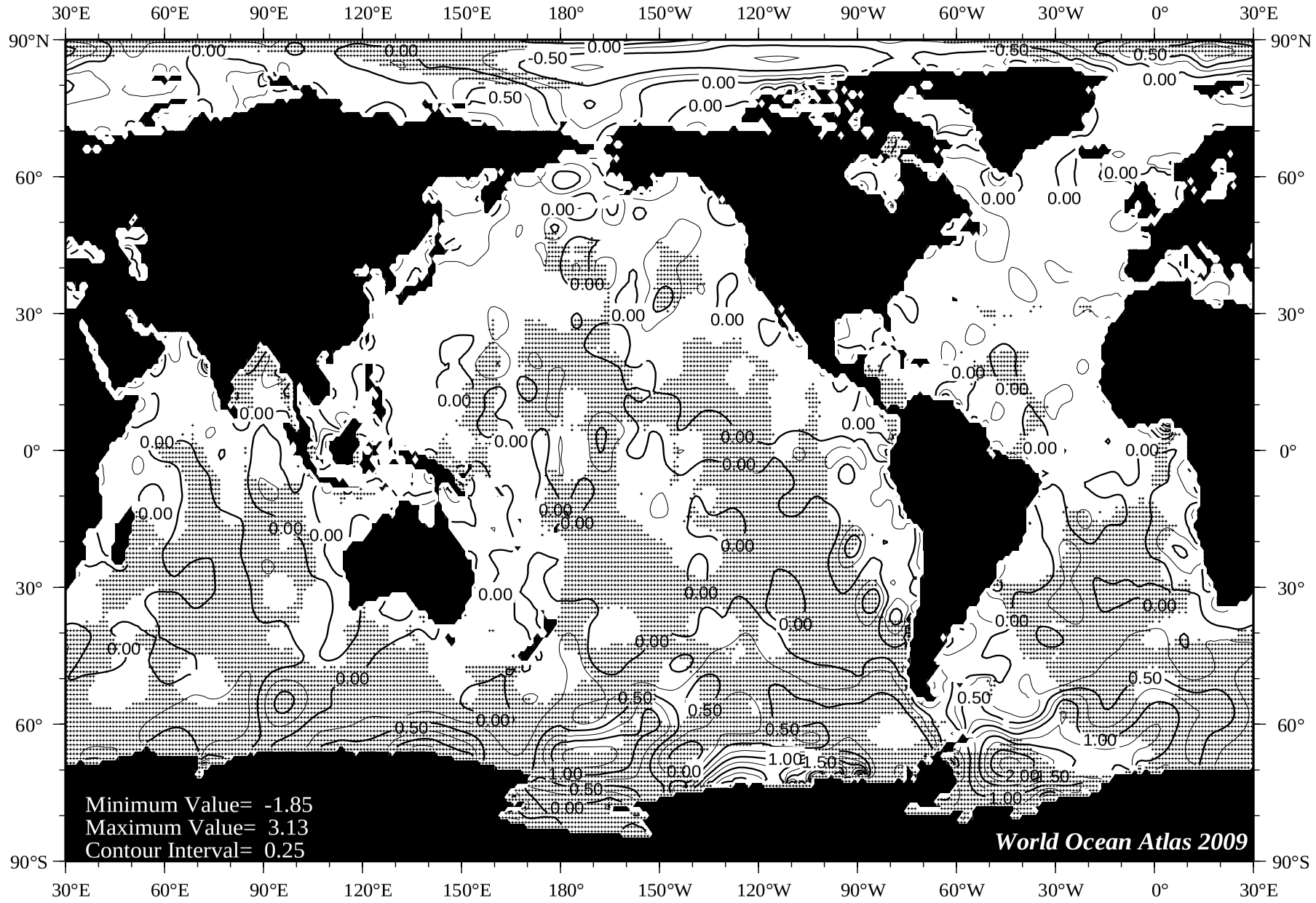

Fig F33 September mean apparent oxygen utilization (ml/l) at the surface.

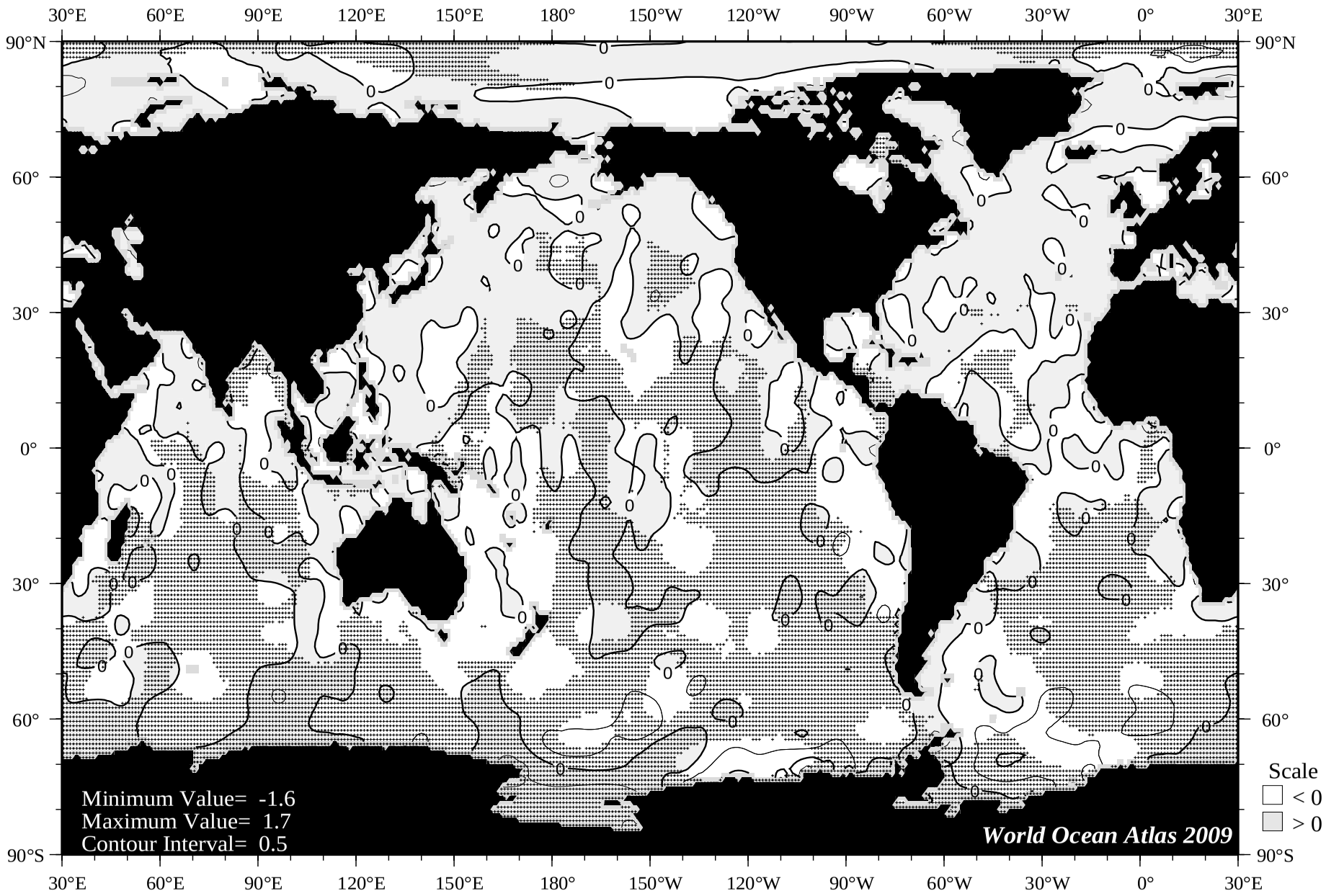

Fig F34 September minus annual AOU at the surface.

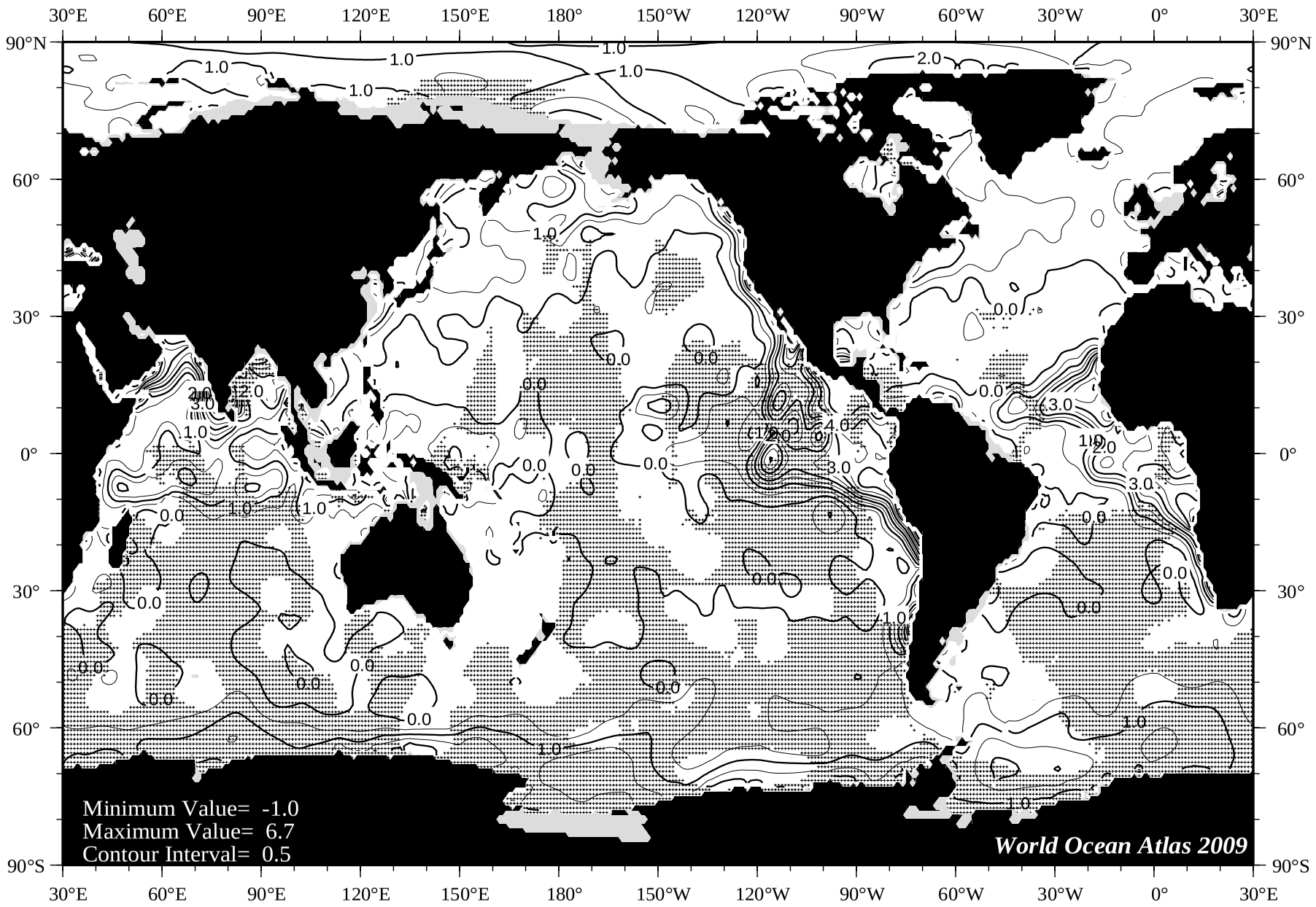

Fig F35 September mean apparent oxygen utilization (ml/l) at 75 m. depth.

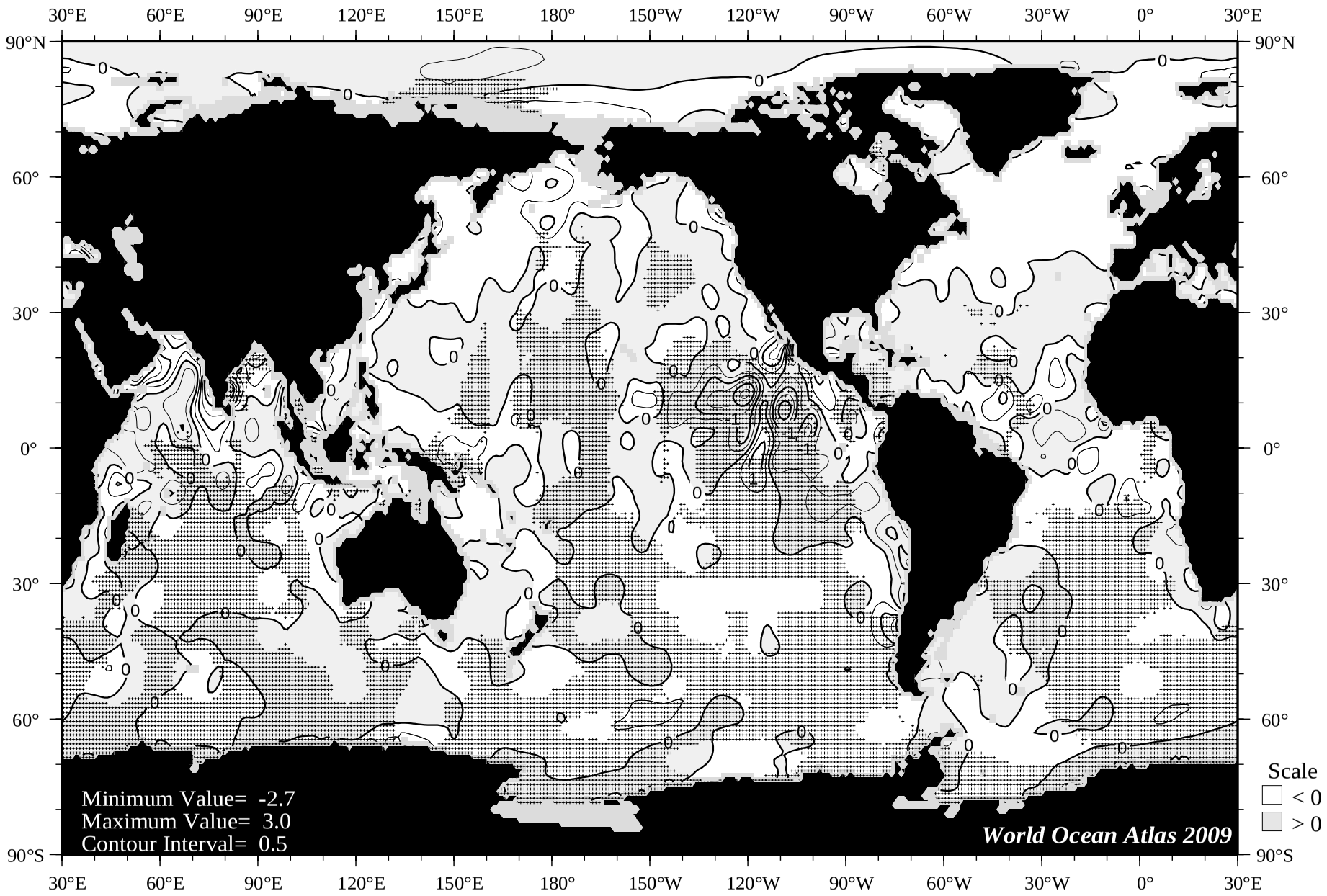

Fig F36 September minus annual AOU at 75 m. depth.

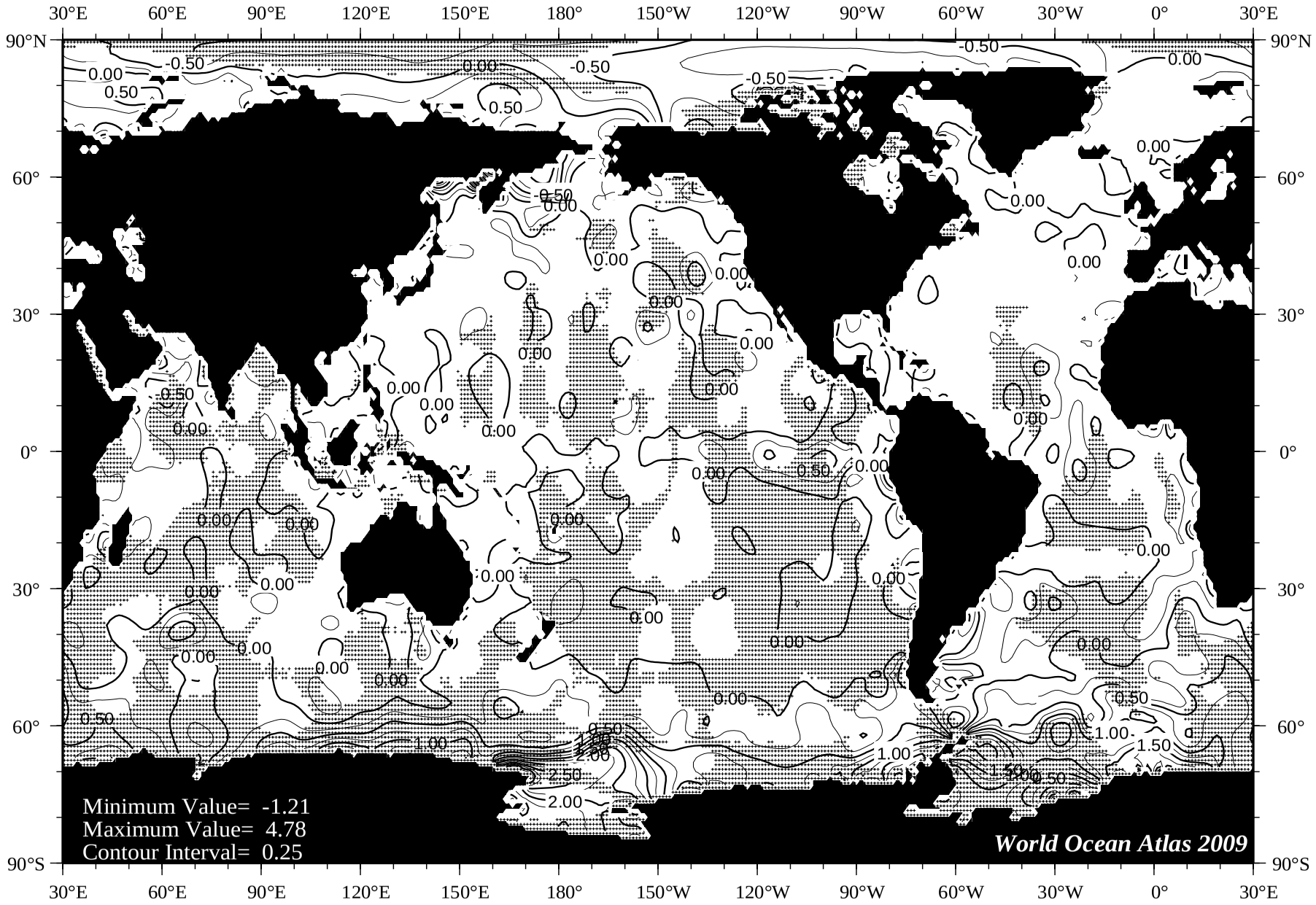

Fig F37 October mean apparent oxygen utilization (ml/l) at the surface.

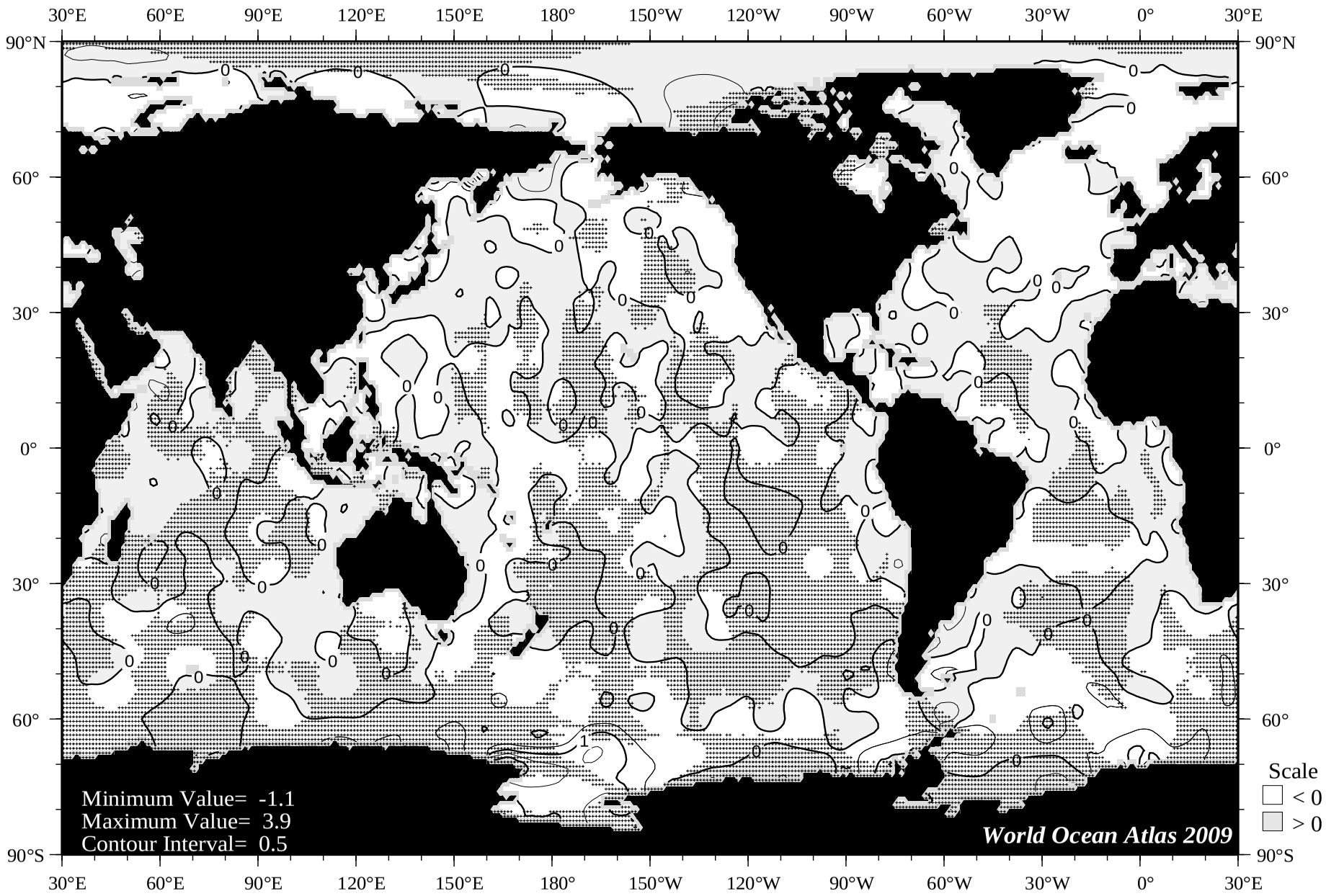

Fig F38 October minus annual AOU at the surface.

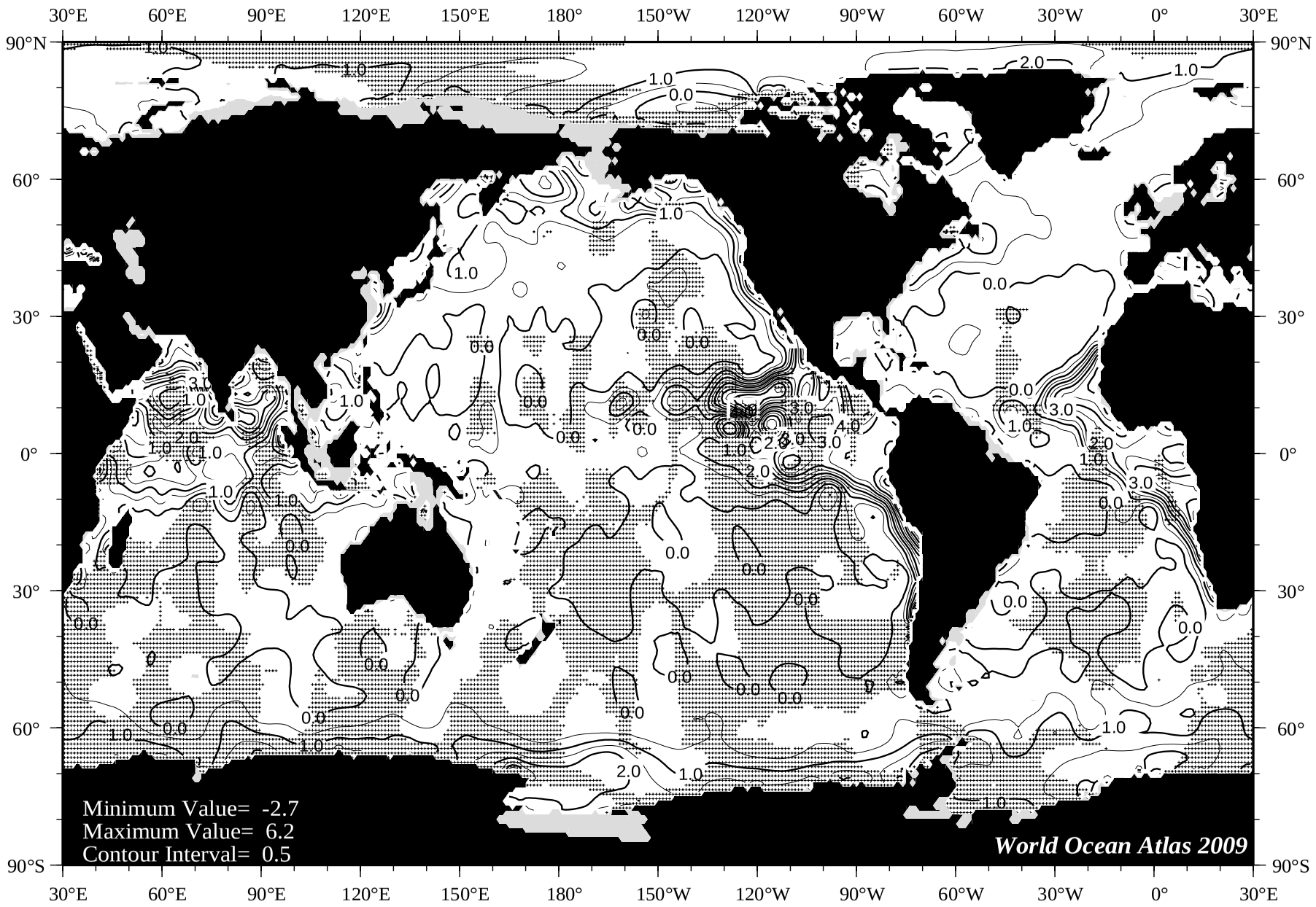

Fig F39 October mean apparent oxygen utilization (ml/l) at 75 m. depth.

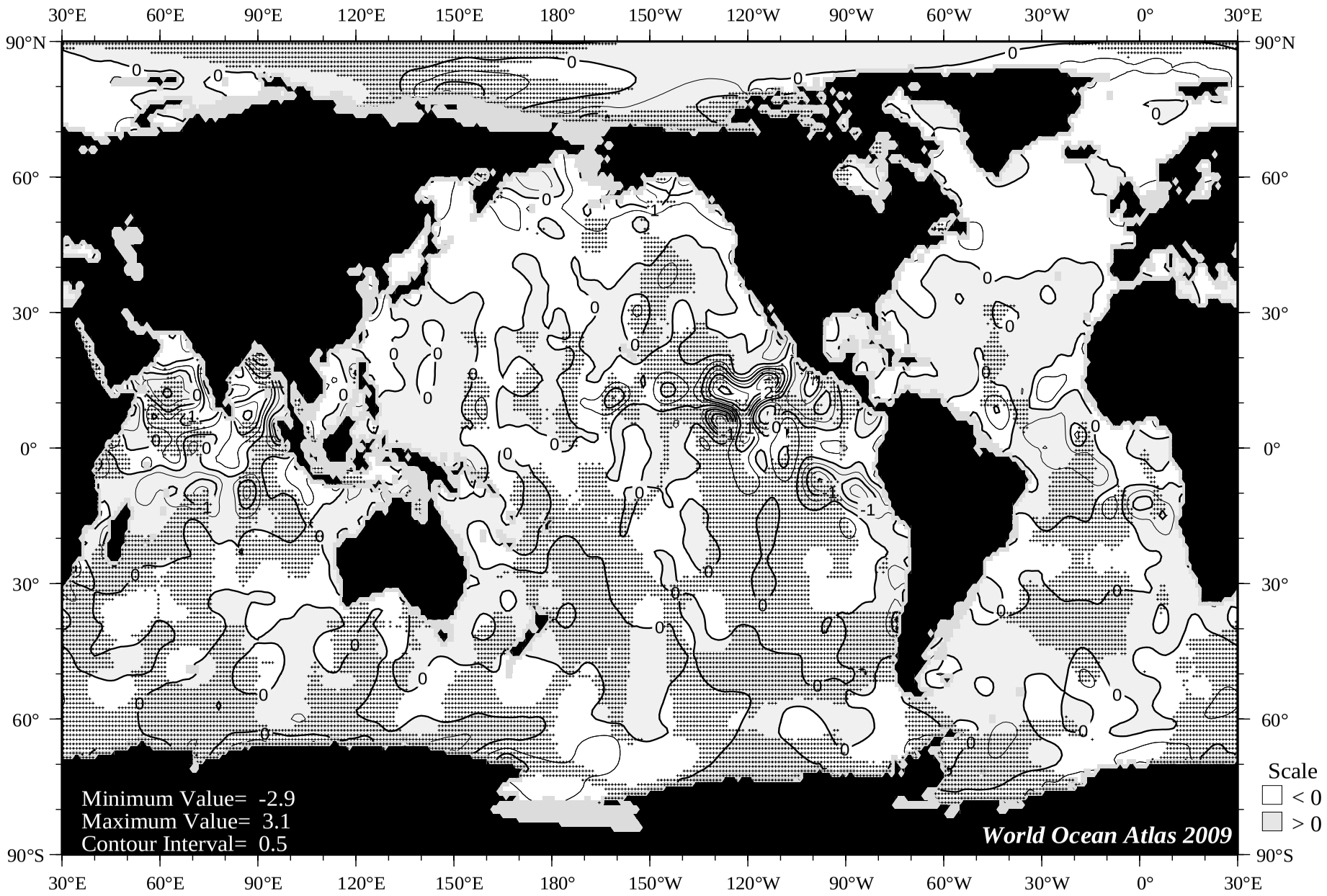

Fig F40 October minus annual AOU at 75 m. depth.

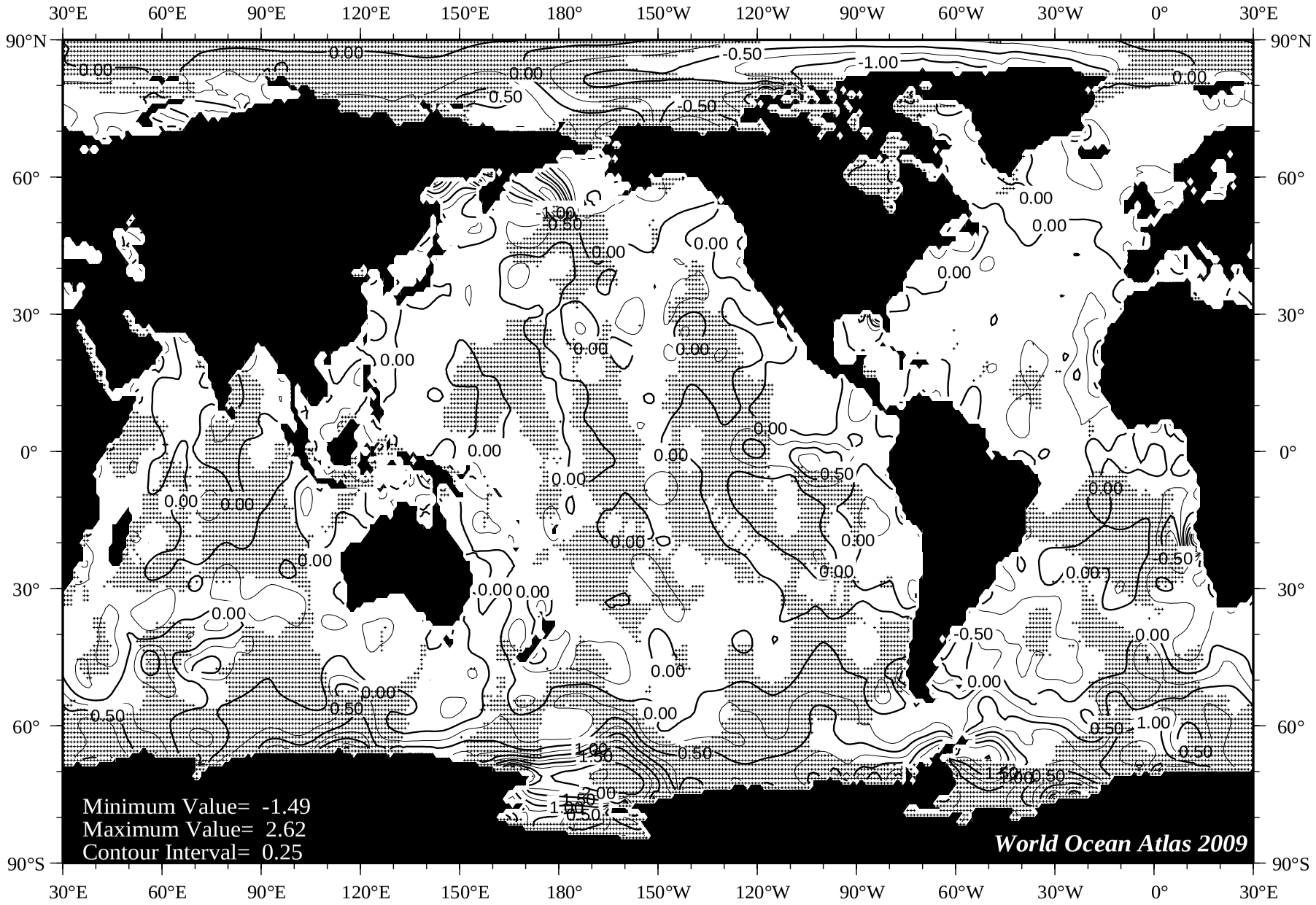

Fig F41 November mean apparent oxygen utilization (ml/l) at the surface.

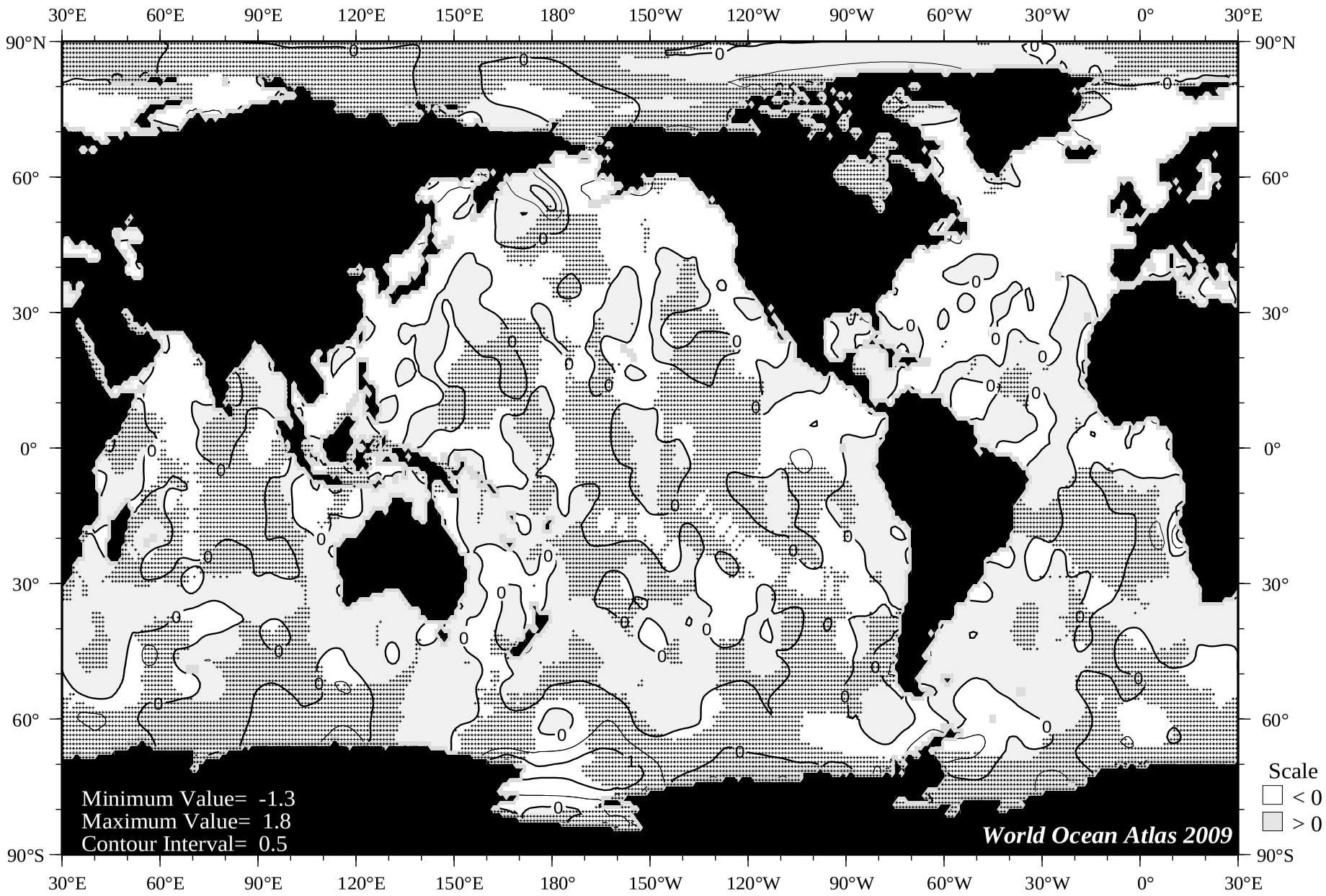

Fig F42 November minus annual AOU at the surface.

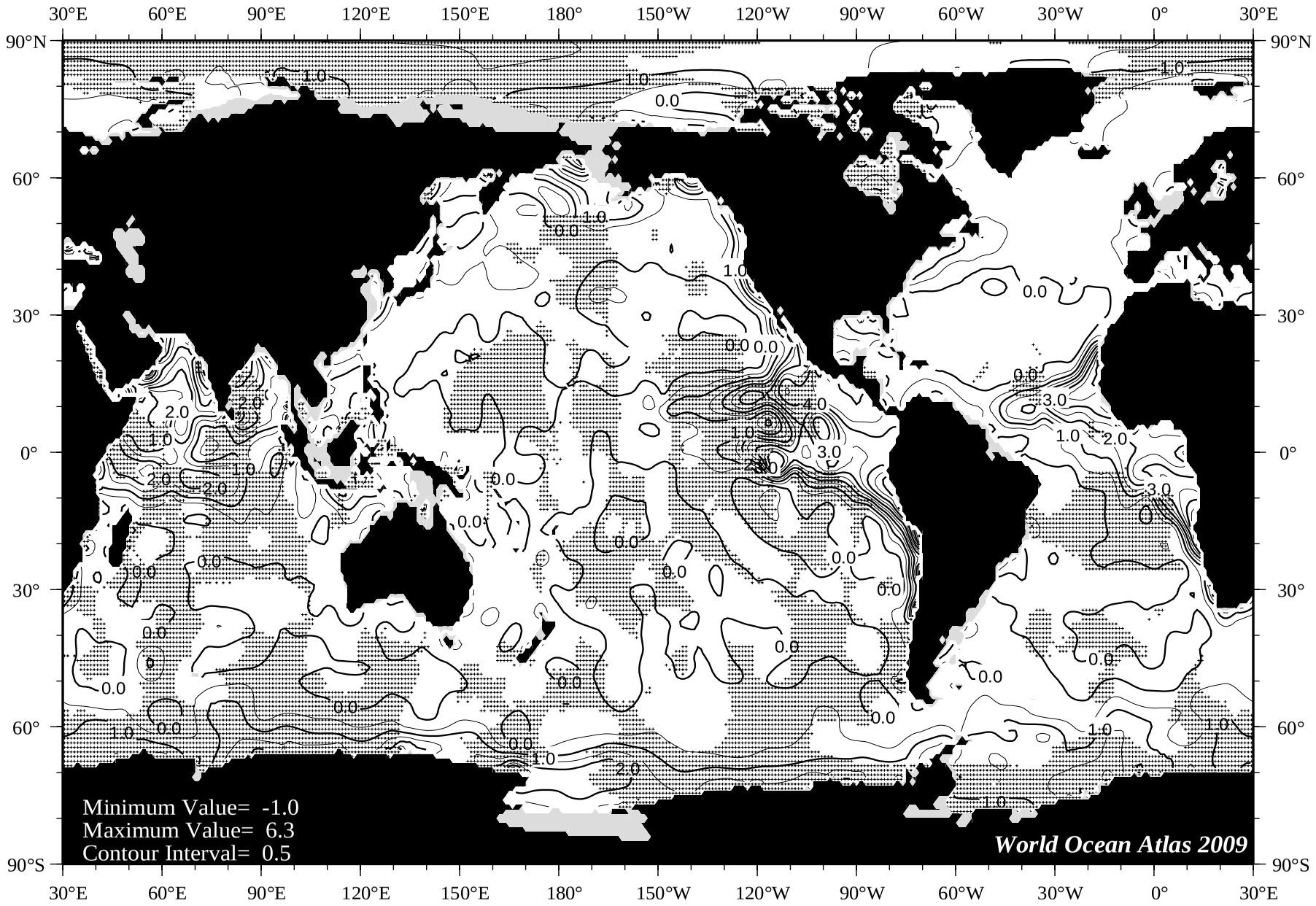

Fig F43 November mean apparent oxygen utilization (ml/l) at 75 m. depth.

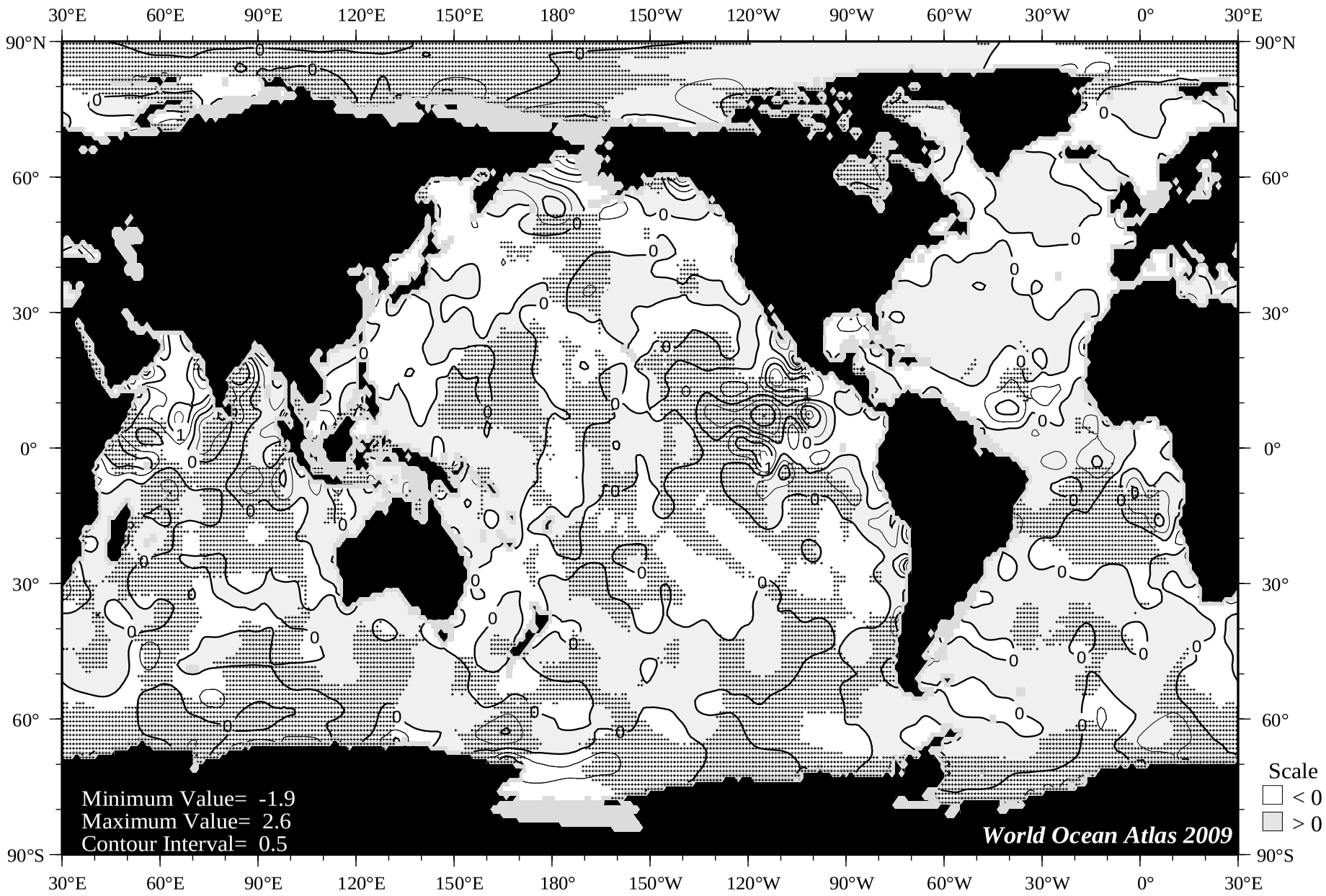

Fig F44 November minus annual AOU at 75 m. depth.

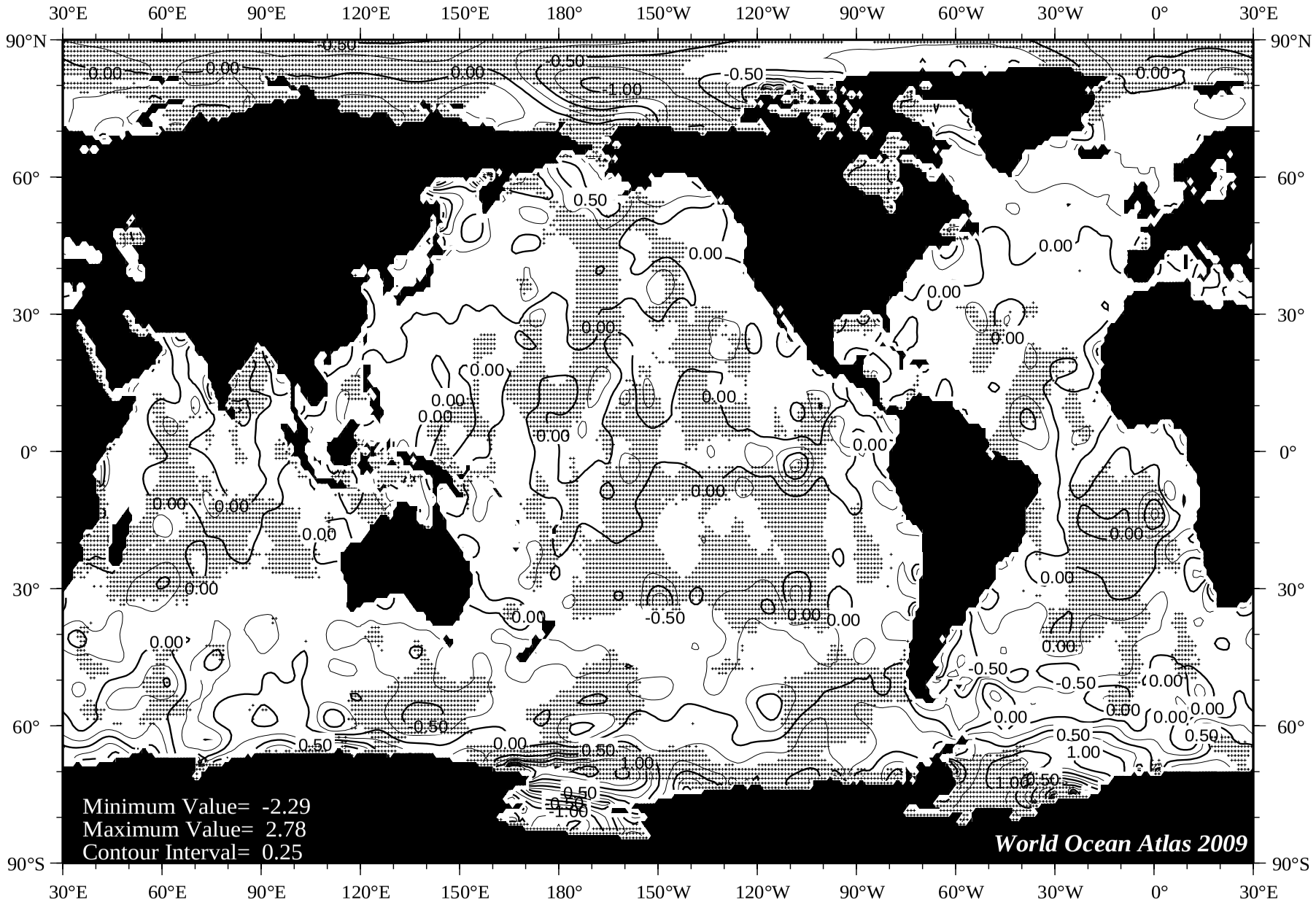

Fig F45 December mean apparent oxygen utilization (ml/l) at the surface.

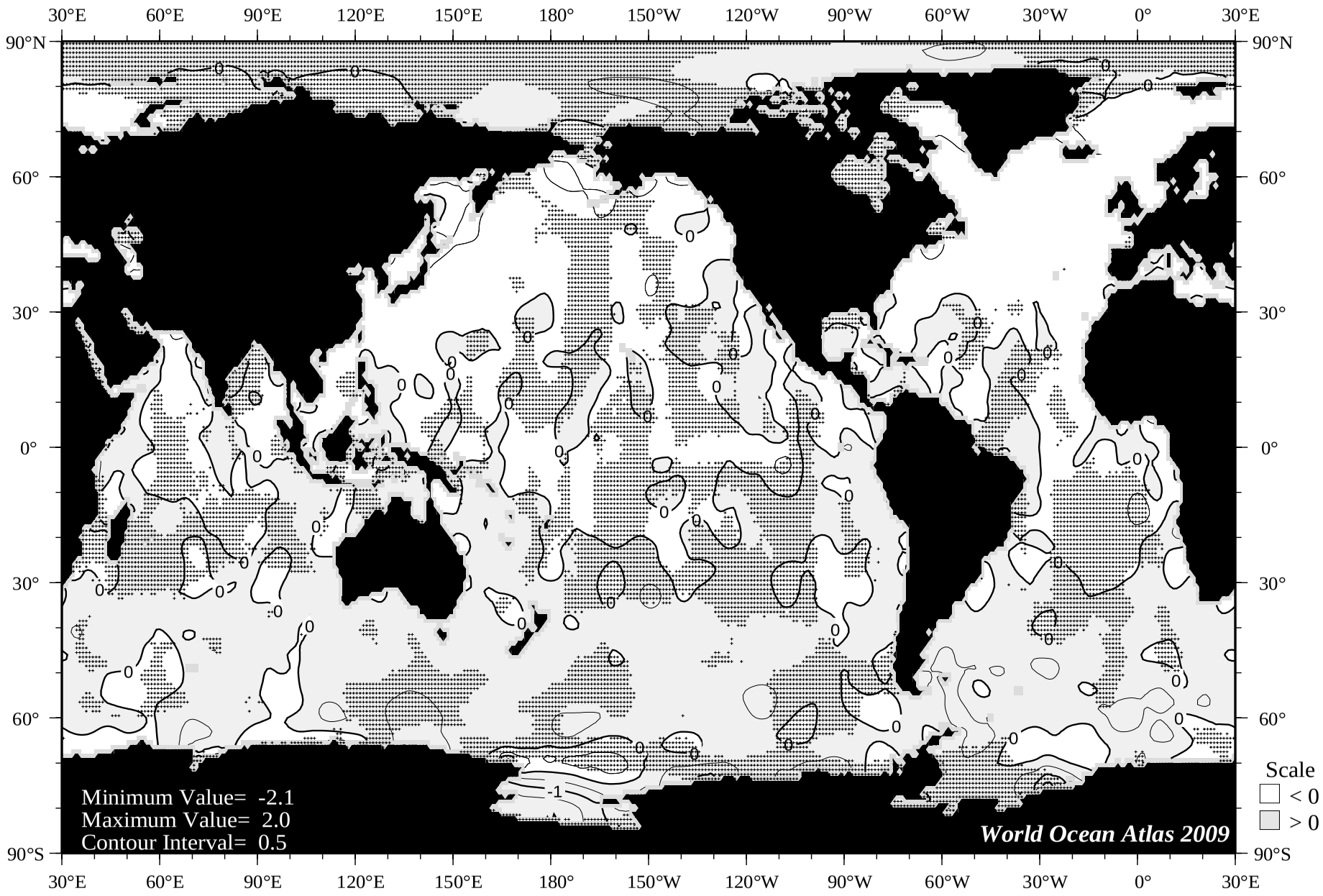

Fig F46 December minus annual AOU at the surface.

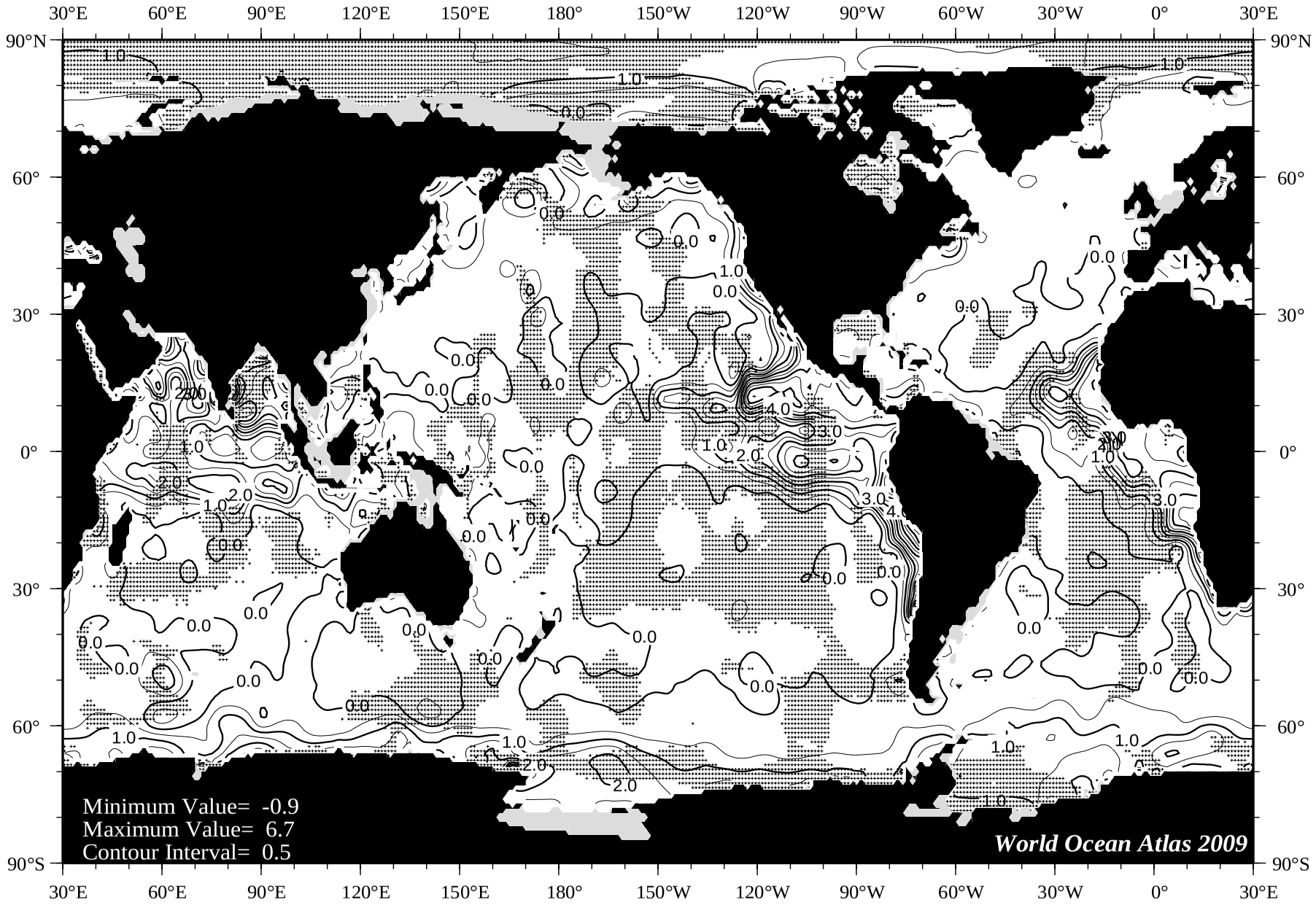

Fig F47 December mean apparent oxygen utilization (ml/l) at 75 m. depth.

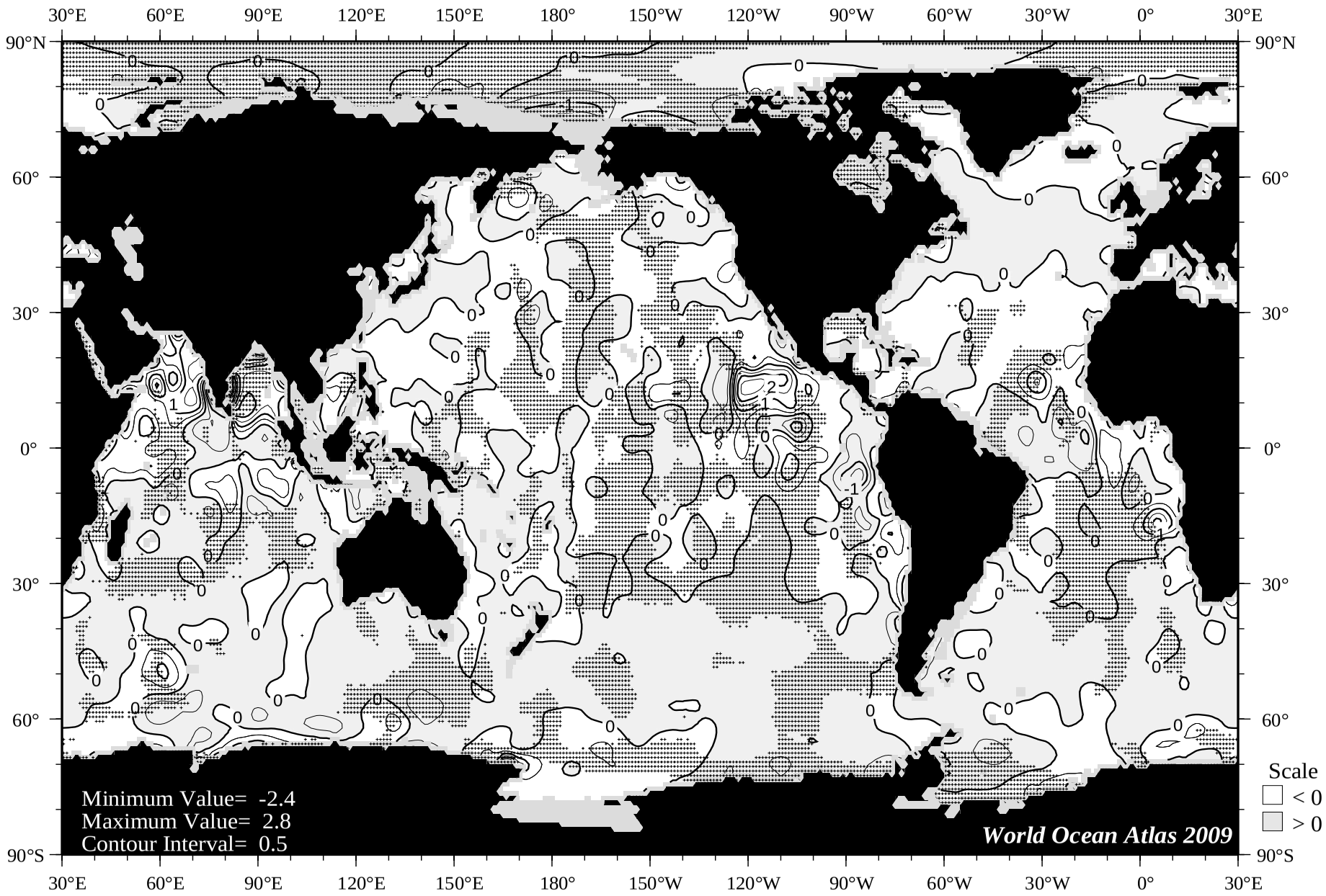

Fig F48 December minus annual AOU at 75 m. depth.

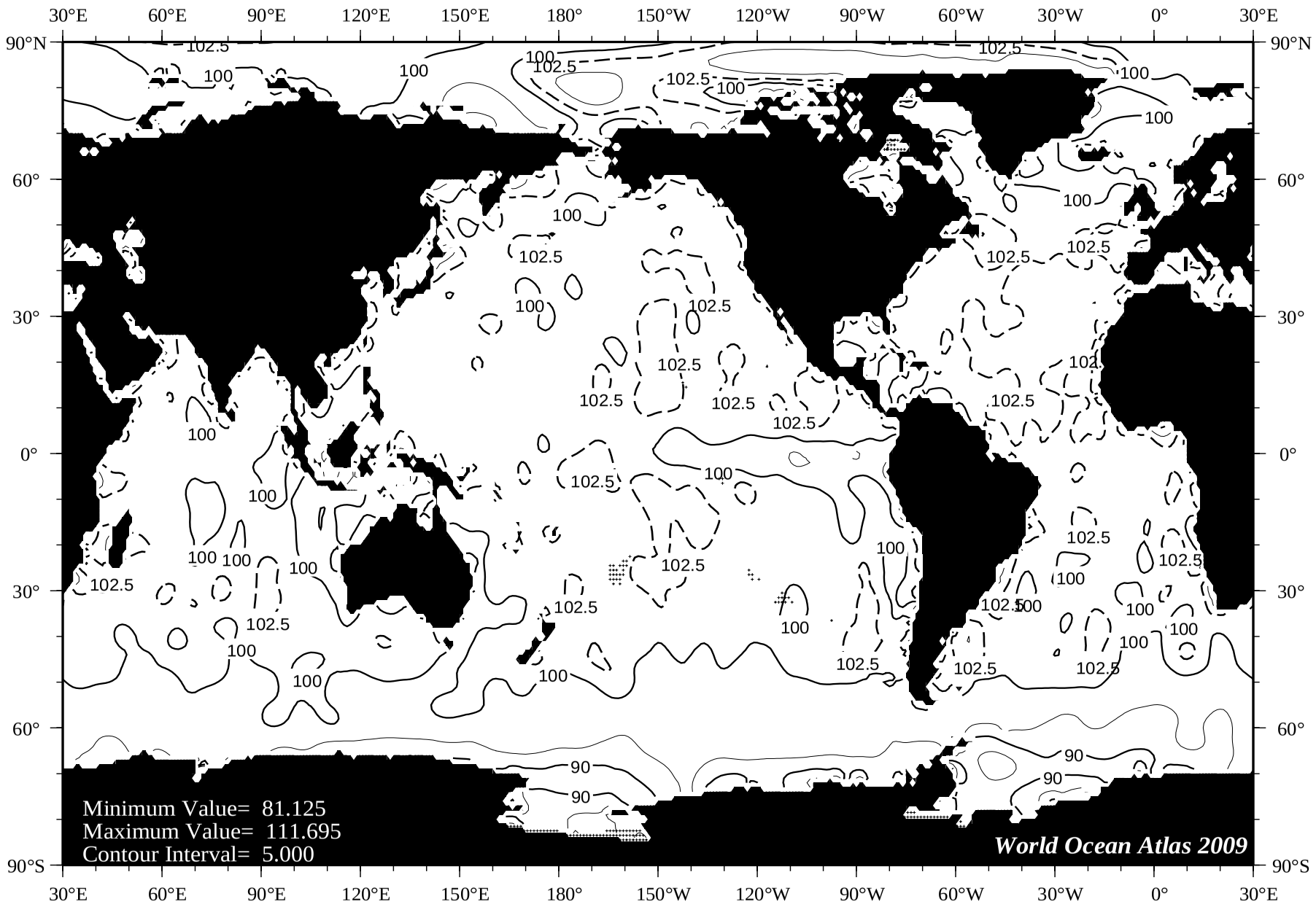

Fig G1 Annual percent oxygen saturation at the surface.

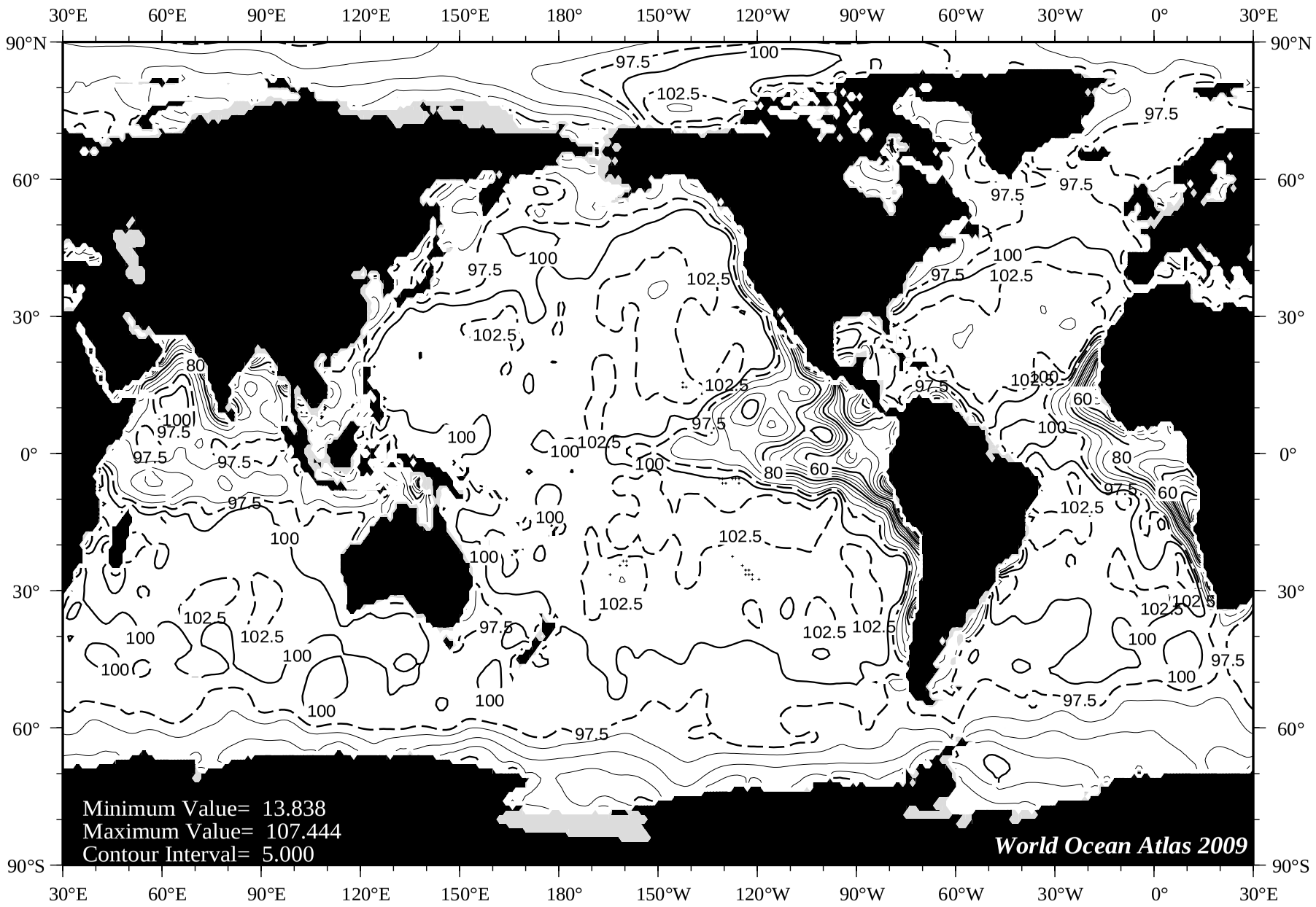

Fig G2 Annual percent oxygen saturation at 50 m. depth.

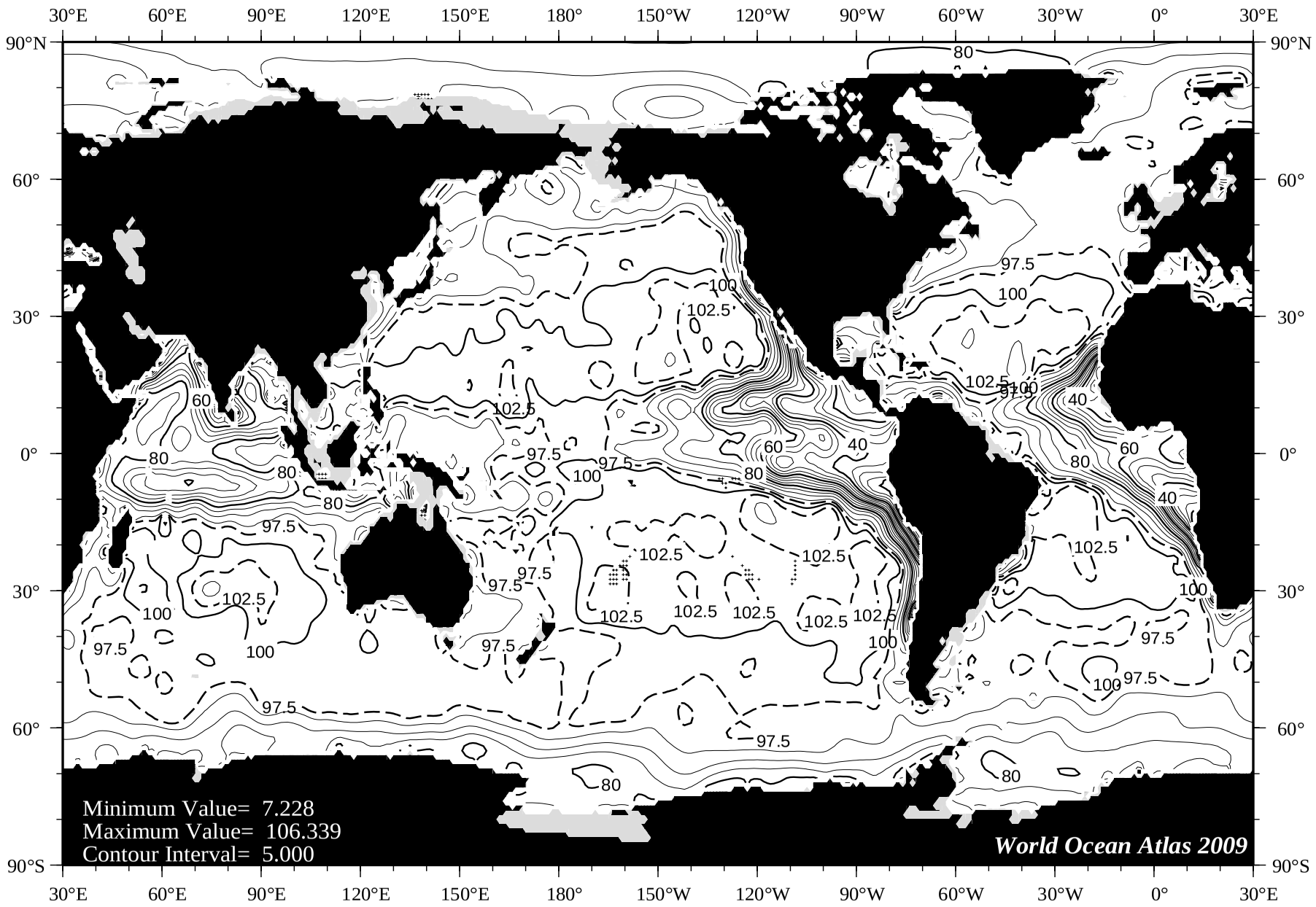

Fig G3 Annual percent oxygen saturation at 75 m. depth.

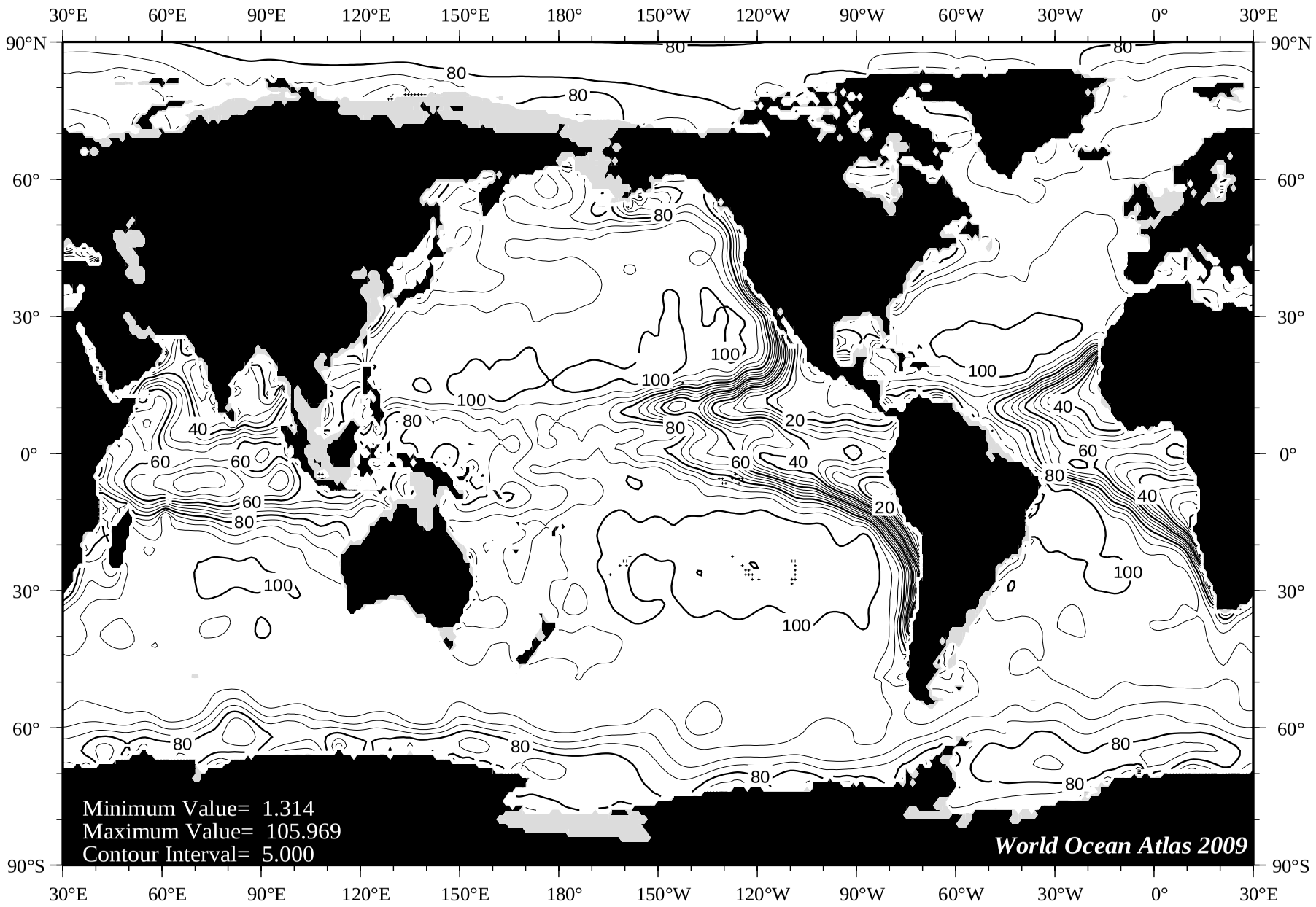

Fig G4 Annual percent oxygen saturation at 100 m. depth.

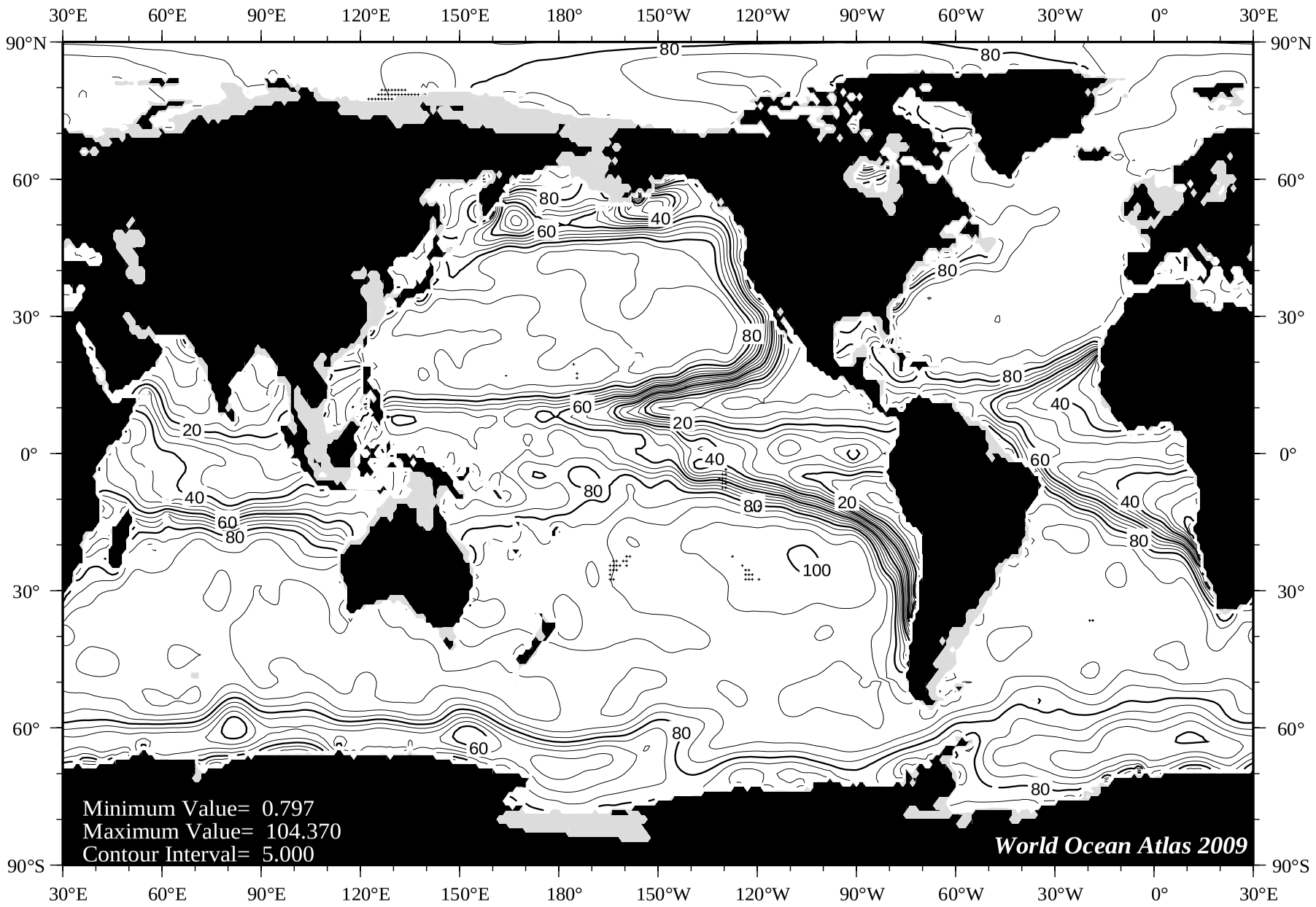

Fig G5 Annual percent oxygen saturation at 150 m. depth.

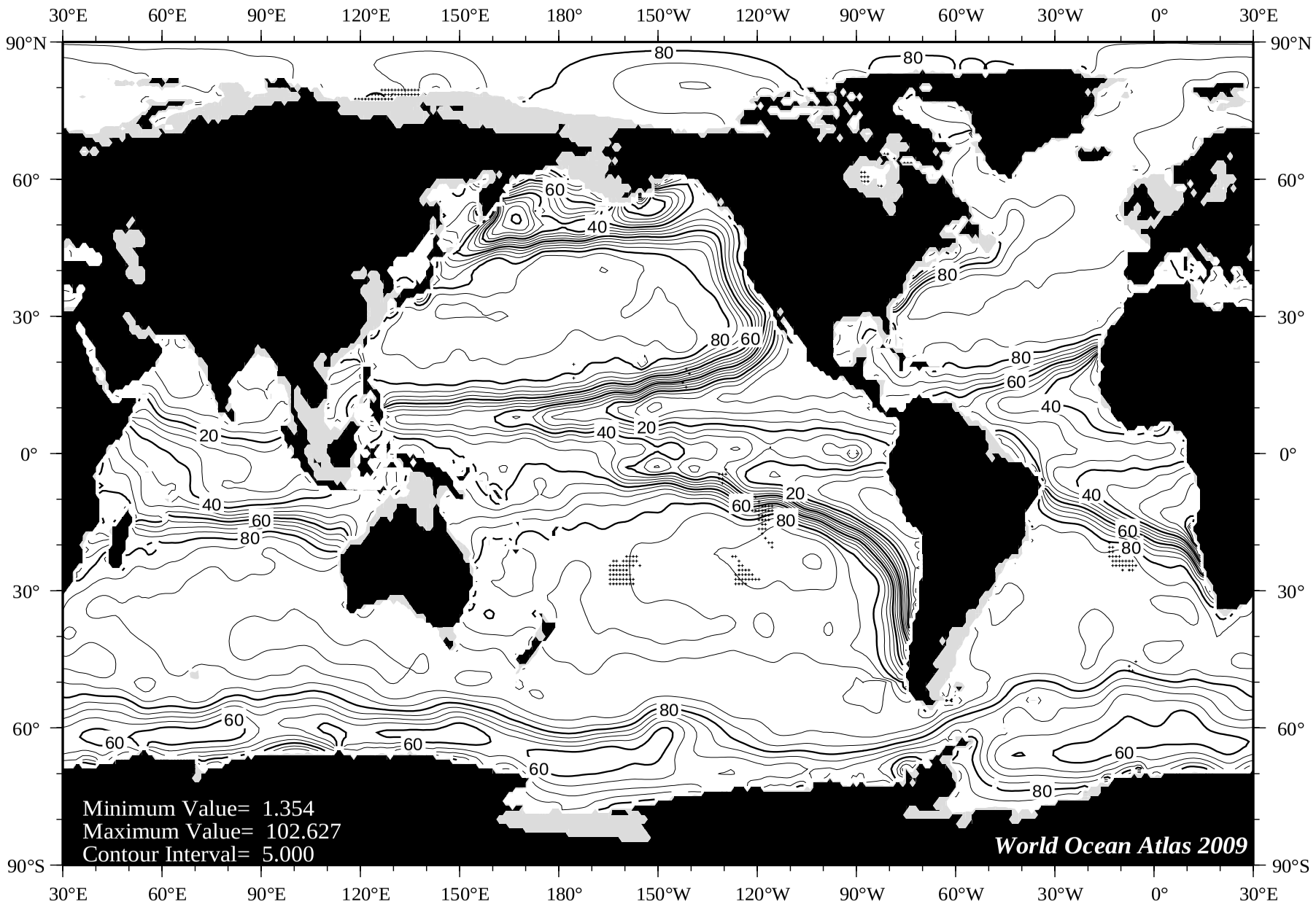

Fig G6 Annual percent oxygen saturation at 200 m. depth.

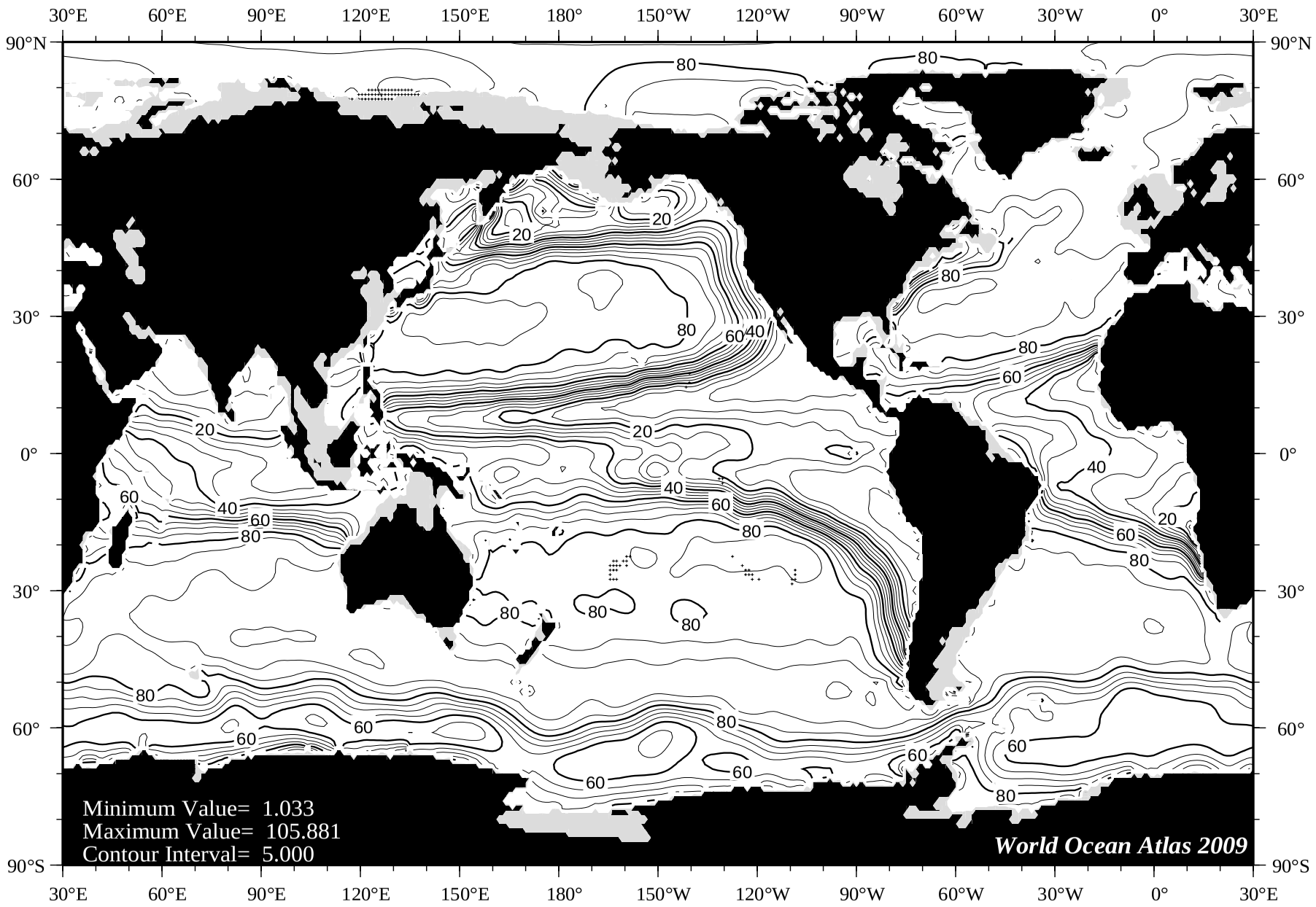

Fig G7 Annual percent oxygen saturation at 250 m. depth.

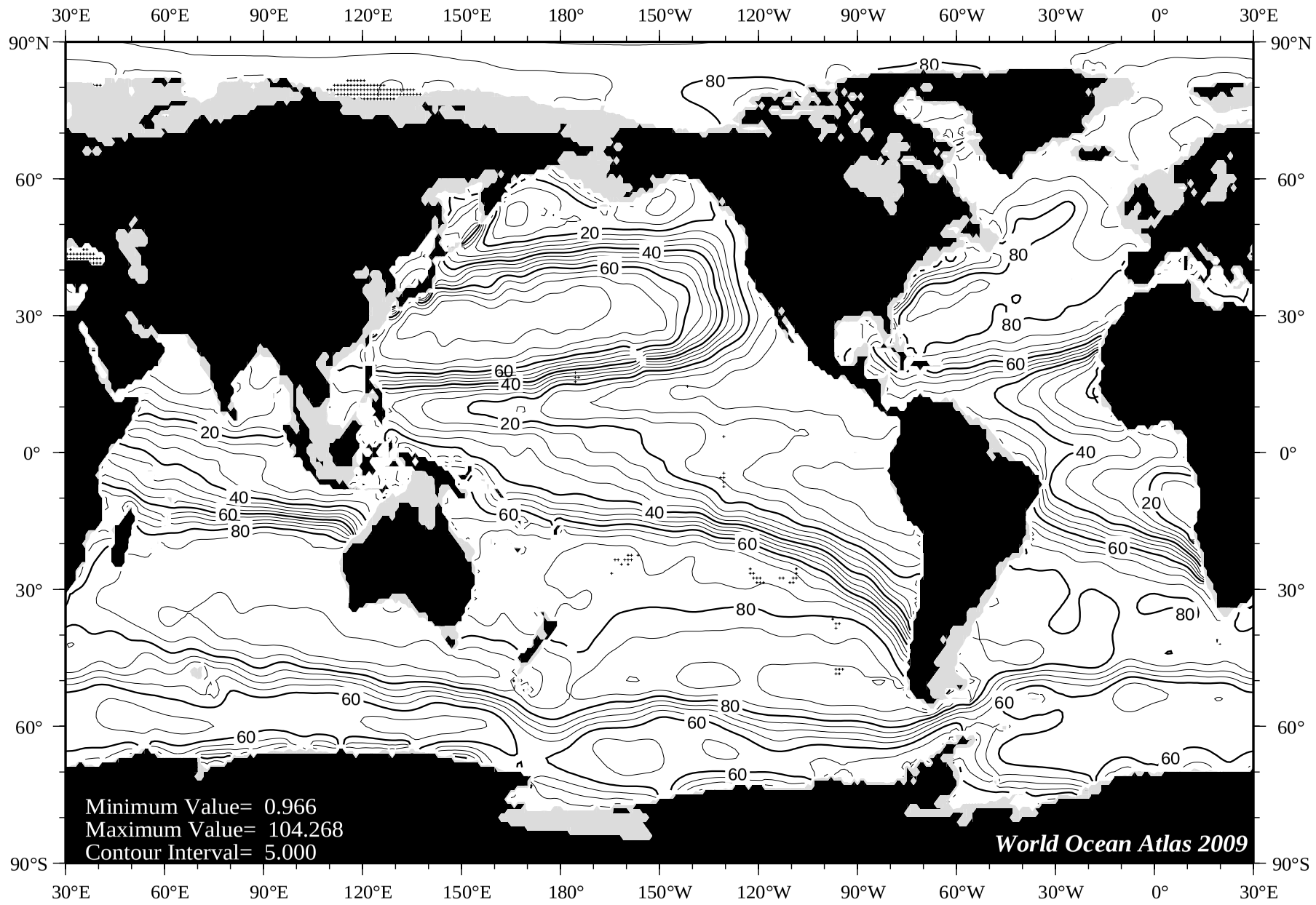

Fig G8 Annual percent oxygen saturation at 400 m. depth.

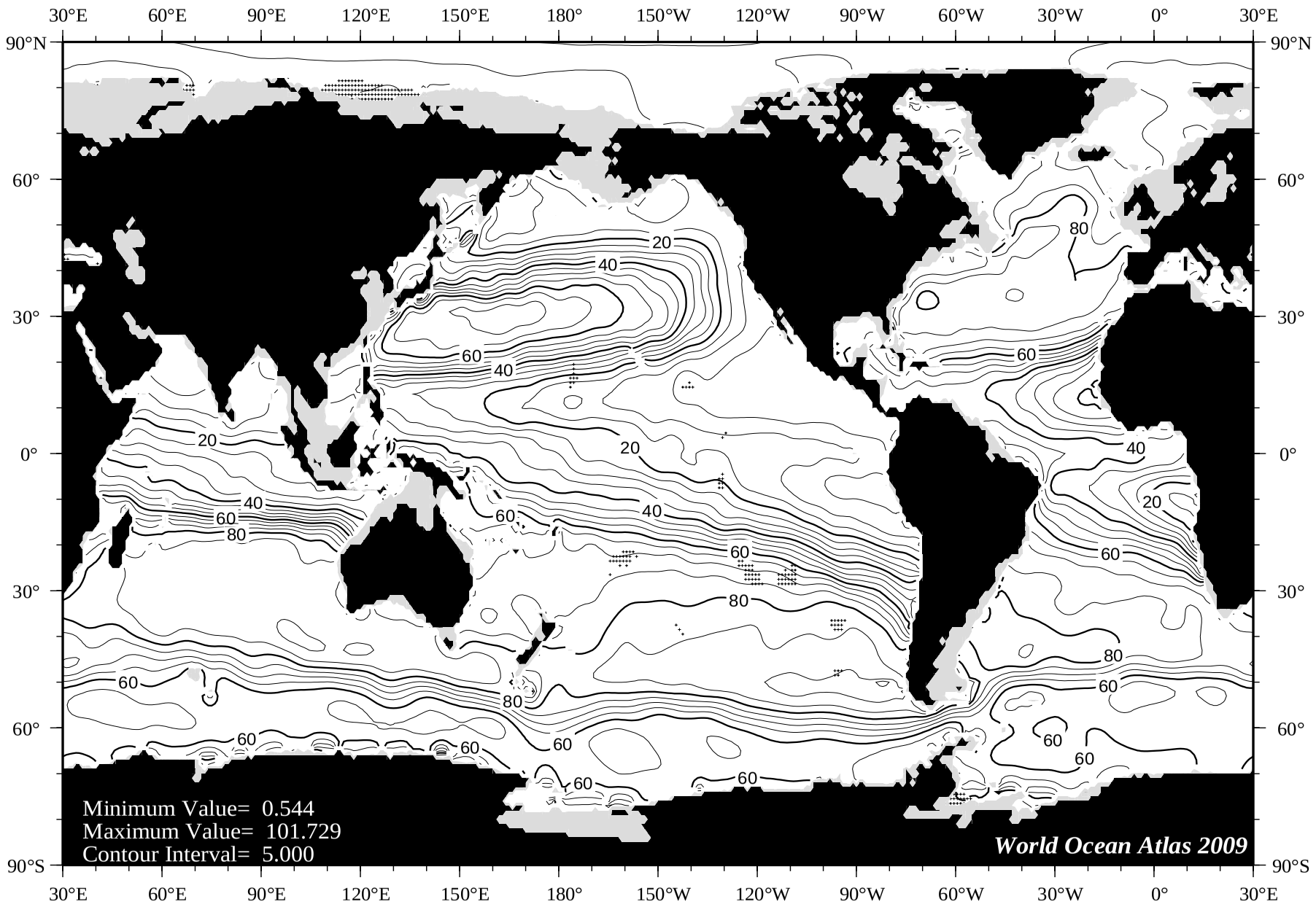

Fig G9 Annual percent oxygen saturation at 500 m. depth.

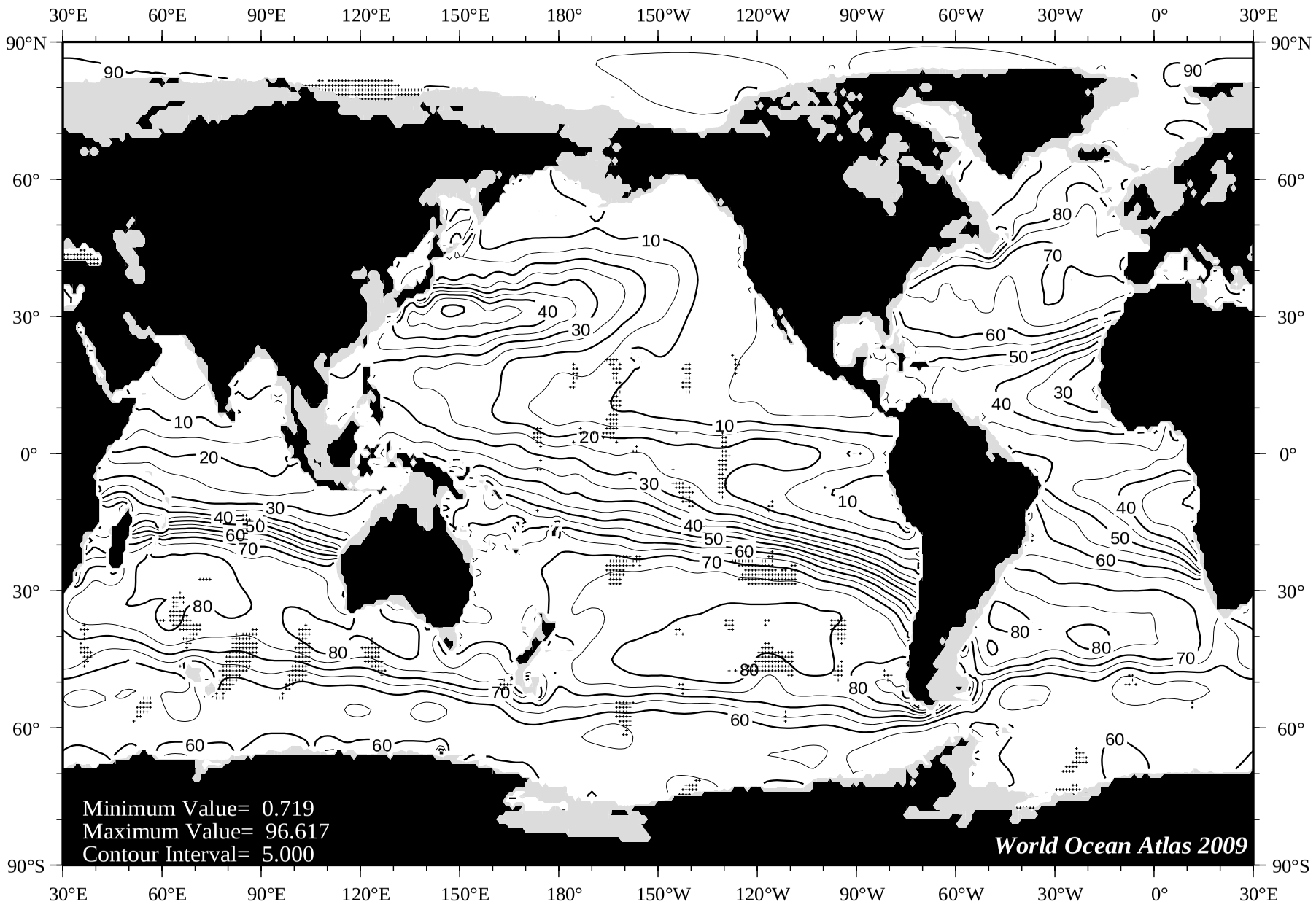

Fig G10 Annual percent oxygen saturation at 700 m. depth.

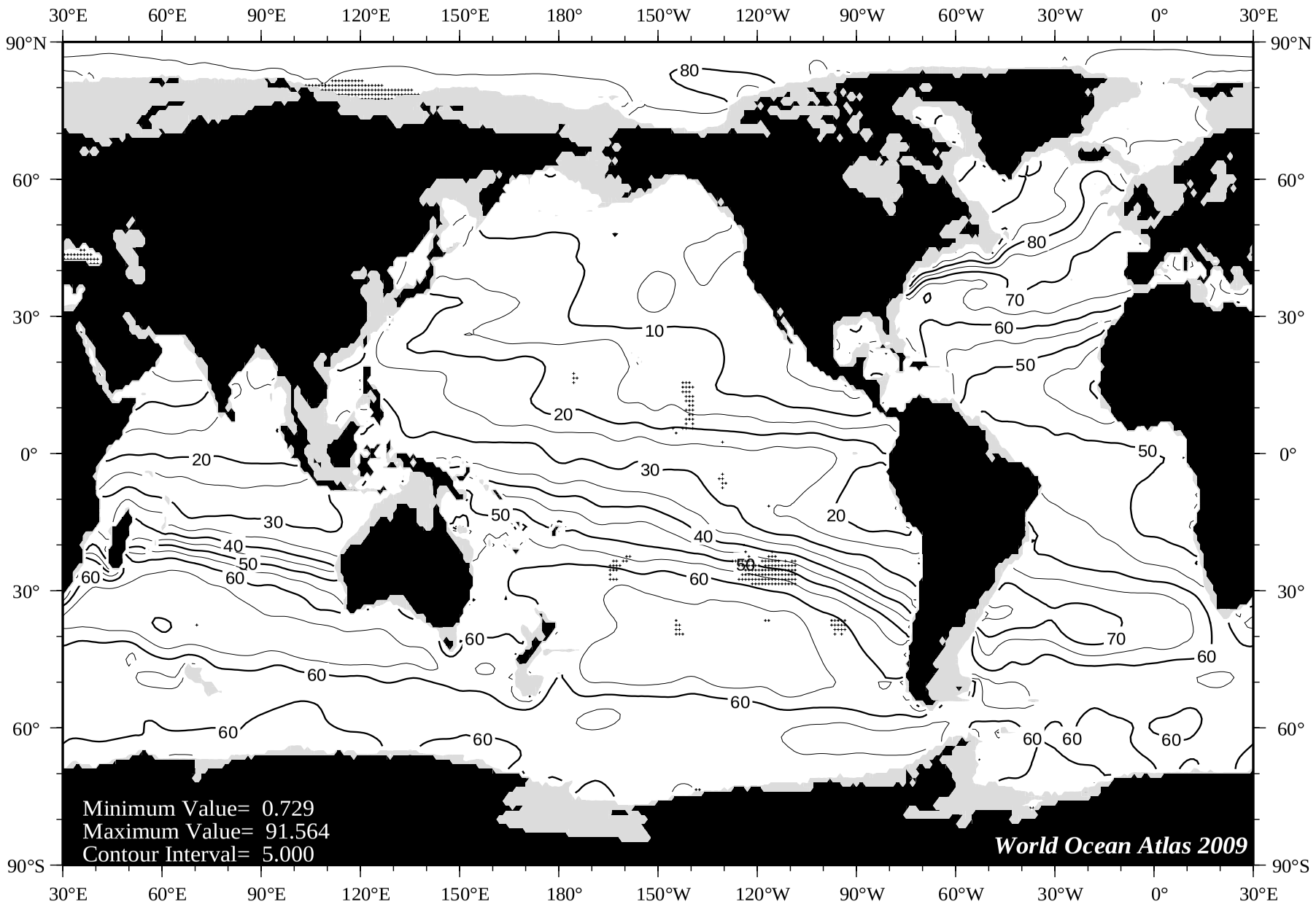

Fig G11 Annual percent oxygen saturation at 1000 m. depth.

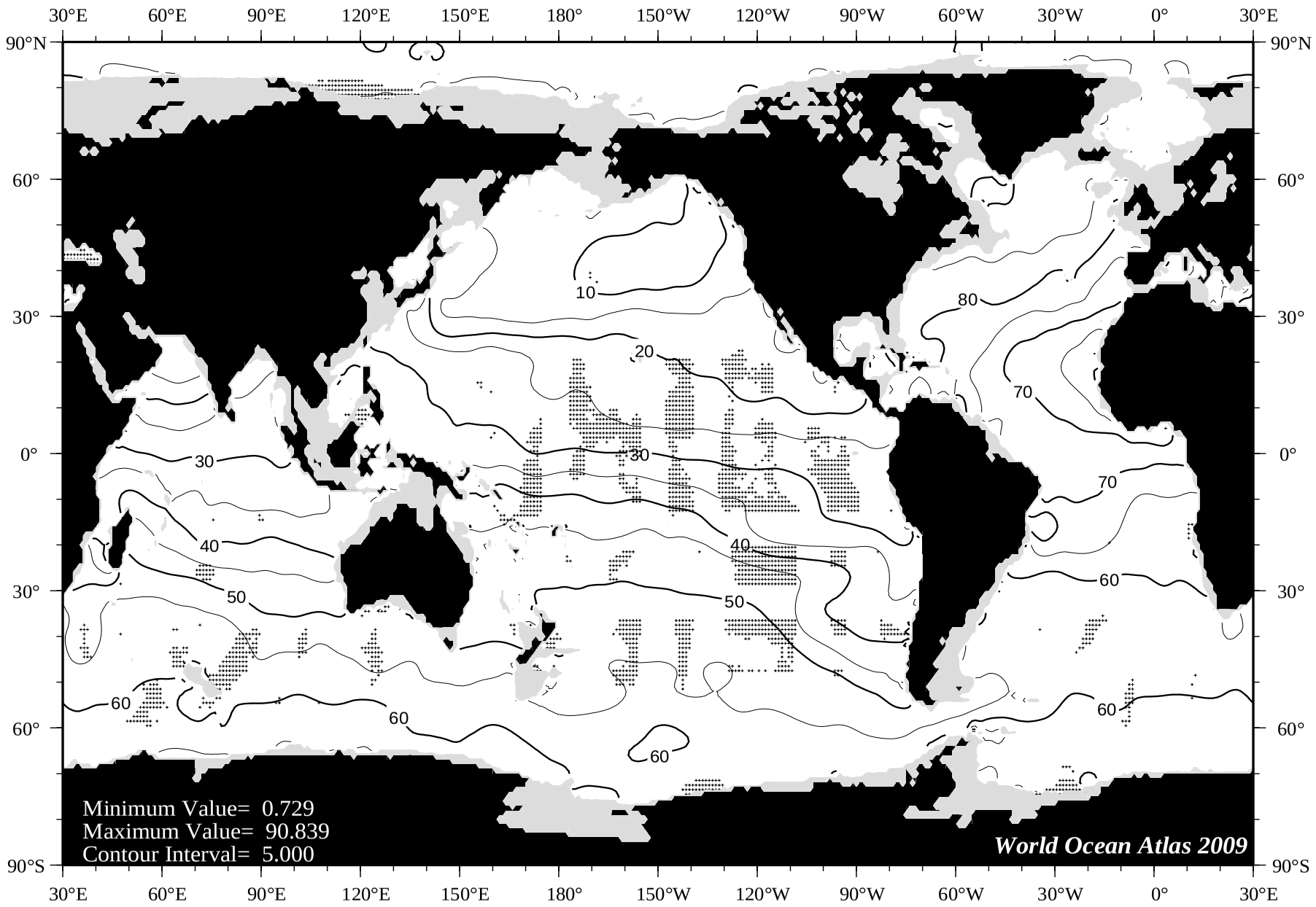

Fig G12 Annual percent oxygen saturation at 1500 m. depth.

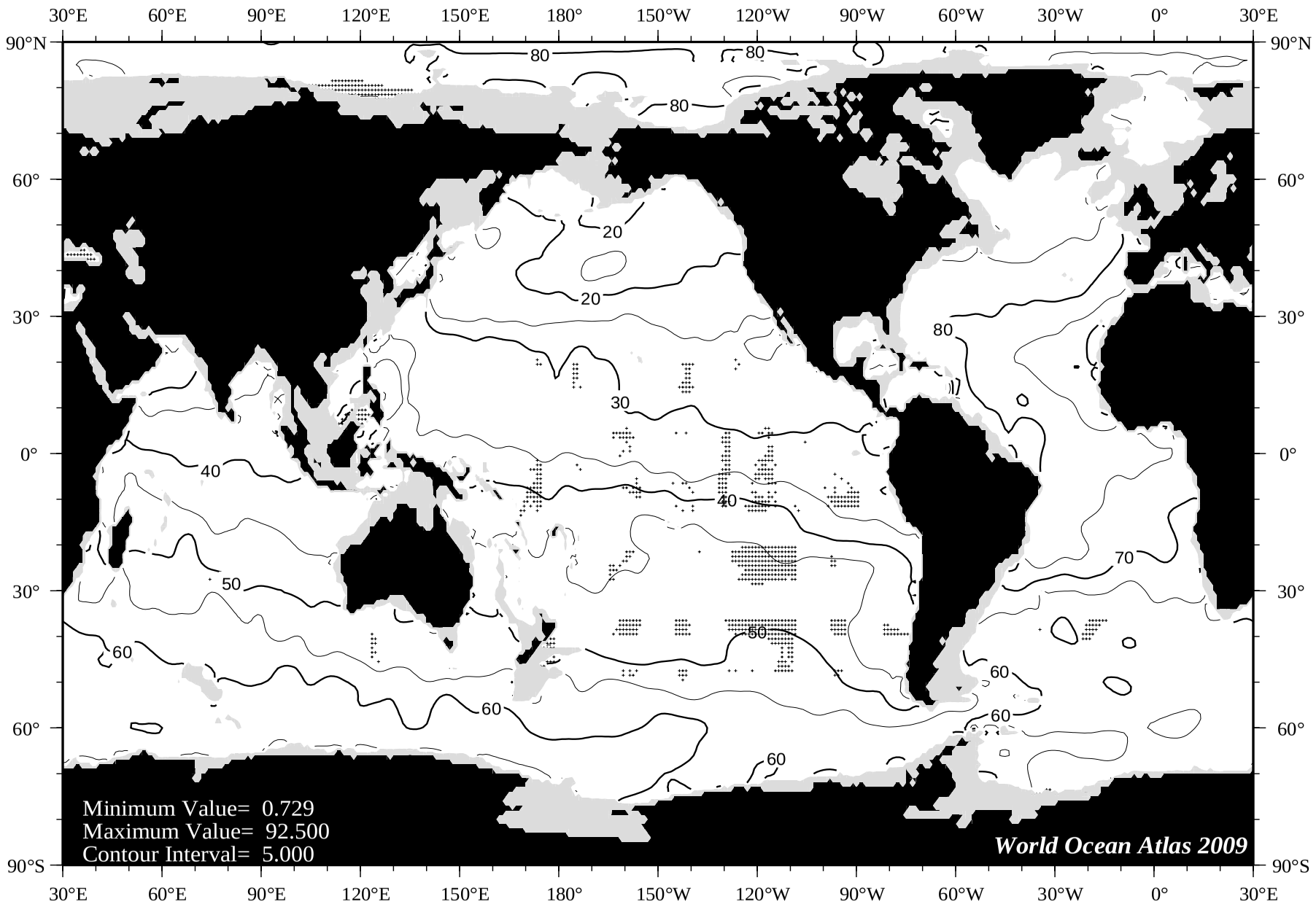

Fig G13 Annual percent oxygen saturation at 2000 m. depth.

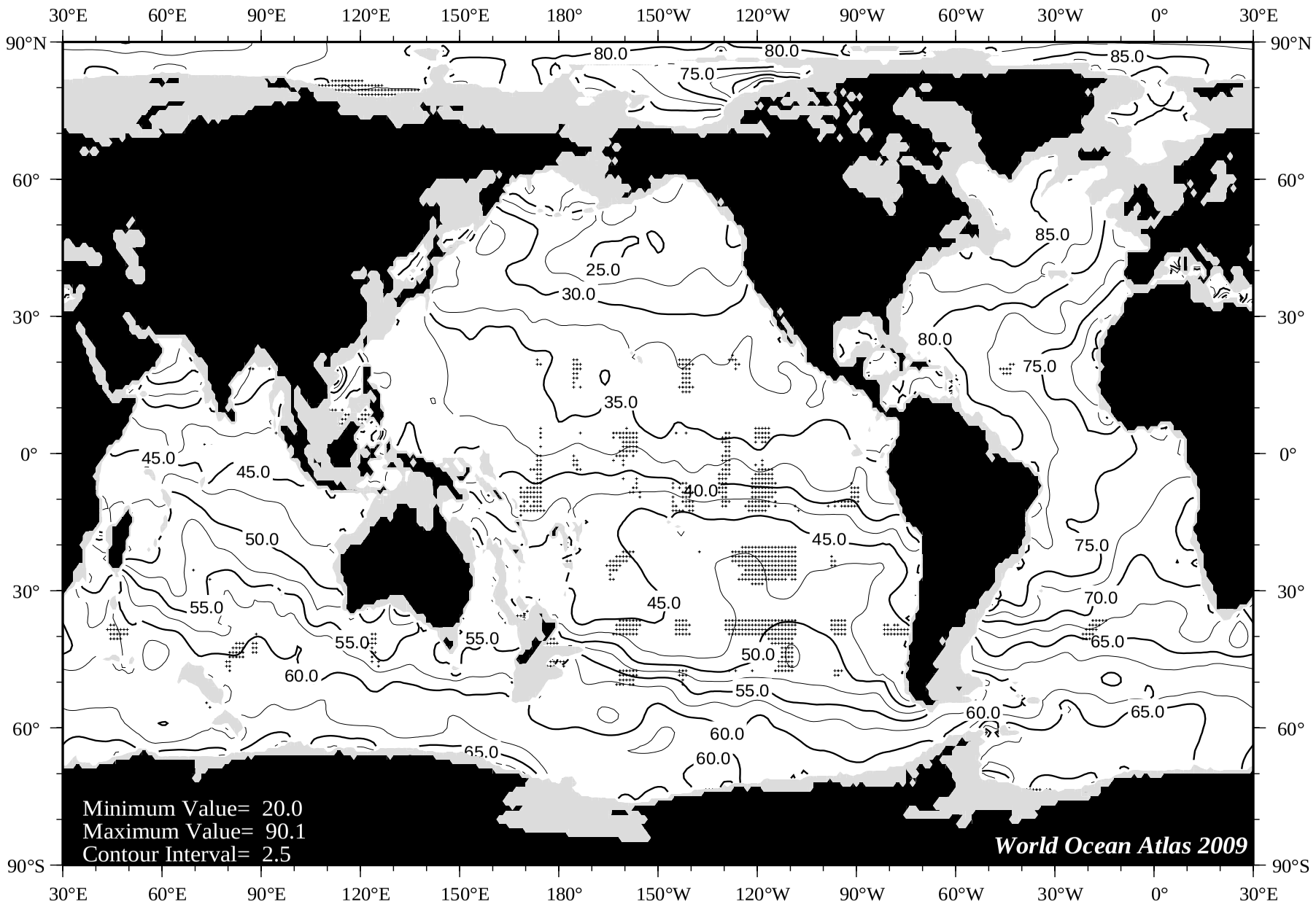

Fig G14 Annual percent oxygen saturation at 2500 m. depth.

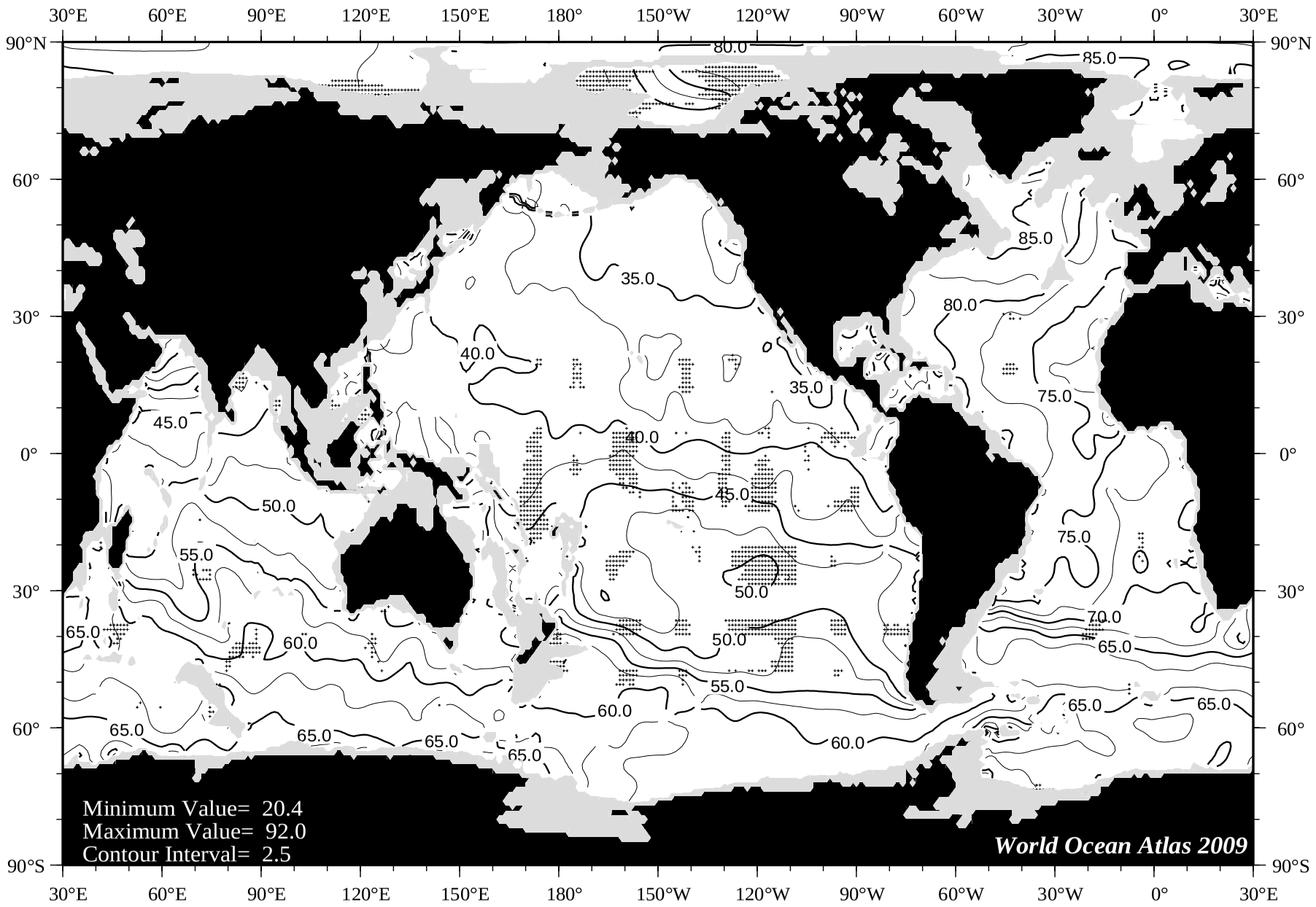

Fig G15 Annual percent oxygen saturation at 3000 m. depth.

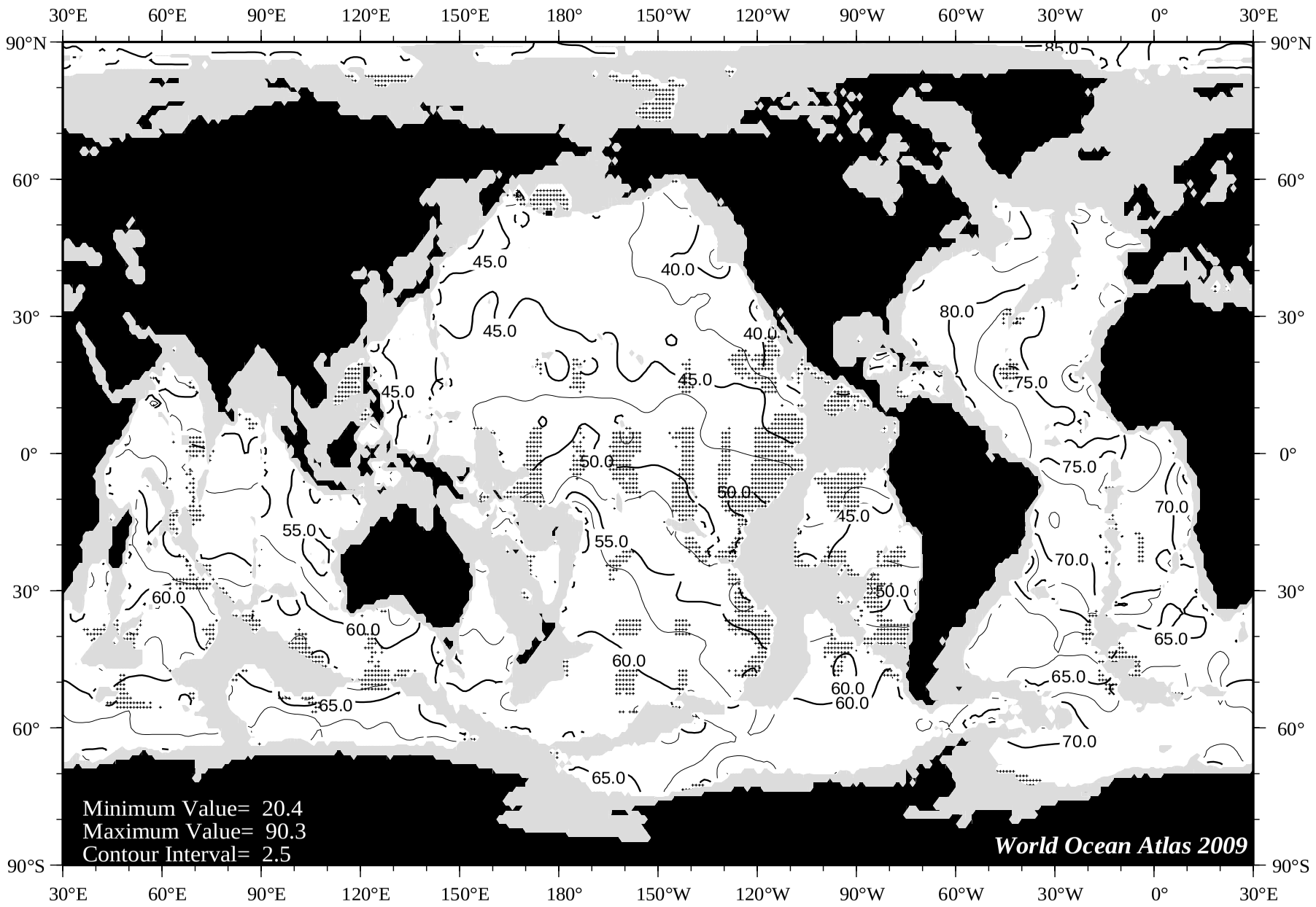

Fig G16 Annual percent oxygen saturation at 4000 m. depth.

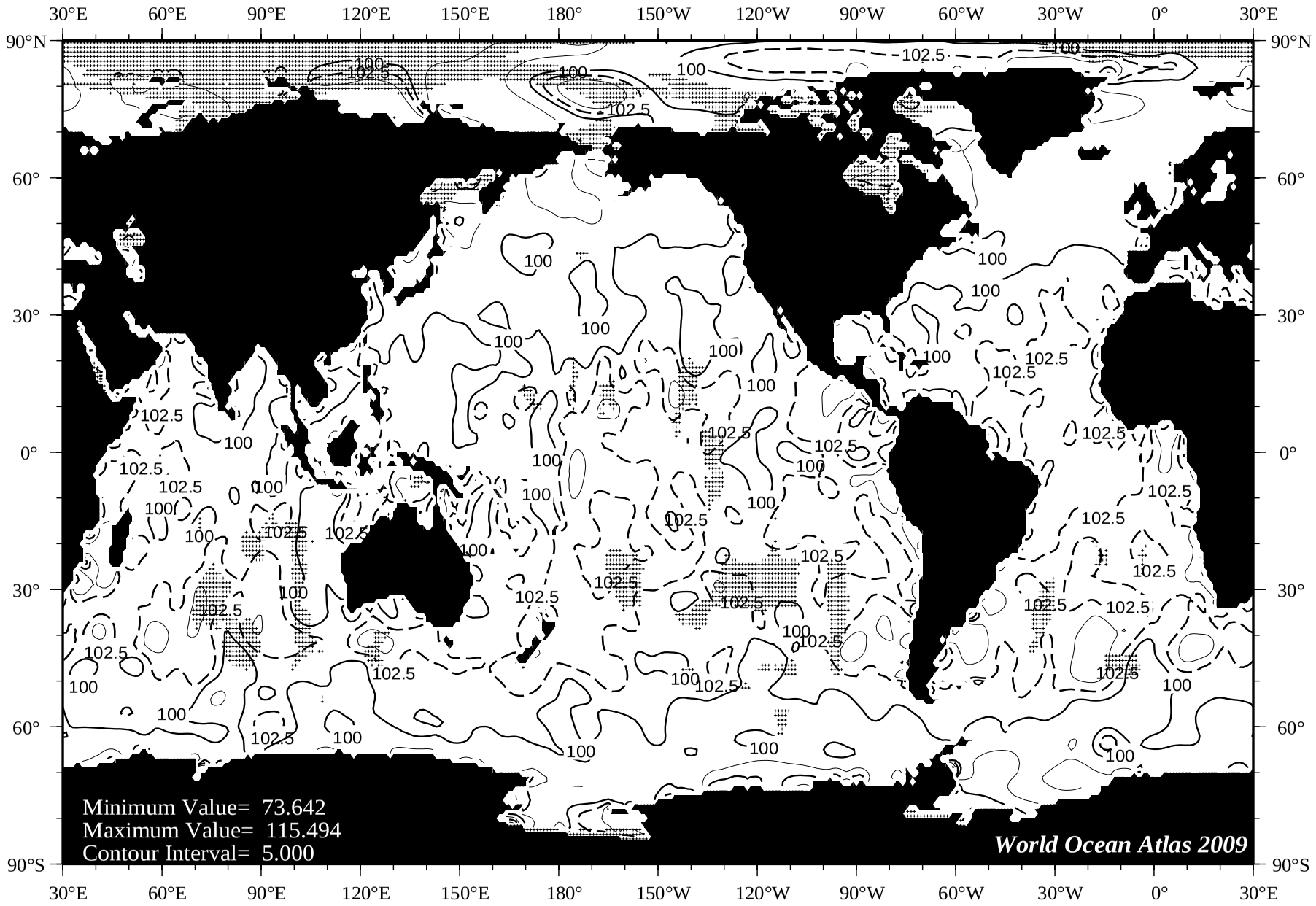

Fig H1 Winter (Jan.-Mar.) percent oxygen saturation at the surface.

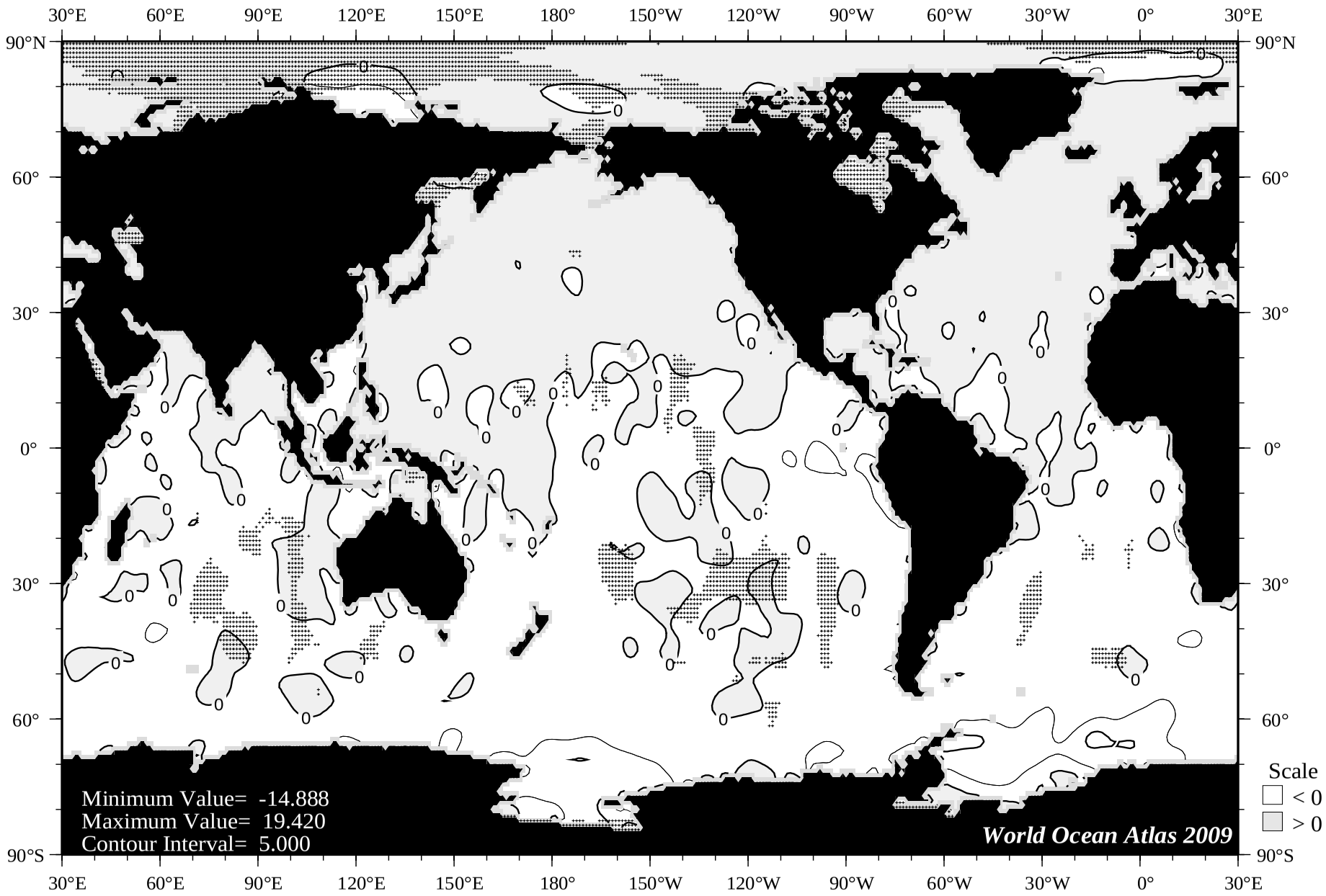

Fig H2 Winter (Jan.-Mar.) minus annual percent oxygen saturation at the surface.

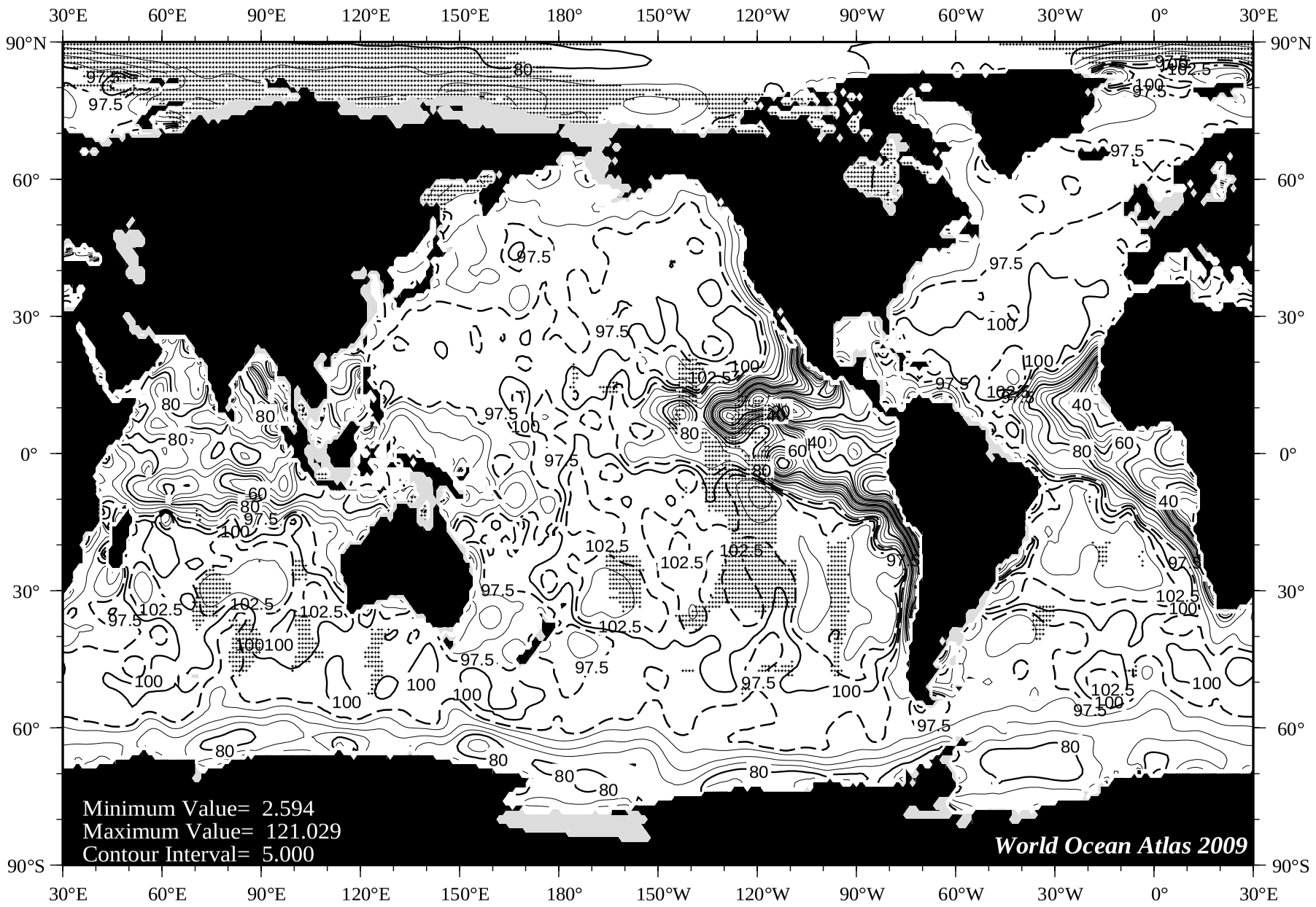

Fig H3 Winter (Jan.-Mar.) percent oxygen saturation at 75 m. depth.

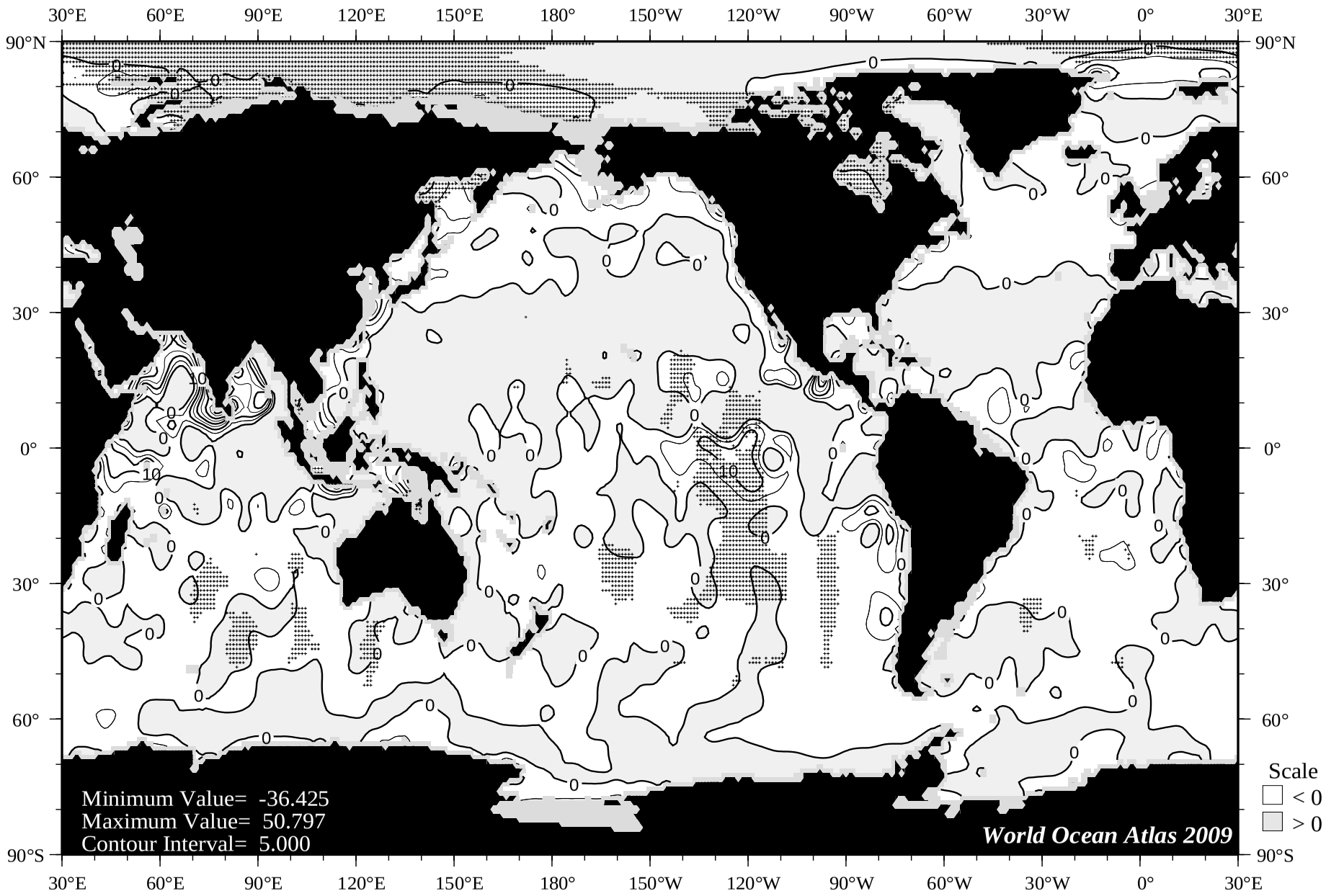

Fig H4 Winter (Jan.-Mar.) minus annual percent oxygen saturation at 75 m. depth.

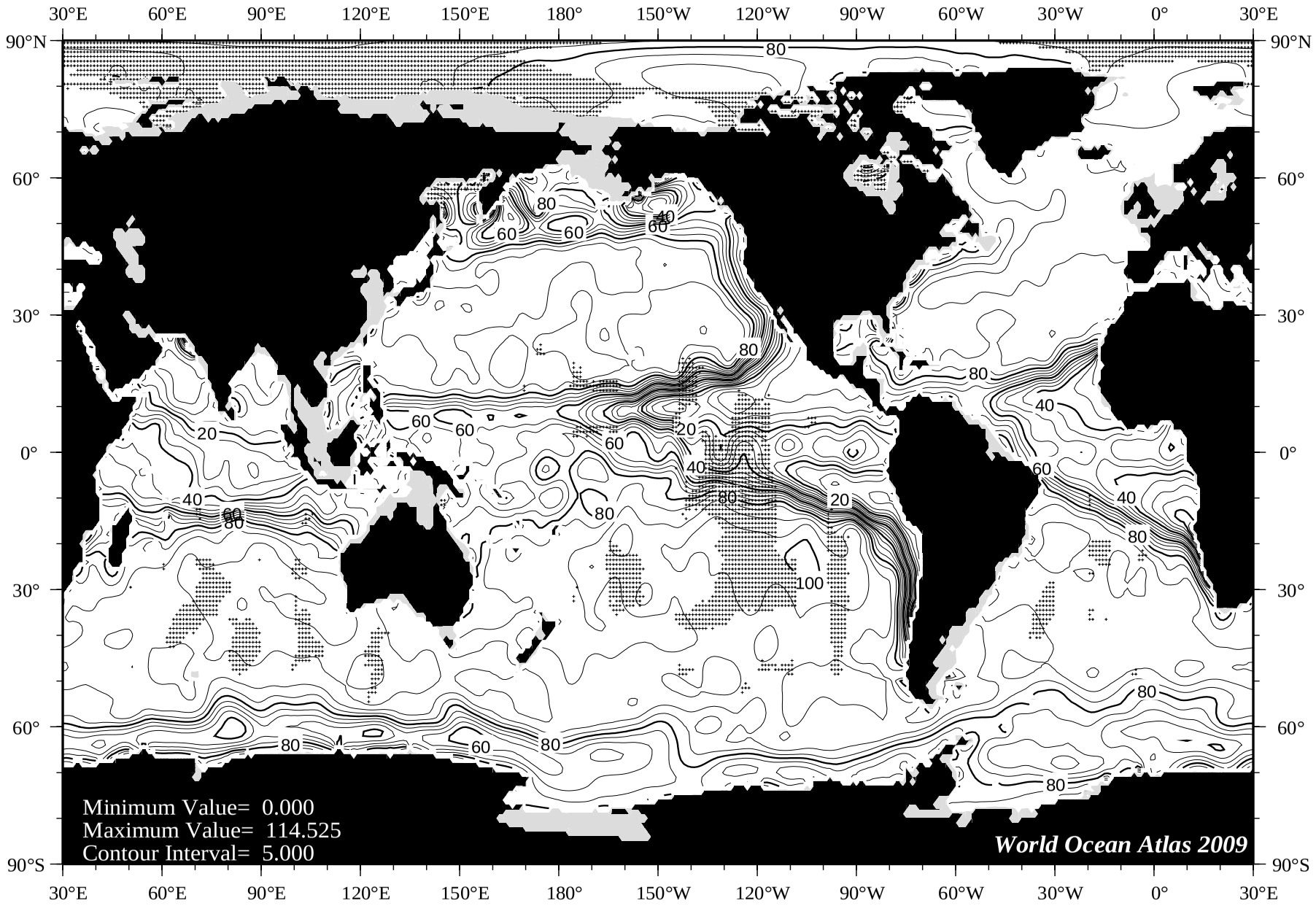

Fig H5 Winter (Jan.-Mar.) percent oxygen saturation at 150 m. depth.

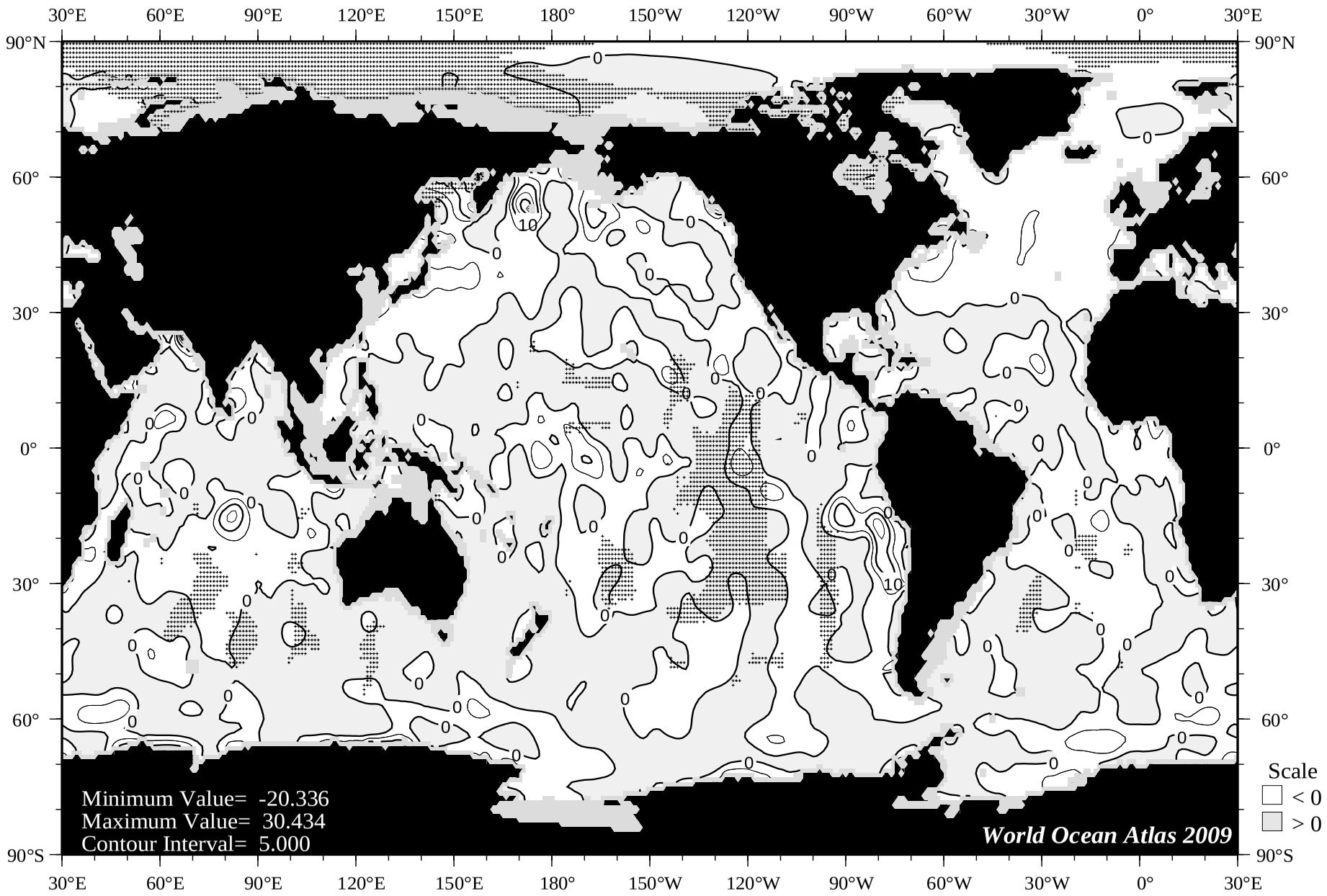

Fig H6 Winter (Jan.-Mar.) minus annual percent oxygen saturation at 150 m. depth.

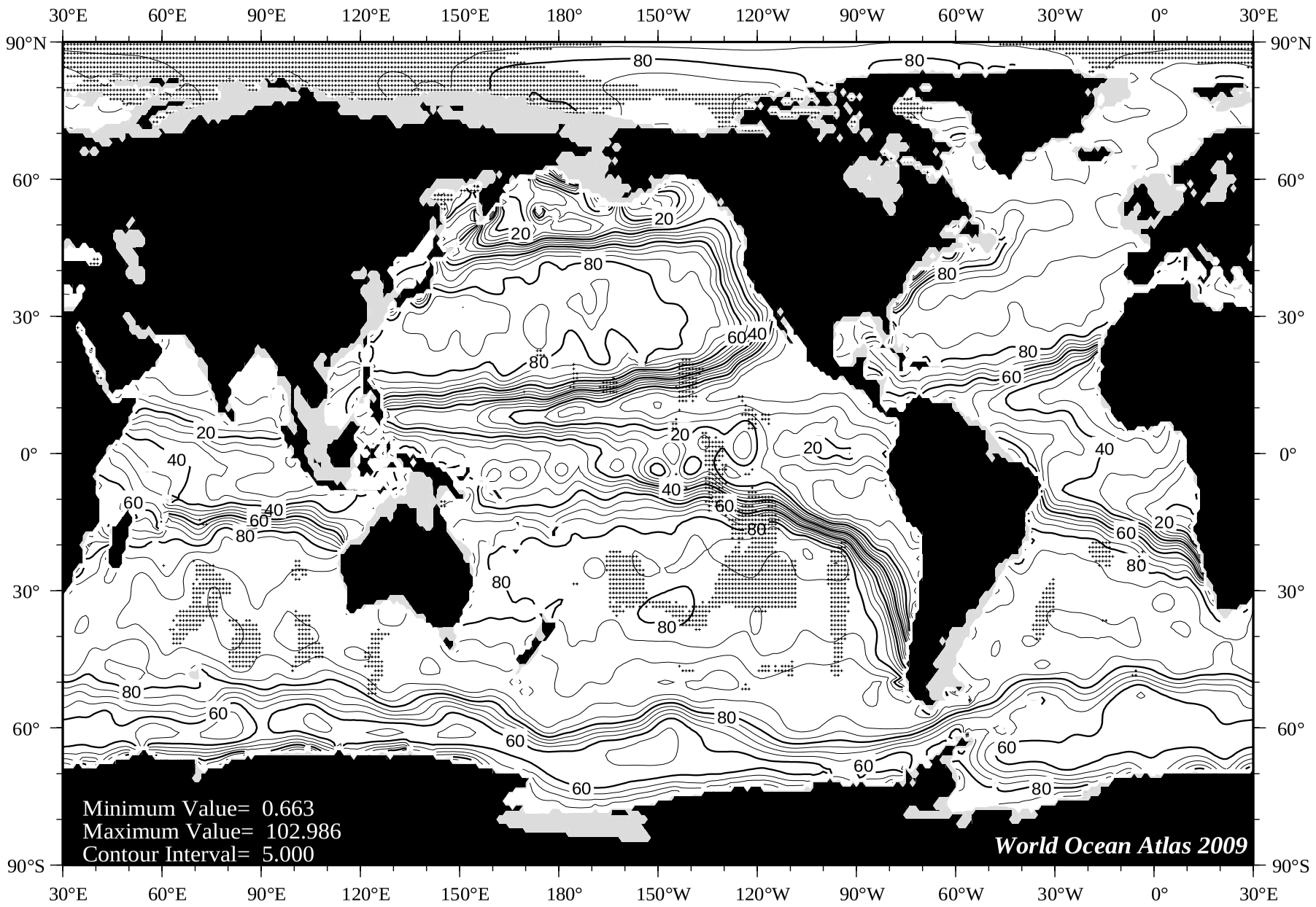

Fig H7 Winter (Jan.-Mar.) percent oxygen saturation at 250 m. depth.

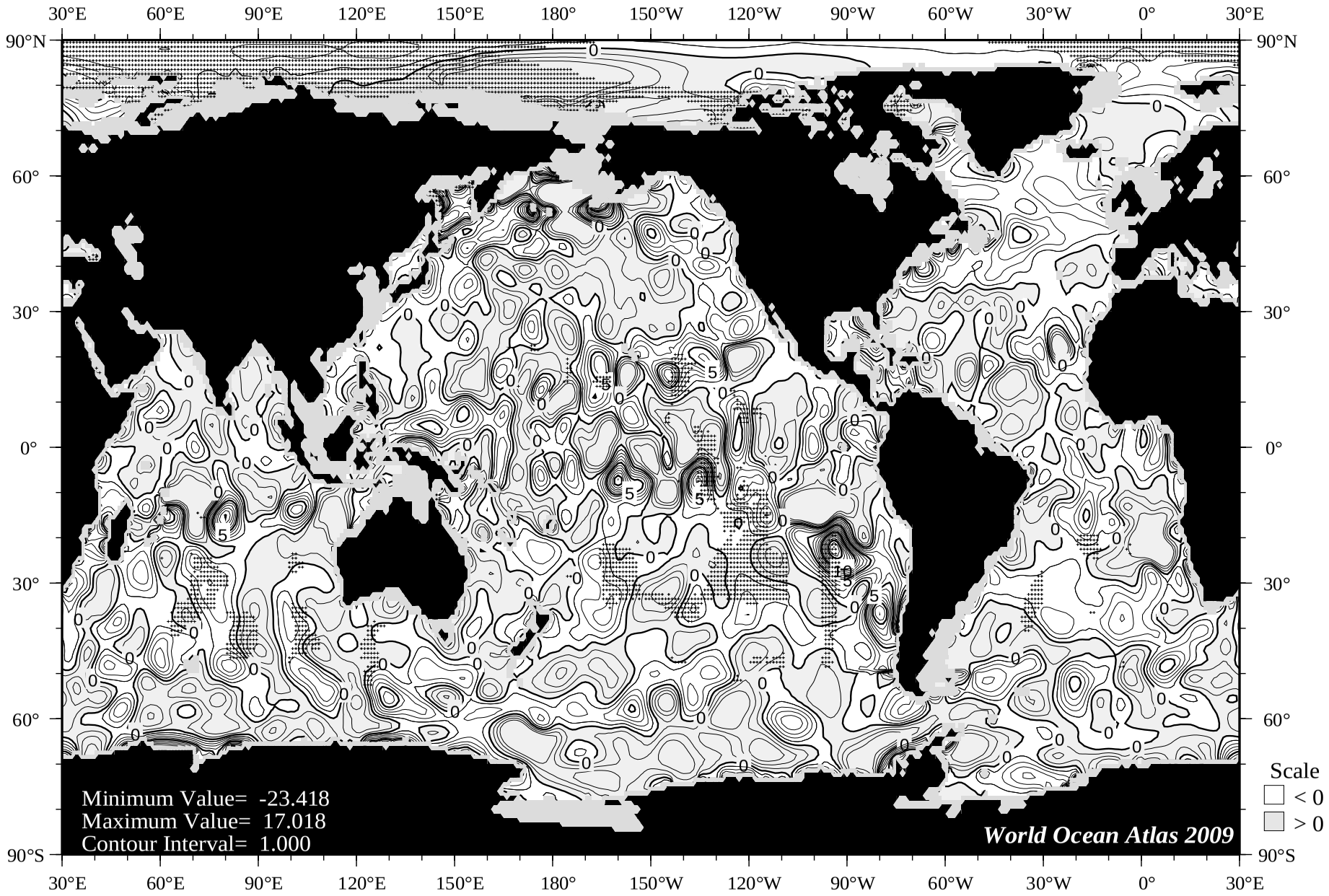

Fig H8 Winter (Jan.-Mar.) minus annual percent oxygen saturation at 250 m. depth.

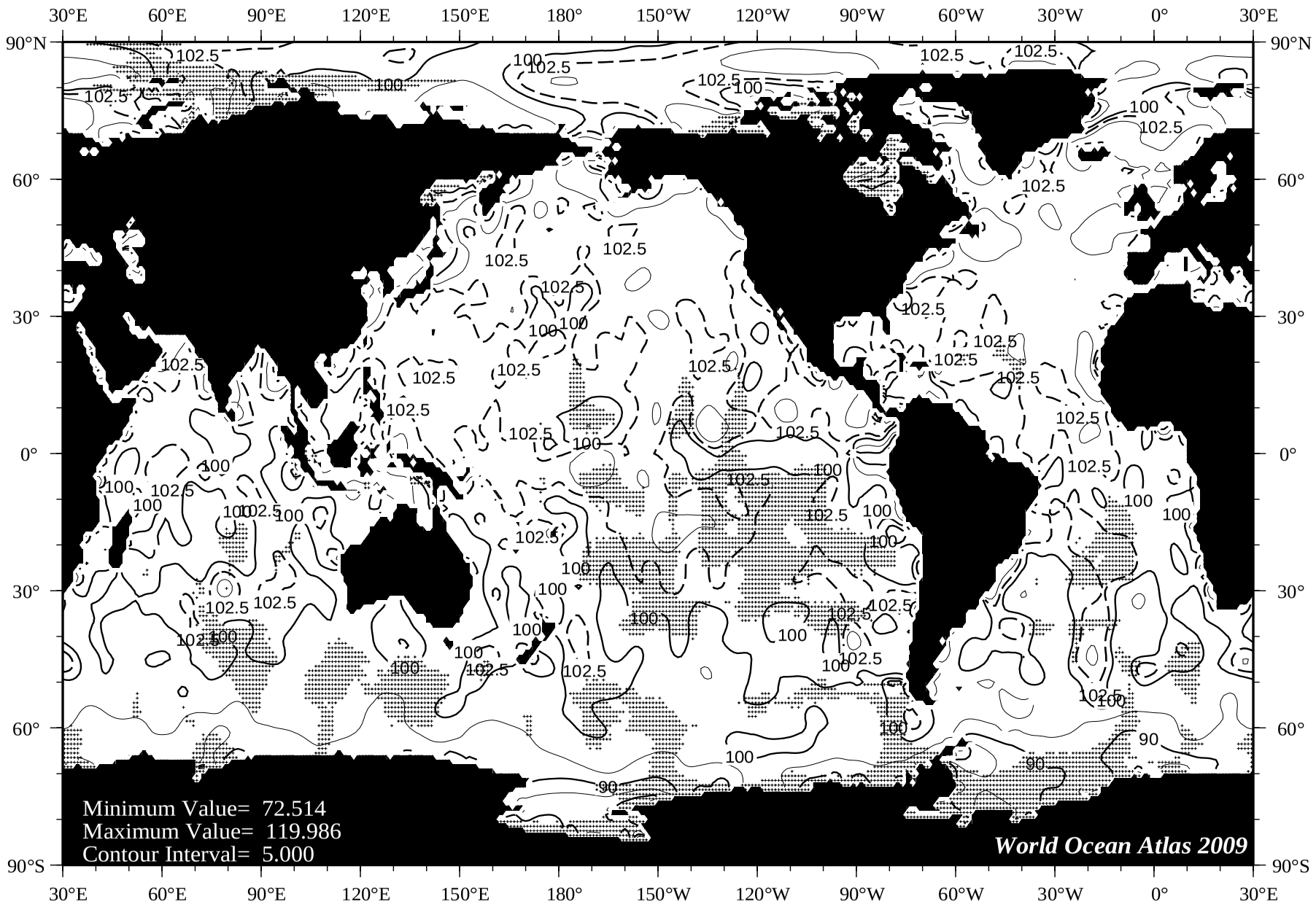

Fig H9 Spring (Apr.-Jun.) percent oxygen saturation at the surface.

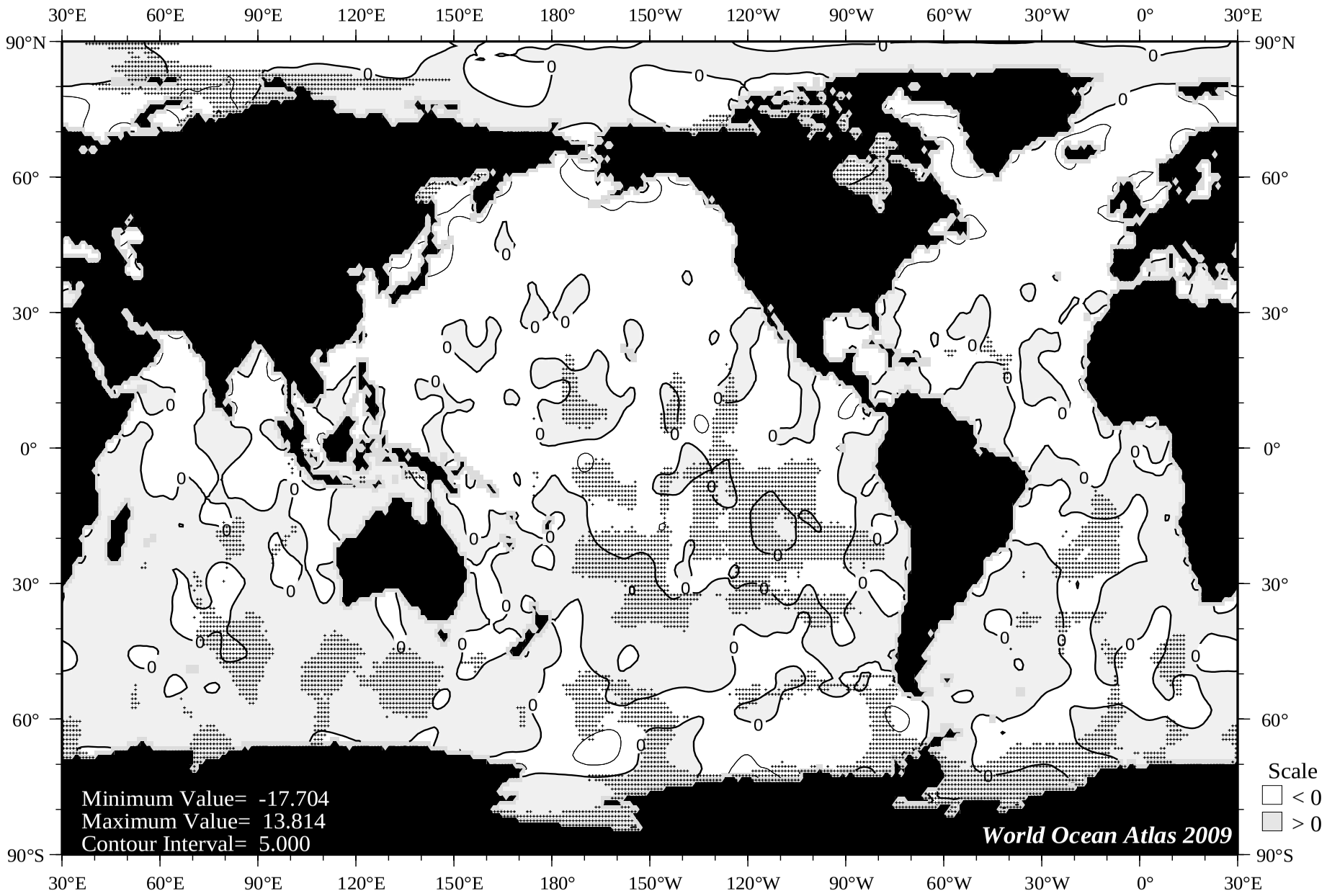

Fig H10 Spring (Apr.-Jun.) minus annual percent oxygen saturation at the surface.

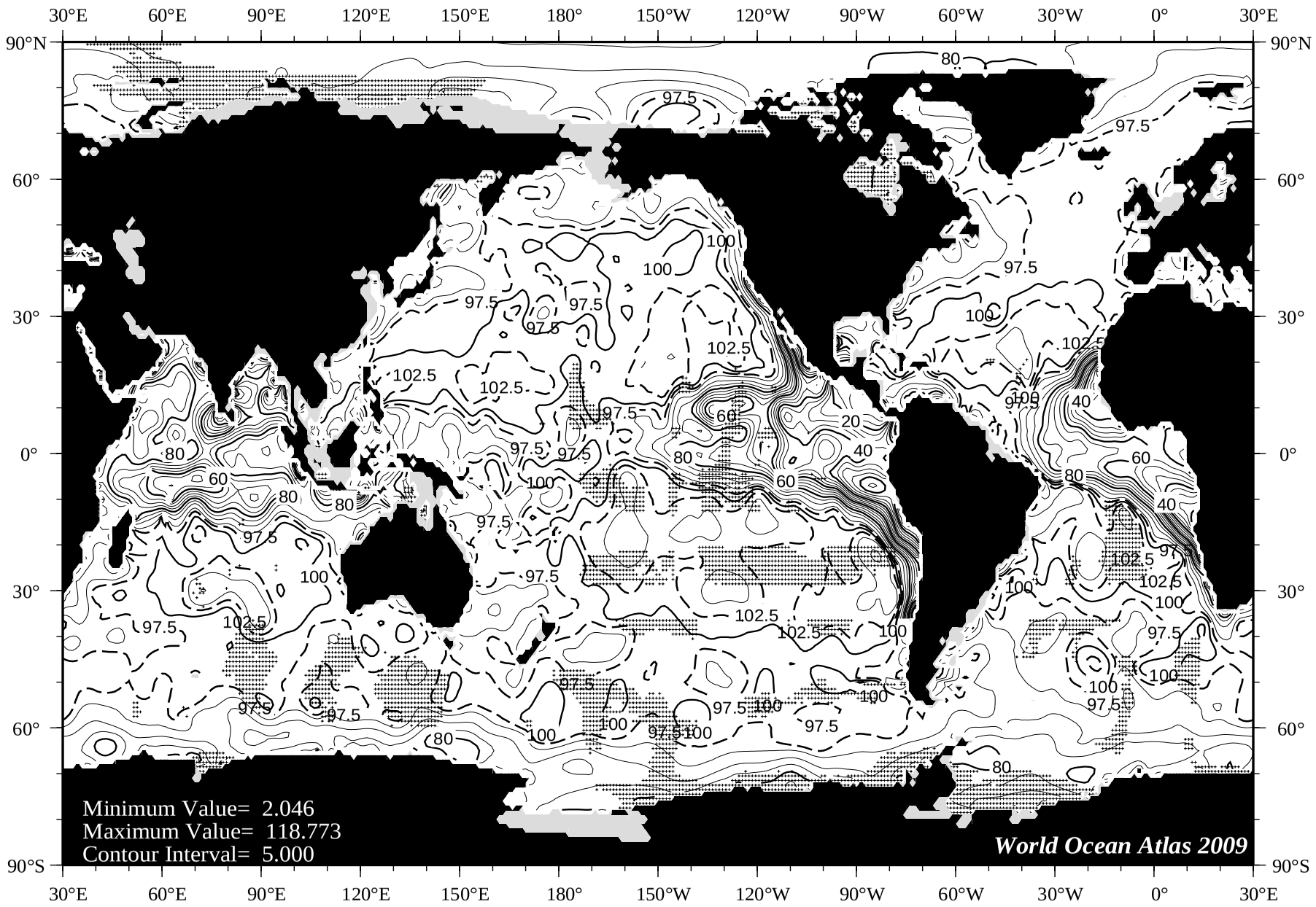

Fig H11 Spring (Apr.-Jun.) percent oxygen saturation at 75 m. depth.

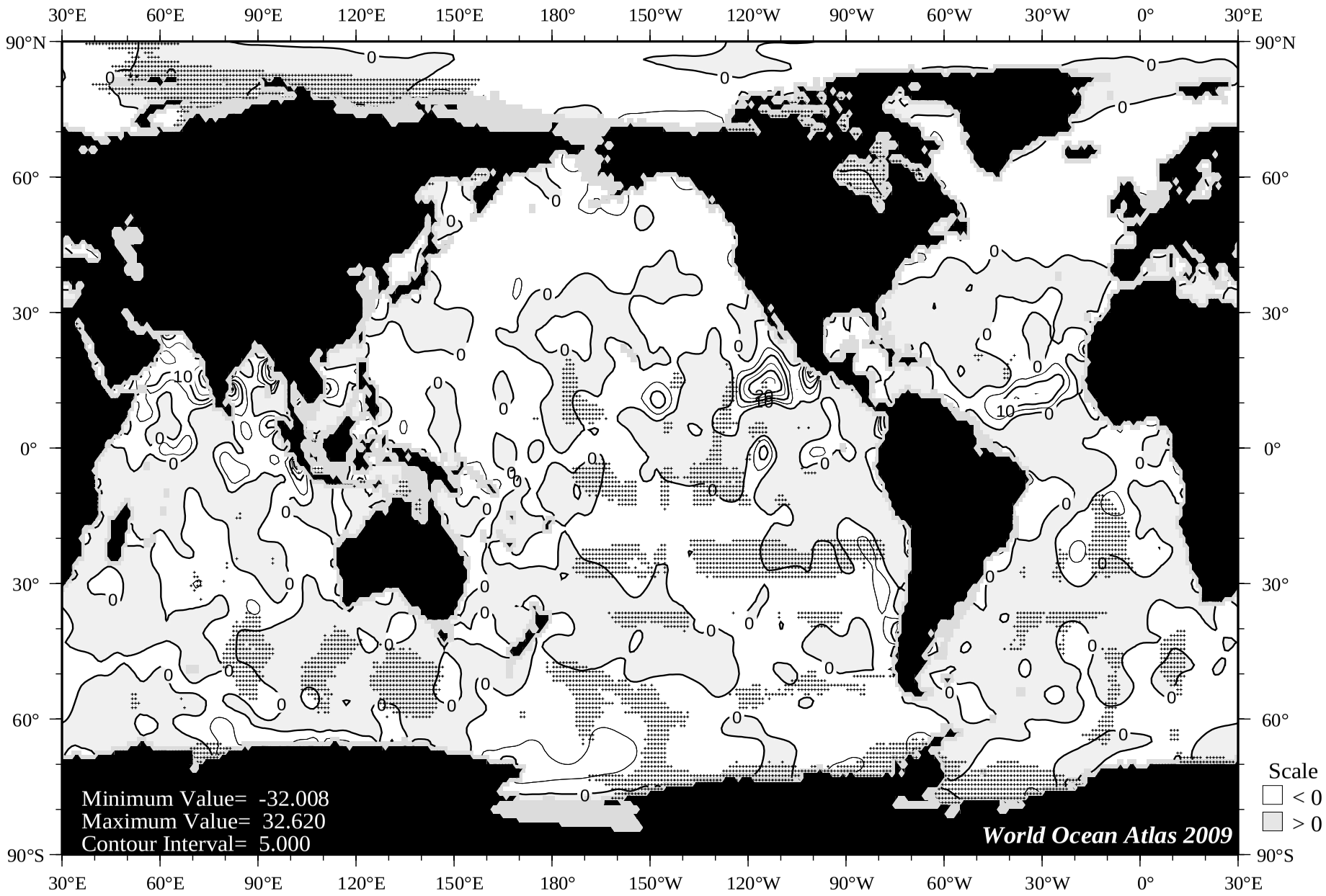

Fig H12 Spring (Apr.-Jun.) minus annual percent oxygen saturation at 75 m. depth.

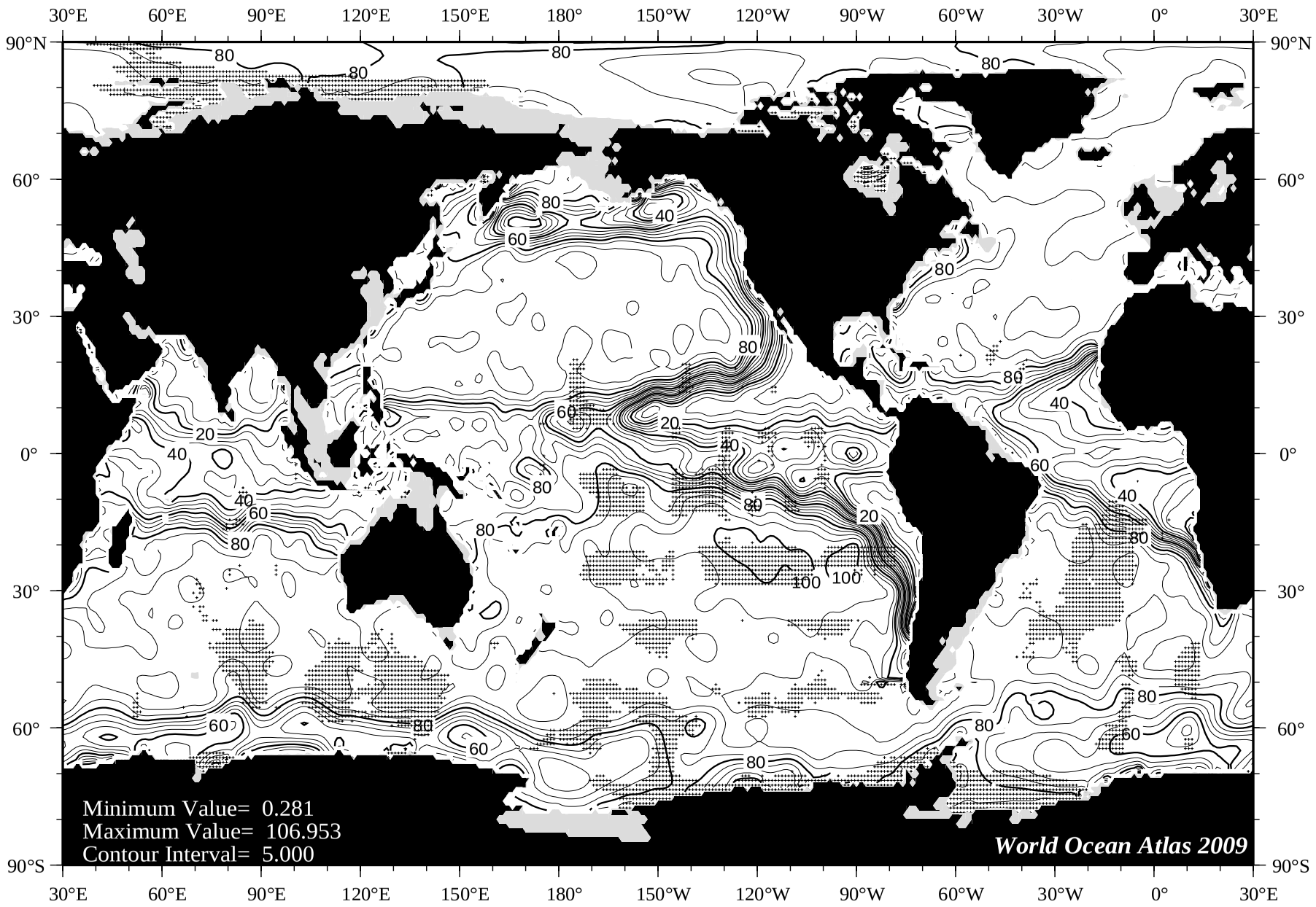

Fig H13 Spring (Apr.-Jun.) percent oxygen saturation at 150 m. depth.

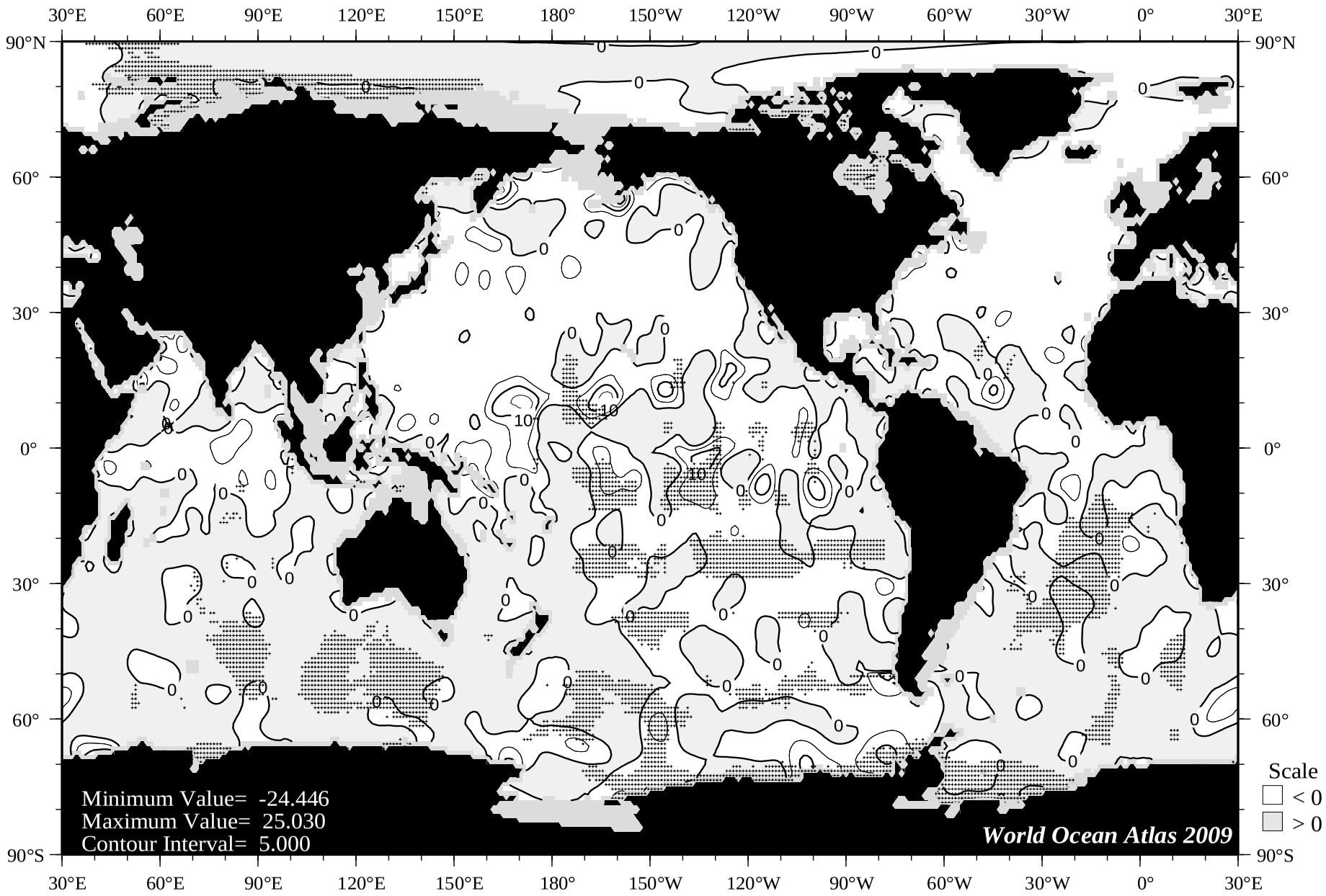

Fig H14 Spring (Apr.-Jun.) minus annual percent oxygen saturation at 150 m. depth.

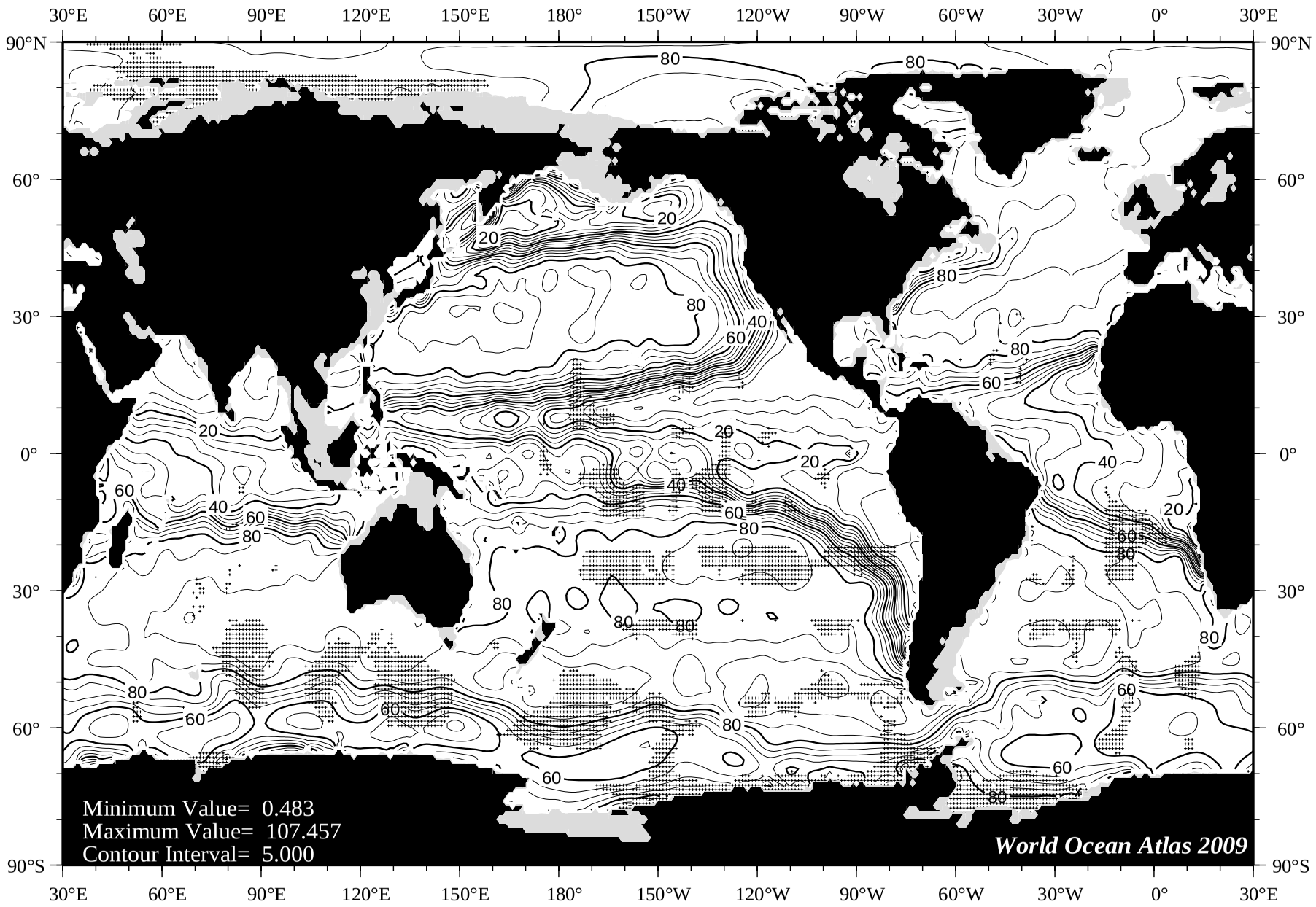

Fig H15 Spring (Apr.-Jun.) percent oxygen saturation at 250 m. depth.

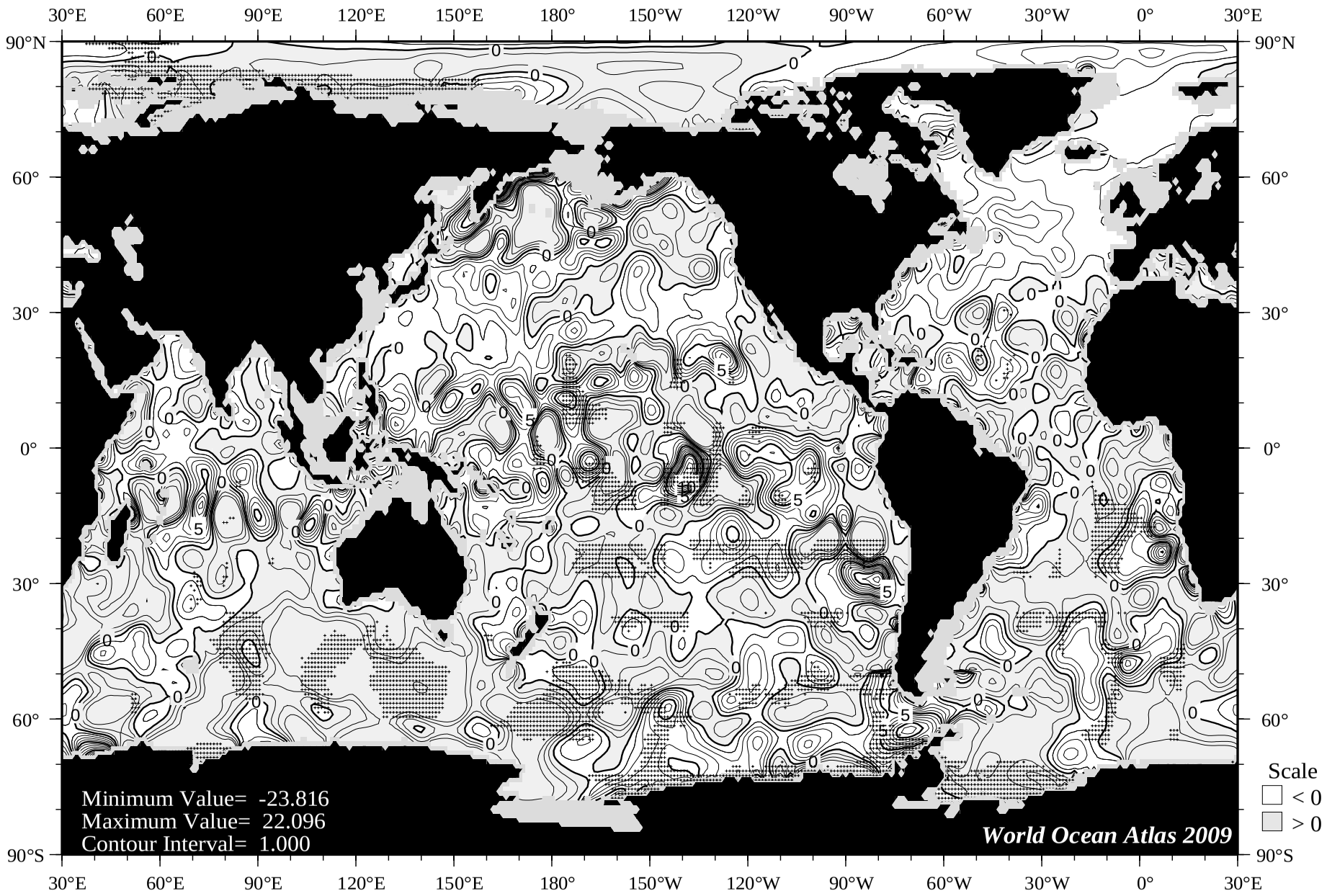

Fig H16 Spring (Apr.-Jun.) minus annual percent oxygen saturation at 250 m. depth.

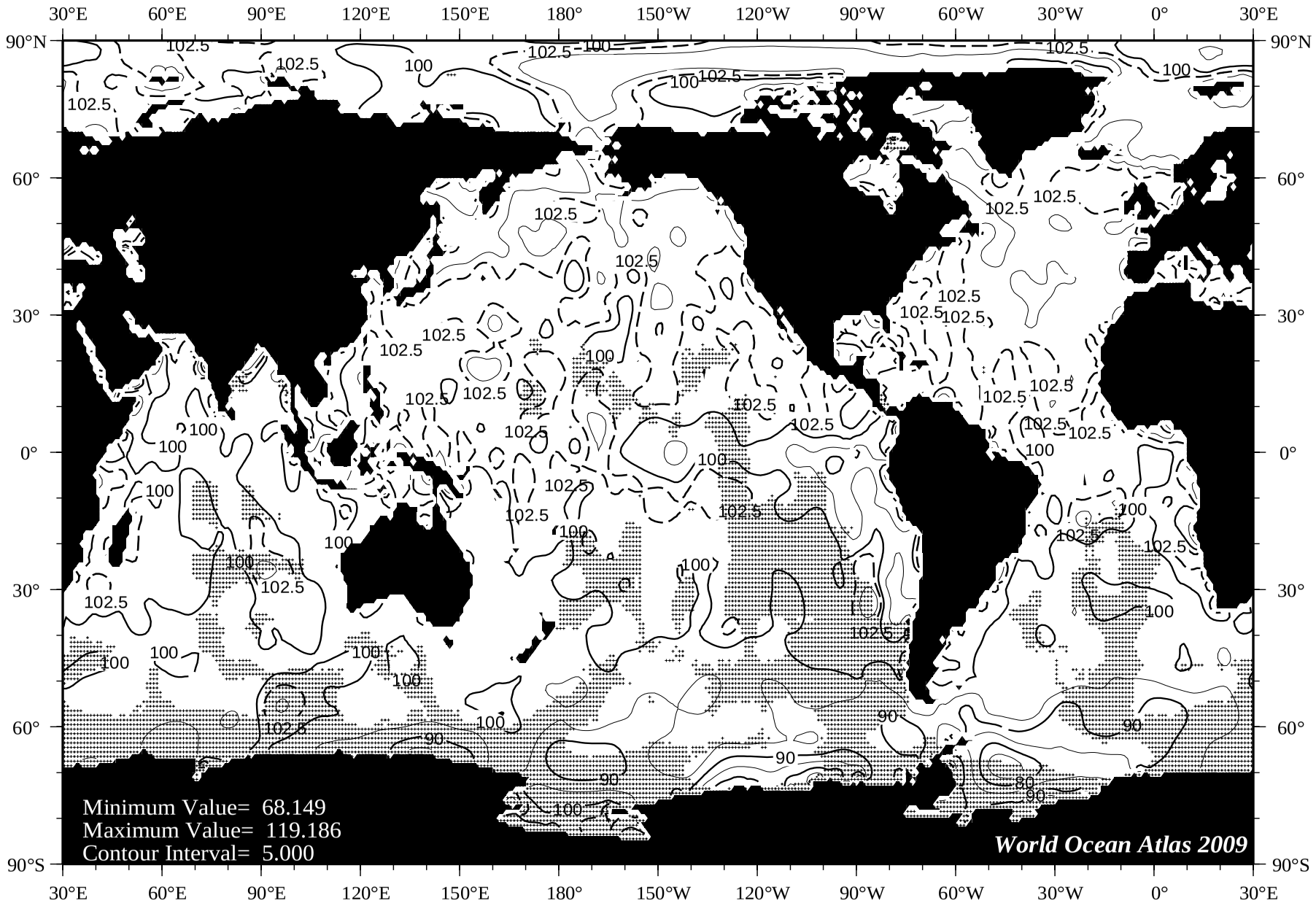

Fig H17 Summer (Jul.-Sep.) percent oxygen saturation at the surface.

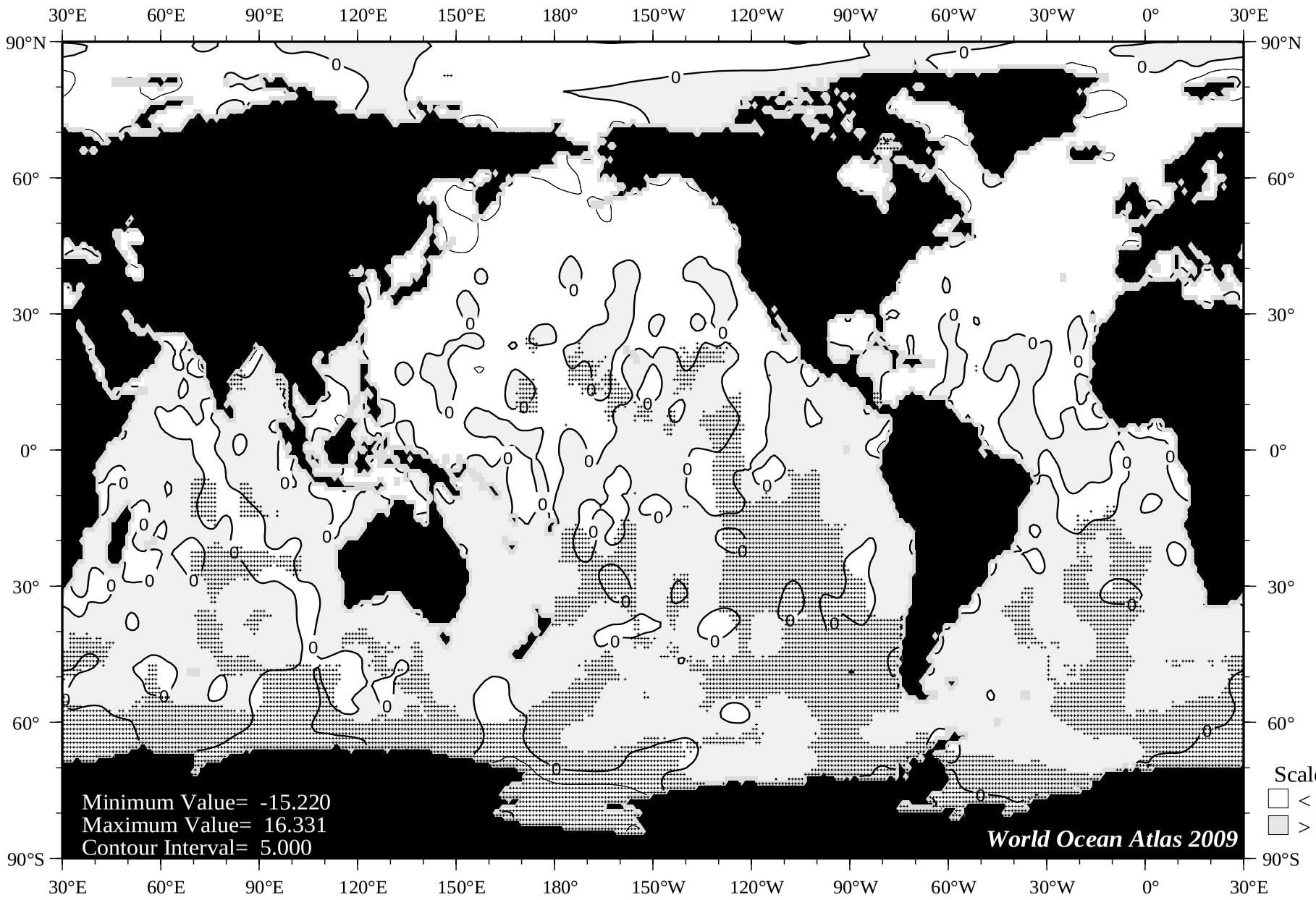

Fig H18 Summer (Jul.-Sep.) minus annual percent oxygen saturation at the surface.

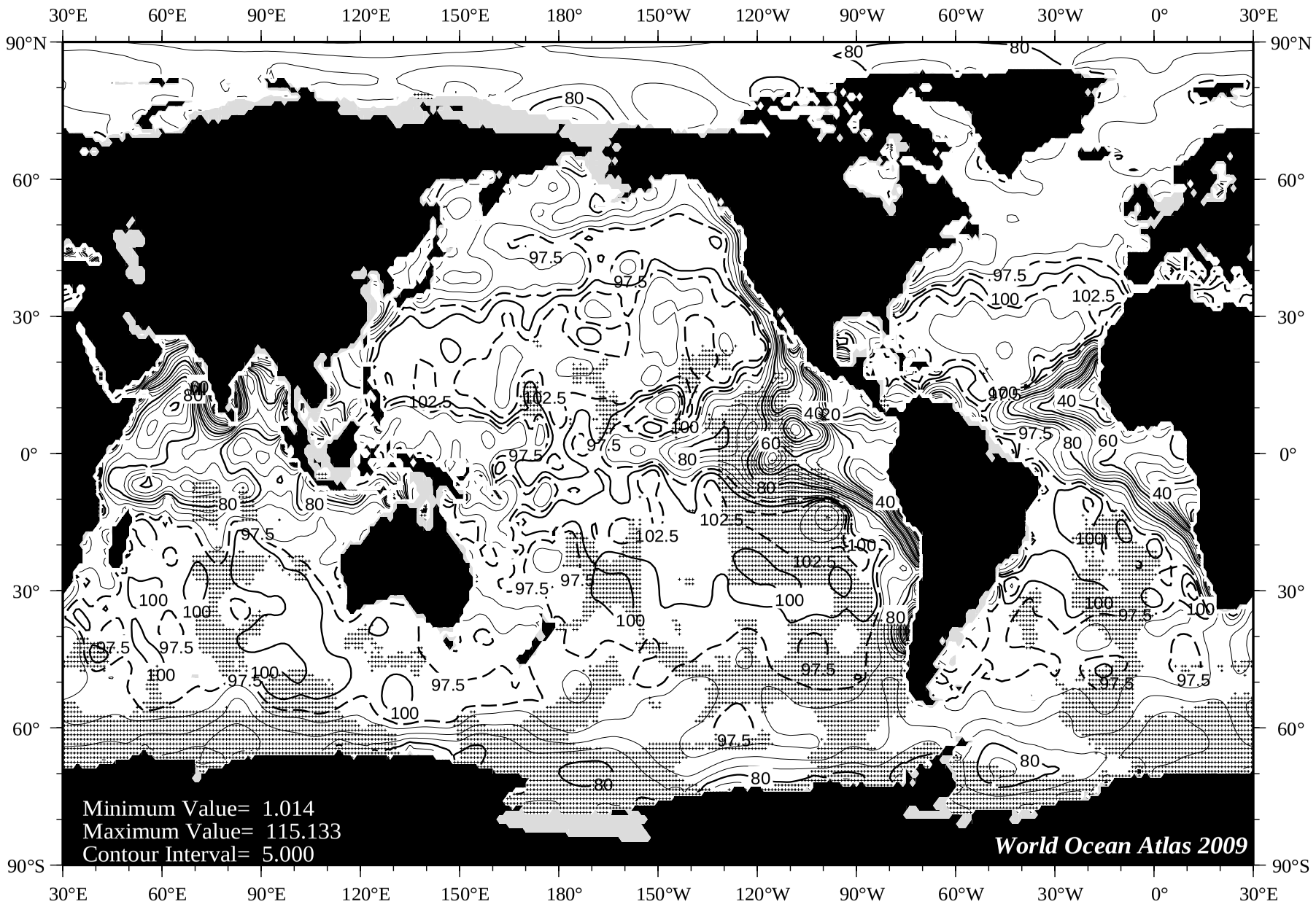

Fig H19 Summer (Jul.-Sep.) percent oxygen saturation at 75 m. depth.

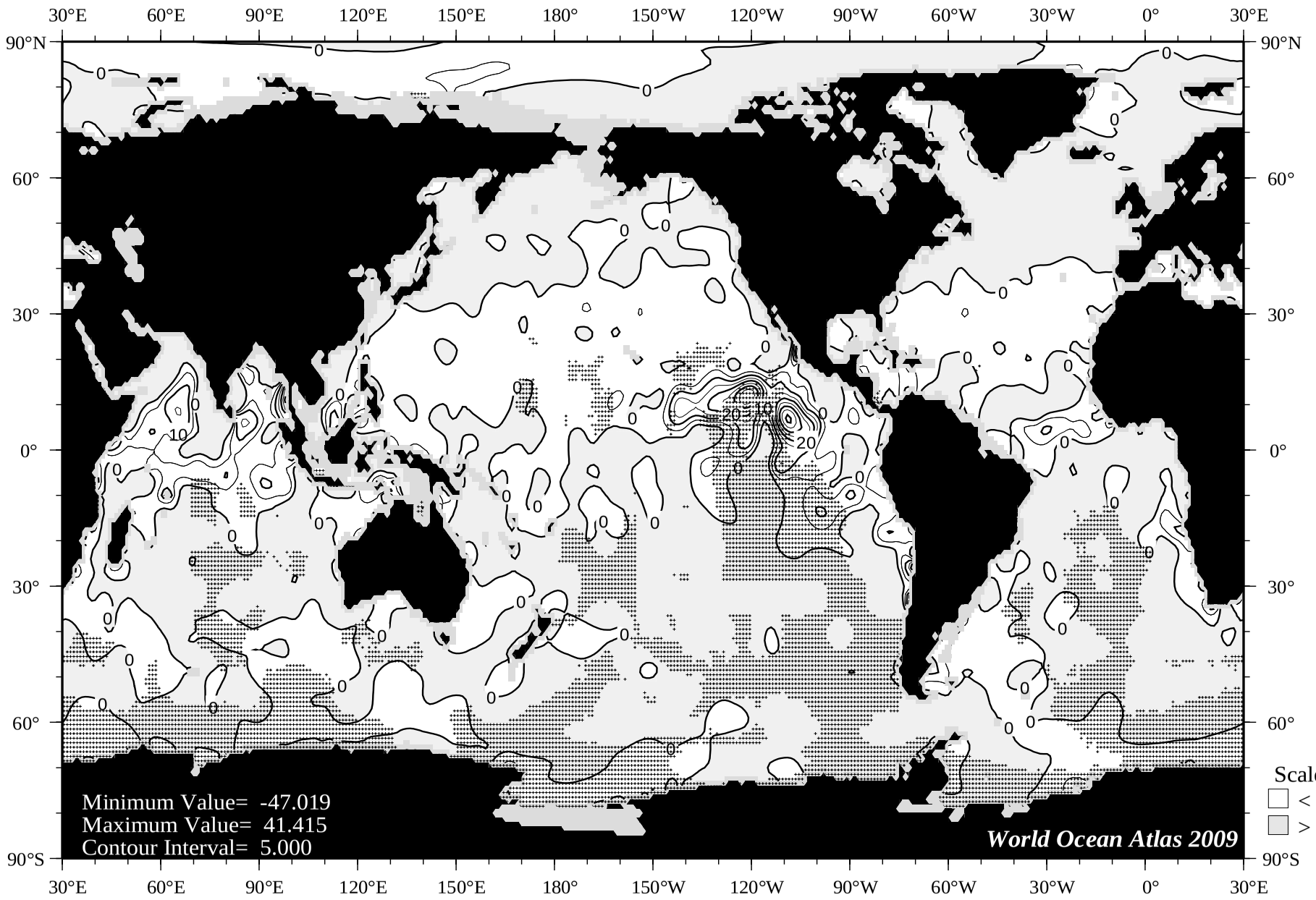

Fig H20 Summer (Jul.-Sep.) minus annual percent oxygen saturation at 75 m. depth.

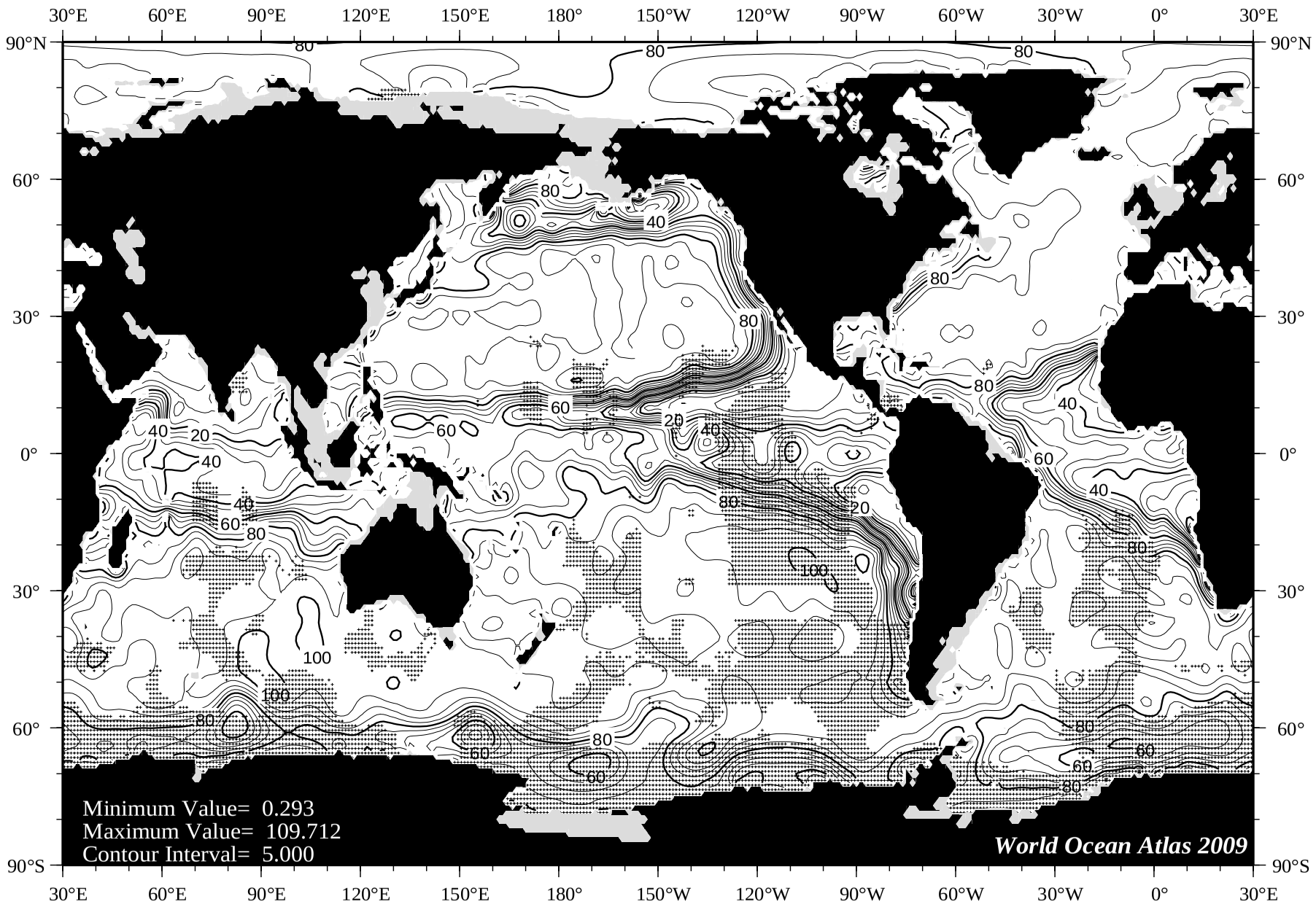

Fig H21 Summer (Jul.-Sep.) percent oxygen saturation at 150 m. depth.

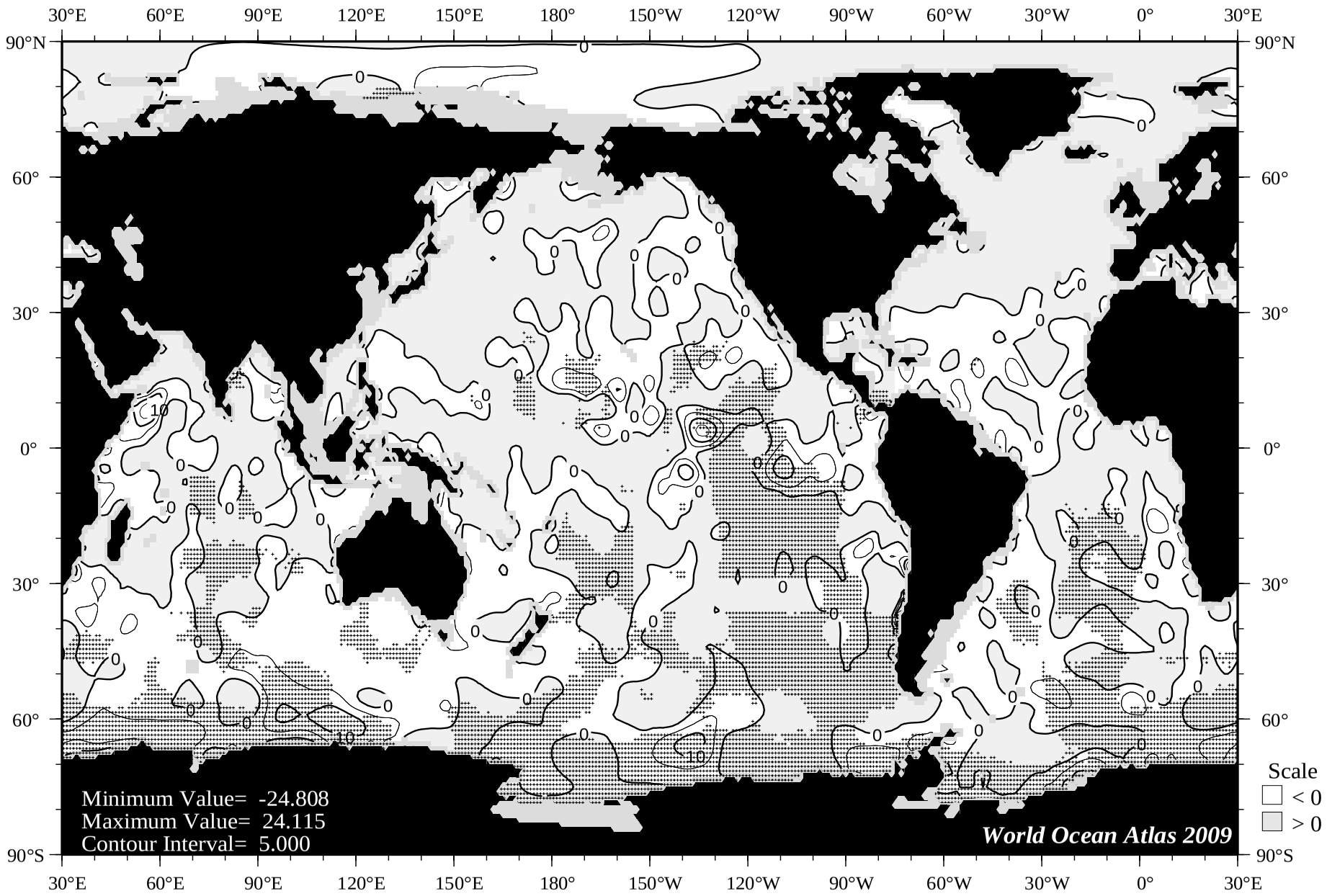

Fig H22 Summer (Jul.-Sep.) minus annual percent oxygen saturation at 150 m. depth.

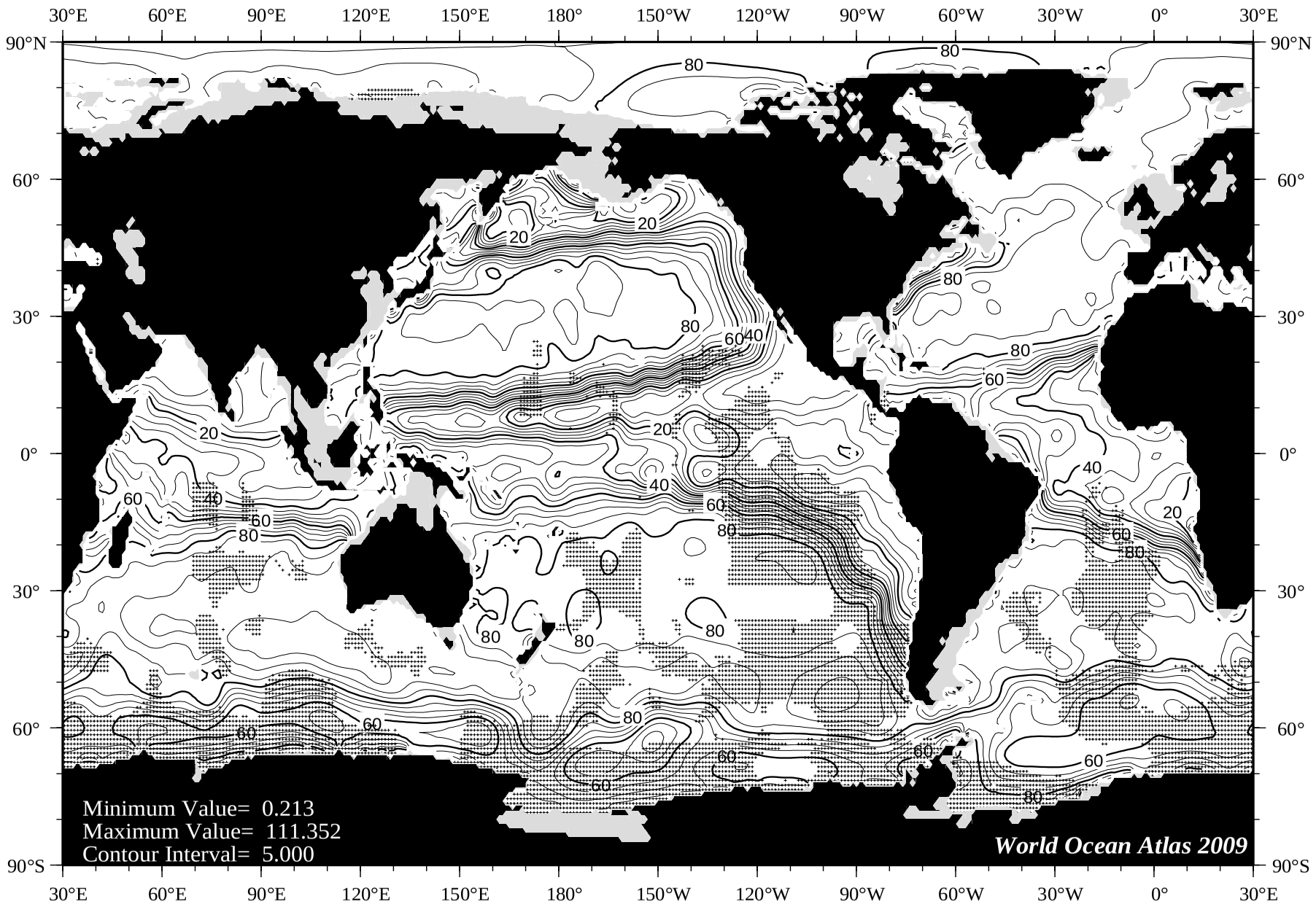

Fig H23 Summer (Jul.-Sep.) percent oxygen saturation at 250 m. depth.

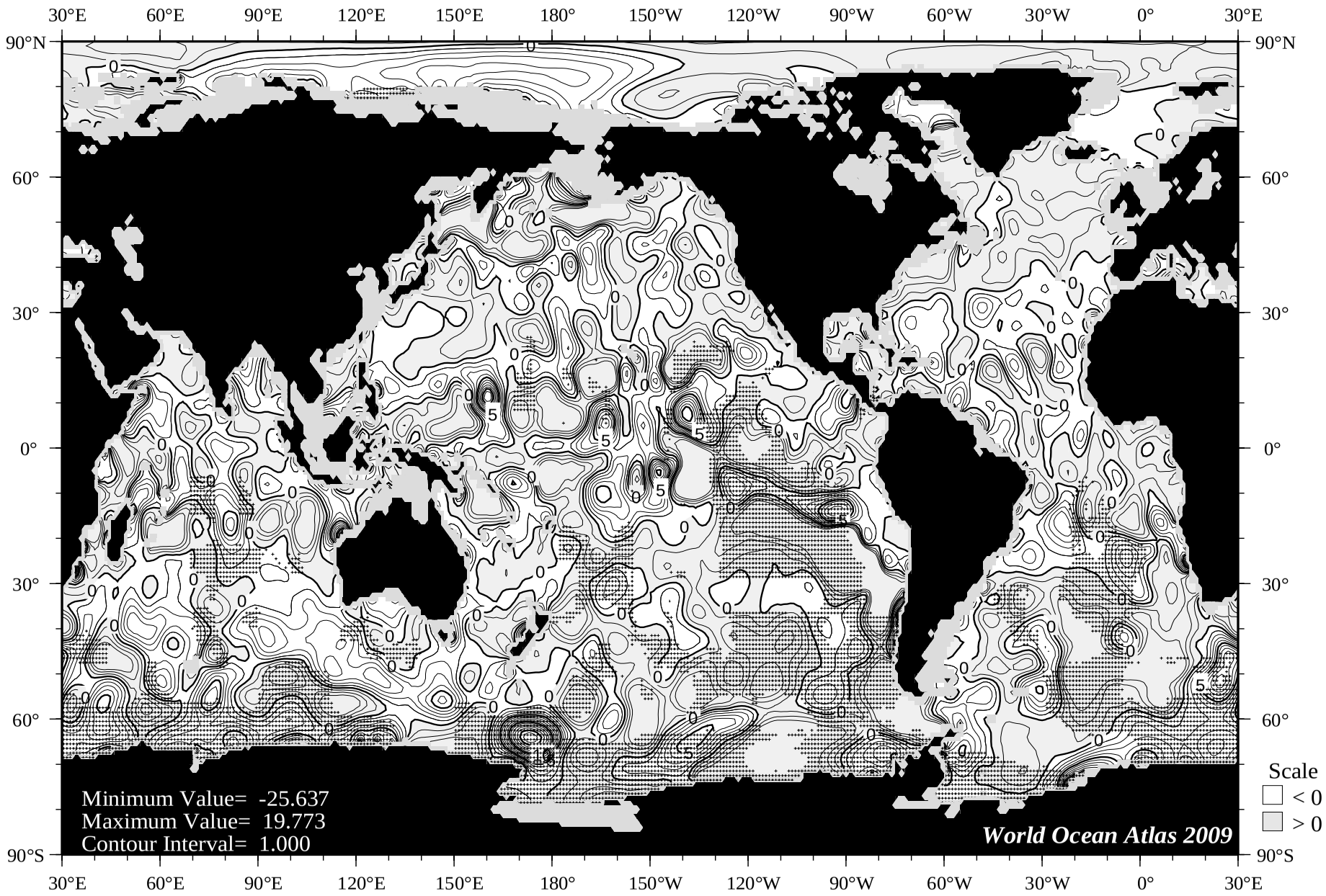

Fig H24 Summer (Jul.-Sep.) minus annual percent oxygen saturation at 250 m. depth.

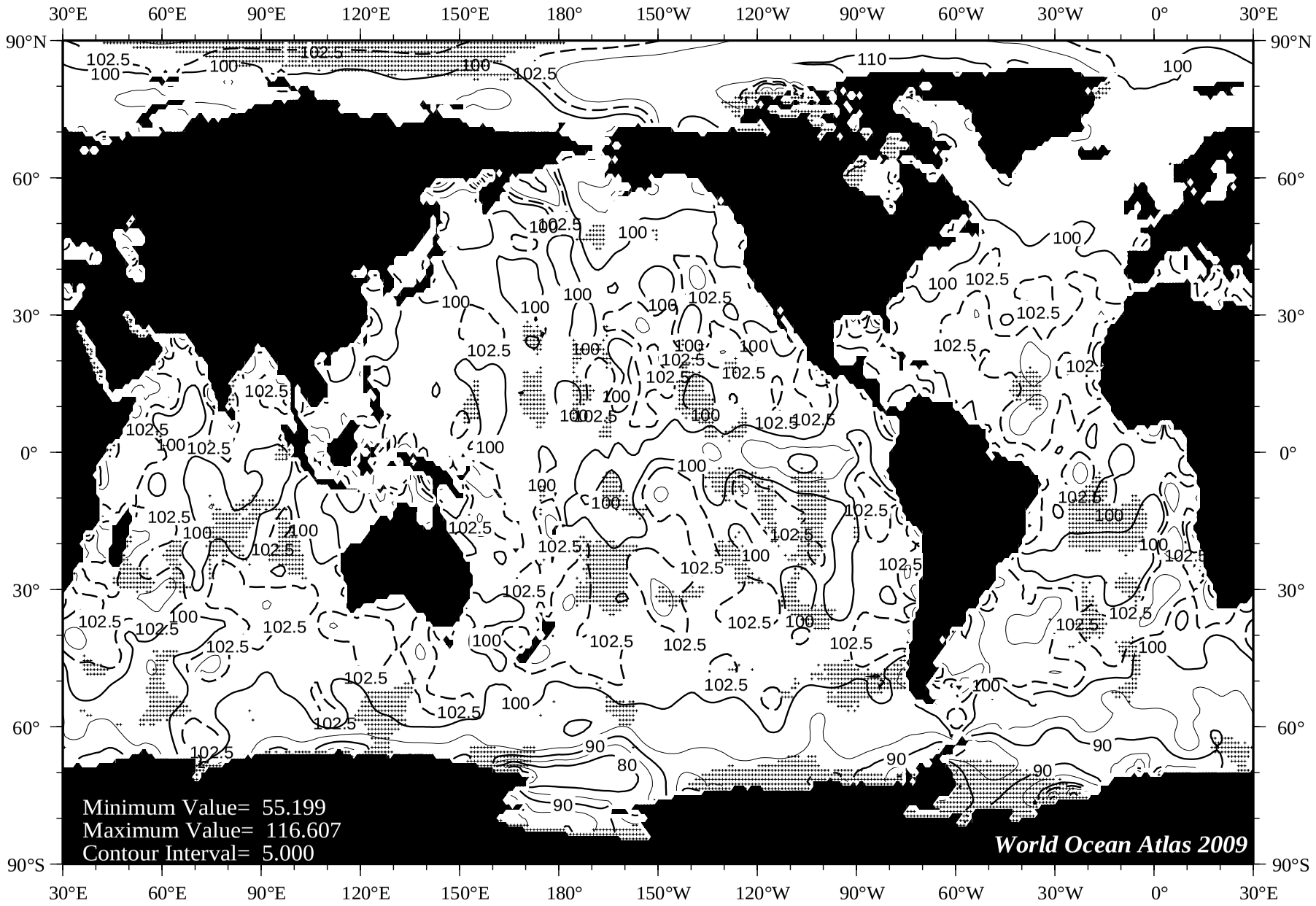

Fig H25 Fall (Oct.-Dec.) percent oxygen saturation at the surface.

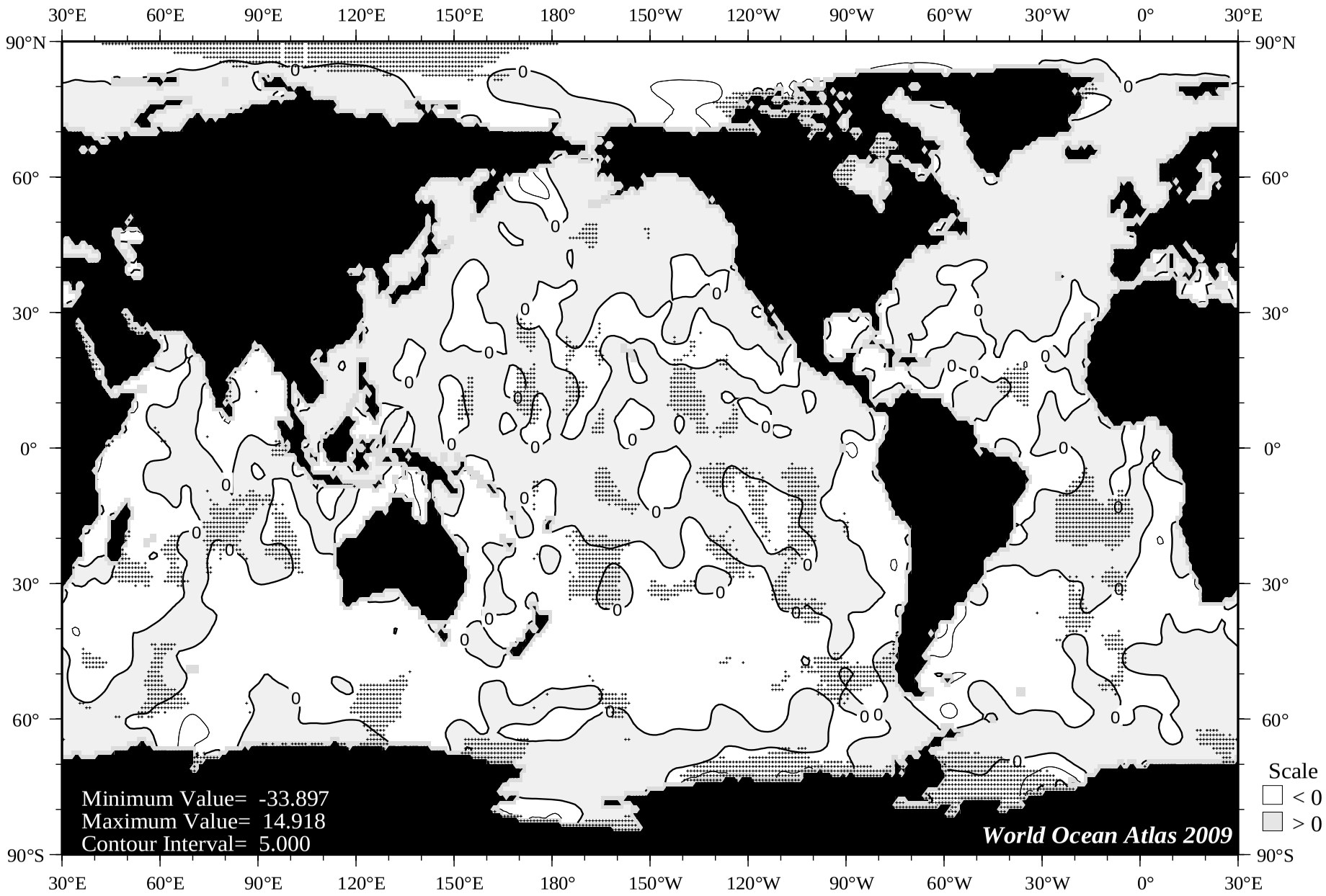

Fig H26 Fall (Oct.-Dec.) minus annual percent oxygen saturation at the surface.

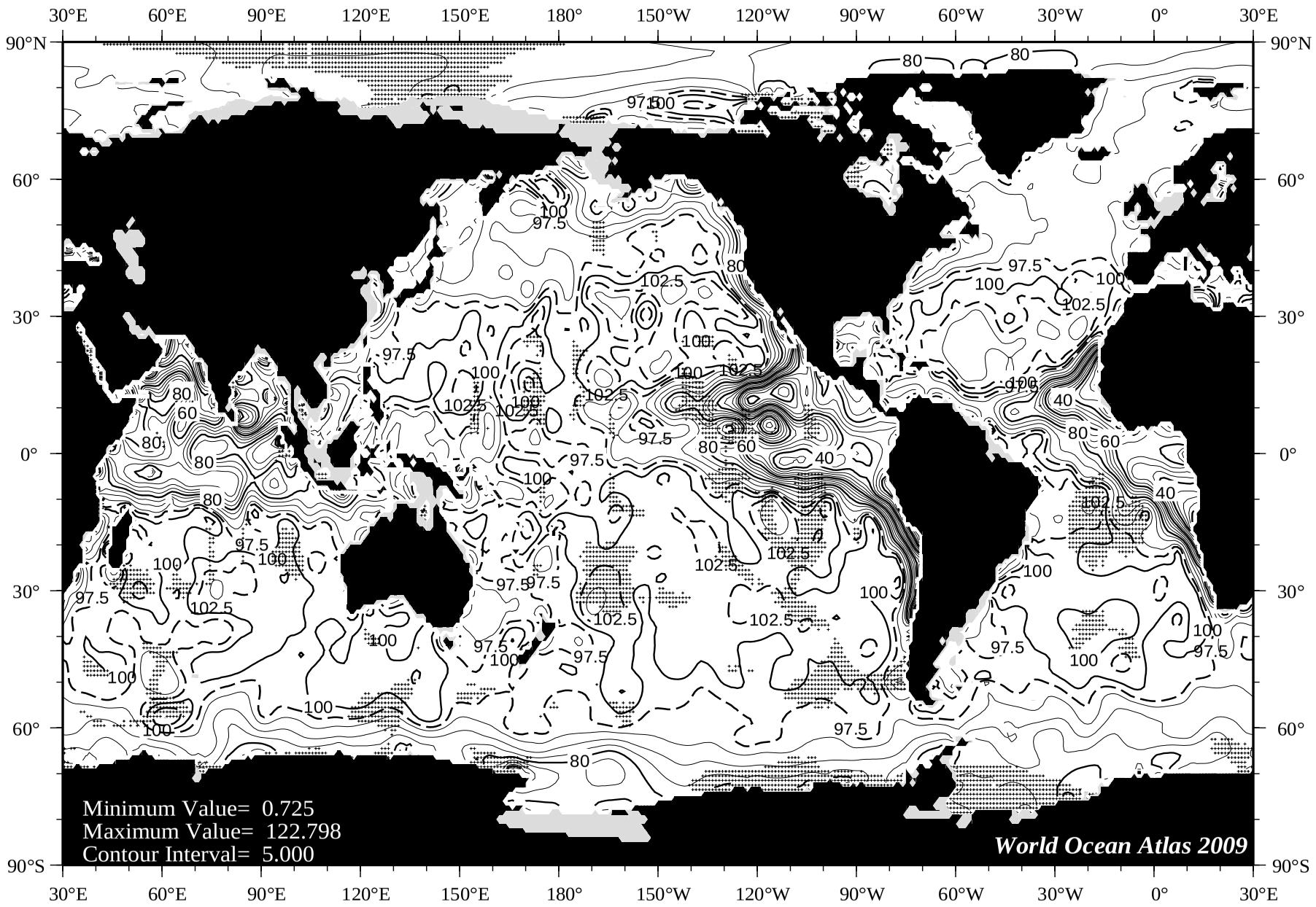

Fig H27 Fall (Oct.-Dec.) percent oxygen saturation at 75 m. depth.

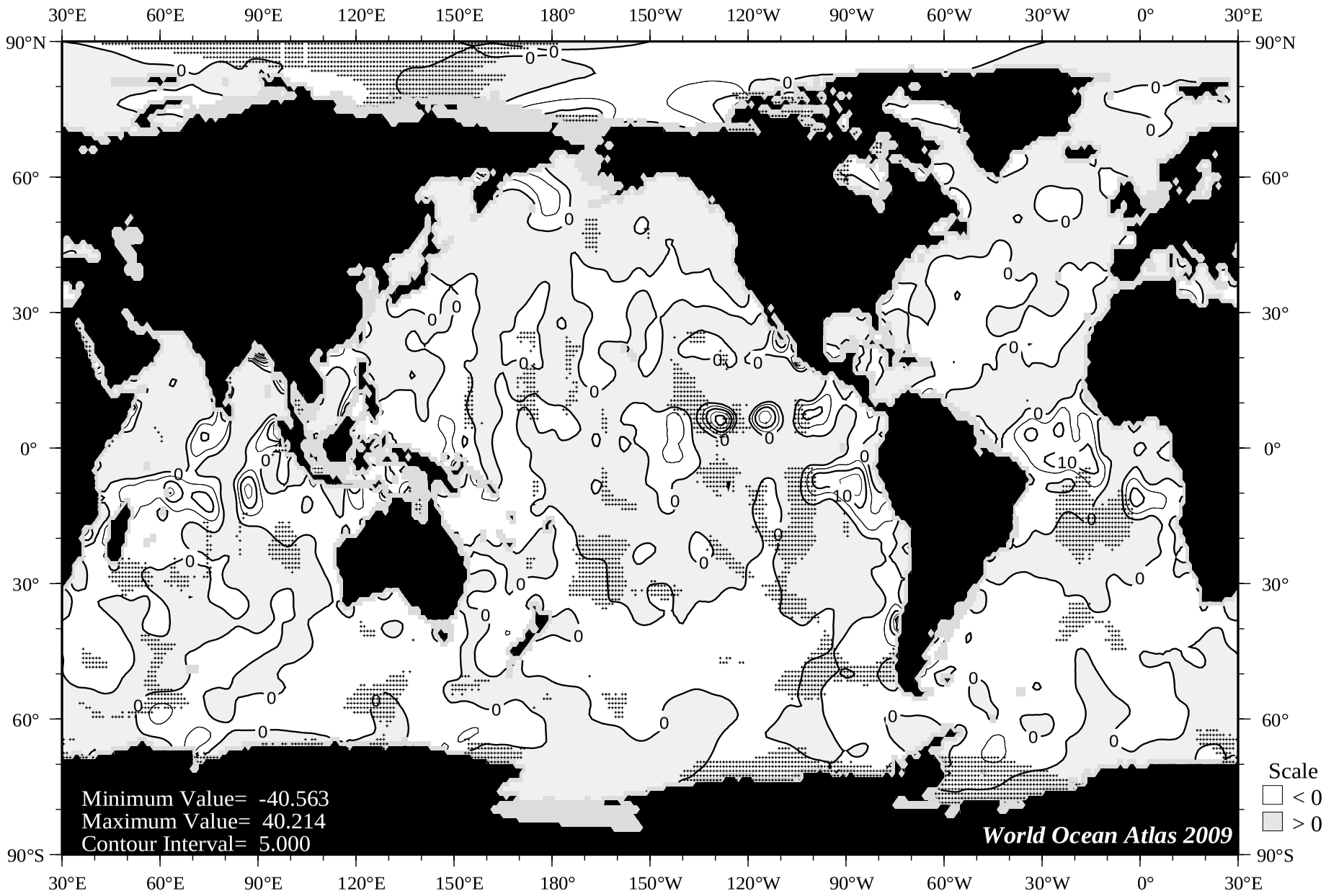

Fig H28 Fall (Oct.-Dec.) minus annual percent oxygen saturation at 75 m. depth.

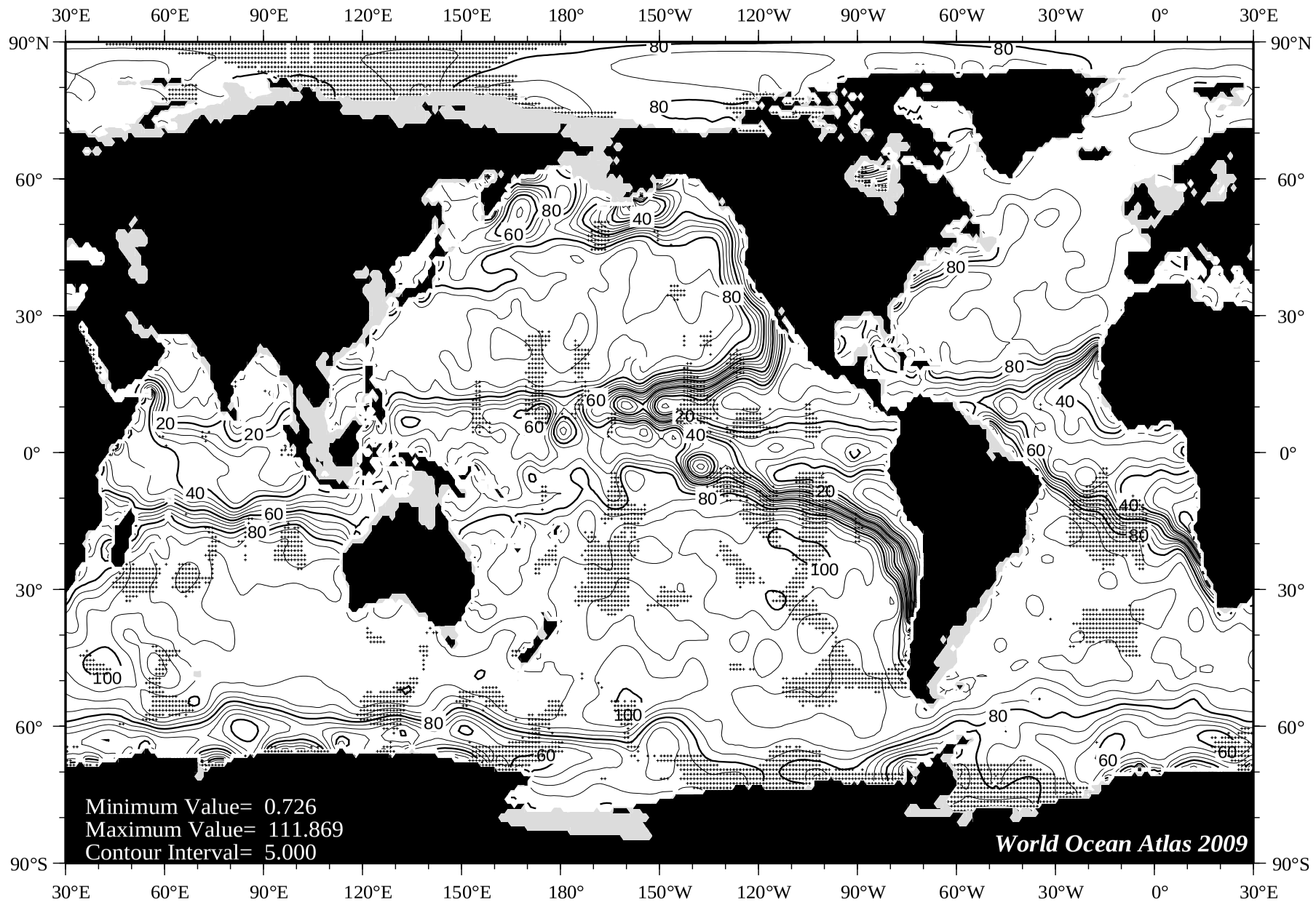

Fig H29 Fall (Oct.-Dec.) percent oxygen saturation at 150 m. depth.

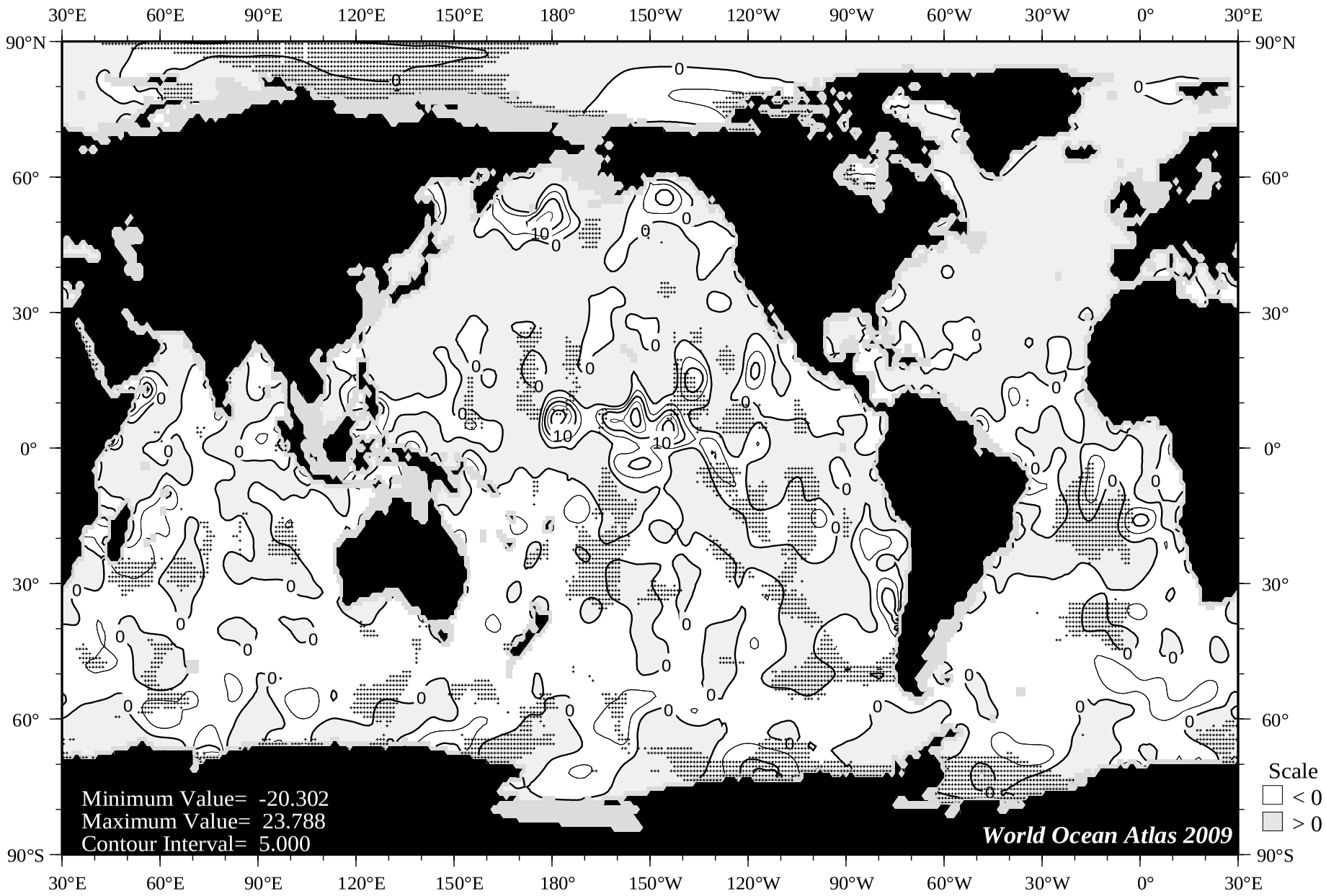

Fig H30 Fall (Oct.-Dec.) minus annual percent oxygen saturation at 150 m. depth.

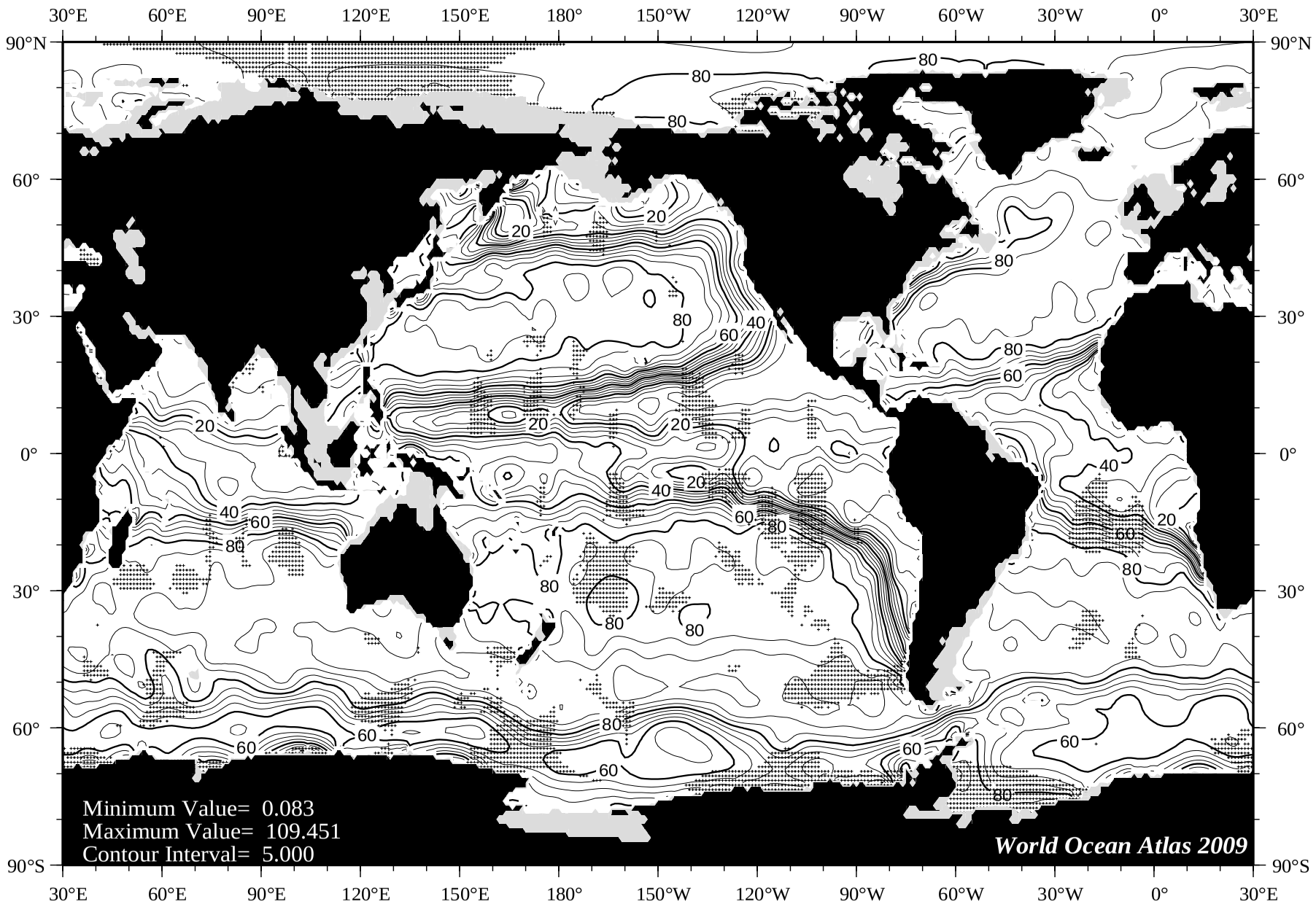

Fig H31 Fall (Oct.-Dec.) percent oxygen saturation at 250 m. depth.

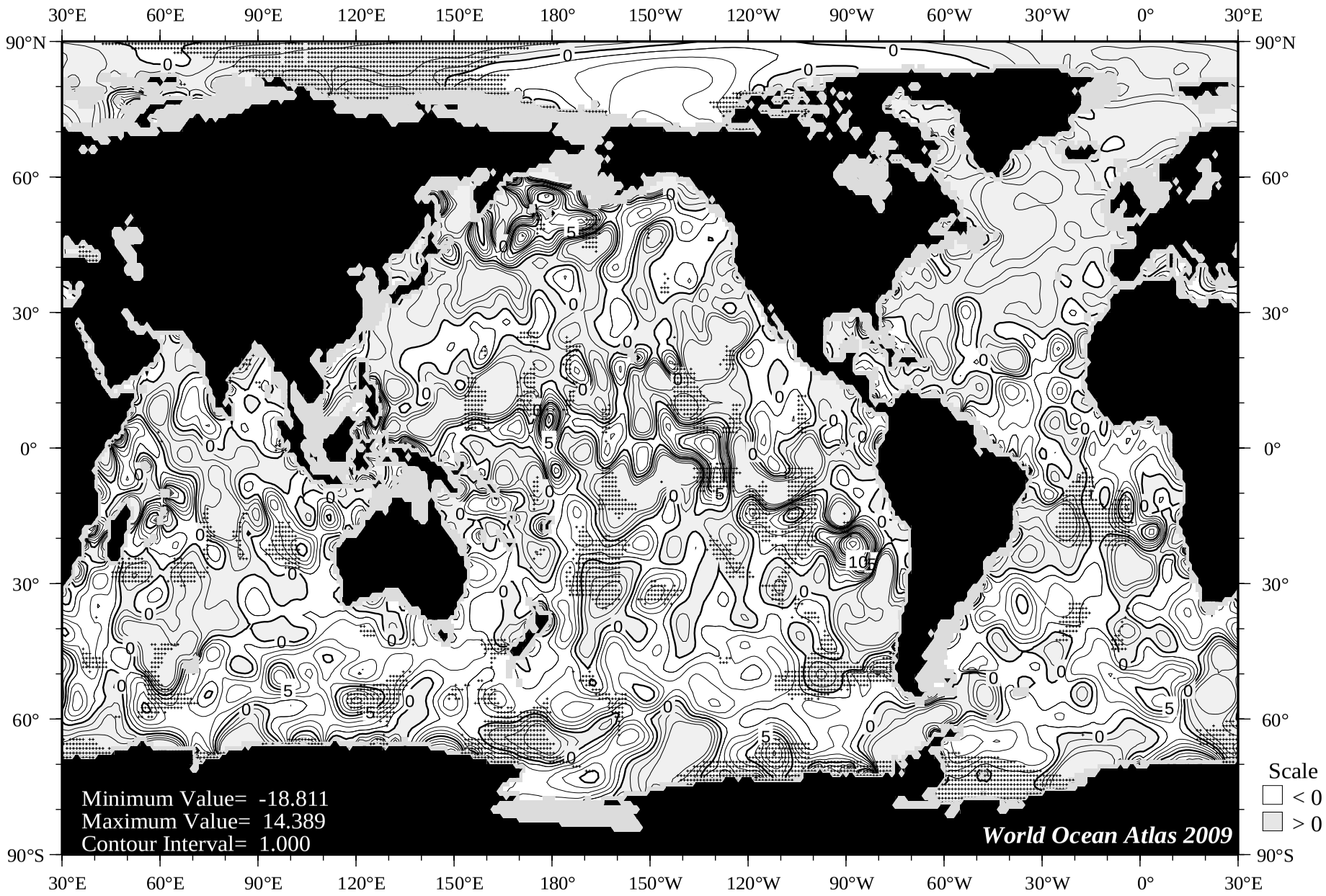

Fig H32 Fall (Oct.-Dec.) minus annual percent oxygen saturation at 250 m. depth.

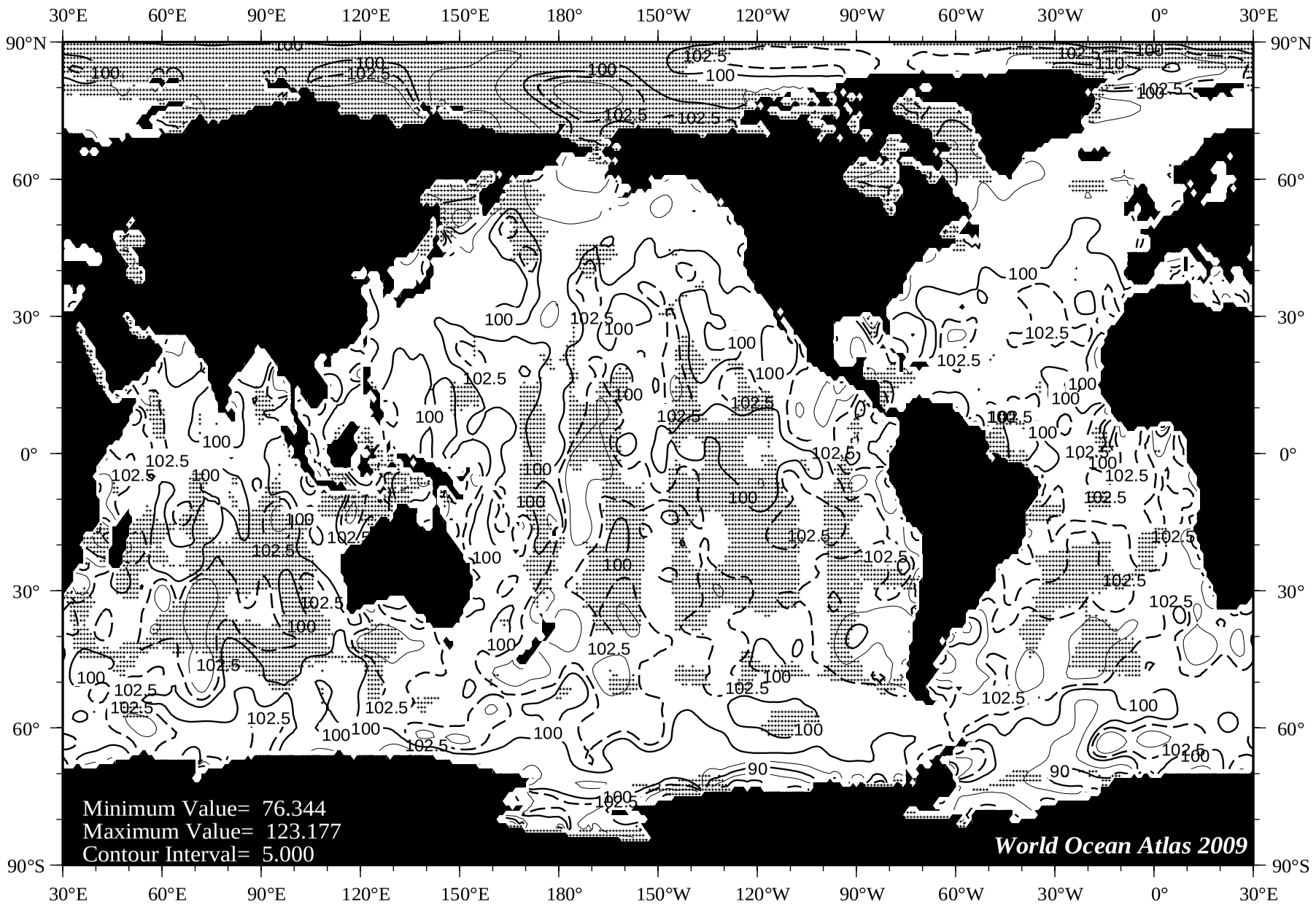

Fig I1 January mean percent oxygen saturation at the surface.

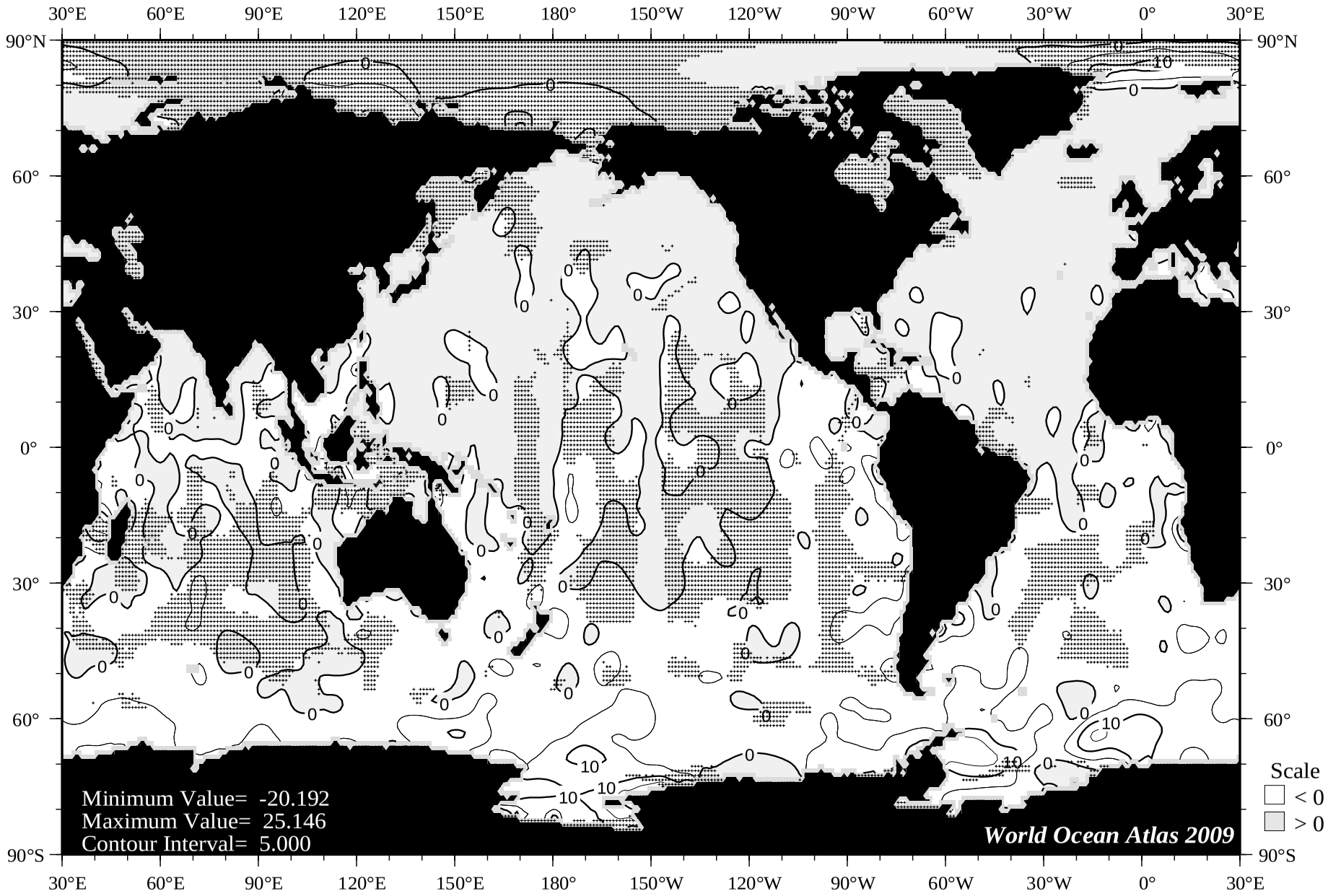

Fig I2 January minus annual percent oxygen saturation at the surface.

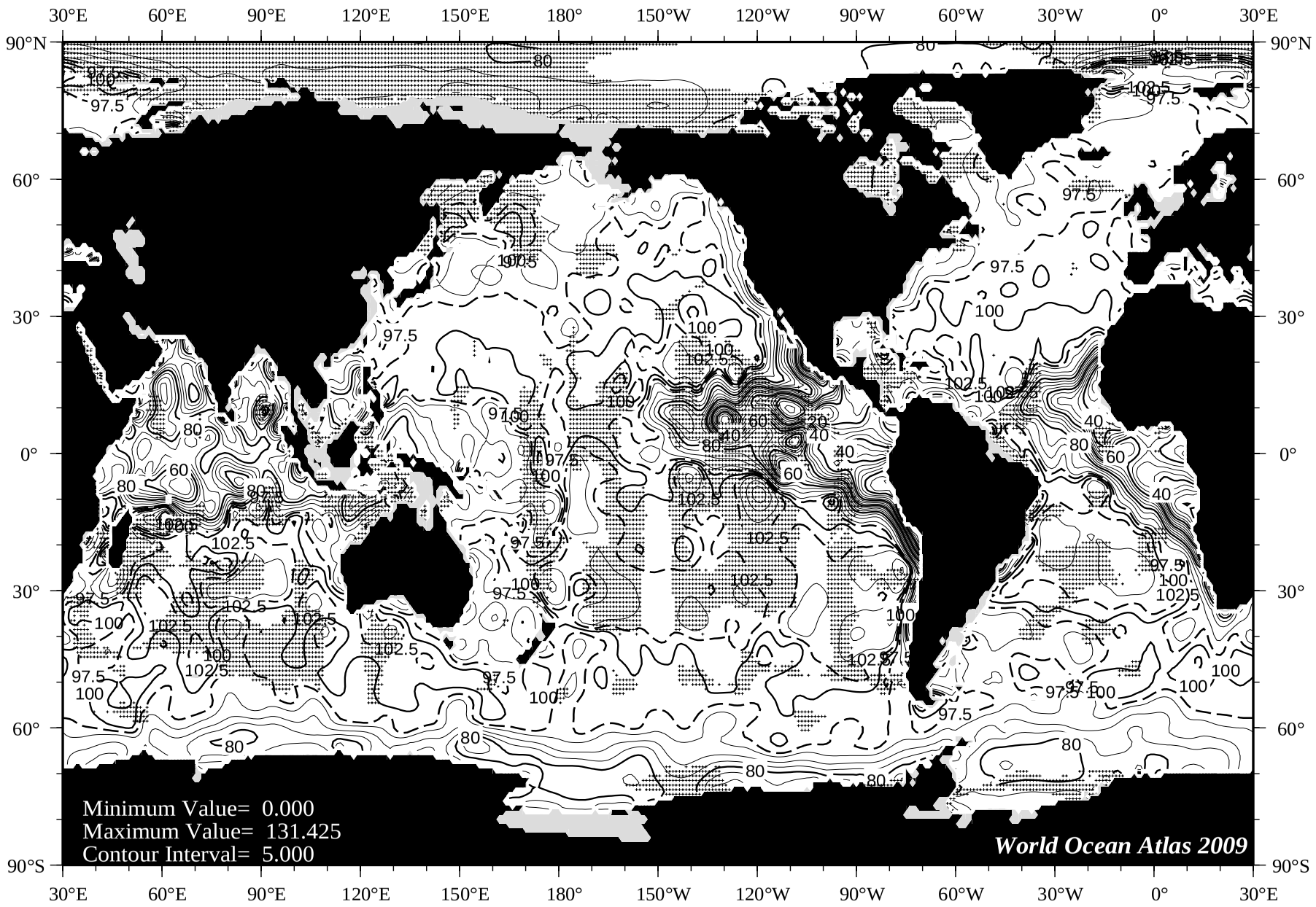

Fig I3 January mean percent oxygen saturation at 75 m. depth.

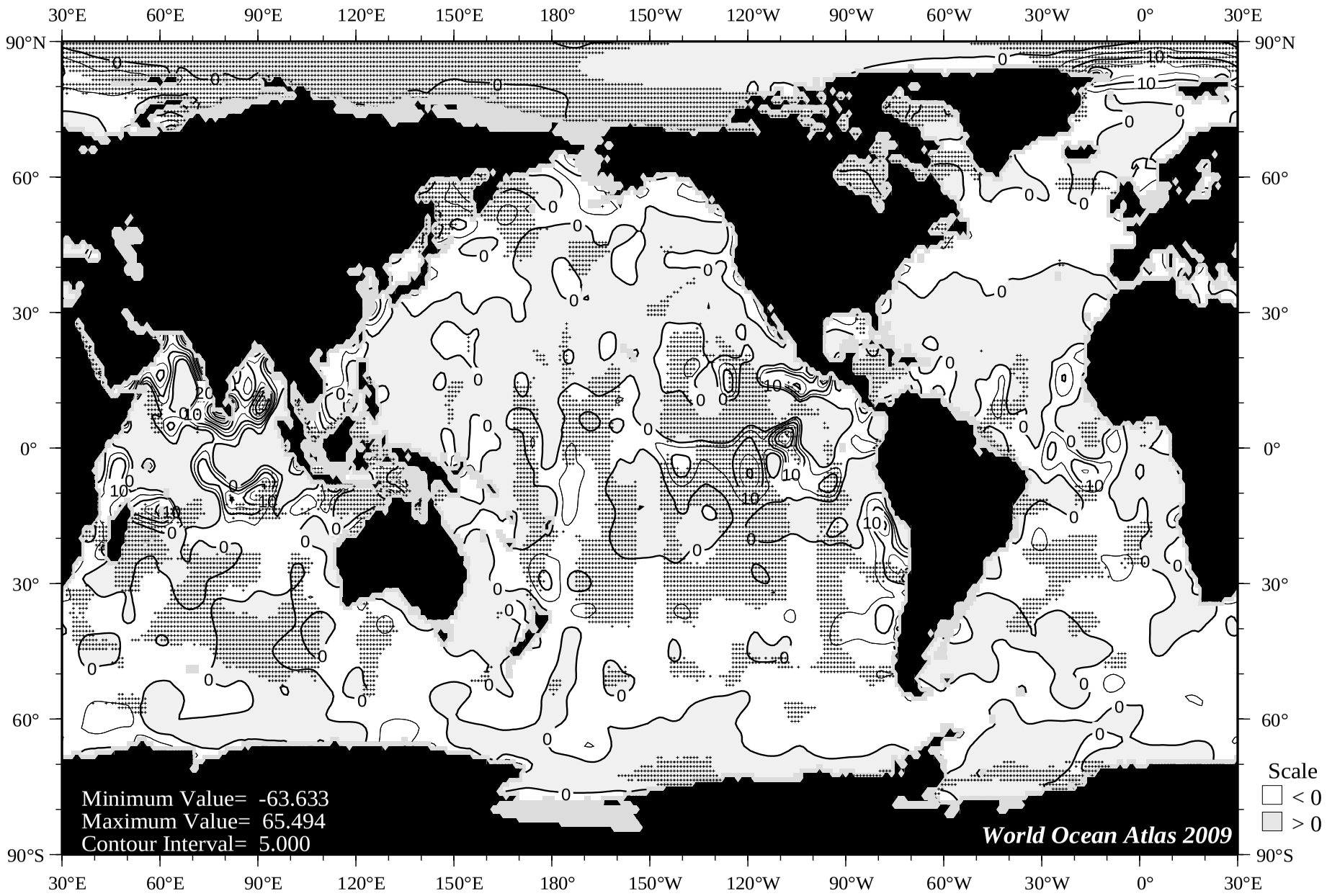

Fig I4 January minus annual percent oxygen saturation at 75 m. depth.

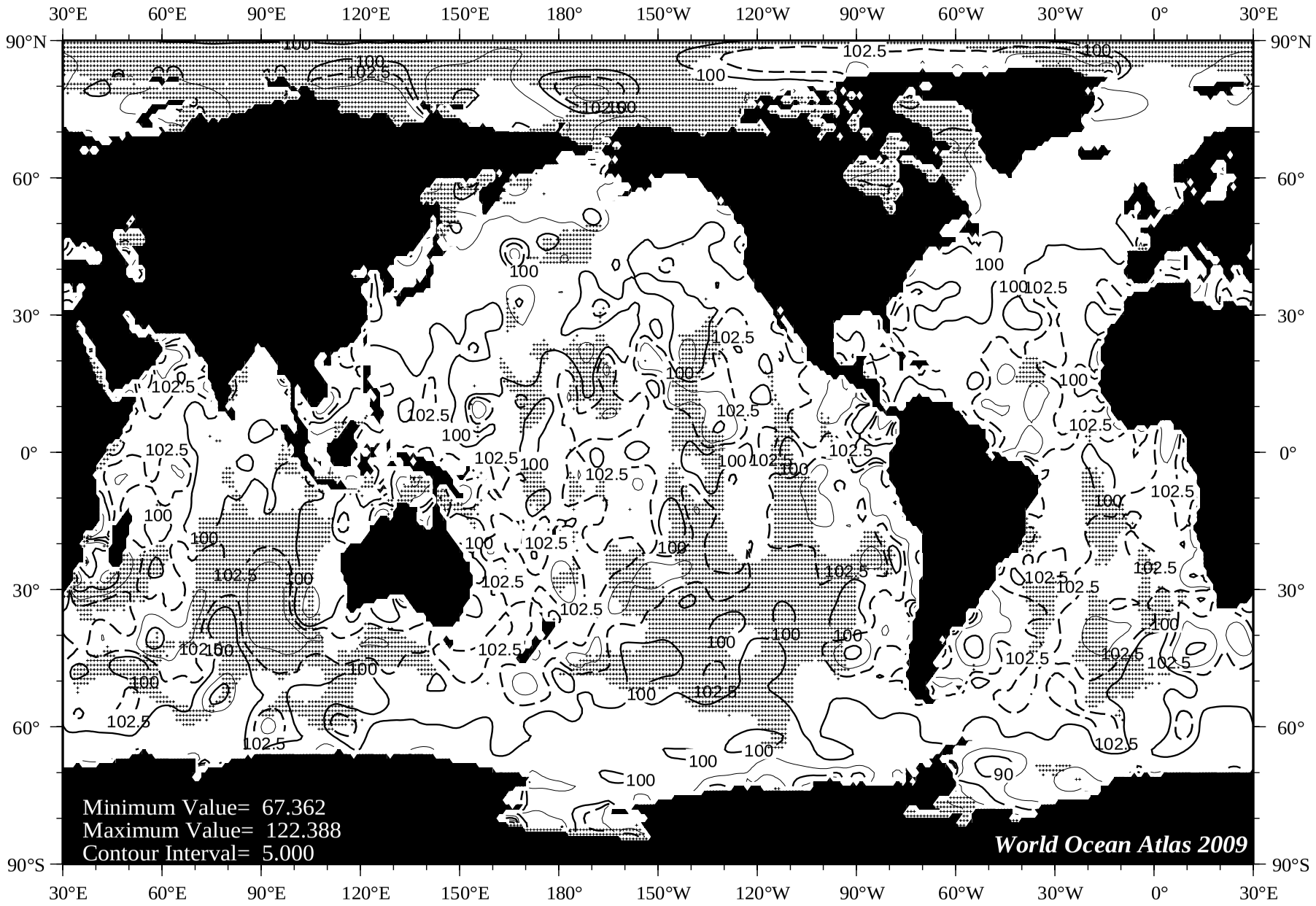

Fig I5 February mean percent oxygen saturation at the surface.

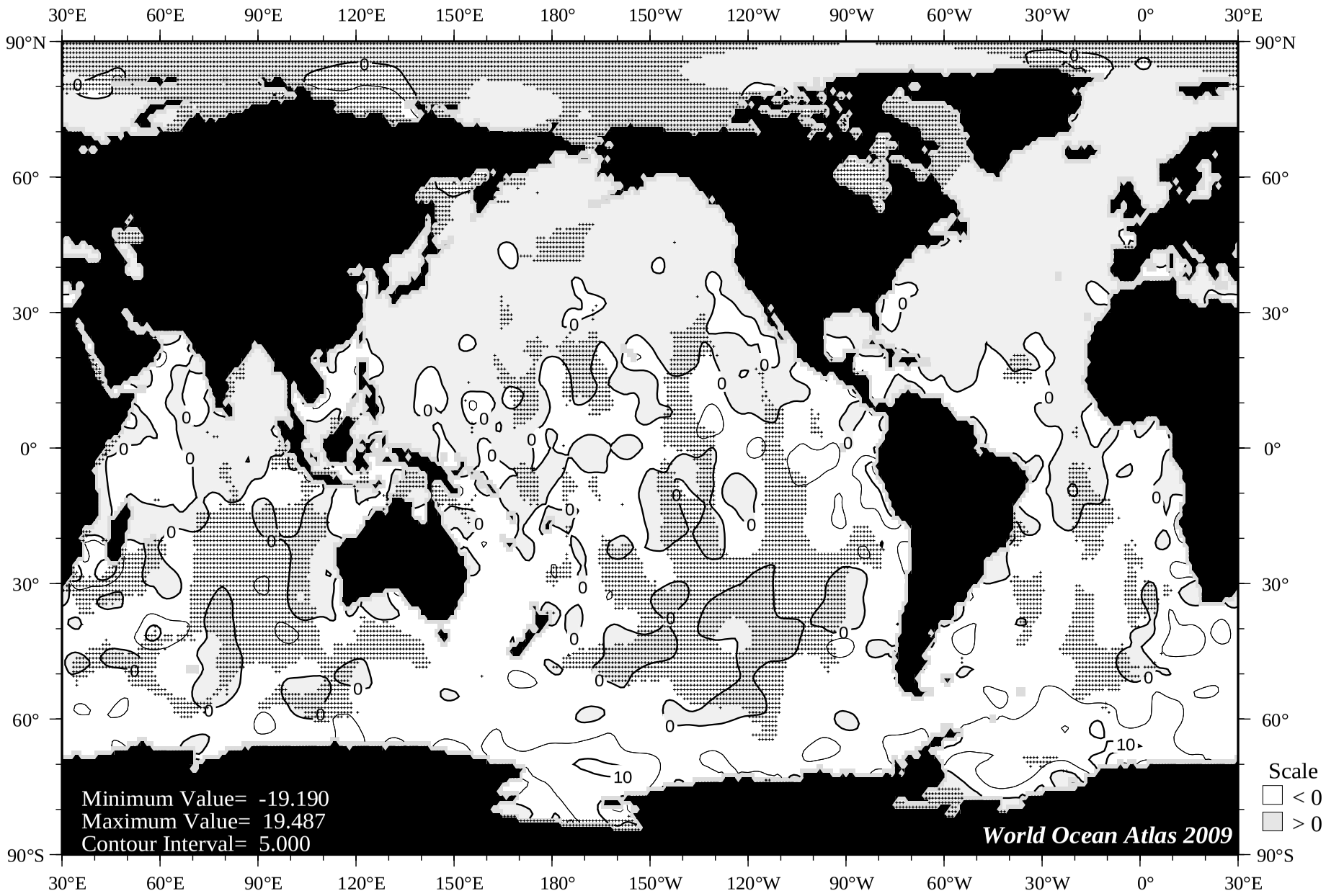

Fig I6 February minus annual percent oxygen saturation at the surface.

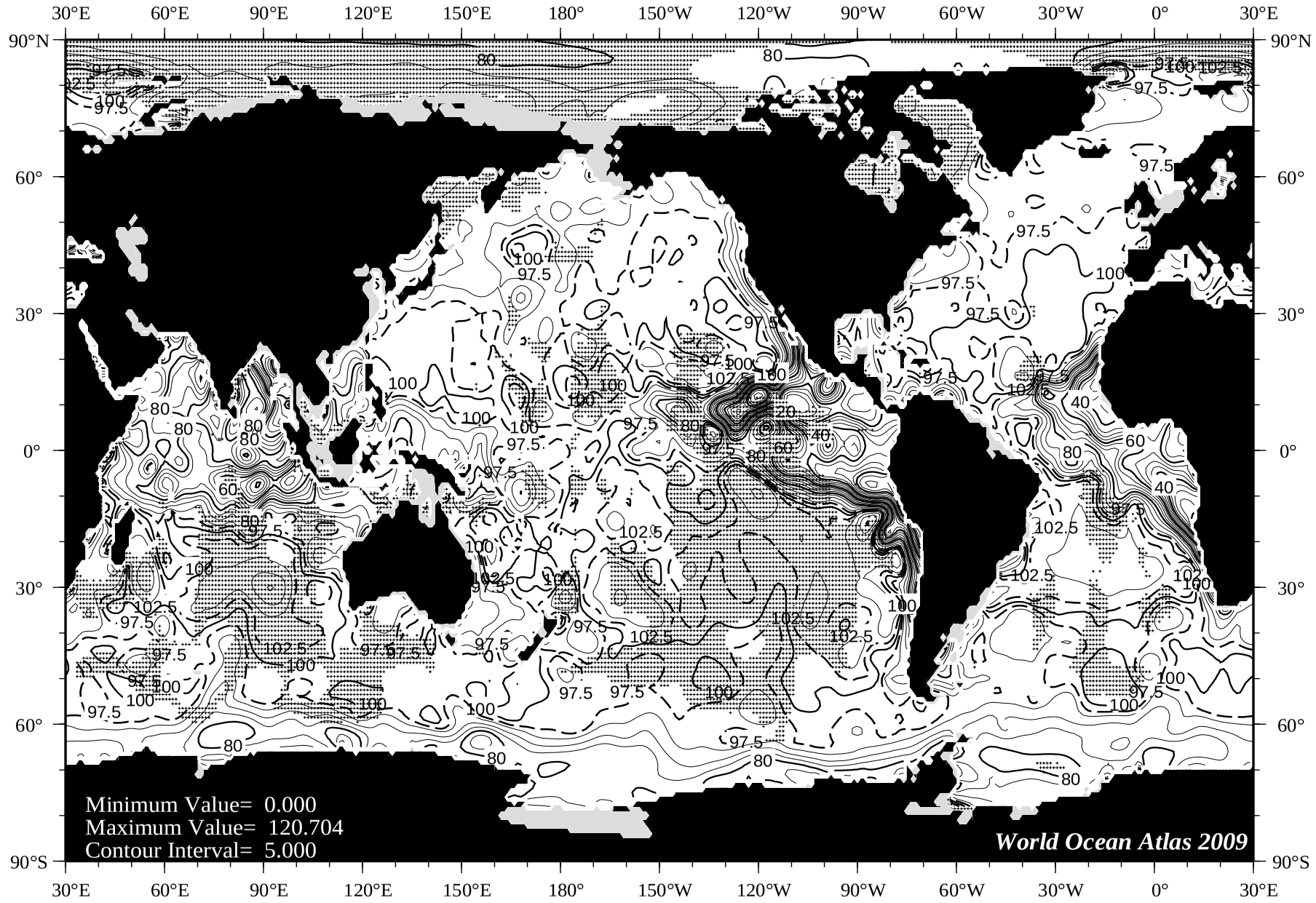

Fig I7 February mean percent oxygen saturation at 75 m. depth.

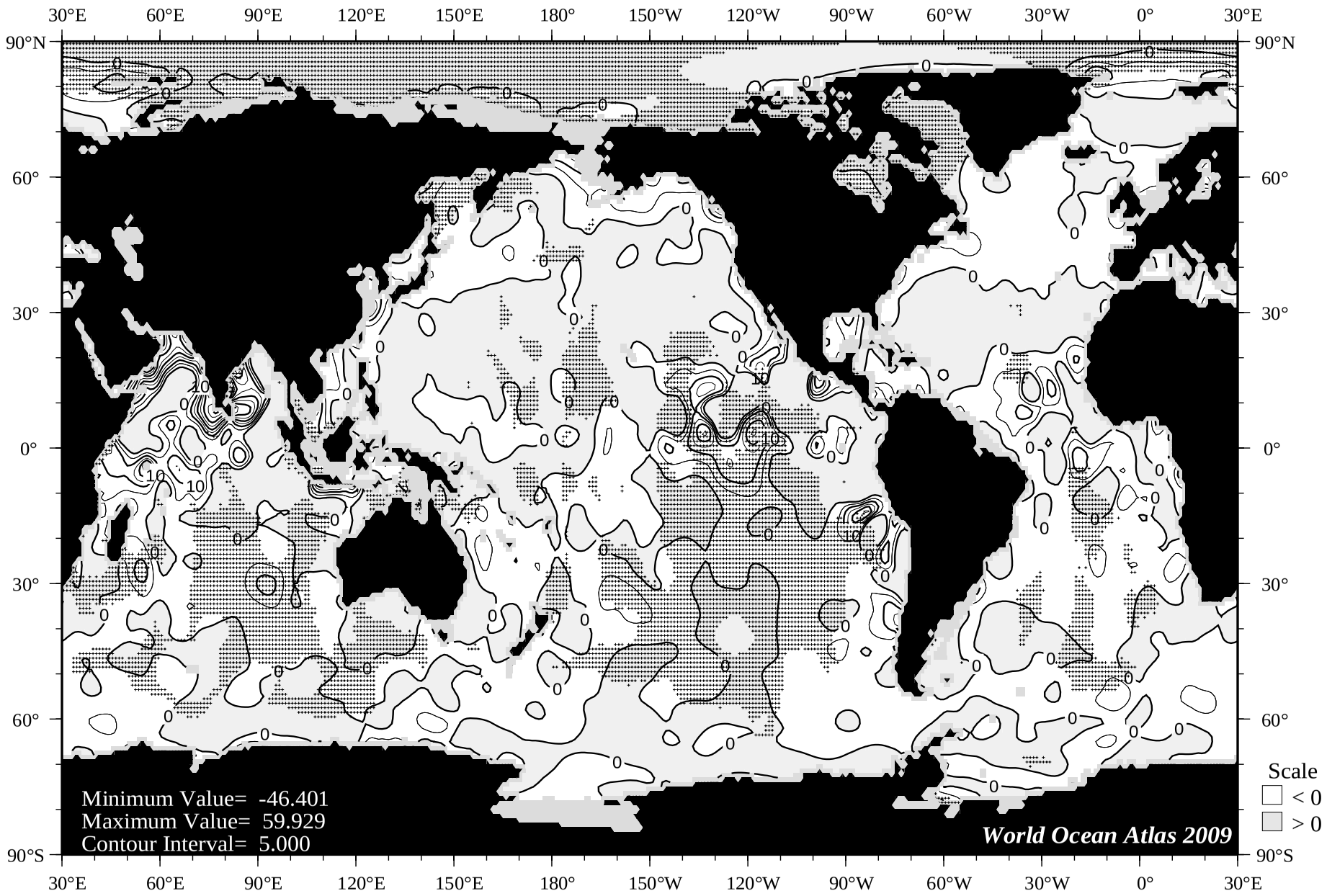

Fig I8 February minus annual percent oxygen saturation at 75 m. depth.

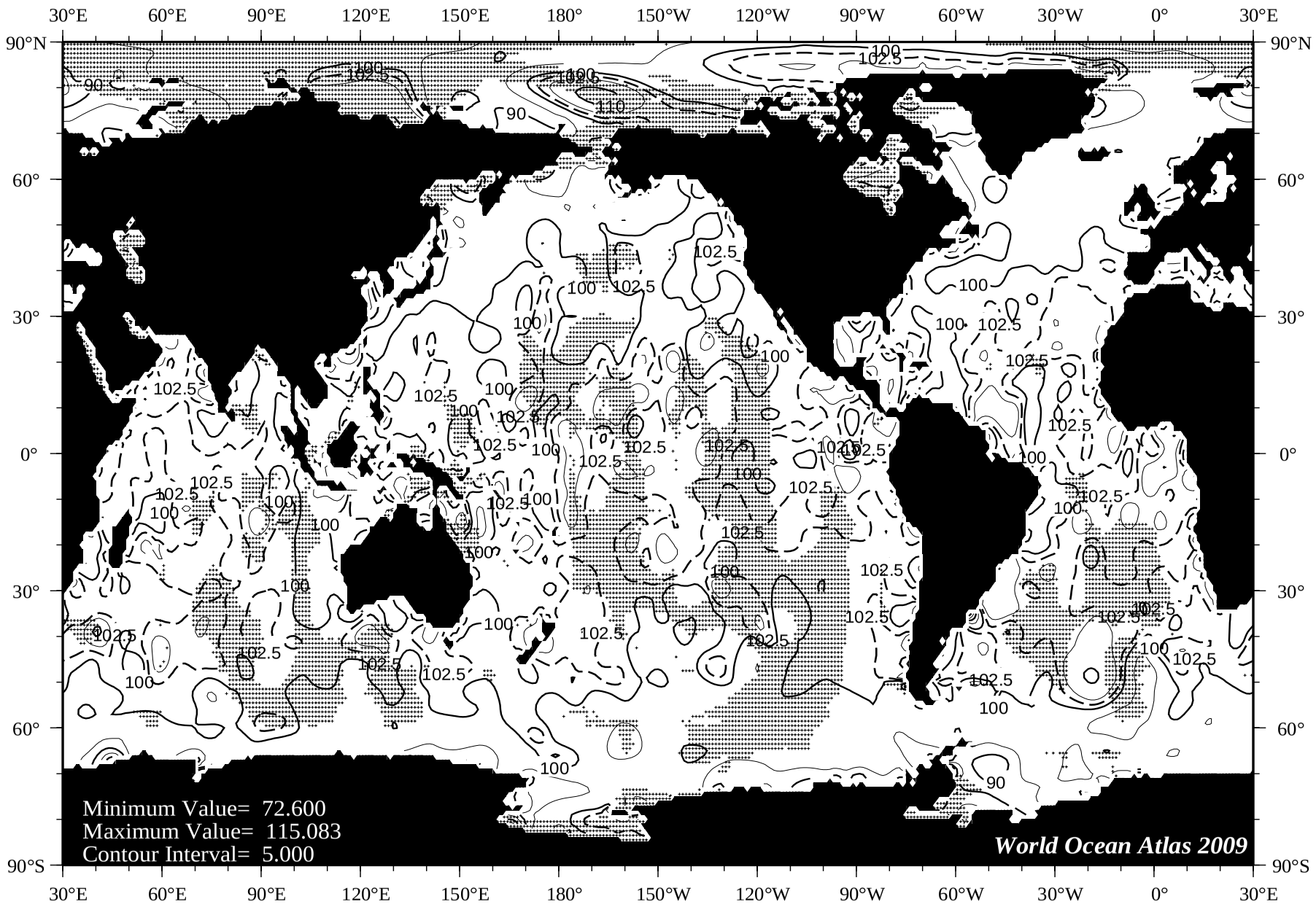

Fig I9 March mean percent oxygen saturation at the surface.

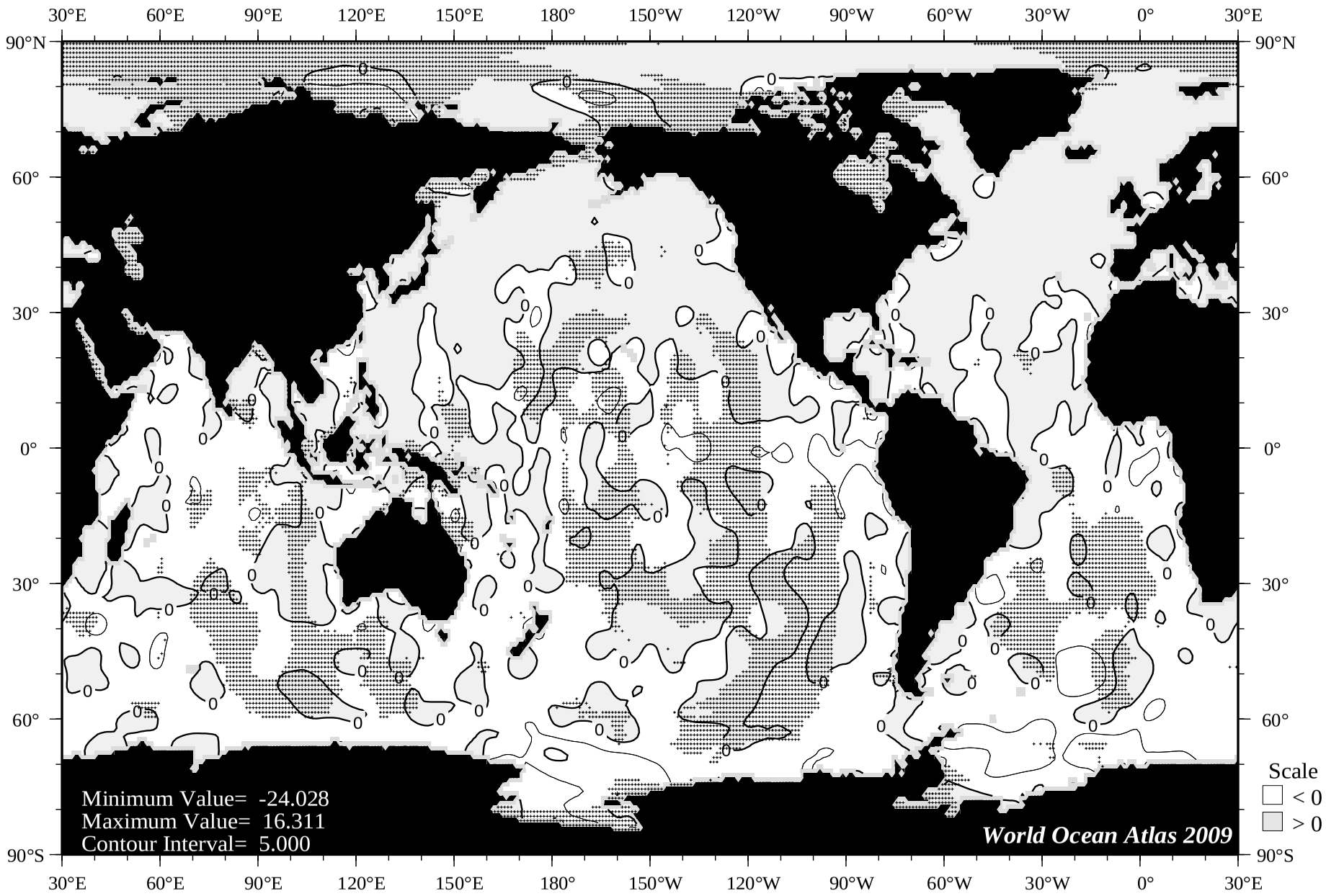

Fig I10 March minus annual percent oxygen saturation at the surface.

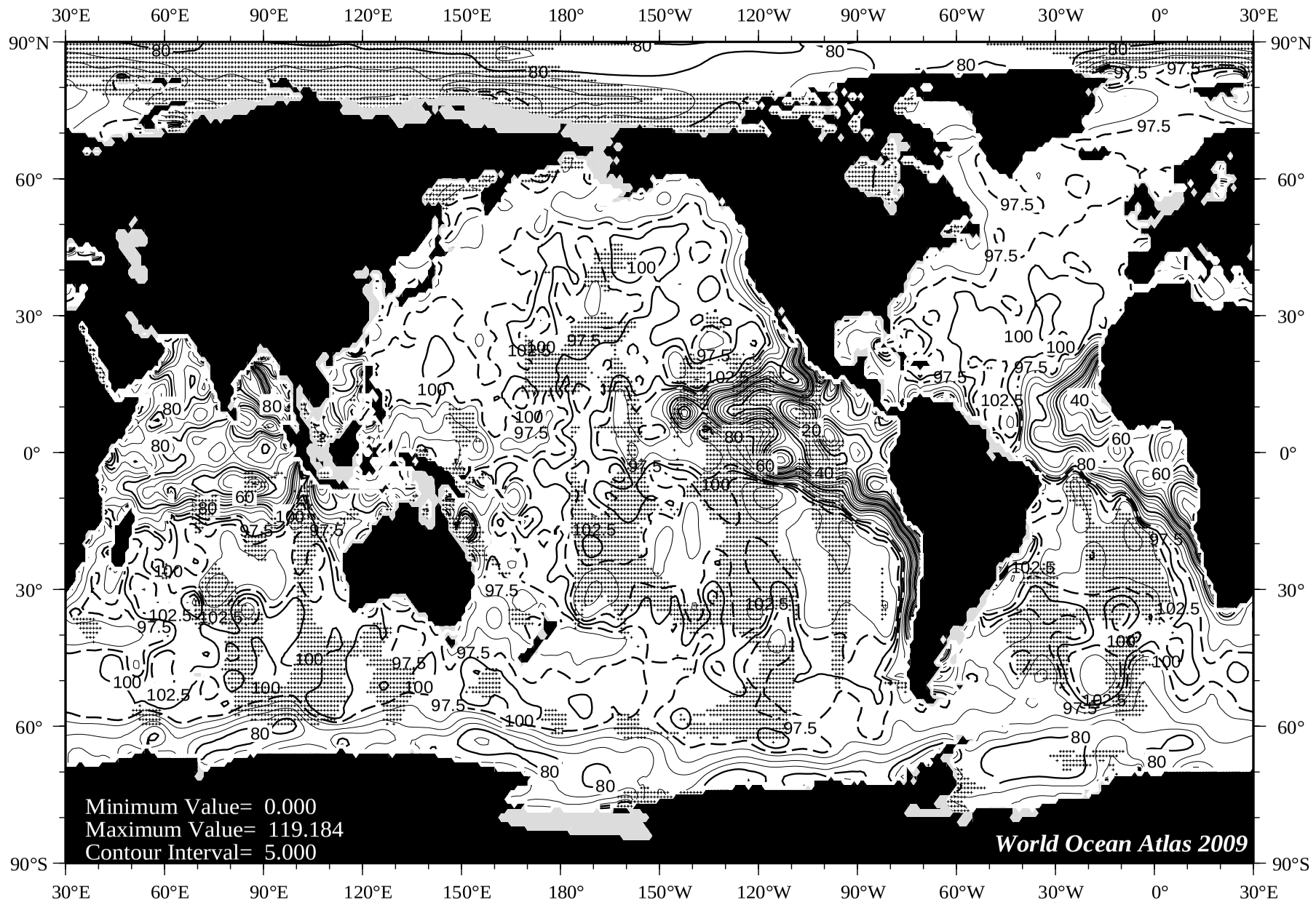

Fig I11 March mean percent oxygen saturation at 75 m. depth.

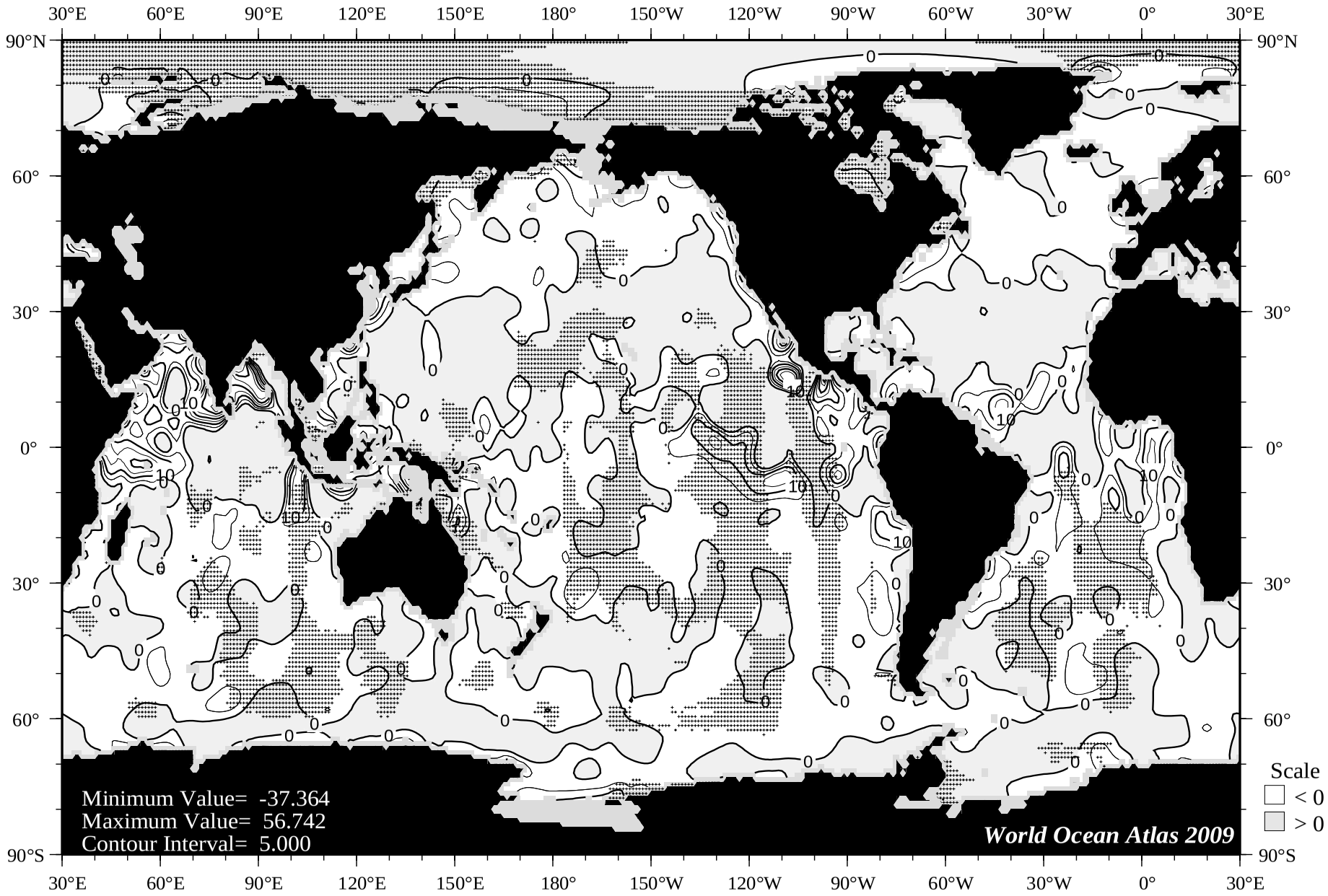

Fig I12 March minus annual percent oxygen saturation at 75 m. depth.

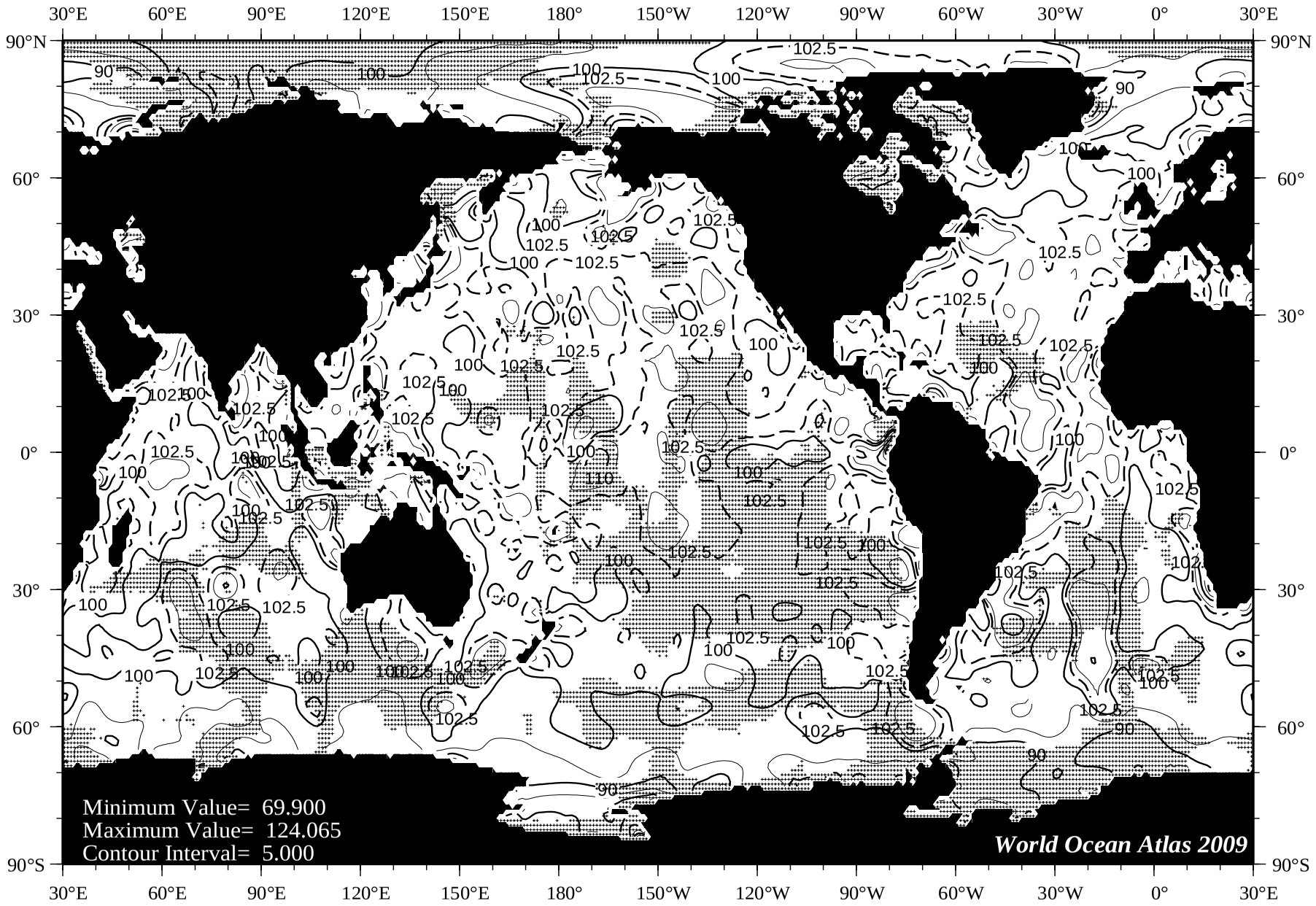

Fig I13 April mean percent oxygen saturation at the surface.

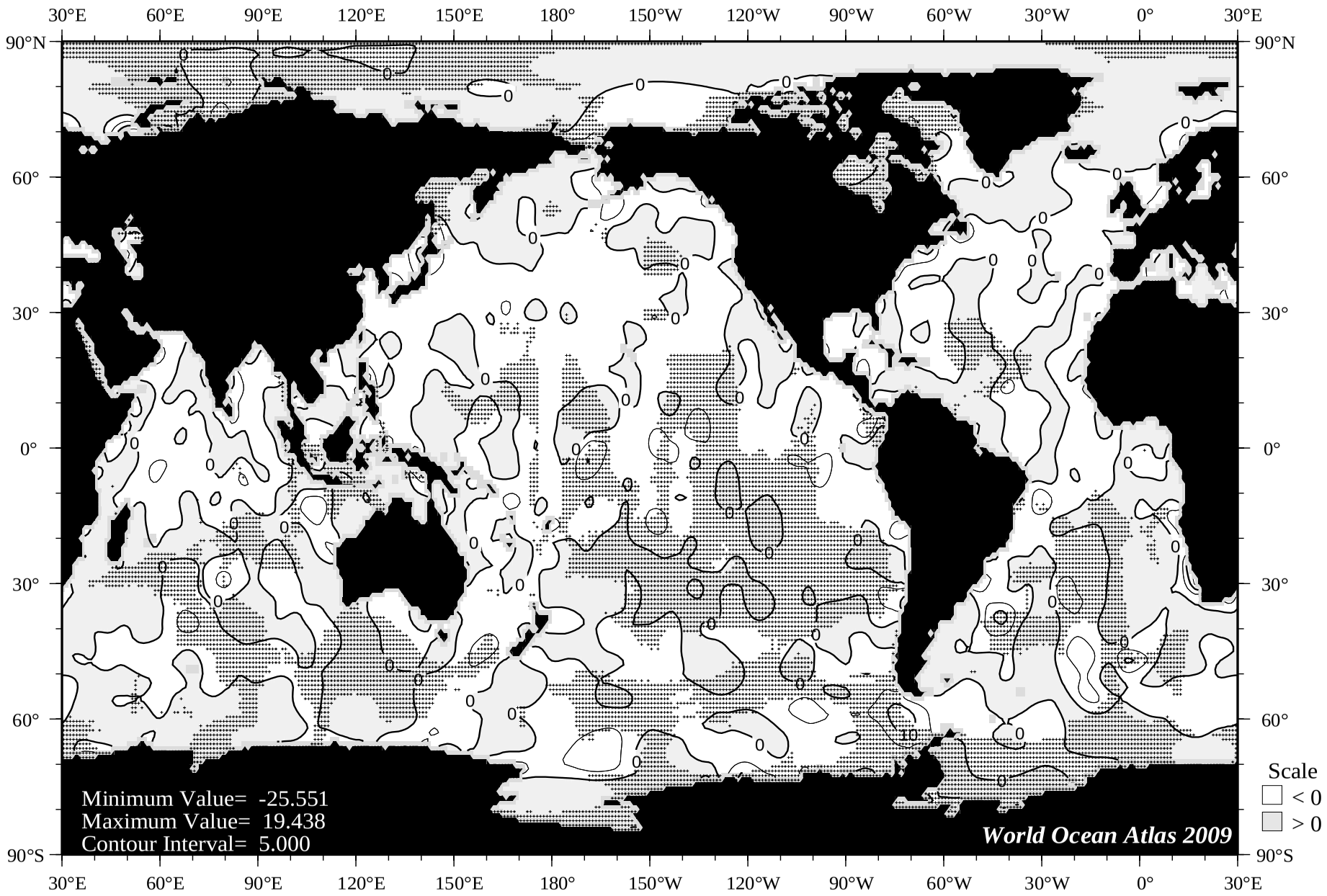

Fig I14 April minus annual percent oxygen saturation at the surface.

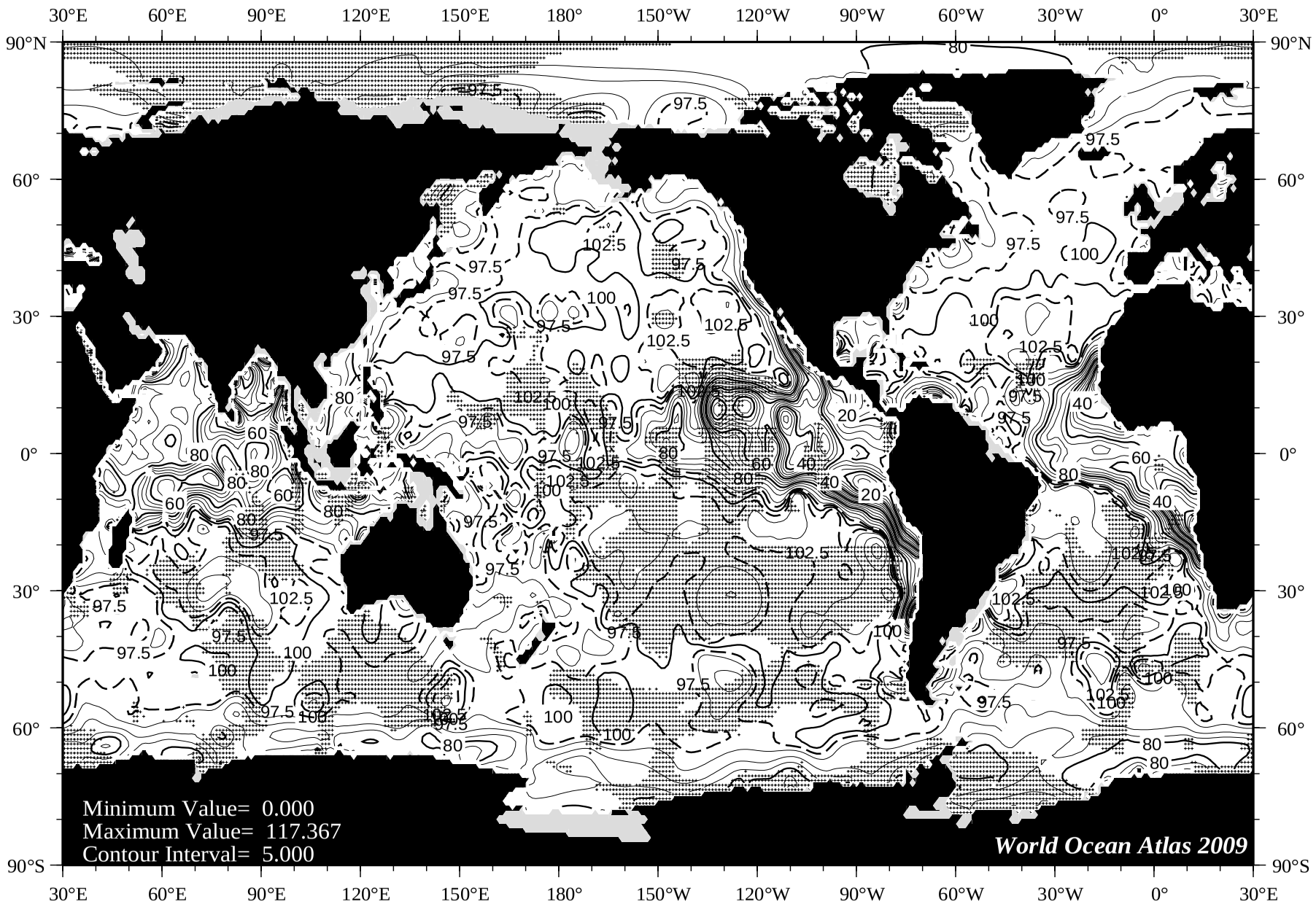

Fig I15 April mean percent oxygen saturation at 75 m. depth.

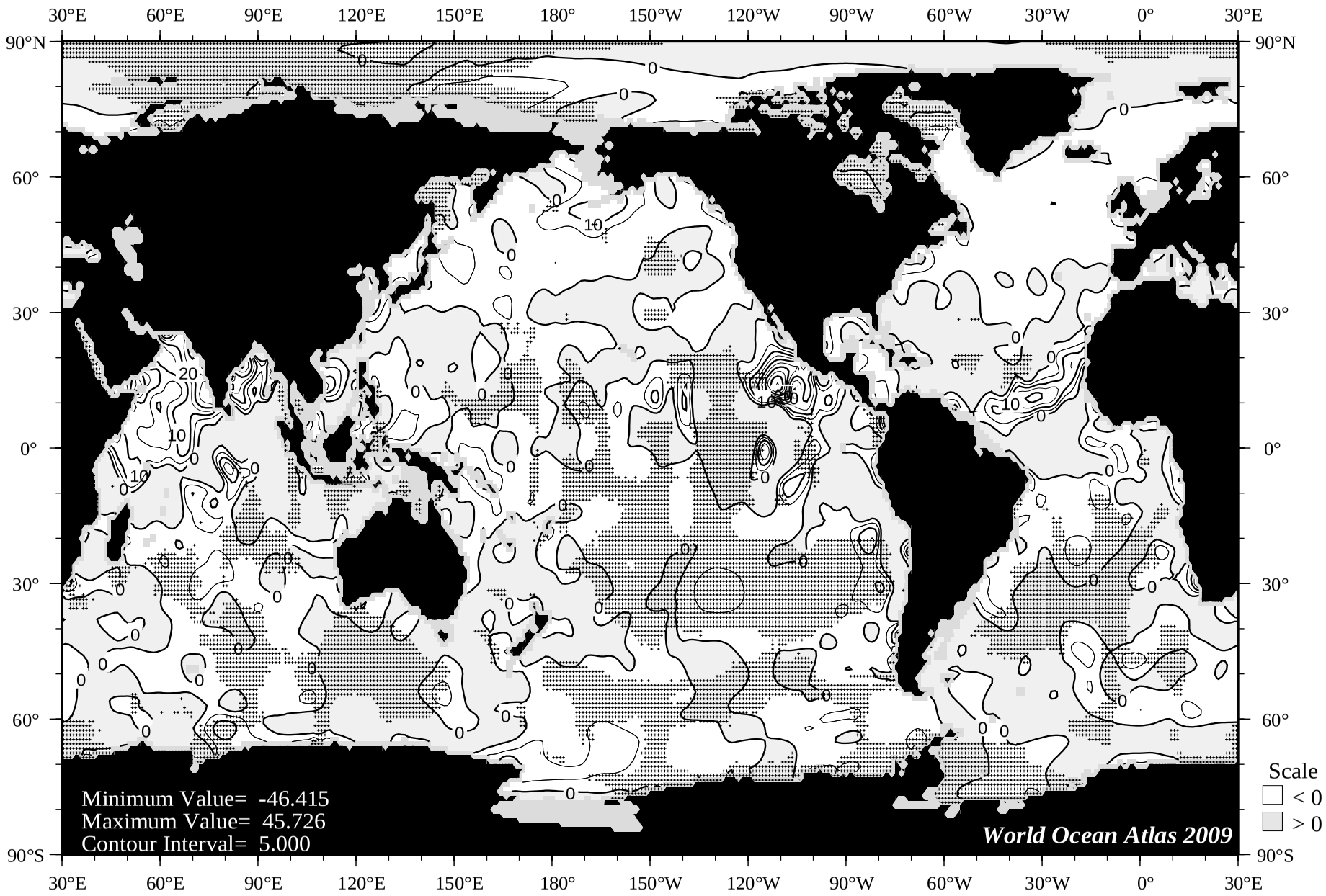

Fig I16 April minus annual percent oxygen saturation at 75 m. depth.

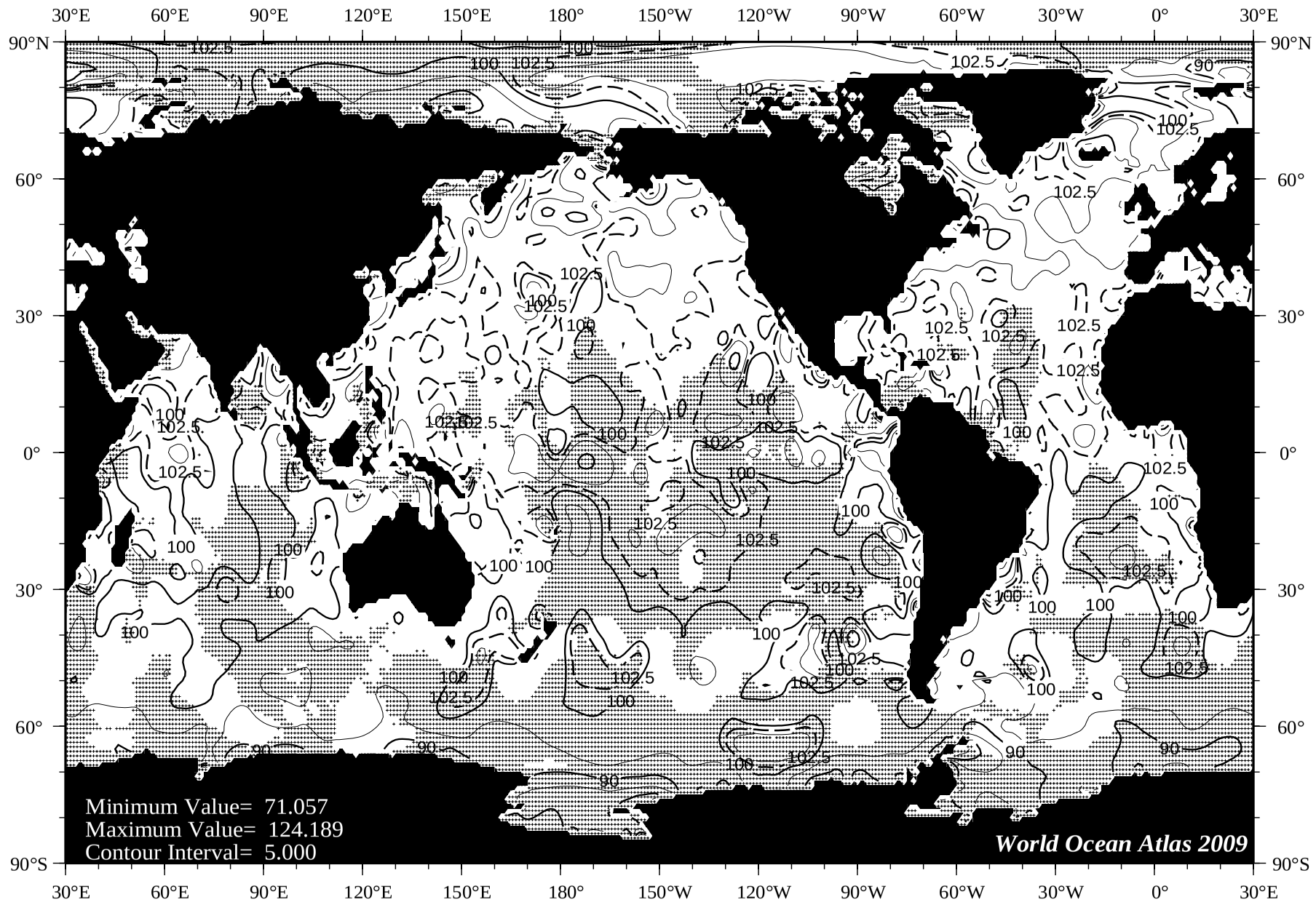

Fig I17 May mean percent oxygen saturation at the surface.

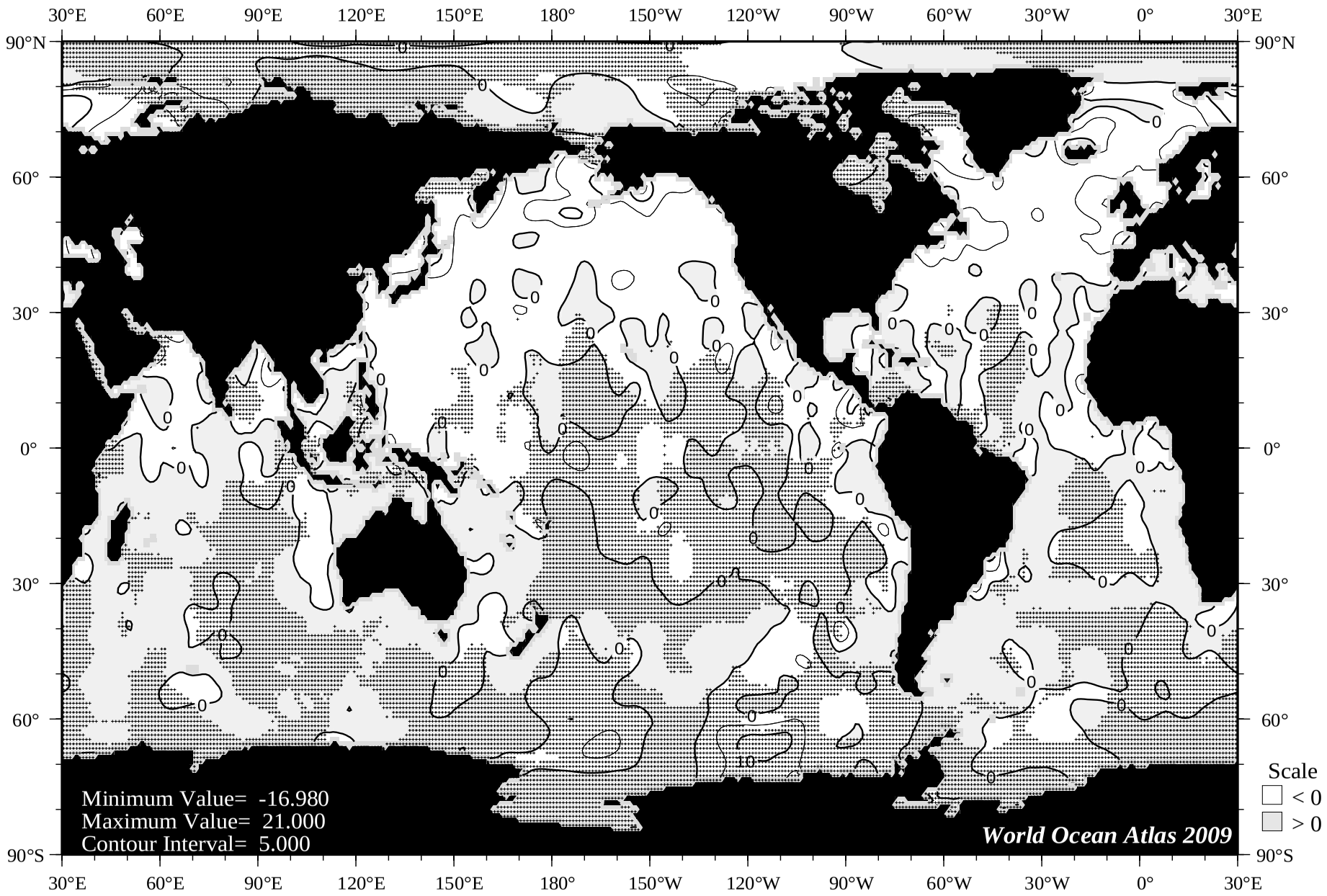

Fig I18 May minus annual percent oxygen saturation at the surface.

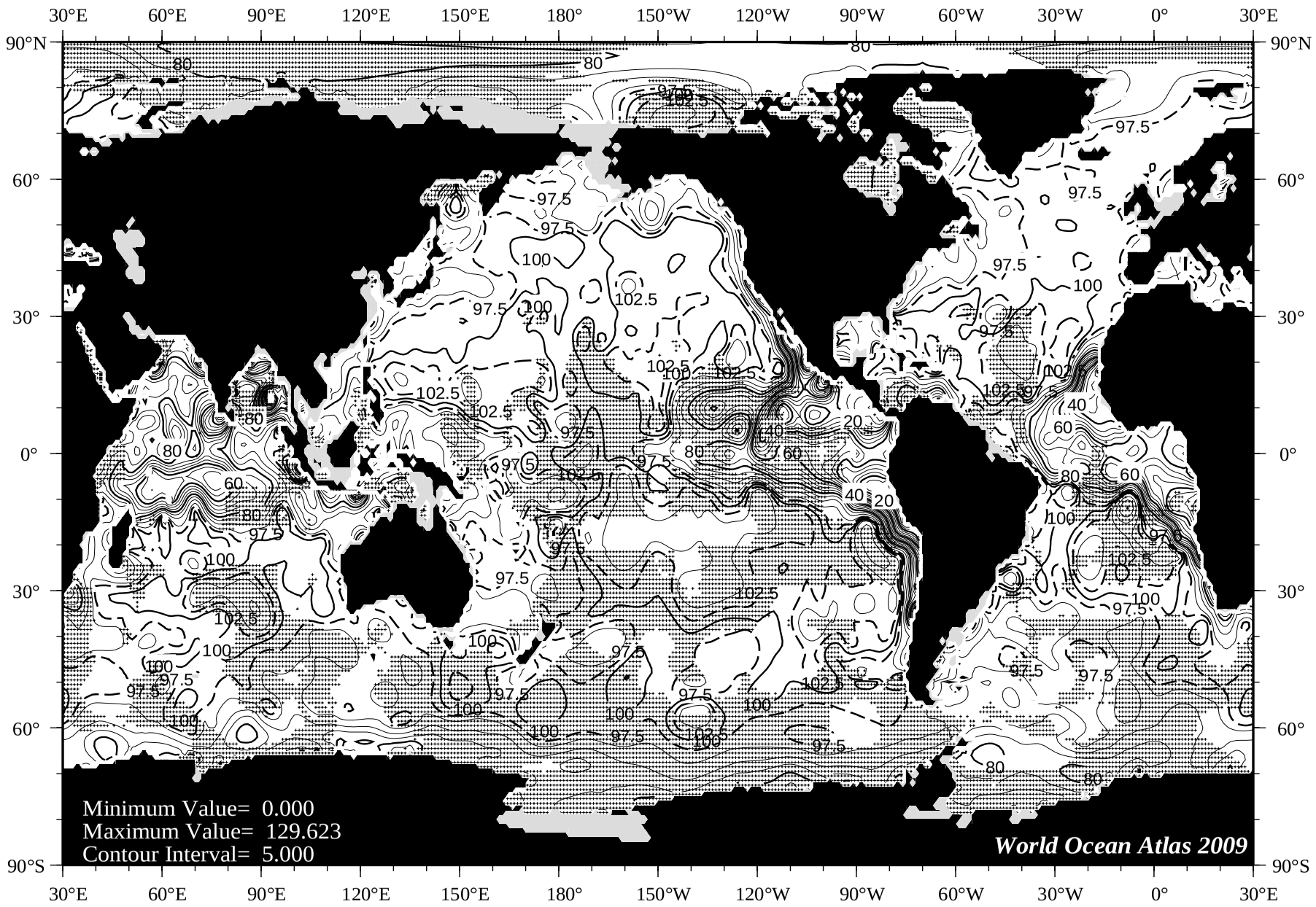

Fig I19 May mean percent oxygen saturation at 75 m. depth.

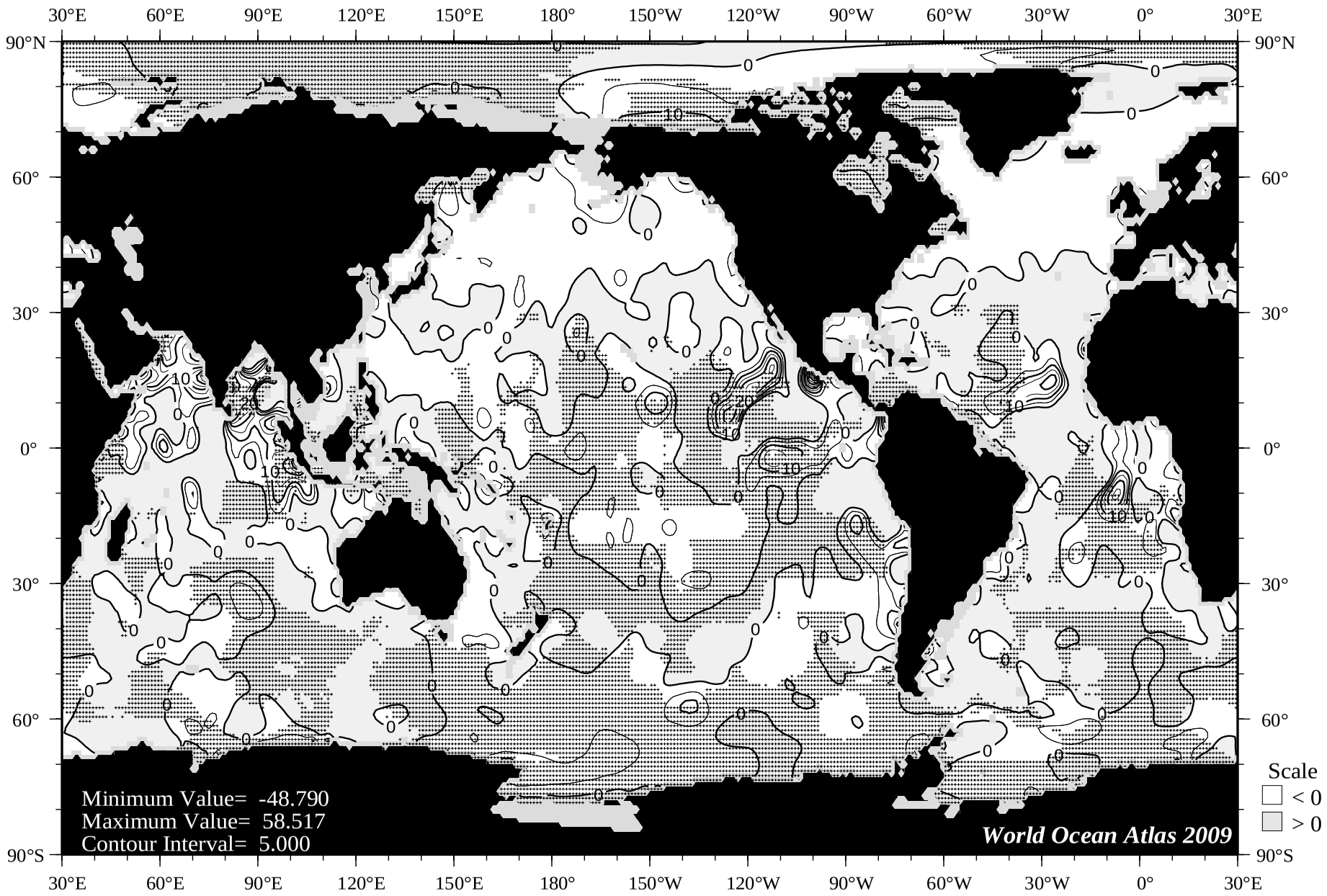

Fig I20 May minus annual percent oxygen saturation at 75 m. depth.

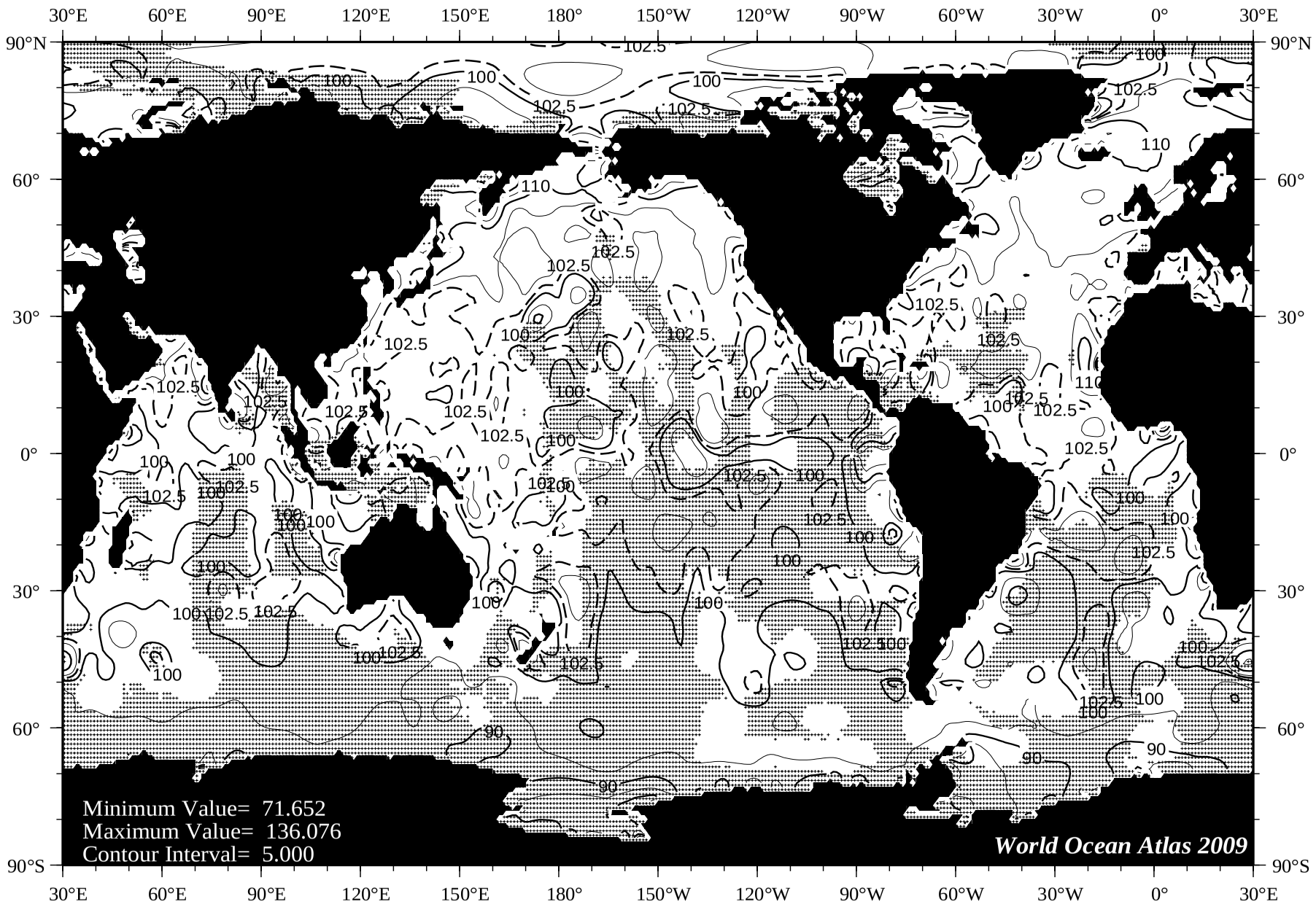

Fig I21 June mean percent oxygen saturation at the surface.

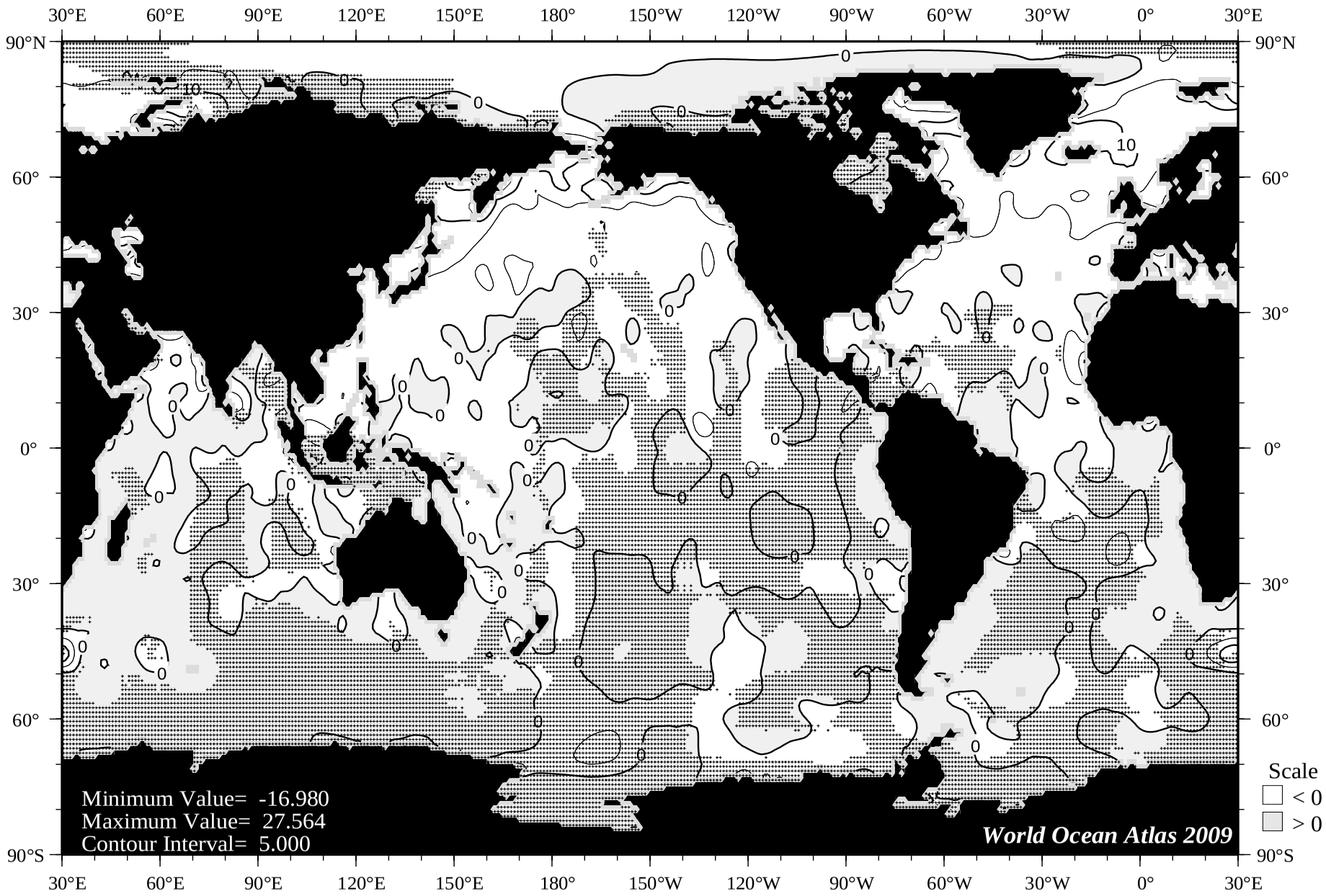

Fig I22 June minus annual percent oxygen saturation at the surface.

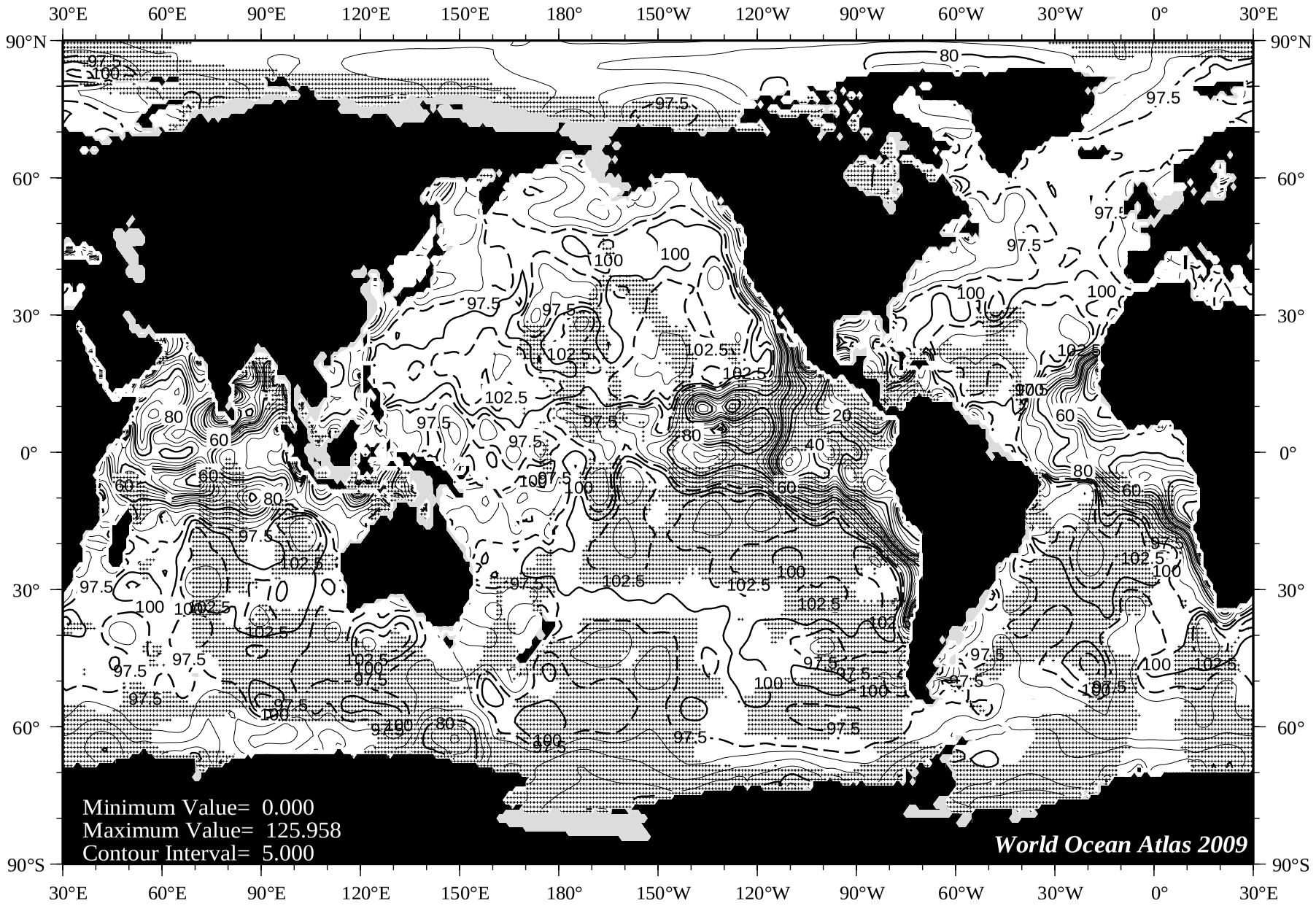

Fig I23 June mean percent oxygen saturation at 75 m. depth.

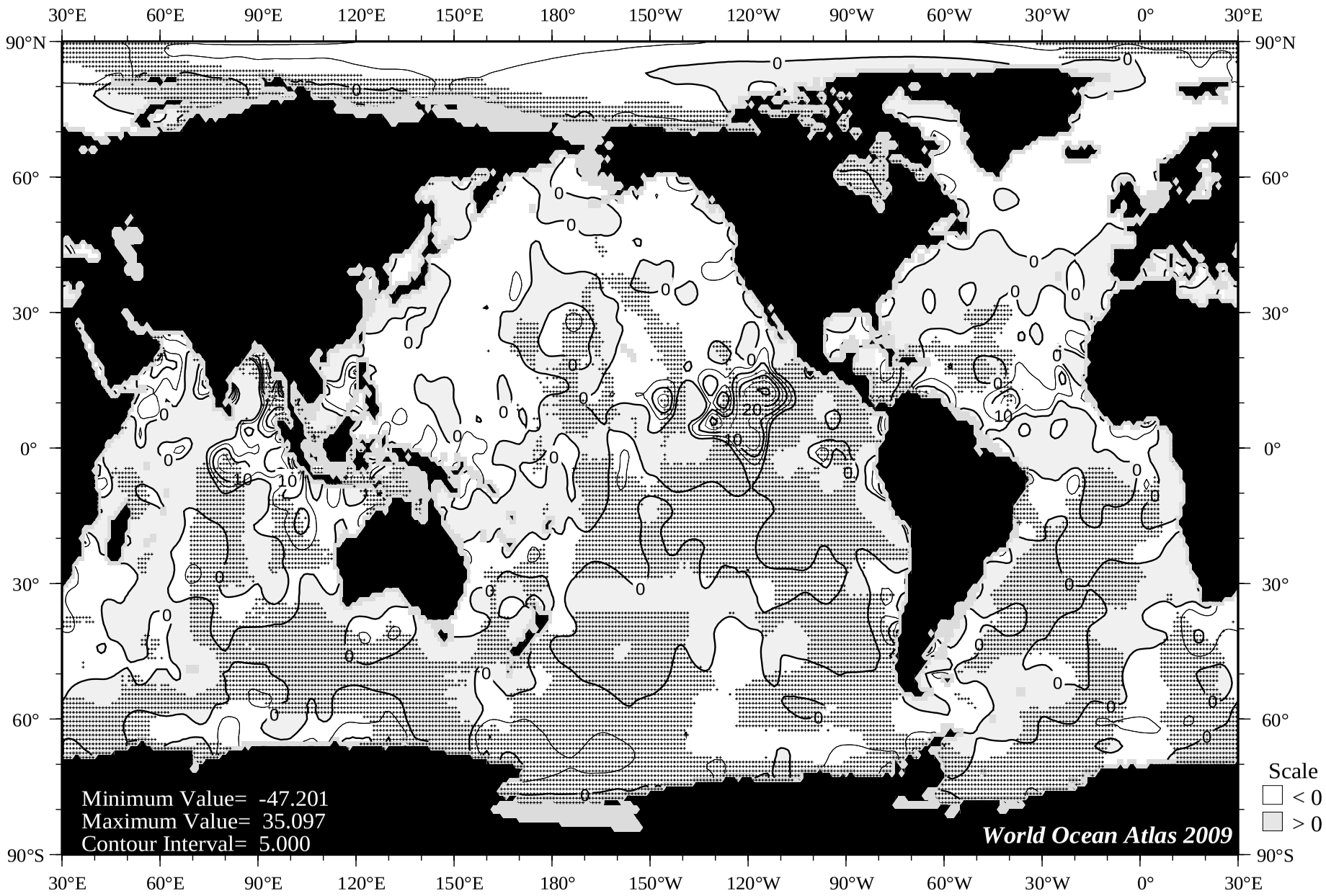

Fig I24 June minus annual percent oxygen saturation at 75 m. depth.

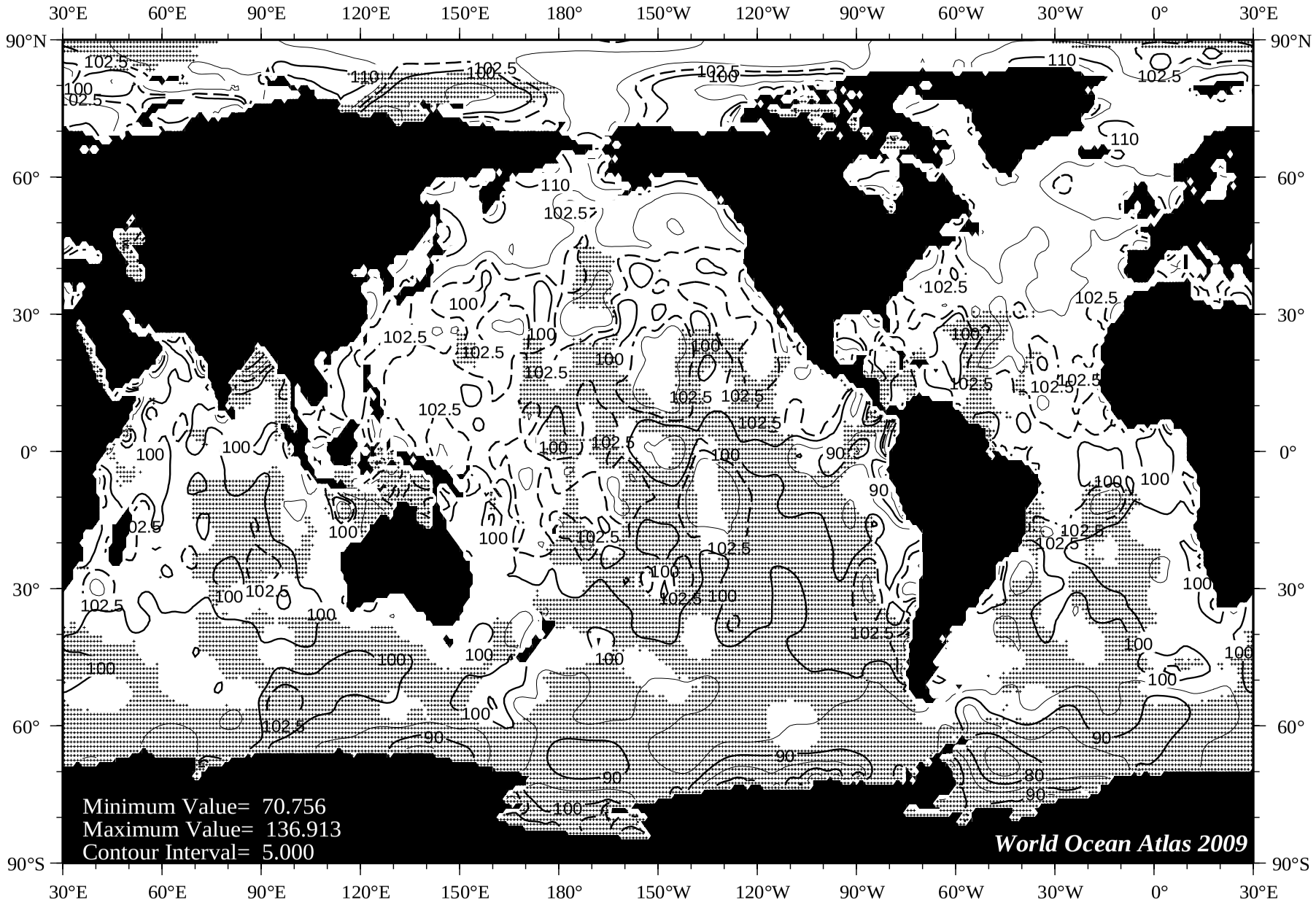

Fig I25 July mean percent oxygen saturation at the surface.

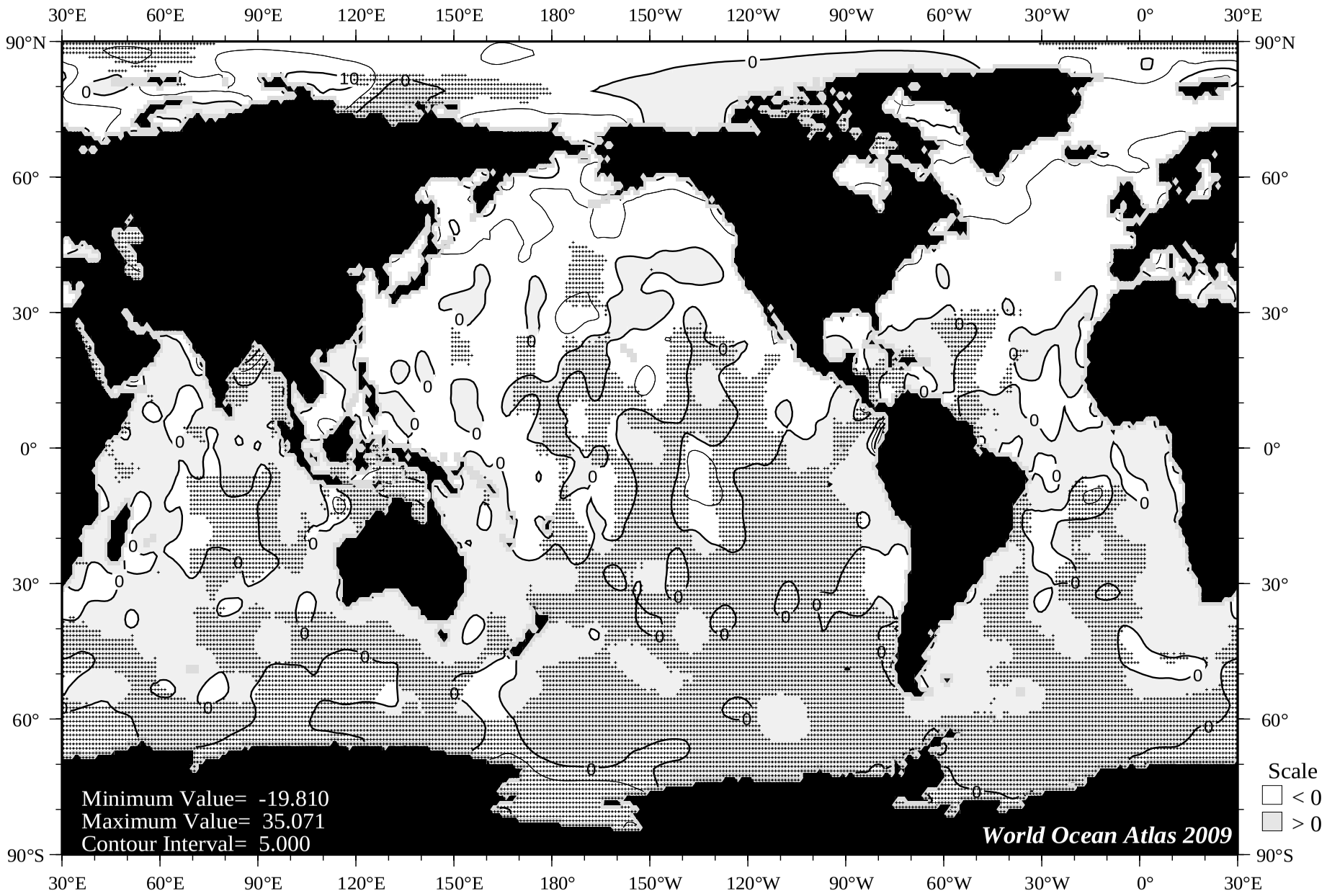

Fig I26 July minus annual percent oxygen saturation at the surface.

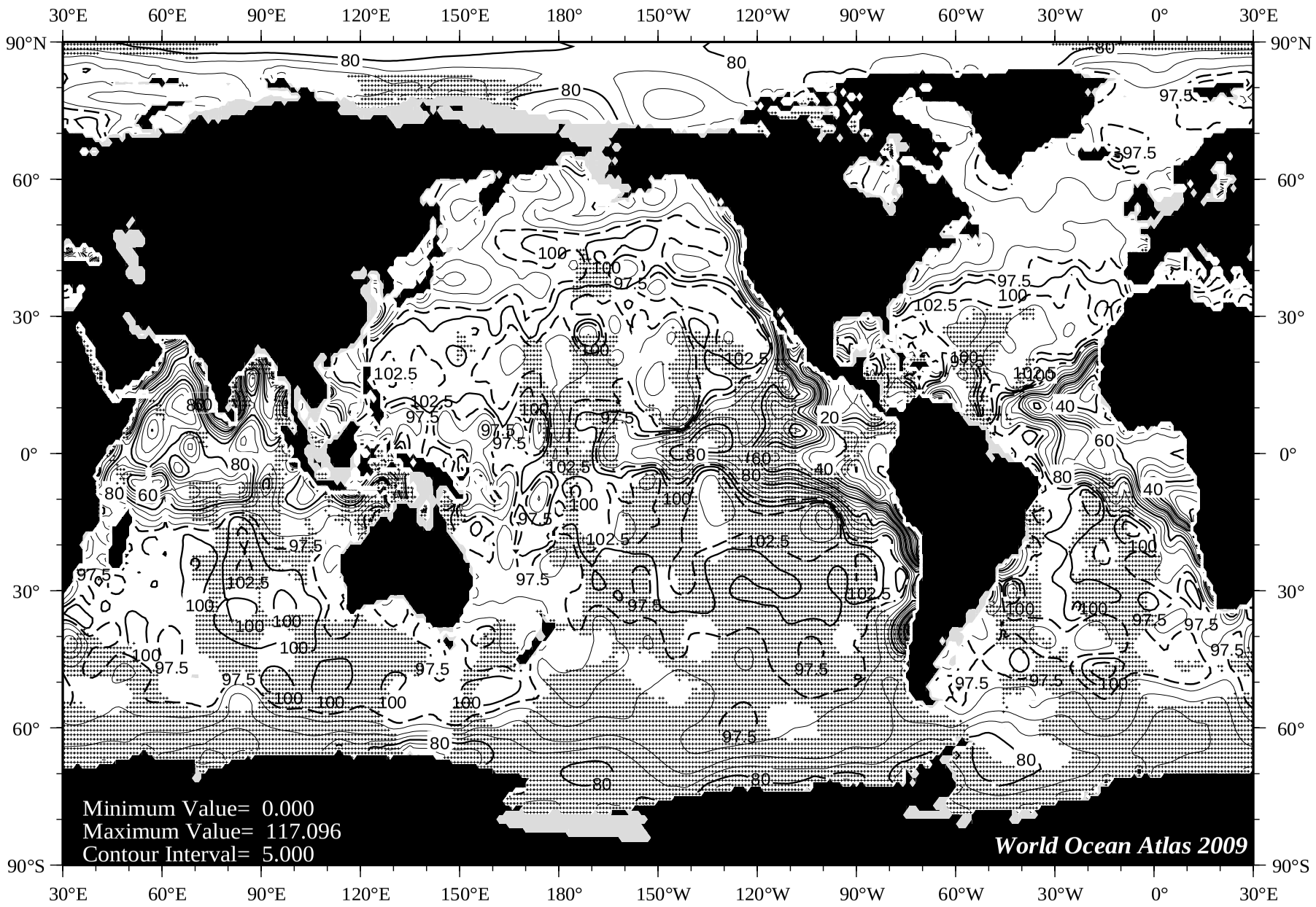

Fig I27 July mean percent oxygen saturation at 75 m. depth.

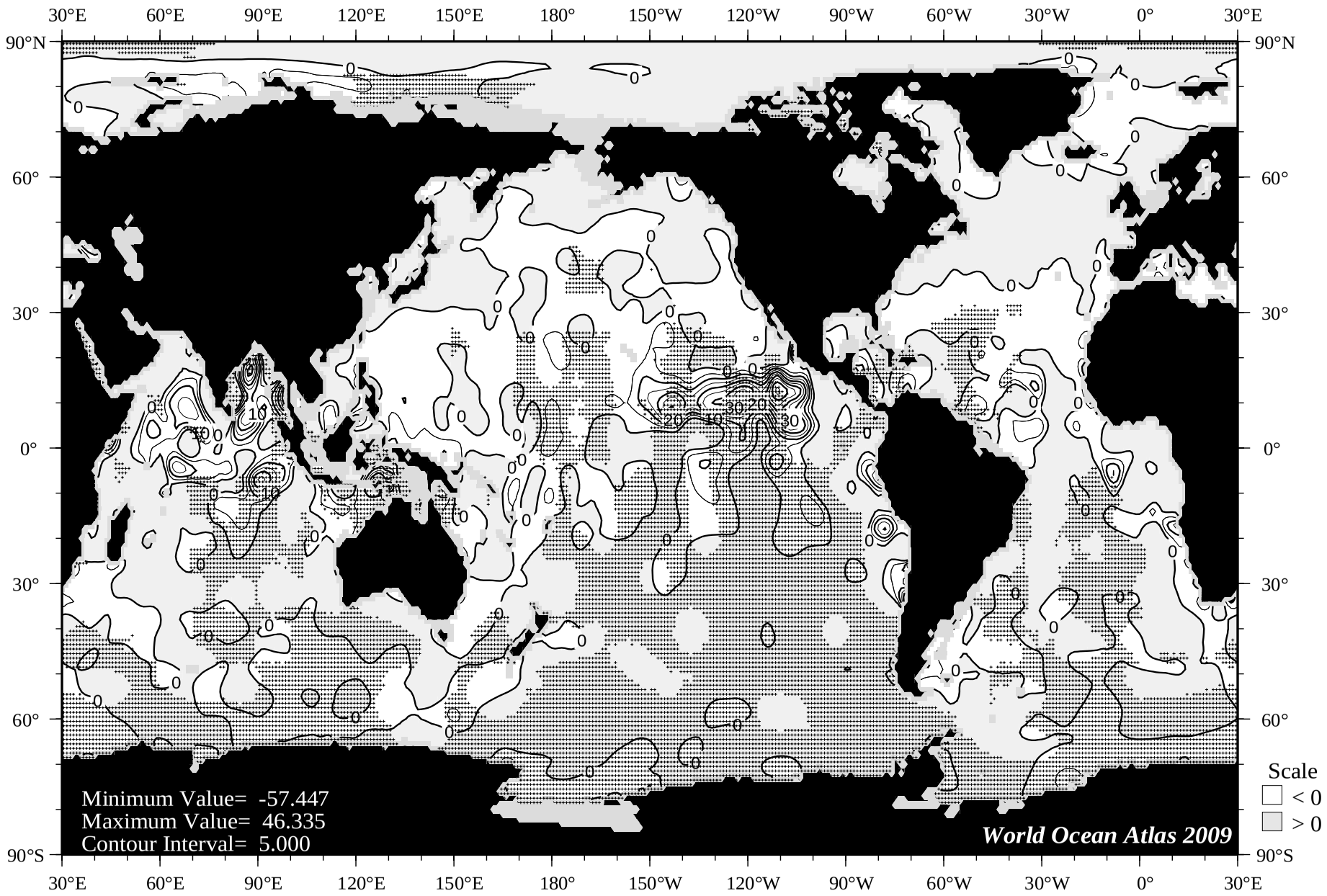

Fig I28 July minus annual percent oxygen saturation at 75 m. depth.

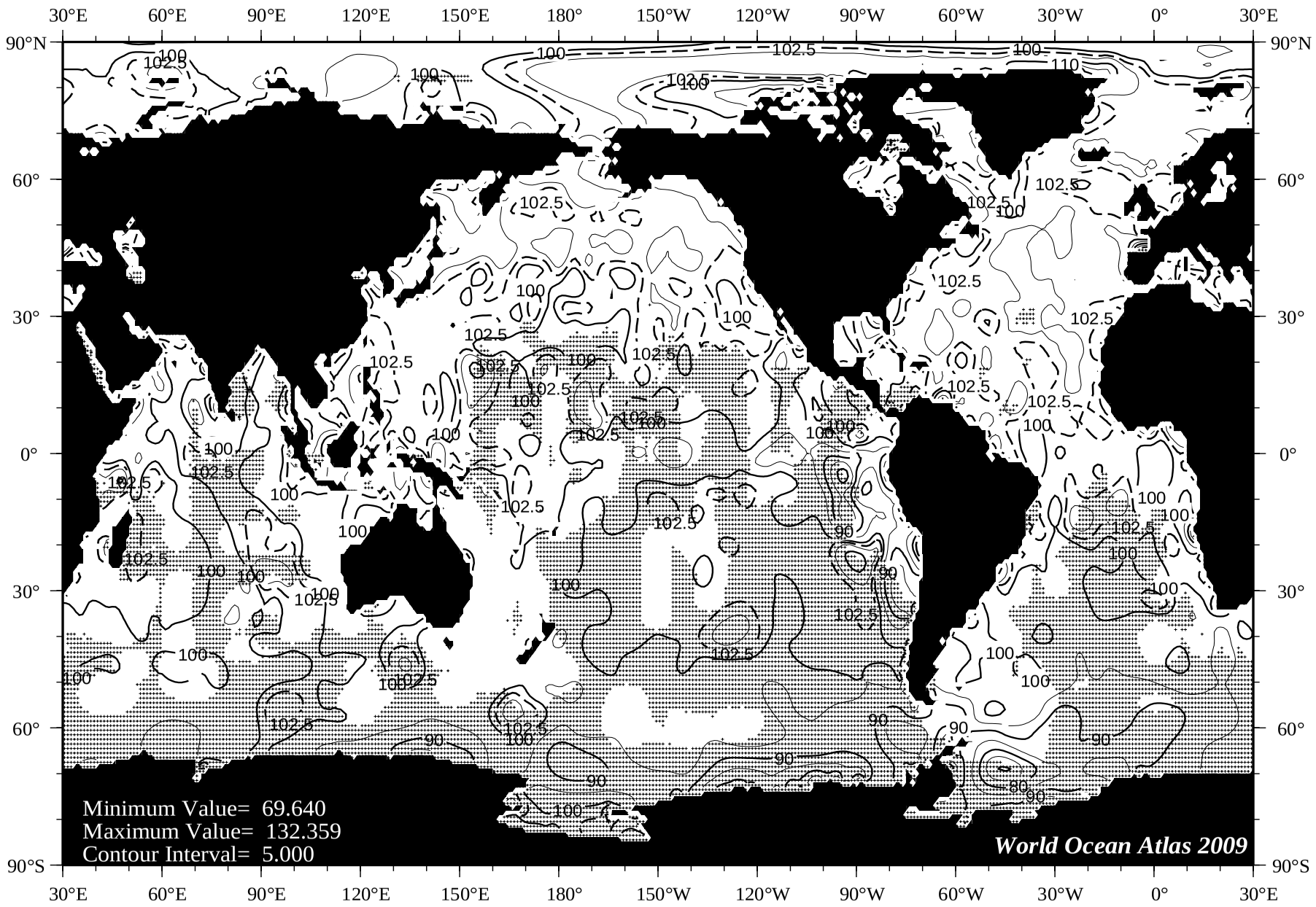

Fig I29 August mean percent oxygen saturation at the surface.

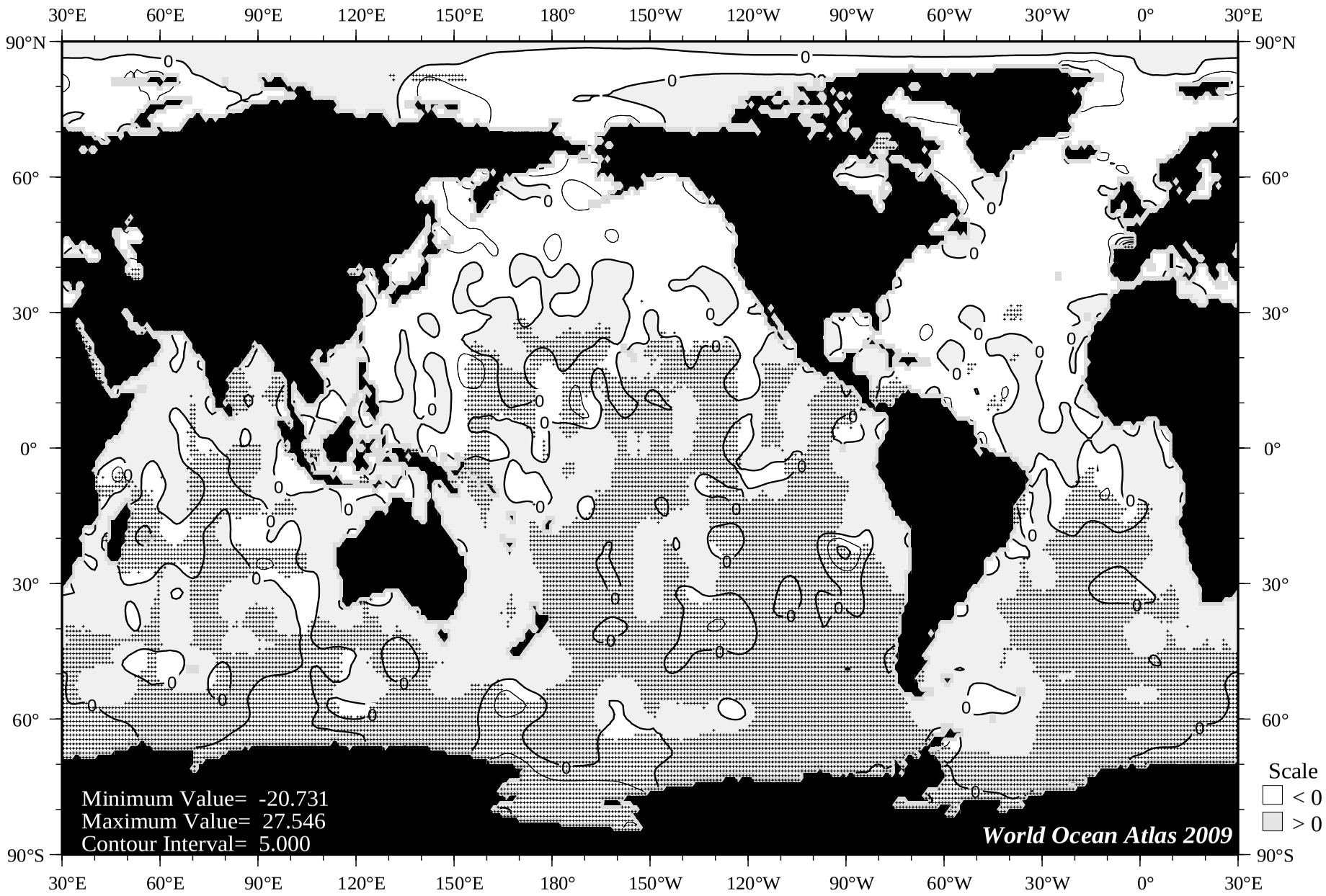

Fig I30 August minus annual percent oxygen saturation at the surface.

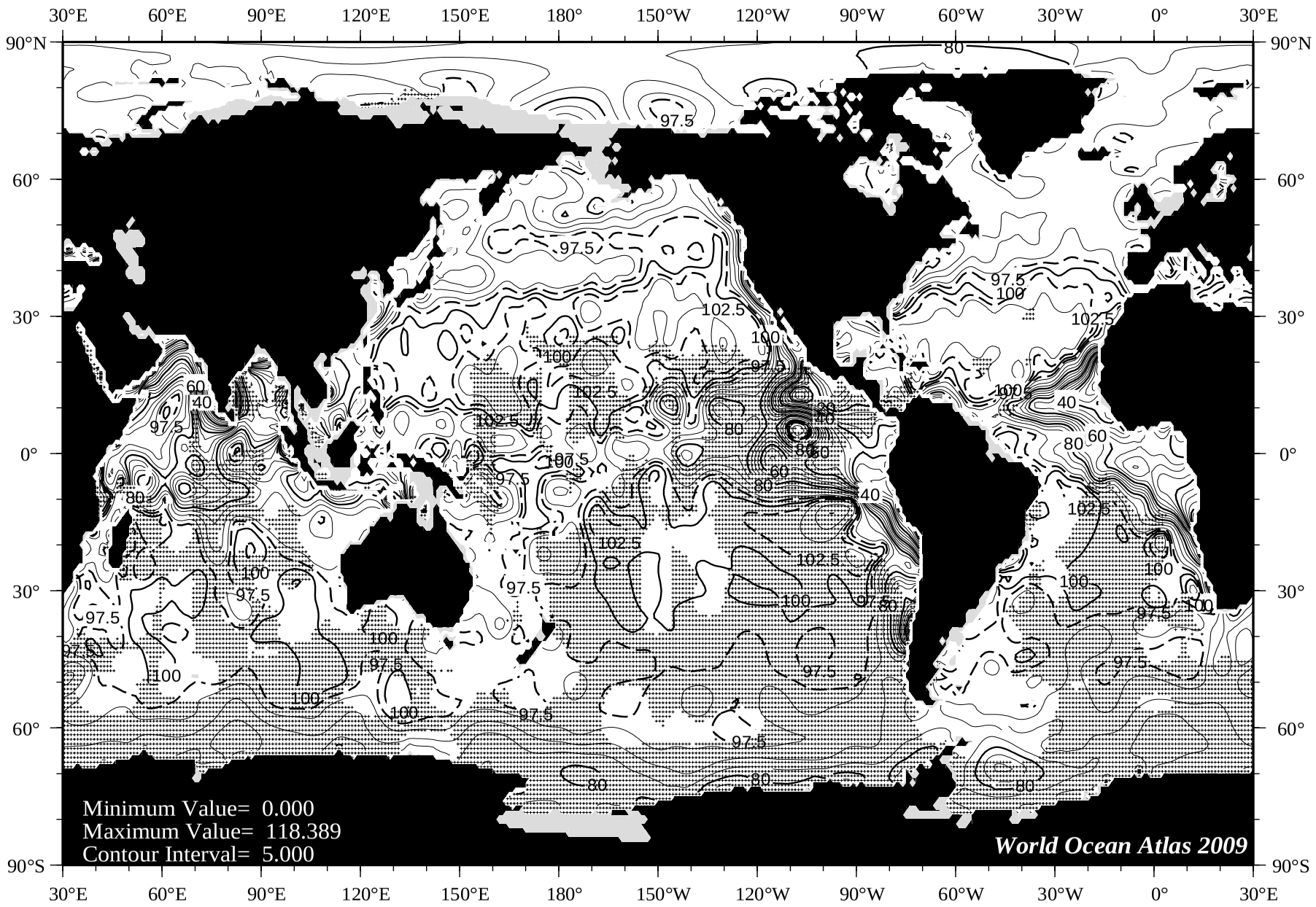

Fig I31 August mean percent oxygen saturation at 75 m. depth.

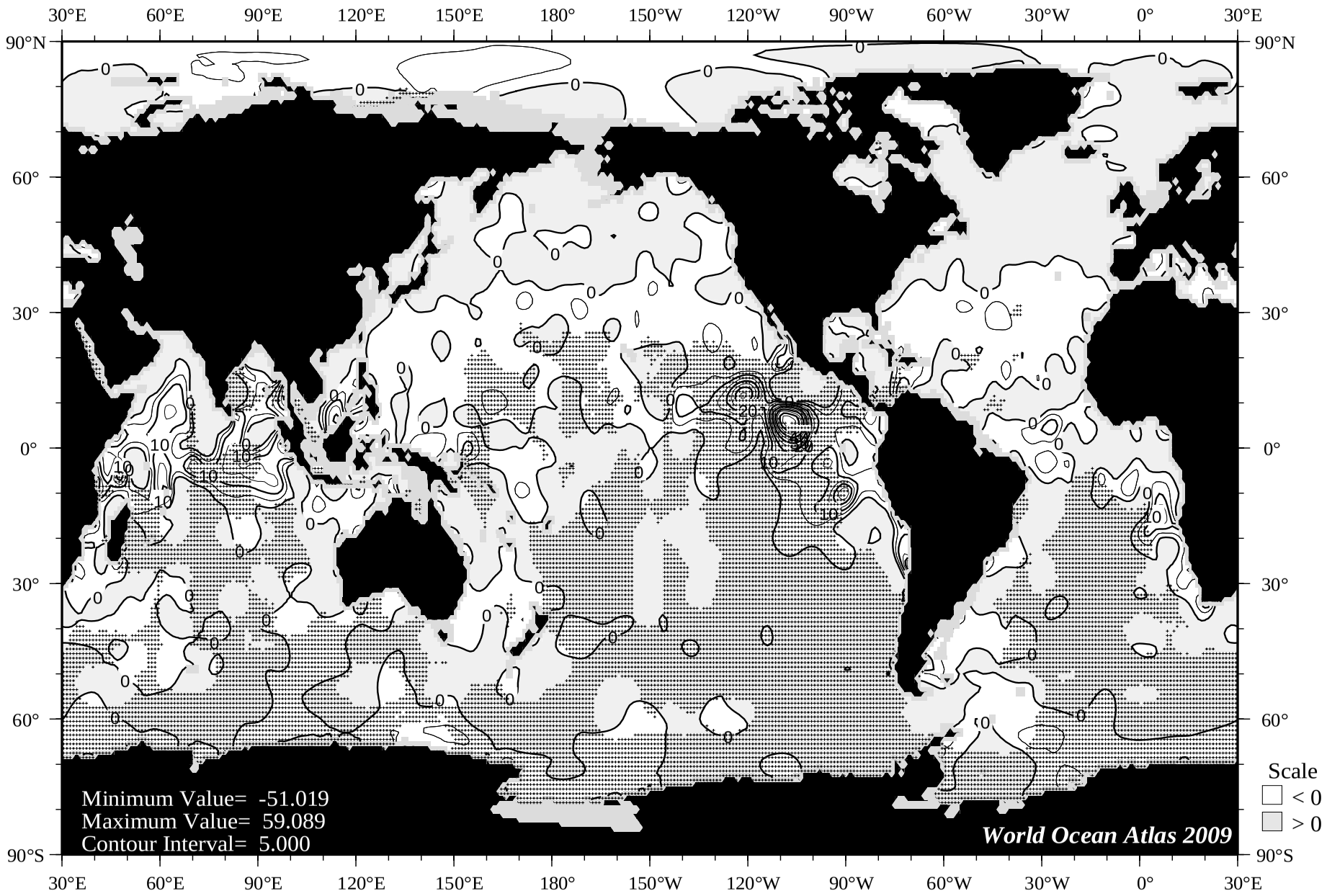

Fig I32 August minus annual percent oxygen saturation at 75 m. depth.

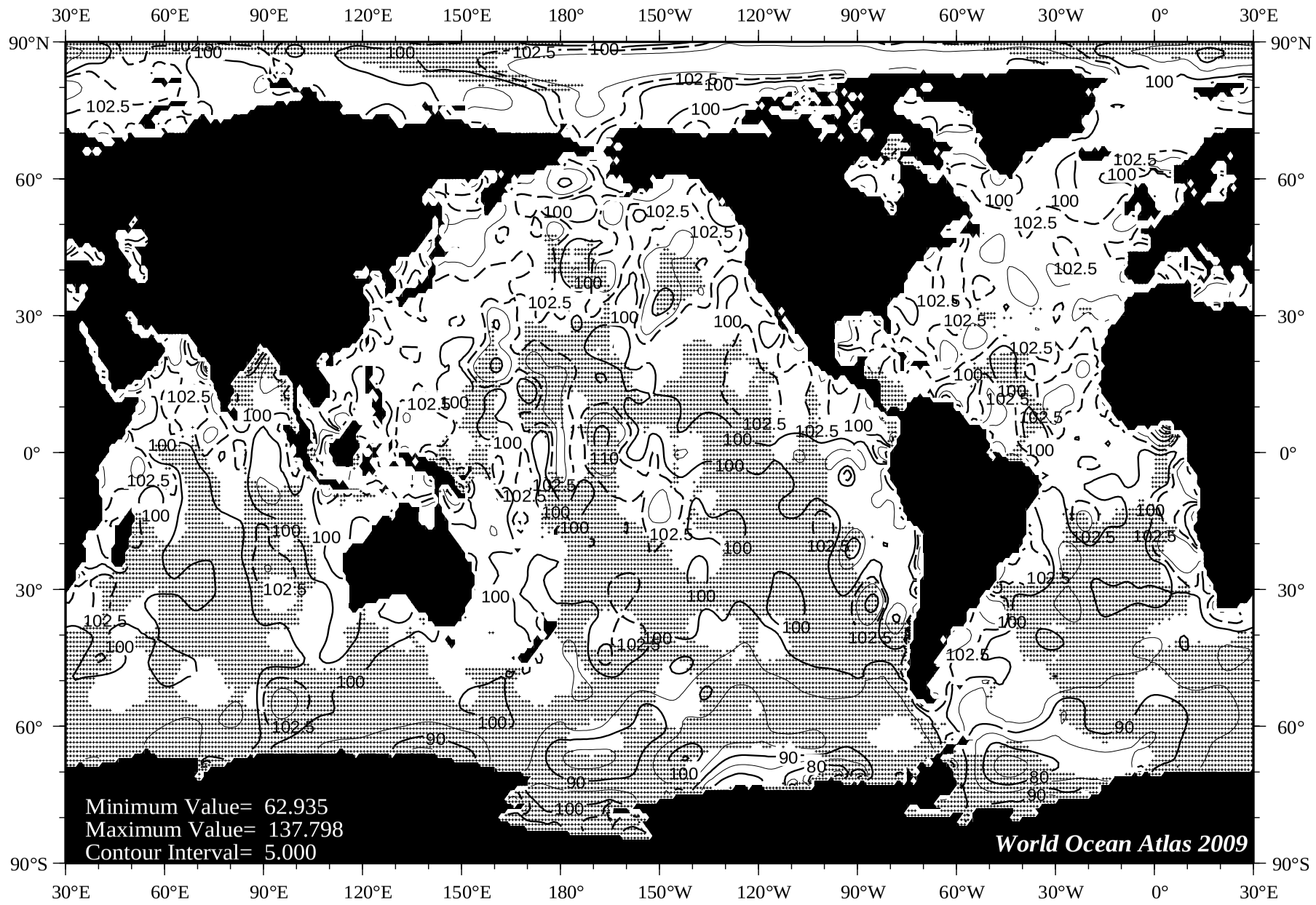

Fig I33 September mean percent oxygen saturation at the surface.

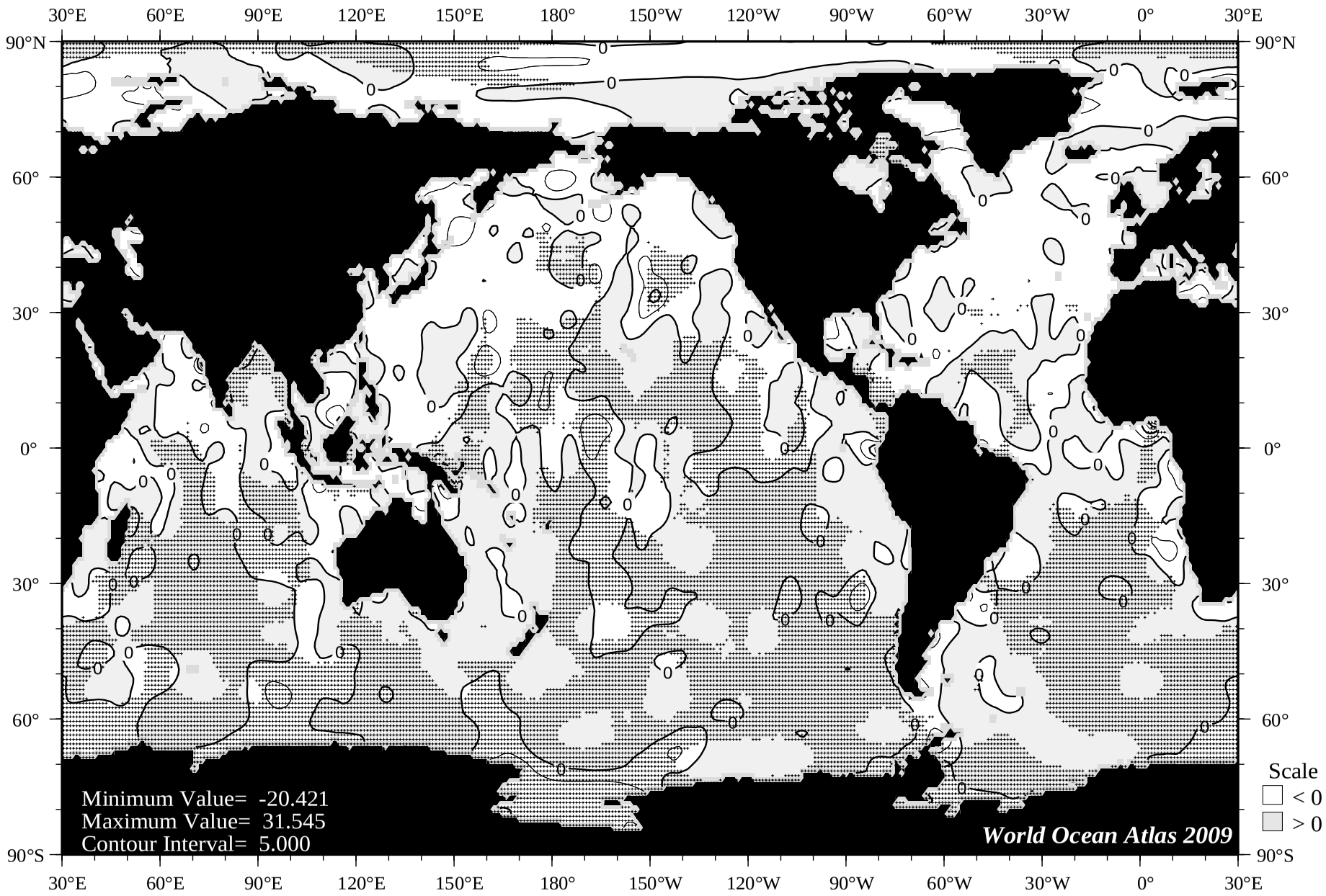

Fig I34 September minus annual percent oxygen saturation at the surface.

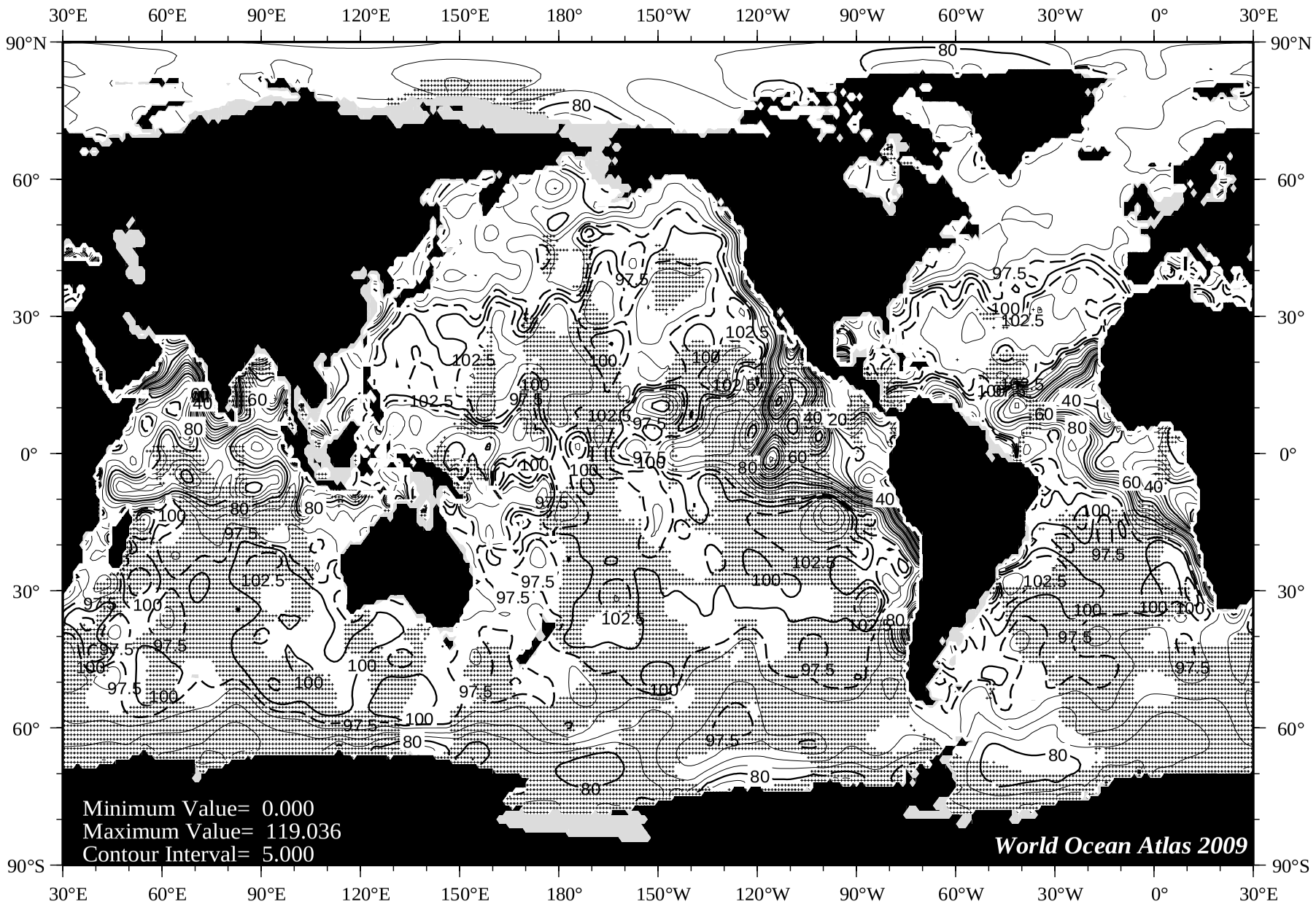

Fig I35 September mean percent oxygen saturation at 75 m. depth.

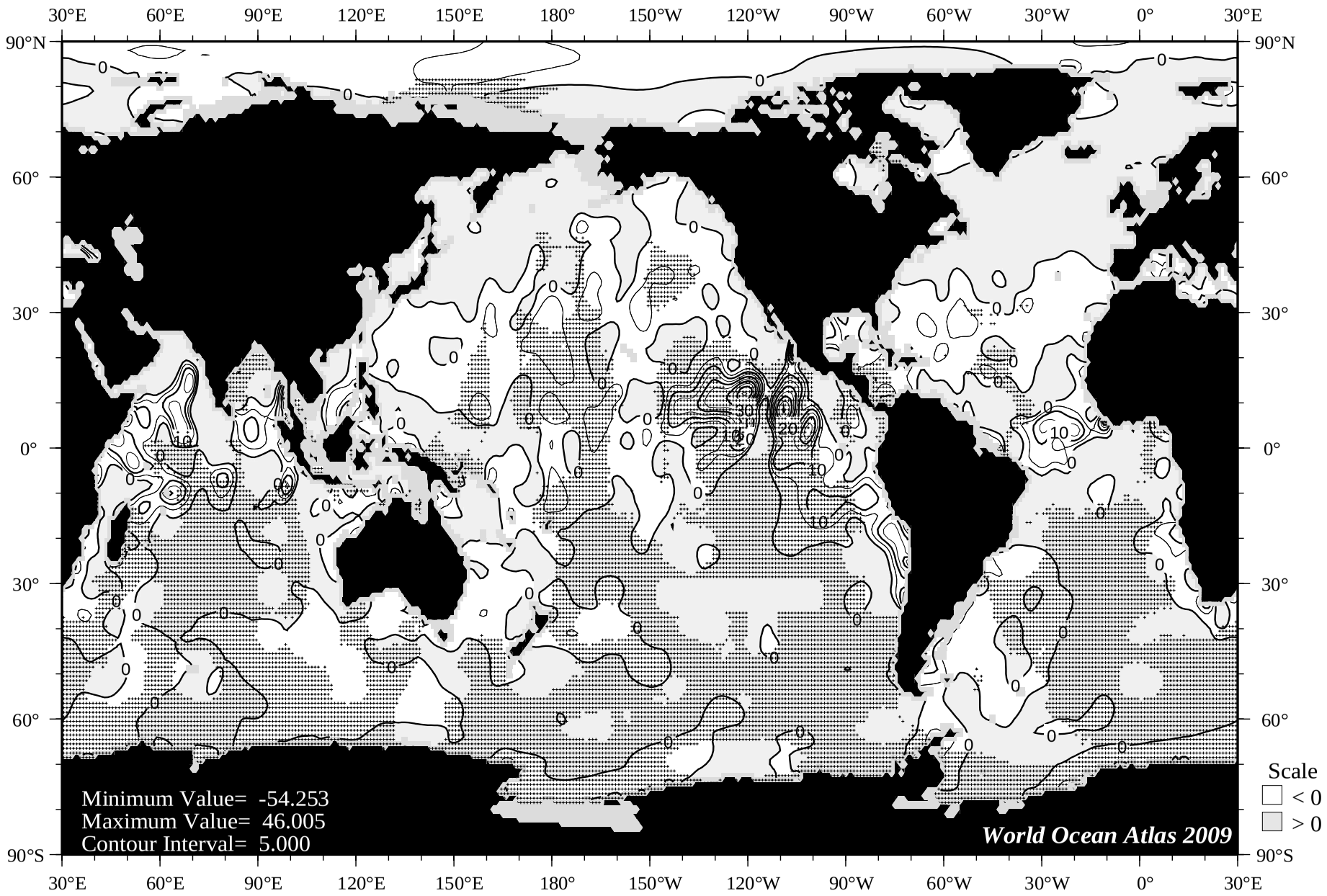

Fig I36 September minus annual percent oxygen saturation at 75 m. depth.

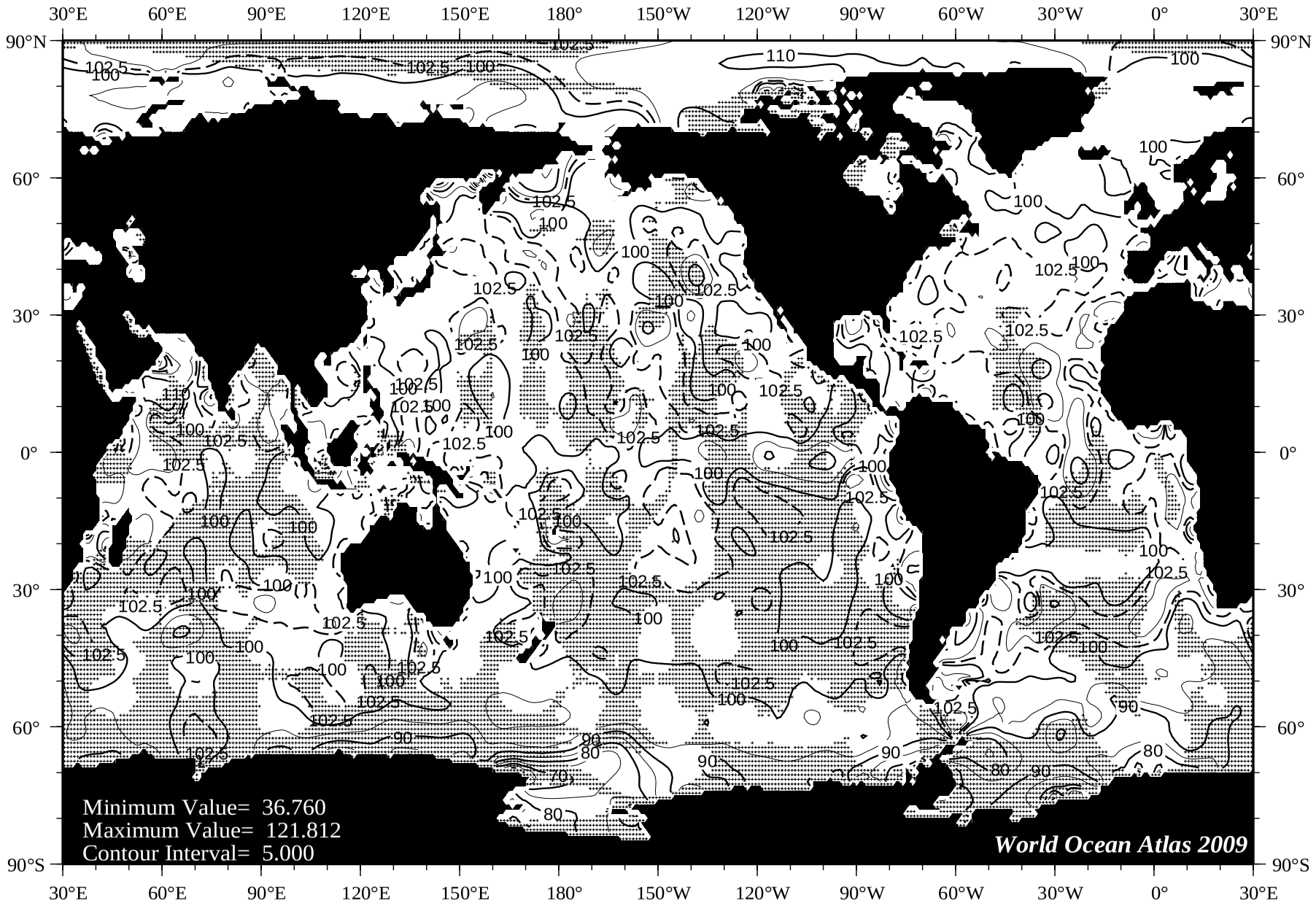

Fig I37 October mean percent oxygen saturation at the surface.

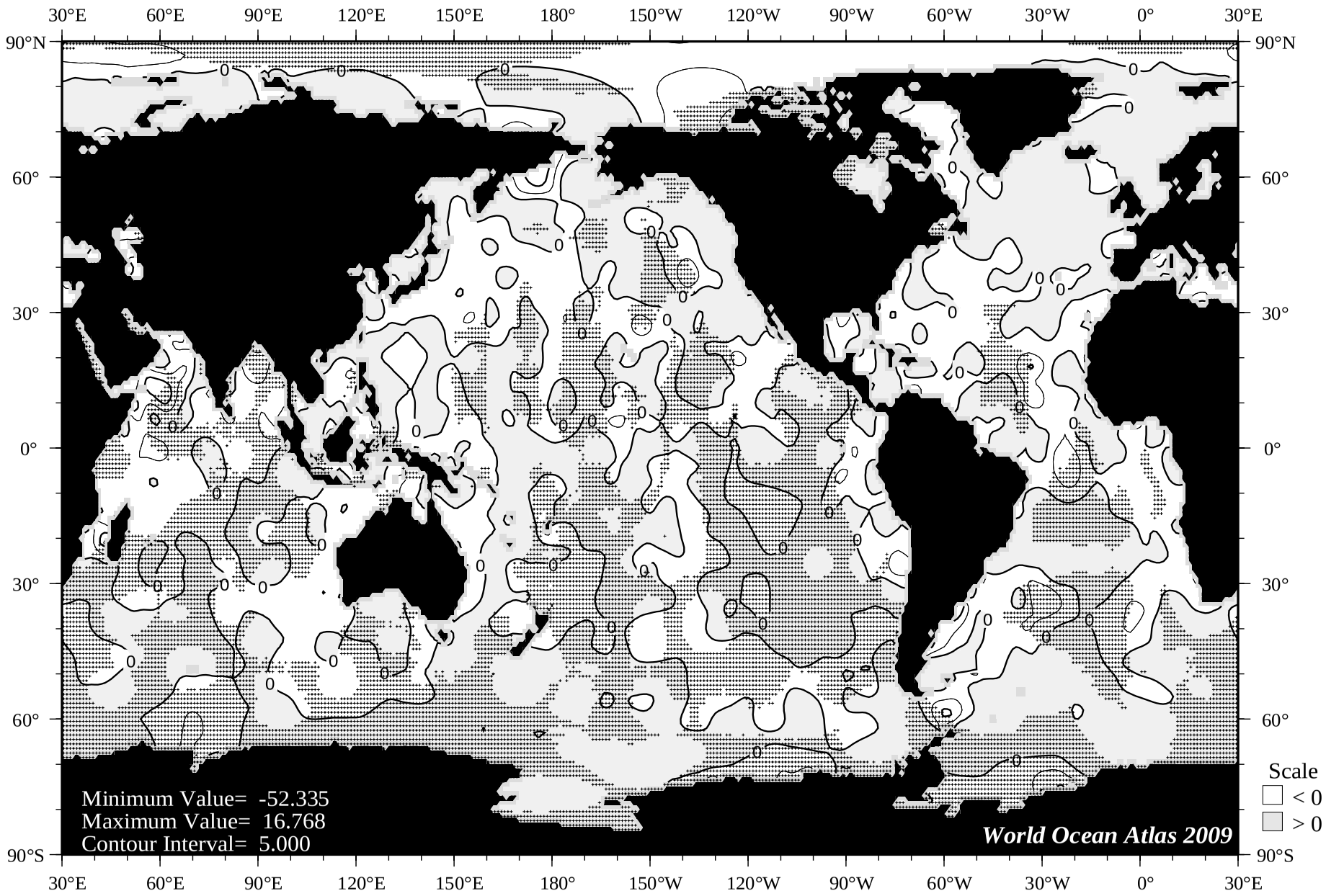

Fig I38 October minus annual percent oxygen saturation at the surface.

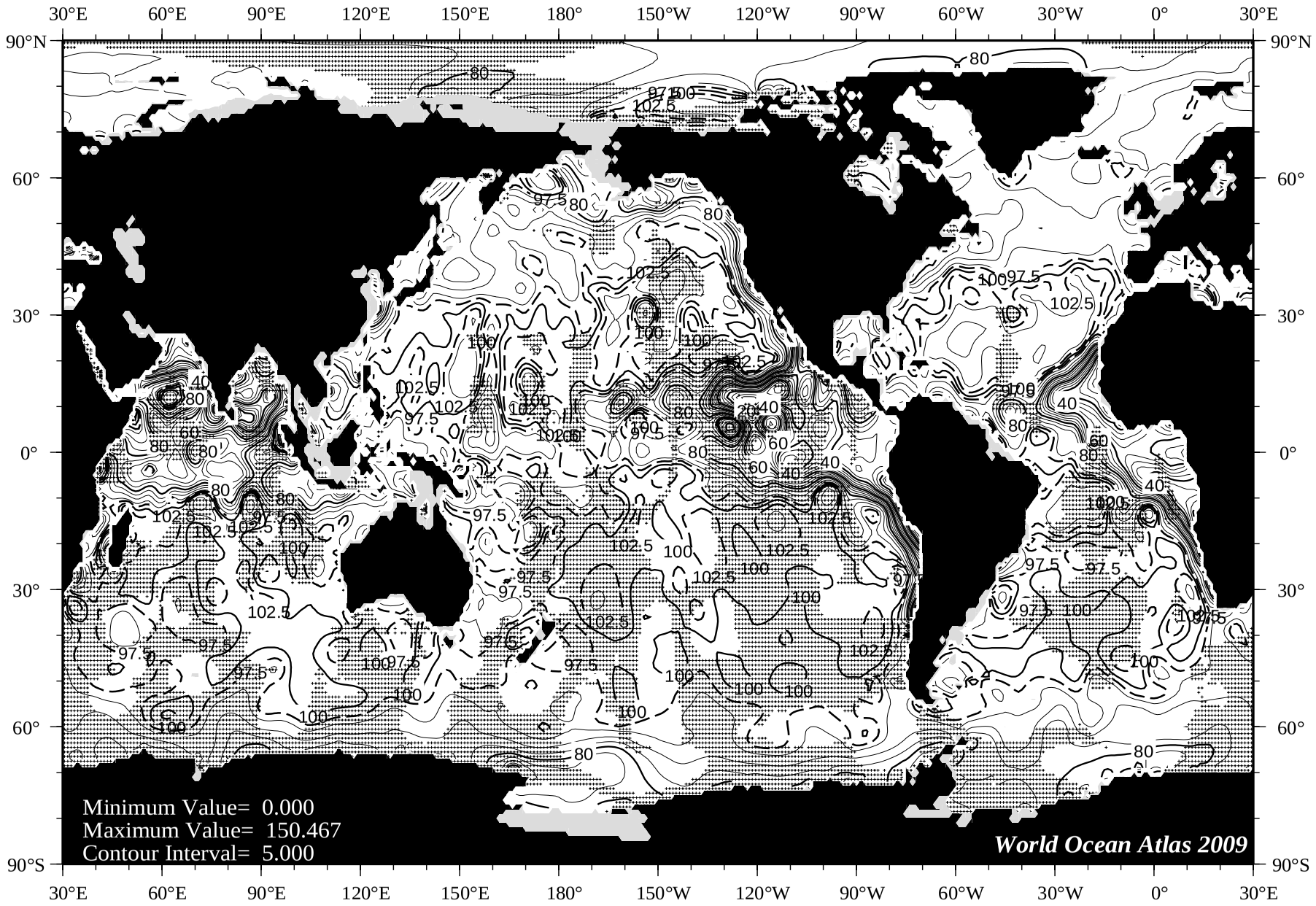

Fig I39 October mean percent oxygen saturation at 75 m. depth.

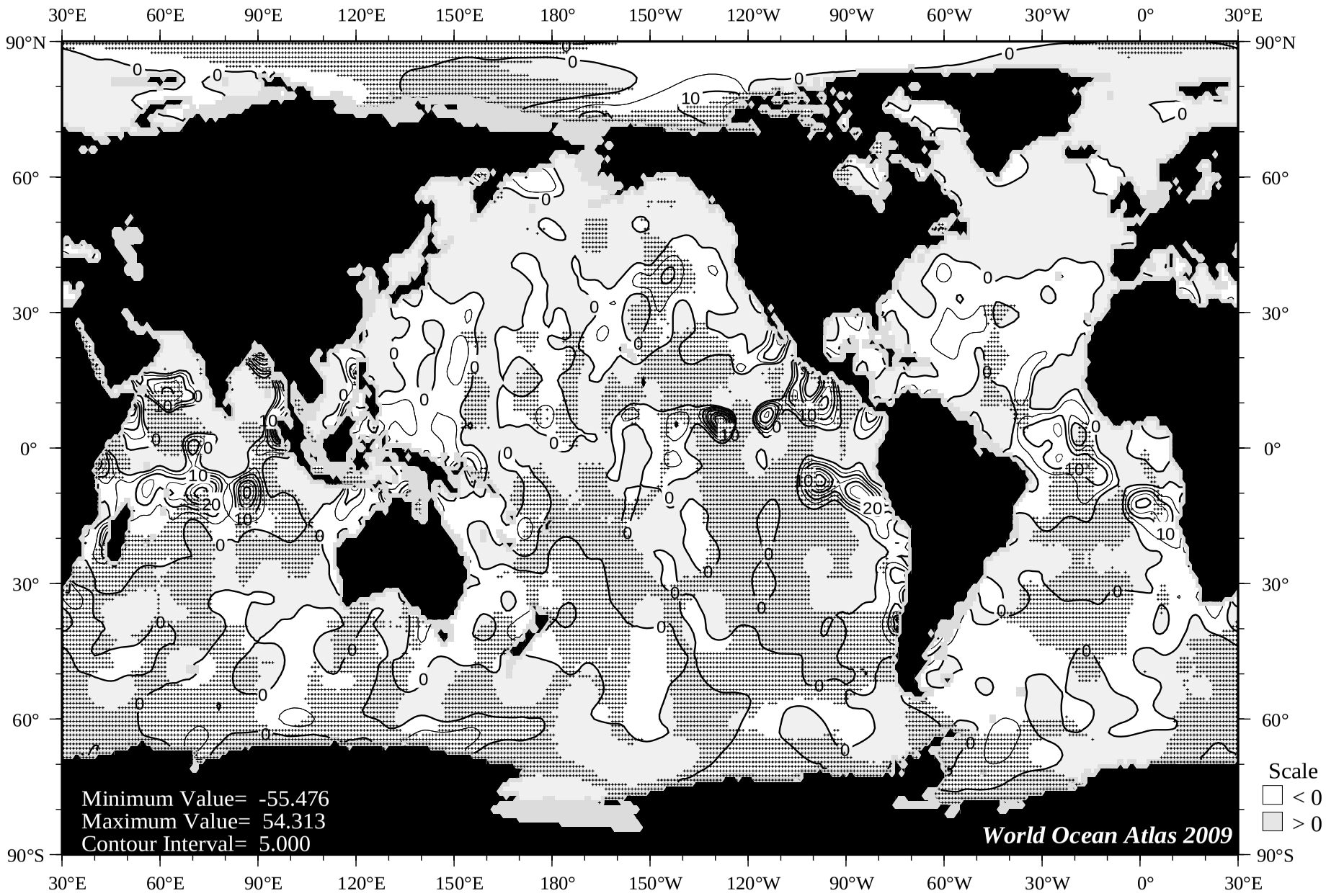

Fig I40 October minus annual percent oxygen saturation at 75 m. depth.

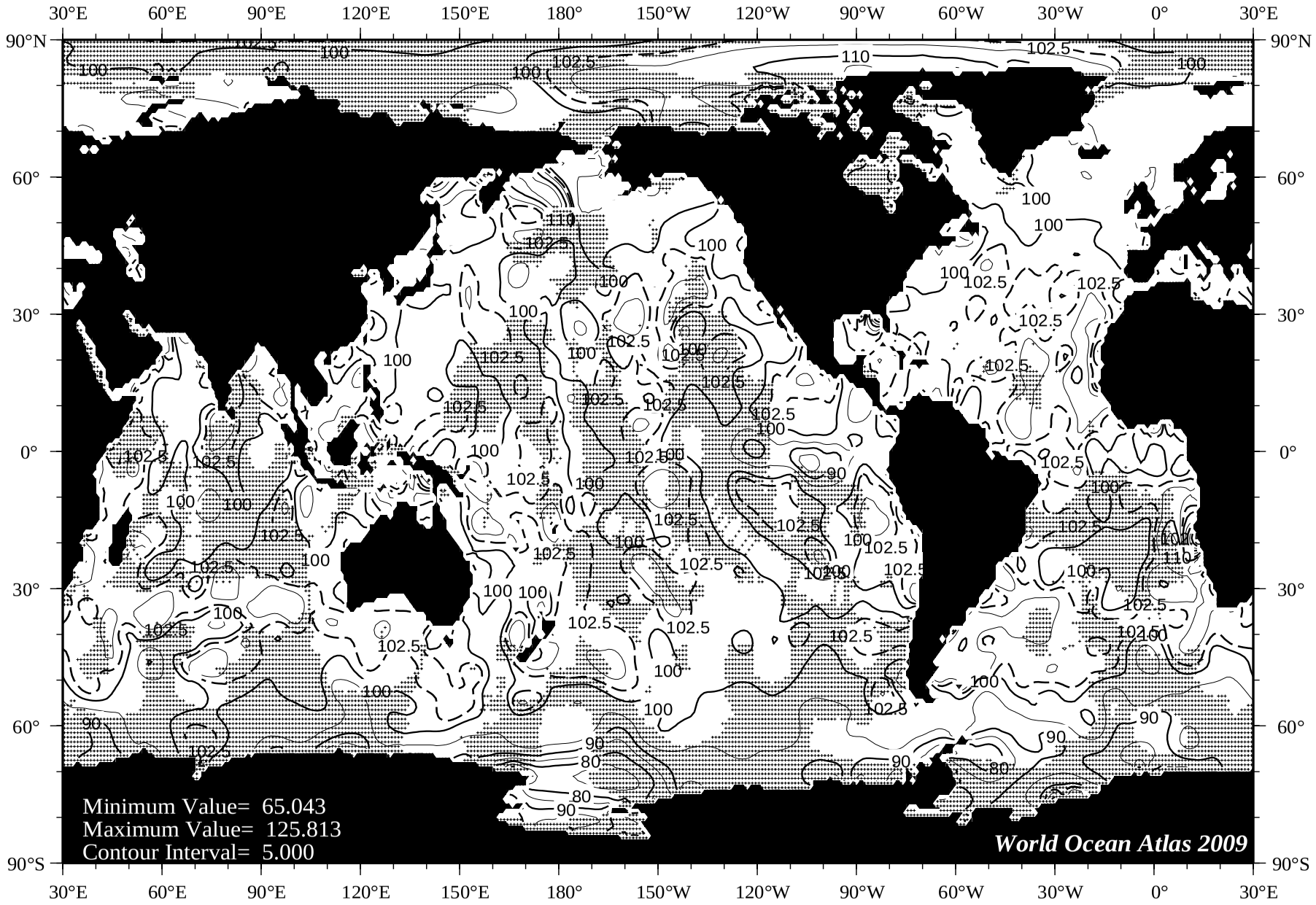

Fig I41 November mean percent oxygen saturation at the surface.

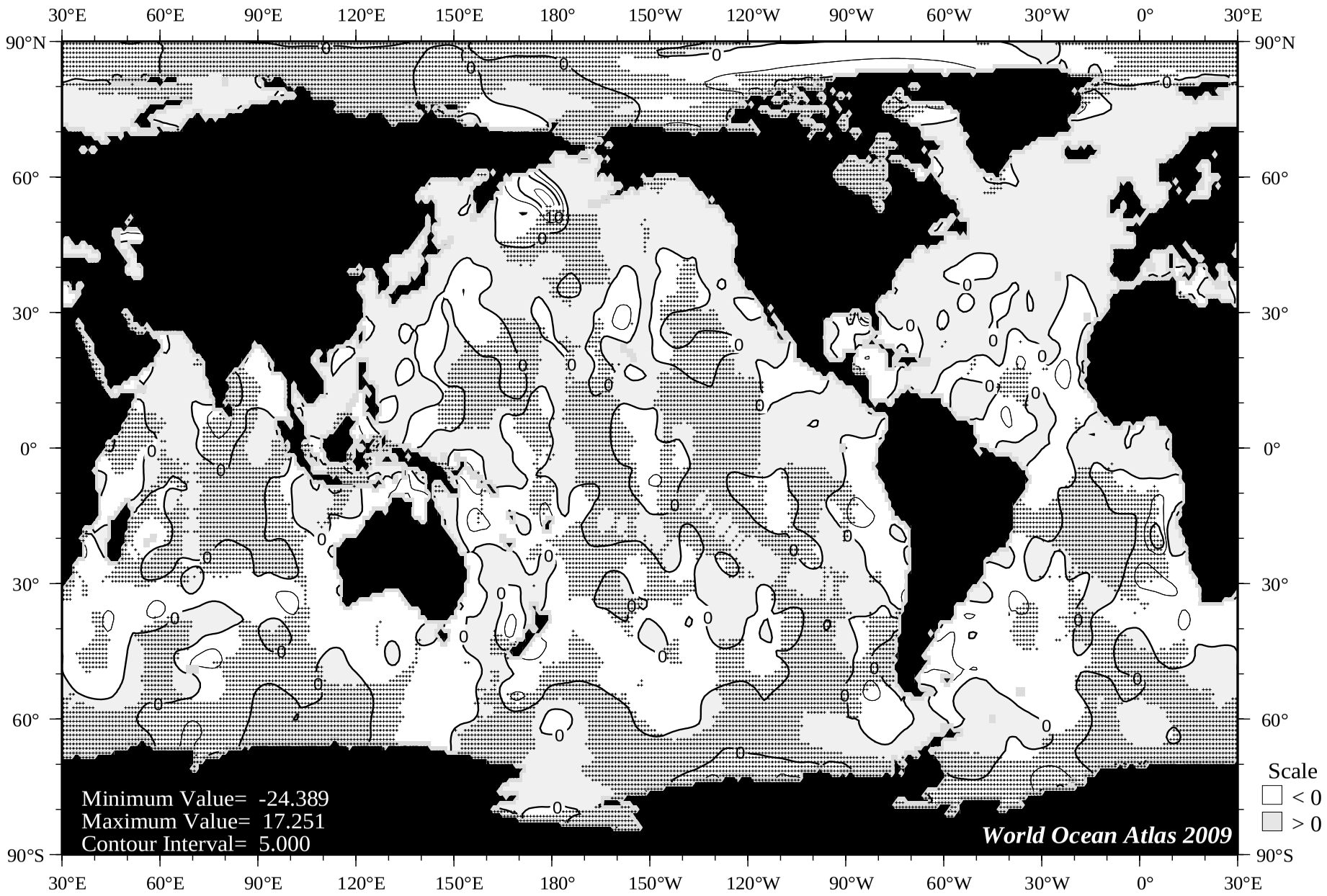

Fig I42 November minus annual percent oxygen saturation at the surface.

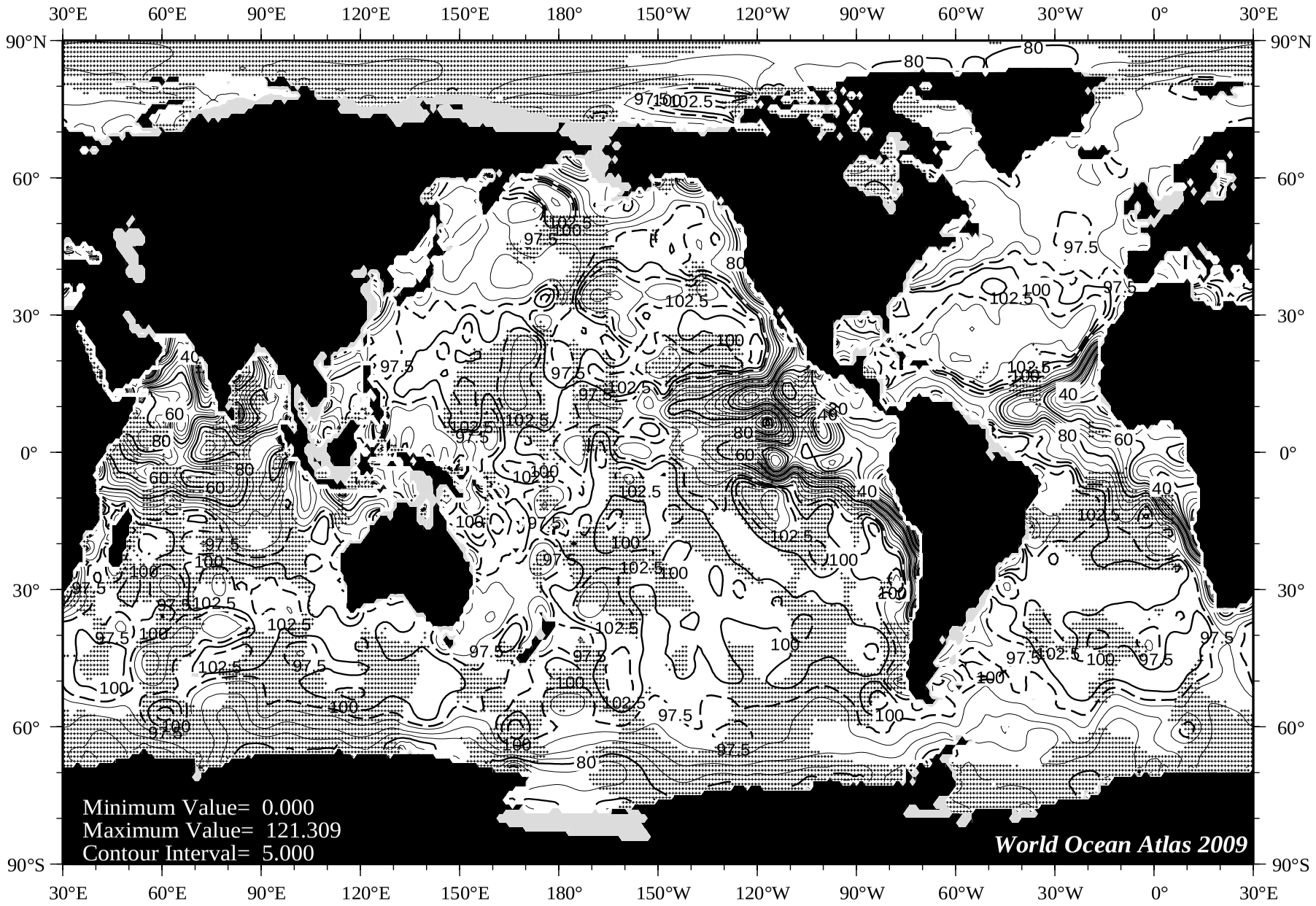

Fig I43 November mean percent oxygen saturation at 75 m. depth.

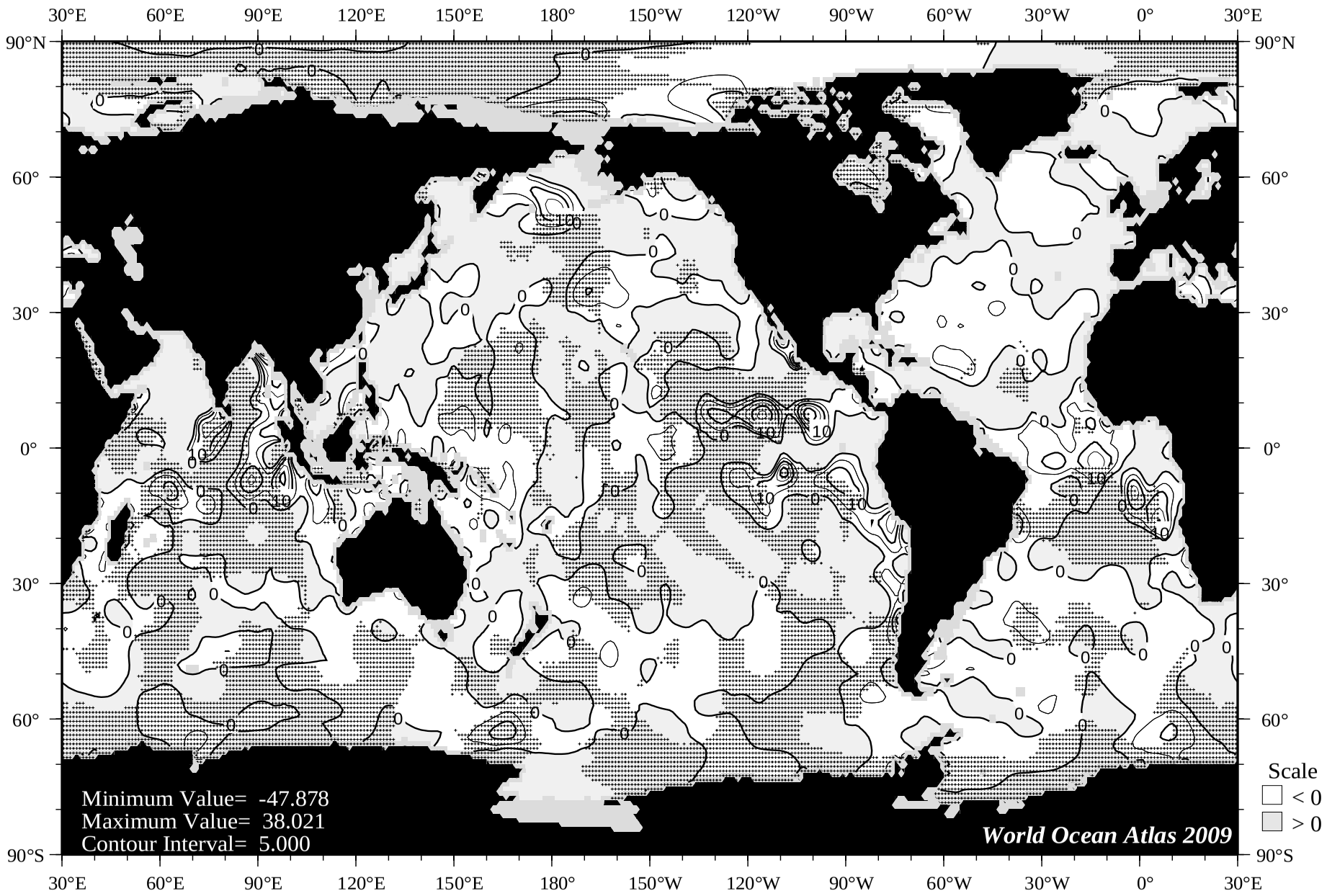

Fig I44 November minus annual percent oxygen saturation at 75 m. depth.

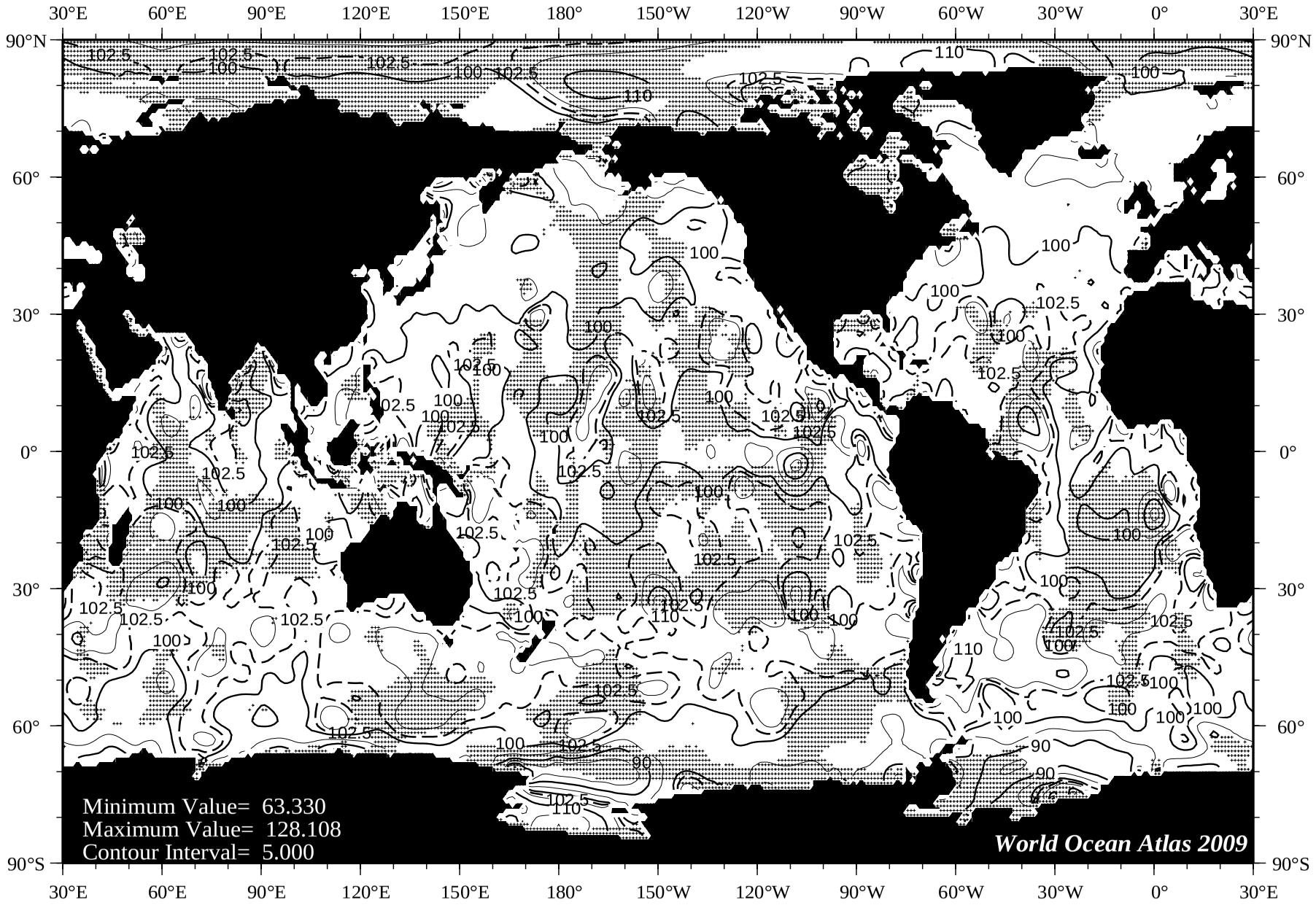

Fig I45 December mean percent oxygen saturation at the surface.

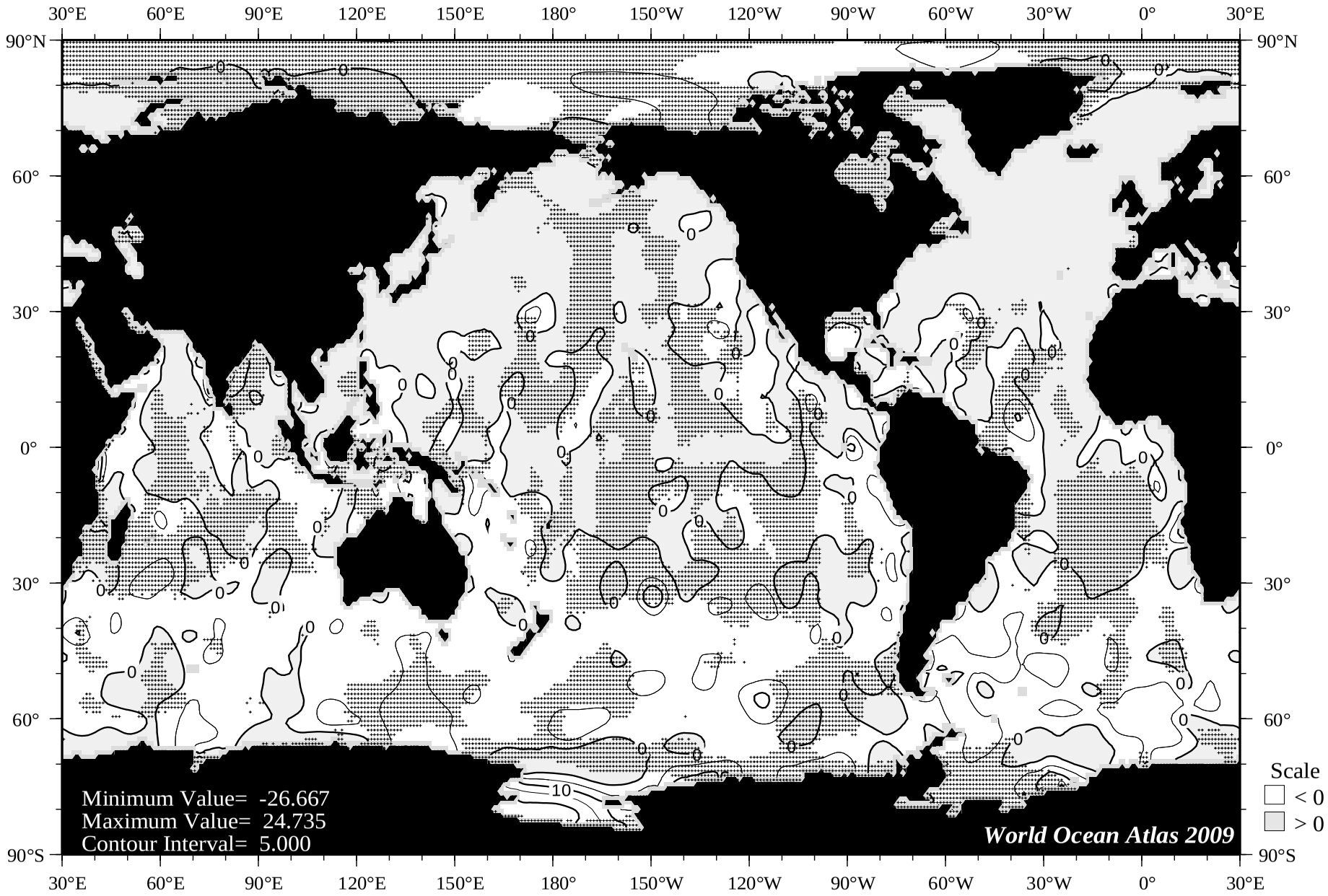

Fig I46 December minus annual percent oxygen saturation at the surface.

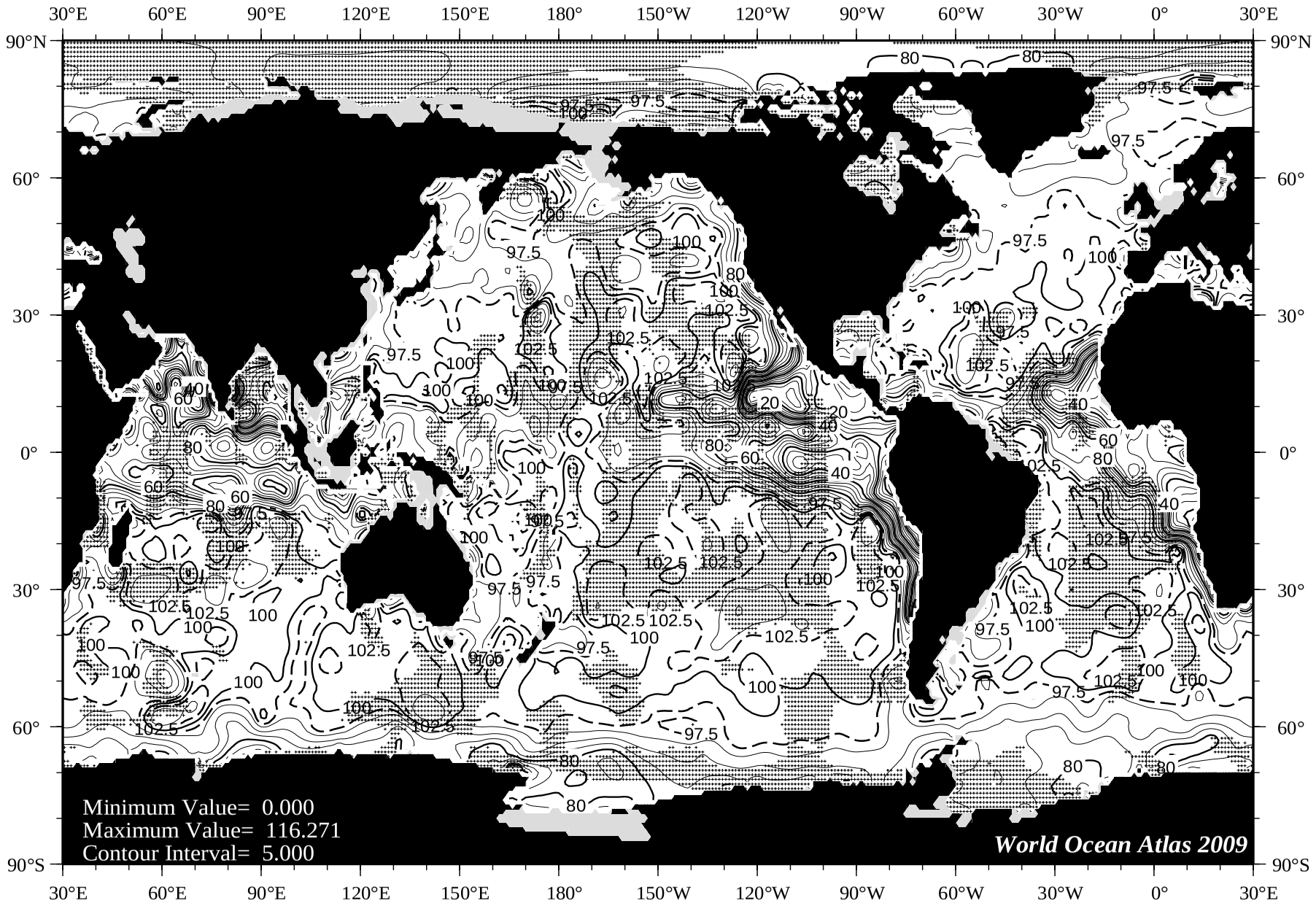

Fig I47 December mean percent oxygen saturation at 75 m. depth.

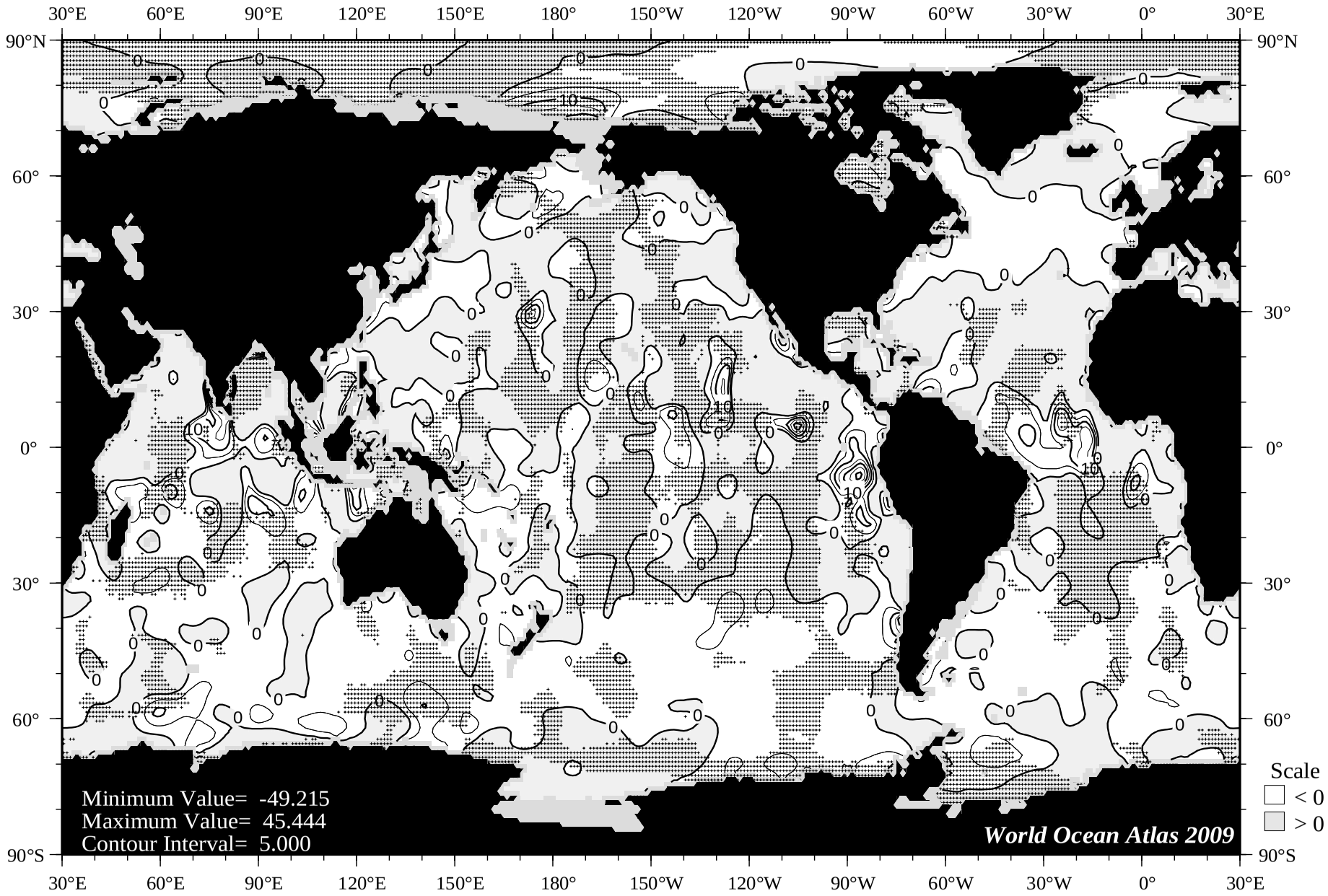

Fig I48 December minus annual percent oxygen saturation at 75 m. depth.